NUREG/CR-24
EPRI NP-2014
WCAP-9992
Vol. 1

PWR FLECHT SEASET 21-Rod Bundle Flow Blockage Task Data and Analysis Report

NRC/EPRI/Westinghouse Report No. 11

Main Report and Appendices A-J

Prepared by M. J. Loftus, L. E. Hochreiter, N. Lee,
M. F. McGuire, A. H. Wenzel, M. M. Valkovic

Jointly Sponsored by
USNRC, EPRI, and Westinghouse

GPO Printed copy price: $20.00

FLECHT SEASET Program
NRC/EPRI/Westinghouse Report No. 11
NUREG/CR-2444, Vol. 1
NP-2014
WCAP-9992

PWR FLECHT SEASET
21-ROD BUNDLE FLOW BLOCKAGE TASK
DATA AND ANALYSIS REPORT

September 1982

M. J. Loftus
L. E. Hochreiter
N. Lee
M. F. McGuire
A. H. Wenzel
M. M. Valkovic

prepared for

United States Nuclear Regulatory Commission
Washington, D. C. 20555

Electric Power Research Institute
3412 Hillview Avenue
Palo Alto, California 94303

and

Westinghouse Electric Corporation
Nuclear Energy Systems
P.O. Box 355
Pittsburgh, Pennsylvania 15230

by

Westinghouse Electric Corporation

under

Contract No. NRC-04-77-127, EPRI Project No. RP959-1

Program Management Group
NRC - L. H. Sullivan
EPRI - K. H. Sun
Westinghouse - D. G. Agate

NRC FIN B6204

NOTICE

ABSTRACT

This report presents data and limited analysis from the 21-Rod Bundle Flow Blockage Task of the Full-Length Emergency Cooling Heat Transfer Separate Effects and Systems Effects Test Program (FLECHT SEASET). The tests consisted of forced and gravity reflooding tests utilizing electrical heater rods with a cosine axial power profile to simulate PWR nuclear core fuel rod arrays. Steam cooling and hydraulic characteristics tests were also conducted. These tests were utilized to determine effects of various flow blockage configurations (shapes and distributions) on reflooding behavior, to aid in development/assessment of computational models in predicting reflooding behavior of flow blockage configurations, and to screen flow blockage configurations for future 163-rod flow blockage bundle tests.

ACKNOWLEDGMENTS

The authors acknowledge the efforts of the following Westinghouse Nuclear Energy Systems contributors, especially the continual and sustained efforts of C. E. Conway, D. P. Kitzmiller, J. Carovac, and A. Villella:

NTD PROJECTS
H. W. Massie, Jr.
L. Chajson
J. Cohen

SAFEGUARDS ENGINEERING
M. Y. Young/R. P. Vijuk
E. R. Rosal
T. S. Sobek
A. Tong
K. F. McNamee
D. P. Remlinger
D. W. Sklarsky
S. C. Yao

TEST ENGINEERING
L. R. Katz
J. T. Martin
B. R. Sinwell

TEST OPERATIONS
P. F. Orangio
A. C. Toth
H. F. Andrew
R. V. Rulis
R. J. Priddy
R. Freudenberg
J. Kalo
J. Latta
J. Thomas
W. Hamilton
D. C. Kalo

NUCLEAR FUEL DIVISION
D. L. Burman
P. Heasely

PUBLICATION PROGRAMS
J. G. Nagle

The work of the following members of the Program Management Group, their colleagues, and their consultants is hereby acknowledged:

EPRI - K. H. Sun
NRC-RSR - M. L. Picklesimer, L. H. Sullivan, A. L. M. Hon
NRC-NRR - W. Hodges, D. A. Powers
ORNL - R. W. McCulloch, S. D. Snyder
Battelle - C. Stewart
ITI - P. Davis

GLOSSARY

This glossary explains definitions, acronyms, and symbols included in the text which follows.

Axial peaking factor -- ratio of the peak-to-average power for a given power profile

Blocked -- a situation in which the flow area in the rod bundle or single tube is purposely obstructed at selected locations so as to restrict the flow

Bottom of core recovery (BOCR) -- a condition at the end of the refill period in which the lower plenum is filled with injected ECC water as the water is about to flood the core

Carryout rate fraction -- the fraction of the inlet flooding flow rate which flows out the rod bundle exit by upflowing steam

Carryover -- the process in which the liquid is carried in a two-phase mixture out of a control volume, that is, the test bundle

Core rod geometry (CRG) -- a nominal rod-to-rod pitch of 12.6 mm (0.496 inch) and outside nominal diameter of 9.50 mm (0.374 inch) representative of various nuclear fuel vendors' new fuel assembly geometries (commonly referred to as the 17 x 17 or 16 x 16 assemblies)

Cosine axial power profile -- the axial power distribution of the heater rods in the CRG bundle that contains the maximum (peak) linear power at the midplane of the active heated rod length. This axial power profile will be used on all FLECHT SEASET tests as a fixed parameter.

ECC -- emergency core cooling

Entrainment -- the process by which liquid, typically in droplet form, is carried in a flowing stream of gas or two-phase mixture

Fallback -- the process whereby the liquid in a two-phase mixture flows countercurrent to the gas phase

FLECHT -- Full-Length Emergency Core Heat Transfer test program

FLECHT SEASET -- Full-Length Emergency Core Heat Transfer - Systems Effects and Separate Effects Tests

Loss-of-coolant accident -- a break in the pressure boundary integrity resulting in loss of core cooling water

PMG -- Program Management Group

Separation -- the process whereby the liquid in a two-phase mixture is separated and detached from the gas phase

Silicon-controlled rectifier (SCR) -- a rectifier control system used to supply dc current to the bundle heater rods

Spacer grids -- the metal matrix assembly (egg crate design) used to support and space the heater rods in a bundle array

TABLE OF CONTENTS
Volume 1

TABLE OF CONTENTS (cont)

TABLE OF CONTENTS (cont)

TABLE OF CONTENTS (cont)

TABLE OF CONTENTS (cont)
VOLUME 2

LIST OF ILLUSTRATIONS

LIST OF ILLUSTRATIONS (cont)

LIST OF ILLUSTRATIONS (cont)

LIST OF ILLUSTRATIONS (cont)

LIST OF ILLUSTRATIONS (cont)

LIST OF ILLUSTRATIONS (cont)

LIST OF ILLUSTRATIONS (cont)

LIST OF ILLUSTRATIONS (cont)

LIST OF ILLUSTRATIONS (cont)

LIST OF ILLUSTRATIONS (cont)

LIST OF TABLES

SECTION 1
SUMMARY

As part of the NRC/EPRI/Westinghouse FLECHT SEASET reflood heat transfer and hydraulic program,[1] a series of forced flow and gravity feed reflooding tests, steam cooling tests, and hydraulic characteristics tests with flow blockage were conducted on a 21-rod bundle whose dimensions were typical of current PWR fuel rod arrays. The purpose of these tests was to screen various fuel rod flow blockage configurations which are postulated to occur in a hypothetical loss-of-coolant accident (LOCA), to determine which configuration provides the least favorable heat transfer characteristics. This blockage configuration will subsequently be placed in a larger 163-rod bundle[2] to evaluate the additional effect of flow bypass.[3] The 21-rod bundle data will also be utilized to develop a blockage heat transfer model. This blockage model will be assessed through comparison and analysis of the 163-rod blocked bundle data.

In this particular test program, a facility was built to accept a 21-rod bundle whose dimensions are typical of the PWR fuel rod array sizes currently in use by PWR and PWR fuel vendors. This test facility was very similar to the facility used in the 161-rod unblocked bundle task[4] and the flow areas were scaled appropriately. The

---

1. Conway, C. E., et al., "PWR FLECHT Separate Effects and Systems Effects Test (SEASET) Program Plan," NRC/EPRI/Westinghouse-1, December 1977.

2. Hochreiter, L. E., et al., "PWR FLECHT SEASET 161-Rod Bundle Flow Blockage Task: Task Plan Report," NRC/EPRI/Westinghouse-6, September 1980.

3. The 161-rod blocked bundle was changed to a 163-rod bundle by substituting two heater rods for two thimbles in order to provide better comparison with the 21-rod bundle, as discussed in section 3.

4. Loftus, M. J., et al., "PWR FLECHT SEASET Unblocked Bundle, Forced and Gravity Reflood Task Data Report," NRC/EPRI/Westinghouse-7, June 1980.

instrumentation plan was developed such that local thermal-hydraulic parameters could be calculated from the experimental data. Sufficient instrumentation was installed in the test facility to perform mass and energy balances from the data.

The forced reflood tests examined the two-phase flow effects of flow blockage on system pressure, rod power, flooding rate, coolant subcooling, and variable flooding rate. Steam cooling tests were also conducted to determine the single-phase flow effects of blockage as a function of the Reynolds number. Hydraulic characteristics tests were performed to determine the bundle friction factor, grid loss coefficient, and blockage loss coefficient.

Sample data obtained in tests which met the specified conditions are reported herein, including clad temperature, turnaround and quench times, heat transfer coefficients, flooding rates, exit steam flow, mass balance, differential pressures and calculated void fractions, steam temperatures, housing temperatures, blockage temperatures, pressure loss coefficients, and enhancement factors. All the valid data are available in the NRC Data Bank.

SECTION 2
INTRODUCTION

2-1. BACKGROUND

The flow blockage tasks in the FLECHT SEASET program are intended to provide sufficient data and resulting analysis such that the existing Appendix K, 10CFR50.46, flow blockage model (steam cooling requirements used in PWR safety analyses) can be reassessed and replaced by a suitably conservative but more physically realistic safety analysis model.

The FLECHT SEASET flow blockage test program has been coordinated with the programs conducted in Germany's FEBA tests[1] and Japan's SCTF tests.[2] The FEBA tests have been conducted on a 1 x 5 rod bundle and a 5 x 5 rod bundle with 62 percent and 90 percent blockage of the corner nine rods. The Japanese Slab Core Tests are being conducted on eight full-size simulated fuel rod bundles arranged in a row with two adjacent bundles blocked 62 percent in a coplanar fashion.

Appendix K requires that any effect of fuel rod flow blockage must be explicitly accounted for in safety analysis calculations when the core flooding rate drops below 25 mm/sec (1 in./sec). The rule also requires that a pure steam cooling calculation be performed in this case. To comply with this requirement, PWR vendors have developed semi-empirical methods of treating fuel rod flow blockage and steam cooling. Experimental data on single- and multirod burst test behavior have been correlated into

---

1. Ihle, P., et al., "FEBA - Flooding Experiments with Blocked Arrays - Heat Transfer in Partly Blocked 25-Rod Bundle," presented at 19th National Heat Transfer Conference, Orlando, FL, July 27, 1980.

2. Adachi, H., "SCTF - Core-1 Test Results," presented at Ninth Water Reactor Safety Research Information Meeting, Gaithersburg, MD, October 26-30, 1981.

a burst criterion which yields a worst planar blockage, given the burst temperature and internal rod pressure of the average power rod in the hot assembly. The test data used to establish this burst criterion indicate that the rod burst is random and noncoplanar, and is distributed over the axial length of the hot zone. When calculating the flow redistribution due to flow blockage, PWR vendors used multichannel codes to obtain the blocked channel flow.

Simpler models developed by Gambill[1] have also been used for flow redistribution calculations. In its ECCS evaluation model, Westinghouse modeled noncoplanar blockage as a series of planar blockages distributed axially over the region of interest, with each plane representing a given percentage blockage. The flow distribution effect was then calculated from a series of proprietary THINC-IV[2] computer runs and correlated into a simple expression for flow redistribution. The hot assembly was used as the unit cell in these calculations so that the individual subchannel flow redistribution effects generated by the noncoplanar blockage at a given plane are averaged and each subchannel has the same flow reduction. However, it should be remembered that the percentage of blockage simulated in these calculations was derived by examination of noncoplanar multirod burst data.

The resulting flow redistribution is then used to calculate a hot assembly enthalpy rise as part of the steam cooling calculation. The resulting fluid sink temperature and a radial conduction fuel rod model are then used to predict the clad peak temperature. Again, the flow redistribution or blockage effects and the steam cooling calculation are only used when the core flooding rate drops below 25 mm/sec (1 in./sec). Above 25 mm/sec (1 in./sec), the unblocked FLECHT heat transfer data are used.

---

1. Gambill, W. R., "Estimate of Effect of Localized Flow Blockages on PWR Clad Temperatures During the Reflood," CONF-730304-4, 1973.

2. Chelemer, H., et al., "An Improved Thermal-Hydraulic Analysis Method for Rod Bundle Cores," Nucl. Eng. Des. 41, 219-229 (1977).

A review of flow blockage literature[1,2,3,4] indicates that there are four primary heat transfer effects which need to be examined for both forced and gravity reflooding:

-- Flow redistribution effects due to blockage and their effect on the enthalpy rise of the steam behind the blockage. Bypass of steam flow could result in increased superheating of the remaining steam flow behind the blockage region. The higher the downstream steam temperature, the lower the rod heat flux and resulting heat transfer behind the blockage.

-- Effect of blockage downstream of the blockage zone and the resulting mixing of the steam and droplet breakup behind the blockage. The breakup of the entrained water droplets will increase the liquid surface area so that the drops will become a more effective heat sink for the steam. The breakup should desuperheat the steam; this would result in greater rod heat transfer behind the blockage zone in the wake of the blockage.

-- The heat transfer effects in the immediate blockage zone due to droplet impact, breakup, mixing, and cooling due to increased slip, as well as the increased steam velocity due to blockage flow area changes. The droplet breakup is a localized effect primarily caused by the blockage geometry; it will influence the amount of steam cooling which can occur farther downstream of the blockage.

---

1. Gambill, W. R., "Estimate of Effect of Localized Flow Blockages on PWR Clad Temperatures During the Reflood," CONF-730304-4, 1973.

2. Davis, P. R., "Experimental Studies of the Effect of Flow Restrictions in a Small Rod Bundle Under Emergency Core Coolant Injection Conditions," Nucl. Technol. 11, 551-556 (1971).

3. Rowe, D. S., et al., "Experimental Study of Flow and Pressure in Rod Bundle Subchannels Containing Blockages," BNWL-1771, September 1973.

4. Hall, P. C., and Duffey, R. B., "A Method of Calculating the Effect of Clad Ballooning on Loss-of-Coolant Accident Temperature Transients," Nucl. Sci. Eng. 58, 1-20 (1975).

-- Effect of blockage on the upstream region of the blockage zone due to steam bypass, droplet velocities, and sizes

In summary, the flow blockage heat transfer effects are a combination of two key thermal-hydraulic phenomena:

-- A flow bypass effect, which reduces the mass flow in the blocked region and consequently tends to decrease the heat transfer

-- A flow blockage effect, which can cause flow acceleration, droplet breakup, improved mixing, steam desuperheating, and establishment of new boundary layers, which consequently tends to increase the heat transfer

These two effects are dependent on blockage geometry and distribution and counteract each other such that it is not evident which effect dominates over a range of flow conditions.

2-2. TASK OBJECTIVES

The primary objectives of the 21-rod bundle tests were threefold:

-- To obtain, evaluate, and analyze thermal hydraulic data using 21-rod bundles to determine the effects of flow blockage geometry variation on the reflood heat transfer

-- To guide the selection of a blockage shape for use in the large blocked bundle task[1]

-- To develop an analytical or empirical method for use in analyzing the blocked bundle heat transfer data

---

1. Hochreiter, L. E., et al., "PWR FLECHT SEASET 161-Rod Bundle Flow Blockage Task: Task Plan Report," NRC/EPRI/Westinghouse-6, September 1980.

To achieve these objectives, the fuel rod burst and blockage literature and test programs were studied to find the most representative blockage shapes, which would be candidates for testing in the 21-rod bundle test facility. The shapes which were chosen and the bases for the choices are given in section 3. Many different shapes and distributions of the blockage sleeves are possible; these combinations have been reduced to a total of six test series in the 21-rod bundle through engineering judgment, examination of postulated flow blockage effects (paragraph 2-1), and examination of the existing flow blockage model or method of calculation suggested by Hall and Duffey.[1] The six 21-rod bundle test series are listed in table 2-1 with an explanation of the different effects which were expected to be observed from the experiments. The exact geometric description of each shape is given in section 3.

As shown in table 2-1, three of the five blockage configurations utilized a noncoplanar blockage sleeve distribution. This type of distribution was employed since most of the out-of-pile data indicated that burst occurs in a noncoplanar fashion. A noncoplanar blockage distribution has recently been observed in the in-pile NRU tests[2] being conducted in Canada. In the FLECHT SEASET flow blockage program, coplanar blockage is defined as bursts located at the same exact elevation. Noncoplanar blockage is defined as bursts located at different elevations; however, the blockage strain may overlap from rod to rod. The sleeves for all test series were smooth, and no attempt was made to simulate the burst opening in the clad. Tests were conducted with no blockage in the same facility at the same thermal-hydraulic conditions, to serve as a basis for evaluation of the flow blockage heat transfer.

To help ascertain both the hydraulic and the heat transfer effects of the flow blockage configurations relative to the unblocked bundle, single-phase hydraulic tests, steam cooling, forced reflood, and gravity reflood scoping tests were performed on each of the six bundles (with the exception that gravity reflood tests were not performed on the

1. Hall, P. C., and Duffey, R. B., "A Method of Calculating the Effect of Clad Ballooning on Loss-of-Coolant Accident Temperature Transients," Nucl. Sci. Eng. 58, 1-20 (1975).

2. "LOCA Simulation in the NRU Reactor," NUREG/CR-2152, PNL-3835, Volume 1, October 1981.

TABLE 2-1

BLOCKAGE SHAPES AND CONFIGURATIONS
TESTED IN 21-ROD BUNDLE

Test Series	Configuration Description	Comments
A	No blockage on the rods	This configuration served as a reference.
B	Short concentric sleeve, coplanar blockage on center nine rods	This series provided for both blockage effect and some bypass effects.
C	Short concentric sleeve, coplanar blockage on all 21 rods	This series was easiest to analyze, since it provides no flow bypass effects with maximum flow blockage effect at one axial plane.
D	Short concentric sleeve, noncoplanar blockage on all 21 rods	This test series examined a noncoplanar blockage distribution and was comparable to series C.
E	Long nonconcentric blockage sleeve, noncoplanar blockage on all 21 rods	This test series permitted a one-to-one comparison with series D in which all rods were blocked. Comparison of series D and E with unblocked data indicated the worst shape.
F	Test series E with increased blockage sleeve strain, noncoplanar blockage on all 21 rods	This test series increased the blockage effect relative to series E.

final configuration). The hydraulic tests were used to characterize the bundle in a hydraulic fashion by measuring the blockage pressure loss coefficient, grid loss coefficients, and the 21-rod bundle friction factor. These hydraulic parameters were then input to a COBRA-IV[1] model of the 21-rod bundle test facility. The COBRA-IV code (appendix A) was then used to calculate the single-phase flow redistribution in and around the blockage zone for each configuration. In this fashion, the measured local heat transfer was associated with a calculated local flow (single-phase) from COBRA to explain the heat transfer behavior.

The COBRA-IV calculations performed were single-phase steam flow redistribution calculations. Although the flow during reflooding was two-phase for most of the test time, the flow regime which existed above the quench front was highly dispersed flow. A typical void fraction above the quench front for the low flooding rate test conditions was 0.95. Therefore, steam flow was in the continuous phase and the relatively few droplets were not expected to affect the macroscopic (subchannel average) steam flow and/or flow redistribution. Sample calculations were performed and reported in the FLECHT SEASET program plan on the effect of steam redistribution on droplets. It was shown that, except for the extremely small drops, the liquid phase does not redistribute with the steam flow. The drops have sufficient inertia to continue their flight through the blockage zone without any significant deviations.

Single-phase steam cooling tests were conducted to provide a reference heat transfer environment compared to two-phase reflooding heat transfer data. In this manner, both the single- and two-phase effects of the blockage on the local rod heat transfer could be evaluated. Similarly, the gravity-driven blocked reflood tests permit one-to-one comparisons with the unblocked gravity reflood tests in the 21-rod bundle test facility for each blockage configuration.

The emphasis in the 21-rod bundle was on forced reflooding tests, since most of today's safety analysis evaluation models calculate a quasi-steady, decreasing flooding rate

1. Wheeler, C. L., et al., "COBRA-IV-I: An Interim Version of COBRA for Thermal-Hydraulic Analysis of Rod Bundle Nuclear Fuel Elements and Cores," BNWL-1962, March 1976.

into the reactor core. Also, forced flooding rate tests are easier to analyze and can be used more effectively to develop a flow blockage model or method of analysis through comparisons with identical unblocked forced reflooding tests. The gravity reflood scoping tests were performed to ensure that no additional hidden flow effects could cause a worst-case heat transfer situation as compared to the forced flooding test data. The data analysis emphasis in these experiments will be on calculation of the fluid conditions at each instrumented bundle axial plane, to help develop a model and a mechanistic explanation of the flow blockage effect in the bundle. The mechanistic model or empirical method of predicting blockage heat transfer will be evaluated in the larger 163-rod bundle test, where ample flow bypass can occur.

2-3. TEST FACILITY

The tests performed in this task are classified as separate effects tests. In this case, the bundle is isolated from the system and the thermal-hydraulic conditions are prescribed at the bundle entrance and exit. Within the bundle, the dimensions are full scale (compared to a PWR), with the exception of overall radial dimension. The low mass housing used in this test series was designed to minimize the wall effects. The housing was heated by radiation from the bundle to reduce the radial temperature gradient across the bundle and to minimize premature housing quench. To preserve proper thermal scaling of the FLECHT facility with respect to a PWR, the power to flow area ratio was made to be nearly the same as that of a PWR fuel assembly.

The locations of bundle instrumentation, such as heater rod thermocouples and steam temperature probes, were designed to be nearly the same for each blockage configuration. The instrumentation in the test facility loop, housing, flow system, and controls was identical for all test series. Through replicate tests at the same conditions in the same facility, the local heat transfer on a given blocked rod was compared to that on an unblocked rod, to obtain the effect of the flow blockage. Comparisons of this type, on a one-to-one basis with unblocked data, allowed the determination of which shape or distribution results in the poorest heat transfer relative to the unblocked geometry.

The tests in the 21-rod bundle flow blockage task utilized a core rod geometry, CRG,[1] that is typified by the Westinghouse 17 x 17 fuel rod design, as shown in table 2-2. This CRG is representative of all current vendors' PWR fuel assembly geometries.

TABLE 2-2

COMPARISON OF PWR VENDORS' FUEL ROD GEOMETRIES

Vendor	Rod Diameter [mm (in.)]	Rod Pitch [mm (in.)]
Westinghouse	9.50 (0.374)	12.6 (0.496)
Babcock & Wilcox	9.63 (0.379)	12.8 (0.502)
Combustion Engineering	9.70 (0.382)	12.9 (0.506)
Exxon	9.45 (0.372)	12.6 (0.496)

2-4. REFERENCE REFLOOD TEST CONDITIONS

Most of the tests in the 21-rod bundle test matrix were constant forced flooding reflood tests. The test conditions represent typical safety evaluation model assumptions and initial conditions.

The reflood phase of the PWR design basis LOCA transient is calculated to start approximately 30 seconds after initiation of a hypothetical break. At this time, the lower plenum, which had emptied during the blowdown, has refilled to the bottom of the

1. The CRG is defined in this program as a nominal rod-to-rod pitch of 12.6 mm (0.496 in.) and outside nominal diameter of 9.5 mm (0.374 in.), representative of various nuclear fuel vendors' new fuel assembly geometries and commonly referred to as the 17 x 17 or 16 x 16 assemblies.

core. The applicable reference assumptions for the reflood transient for a worst-case analysis of a hypothetical LOCA typical of a Westinghouse 17 x 17 four-loop PWR or other PWR vendor plant are as follows:

-- The core hot assembly was simulated in terms of peak linear power and initial temperature at the time of core recovery.

-- Decay power was ANS + 20 percent, as specified by appendix K of 10CFR50.46 and shown in figure 2-1.

-- The initial rod clad temperature is primarily dependent on the full-power linear heating rate at the time of core recovery. For the period from 30 seconds to core recovery or when the reflood water begins to flood the core, typical calculations yield an initial clad temperature in the hot assembly of 871°C (1600°F).

-- Coolant temperature was selected to maintain a constant subcooling to facilitate the determination of parametric effects.

-- Coolant was injected directly into the test section lower plenum for the forced flooding rate tests, and into the bottom of the downcomer for the gravity reflood tests. Injection into the bottom of the downcomer was used for better test facility pressure control.

-- Upper plenum pressure at the end of blowdown is approximately 0.14 MPa (20 psia) for an ice condenser plant, and about 0.28 MPa (40 psia) for a dry containment plant.

-- The tests were performed with a uniform radial power profile.

-- The axial power shape built into the heater rod was the modified cosine with a power peak-to-average ratio of 1.66, as shown in figure 2-2.

The use of the 1.66 axial profile will allow comparisons with the 161-rod unblocked and the 163-rod blocked bundle test data, since the bundle sizes are the primary difference among these tests.

The initially proposed reference test conditions and range of test conditions are listed in table 2-3, based upon the above reference assumptions.

2-5. HYDRAULIC CHARACTERISTICS TEST CONDITIONS

To evaluate the pressure losses associated with the rod friction, grids, and blockage sleeves, isothermal single-phase (water) tests were conducted for the one unblocked configuration and the five blockage configurations prior to the heat transfer tests. These hydraulic tests were conducted at a Reynolds number in the same range as that expected in the heat transfer tests. The expected range of Reynolds numbers was 2,000 to 15,000, which when simulated by 21°C (70°F) water provides flows from 4.7×10^{-4} to 3.5×10^{-3} m^3/sec (7.5 to 55 gal/min). This range of Reynolds numbers was based on the calculation from the 161-rod unblocked bundle,[1] which showed that approximately half of the injected water is evaporated into steam. These Reynolds numbers envelop flooding rates from 10 to 38 mm/sec (0.4 to 1.5 in./sec). Although the range of test conditions shown in table 2-3 includes a test at 152 mm/sec (6 in./sec), which corresponds to a Reynolds number of approximately 50,000, it was expected that the pressure loss coefficients would not vary significantly for turbulent flow Reynolds numbers greater than 10,000.

2-6. STEAM COOLING TEST CONDITIONS

The steam cooling tests were conducted at a Reynolds number corresponding to the bundle outlet steam phase Reynolds number of the constant flooding rate tests. The temperature of the outlet steam was limited to approximately 204°C (400°F) to prevent

---

1. N. Lee, et al., "PWR FLECHT SEASET Unblocked Bundle, Forced and Gravity Reflood Task Data Evaluation and Analysis Report," NRC/EPRI/Westinghouse-10, September 1981.

TABLE 2-3

REFERENCE AND RANGE OF TEST CONDITIONS FOR
21-ROD BUNDLE FLOW BLOCKAGE TASK

Parameter	Initial Condition	Range of Conditions
Initial clad temperature	871°C (1600°F)	260°C - 871°C (500°F - 1600°F)
Peak power	2.3 kw/m (0.7 kw/ft)	0.88 - 2.3 kw/m (0.27 - 0.7 kw/ft)
Upper plenum pressure	0.28 MPa (40 psia)	0.14 - 0.28 MPa (20 - 40 psia)
Flooding rate:		
-- Constant	25 mm/sec (1 in./sec)	10.2 - 152 mm/sec (0.4 - 6 in./sec)
-- Variable in steps	-	152 to 20 mm/sec (6.0 to 0.8 in./sec)
Injection rate (gravity reflood) - variable in steps	-	0.82 to 0.09 kg/sec (1.8 to 0.2 lb/sec)
Coolant ΔT subcooling	78°C (140°F)	3°C-78°C (5°F-140°F)

failure of the upper seals (made of polyurethane) on the heater rods. The tests were run to steady-state conditions in order to eliminate the effect of energy storage in the facility, and for ease of data analysis.

2-7. GRAVITY REFLOOD TEST DESCRIPTION

The gravity reflood tests were conducted to provide a simulation of the conditions expected to occur in reflooding the core after a LOCA. Coolant was injected into the simulated downcomer at flow rates which are representative of the nuclear power plant accumulators.[1] The downcomer was attached to the test facility lower plenum by the crossover leg, which was designed to provide a pressure loss coefficient equivalent to that of a reactor lower plenum and core inlet, or a value of approximately 11. The system pressure was controlled downstream of the test facility in the simulated containment and the hot leg flow resistance (of approximately 32.5) was simulated by a partially closed gate valve upstream of the simulated containment.

2-8. TEST MATRIX

The originally approved test matrix as developed in the task plan[2] consisted of 23 tests grouped into eight series, as shown in table 2-4. However, during the test program, several modifications and/or additions were made to the test matrix as discussed in the following paragraphs.

In the course of testing the first bundle, a defective turbine meter provided for a higher-than-specified forced reflood injection flow and, because of a coding error in the mass balance program, the test results were misinterpreted such that the rod power was subsequently increased. Most of the forced reflood tests were conducted with the high flow and high power. To provide direct bundle-to-bundle comparison, the forced reflood tests in all subsequent bundles were subjected to these same test conditions.

---

1. Waring, J. P., et al., "PWR FLECHT-SET Phase B1 Data Report," WCAP-8431, December 1974.

2. Hochreiter, L. E., et al., "PWR FLECHT SEASET 21-Rod Bundle Flow Blockage Task: Task Plan Report," NRC/EPRI/Westinghouse-5, March 1980.

TABLE 2-4

TEST MATRIX FOR 21-ROD BUNDLE FLOW BLOCKAGE TASK

Test No.	Pressure [MPa (psia)]	Rod Initial Temperature [°C (°F)]	Rod Peak Power [kw/m (kw/ft)]	Flow Rate [kg/sec (lb/sec)]	Inlet Subcooling [°C (°F)]	Parameter	Test Series
1	0.28 (40)	131 (267)	0.043 (0.013)	0.013 (0.03)	0	Steam	1
2	0.28 (40)	131 (267)	0.088 (0.027)	0.027 (0.06)	0	cooling	
3	0.28 (40)	131 (267)	0.11 (0.034)	0.034 (0.075)	0	test	
				Flooding Rate [mm/sec (in/sec)]			
4	0.28 (40)	871 (1600)	0.88 (0.27)	10 (0.4)	78 (140)	Constant	2
5	0.28 (40)	871 (1600)	1.3 (0.4)	15 (0.6)	78 (140)	flooding	(reference)
6	0.28 (40)	871 (1600)	2.3 (0.7)	20 (0.8)	78 (140)	rate	
7	0.28 (40)	871 (1600)	2.3 (0.7)	25 (1.0)	78 (140)	tests	
8	0.28 (40)	871 (1600)	2.3 (0.7)	38 (1.5)	78 (140)		
9	0.28 (40)	871 (1600)	2.3 (0.7)	152 (6.0)	78 (140)		
10	0.28 (40)	871 (1600)	0.88 (0.27)	10 (0.4)	78 (140)	Pressure	3
11	0.28 (40)	871 (1600)	1.3 (0.4)	15 (0.6)	78 (140)	effect	
12	0.28 (40)	871 (1600)	2.3 (0.7)	25 (1.0)	78 (140)	tests	
13	0.28 (40)	871 (1600)	2.3 (0.7)	25 (1.0)	3 (5)	Subcooling	4
14	0.28 (40)	871 (1600)	2.3 (0.7)	152 (6) 5 sec 20 (0.8) onward	78 (140)	Variable stepped flow	5
15	0.28 (40)	871 (1600)	2.3 (0.7)	25 (1.0)	78 (140)	Repeat test	6

TABLE 2-4 (cont)

TEST MATRIX FOR 21-ROD BUNDLE FLOW BLOCKAGE TASK

Test No.	Pressure [MPa (psia)]	Rod Initial Temperature [°C (°F)]	Rod Peak Power [kw/m (kw/ft)]	Flow Rate [kg/sec (lb/sec)]	Inlet Subcooling [°C (°F)]	Parameter	Test Series
16	0.28 (40)	871 (1600)	2.3 (0.7)	0.82 (1.8) 14 sec 0.095 (0.21) onward	78 (140)	Gravity reflood tests	7
17	0.14 (20)	871 (1600)	2.3 (0.7)	0.82 (1.8) 14 sec 0.095 (0.21) onward	78 (140)		
				Flooding Rate [m^3/sec (gal/min)]			
18	0.10 (15)	21 (70)	0	6.3×10^{-4} (10)	79 (142)	Hydraulic characteristics tests	8
19	0.10 (15)	21 (70)	0	1.3×10^{-3} (20)	79 (142)		
20	0.10 (15)	21 (70)	0	1.9×10^{-3} (30)	79 (142)		
21	0.10 (15)	21 (70)	0	2.5×10^{-3} (40)	79 (142)		
22	0.10 (15)	21 (70)	0	3.2×10^{-3} (50)	79 (142)		
23	0.10 (15)	21 (70)	0	3.8×10^{-3} (60)	79 (142)		

A steam cooling test was added and was conducted at the lowest Reynolds number which was possible in the 21-rod bundle test facility. The system pressure in the steam cooling tests was also reduced from 0.28 MPa (40 psia) to 0.14 MPa (20 psia) because of the upper heater rod seal temperature limit of 134°C (275°F). The temperature rise of the seal plate was greater than the difference between the saturation temperature of 130°C (267°F) at 0.28 MPa (40 psia) pressure and the seal temperature limit of 134°C (275°F).

The effect of the relatively cold housing on the bundle quench front and radial temperature profile was reduced by heating the housing to approximately 538°C (1000°F) peak temperature prior to the initiation of reflooding. The housing was heated by pulsing the heater rod bundle twice to approximately 649°C (1200°F) peak temperature. All reflood tests were conducted with a hot housing except for the 152 mm/sec (6 in./sec) forced flooding rate test, since the quench front progresses very rapidly and it was believed that the initial housing temperature would insignificantly affect the bundle behavior. (See appendix B for an evaluation of the housing effect.)

The 3°C (5°F) subcooling test could not be run in the first bundle, apparently because of the heat losses in the injection line which substantially reduced the temperature of the coolant prior to flood. However, a 28°C (50°F) subcooling test was run in the first bundle and in all subsequent bundles. In order to avoid pressure oscillations in the low subcooling test, the initial peak housing temperature was only 454°C (850°F).

Four additional forced reflood tests were conducted in configuration F instead of the gravity reflood tests, to provide a comparison between the 161-rod unblocked bundle and 163-rod blocked bundle at similar test conditions.

SECTION 3
BLOCKAGE SHAPES AND TEST CONFIGURATIONS

3-1. INTRODUCTION

The high internal pressure and temperature of fuel rods during a postulated PWR LOCA are expected to cause the fuel rods to swell and burst. The resulting rod deformation would reduce the fluid flow area in the rod array. The shape of the rod swelling and burst is referred to as a blockage shape. This flow area reduction (or flow blockage) is governed by the shapes and spatial distribution of blockage. Therefore, to simulate the thermal-hydraulic conditions of the fluid in the blocked rod array, blockage shapes and their spatial distribution must be chosen properly. The number of selected blockage shapes should be minimized to make blockage tests feasible, but it must be sufficient to address the important effects of the flow blockage on heat transfer. The spatial blockage distribution must also be chosen to represent realistic situations and to provide fundamental understanding of blockage effects on the local heat transfer.

The results of several single- and multirod burst tests were used to define the blockage shapes to be simulated in the 21-rod blockage task. Discussions with NRC and EPRI were also considered in the choice of blockage shape. The blockage shapes so determined were simulated by stainless steel sleeves attached to the rods to simulate flow blockage.

3-2. BLOCKAGE SHAPES

Several out-of-pile and in-pile burst tests have been performed to aid the understanding of rod burst phenomena during a LOCA. Out-of-pile tests have employed several heating methods to simulate rod heatup during a reflooding period. The heating methods include a stiff internal heater rod (continuous rigid heating element) method, external radiant heating, and direct resistance heating. The external radiant heating and direct

resistance heatup methods are believed to distort the thermal response of the clad deformation. The internal heater rod may reduce the clad temperature nonuniformity which is expected in the real situation of stacked fuel pellets. Although an out-of-pile test method is not ideal, it is generally agreed that an internal heater method is most representative of the real situation. Therefore the results from the tests using internal heater rod methods were reviewed in the 21-rod blockage task to provide a basis for defining blockage shapes as well as available in-pile test results.

The available results from several rod burst tests showed that there were two distinctive rod swelling patterns, depending on the burst temperature. This is due to the existence of two phases of Zircaloy, whose material properties are quite different from each other. Zircaloy is in the alpha phase at temperatures of less than 832°C (1529°F) and in mixed phase of alpha and beta types between 832°F and 970°C (1529°F and 1779°F). Above 970°C (1779°F), Zircaloy is in beta phase. Alpha phase Zircaloy has anisotropic strain properties. The deformation of Zircaloy at high temperatures is very sensitive to minor temperature irregularities since about 15°C (27°F) temperature difference will about double the strain rate. The anisotropic strain properties of Zircaloy cause the rods to shorten in proportion to the amount of circumferential strain. Thus, if a hot spot occurs on one side of the clad, the rod will bow with the hot side concave. This results in bringing the hot side of the clad closer to the heating rod which, in turn, increases the temperature difference around the clad and localizes the strain on one side of the rod. Although the burst phenomenon in the mixed phase is not well understood, this burst range can be treated essentially as alpha phase burst because of the anisotropic property of the alpha phase. Beta phase Zircaloy has isotropic strain properties. As the clad strains circumferentially, there is no rod shortening and no rod bow. Thus beta phase bursts tend to be more concentric.

Therefore, two typical blockage shapes respresenting alpha and beta phase swelling were chosen to be simulated in the 21-rod tests. The two blockage shapes are shown in figures 3-1 and 3-2. Detailed explanations of the choices are given in the 21-rod bundle flow blockage task plan.[1]

---

1. Hochreiter, L. E., et al., "PWR FLECHT SEASET 21-Rod Bundle Flow Blockage Task: Task Plan Report," NRC/EPRI/Westinghouse-5, March 1980.

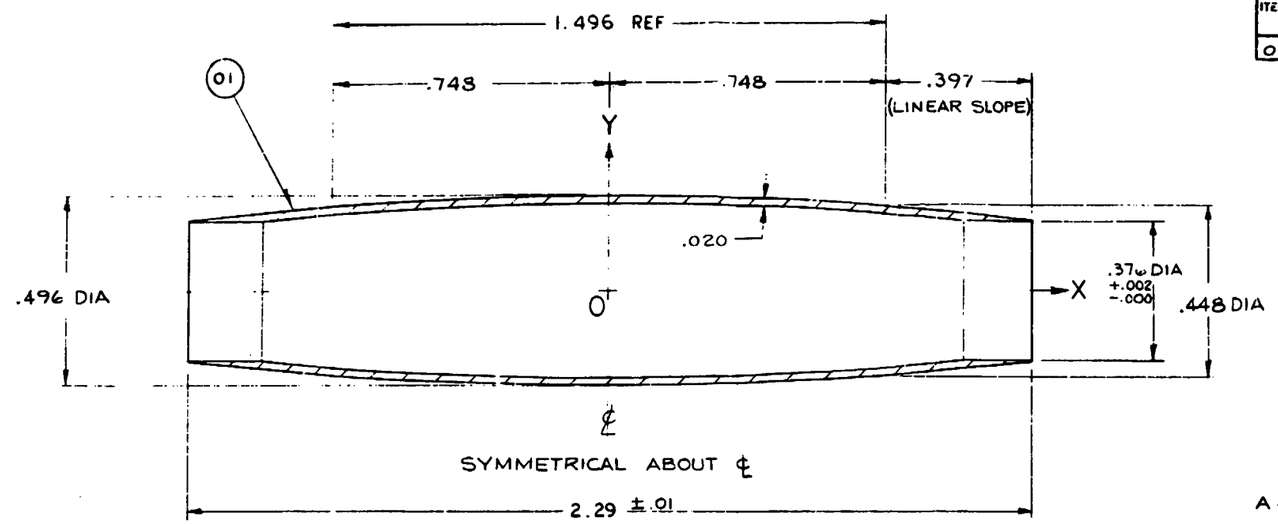

BILL OF MATERIAL						
ITEM	NOTE	PART NAME	DRAWING & GR OR IT.	MATERIAL	REQ 01	REQ 02
01	A	SLEEVE			1	

A - MAKE FR 300 SERIES SST

DIM. O-X	DIM. O-Y
0	.248
.10	.247
.20	.246
.30	.243
.40	.240
.50	.236
.60	.231
.70	.226
.748	.224

FORMULA : $-.748 < X < .748$

$Y = .024 \cos 120.3X + .224$

Figure 3-1. FLECHT SEASET 21-Rod Test Flow Blockage Sleeve

BILL OF MATERIAL								
ITEM	NOTE	PART NAME	DRAWING & SIZE OF IT	MATERIAL	REQ PER GROUP			
					01	02	03	04
01	A	SLEEVE			-			

A - MAKE FR 300 SERIES CST

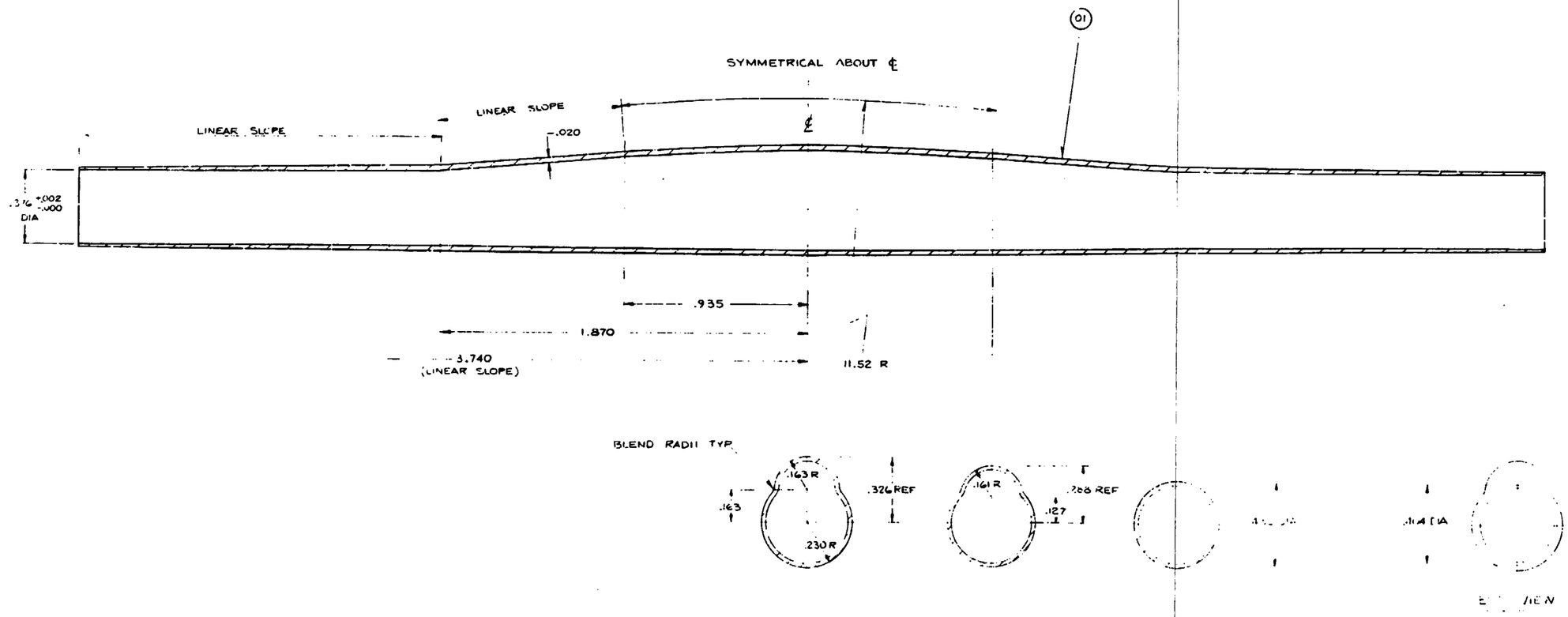

Figure 3-2. FLECHT SEASET 21-Rod Test Nonconcentric Flow Blockage Sleeve

3-3. BLOCKAGE CONFIGURATIONS

The 21-rod bundle task examined the reflooding phenomenon for simple blockage configurations in order to obtain a fundamental understanding of the heat transfer change effected by blockage and to select a worst blockage shape in terms of heat transfer. This selected shape will be used in a separate large blocked bundle test with ample bypass.[1] The effects of blockage on heat transfer are due to flow bypassing in the blockage zone and local flow behavior in and downstream of the blockage. Bypass flow is expected to reduce heat transfer in the blocked region because of reduction of fluid flow, but the geometry blockage itself may increase heat transfer as a result of increased turbulence and droplet disintegration. These two heat transfer effects are counteracting; for a clear understanding it is necessary to determine which effect can dominate under which thermal-hydraulic conditions. Therefore, this test series studied these effects to determine the relative importance of flow bypass and local blockage geometry on reflood heat transfer.

For these purposes, this test program utilized two blockage shapes (concentric and nonconcentric), different strains, and two blockage distributions (coplanar and noncoplanar). In the coplanar blockage distribution, all the sleeves on the rods are at the same axial elevation; the noncoplanar distribution does not have all the sleeves at the same elevation.

The following six blockage configurations were tested:

-- Unblocked (configuration A)[2]

-- Concentric sleeve, 32.6 percent maximum strain, coplanar on nine rods (configuration B)

---

1. Hochreiter, L. E., et al., "PWR FLECHT SEASET 161-Rod Bundle Flow Blockage Task: Task Plan Report," NRC/EPRI/Westinghouse-6, September 1980.

2. See table 2-1.

-- Concentric sleeve, 32.6 percent maximum strain, coplanar on all rods (configuration C)

-- Concentric sleeve, 32.6 percent maximum strain, noncoplanar on all rods (configuration D)

-- Nonconcentric sleeve, 36 percent maximum strain, noncoplanar on all rods (configuration E)

-- Nonconcentric sleeve, 44 percent maximum strain, noncoplanar on all rods (configuration F)

The concentric and nonconcentric sleeves are shown in figures 3-1 and 3-2, respectively.

The unblocked configuration was required as a reference. The next three configurations (B, C, and D) employed concentric sleeves which represent the blockage shape resulting from a high-temperature beta phase burst of Zircaloy clad. The coplanar sleeve location was chosen because of its geometric simplicity, which is advantageous for data analysis. Configuration B was expected to show the effect of a partial bypass of fluid flow. Configuration C, with sleeves on all rods, was designed to study blockage effect without bypass. Configuration D was noncoplanar, to simulate the expected blockage distribution. The method of distributing sleeves in a noncoplanar way is discussed in paragraph 3-4.

Configuration E used long nonconcentric sleeves on 21 rods. The results of this test were compared to those from configuration D to help determine the effect of sleeve shape and geometry on reflood heat transfer. These comparisons showed that the nonconcentric sleeve gave poorer heat transfer than the concentric sleeve, as discussed in appendix C. Therefore the nonconcentric sleeve was used in configuration F with the higher strain, to examine the strain effect.

3-4. Noncoplanar Blockage Distribution

A noncoplanar blockage test configuration requires a method to axially distribute the blockage sleeves. The following paragraphs describe the method of distributing the blockage sleeves on the heater rods. The objective was to locate blockage sleeves in the bundle in such a manner that the statistics of the location coincide with the expected deformation and bursts of a PWR. The basis of this approach is the following statement from the ORNL multirod burst test results: "Posttest deformation measurements showed excellent correlation with the axial temperature distribution, with deformation being extremely sensitive to small temperature variations."[1]

Burman and Olson[2] have studied temperature distributions on rods in a bundle. Their method can be employed to determine the statistics of burst locations in the bundle.

The burst locations so determined were selected without considering the grid effect on burst location which was observed in the German REBEKA tests.[3] It was found that rod burst locations were shifted toward the fluid flow direction because of enhanced heat transfer downstream of the grids.

Incorporation of this hydraulic effect on burst location requires knowledge of the time of rod burst. Rod bursts during blowdown are expected to occur at locations shifted downward, because of the downward fluid flow at the time. Burst at the end of blowdown and during refill may not be affected by fluid flow because there is little fluid flow at these times. During the reflood phase, rod bursts will occur at locations shifted upward.

---

1. Chapman, R.H., "Significant Results from Single-Rod and Multirod Burst Tests in Steam With Transient Heating," paper presented at Fifth Water Reactor Safety Research Information Meeting, Gaithersburg, MD, November 7-10, 1977.

2. Burman, D.L., and Olson, C.A., "Temperature and Cladding Burst Distributions in a PWR Core During LOCA," Specialists Meeting on the Behaviour of Water Reactor Fuel Elements Under Accident Conditions, Norway, September 13, 1976, pp 73-77.

3. Wiehr, K., et al., "Fuel Rod Behavior in the Refill and Flooding Phase of a Loss-of-Coolant Accident," CONF-771252-5, December 1977.

Fuel rods in a PWR can burst at any phase of a LOCA transient, depending on power distribution, operating life, type of break, material strength uncertainties, and the like. Therefore, the hydraulic effect can be incorporated into the determination of burst locations in several ways. However, the primary objective in the present study is the study of local heat transfer under a typical blockage distribution; such an objective can be achieved without considering the hydraulic effect.

To determine burst locations, it is assumed that all rods to be deformed have the same or similar temperature distribution. The ORNL multirod burst tests showed that there were no interactions among rods during burst, so it may be assumed that each rod in a bundle bursts independently. Then the characteristics of one rod may be used to infer the behavior of the rod bundle.

A rod is divided into several sections with the same interval. Burman and Olson computed the probability that a certain section (say, the i-th increment) of a fuel rod is at the highest temperature in the rod as follows:

$$\int_0^\infty \left\{ \frac{1}{\sigma_T\sqrt{2\pi}} \exp\left[\frac{(\mu_i - T)^2}{2\sigma_T^2}\right] \prod_{j=1,N,\, j\neq i} \frac{1}{\sigma_T\sqrt{2\pi}} \int_0^T \exp\left[\frac{-(\mu_i - t)^2}{2\sigma_T^2}\right] dt \right\} dT \quad (3\text{-}1)$$

Here σ_T and μ_i are the standard deviation of local temperature and the mean temperature at the i-th increment, respectively. It can be seen that these two characteristics (σ_T and μ_i) must be known to compute the local probability of highest temperature. As the ORNL test showed, this highest-temperature location can be interpreted as the burst location.

The mean temperature distribution required in equation (3-1) is the axial mean temperature of a nuclear fuel rod at the time of rod burst. The standard deviation of local temperature is included to account for the local temperature fluctuation. Burman and Olson assumed that the fluctuation is normally distributed.

The local temperature can be divided into two components:

$$T_{local} = \bar{T}_{local} + T'_{local} \qquad (3\text{-}2)$$

where $\bar{T}_{local}$ and T'_{local} are the mean and the variation of local temperature, respectively. The mean temperature is obtained from the axial mean temperature distribution. The local temperature variation is a function of the following effects:

-- Manufacturing effects

Initial fuel pellet density
Fuel pellet diameter
Fuel enrichment
Manufacturing variables which affect fuel densification
Clad local ovality
Fuel pellet chemical bonding

-- In-pile effects

Fuel pellet radial offset within clad
Fuel pellet cracking
Fuel densification

Burst probabilities at each rod increment can be computed by equation (3-1) with the inputs of σ_T and μ_i.

Westinghouse has developed a statistical method for the distribution of sleeves in a 163-rod bundle according to the probability distribution calculated above. However, this method cannot be applied directly to the 21-rod bundle, because of the small sample number. Therefore, the method was modified for the small bundle. The method used for the 21-rod bundle maintains the principle of the previous statistical arguments and can be applied to the large bundle to remove the slight dependency of the axial blockage distribution on sample random numbers.

Multiplying the probabilities by the total rod number gives theoretical burst numbers at the corresponding axial increments. These numbers are usually not integers. Therefore, for practical purposes, these numbers are transformed to integers to satisfy the requirement that the total burst number is the same as the total rod number. These integer numbers indicate how many sleeves should be located at specific axial increments. This procedure is shown schematically in figure 3-3. An increment (i-th) is then selected at random. Since it is known from the above calculation that N_i rods have bursts at this increment, N_i rods are selected at random. Each of these selected rods has a sleeve on the i-th increment. Then another increment and corresponding rods are selected at random. This procedure is repeated until all the axial increments where bursts occur have been considered.

A computer program was written to execute this procedure for selection of sleeve locations. This program, called COFARR (Coolant Flow Area Reduction), calculates subchannel blockage with given input strain information of the blockage sleeve. The program is discussed in appendix D.

3-5. Input Data

The mean temperature distribution at time of burst and local temperature fluctuation data are required to compute burst probability from equation (3-1). In addition, strain information is required to compute actual blockage distribution and subchannel area.

Westinghouse requested that the three other PWR fuel vendors (Babcock & Wilcox, Combustion Engineering, and Exxon) provide relevant information to calculate a noncoplanar blockage distribution.

Westinghouse calculated a mean temperature distribution at the time of burst (figure 3-4) by analyzing a LOCA. Burst was calculated to occur at the end of blowdown. Babcock & Wilcox[1] calculated an axial temperature distribution for its

1. Personal communication from J. J. Cudlin, Babcock & Wilcox, to H. W. Massie, Jr., Westinghouse, April 5, 1978.

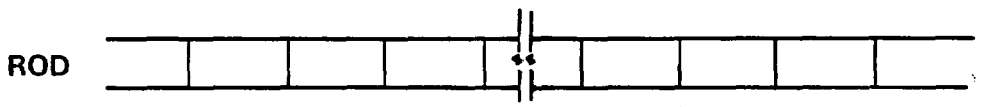

INCREMENT NUMBER	1	2	3		L-1	L
BURST PROBABILITY [EQ. (4-7)]	P_1	P_2	P_3		P_{L-1}	P_L
N P_i	X_1	X_2	X_3		X_{L-1}	X_L
SLEEVE NUMBER AT THE i-th INCREMENT	n_1	n_2	n_3		n_{L-1}	n_L

$\left(\sum_{L=1}^{L} n_i = N \right)$ N: TOTAL ROD NUMBER

Figure 3-3. Procedure for Determining Sleeve Numbers on Each Axial Increment

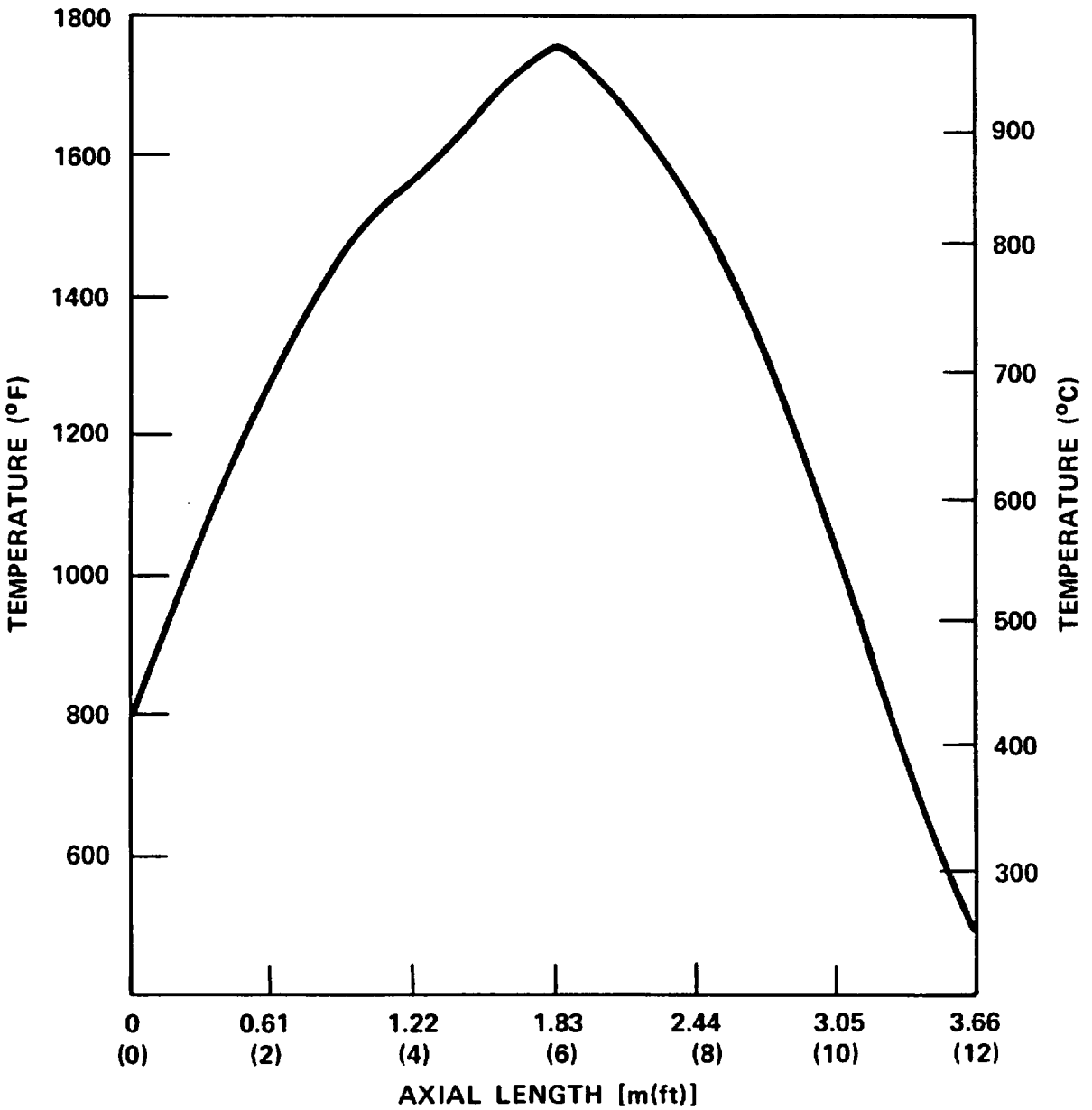

Figure 3-4. Westinghouse Mean Temperature Distribution

plant (15 x 15 fuel) for a 0.794 m^2 (8.55 ft^2) double-ended cold leg break. Babcock & Wilcox also analyzed a plant with 17 x 17 fuel for the same accident case. Clad rupture was calculated to occur during blowdown. Combustion Engineering[1] analyzed its 16 x 16 fuel assembly for a worst-temperature distribution using LOCA licensing analysis codes and input data. Exxon[2] also used its WREM ECCS model to get a mean temperature distribution for a 15 x 15 fuel assembly at the time of rod rupture. Comparisons of the available mean temperature data reveal that Westinghouse and Babcock & Wilcox plants are expected to have the most peaked axial temperature distributions. The Westinghouse temperature distribution was chosen to be a reference case. Detailed discussion of this analysis can be found in the task plan.

Manufacturing quality assurance records were reviewed by Burman and Olson to determine the realistic distribution for pellet parameters which would have an effect on local temperature variation, such as enrichment (negligible), initial density, sintering characteristics, diameter, and surface roughness. The variations thus obtained were input into Westinghouse standard design codes to determine their effect on operating temperature. Perturbation studies were analyzed to determine the effect of small variations in initial power and temperature on the clad temperature at the time of burst, for cases in which burst occurred during refill. The initial temperature distributions were then modified to account for these effects. The resulting responses were statistically combined to obtain the overall temperature uncertainty just prior to the accident due to manufacturing variables. The resulting standard deviation in temperature was found to be approximately 9.80°C (17.6°F).

Of the various uncertainties in pellet temperature due to in-pile effects, only the standard deviation in pellet temperature due to pellet offset was analyzed. Using a finite difference program, the effect of pellet eccentricity on pellet average temperature during normal operation was calculated, assuming various degrees of pellet clad eccentricity. The resulting temperature distribution was convoluted with that arising

---

1. Personal communication from J. H. Holderness, Combustion Engineering, to H. W. Massie, Jr., Westinghouse, April 11, 1978.

2. Personal communication from R. E. Collingham, Exxon Nuclear, to M. W. Hodges, USNRC, August 3, 1978.

from manufacturing uncertainties and the convoluted sum corrected to account for the temperature variability at burst time for a given temperature variability at power. This variation was determined to be 9.11°C (16.4°F). When statistically combined with the uncertainties due to manufacturing variables, the total standard deviation in local temperature becomes 13°C (24°C) at the time of blowdown or 7°C (12°F) at the time of burst.

In summary, the mean temperature distribution of Westinghouse (figure 3-4) and a standard deviation of 7°C (12°F) were chosen as a case to calculate a noncoplanar blockage distribution.

Strain data were used to finalize the sleeve shapes discussed in this chapter. A real blockage distribution can be calculated by COFARR with input sleeve geometries which were selected for the 21-rod bundle (paragraph 3-2).

It is expected that rod bursts in a bundle will show a range of strain and shape sizes; however, a single size strain was suggested for all rods in the present tests for simplicity of both experimental setup and data analysis. The effect of different sleeve sizes was indirectly addressed by tests with a higher-strain sleeve.

Strain data are available from various rod burst tests. The results of the ORNL multi-rod burst tests are plotted in figure 3-5, along with the German in-pile test results. In the ORNL in-pile test, strains ranging from 26 to 42 percent were observed. The German in-pile test showed relatively low strains, ranging from 8 to 32 percent.

The most representative strain value is considered to be about 36 percent, with a standard deviation of 8 percent, assuming that strains are distributed normally.

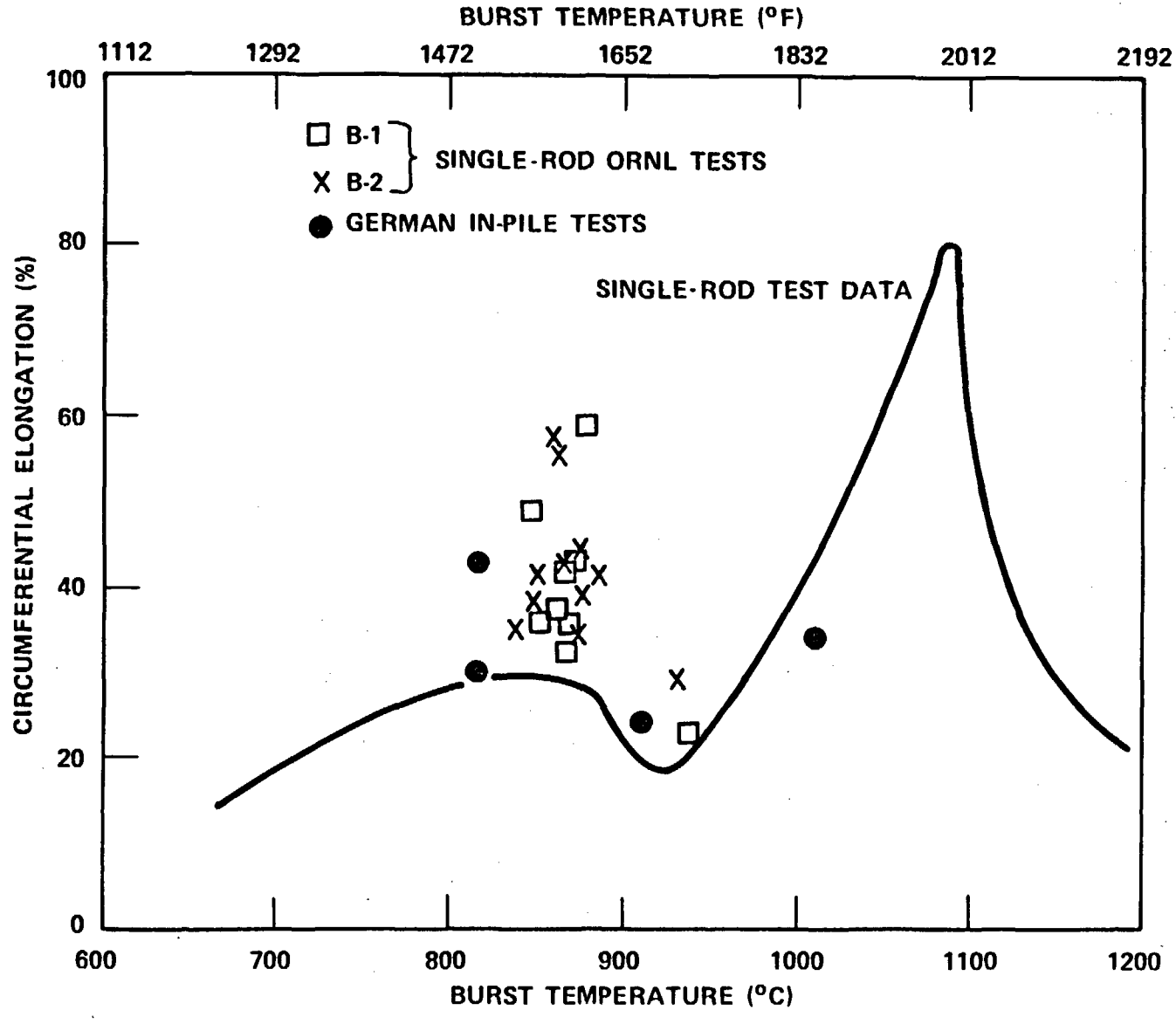

Figure 3-5. Strain Data From ORNL Rod Burst Tests and German In-Pile Tests

16,047-28

This is also consistent with the data of the REBEKA test.[1,2] Therefore, a strain of 36 percent was chosen as a reference case for tests with nonconcentric sleeves. A strain of 44 percent was selected for the higher-strain nonconcentric sleeve. The strain relation between the concentric and nonconcentric sleeves is discussed in the following paragraphs.

3-6. Relationships Between Different Configurations

Several configurations and sleeve shapes were employed in this series, as explained above. The results obtained from these tests were intended to be used to determine a blockage shape heat transfer and to obtain a better understanding of heat transfer in blocked bundles. Therefore one must establish the bases of comparison between different test conditions for these purposes.

Two distinct pairs of test configurations are significant: concentric versus nonconcentric sleeve shapes and coplanar versus noncoplanar sleeve arrangements.

3-7. Concentric Versus Nonconcentric Sleeve Shapes -- As noted above, the 21-rod test results were intended to be used to determine a blockage shape which provides the least favorable heat transfer. To select the sleeve shape, it is necessary to establish a certain basis of comparison.

The blockage configurations allow one set of sleeve comparisons: test configurations A and D versus test configurations A and E.

As discussed earlier, the sleeve locations for configurations D and E are the same, since the inputs of mean temperature and standard deviation are the same for both cases.

---

1. Erbacher, F., et al., "Interaction Between Thermohydraulics and Fuel Clad Ballooning in a LOCA, Results of REBEKA Multi-Rod Burst Tests With Flooding," presented at Sixth Water Reactor Safety Research Meeting, Gaithersburg, MD, November 1978.

2. Wiehr, K., "Results of REBEKA Test 3," presented at Zircaloy Cladding Research Review Meeting, Idaho Falls, ID, June 1979.

Also, the reference strain of the nonconcentric sleeve was taken as 36 percent. Therefore the remaining question is what strain should be used for the concentric sleeve to provide a meaningful comparison between the two sleeves. The following two alternatives were considered:

-- Maintain the maximum blockage from the single concentric sleeve the same as that of the nonconcentric one.

-- Maintain the bundle-wide maximum blockage the same.

Each alternative is a valid basis for comparison. However, the second case requires that the strain be determined as a function of number of sleeves and axial sleeve distribution. That is, this comparison provides a very restricted case. The first case is not affected by these parameters and considered to be more general.

Therefore the strain of the concentric sleeve was selected to have the same maximum flow blockage as the maximum blockage of the nonconcentric sleeve, as indicated in figure 3-6. This gives the maximum strain of the concentric sleeve as 32.6 percent.

The resultant tests of configurations D and E were evaluated by calculating the enhancement factor, Ne, which is defined by the following equation according to the Hall and Duffey approach:[1]

$$\frac{h_b}{h_o} = \left(\frac{G_b}{G_o}\right)^m Ne \qquad (3\text{-}3)$$

where h and G are the heat transfer coefficient and fluid flow rate, respectively; m is a constant. Subscripts b and o represent blocked and unblocked bundles, respectively. Detailed discussions are provided in section 6.

---

1. Hall, P. C., and Duffey, R. B., "A Method of Calculating the Effect of Clad Ballooning on Loss-of-Coolant Accident Temperature Transients," Nucl. Sci. Eng. 58, 1-20 (1975).

A. CROSS-SECTIONAL VIEW AT MAXIMUM BLOCKAGE FOR CONCENTRIC SLEEVE

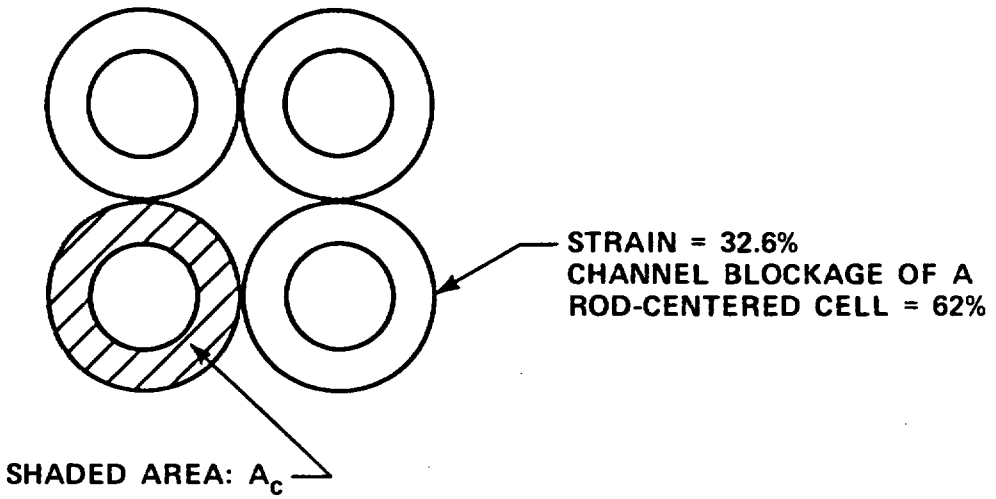

B. CROSS-SECTIONAL VIEW AT MAXIMUM BLOCKAGE FOR NONCONCENTRIC SLEEVE

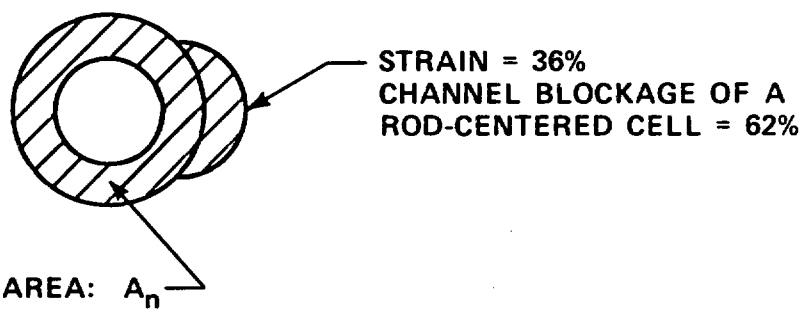

NOTE: $A_c = A_n$

Figure 3-6. Blockage Sleeve Maximum Strain

3-8. Coplanar Versus Noncoplanar Sleeve Distributions -- When coplanar and noncoplanar sleeve test results are compared, one parameter must be kept constant. The parameter may be either sleeve strain or overall pressure drop. However, keeping the pressure drop constant is difficult, because the total pressure drop is expected to be small and it is difficult to predict such a small pressure drop with good accuracy. Keeping the strain constant is straightforward. It is also a sensible way to study heat transfer phenomena, with the degree of noncoplanarity as a parameter. The coplanar arrangement is a special case in which the noncoplanarity (or local temperature uncertainty) is zero.

3-9. Sleeve Distributions

The following paragraphs describe the actual sleeve distribution used in each bundle as a result of the analysis of the preceding paragraphs.

3-10. Configurations B and C -- Configuration B had sleeves on the center nine rods, and configuration C had sleeves on all the rods. The sleeves on the eight corner rods were modified to fit into the housing, as shown in figure 3-7. The centers of the concentric sleeves were located at 1.85 m (73 in.) from the bottom of the bundle for both cases.

3-11. Configurations D, E, and F -- A noncoplanar sleeve distribution was calculated using COFARR (appendix D), as shown in figure 3-8, using a 25 mm (1 in.) node length. As indicated above, the same sleeve distribution was used for all these configurations. That is, the middle of a sleeve was located at the middle of the indicated node on each rod.

The sleeves on the eight corner rods for these configurations were also modified to fit into the housing, as in configurations B and C.

3-12. Bulge Directions for Nonconcentric Sleeves -- Data from Westinghouse multirod burst tests[1] showed a thimble effect on circumferential burst location (appendix E). The burst locations were not random, and were usually directed away from thimbles. This indicated that the thimbles were good heat sinks, causing nonuniform circumferential temperature distributions on neighboring rods. It must be noted that a burst occurs at the hottest point of a rod; major flow blockage due to burst is on the opposite side of the burst location.

Observations from the Westinghouse tests indicate that burst can occur toward either adjacent subchannels or rods. For the present purpose it was proposed that bursts be restricted to occur only toward adjacent subchannels for the following reasons:

-- Blockage study is not intended to investigate detailed variations in a subchannel but to determine average subchannel behavior.

-- The additional parameter of burst orientation makes data analysis complicated without an apparent improvement of understanding.

-- There are physical limitations in installing the blockage sleeves on the rods.

The above finding and proposal provided the bases for selecting bulge directions of the nonconcentric sleeves in the 21-rod bundle. First it is necessary to find the hottest subchannel out of the four subchannels surrounding each rod. Then the bulge direction is the opposite side of the hottest point.

Since an effort had been made to couple the 21-rod bundle to the 163-rod bundle to maximize data utilization,[2] it was better to consider the relative location of the 21-rod island in a fuel assembly in applying the present method to the small bundle

---

1. Schreiber, R. E., et al., "Performance of Zircaloy Clad Fuel Rods During a Simulated Loss-of-Coolant Accident -- Multirod Burst Tests," WCAP-7495-L, April 1970.

2. L. E. Hochreiter, et al., "PWR FLECHT SEASET 161-Rod Bundle Flow Blockage Task: Task Plan Report," NRC/EPRI/Westinghouse-6, September 1980. NUREG/CR-1531.

BILL OF MATERIAL								
ITEM	NOTE	PART NAME	DRAWING # OR SPEC	MATERIAL	REQ PER GROUP			
					01	02	03	04
01	C	SLEEVE		304 SST	1			

C - MAKE FROM .500 O.D. x .065 WALL

DIM. O-X	DIM. O-Y
0	.248
.10	.247
.20	.246
.30	.243
.40	.240
.50	.236
.60	.231
.70	.226
.748	.224

FORMULA:
$-.748 < x < .748$
$Y = .024 \cos 120 .3X + .224$

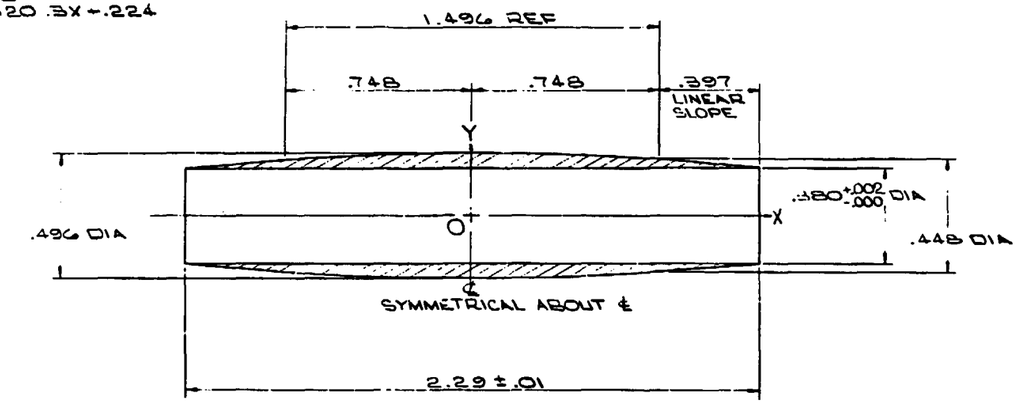

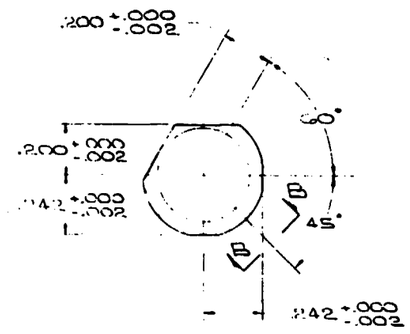

SECTION A-A

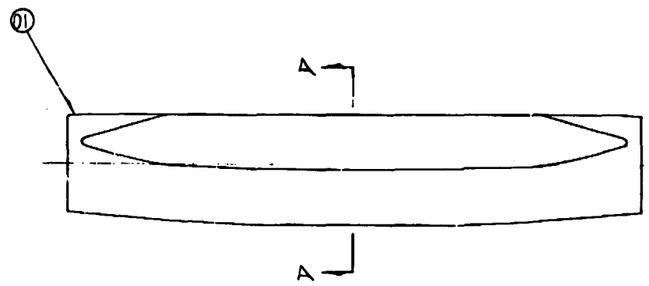

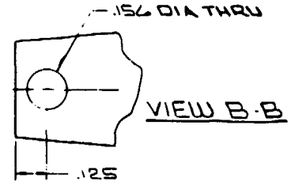

VIEW B-B

Figure 3-7. Modified Blockage Sleeve on Eight Peripheral Heater Rods

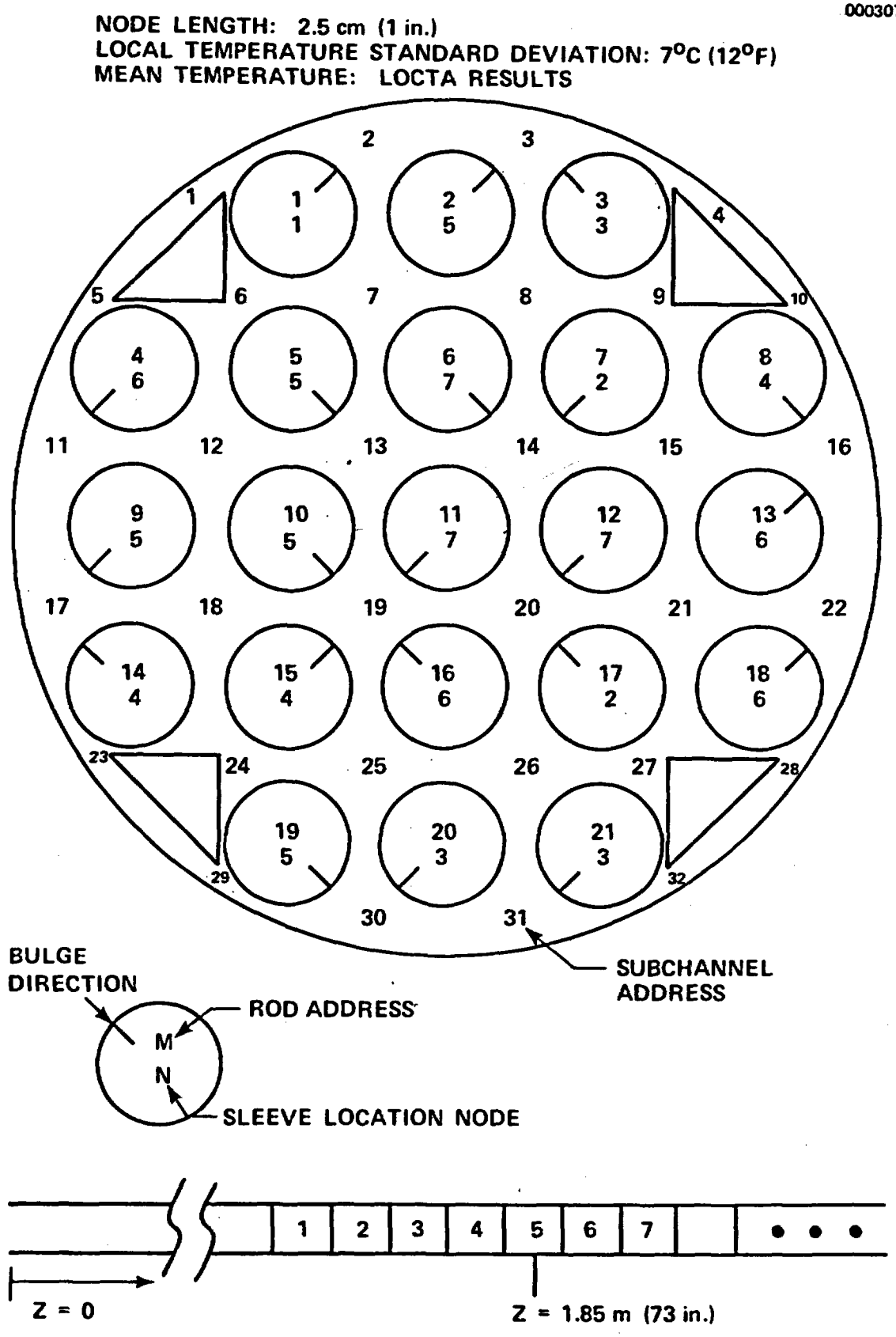

Figure 3-8. Noncoplanar Sleeve Distribution and Bulge Direction for Nonconcentric Sleeves

(figure 3-9). For this case it was straightforward to find out the hottest subchannel (or subchannels) associated to each rod, because of the unique distribution of the thimbles.

The above arguments were used to determine the possible bulge directions in the 21-rod bundle, as indicated by dots in figure 3-9. The bulge directions of some rods were determined uniquely; others had several possible locations. Bulge directions of the rods with multiple choices could be chosen from the possible locations so that the four center subchannels have high blockages. The locations of the peripheral rods with multiple choice could be chosen arbitrarily from the possible locations. The resulting bulge directions are shown in figure 3-8.

3-13. Bundle-Wide Blockage Distributions -- The resulting bundle-wide blockage distributions of configurations C through F were calculated, and are shown in figure 3-10.

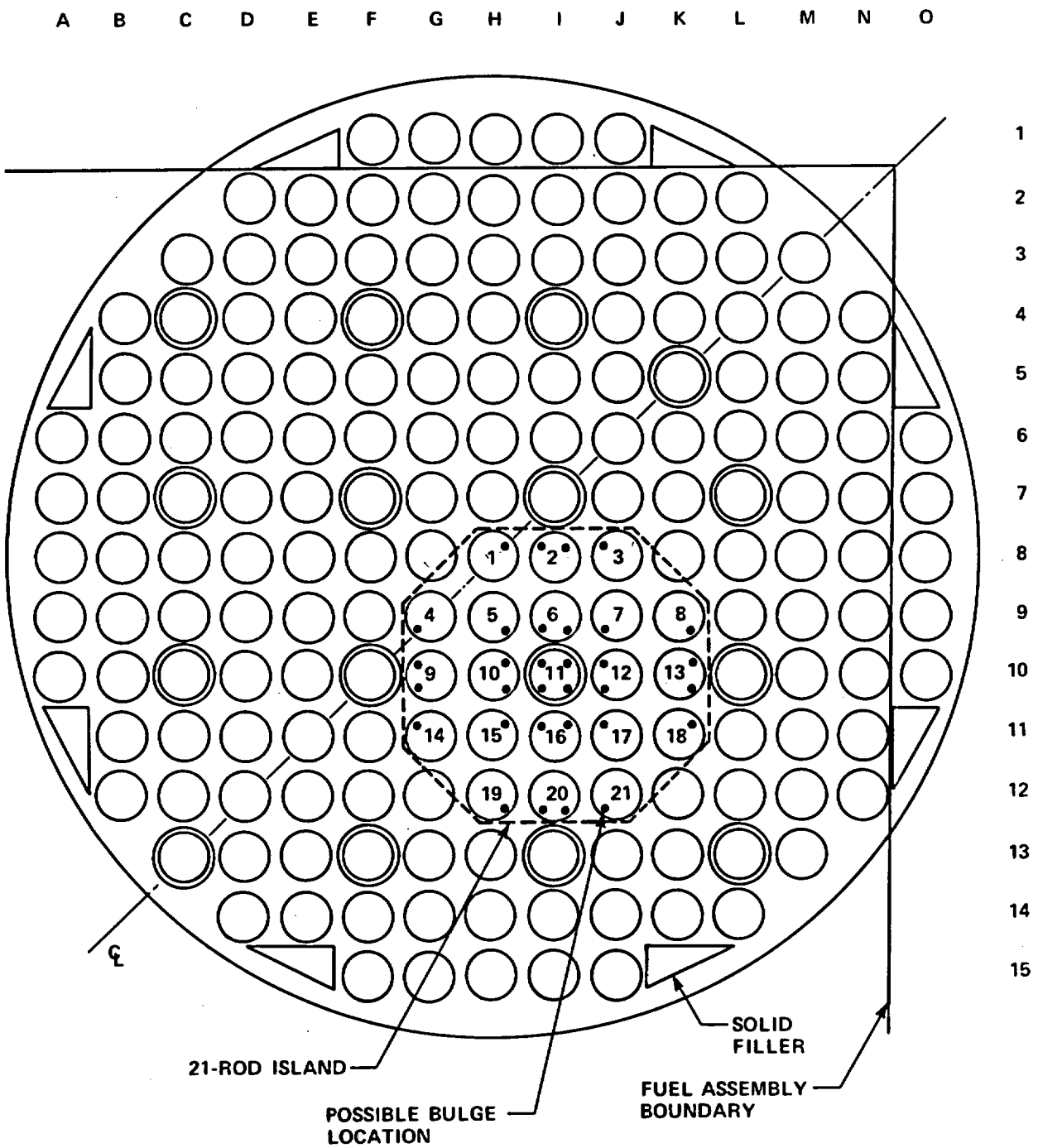

Figure 3-9. Potential Bulge Directions and Comparison Between the Two Bundles

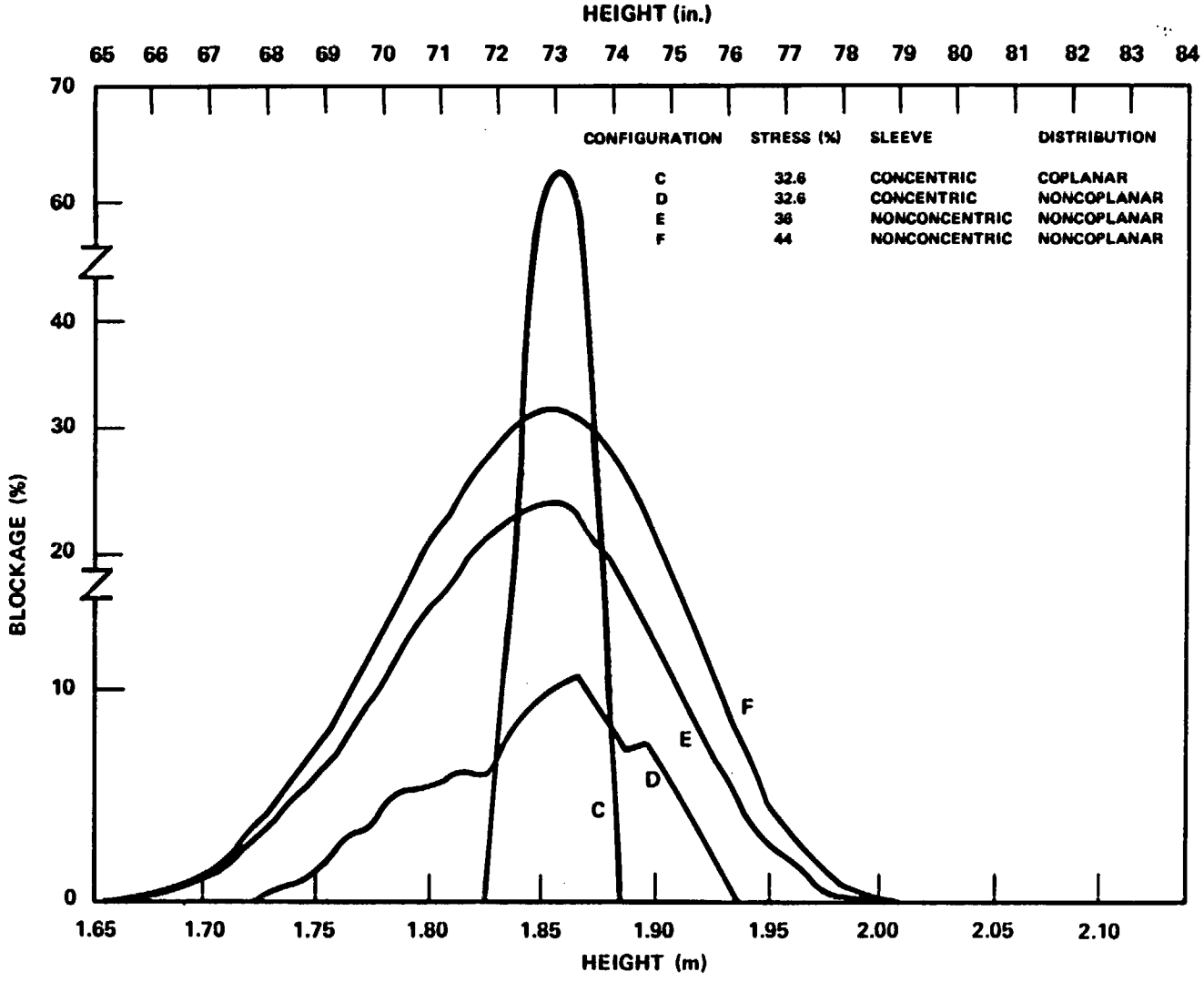

Figure 3-10. Bundle-Wide Blockage Distribution

SECTION 4
SYSTEM DESCRIPTION

4-1. INTRODUCTION

The FLECHT SEASET 21-rod bundle test facility was, in general, a scaled-down version of the FLECHT SEASET 161-rod unblocked bundle test facility,[1] as shown schematically in figure 4-1. The test facility consisted of the following major components:

-- A heater rod bundle and flow blockage sleeves

-- A low mass housing, an upper plenum, and a lower plenum

-- A coolant injection system and a steam injection system

-- A phase separation and liquid collection system

-- A downcomer and crossover leg

All of the above components were thoroughly instrumented, in order to measure flow blockage effects within the bundle and respective boundary conditions at the bundle inlet and outlet.

The test section, upper and lower plenums, liquid collection tanks, and the downcomer and crossover leg have approximately the same volume to flow area ratio as the 161-rod unblocked bundle facility.

---

1. Loftus, M. J., et al., "PWR FLECHT SEASET Unblocked Bundle, Forced and Gravity Reflood Task Data Report," NRC/EPRI/Westinghouse-7, June 1980, NUREG/CR-1532, Volumes 1 and 2.

The facility is capable of performing steam cooling, forced flooding, and gravity reflood tests similar to those performed in the 161-rod unblocked bundle facility, and also capable of performing hydraulic characteristics tests. Paragraphs 4-2 through 4-5 briefly describe each type of test.

4-2. HYDRAULIC CHARACTERISTICS TESTS

The hydraulic characteristics tests were performed at the beginning of each test series to determine the pressure losses associated with rod friction, grids, and blockage sleeves. The test section, exhaust piping, and components were filled solid with room-temperature water. Steady-state flows between 6.3×10^{-4} and 3.8×10^{-3} m^3/sec (10 and 60 gal/min) were established through the test section, utilizing the coolant injection system. The housing differential pressure transmitters measured the pressure drop for each 0.30 m (12 in.) increment. Testing was terminated after at least 60 seconds of steady-state data had been collected.

4-3. STEAM COOLING TESTS

The steam cooling tests were performed to measure the single-phase flow heat transfer effects of the flow blockage. Steam flow was initially established in the test section utilizing the steam injection system while system pressure was maintained by the pneumatically operated control valve located in the exhaust line. A constant low power (1.37 to 6.07 kw) was set in the rod bundle with an auto transformer. The steam cooling tests were terminated after steady-state heater rod temperatures had been achieved.

4-4. FORCED REFLOOD TESTS

The forced reflood tests were performed to measure the two-phase flow heat transfer effects of the flow blockage during forced flow injection. The forced reflood tests utilized all the major facility components, with the exception of the steam injection system, downcomer, and crossover leg.

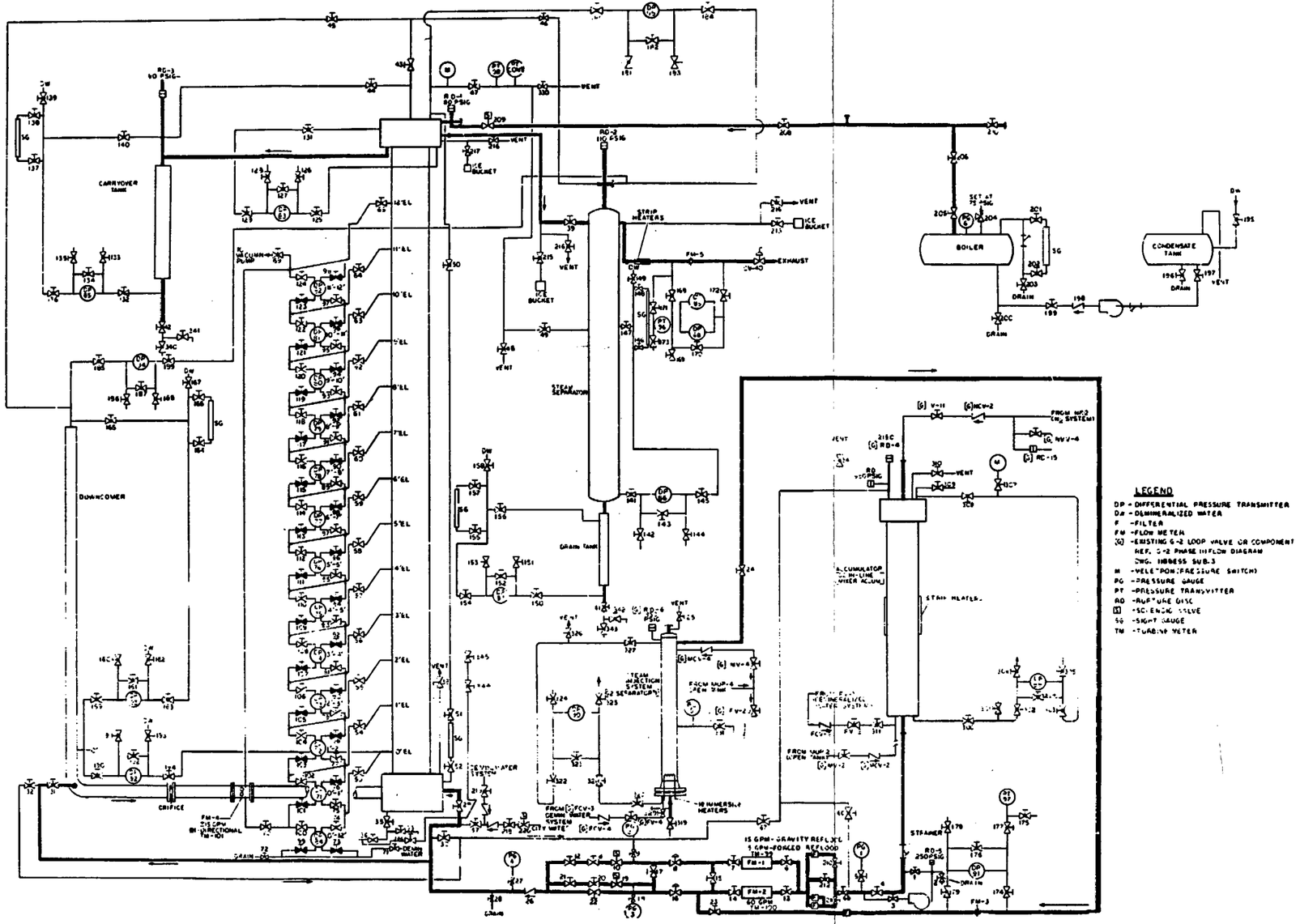

Figure 4-1. Schematic Diagram -- FLECHT SEASET 21-Rod Bundle Flow Diagram

Coolant flow from the 0.38 m^3 (100 gal) capacity water supply accumulator entered the test section housing through a series of hand valves and through a pneumatically operated control valve and a series of solenoid valves. Coolant flow was measured by a turbine meter located in the injection line. Test section pressure was initially established by a steam boiler connected to the upper plenum of the test section. During the reflood test, the boiler was isolated from the system and pressure was maintained by a pneumatically operated control valve located in the exhaust line. Liquid effluent leaving the test section was separated in the upper plenum and collected in a close-coupled carryover tank. An entrainment separator located in the exhaust line was used to separate any remaining liquid entrained in the vapor. Dry steam flow leaving the separator was measured by an orifice meter before it was exhausted to the atmosphere. A more detailed explanation of forced reflood facility operation is presented in paragraph 4-32.

4-5. GRAVITY REFLOOD TESTS

The gravity reflood tests were performed to measure the two-phase flow heat transfer effects of the flow blockage during the PWR-simulated gravity flow injection.

For gravity reflood tests, the downcomer and crossover pipe were connected to the test section lower plenum. Coolant was then injected into the test section through the downcomer. A full-bore gate valve, installed in the exhaust line, was partially closed for these tests to simulate the PWR hot leg flow resistance of approximately 32.5. A vent path was also established between the top of the downcomer and the entrainment separator to prevent overpressurization in the downcomer. Facility operation was essentially the same as that in forced reflood tests.

4-6. FACILITY COMPONENT DESCRIPTION

The various components of the 21-rod bundle test facility are described in the following paragraphs. The key instrumentation for each component is also listed.

4-7. Heater Rod Bundle

The bundle was composed of 21 instrumented heater rods and four solid triangular fillers (figure 4-2) and eight FLECHT-type grids (figure 4-3).

Details of the heater rod design are shown in appendix F, figures F-1, F-2, and F-3. The thermophysical properties of the heater rod materials are listed in table 4-1.

In the heater rod design utilized for configurations A through D (figure F-2), 0.63 mm (0.025 in.) diameter sheathed thermocouples were used. For configurations E and F, several design changes were made to the heater rod to minimize heater rod thermocouple failures. The thermocouple diameter was increased to 1.0 mm (0.040 in.). To incorporate this increase in thermocouple diameter and maintain heater element isolation integrity, the heater element coil diameter was decreased from 4.32 mm (0.170 in.) to 3.43 mm (0.135 in). To reduce the coil diameter, the element wire diameter was decreased from 1.0 mm (0.040 in.) to 0.91 mm (0.036 in.).

All the heater rods in the 21-rod bundle test program were annealed after manufacture at low temperatures [450°C (842°F) for 60 hours] to remove the residual stresses. The annealing process was believed to reduce premature thermocouple failure by counteracting grain structure embrittlement caused by cold working of the thermocouples during the manufacturing process.[1] An infrared scan of each heater rod was also performed by Oak Ridge National Laboratory to check heater coil integrity and density of boron nitride insulation. These two procedures were incorporated into the 21-rod bundle test program to eliminate heater rod failures and thermocouple failures, which had occurred in the 161-rod unblocked bundle tests. These procedures were apparently successful, since there were no heater rod failures and minimal thermocouple failures in the 21-rod bundle test program. However, the heater rod temperatures were lower in 21-rod bundle program than in the 161-rod bundle program; this could also affect rod performance.

---

1. McCulloch, R. W., et al., Proceedings of the International Symposium on Fuel Rod Simulators - Development and Application, Gatlinburg, TN, October 1980, pp 435-439.

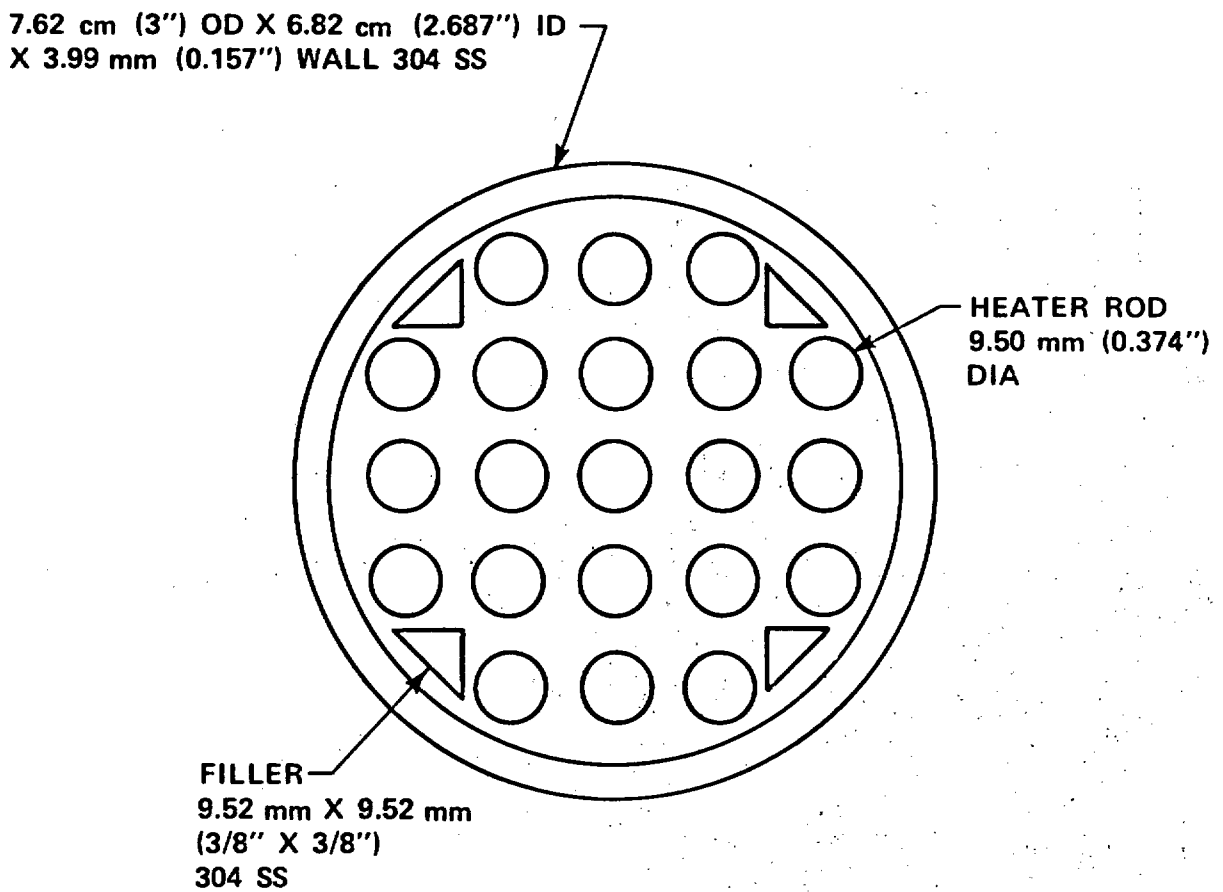

Figure 4-2. 21-Rod Bundle Test Section Cross Section

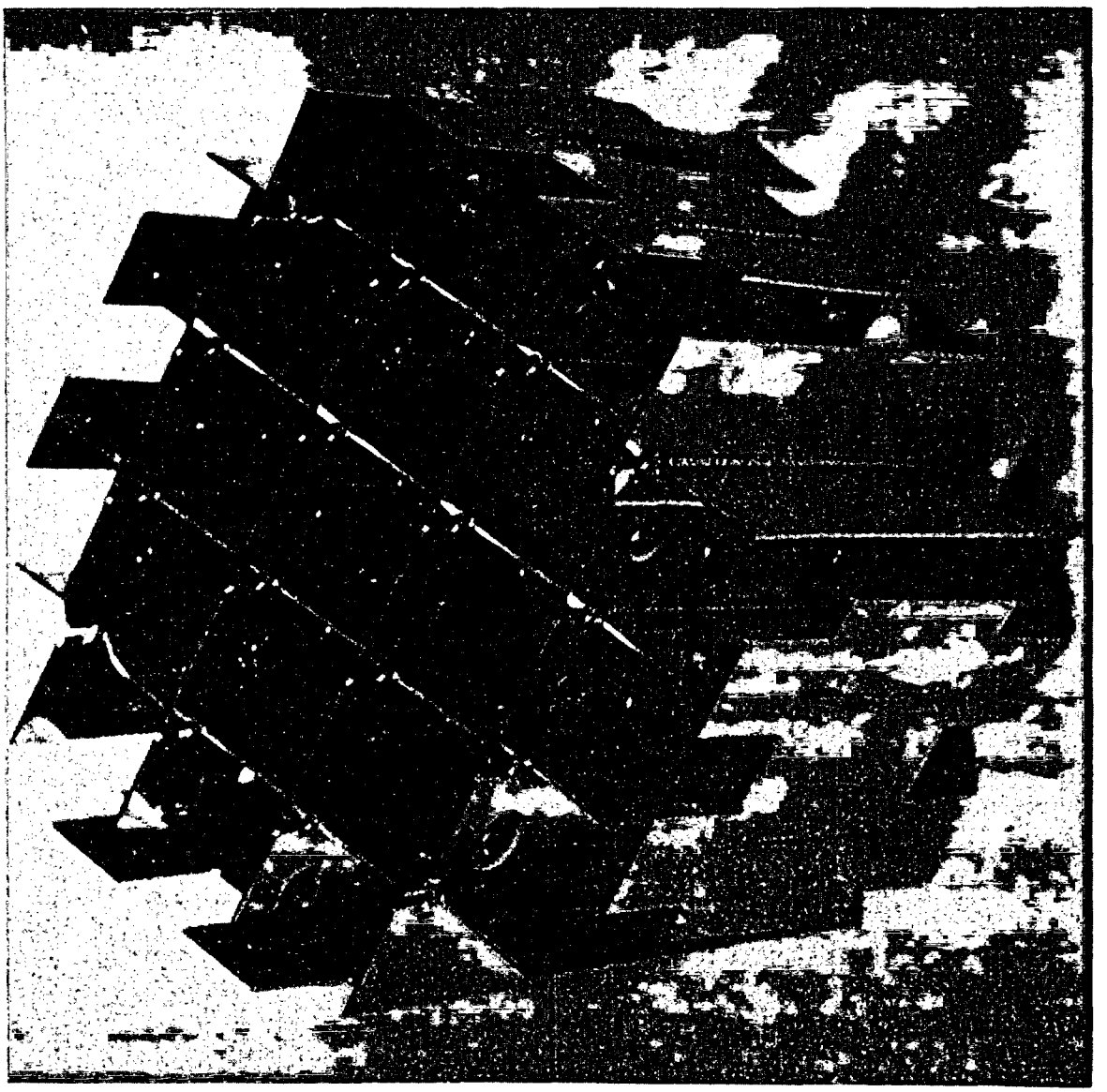

Figure 4-3. FLECHT-Type Grid

TABLE 4-1

THERMOPHYSICAL PROPERTIES OF HEATER ROD MATERIALS[a]

Material	Density [kg/m^3(lbm/ft^3)]	Thermal Specific Heat [J/kg-^{o}C(Btu/lbm-^{o}F)]	Conductivity [W/m-^{o}C(Btu/hr-ft-^{o}F)]
Kanthal	7144.24 (446)	456.36 + 0.45674 T for T $\leq$ 649^{o}C (0.109 + 0.000059 T for T $\leq$ 200^{o}F) 4161.68 - 3.843 T for 649^{o}C < T < 871^{o}C (0.994 - 0.00051 T for 1200^{o}F < T < 1600^{o}F) 664.86 + 0.0904 T for T $\geq$ 871^{o}C (0.1588 + 0.000012 T for T $\geq$ 1600^{o}F)	16.784 + 0.0134 T (9.7 + 0.0043 T)
Boron nitride	2212.15 (138.1)	2017.74 - 1396.26e (- 0.00245 T) [0.48193 - 0.333492e (-0.0013611 T)]	25.571 - 0.00276 T (14.7778 - 0.000889 T)
Stainless steel	8025.25 (501.0)	443.8 + 0.2888 T for T < 315^{o}C (0.106 + 3.833 x 10^{-5} T for T < 599.25^{o}F) 484.4 + 0.1668 T for T $\geq$ 315^{o}C (0.1157 + 2.2143 x 10^{-5} T for T $\geq$ 599.25^{o}F)	14.535 + 0.01308 T (8.4 + 0.0042 T)

a. See table E-1 for data sources.

The triangular fillers were split and pin-connected to each other midway between grids to accommodate thermal growth, and welded to the grids to maintain the proper grid location. The fillers reduced the amount of excess flow area[1] in the housing, and also supported test bundle instrumentation leads. The excess flow area was approximately 12.4 percent with the fillers. Bundle assembly and filler details are shown in figures F-4 and F-5. The fillers were instrumented with several thermocouples (except in the first bundle), to measure filler thermal response. The grid design, essentially the same as that utilized in the 161-rod unblocked bundle, is shown in figure F-6.

4-8. Flow Blockage Sleeves

The blockage sleeve shapes tested consisted of concentric short sleeves and nonconcentric long sleeves as previously described in section 3 and shown in figure 4-4. Configurations B, C, and D utilized the short concentric blockage sleeve design. Both sleeves were made by hydroforming, in which 0.76 mm (0.030 in.) tubing was hydraulically expanded into a mold. Configuration B, with coplanar blockage on the nine center rods, utilized the hydroformed short, concentric sleeve shown in figure F-7. Configuration C, with coplanar blockage on all 21 rods, used 13 hydroformed short, concentric sleeves like those in configuration B; the eight corner rods used machined short sleeves with two flats as shown in figure F-8, to fit adjacent to the triangular filler rods. For the noncoplanar, all-rods-blocked confiquration D, the hydroformed and machined corner sleeve design of figures F-7 and F-8 was used.

Configurations E and F, all rods blocked, noncoplanar blockage, utilized long nonconcentric hydroformed and machined sleeves. In configuration E, the hydroformed sleeve shown in figure F-9 was used for all but the eight corner rods, where a machined sleeve design (figure F-10) was used. Configuration F was the same as configuration E except that the circumferential strain (blockage) was increased, as shown in figures F-11 and F-12.

1. Excess flow area is that area which is in excess of the area occupied by 21 rods in a large rod array.

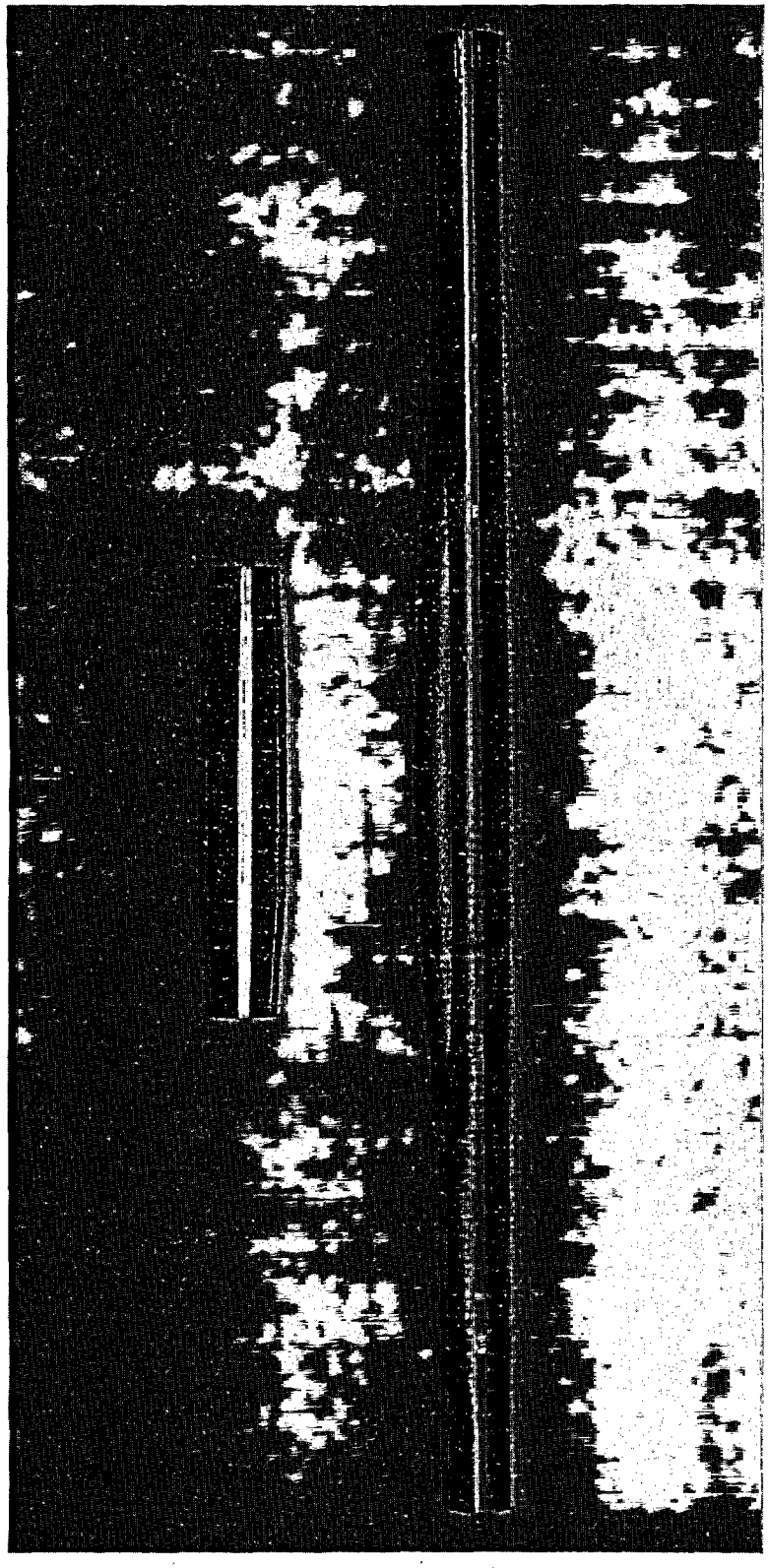

Figure 4-4. Flow Blockage Sleeves

On instrumented blockage sleeves, a groove was milled into the sleeve wall at the point of maximum strain, and thermocouples were then Nicrobrazed into the groove. The effect of instrumenting the blockage sleeves was found to be negligible in a single-rod test, as discussed in appendix G.

Sleeves were attached to the rods by applying a weld bead to the heater rod sheath through a hole predrilled in the sleeve wall. The weld bead was high enough so that the sleeve could not slide over it.

Since an annular gap may exist between this flow blockage sleeve and the heater rod, steam may flow through this gap. The amount of steam flow between the sleeve and the rod was calculated utilizing a simple parallel flow path model. The bundle frictional pressure drop provided the flow between the sleeve, and the rod was modelled (for the short, concentric sleeve) as shown below:

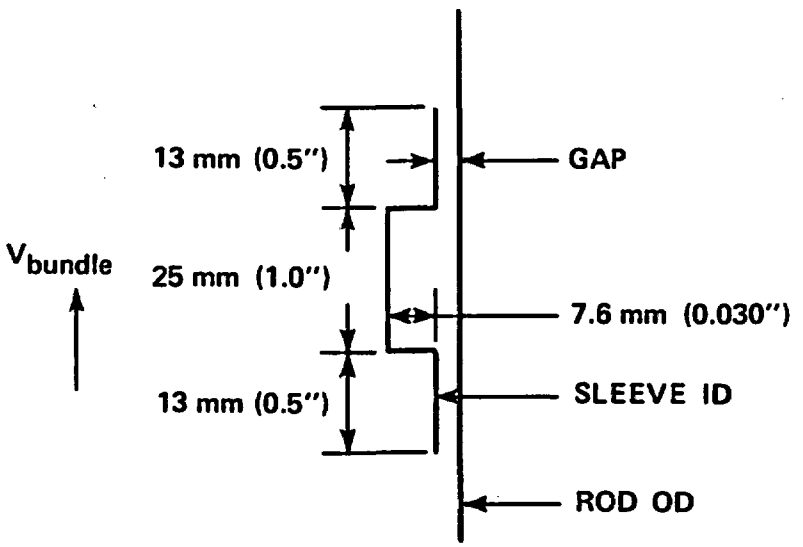

The bundle conditions were assumed to be 865°C (1590°F) and 0.28 MPa (40 psia), and a velocity of 12 m/sec (40 ft/sec). The width of the gap was varied in this calculation between 0.1 mm (0.005 in.) and 0.6 mm (0.025 in.). The results of this calculation are shown in figure 4-5 as a function of gap width. The mass flow between the sleeve and the rod was calculated as a percentage of the bundle mass flow rate. The bundle

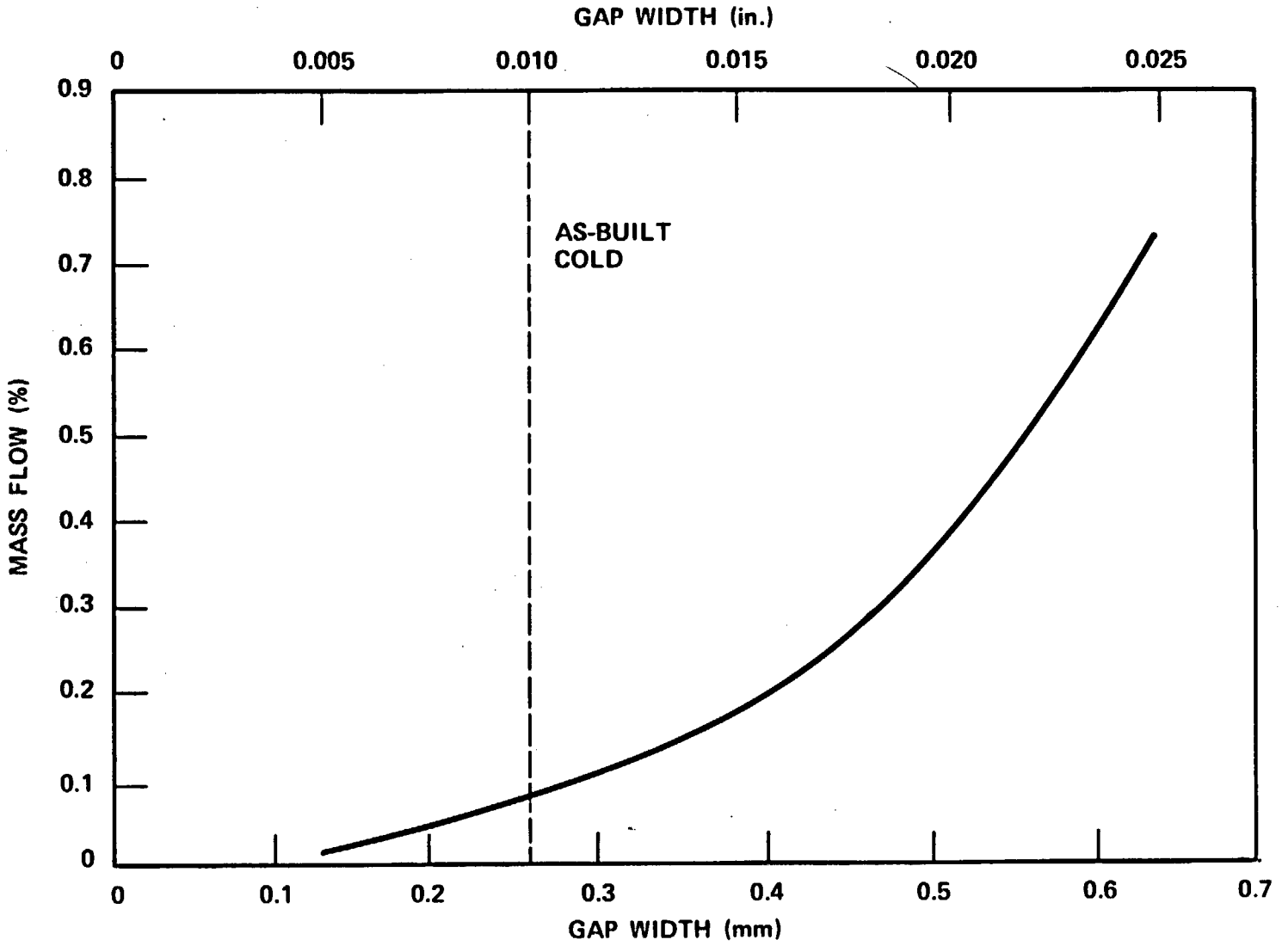

Figure 4-5. Percent Mass Flow Between Blockage Sleeve and Heater Rod

[hydraulic diameter = 8.5 mm (0.34 in.)] frictional pressure drop was used as the driving force. Figure 4-5 shows that the mass flow beneath the sleeve is a strong function of the gap width, but is generally less than 0.5 percent of the bundle flow. Based on the as-built heater rod and blockage sleeve dimensions, it was expected that the gap width at cold conditions was no greater than 0.25 mm (0.010 in.). Since the heater rod was at a higher temperature than the blockage sleeve, the thermal expansion would tend to reduce this gap by approximately 0.01 mm (0.0004 in.) Generally, the flow between the sleeve and the heater rod was insignificant.

4-9. Test Section

The low mass housing, together with the lower and upper plenums (figure F-13) constituted the test section (figure F-14). The low mass housing (figure F-15) was a cylindrical vessel with a nominal inside diameter of 6.825 cm (2.687 in.) and a 0.399 cm (0.157 in.) wall, constructed of 304 stainless steel rated for 0.55 MPa (80 psi) at 815°C (1500°F). The wall thickness was the minimum allowed by the ASME pressure vessel code so that the housing would absorb, and hence release, the minimum amount of heat compared with the rod bundle. The inside diameter of the housing was made as close to the rod bundle outer dimensions as possible to minimize excess flow area. The housing was instrumented with 38 thermocouples in all six bundles to measure the housing thermal response. These 38 thermocouples were distributed axially and azimuthally over the housing to compute housing energy storage and release.

The housing and the plenum were insulated with 5 cm (2 in.) of high-temperature Fiberfax insulation. The insulation was subsequently enclosed with thin stainless steel sheathing to protect the insulation from environmental effects. The sheathing was instrumented with 12 thermocouples in all six bundles to measure the energy loss from the heater rod bundle.

Because of the high temperature conditions placed on the housing, as discussed in appendix B, and the necessity of removing bundles for each test series, it was necessary to replace the housing for every other test series. Consequently, three housings were used during the course of the 21-rod bundle test program. Volumetric checks were performed on each of the housings to determine the average inside diameter. Also, after

installation of each test bundle, the average flow area was calculated from volumetric data. These flow areas were used to determine the coolant injection rates for each bundle and were also utilized in the respective data reduction codes (as described in section 5). The results of the housing average inside diameter and flow area volumetric checks are shown in table 4-2.

To help eliminate thermal buckling and distortion, the test section was supported from the upper plenum to permit the housing to freely expand downward as it heated up. Also, three horizontal supports were provided at 1.22 m (48 in.) increments to prevent bowing of the housing. These horizontal supports were simply rings which encircled the housing with three lateral support arms located 120 degrees apart. The rings provided support for the housing, but still allowed the housing to thermally expand axially.

The upper plenum provided the initial phase separation for the flow exiting the heater rod bundle. The flow expansion from the bundle flow area of approximately 20 cm^2 (3.2 $in.^2$) to the upper plenum cross-sectional area of 323 cm^2 (50 $in.^2$) decelerated the two-phase flow such that the water droplets could no longer be suspended. The water was collected at the bottom of the upper plenum and prevented from flowing back into

TABLE 4-2

HOUSING DIAMETER AND BUNDLE FLOW AREA

Housing No.	Configuration	Housing Diameter [cm(in.)]	Average Bundle Flow Area [cm^2($in.^2$)]
1	A	6.88 (2.71)	20.8 (3.22)
	B		20.6 (3.19)
2	C	6.88 (2.71)	20.7 (3.21)
	D		20.6 (3.19)
3	E	6.93 (2.73)	20.6 (3.20)
	F		20.6 (3.19)

the bundle by the upper plenum extension (see figure F-27), as shown in figure 4-6. Two flow holes in the bottom of the upper plenum allowed water to drain into the carryover tank. The two-phase flow was further separated by means of the upper plenum baffle (see figure F-27), as also shown in figure 4-6.

Flow was injected into the lower plenum perpendicular to the heater rod bundle (figure F-25). The lower plenum extension (figure F-27), which was a cylinder attached to the top of the lower plenum extending to the lower seal plate, was perforated with 192 3.6 mm (0.14 in.) diameter holes to provide a more uniform flow distribution into the rod bundle.

4-10. Carryover Tank

The function of the carryover tank was to collect liquid overflow from the test section. The carryover vessel was a dual-diameter vessel which provided sufficient capacity for high-flow-rate tests and also accurate measurement for low-flow-rate tests. The large-diameter vessel was 7.6 cm (3 in.) diameter schedule 40 carbon steel pipe and was 2.16 m (85 in.) long. The small-diameter vessel was 6.4 cm (2.5 in.) diameter schedule 40 carbon steel pipe and was 2.24 m (88 in.) long. The vessel was close-coupled to the upper plenum by a stainless steel flexible hose as shown in figure F-16. The carryover tank was instrumented with a differential pressure transmitter to measure liquid carryover. A volumetric check of the carryover tank indicated an average cross-sectional area of 0.00225 m^2 (0.0242 ft^2) for the small-diameter vessel and 0.004842 m^2 (0.05212 ft^2) for the large-diameter vessel.

4-11. Steam Separator

The separator was designed to remove the remaining water droplets from the two-phase flow exiting the upper plenum, as shown in figure F-16, so that a meaningful single-phase flow measurement could be obtained by an orifice section downstream of the separator. The vessel shell was 15 cm (6 in.) schedule 40 carbon steel pipe and the vessel volume was 0.02843 m^3 (1.004 ft^3). The separator utilized centrifugal action to force the moisture against the wall, where it drained to the bottom. The water was collected in a separator drain tank directly connected to the bottom of the separator.

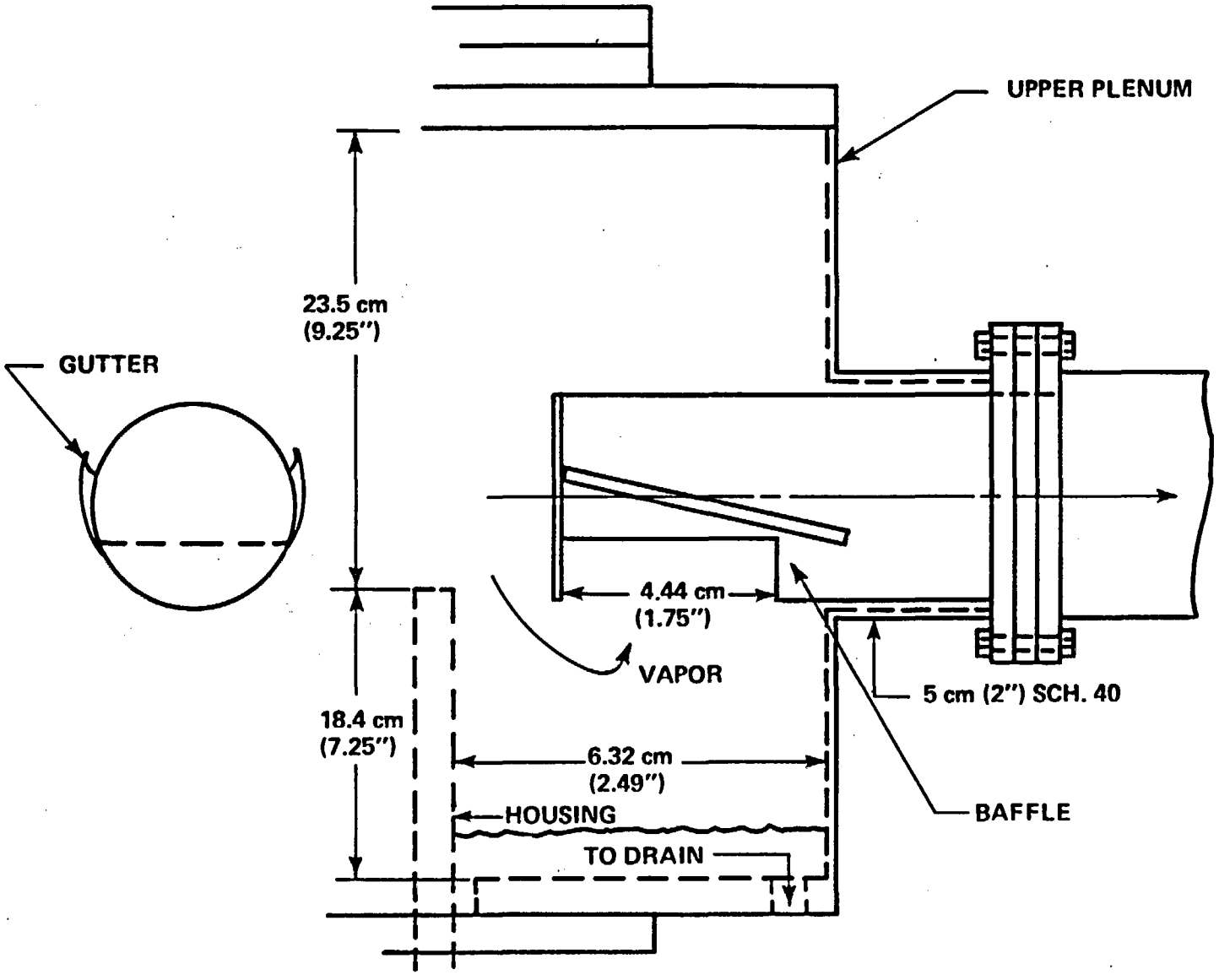

Figure 4-6. 21-Rod Bundle Upper Plenum Baffle

The drain tank shell was a 3.8 cm (1.5 in.) carbon steel pipe and the volume was 0.018 m^3 (0.065 ft^3). The steam separator was instrumented with a differential pressure transmitter to measure separated liquid.

4-12. Exhaust Line

Test section effluent discharged to the atmosphere through 5 cm (2 in.) exhaust line piping, as shown schematically in figure 4-1. A nozzle penetration on the upper plenum provided the attaching point for the exhaust line piping. Sandwiched between the two mating flanges was a plate which served as a structural attachment for the upper plenum baffle, as shown in figure 4-6. This baffle served to improve the liquid carryout separation and minimize liquid entrainment in the exhaust vapor. After passing through the upper plenum baffle pipe, the exhaust vapor passed through a 90-degree elbow and a straight run of pipe into the entrainment separator.

Steam leaving the separator passed through a 90-degree elbow and along a straight run of heated pipe to an orifice flange assembly utilized to measure flow rate. Clamp-on strip heaters on the pipe were used to heat the pipe to 260°C (500°F), to assure single-phase steam flow through the orifice. Steam then exhausted to the atmosphere through a pressure control valve. The control valve was an air-operated V-ball control valve of the type used successfully on the 161-rod unblocked bundle test series to minimize the pressure oscillations during a test run. Aspirating steam probes were located in each of the two 90-degree elbows to measure the temperature of the exhaust steam. A full-bore gate valve installed at the entrainment separator inlet flange was employed to simulate the PWR hot leg flow resistance of 32.5 for the gravity reflood tests. Figure F-16 shows details of the exhaust line.

4-13. Coolant Injection System

The coolant injection system provided water to quench the rod bundle during reflood testing. Coolant injection water was supplied by the 0.378 m^3 (100 gal) accumulator through a series of valves and turbine meters, as shown in figure 4-1. Nitrogen overpressure on the accumulator provided the necessary driving head to attain the required

injection rates. The injection line was constructed of stainless steel tubing downstream of the filter to prevent contamination of the test section. Figure F-16, sheet 1, shows details of the injection system.

Constant or stepped injection flow was accomplished by the proper sequencing of solenoid valves, which were located in a piping manifold arrangement (figure 4-1). A pneumatically operated control valve was used to fine tune and maintain the specified flow during the test. In the automatic control mode, the valve used a feedback signal from the injection line turbine meter to maintain the preset flow. Two injection line turbine meters were used for ECCS simulation flow rate measurement, one with a range of 1.6×10^{-5} to 3.2×10^{-4} m^3/sec (0.25 to 5.0 gal/min) for forced flooding tests and one with a range of 1.6×10^{-5} to 9.5×10^{-4} m^3/sec (0.25 to 15 gal/min) for gravity reflood tests. A flow check was performed prior to each reflood test to ensure that the turbine meter was operating properly.

A full-bore 38 mm (1.5 in.) diameter bidirectional turbine meter with a range of 3.1×10^{-5} to 9.5×10^{-4} m^3/sec (0.5 to 15 gal/min) was installed in the crossover leg during gravity reflood tests to measure flow into the test section and any reverse flow from the test section into the downcomer.

For hydraulic characteristics tests, a 3.8×10^{-5} to 3.8×10^{-3} m^3/sec (0.6 to 60 gal/min) turbine meter was installed in the injection line to measure flow into the test section.

4-14. Downcomer and Crossover Leg

The downcomer and crossover leg were connected to the test section lower plenum for the gravity reflood tests, as shown in figure F-16. The crossover leg and lower plenum were designed to provide approximately the same flow resistance (a value of 11) as in the PWR lower plenum and core inlet. The downcomer and crossover leg were fabricated from 5 cm (2 in.) schedule 40 pipe with a 90-degree long radius elbow in between. A flexible rubber pipe connected the crossover leg to the lower plenum and allowed for downward thermal expansion of the test section. The horizontal crossover leg was 2.21 m (87 in.) long and the vertical downcomer was approximately 6.1 m (240 in.). Coolant injection water entered the downcomer through a nozzle located in the elbow.

The bidirectional turbine meter was located in the crossover leg. The downcomer was instrumented with a differential pressure transmitter to measure accumulated liquid.

4-15. Facility Heating Boiler

The boiler was a Reimers Electric steam boiler with a steam capacity of approximately 1.51×10^{-3} kg/sec (125 lb/hr) at 100°C (212°F). The boiler was used to pressurize the facility and for pretest facility heatup. This was accomplished by valving the boiler into the upper plenum of the test section. A solenoid valve was used to isolate the boiler from the test facility at initiation of testing, at which time the steam generated in the test section in combination with the control valve in the exhaust line was sufficient to maintain facility pressure.

4-16. Steam Injection System

The steam injection system was composed of a large-volume tank with immersible electric heaters capable of providing saturated steam to the rod bundle during steam cooling tests in the range of approximately 0.0045 kg/sec (0.01 lb/sec) to 0.045 kg/sec (0.10 lb/sec). The steam injection boiler was an existing component previously used on another test program.

4-17. BUNDLE REPLACEMENT

As discussed in section 3, six bundle configurations were tested during the course of the 21-rod bundle test program. Assembly of each bundle was performed in parallel with testing of the preceding bundle to minimize downtime between test series. Each bundle was built in the horizontal position in a fixture called a strongback, as shown in figure F-17.

A deficiency which was apparent upon removal of all the bundles from the housing was the separation of the fillers at the pin joints at the 1.80 m (71 in.) elevation. It is believed that the pin joints sheared as a result of frictional forces between the heater rods and grids at and below 1.57 m (62 in.). However, increasing the clearance between the rods and grids after test series A was not sufficient to alleviate the problem. Some

heater rod bowing was present as a result of the filler separation; however, it was felt that the pin joint filler design minimized this bowing by relieving stresses which would have otherwise caused more significant bowing.

Figure 4-7 shows a typical filler joint detail before and after testing. Filler joint separations as high as 69.8 mm (2.75 in.) were measured after bundle removal. After test series A, however, mechanical stops were welded to the bottom seal plate, which prevented the fillers from separating more than 51 mm (2 in.). The effect of bundle geometry changes is discussed in appendix H.

4-18. DATA ACQUISITION AND PROCESSING SYSTEM

Three types of systems monitored the instrumentation and recorded data on the FLECHT SEASET 21-rod bundle test facility: a Computer Data Acquisition System (CDAS), a Fluke data logger, and four Texas Instruments stripchart pen recorders.

4-19. Computer Data Acquisition System

The CDAS, the primary data collecting system used on the FLECHT facility, consisted of a PDP-11 computer and associated equipment. The system could record 364 channels of analog input data representing bundle and system temperatures, bundle power, flows, and absolute and differential pressures. The computer was capable of storing approximately 2500 data scans for each of the 364 analog input channels.

Typically, each data channel could be recorded once every second until flood, then once every half-second for 200 seconds, and then back to once every second thereafter to a maximum of 2500 data points.

The computer software had the following features:

- A calibration file to convert raw data into engineering units

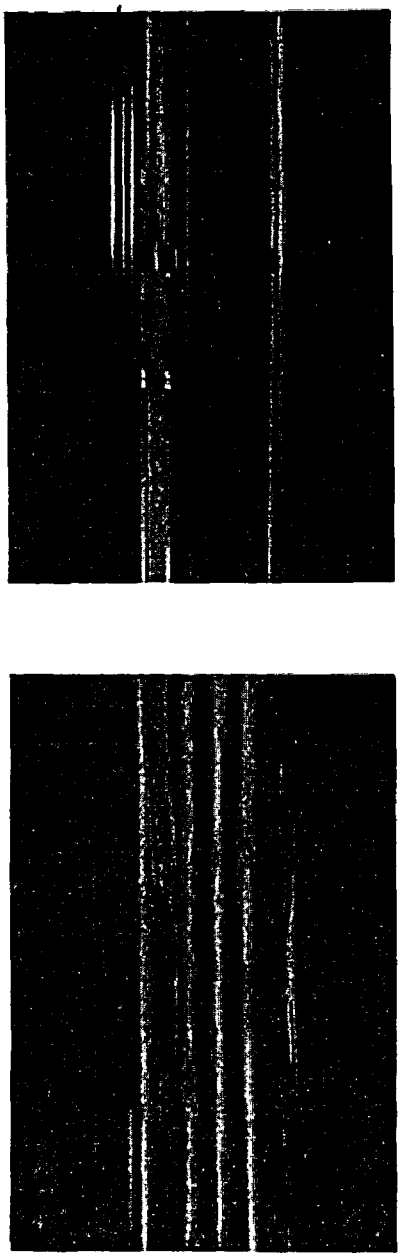

Figure 4-7. Pretest and Posttest Filler Joint Separation

-- A preliminary data reduction program which transferred the raw data stored on disk to a magnetic tape, in a format compatible for entry into a Control Data Corporation 7600 computer

-- A program called XLOOK which reduced raw data into engineering units; a program called XVALID which printed out key data used in validating FLECHT SEASET runs; and a PLOT program, which plotted up to four data channels on a single graph. All three programs were utilized to quickly understand and evaluate test runs.

A mass balance program was written after the first bundle had been tested to provide a quick check on the system measurements and allow for the continual running of reflood tests. This mass balance program prevented the problems which had occurred in the first test series, with a calibration shift in the turbine meter.

In addition to its role as a data acquisition system, the computer also controlled the performance of an experimental run. Important control functions included initiation and control of reflood flow and power decay as well as termination of bundle power in the event of a heater rod overtemperature condition. Figure 4-8 shows the hardware interfaces of the CDAS.

4-20. Fluke Data Logger

The Fluke data logger had 60 channels of analog input for monitoring loop heatup and aiding in equipment troubleshooting. The Fluke data logger recorded key facility vessel and fluid temperatures, displaying temperature directly in degrees Fahrenheit. This made the task of monitoring loop heatup more efficient. The Fluke data logger also recorded millivolt data from the test section differential pressure cells, allowing the operator to keep a check on their operation and repeatability. The Fluke data logger was further used to troubleshoot problems with loop equipment in a quick and convenient manner.

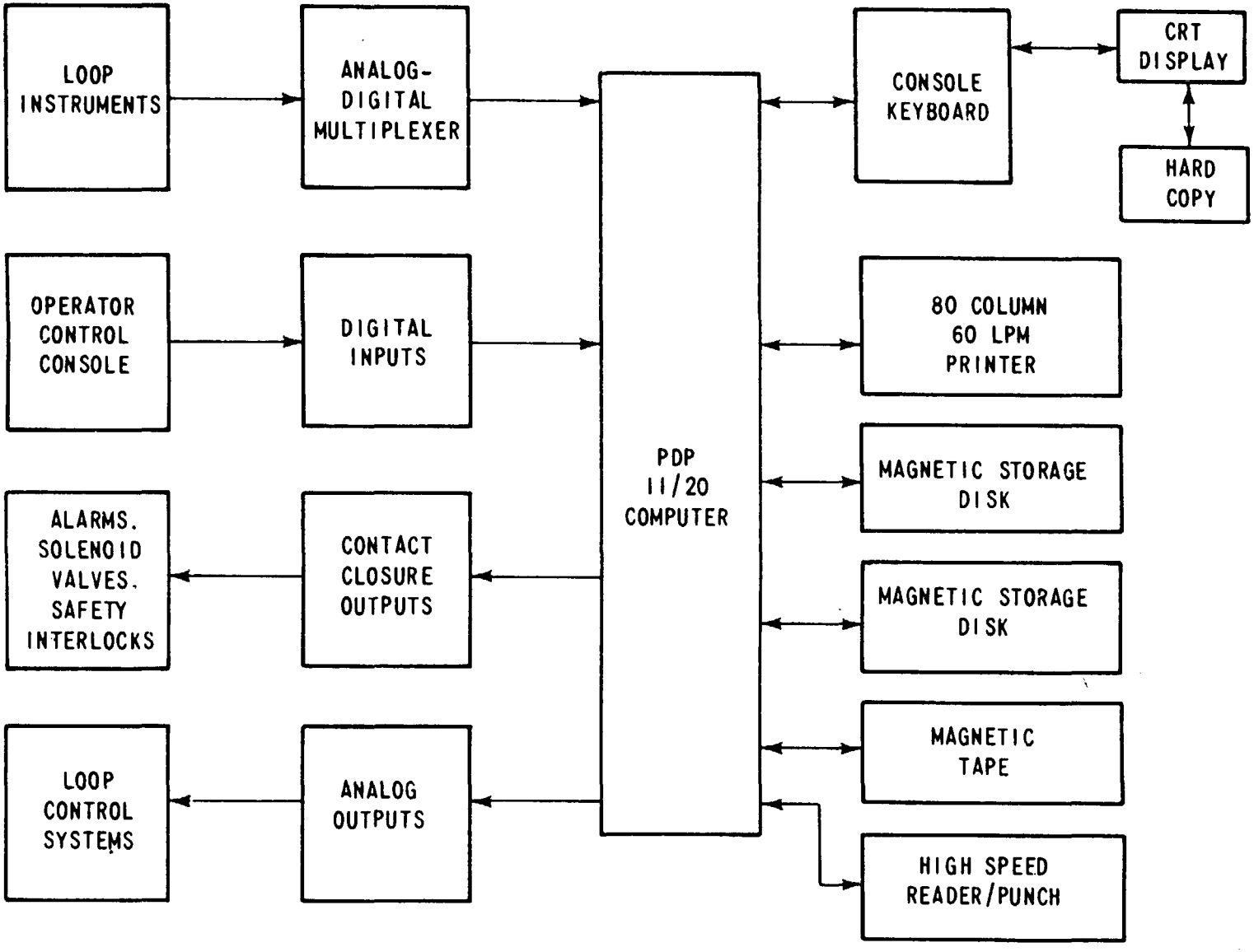

Figure 4-8. FLECHT SEASET Computer Hardware Interface for 21-Rod Bundle Flow Blockage Task

4-21. Multiple-Pen Stripchart Recorders

Four Texas Instruments stripchart recorders were used to record bundle power; selected bundle thermocouples; reflood turbine meter flows; accumulator, separator drain tank, housing, and carryover tank levels; and exhaust orifice differential pressure. These recorders gave the loop operators and test directors immediate information on test progress and warning in the event of system anomalies. The stripcharts provided an analog recording of critical data channels as a backup to the computer. Stripcharts were also needed during the heatup phase of the facility when the computer was not available.

4-22. INSTRUMENTATION

The instrumentation on the 21-rod bundle facility was designed to measure temperature, power, flow, fluid level, and pressure. The temperature data were measured by type K, Chromel-Alumel, ungrounded thermocouples using 66°C (150°F) reference junctions.

Power input to the bundle heater rods was measured by Hall-effect watt transducers, which produce a direct current electrical output proportional to power input. The voltage and current input to the watt transducer is scaled down by transformers so that the range of the watt transducer matches the bundle power. The scaling factor of the transformers is accounted for when the raw data (millivolts) are converted to engineering units.

Reflood injection flow was measured by turbine meters. The turbine meter was connected to a preamplifier and flow rate monitor for conversion of turbine blade pulses into flow rate in engineering units. The turbine meter flow rate monitor analog signal was proportional to the speed and direction of flow in the downcomer crossover leg. Calibration of the turbine meter by the manufacturer provided for data conversion to volumetric flows for the turbine meter analog signal.

System static and differential pressures were measured with Rosemount model 1151 pressure transmitters. The differential pressure transmitters measured water level in the vessels, bundle pressure drops, and pressure drops across orifice sections and other system components.

Standard thermocouple calibration table entries and the corresponding coefficients were used to compute the temperature values. All other channel calibration files were straight-line interpolations of calibration data. The slope, intercept, and zero for the least-squares fit of a straight line to the equipment calibration data were computed for each channel and entered into its calibration file. The CDAS software used this straight-line formula to convert millivolts to engineering units.

4-23. Loop Instrumentation

Figure 4-9 shows schematically the forced reflood and gravity reflood test loop instrumentation arrangement.

Forty computer channels were assigned to the collection of temperature, flow, and pressure data throughout the loop, exclusive of the instrumentation found in the upper and lower plenum, bundle, and housing.

This instrumentation included 13 fluid thermocouples, 9 wall thermocouples, 4 turbine meters, 11 differential pressure cells, and 3 absolute pressure cells.

The 13 fluid thermocouples were placed in the water and steam supply systems, the exhaust line, the carryover tank, the steam separator, the steam separator drain tank, the crossover leg (gravity reflood tests), and the downcomer (gravity reflood tests). The fluid thermocouples were utilized to measure the temperature of either stored or injected flow. Two of these thermocouples were utilized in aspirating steam probes placed in the elbows of the exhaust line on either side of the steam separator. These steam probes were designed to measure vapor nonequilibrium in the test section exit and the desuperheating effect of the steam separator. This steam probe was similar to that used in the 161-rod unblocked bundle test series.

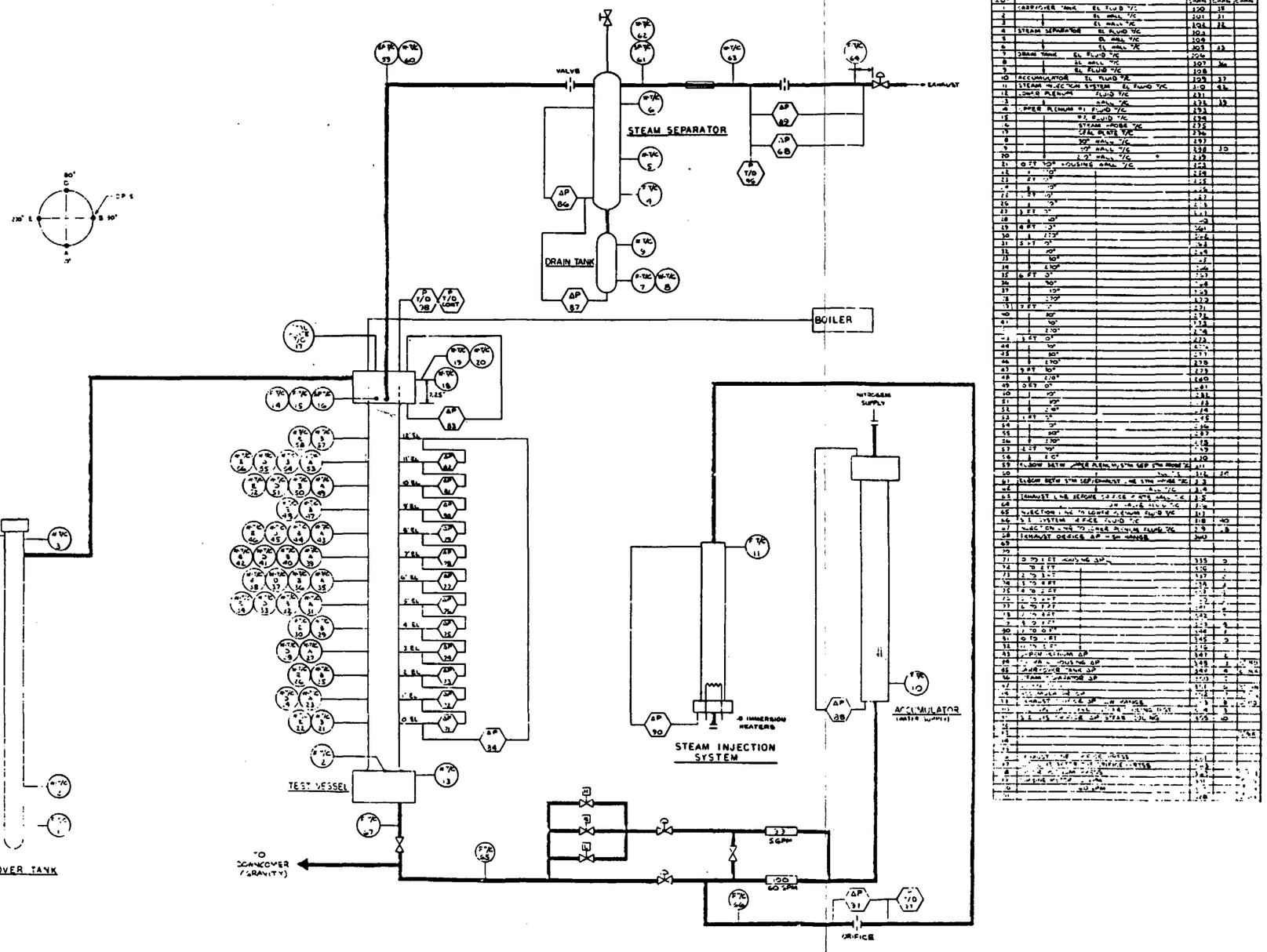

Figure 4-9. 21-Rod Bundle Flow Blockage Task Instrumentation Schematic Diagram (sheet 1 of 2)

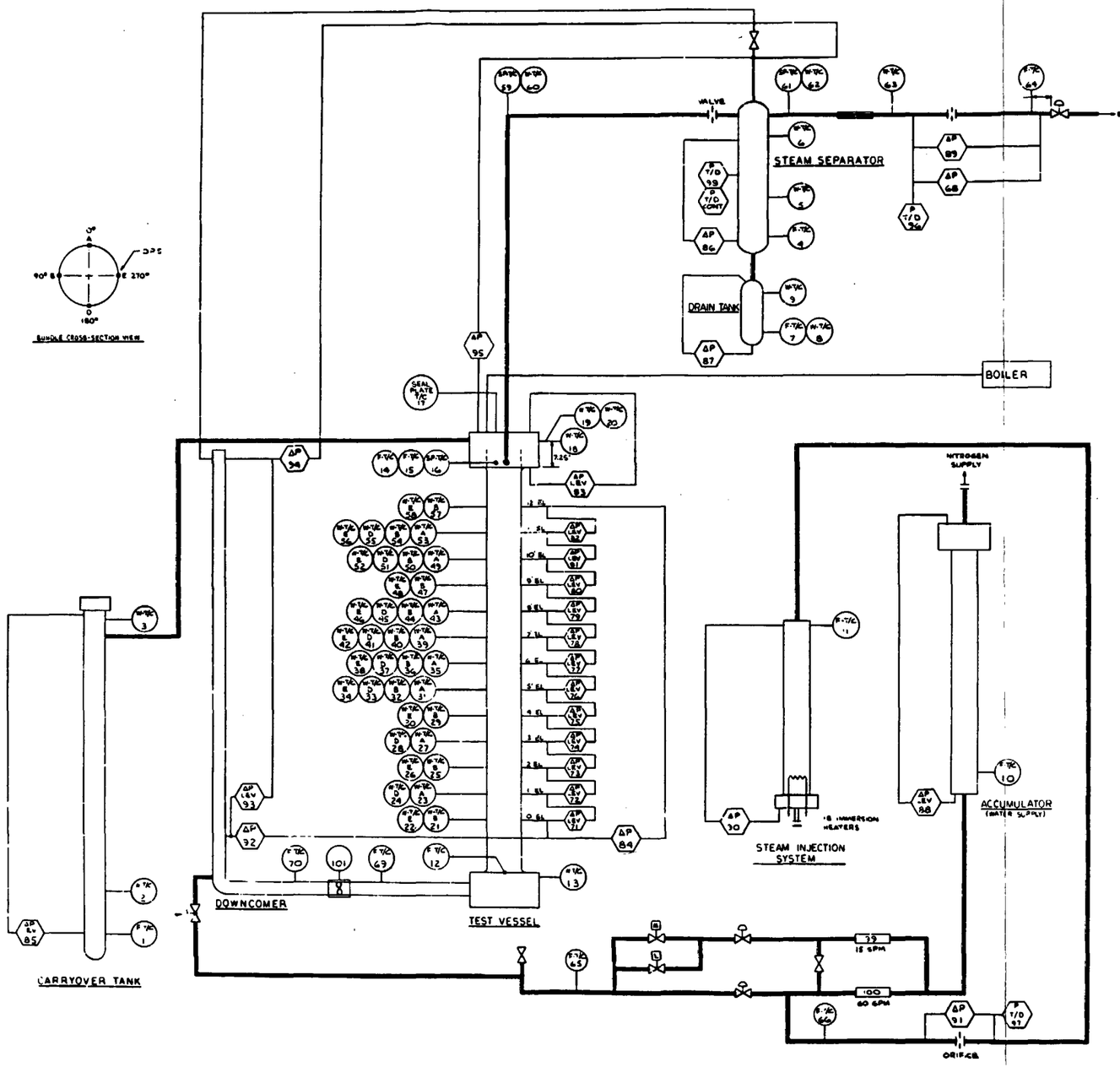

LOOP & ID #	DESCRIPTION	COMP CH	FLUID CH	T/C CH
1	CARRYOVER TANK 0' EL FLUID T/C	300	15	
2	0' EL WALL T/C	301	31	
3	10' EL WALL T/C	302	32	
4	STEAM SEPARATOR 0' EL FLUID T/C	303		
5	1' EL WALL T/C	304		
6	4' EL WALL T/C	305	33	
7	DRAIN TANK 0' EL FLUID T/C	306		
8	0' EL WALL T/C	307	34	
9	4' EL WALL T/C	308		
10	ACCUMULATOR 1' EL FLUID T/C	309	37	
11	STEAM AT 5'4 TOP EL FLUID T/C	310	42	
12	LOWER PLENUM BUNDLE FLUID T/C	311		
13	WALL T/C	312	39	
14	UPPER PLENUM BUNDLE FLUID T/C	313		
15	HOUSING EXTENSION T/C	314		
16	STEAM PROBE T/C	315		
17	SEAL PLATE T/C	316		
18	30° WALL T/C	317		
19	80° WALL T/C	318	30	
20	170° WALL T/C	319		
21	0 FT 90° HOUSING WALL T/C	251		
22	" 270°	252		
23	1 FT 0°	253		
24	" 90°	254		
25	2 FT 90°	255		
26	" 270°	256		
27	3 FT 0°	257		
28	" 90°	258		
29	4 FT 90°	259		
30	" 270°	260		
31	5 FT 0°	261		
32	" 90°	262		
33	" 180°	263		
34	" 270°	264		
35	6 FT 0°	265		
36	" 90°	266		
37	" 180°	267		
38	" 270°	268		
39	7 FT 0°	269		
40	" 90°	270		
41	" 180°	271		
42	" 270°	272		
43	8 FT 0°	273		
44	" 90°	274		
45	" 180°	275		
46	" 270°	276		
47	9 FT 90°	277		
48	" 270°	280		
49	10 FT 0°	281		
50	" 90°	282		
51	" 180°	283		
52	" 270°	284		
53	11 FT 0°	285		
54	" 90°	286		
55	" 180°	287		
56	" 270°	288		
57	12 FT 90°	289		
58	" 270°	290		
59	ELBOW BETW UPPER PLENUM/STM SEP STM PROBE T/C	311		
60	" WALL T/C	312	34	
61	ELBOW BETW STM SEP/EXHAUST LINE STM PROBE T/C	313		
62	" WALL T/C	314		
63	EXHAUST LINE BEFORE ORIFICE PLATE WALL T/C	315		
64	" FLOW VALVE FLUID T/C	316		
65	INJECTION LINE TO LOWER PLENUM FLUID T/C	317		
66	5'2 STD ORIFICE FLUID T/C	318		
67				
68	EXHAUST ORIFICE ΔP HIGH RANGE	320		
69	DOWNCOMER LINE AFTER TURBO PROBE FLUID T/C	320	4	
70	" BELOWS	321	1	
71	0 TO 1 FT HOUSING ΔP	335	0	
72	1 TO 2 FT	336		
73	2 TO 3 FT	337	2	
74	3 TO 4 FT	338	3	
75	4 TO 5 FT	339	4	
76	5 TO 6 FT	340	5	
77	6 TO 7 FT	341	6	
78	7 TO 8 FT	342	7	
79	8 TO 9 FT	343	8	
80	9 TO 10 FT	344	9	
81	10 TO 11 FT	345	10	
82	11 TO 12 FT	346	11	
83	UPPER PLENUM ΔP	347	12	
84	OVERALL HOUSING ΔP	348	13	1" W/D
85	CARRYOVER TANK ΔP	349	14	1" Hg
86	STEAM SEPARATOR ΔP	350	15	
87	DRAIN TANK ΔP	351	16	5" WM
88	ACCUMULATOR ΔP	352	17	5" H2O
89	EXHAUST ORIFICE ΔP LOW RANGE	353	18	5" H2O
90	0 TO 1.5 ΔP FUEL STEAM COOLING TEST	354	19	
91	0 TO 1.5 ORIFICE ΔP STEAM COOLING	355	20	
92	DOWNCOMER/TOP EL ΔP	356	21	
93	5'/EL ΔP	357	22	5" WM
94	5'/STEAM SEPARATOR ΔP	358	23	
95	UPPER PLENUM/STEAM SEPARATOR ΔP	359	24	
96	EXHAUST LINE ORIFICE PRESS	35		
97	0-1 LINE AFTER THE ORIFICE PRESS	363		
98	STEAM SEPARATOR PRESS	362		5" SUR
99	TURBINE METER 3 GPM	332		5" WM
100	" 60 GPM	333		5" WM
101	IN SPECIAL T/C PROBE	287		5" WM

Figure 4-9. 21-Rod Bundle Flow Blockage Task Instrumentation Schematic Diagram (sheet 2 of 2)

The nine wall thermocouples monitored by the computer were placed on the carryover tank, steam separator, steam separator drain tank, and exhaust line. This instrumentation was utilized to control the heatup period such that component wall temperatures were at saturation temperature. This instrumentation was also used to estimate the heat release from the fluid to the loop components during the test.

The four turbine meters were utilized to measure the flow rate of injected water in the hydraulic characteristics, forced flooding, and gravity reflooding tests. One turbine meter was used to measure the injected flow for the hydraulic characteristics tests; another meter was used for the forced flooding tests; and two turbine meters, one in the injection line and one in the crossover leg, were used to measure flow for the gravity reflooding tests. The turbine meter in the crossover leg was bidirectional, to measure both forward and reverse flow into and out of the test section. Together, these turbine meters utilized four computer channels.

The 11 differential pressure cells were used to measure loop pressure drops, flow, or separated water accumulation. The accumulator tank had a differential pressure cell which was utilized as a backup to or a check on the injection line turbine meters. The steam injection system for the steam cooling test utilized an orifice plate coupled with a differential pressure cell, fluid thermocouple, and pressure cell to measure the injected steam flow. The three storage tanks on the downstream side of the bundle, the carryover tank, the steam separator, and the steam separator drain tank were each instrumented with differential pressure cells to measure liquid accumulation. The exit steam flow was measured downstream of the steam separator utilizing an orifice plate, differential pressure cell, fluid thermocouple, and pressure cell. Four additional differential pressure cells were utilized in the gravity reflood tests to measure mass accumulated in the downcomer, and to measure differential pressures between the downcomer and bundle, between the upper plenum and steam separator, and between the top of the downcomer and the steam separator.

The three loop pressure cells were utilized to measure the absolute pressure at the orifice plates on the bundle inlet for steam cooling tests and outlet for reflood tests, and in the upper plenum or steam separator for the gravity reflood tests.

The loop instrumentation was set up to provide redundant measurements and eliminate computer channel reassignments between forced flooding tests and gravity reflood tests, as required in previous FLECHT tests. This instrumentation design provided for efficient facility turnaround for conducting the tests.

4-24. Bundle Instrumentation

The bundle instrumentation consisted of heater rod thermocouples, steam temperature measurements, blockage sleeve thermocouples, differential pressure cells, power measurements, and plenum fluid thermocouples.

The locations of the heater rod thermocouples, steam probes, and blockage sleeve thermocouples for each of the six bundles are shown in figures F-18 through F-23 in appendix F. Also included is the complete listing of computer data acquisition system channel assignments.

4-25. Heater Rod Thermocouples

All 21 heater rods in this task were instrumented with eight thermocouples each, for a total of 168. All available thermocouples were connected to the computer. The placement of the heater rod thermocouples was based on the following objectives:

-- Achieving an overall axial distribution the same as in the 161-rod unblocked bundle reflood tests

-- Achieving a radial distribution such that rods in both the center and periphery of the bundle were instrumented

-- Achieving a sufficient number of thermocouples upstream and downstream of the blockage zone to determine the axial effects of blockage sleeves

The heater rod thermocouples in the blockage zone for configurations D and E and their locations relative to the blockage sleeves are shown in a three-dimensional perspective in figures 4-10 and 4-11, respectively.

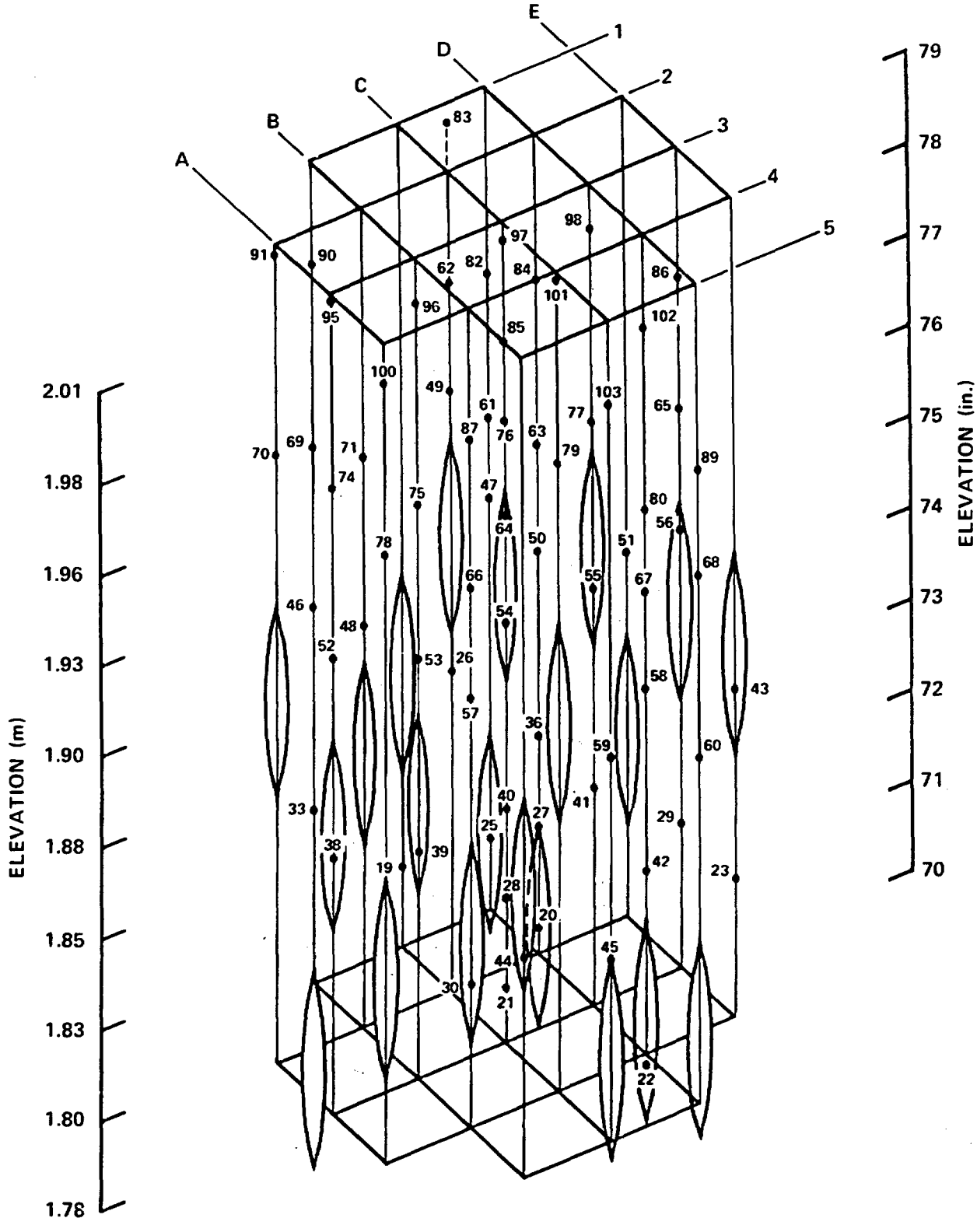

Figure 4-10. Configuration D Blockage Distribution and Instrumentation

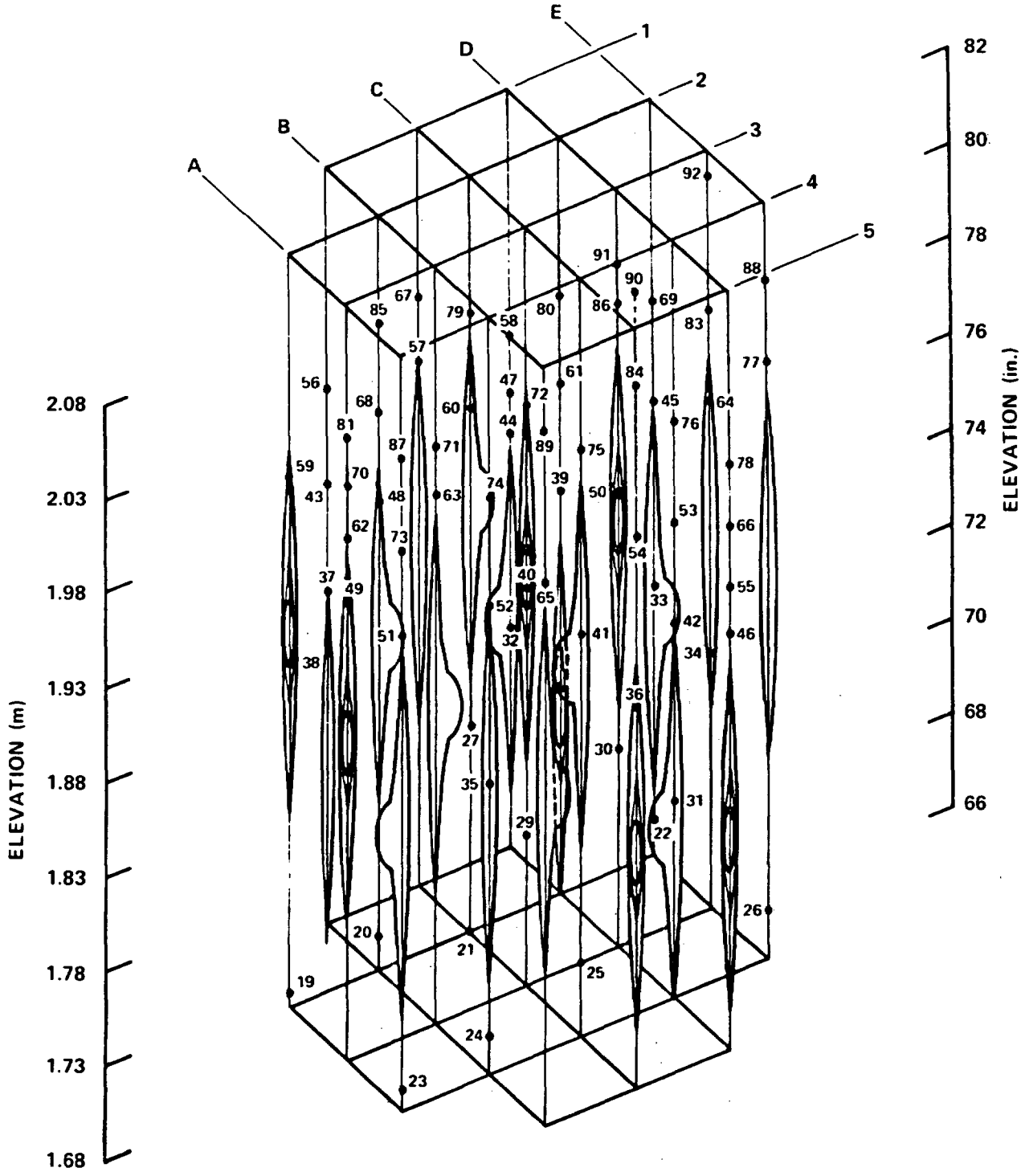

Figure 4-11. Configuration E Blockage Distribution and Instrumentation

For configurations A through D, the azimuthal orientations of the heater rod thermocouples were arranged such that the thermocouples were directed toward the subchannel instead of toward an adjacent heater rod. Heat conduction calculations (appendix I) later showed that azimuthal orientation was not an important consideration; therefore, no attempt was made to azimuthally orient thermocouples in configurations E and F. Checks were performed during test series D and E on selected rods (bundle locations 3A and 3E). The checks indicated that although the rods were fixed at the top of the bundle, rod rotations as high as 25 degrees were seen at the lower end where the rods were by necessity left free to grow and rotate. This indicated that, although it was possible to assemble a bundle with known initial azimuthal thermocouple locations, it was not possible to accurately predict thermocouple azimuthal locations after a bundle was thermally cycled. It was also possible that rod rotations higher than the posttest cold measurement could have occurred. These rod rotations would not have had any effect on the nonconcentric sleeve blockage, since the bulge could rotate an insignificant amount in the flow channel.

4-26. Steam Temperature Instrumentation

Steam temperature data required for data analysis and evaluation efforts were measured by means of a steam probe specifically designed for the 21-rod bundle task and unshielded thermocouples. This instrumentation provided data for evaluation of the following:

-- Mass and energy balances

-- Nonequilibrium vapor properties

-- Radial and axial steam temperature variation

-- Effect of flow blockage sleeves

Unlike the steam probes in the 161-rod unblocked bundle task, which were located within a thimble tube and aspirated steam to the atmosphere, the 21-rod bundle steam

probe was enclosed within a 2.381 mm (0.09375 in.) hollow tube, and relied on the frictional pressure drop across a 0.64 cm (0.25 in.) length to drive steam flow. A simplified sketch of the steam probe is shown in figure 4-12. A 0.81 mm (0.032 in.) thermocouple was enclosed within a 2.381 mm (0.09375 in.) OD hollow tube of 0.2 mm (0.006 in.) wall thickness. The two flow holes spaced 6.4 mm (0.25 in.) apart were diametrically opposed. The thermocouple junction was located midway between the two flow holes, thereby providing radiation shielding and protection from water droplets. Figure F-24 shows the construction details of the self-aspirating steam probes as well as the details of the unshielded fluid thermocouples, which were also used to measure vapor temperatures.

Steam probe and bare fluid thermocouples were, in general, located in subchannels at elevations where heater rod temperatures were being measured. They were concentrated immediately upstream and downstream of the blockage zone to determine axial and radial effects of blockage on steam temperatures. The steam probes and fluid thermocouples were attached to the nearest grid and centered in the subchannel. The thermocouple leads lay on the top or bottom of the grid and ran to the corner fillers. The leads subsequently were routed in scallops in the fillers and exitted the test section through seal glands in the top or bottom seal plates. Appendix J presents the evaluation of the self-aspirating steam probe and unshielded fluid thermocouples.

4-27. Blockage Sleeve Instrumentation

The placement of blockage sleeves on the heater rod to simulate prototypical subchannel flow blockage added a thermal resistance to the heater rod. Since this thermal resistance is a function of the sleeve temperature, it was necessary to measure the temperature of the blockage sleeve so that the heat transfer to the coolant could be determined. Also, it was desirable to know the quench temperature and quench time of the sleeve.

A 0.81 mm (0.032 in.) diameter thermocouple was embedded in selected blockage sleeves at the point of maximum strain. The thermocouple lead was routed downstream of the blockage sleeve along a filler rod and through the seal plate in the same manner as the steam probe and unshielded fluid thermocouples.

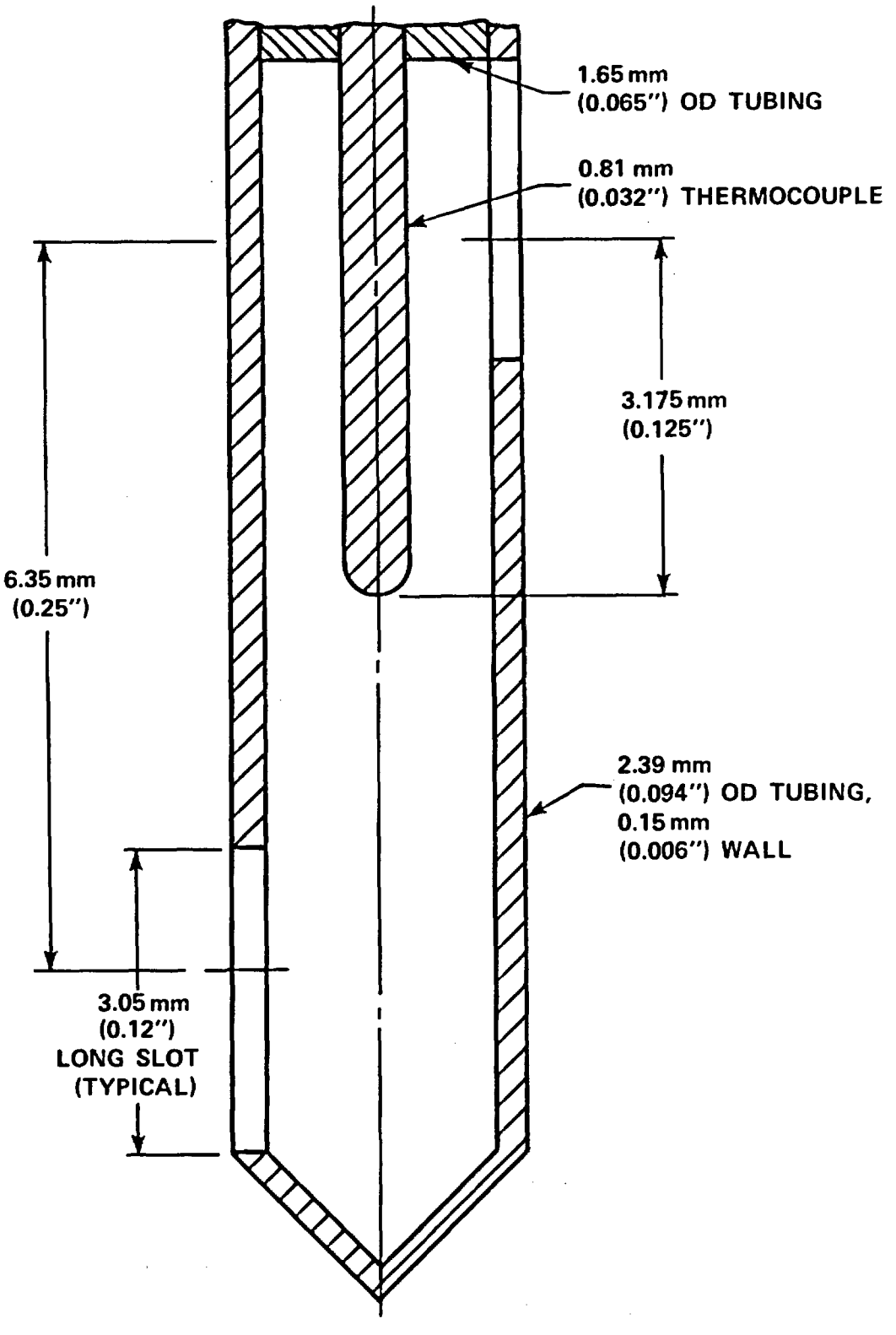

Figure 4-12. Steam Probe Design for 21-Rod Bundle Flow Blockage Task

4-28. Differential Pressure Measurements

Differential pressure measurements were made every 0.30 m (12 in.) along the length of the bundle to determine mass accumulation in the bundle during reflood tests. Differential pressure transmitters [±3.7 MPa (±15 in. H_2O)] were utilized to obtain an accurate mass accumulation measurement representative of an average across the bundle. An additional cell measured the overall pressure drop from the bottom to the top of the heated length.

These transmitters were also used to measure the frictional and form losses across the grid, rods, and blockage sleeves in hydraulic characteristic tests, which were performed prior to the single-phase steam and heat transfer tests. These pressure transmitters were accurate to ±0.20 percent of full scale.

4-29. Power Measurements

Three instrumentation channels were devoted to measurement of power into the bundle. One was used as a primary measurement from which power was controlled by the computer software. One independent power measurement was used for data reduction purposes for forced and gravity reflood tests. The third power measurement channel was used exclusively for the low-power steam cooling tests.

4-30. Upper Plenum Instrumentation

The upper plenum (figure 4-13) was an important component of the FLECHT loop. The upper plenum was utilized to separate the liquid and steam phases in close proximity to the test section so that accurate mass and energy balances could be accomplished. A differential pressure cell connected between the top and bottom of the upper plenum was used to measure liquid accumulation within this component. Liquid collected at the bottom of the upper plenum before draining into the carryover tank. System pressure was controlled by a pressure transmitter located in the upper plenum for all tests except gravity reflood tests. Another pressure transmitter was connected to the computer for measuring system pressure.

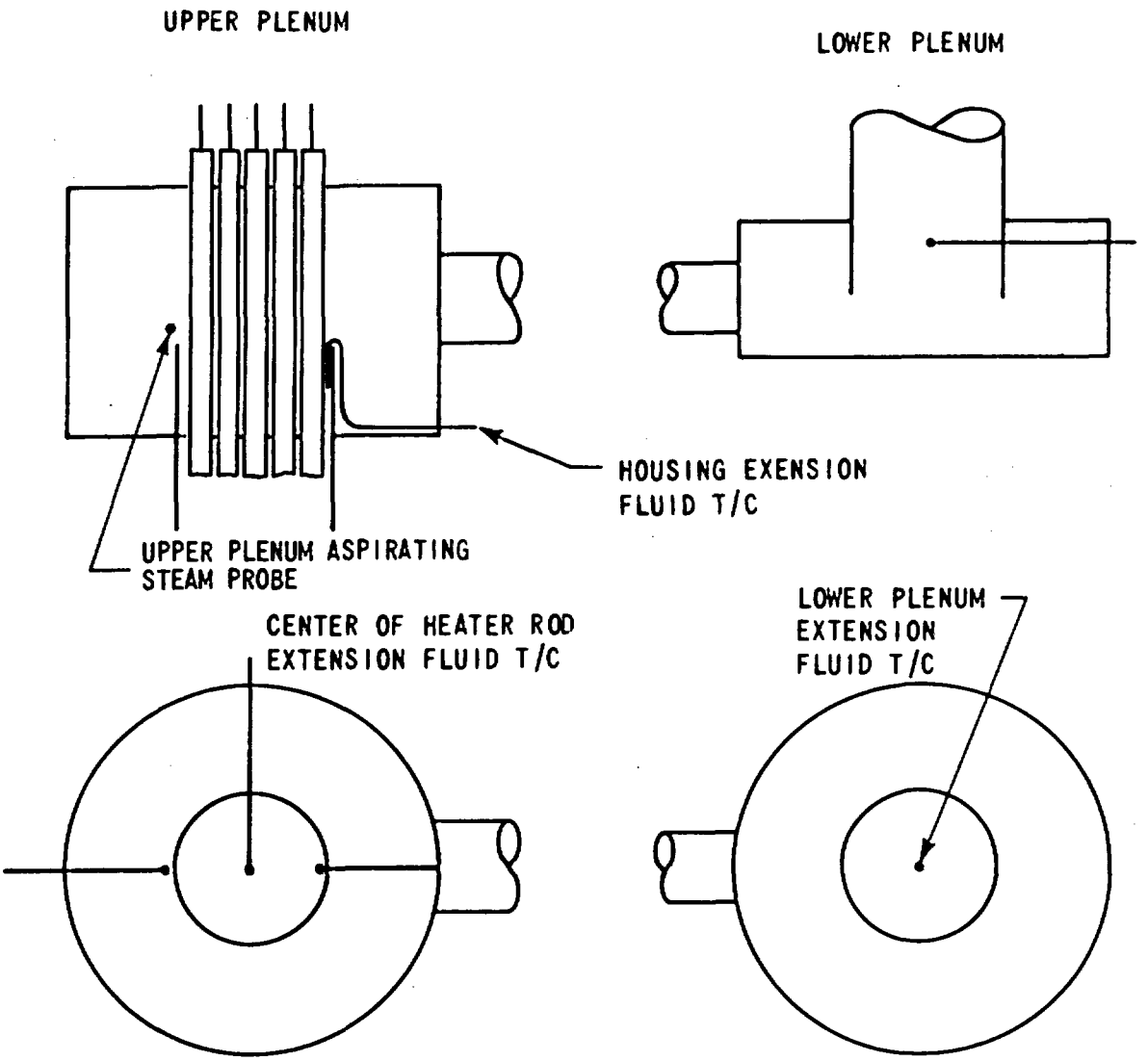

Figure 4-13. Upper and Lower Plenum Thermocouple Location for 21-Rod Flow Blockage Task

Two upper plenum thermocouples were designed to measure the fluid temperature at upper plenum exit and in the upper plenum extension. These thermocouples indicated the location and presence of liquid in the upper plenum and housing extension. An aspirating steam probe located in the upper plenum at the bundle exit was utilized to measure vapor nonequilibrium temperature. Three wall thermocouples were used to ensure that the plenum was at a uniform temperature prior to and during testing. A thermocouple was imbedded in one of the upper heater rod O-ring seals to monitor the seal temperature. A seal temperature limit of 135°C (275°F) was established for the steam cooling tests to prevent failure of the polyurethane sealing material.

4-31. Lower Plenum Instrumentation

The lower plenum was instrumented with a wall thermocouple for helping to establish initial test conditions, and a fluid thermocouple located in the center of the lower plenum extension (figure 4-13) for measuring inlet subcooling as water flooded the bundle. Two additional fluid thermocouples located in the injection piping were utilized as backups to the lower plenum fluid thermocouple.

4-32. FACILITY OPERATION

The following general procedure was used to conduct a typical forced reflood test:

(1) Fill accumulator with water and heat to desired coolant temperature, 53°C (127°F) nominal.

(2) Turn on boiler and bring the pressure up to 0.62 MPa (75 psig) nominal gage pressure.

(3) Steam heat the carryover vessel, entrainment separator, separator drain tank, test section plenum, and test section outlet piping (located before the entrainment separator) while empty to slightly above the saturation temperature corresponding to the test run pressure. The exhaust line between the separator and exhaust orifice is electrically heated to 260°C (500°F) nominal; the test section lower plenum is heated to the temperature of the coolant in the accumulator.

(4) Pressurize the test section, carryover vessel, and exhaust line components to the specified test run pressure by valving in the boiler and setting the exhaust line control valve to the specified pressure.

(5) Scan all instrumentation channels by the computer to check for defective instrumentation. The differential pressure and static pressure cell zero readings are taken and entered into the computer calibration file. These zero readings are compared with the component calibration zero reading. The straight-line conversion to engineering units is changed to the new zero when the raw data are converted to engineering units. This zero shift process accounts for errors due to transmitter zero shifts and compensates for reference leg levels, enabling the engineering units to start with an empty reading.

(6) Power bundle twice to heater rod temperature of 649°C (1200°F) to achieve housing 1.83 m (72 in.) wall temperatures of between 482°C and 538°C (900°F and 1000°F).

(7) Apply power to the test bundle at a peak rate of 1.3 kw/m (0.4 kw/ft) and allow rods to heat up. When the temperature in any 2 of 28 designated bundle thermocouples reaches the desired test flood temperature, 871°C (1600°F), the computer automatically initiates flood, sets power at initial value as specified, and controls power decay. The exhaust control valve regulates the system pressure at the preset value by releasing steam to the atmosphere.

(8) Ascertain that all designated rods have quenched (indicated by the computer printout of bundle temperature).

(9) Cut power from heaters, terminate coolant injection, and depressurize the entire system.

(10) Drain and weigh water from all components.

The procedure was exactly the same as above for the gravity reflood tests except for the addition of the crossover leg and downcomer, in which the coolant was injected into a water-filled crossover leg and downcomer (equivalent to the bottom of the heated length).

4-33. KEY FACILITY OPERATING LIMITATIONS AND SAFETY FEATURES

All vessels in the FLECHT SEASET 21-rod bundle facility were designed and built to the ASME Boiler and Pressure Vessel Code. Facility piping conformed to the latest edition of the Code for Power Piping, ANSI B31.1. Facility operating limits were set by either design criteria and/or component material limitations. Primary loop (test section and exhaust piping and components) design pressure was limited to 0.65 MPa (80 psig) because of the thin-walled low mass housing design, which was rated 0.65 MPa (80 psig) with an 815°C (1500°) midplane temperature. This temperature was a maximum material limitation set by the ASME Code. All 21-rod facility tests were run at or below 0.27 MPa (25 psig).

Both the steam cooling and water injection system piping and components were designed for 6.65 MPa (950 psig) and minimum temperature of 177°C (350°F). The systems were operated well within these design limits.

Heater rod O-ring seals were made of ethylene propylene, which limited the test section upper seal plate temperature to 135°C (275°F) during steam cooling tests. This, in turn, limited test section exhaust steam temperatures to approximately 204°C (400°F).

The Kanthal heater rod element material limited operation of the test bundle heater rods to 1232°C (2250°F).

Personnel as well as facility safety were prime considerations in the design of the FLECHT SEASET 21-rod bundle facility. Accordingly, the following safety devices and/or features were designed into the facility:

- Test section:
  Rupture disk with a burst pressure of 0.65 MPa (80 psig) at 22°C (72°F)

Pressure switch, set to sound an alarm at 0.62 MPa (75 psig)

-- Carryover tank:
Rupture disk with a burst pressure of 0.65 MPa (80 psig) at 22°C (72°F)

-- Entrainment separator:
Rupture disk with a burst pressure of 0.86 MPa (110 psig) at 22°C (72°F)

-- Facility heating boiler:
Relief valve set at 0.79 MPa (100 psig)

-- Steam cooling steam supply boiler:
Rupture disk with a burst pressure of 6.65 MPa (950 psig) at 22°C (72°F)

-- Water supply vessel:
Rupture disk with a burst pressure of 6.65 MPa (950 psig) at 22°C (72°F)

-- Upper heater rod O-ring seal plate:
Thermocouple temperature controller circuit to shut off bundle power and sound alarm when seal plate temperature exceeds 135°C (275°F)

-- Heater rod bundle:
Overcurrent limit to protect rods from failure from an overpowered SCR by shutting off bundle power and sounding alarm
Computer-monitored and activated overtemperature trip set to shut off bundle power and sound alarm at 1232°C (2250°F)
Provision for shutting off bundle power and sounding alarm in case of computer power failure
Circuitry design to shut off bundle power in case of control panel voltage (100 v) failure

SECTION 5
TEST RESULTS

5-1. INTRODUCTION

The data from 87 forced reflood, 10 gravity reflood, 24 steam cooling, and 43 hydraulic characteristics tests performed during the FLECHT SEASET 21-rod bundle test program met the specified test conditions and are reported herein. The data from 22 forced reflood tests, 2 gravity reflood, and 22 steam cooling tests did not meet the test matrix specifications for the reasons specified in table K-7 of appendix K.

5-2. DATA REDUCTION

Data collected for each run at the test site were compiled on a binary magnetic tape in engineering units by the CDAS. This magnetic tape was processed by a CDC-7600 computer and the following series of data reduction programs were utilized for forced and gravity reflood tests:

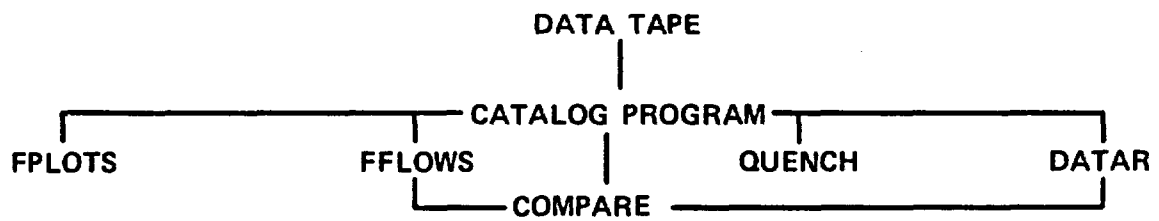

The CATALOG program converted the data to a form compatible with the CDC computer. The FPLOTS program simply printed and plotted all the recorded data as a function of time.

The hydraulic characteristics and steam cooling tests utilized only the CATALOG and FPLOTS programs from above. The as-run test conditions for these single-phase tests

are shown in tables 5-1 and 5-2. The test conditions were modified in configurations E and F for matrix tests 01 and 02, to provide a wider range of Reynolds numbers. However, the power-to-flow ratio was held constant for all tests. (See paragraph 6-12 for actual flows.) The hydraulic characteristics test data were reduced by the HYCHAR code as described in paragraph 5-7. The steam cooling test data were reduced by the STMCOOL code as described in paragraph 5-8.

The following paragraphs describe the other four reflood programs and a sampling of reduced data. The as-run test conditions for the reflood tests are shown in table 5-3. The instrumentation error analysis associated with the recorded data is discussed in appendix L.

The test numbers comprise six characters each. The first character, 4, refers to the 21-rod bundle test program, the second and third refer to the sequential bundle cycle number, the fourth and fifth are the test matrix number, and the sixth character refers to the blockage configuration. For example, run 41909A is matrix test number 09 in the 19th cycle of configuration A 21-rod bundle tests.

5-3. FFLOWS Program and Results

The FFLOWS program was utilized primarily to calculate the mass balance for each reflood test. The mass balance was calculated by the following formulation:

$$\text{percent mass imbalance} = \frac{\text{mass difference}}{\text{mass injected}} \times 100$$

where

mass difference = injected mass - (collected liquid mass + mass in bundle + steam mass out + steam probe mass)

collected liquid mass = upper plenum mass + carryover tank mass + steam separator mass

TABLE 5-1

AS-RUN CONDITIONS FOR HYDRAULIC CHARACTERISTICS TESTS

Test Matrix No. and Bundle	Test Run No.	Upper Plenum Pressure [MPa (psia)]	Flow Rate [m^3/sec(gal/min)]	Average Coolant Temperature [C^o(^{o}F)]	Reynolds Number
18A	40618A	0.13(19)	6.3×10^{-4}(10)	23(73)	2645
18B	40818B	0.20(29)	6.69×10^{-4}(10.6)	26(78)	3037
18C	40718C	0.12(18)	6.37×10^{-4}(10.1)	30(86)	3205
18D	40718D	0.14(20)	6.37×10^{-4}(10.1)	23(74)	2685
18E	42818E	0.15(22)	6.75×10^{-4}(10.7)	27(81)	3126
18F	40618F	0.12(17)	5.90×10^{-4}(9.35)	25.7(78.2)	2617
19A	40419A	0.13(19)	1.3×10^{-3}(20)	23(74)	5431
19B	40619B	0.26(37)	1.32×10^{-3}(20.9)	25(77)	5866
19C	40519C	0.15(22)	1.25×10^{-3}(19.8)	30(86)	6251
19D	40519D	0.14(21)	1.27×10^{-3}(20.2)	23(73)	5300
19E	43219E	0.11(16)	1.29×10^{-3}(20.5)	26(79)	5793
19F	40419F	0.097(14)	1.20×10^{-3}(19.0)	28.7(83.6)	5682
20A	40220A	0.12(18)	1.9×10^{-3}(30)	25(77)	8518
	40720A	0.17(24)	1.9×10^{-3}(30)	22(71)	7835
20B	40420B	0.20(29)	1.87×10^{-3}(29.7)	26(78)	8452
	40920B	0.19(27)	1.96×10^{-3}(31.1)	25(77)	8759
20C	40320C	0.12(18)	1.91×10^{-3}(30.3)	30(86)	9525
	40820C	0.12(18)	1.92×10^{-3}(30.4)	29(85)	9571
20D	40220D	0.12(17)	1.96×10^{-3}(31.1)	24(75)	8430
	40820D	0.12(18)	1.97×10^{-3}(31.2)	23(73)	8246
20E	42920E	0.28(40)	2.00×10^{-3}(31.7)	27(81)	9260
	43420E	0.12(18)	1.93×10^{-3}(30.6)	25(77)	8458
20F	40220F	0.17(25)	1.84×10^{-3}(29.2)	28.1(82.5)	8389
	40720F	0.121(17.5)	1.88×10^{-3}(29.8)	25.7(78.2)	8650

TABLE 5-1 (cont)

AS-RUN CONDITIONS FOR HYDRAULIC CHARACTERISTICS TESTS

Test Matrix No. and Bundle	Test Run No.	Upper Plenum Pressure [MPa (psia)]	Flow Rate [m^3/sec(gal/min)]	Average Coolant Temperature [C°(°F)]	Reynolds Number
21A	40121A	0.19(27)	2.5×10^{-3}(40)	26(78)	11464
21B	40321B	0.18(26)	2.49×10^{-3}(39.4)	24(76)	10941
21C	40221C	0.22(32)	2.48×10^{-3}(39.3)	30(86)	12436
21D	40121D	0.28(40)	2.49×10^{-3}(39.5)	25(77)	10993
21E	43021E	0.19(28)	2.57×10^{-3}(40.8)	27(80)	11762
21F	40121F	0.176(25.5)	2.48×10^{-3}(39.3)	27.4(81.4)	11403
22A	40322A	0.18(26)	3.2×10^{-3}(50)	24(75)	13695
22B	40522B	0.28(40)	3.17×10^{-3}(50.3)	24(75)	13757
22C	40422C	0.23(33)	3.24×10^{-3}(51.3)	29(84)	15918
22D	40422D	0.17(25)	3.17×10^{-3}(50.3)	26(78)	12996
22E	43122E	0.27(39)	3.2×10^{-3}(50)	26(79)	14158
22F	40322F	0.21(30)	3.11×10^{-3}(49.3)	28.1(82.5)	14598
23A	40523A	0.21(31)	3.8×10^{-3}(60)	23(74)	16287
23B	40723B	0.34(50)	3.76×10^{-3}(59.6)	25(77)	16759
23C	40623C	0.28(40)	3.72×10^{-3}(58.9)	31(87)	18870
23D	40623D	0.22(32)	3.8×10^{-3}(60)	23(73)	15774
	40322D[a]	0.28(40)	3.8×10^{-3}(60)	23(73)	15749
23E	43323E	0.28(41)	3.51×10^{-3}(55.6)	25(77)	15394
23F	40523F	0.23(34)	3.77×10^{-3}(59.8)	28.1(82.5)	17682

a. Misnumbered test; should be 40323D

A mass balance plot for the reference run in configuration A (run 42430A) is shown in figure 5-1. The percent mass imbalances at the end of injection for all of the reflood tests in all six bundles are shown in figure 5-2. The average mass imbalance was found to be approximately 2.4 percent at the end of injection for all forced reflood tests, and approximately 1.4 percent for all gravity reflood tests. Although there were some tests which had mass imbalances between 5 and 10 percent at the end of injection, the mass imbalances for these tests during the run were generally less than that at the end of injection.

The details of these mass balance calculations as well as the other features of the FFLOWS program are provided in appendix M.

5-4. QUENCH Program and Results

The heater rod and housing thermocouple data for reflood tests were reduced by the QUENCH program. The QUENCH program was designed to determine the characteristics of temperature histories of the thermocouple data. These characteristics include the initial temperature, maximum temperature, quench temperature, turnaround time, and quench time. The temperature history of the hottest rod thermocouple for the reference run in configuration A (run 42430A) is shown in figure 5-3 with the actual data points chosen by the QUENCH program. A tabulation of the hot rod characteristics from the QUENCH program for all gravity and forced reflood tests is provided in table 5-3. The QUENCH program calculates the statistics of these characteristics for each instrumentation elevation, such as average turnaround time. These statistics are tabulated for each reflood test in appendix K.

The QUENCH program also calculates a quench front curve (from a cubic spline curve fit) from the average of the quench times at a given elevation, and subsequently calculates a quench front velocity which is utilized in the FLEMB code for calculating an energy balance (section 6). Examples of the calculated quench curve and quench front velocity are shown in figures 5-4 and 5-5, respectively, for run 42430A.

The details of the criteria used for choosing quench time and temperature are provided in appendix M.

TABLE 5-2

AS-RUN CONDITIONS FOR STEAM COOLING TESTS

Test Matrix No. and Bundle	Test Run No.	Upper Plenum Pressure [MPa (psia)]	Rod Peak Power [kw/m (kw/ft)]	Flow Rate [kg/sec (lb/sec)]	Average Coolant Temperature [°C (°F)]	Inlet Reynolds Number
01A	44401A	0.145(21.1)	0.0525(0.0160)	0.014(0.031)	110(230)	4790
01B	41401B	0.141(20.4)	0.0522(0.0159)	0.0141(0.0312)	111(231)	4700
01C	41201C	0.140(20.3)	0.0531(0.0162)	0.014(0.031)	111(232)	4630
01D	43401D	0.141(20.4)	0.0531(0.0162)	0.0143(0.0316)	110(230)	4645
01E	40601E	0.141(20.5)	0.043(0.013)	0.012(0.026)	110(230)	3796
01F	40901F	0.142(20.6)	0.0413(0.0126)	0.0119(0.0263)	113(236)	3811
02B	43202B	0.143(20.7)	0.103(0.0313)	0.0280(0.0618)	112(233)	9180
02C	43902C	0.140(20.3)	0.105(0.0320)	0.028(0.062)	112(233)	9260
02D	41202D	0.148(21.4)	0.104(0.0318)	0.028(0.062)	112(234)	9054
02E	40102E	0.144(20.9)	0.075(0.023)	0.021(0.046)	112(233)	6695
02F	41002F	0.1410(20.45)	0.0741(0.0226)	0.0207(0.0456)	112(234)	6629
03A	44303A	0.143(20.8)	0.13(0.040)	0.034(0.076)	114(238)	11590
03B	41103B	0.141(20.4)	0.131(0.0399)	0.035(0.077)	114(237)	11330
03C	41003C	0.147(21.3)	0.13(0.040)	0.035(0.077)	112(234)	11460

TABLE 5-2 (cont)

AS-RUN CONDITIONS FOR STEAM COOLING TESTS

Test Matrix No. and Bundle	Test Run No.	Upper Plenum Pressure [MPa (psia)]	Rod Peak Power [kw/m (kw/ft)]	Flow Rate [kg/sec (lb/sec)]	Average Coolant Temperature [°C (°F)]	Inlet Reynolds Number
03D	41103D	0.148(21.4)	0.125(0.0382)	0.035(0.077)	122(251)	10958
03E	40503E	0.143(20.7)	0.125(0.0380)	0.034(0.076)	112(233)	11061
03F	41103F	0.1406(20.39)	0.129(0.0393)	0.0344(0.0759)	118.5(245.4)	10822
29A[a]	44529A	0.141(20.4)	0.03(0.009)	0.00807(0.0178)	109.8(229.6)	2760
29B[a]	43129B	0.139(20.1)	0.029(0.0089)	0.00807(0.0178)	111(231)	2680
29C[a]	41329C	0.144(20.9)	0.03(0.009)	0.0082(0.018)	113(235)	2680
29D[a]	41529D	0.146(21.2)	0.031(0.0094)	0.0082(0.018)	118(244)	2586
29E[a]	43929E	0.138(20.0)	0.0310(0.00945)	0.0086(0.019)	112(233)	2755
	44029E	0.137(19.9)	0.0307(0.00935)	0.0086(0.019)	112(234)	2751
29F[a]	41229F	0.1414(20.51)	0.029(0.0089)	0.00853(0.0188)	113.2(235.8)	2724

a. See page 6-26.

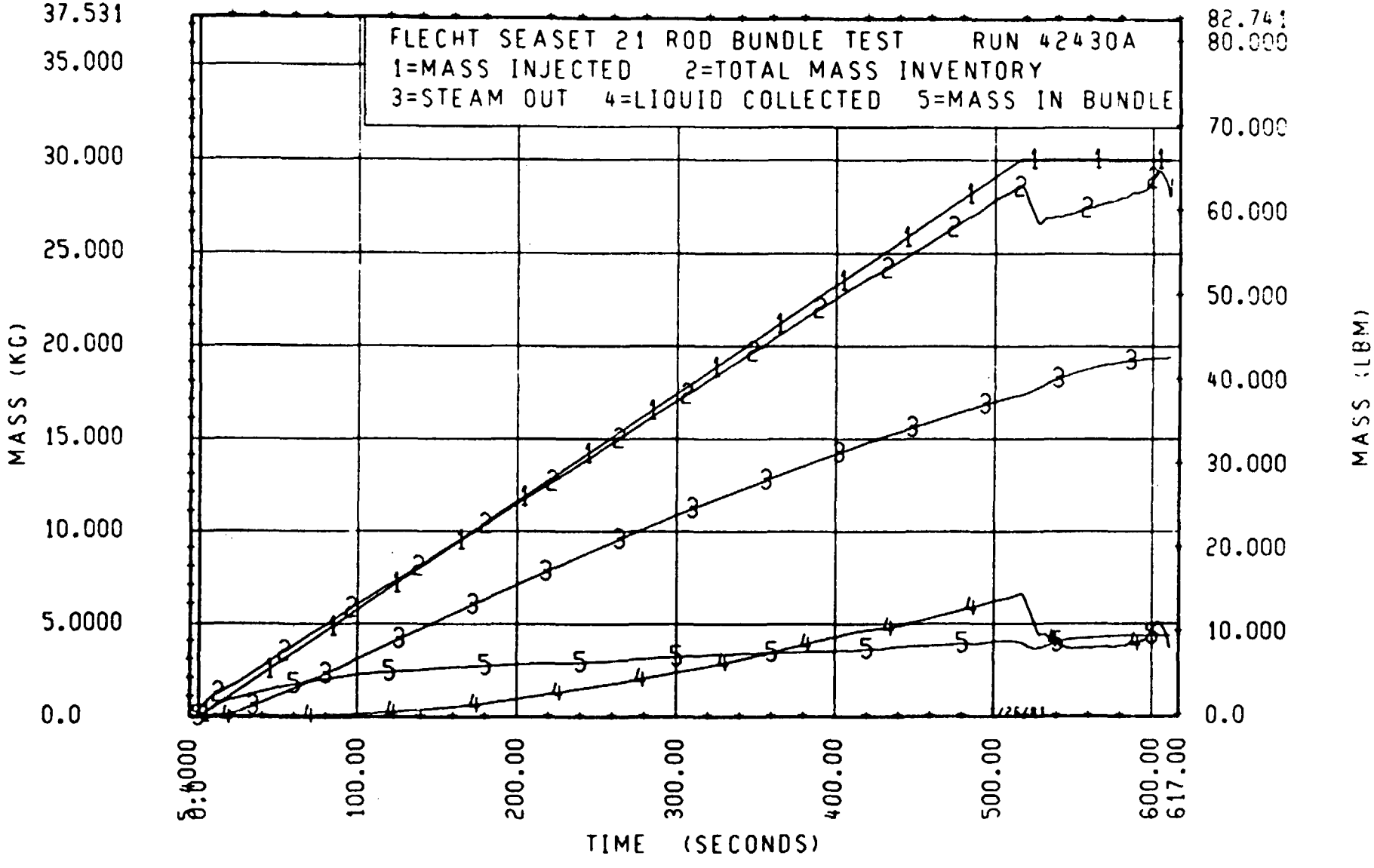

Figure 5-1. Mass Balance, Run 42430A

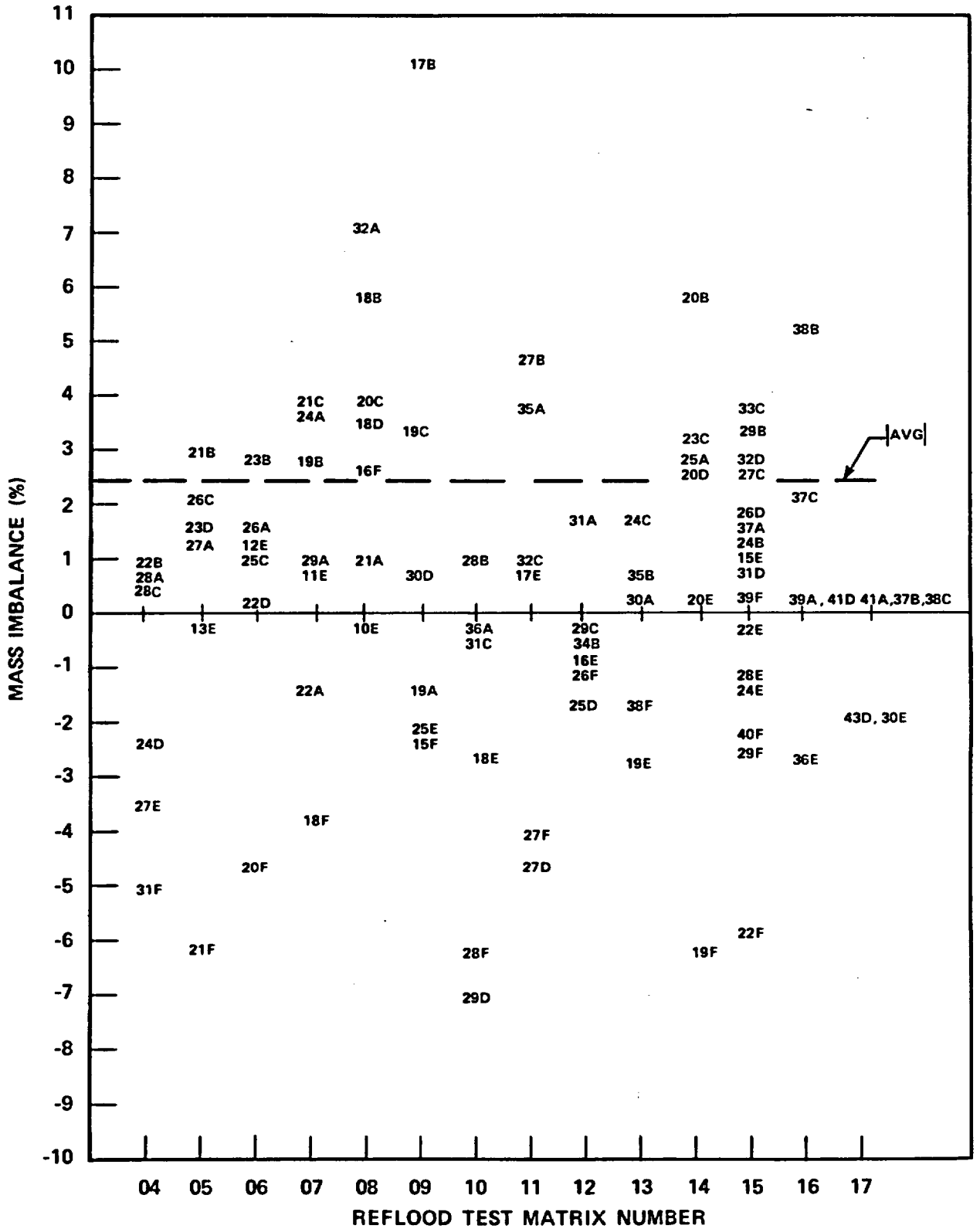

Figure 5-2. Forced and Gravity Reflood Tests Mass Imbalance

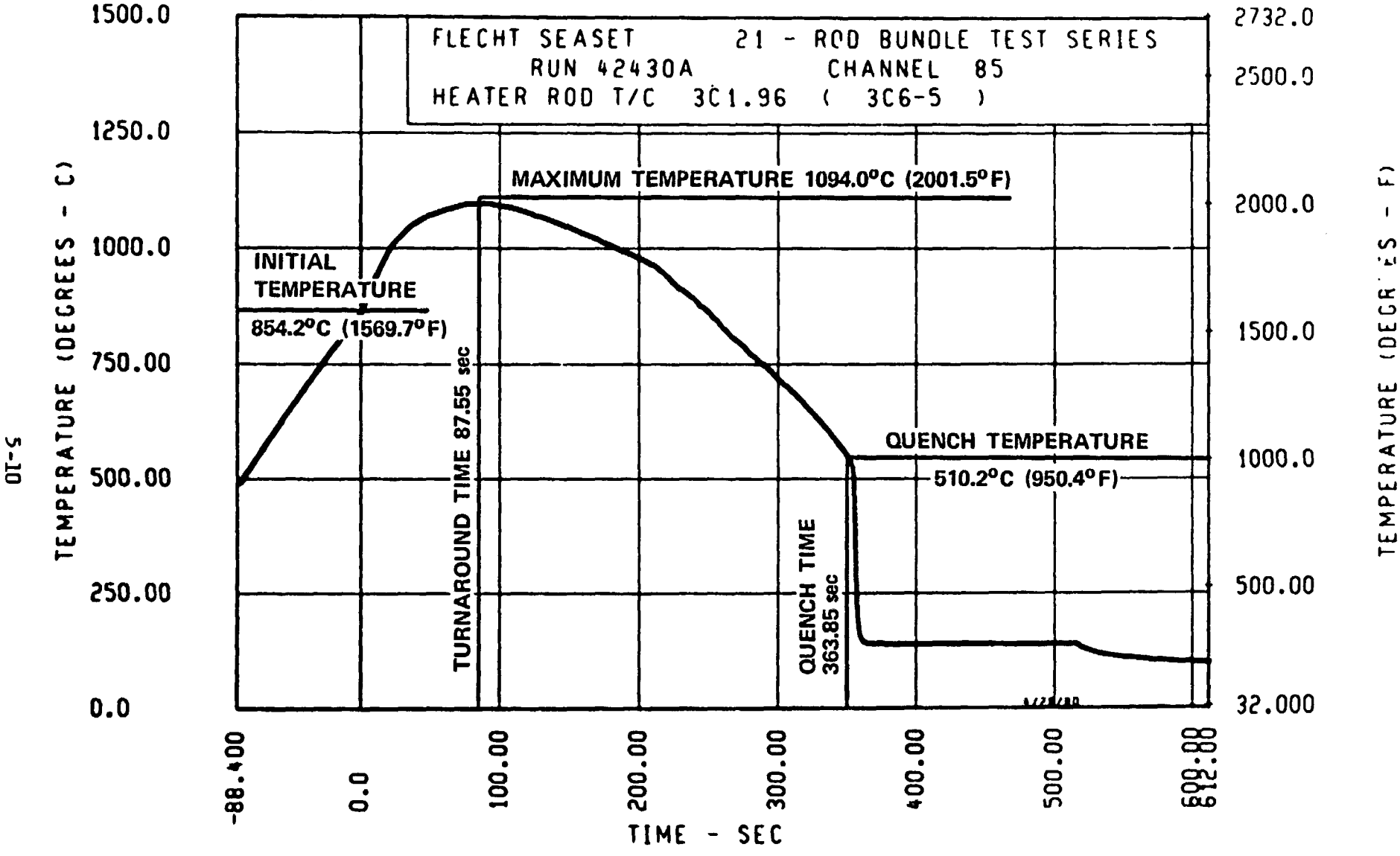

Figure 5-3. Hot Rod Thermocouple Characteristics, Run 42430A

TABLE 5-3a[(a)]

SUMMARY OF RUN CONDITIONS AND RESULTS FOR REFLOOD TESTS

Test Matrix No. and Bundle	Test Run No.	As-Run Test Conditions					Results							
		Upper Plenum Pressure (MPa)	Rod Initial Temperature (°C)	Rod Peak Power (kw/m)	Flooding Rate (mm/sec)	Average Coolant Temperature (°C)	Average Housing Initial Temperature at 1.83 m (°C)	Hottest Rod and Nominal Elevation (m)	Hot Rod Initial Temperature (°C)	Hot Rod Maximum Temperature (°C)	Hot Rod Temperature Rise (°C)	Hot Rod Turnaround Time (sec)	Hot Rod Quench Time (sec)	Bundle Quench Time (sec)
CONSTANT FLOODING RATE EFFECT TESTS														
04A	42804A	0.273	873	1.0	13	50	522	3C-1.96	858	983	125	95	338	536
04B	42204B	0.274	878	0.98	13	52	548	3C-1.88	828	961	133	107	327	583
04C	42804C	0.273	876	0.98	13	49	529	3C-1.98	854	965	112	91	367	551
04D	42404D	0.278	878	1.0	13	51	541	3C-1.911	838	970	133	97	604	548
04E	42704E	0.278	874	0.98	13	49	542	3C-2.13	818	960	143	99	362	528
04F	43104F	0.276	877	1.0	13	49	536	3C-2.03	872	956	85	93	340	555
05A	42705A	0.273	873	1.5	18	50	498	3C-1.96	859	1024	164	85	321	452
05B	42105B	0.274	880	1.5	19	49	486	3C-1.98	854	992	138	86	346	474
05C	42605C	0.275	884	1.5	19	50	487	3C-1.78	871	1000	128	75	282	458
05D	42305D	0.279	878	1.5	18	51	492	3C-1.911	827	1019	188	110	542	481
05E	41305E	0.276	872	1.5	19	49	471	3D-2.03	829	993	164	102	350	467
05F	42105F	0.279	874	1.44	19	50	479	3C-1.78	874	968	96	67	260	448
06A	42606A	0.273	872	2.6	23	50	502	3C-1.96	860	1157	296	99	426	632
06B	42306B	0.274	875	2.6	23	50	529	3C-1.98	860	1128	268	117	463	677
06C	42506C	0.268	874	2.6	23	50	519	3C-1.78	867	1119	253	98	352	643
06D	42206D	0.278	878	2.6	23	50	503	3C-1.98	870	1133	262	116	433	662
06E	41206E	0.279	871	2.6	23	50	509	3D-2.03	796	1103	307	133	470	639
06F	42006F	0.278	875	2.6	23	50	525	3C-2.03	860	1074	213	93	416	603

a. Data are presented in English units in table 5-3b.

TABLE 5-3a[(a)] (cont)

SUMMARY OF RUN CONDITIONS AND RESULTS FOR REFLOOD TESTS

Test Matrix No. and Bundle	Test Run No.	As-Run Test Conditions					Results							
		Upper Plenum Pressure (MPa)	Rod Initial Temperature (°C)	Rod Peak Power (kw/m)	Flooding Rate (mm/sec)	Average Coolant Temperature (°C)	Average Housing Initial Temperature at 1.83 m (°C)	Hottest Rod and Nominal Elevation (m)	Hot Rod Initial Temperature (°C)	Hot Rod Maximum Temperature (°C)	Hot Rod Temperature Rise (°C)	Hot Rod Turnaround Time (sec)	Hot Rod Quench Time (sec)	Bundle Quench Time (sec)
CONSTANT FLOODING RATE EFFECT TESTS (cont)														
07A	42207A	0.273	871	2.3	28.2	52	222	3C-1.96	871	1019	148	55	274	396
	42430A[(b)]	0.276	872	2.6	28.2	50	501	3C-1.96	864	1098	235	82	354	513
07B	41907B	0.276	874	2.6	28.4	50	533	3C-1.98	860	1065	206	95	387	557
07C	42107C	0.270	884	2.6	27.7	51	498	3C-1.78	871	1070	199	69	318	559
07F	41807F	0.277	873	2.6	28.07	49	502	3C-2.03	866	1029	162	85	363	518
08A	42108A	0.269	872	2.3	39.4	52	221	3C-1.96	872	963	92	24	204	308
	43208A	0.280	873	2.3	38.1	50	525	3C-1.96	858	991	133	54	252	367
08B	41808B	0.273	873	2.3	37.3	49	537	3C-1.98	862	970	109	38	278	394
08C	42008C	0.275	883	2.3	37.8	49	514	3C-1.78	869	971	101	39	224	384
08D	41808D	0.278	884	2.3	37.8	52	502	4D-1.78	869	983	113	34	574	428
08E	41008E	0.281	872	2.3	37.8	49	511	2B-1.70	862	947	86	39	208	355
08F	41608F	0.279	875	2.3	38.1	50	526	2B-1.70	870	947	76	37	207	353
09A	41909A	0.270	871	2.3	147	54	217	3C-1.96	863	876	13	3	72	103
09B	41709B	0.273	877	2.3	147	51	333	3C-1.96	877	889	13	3.5	45	110
09C	41909C	0.275	881	2.3	152	51	208	4C-1.70	880	895	14	4	59	108
09D	43009D	0.279	872	2.3	147	52	293	3C-1.98	872	881	9	2.5	33	109
09E	42509E	0.279	879	2.3	142	51	261	2C-1.70	879	891	12	3.5	59	108
09F	41509F	0.276	878	2.3	146	52	351	3C-2.03	878	888	11	2.5	47	115

b. Misnumbered test

TABLE 5-3a[(a)] (cont)

SUMMARY OF RUN CONDITIONS AND RESULTS FOR REFLOOD TESTS

Test Matrix No. and Bundle	Test Run No.	As-Run Test Conditions					Results							
		Upper Plenum Pressure (MPa)	Rod Initial Temperature (°C)	Rod Peak Power (kw/m)	Flooding Rate (mm/sec)	Average Coolant Temperature (°C)	Average Housing Initial Temperature at 1.83 m (°C)	Hottest Rod and Nominal Elevation (m)	Hot Rod Initial Temperature (°C)	Hot Rod Maximum Temperature (°C)	Hot Rod Temperature Rise (°C)	Hot Rod Turnaround Time (sec)	Hot Rod Quench Time (sec)	Bundle Quench Time (sec)
PRESSURE EFFECT AT CONSTANT FLOODING RATE TESTS														
10A	43610A	0.142	872	0.89	10	31	552	3C-1.96	855	982	127	118	494	754
10B	42810B	0.137	878	0.89	10	32	568	3C-1.88	835	968	133	147	477	775
10C	43110C	0.137	871	0.89	10.3	29	526	3C-1.83	812	964	152	136	747	721
10D	42910D	0.143	877	0.89	10	31	538	3C-1.911	843	969	126	120	747	730
10E	41810E	0.141	873	0.89	10	31	538	3D-2.03	855	967	113	141	569	756
10F	42810F	0.139	877	0.89	10	31	543	3C-1.78	875	952	77	76	419	794
11A	43511A	0.142	873	1.3	15	32	523	3C-1.96	850	1029	179	117	476	654
11B	42711B	0.138	875	1.3	15	31	528	3C-1.88	823	995	173	141	442	658
11C	43211C	0.14	874	1.3	15	32	513	3C-1.98	864	989	124	109	417	660
11D	42711D	0.144	875	1.3	15	31	511	3C-1.911	885	1003	174	119	663	628
11E	41711E	0.142	876	1.3	15	32	518	3D-2.03	850	992	143	129	532	672
11F	42711F	0.141	876	1.3	15	31	513	3C-2.03	869	972	103	104	471	660
12A	43112A	0.139	873	2.6	27.9	32	528	3C-1.96	853	1119	267	100	530	771
12B	43412B	0.140	876	2.6	28.2	31	528	3C-1.78	876	1079	203	99	451	825
12C	42912C	0.137	878	2.6	27.9	32	546	3C-1.78	870	1084	215	109	481	886
12D	42512D	0.143	877	2.6	27.9	31	536	3C-1.911	834	1048	214	75	866	807
12E	41612E	0.140	878	2.6	27.9	32	524	2B-1.70	863	1028	170	95	423	857
12F	42612F	0.139	877	2.6	27.9	32	524	2B-1.70	871	1026	155	71	412	753

TABLE 5-3a[(a)] (cont)

SUMMARY OF RUN CONDITIONS AND RESULTS FOR REFLOOD TESTS

Test Matrix No. and Bundle	Test Run No.	As-Run Test Conditions					Results							
		Upper Plenum Pressure (MPa)	Rod Initial Temperature (°C)	Rod Peak Power (kw/m)	Flooding Rate (mm/sec)	Average Coolant Temperature (°C)	Average Housing Initial Temperature at 1.83 m (°C)	Hottest Rod and Nominal Elevation (m)	Hot Rod Initial Temperature (°C)	Hot Rod Maximum Temperature (°C)	Hot Rod Temperature Rise (°C)	Hot Rod Turnaround Time (sec)	Hot Rod Quench Time (sec)	Bundle Quench Time (sec)
SUBCOOLING EFFECT TESTS														
13A	43013A	0.273	871	2.6	27.9	107	437	3C-1.96	846	1073	227	79	443	603
13B	43513B	0.274	874	2.6	28.4	110	443	3C-1.98	861	1053	192	77	416	624
13C	42413C	0.281	880	2.6	27.9	98	402	3C-1.78	864	1049	186	69	376	599
13D	43813D	0.277	873	2.6	27.9	98	423	3C-1.98	870	1017	147	45	316	559
13E	41913E	0.280	873	2.6	27.9	100	432	3D-2.03	855	1023	170	68	455	609
13F	43813F	0.277	870	2.6	27.9	99	446	3C-1.78	871	990	118	41	342	512
VARIABLE FLOODING RATE EFFECT TESTS														
14A	42514A	0.281	873	2.6	160 5 sec 23 onward	49	486	3C-1.96	862	1048	186	103	374	559
14B	42014B	0.275	872	2.6	147 5 sec 23 onward	49	519	3C-1.98	860	1034	175	106	414	620
14C	42314C	0.274	876	2.6	153 5 sec 22 onward	49	501	3C-1.98	861	1024	164	89	419	636
14D	42014D	0.274	878	2.6	153 5 sec 22 onward	50	499	4D-1.98	871	1040	171	76	747	637
14E	42014E	0.279	872	2.6	142 5 sec 23 onward	49	491	3D-2.03	829	1040	211	102	440	600
14F	41914F	0.278	872	2.6	143 5 sec 24 onward	49	503	3C-2.03	857	973	116	91	359	535

TABLE 5-3a[a] (cont)

SUMMARY OF RUN CONDITIONS AND RESULTS FOR REFLOOD TESTS

Test Matrix No. and Bundle	Test Run No.	As-Run Test Conditions					Results							
		Upper Plenum Pressure (MPa)	Rod Initial Temperature (°C)	Rod Peak Power (kw/m)	Flooding Rate (mm/sec)	Average Coolant Temperature (°C)	Average Housing Initial Temperature at 1.83 m (°C)	Hottest Rod and Nominal Elevation (m)	Hot Rod Initial Temperature (°C)	Hot Rod Maximum Temperature (°C)	Hot Rod Temperature Rise (°C)	Hot Rod Turnaround Time (sec)	Hot Rod Quench Time (sec)	Bundle Quench Time (sec)
REPEAT TESTS														
15A	42907A[b]	0.274	871	2.6	27.9	51	490	3C-1.96	847	1096	249	80	364	517
	43715A	0.279	872	2.6	29.0	52	534	3C-1.96	859	1100	239	84	363	520
15B	42415B	0.274	875	2.6	28.2	49	531	3C-1.98	854	1075	222	91	380	547
	42915B	0.275	875	2.6	27.9	50	529	3C-1.98	804	1073	219	96	395	569
15C	42715C	0.275	874	2.6	28.2	49	503	3C-1.78	810	1070	205	79	305	550
	43315C	0.274	874	2.54	28.2	49	513	3C-1.78	867	1073	205	75	314	572
15D	42615D	0.279	872	2.5	28.2	49	500	3C-1.911	829	1052	223	71	604	520
	43115D	0.279	872	2.6	27.9	50	511	3C-1.98	864	1052	188	59	359	537
	43215D	0.277	873	2.6	27.9	51	515	2D-1.78	823	1047	224	74	655	546
15E	41515E	0.276	873	2.6	27.9	51	517	3D-2.03	830	1072	236	110	422	555
	42215E	0.279	875	2.6	28.2	51	516	3D-2.03	843	1049	206	98	409	543
	42315E	0.280	873	2.6	28.2	49	509	3D-2.03	838	1048	211	101	403	533
	42415E	0.279	872	2.6	28.2	50	503	3D-2.03	845	1049	204	105	405	542
15F	42215F	0.276	873	2.6	27.9	51	504	2B-1.70	872	1026	154	63	271	515
	42915F	0.276	878	2.55	28.2	49	523	2B-1.70	871	1013	142	59	262	485
	43915F	0.278	878	2.55	27.9	50	526	3C-1.78	878	1004	126	45	290	491
	44015F	0.278	875	2.6	27.9	48	529	3C-1.98	850	1006	156	62	295	479

h. Misnumbered test

TABLE 5-3a[(a)] (cont)

SUMMARY OF RUN CONDITIONS AND RESULTS FOR REFLOOD TESTS

Test Matrix No. and Bundle	Test Run No.	As-Run Test Conditions					Results							
		Upper Plenum Pressure (MPa)	Rod Initial Temperature (°C)	Rod Peak Power (kw/m)	Flooding Rate (mm/sec)	Average Coolant Temperature (°C)	Average Housing Initial Temperature at 1.83 m (°C)	Hottest Rod and Nominal Elevation (m)	Hot Rod Initial Temperature (°C)	Hot Rod Maximum Temperature (°C)	Hot Rod Temperature Rise (°C)	Hot Rod Turnaround Time (sec)	Hot Rod Quench Time (sec)	Bundle Quench Time (sec)
LARGE BUNDLE FORCED REFLOOD COMPARISON TESTS														
31F	43631F	0.280	872	2.29	25	49	519	3C-2.03	856	1004	148	60	301	467
32F	43432F	0.277	871	2.29	21	49	515	3C-2.03	857	1070	214	92	397	596
33F	43333F	0.276	874	1.32	15.1	48	527	3C-2.03	863	993	130	92	344	539
34F	43534F	0.142	873	2.3	25	31	510	2B-1.70	871	998	127	64	376	675
GRAVITY REFLOOD TESTS					Injection Rate (kg/sec)									
16A	43916A	0.281	872	2.3	0.789 14 sec 0.091 onward	52	543	3C-1.83	872	880	7	2	165	269
16B	43816B	0.276	876	2.3	0.839 14 sec 0.0961 onward	51	496	3C-1.78	877	888	12	3	155	255
16C	43716C	0.279	871	2.3	0.830 14 sec 0.095 onward	52	508	4C-1.70	878	884	7	2	145	244
16D	44116D	0.281	873	2.3	0.839 15 sec 0.095 onward	52	517	3C-1.78	873	880	7	2.5	151	245
16E	43616E	0.280	873	2.3	0.816 15 sec 0.095 onward	52	518	4C-1.70	873	883	10	3	129	225

TABLE 5-3a[(a)] (cont)

SUMMARY OF RUN CONDITIONS AND RESULTS FOR REFLOOD TESTS

Test Matrix No. and Bundle	Test Run No.	As-Run Test Conditions					Results							
		Upper Plenum Pressure (MPa)	Rod Initial Temperature (°C)	Rod Peak Power (kw/m)	Injection Rate (kg/sec)	Average Coolant Temperature (°C)	Average Housing Initial Temperature at 1.83 m (°C)	Hottest Rod and Nominal Elevation (m)	Hot Rod Initial Temperature (°C)	Hot Rod Maximum Temperature (°C)	Hot Rod Temperature Rise (°C)	Hot Rod Turnaround Time (sec)	Hot Rod Quench Time (sec)	Bundle Quench Time (sec)
GRAVITY REFLOOD TESTS (cont)														
17A	44117A	0.142	871	2.3	0.821 14 sec 0.095 onward	32	545	3C-1.83	866	887	22	8	251	425
17B	43717B	0.141	875	2.3	0.830 14 sec 0.10 onward	31	502	3C-1.78	875	890	14	6	210	403
17C	43817C	0.142	872	2.3	0.880 15 sec 0.095 onward	31	505	4C-1.70	875	884	9	3	209	424
17D	44317D	0.143	873	2.3	0.807 15 sec 0.095 onward	32	506	3C-1.96	873	887	13	6	69	411
17E	43817E	0.144	874	2.3	0.812 15 sec 0.095 onward	32	521	2C-1.70	870	887	16	11	247	378

TABLE 5-3b[a]

SUMMARY OF RUN CONDITIONS AND RESULTS FOR REFLOOD TESTS

Test Matrix No. and Bundle	Test Run No.	As-Run Test Conditions					Results							
		Upper Plenum Pressure (psia)	Rod Initial Temperature (°F)	Rod Peak Power (kw/ft)	Flooding Rate (in./sec)	Average Coolant Temperature (°F)	Average Housing Initial Temperature at 72 in. (°F)	Hottest Rod and Nominal Elevation (in.)	Hot Rod Initial Temperature (°F)	Hot Rod Maximum Temperature (°F)	Hot Rod Temperature Rise (°F)	Hot Rod Turnaround Time (sec)	Hot Rod Quench Time (sec)	Bundle Quench Time (sec)
CONSTANT FLOODING RATE EFFECT TESTS														
04A	42804A	39.6	1604	0.32	0.52	122	971	3C-77	1576	1801	225	95	338	536
04B	42204B	39.7	1612	0.30	0.52	125	1016	3C-74	1522	1762	240	107	327	583
04C	42804C	39.6	1609	0.30	0.52	121	984	3C-78	1569	1770	201	91	367	551
04D	42404D	40.3	1612	0.31	0.51	124	1006	3C-75.25	1541	1779	240	97	604	548
04E	42704E	40.3	1605	0.30	0.53	120	1008	3C-84	1505	1760	257	99	362	528
04F	43104F	40.1	1611	0.31	0.52	120	997	3C-80	1602	1753	153	93	340	555
05A	42705A	39.6	1603	0.45	0.72	122	928	3C-77	1579	1875	296	85	321	452
05B	42105B	39.8	1617	0.45	0.73	120	906	3C-78	1570	1818	249	86	346	474
05C	42605C	39.9	1623	0.45	0.73	122	909	3C-70	1600	1832	230	75	282	458
05D	42305D	40.5	1612	0.45	0.70	124	917	3C-75.25	1520	1858	339	110	542	481
05E	41305E	40.1	1601	0.45	0.73	120	880	3D-80	1524	1819	295	102	350	467
05F	42105F	40.4	1606	0.440	0.73	122	894	3C-70	1605	1777	172	67	260	448
06A	42606A	39.6	1601	0.78	0.91	122	935	3C-77	1581	2114	533	99	426	632
06B	42306B	39.8	1607	0.78	0.91	122	984	3C-78	1580	2062	482	117	463	677
06C	42506C	38.9	1606	0.78	0.91	122	967	3C-70	1593	2046	456	98	352	643
06D	42206D	40.3	1612	0.78	0.90	122	938	3C-78	1599	2072	472	116	433	662
06E	41206E	40.4	1600	0.78	0.92	122	949	3D-80	1465	2017	552	133	470	639
06F	42006F	40.3	1607	0.78	0.90	122	977	3C-80	1581	1965	384	93	416	603

a. Data are presented in metric units in Table 5-3a.

TABLE 5-3b[a] (cont)

SUMMARY OF RUN CONDITIONS AND RESULTS FOR REFLOOD TESTS

Test Matrix No. and Bundle	Test Run No.	As-Run Test Conditions					Results							
		Upper Plenum Pressure (psia)	Rod Initial Temperature (°F)	Rod Peak Power (kw/ft)	Flooding Rate (in./sec)	Average Coolant Temperature (°F)	Average Housing Initial Temperature at 72 in. (°F)	Hottest Rod and Nominal Elevation (in.)	Hot Rod Initial Temperature (°F)	Hot Rod Maximum Temperature (°F)	Hot Rod Temperature Rise (°F)	Hot Rod Turnaround Time (sec)	Hot Rod Quench Time (sec)	Bundle Quench Time (sec)
CONSTANT FLOODING RATE EFFECT TESTS (cont)														
07A	42207A	39.6	1600	0.70	1.11	125	431	3C-77	1600	1867	267	55	274	396
	42430A[b]	40.0	1603	0.78	1.11	122	933	3C-77	1587	2009	423	82	354	513
07B	41907B	40.1	1605	0.78	1.12	122	992	3C-78	1580	1949	370	95	387	557
07C	42107C	39.2	1623	0.78	1.09	124	928	3C-70	1600	1959	359	69	318	559
07F	41807F	40.2	1603	0.78	1.105	121	936	3C-80	1591	1884	292	85	363	518
08A	42108A	39.0	1601	0.70	1.55	125	429	3C-77	1602	1765	166	24	204	308
	43208A	40.6	1604	0.70	1.50	122	977	3C-77	1576	1816	240	54	252	367
08B	41808B	39.6	1603	0.70	1.47	121	999	3C-78	1583	1779	197	38	278	394
08C	42008C	39.9	1619	0.69	1.49	121	957	3C-70	1597	1780	181	39	224	384
08D	41808D	40.3	1623	0.70	1.49	126	936	4D-70	1597	1801	204	34	574	428
08E	41008E	40.8	1602	0.70	1.49	121	952	2B-67	1583	1737	154	39	208	355
08F	41608F	40.4	1607	0.69	1.50	122	978	2B-67	1599	1736	136	37	207	353
09A	41909A	39.2	1600	0.69	5.80	130	423	3C-77	1586	1609	23	3	72	103
09B	41709B	39.6	1609	0.69	5.79	124	631	3C-77	1610	1632	24	3.5	45	110
09C	41909C	39.9	1618	0.69	5.98	123	407	4C-67	1617	1643	26	4	59	108
09D	43009D	40.4	1602	0.69	5.78	125	560	3C-78	1602	1618	16	2.5	33	109
09E	42509E	40.4	1614	0.70	5.60	124	502	2C-67	1614	1636	22	3.5	59	108
09F	41509F	40.0	1613	0.69	5.73	125	663	3C-80	1613	1630	19	2.5	47	115

b. Misnumbered test

TABLE 5-3b[(a)] (cont)

SUMMARY OF RUN CONDITIONS AND RESULTS FOR REFLOOD TESTS

Test Matrix No. and Bundle	Test Run No.	As-Run Test Conditions					Results							
		Upper Plenum Pressure (psia)	Rod Initial Temperature (°F)	Rod Peak Power (kw/ft)	Flooding Rate (in./sec)	Average Coolant Temperature (°F)	Average Housing Initial Temperature at 72 in. (°F)	Hottest Rod and Nominal Elevation (in.)	Hot Rod Initial Temperature (°F)	Hot Rod Maximum Temperature (°F)	Hot Rod Temperature Rise (°F)	Hot Rod Turnaround Time (sec)	Hot Rod Quench Time (sec)	Bundle Quench Time (sec)
PRESSURE EFFECT AT CONSTANT FLOODING RATE TESTS														
10A	43610A	20.6	1601	0.27	0.40	88	1026	3C-77	1571	1800	229	118	494	754
10B	42810B	19.9	1612	0.27	0.40	89	1054	3C-74	1535	1774	239	147	477	775
10C	43110C	19.9	1600	0.27	0.405	84	978	3C-72	1494	1767	273	136	747	721
10D	42910D	20.7	1611	0.27	0.40	88	1000	3C-75.25	1550	1777	227	120	747	730
10E	41810E	20.4	1604	0.27	0.41	88	1001	3D-80	1571	1772	203	141	569	756
10F	42810F	20.2	1609	0.27	0.40	88	1009	3C-70	1608	1746	138	76	419	794
11A	43511A	20.6	1603	0.40	0.60	89	974	3C-77	1562	1885	323	117	476	654
11B	42711B	20.0	1607	0.40	0.60	88	982	3C-74	1514	1823	311	141	442	658
11C	43211C	20	1605	0.40	0.61	90	955	3C-70	1588	1812	224	109	417	660
11D	42711D	20.9	1607	0.40	0.61	88	951	3C-75.25	1525	1837	314	119	663	628
11E	41711E	20.6	1609	0.40	0.60	90	964	3D-80	1563	1818	258	129	532	672
11F	42711F	20.5	1609	0.40	0.60	88	956	3C-80	1597	1782	185	104	471	660
12A	43112A	20.2	1604	0.78	1.10	90	983	3C-77	1567	2047	480	100	530	771
12B	43412B	20.3	1609	0.78	1.11	88	982	3C-70	1609	1974	365	99	451	825
12C	42912C	19.9	1613	0.78	1.10	90	1015	3C-70	1599	1984	387	109	481	886
12D	42512D	20.7	1611	0.78	1.10	88	996	3C-75.25	1533	1919	386	75	866	807
12E	41612E	20.3	1612	0.78	1.10	90	976	2B-67	1586	1892	306	95	423	857
12F	42612F	20.2	1610	0.78	1.10	89	975	2B-67	1600	1879	279	71	412	753

TABLE 5-3b[(a)] (cont)

SUMMARY OF RUN CONDITIONS AND RESULTS FOR REFLOOD TESTS

Test Matrix No. and Bundle	Test Run No.	As-Run Test Conditions					Results							
		Upper Plenum Pressure (psia)	Rod Initial Temperature (°F)	Rod Peak Power (kw/ft)	Flooding Rate (in./sec)	Average Coolant Temperature (°F)	Average Housing Initial Temperature at 72 in. (°F)	Hottest Rod and Nominal Elevation (in.)	Hot Rod Initial Temperature (°F)	Hot Rod Maximum Temperature (°F)	Hot Rod Temperature Rise (°F)	Hot Rod Turnaround Time (sec)	Hot Rod Quench Time (sec)	Bundle Quench Time (sec)
SUBCOOLING EFFECT TESTS														
13A	43013A	39.6	1600	0.78	1.10	225	818	3C-77	1555	1964	409	79	443	603
13B	43513B	39.8	1605	0.78	1.12	230	830	3C-78	1582	1928	346	77	416	624
13C	42413C	40.8	1617	0.78	1.10	208	756	3C-70	1587	1920	334	69	376	599
13D	43813D	40.2	1604	0.78	1.10	208	793	3C-78	1599	1863	265	45	316	559
13E	41913E	40.6	1604	0.78	1.10	212	810	3D-80	1571	1875	306	68	455	609
13F	43813F	40.2	1616	0.78	1.10	210	835	3C-70	1600	1814	213	41	342	512
VARIABLE FLOODING RATE EFFECT TESTS														
14A	42514A	40.8	1603	0.78	6.3 5 sec 0.89 onward	120	906	3C-77	1583	1918	335	103	374	559
14B	42014B	39.9	1602	0.78	5.8 5 sec 0.91 onward	120	966	3C-78	1581	1894	315	106	414	620
14C	42314C	39.8	1609	0.78	6.01 5 sec 0.87 onward	120	933	3C-78	1582	1875	295	89	419	636
14D	42014D	39.8	1612	0.78	6.04 5 sec 0.88 onward	122	931	4D-70	1600	1904	307	76	747	637
14E	42014E	40.5	1601	0.78	5.6 5 sec 0.89 onward	121	915	3D-80	1525	1905	380	102	440	600
14F	41914F	40.3	1602	0.78	5.64 5 sec 0.95 onward	121	937	3C-80	1575	1784	209	91	359	535

TABLE 5-3b[a] (cont)

SUMMARY OF RUN CONDITIONS AND RESULTS FOR REFLOOD TESTS

Test Matrix No. and Bundle	Test Run No.	As-Run Test Conditions					Results							
		Upper Plenum Pressure (psia)	Rod Initial Temperature (°F)	Rod Peak Power (kw/ft)	Flooding Rate (in./sec)	Average Coolant Temperature (°F)	Average Housing Initial Temperature at 72 in. (°F)	Hottest Rod and Nominal Elevation (in.)	Hot Rod Initial Temperature (°F)	Hot Rod Maximum Temperature (°F)	Hot Rod Temperature Rise (°F)	Hot Rod Turnaround Time (sec)	Hot Rod Quench Time (sec)	Bundle Quench Time (sec)
REPEAT TESTS														
15A	42907A[b]	39.8	1600	0.78	1.10	124	914	3C-77	1557	2005	448	80	364	517
	43715A	40.5	1601	0.78	1.14	125	994	3C-77	1578	2011	431	84	363	520
15B	42415B	39.7	1608	0.78	1.11	120	988	3C-78	1569	1967	399	91	380	547
	42915B	39.9	1607	0.78	1.10	122	985	3C-78	1580	1965	394	96	395	569
15C	42715C	39.9	1606	0.78	1.11	121	937	3C-70	1590	1959	369	79	305	550
	43315C	39.8	1606	0.775	1.11	121	956	3C-70	1592	1963	369	75	314	572
15D	42615D	40.5	1602	0.77	1.11	121	932	3C-75.25	1524	1926	402	71	604	520
	43115D	40.4	1602	0.78	1.10	122	951	3C-78	1588	1925	338	59	359	537
	43215D	40.2	1604	0.78	1.10	123	959	2D-70	1513	1916	403	74	655	546
15E	41515E	40.1	1604	0.78	1.10	123	962	3D-80	1526	1951	425	110	422	555
	42215E	40.4	1608	0.78	1.11	124	960	3D-80	1550	1920	371	98	409	543
	42315E	40.6	1604	0.78	1.11	120	948	3D-80	1540	1919	379	101	403	533
	42415E	40.4	1601	0.78	1.11	122	937	3D-80	1554	1921	367	105	405	542
15F	42215F	40.0	1603	0.78	1.10	124	939	2D-67	1601	1879	278	63	271	515
	42915F	40.1	1613	0.777	1.11	120	973	2D-67	1600	1855	255	59	262	485
	43915F	40.3	1613	0.778	1.10	122	978	3C-70	1613	1840	226	45	290	491
	44015F	40.3	1608	0.78	1.10	119	984	3C-78	1562	1843	281	62	295	479

b. Misnumbered test

TABLE 5-3b[(a)] (cont)

SUMMARY OF RUN CONDITIONS AND RESULTS FOR REFLOOD TESTS

Test Matrix No. and Bundle	Test Run No.	As-Run Test Conditions					Results							
		Upper Plenum Pressure (psia)	Rod Initial Temperature (°F)	Rod Peak Power (kw/ft)	Flooding Rate (in./sec)	Average Coolant Temperature (°F)	Average Housing Initial Temperature at 72 in. (°F)	Hottest Rod and Nominal Elevation (in.)	Hot Rod Initial Temperature (°F)	Hot Rod Maximum Temperature (°F)	Hot Rod Temperature Rise (°F)	Hot Rod Turnaround Time (sec)	Hot Rod Quench Time (sec)	Bundle Quench Time (sec)
LARGE BUNDLE FORCED REFLOOD COMPARISON TESTS														
31F	43631F	40.6	1602	0.697	1.0	120	966	3C-80	1573	1840	267	60	301	467
32F	43432F	40.2	1600	0.699	0.81	121	959	3C-80	1575	1959	386	92	397	596
33F	43333F	40.1	1606	0.402	0.595	119	981	3C-80	1585	1819	234	92	344	539
34F	43534F	20.6	1604	0.70	1.0	88	950	2B-67	1600	1829	229	64	376	675
GRAVITY REFLOOD TESTS					Injection Rate (lb/sec)									
16A	43915A	40.8	1602	0.70	1.74 14 sec 0.20 onward	126	1010	3C-72	1602	1616	13	2	165	269
16B	43816B	40.1	1609	0.70	1.85 14 sec 0.212 onward	123	923	3C-70	1611	1630	21	3	155	255
16C	43716C	40.4	1600	0.70	1.83 14 sec 0.21 onward	125	947	4C-67	1612	1623	12	2	145	244
16D	44116D	40.7	1604	0.69	1.85 15 sec 0.21 onward	123	963	3C-70	1604	1617	13	2.5	151	245

TABLE 5-3b[a] (cont)

SUMMARY OF RUN CONDITIONS AND RESULTS FOR REFLOOD TESTS

Test Matrix No. and Bundle	Test Run No.	As-Run Test Conditions					Results							
		Upper Plenum Pressure (psia)	Rod Initial Temperature (°F)	Rod Peak Power (kw/ft)	Injection Rate (lb/sec)	Average Coolant Temperature (°F)	Average Housing Initial Temperature at 72 in. (°F)	Hottest Rod and Nominal Elevation (in.)	Hot Rod Initial Temperature (°F)	Hot Rod Maximum Temperature (°F)	Hot Rod Temperature Rise (°F)	Hot Rod Turnaround Time (sec)	Hot Rod Quench Time (sec)	Bundle Quench Time (sec)
GRAVITY REFLOOD TESTS (cont)														
16E	43616E	40.6	1603	0.70	1.80 15 sec 0.21 onward	125	964	4C-67	1603	1621	18	3	129	225
17A	44117A	20.6	1600	0.70	1.81 14 sec 0.21 onward	89	1013	3C-72	1591	1629	40	8	251	425
17B	43717B	20.4	1608	0.70	1.83 14 sec 0.22 onward	88	936	3C-70	1608	1634	26	6	210	403
17C	43817C	20.6	1601	0.70	1.94 15 sec 0.21 onward	88	941	4C-67	1607	1624	17	3	209	424
17D	44317D	20.8	1604	0.70	1.78 15 sec 0.21 onward	90	943	3C-77	1604	1628	24	6	69	411
17E	43817E	20.9	1605	0.70	1.79 15 sec 0.21 onward	89	969	2C-67	1599	1628	29	11	247	378

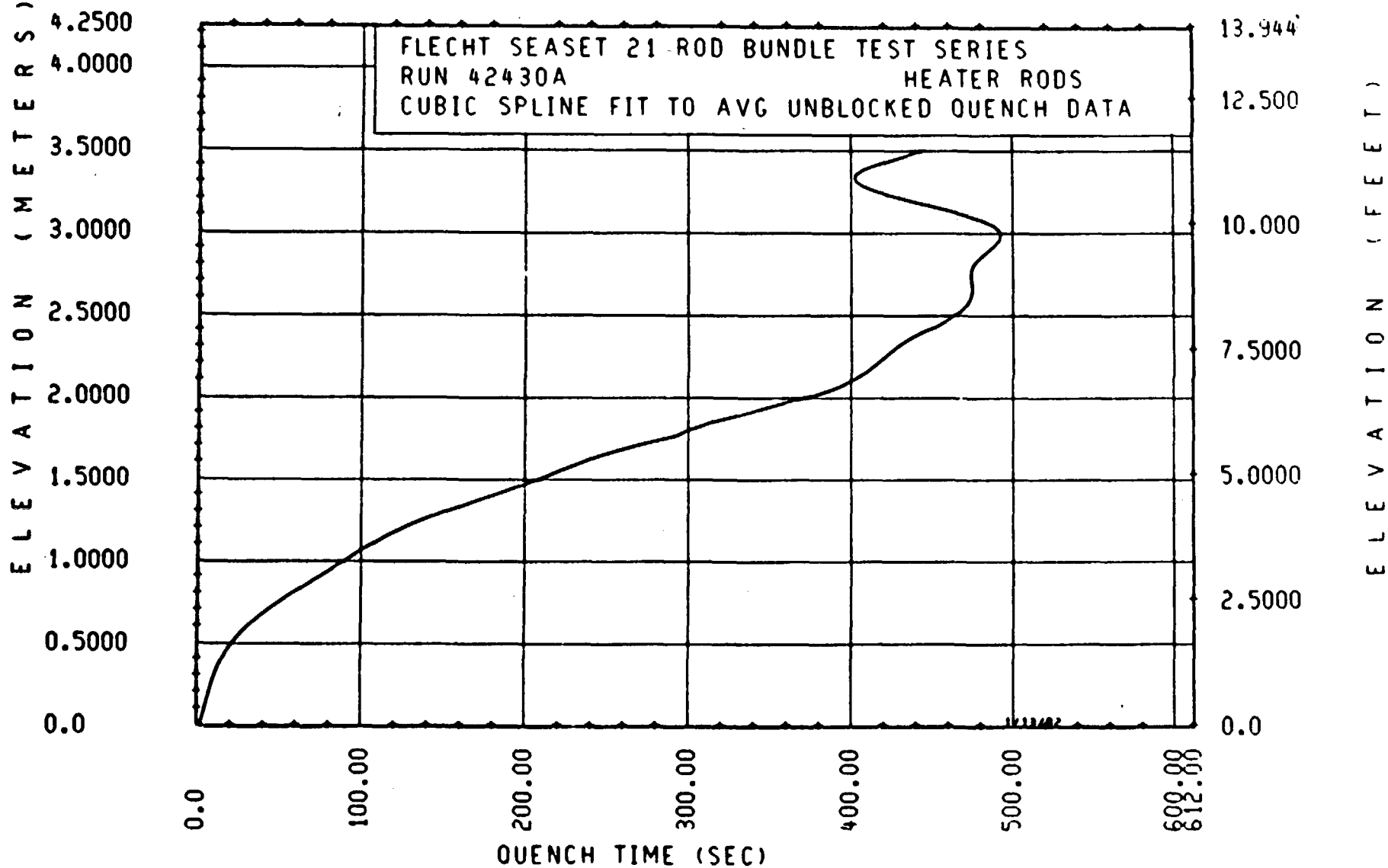

Figure 5-4. Quench Front Curve, Run 42430A

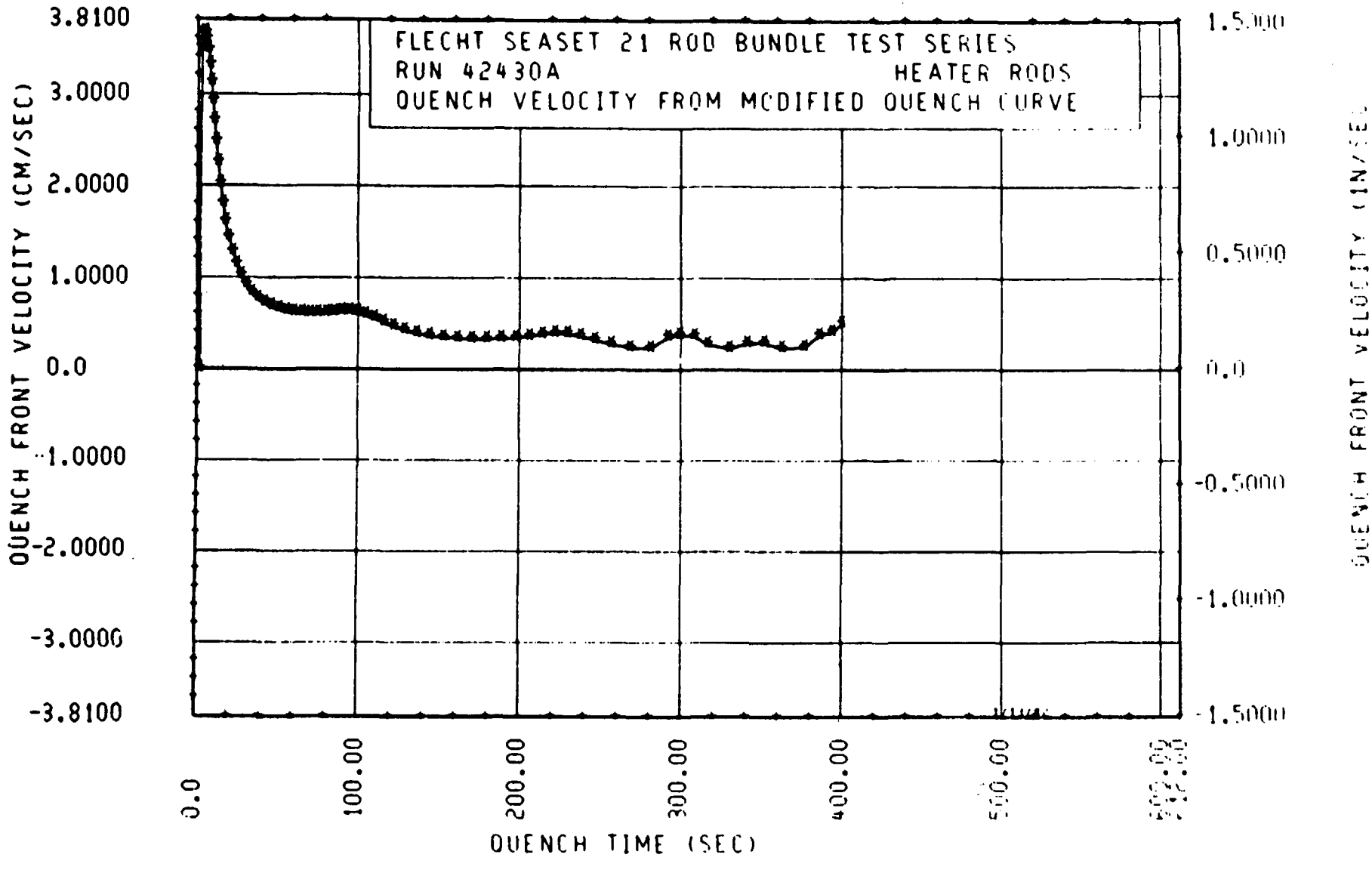

Figure 5-5. Quench Front Velocity, Run 42430A

5-5. DATAR Program and Results

The DATAR program was used to calculate the heat transfer coefficients for the reflood tests. The program employs a finite difference method to solve the inverse conduction problem utilizing the measured rod power, temperature, and physical dimensions to calculate the rod heat flux. The change in the thermocouple diameter after the first four configurations was accommodated in the DATAR code rod model by incorporating the thermocouple diameter, coil diameter, wire diameter, and Kanthal fraction. The calculated heat transfer coefficient is referenced to the measured saturation temperature. The heat transfer coefficient for the hottest rod thermocouple from run 42430A is shown in figure 5-6. The sharp decrease in the heat transfer coefficient immediately after flood is attributed to the step increase in the power. The power was lower than specified prior to flood in order to dry out the steam probes during a slow heatup rate. The effect of this power step is believed to negligible, as discussed in appendix M.

To provide heat transfer coefficient data more suitable for analysis and evaluation, the data were smoothed (or averaged) over a total time of 10 seconds. This smoothing technique consisted of replacing each data point with an average value of the original data point and a specified number of points before and after the time of interest. An example of the original data and smoothed data is shown in figure 5-7 for the hottest rod thermocouple from run 42430A.

The details of the DATAR program calculations, as well as the details on the data smoothing technique, are given in appendix M.

The heat transfer coefficient error analysis as previously performed for the 161-rod unblocked bundle (figure 5-8) is applicable to the 21-rod bundle, since the heater rod dimensions and materials are exactly the same for the first four test configurations. In configurations E and F, the thermocouple diameter was increased to 1.0 mm (0.040 in.) from 0.69 mm (0.025 in.) and the heating coil diameter was subsequently reduced, but it is believed that the errors associated with these changes are negligible.

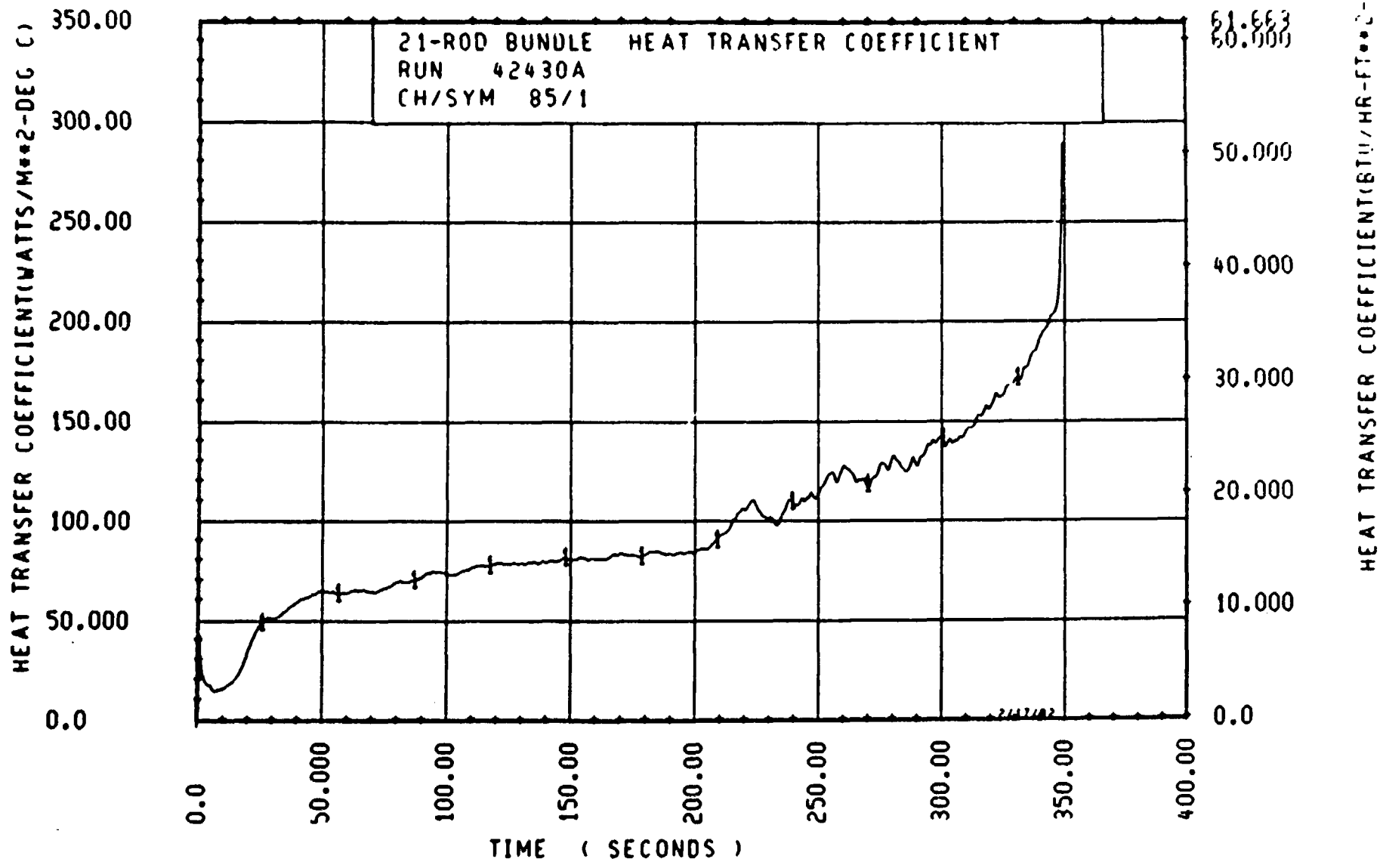

Figure 5-6. Hot Rod Thermocouple Heat Transfer Coefficient, Run 42430A

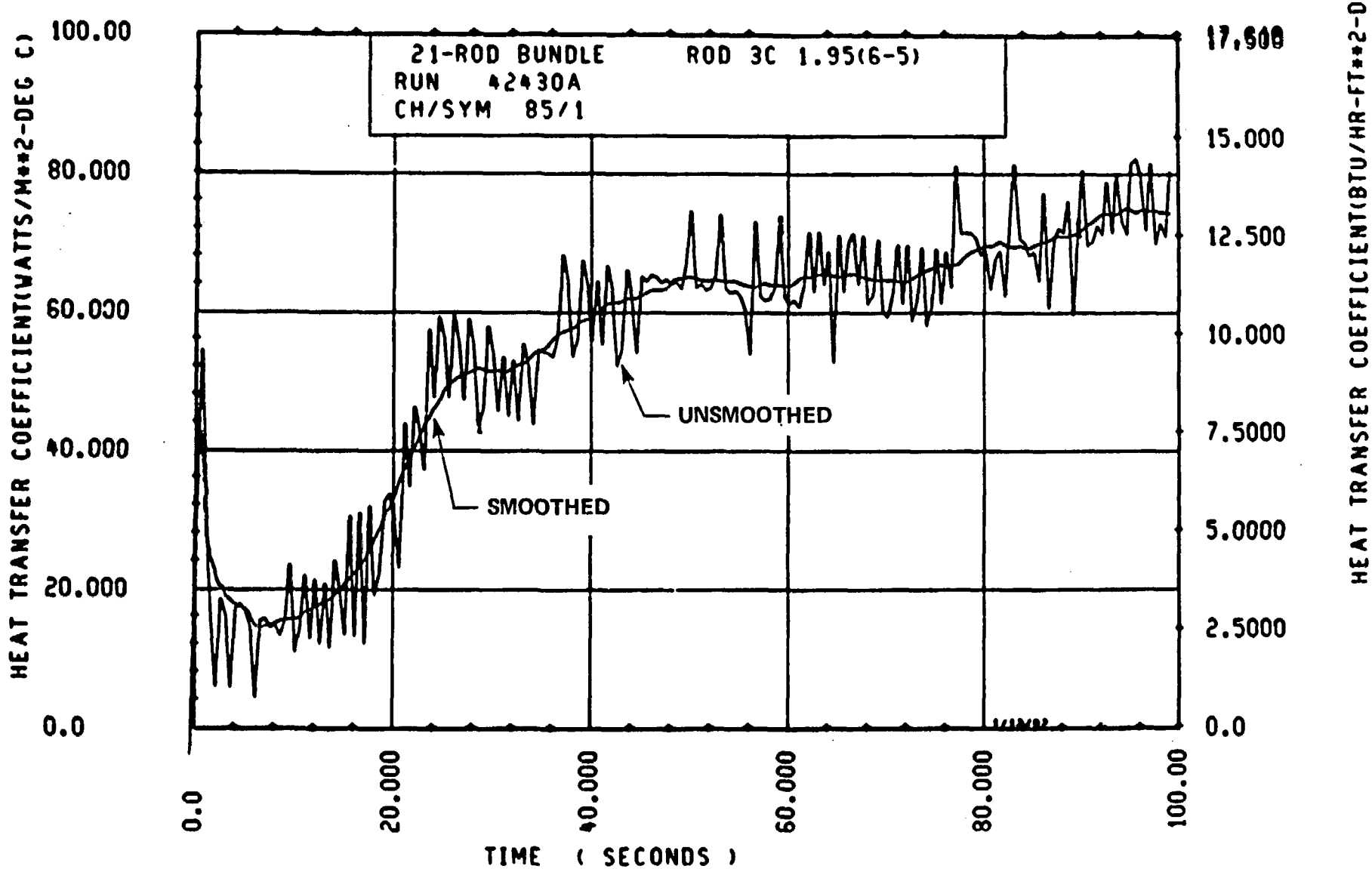

Figure 5-7. Smoothed and Unsmoothed Heat Transfer Coefficient, Run 42430A

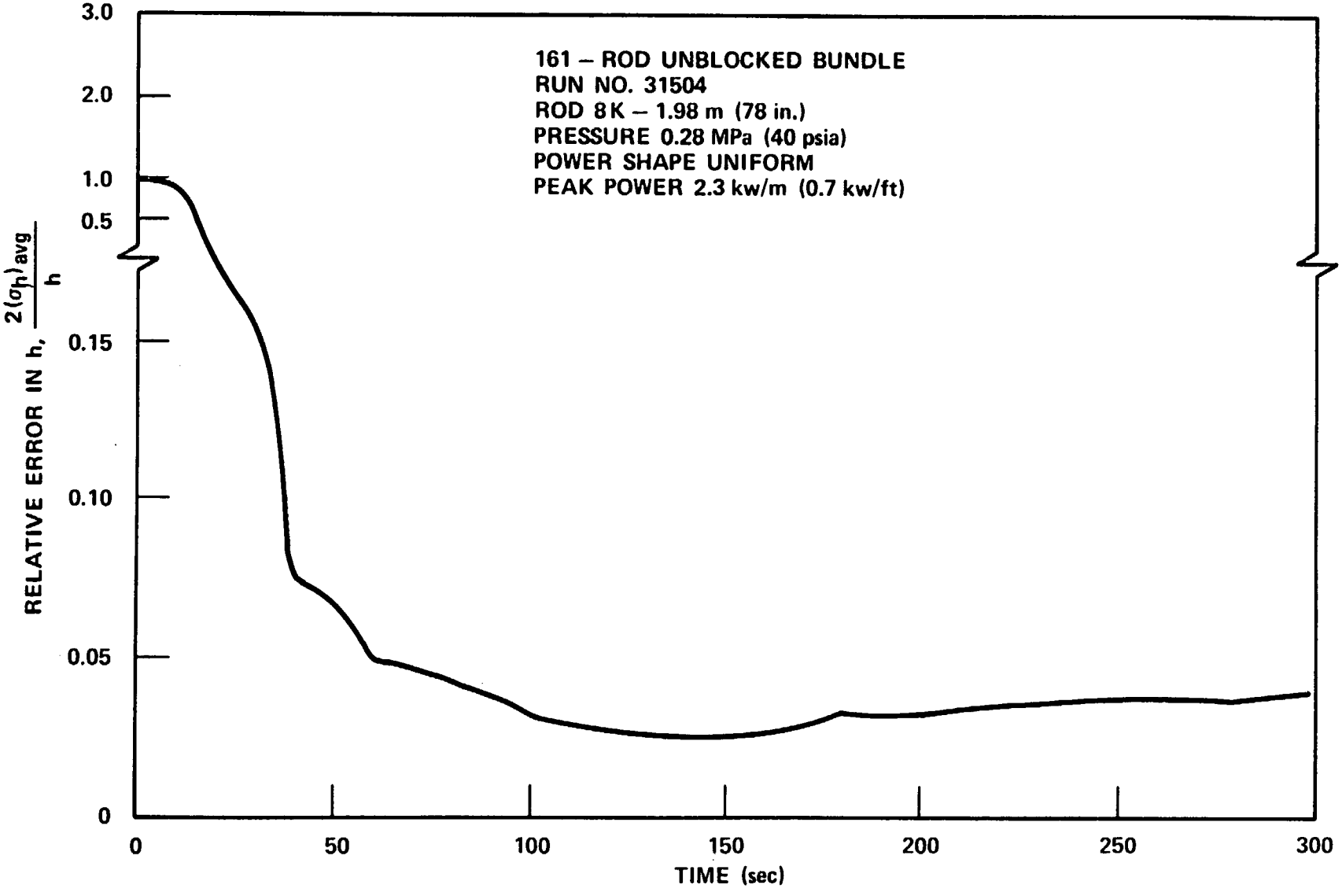

Figure 5-8. Relative Error in Heat Transfer Coefficient as a Function of Time

5-6. COMPARE Program

The COMPARE program was utilized to compare data within a test run, between test runs, and/or between test series by plotting the respective data as a function of time. The automated comparison of data provided for not only quick and efficient validation of tests, but also thorough analysis of large quantities of data. In the 21-rod bundle tests, data from approximately 125 tests were validated for the six configurations during the testing and rebuilding period of approximately 10 months.

The COMPARE program was utilized to calculate the heat transfer coefficient ratio between blocked bundles and the unblocked bundle in the analysis of the flow blockage effects, and in the calculation of the enhancement factor, as described in section 3.

5-7. SUMMARY OF RUN CONDITIONS AND TEST RESULTS FOR REFLOOD TESTS

The as-run conditions and the summary results for the reflood tests are listed in table 5-3.

The summary results for the forced and gravity reflood tests include the following information:

- Location of the hottest temperature recorded during the test, which is characterized by the radial location of the rod in the bundle and the thermocouple nominal elevation with respect to the bottom of the heated length

- Initial and maximum temperatures of the hot rod

- Turnaround time, which is the time after the start of flooding at which the hot rod maximum temperature was recorded

- Hottest rod quench time, which is the time after the start of flooding at which the temperature of the hottest rod started to decrease very rapidly

-- Bundle quench time, which is the time after the start of flooding at which all thermocouples in the bundle had quenched. On the average, the thermocouples located at the 3.05 m (120 in.) elevation quenched last.

A sample of gravity reflood test results is provided in paragraph 5-10.

5-8. HYDRAULIC CHARACTERISTICS TEST RESULTS

The data from the hydraulic characteristics tests were reduced using the HYCHAR program. The HYCHAR program calculated the friction factor, grid pressure loss coefficient, and blockage loss coefficient, utilizing the measured steady-state differential pressures and velocity. The details of the HYCHAR program are provided in appendix M.

The results of the hydraulic characteristics tests for all six bundles are shown in figures 5-9 through 5-15. Figure 5-9 shows the measured friction factor as a function of Reynolds number. Figure 5-10 shows the 0.53 m (21 in.) grid as a function of Reynolds number and figure 5-11 shows the 1.07 m (42 in.) grid as a function of Reynolds number. Figure 5-11 shows that data from test series A and B were generally above the data for the other four bundles.

This difference is attributed to the grid design, which was modified after the second test series to allow the heater rods to grow axially through the grids more easily. The dimples on the grid for the outside 12 rods were removed and the dimples for the inside 9 rods were reduced. The 0, 1.07, and 1.57 m (0, 42, and 62 in.), elevation grids were modified in this fashion. On the 0.53 m (21 in.) elevation grid, only the dimples for the outside 12 rods were reduced, in order to provide rod-to-rod spacing in the lower half of the heater rod bundle. The grids in the upper half of the bundle were not modified. Figure 5-12 shows the measured grid loss coefficient for the 1.57 m (62 in.) and 2.11 m (83 in.) grids for configuration A. The 1.57 m (62 in.) and 2.11 m (83 in.) grid loss coefficients could be measured only in configuration A because of the relative location of the respective pressure tap at 1.83 m (72 in.) and the blockage zone centerline at

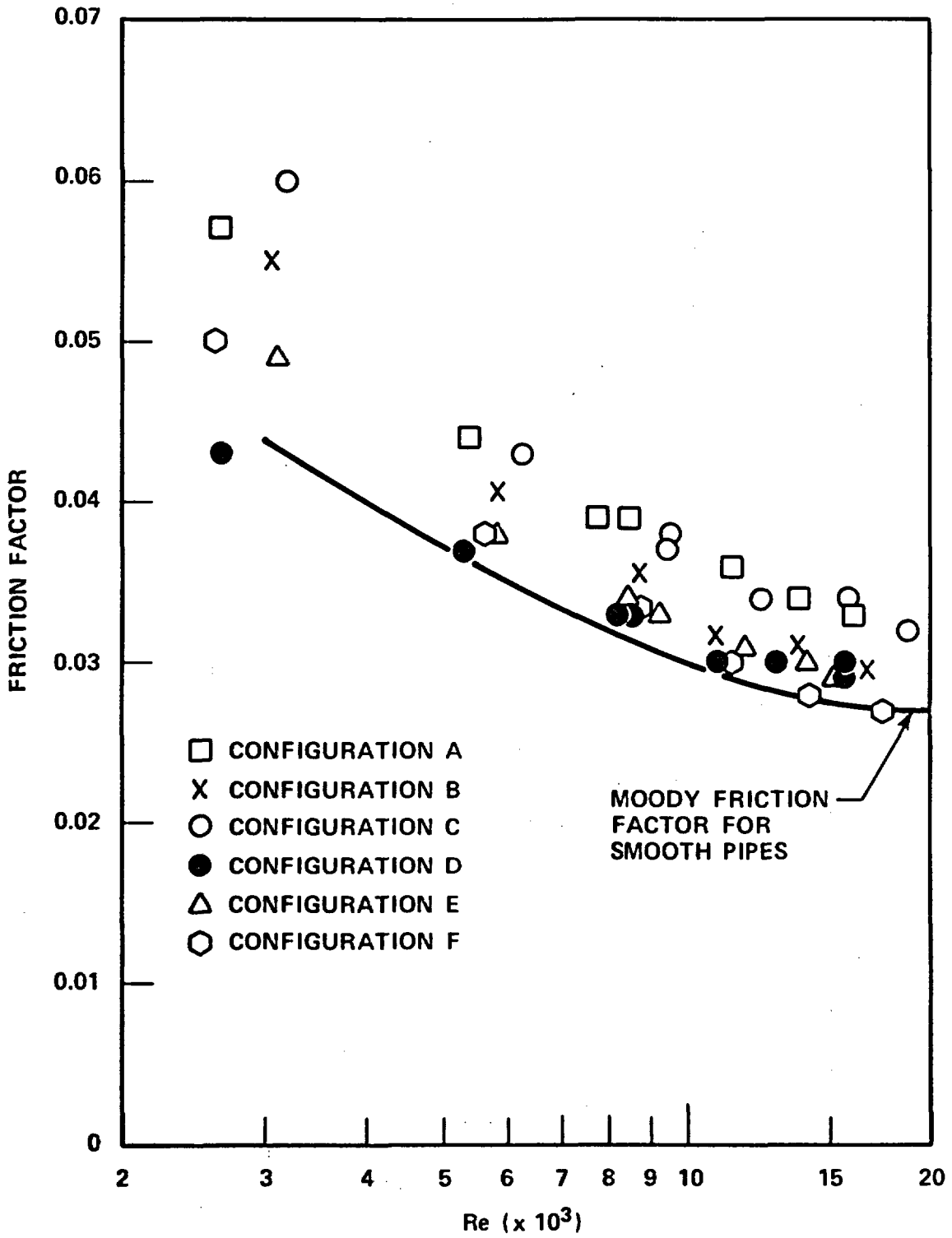

Figure 5-9. Average Bundle Friction Factor Versus Reynolds Number

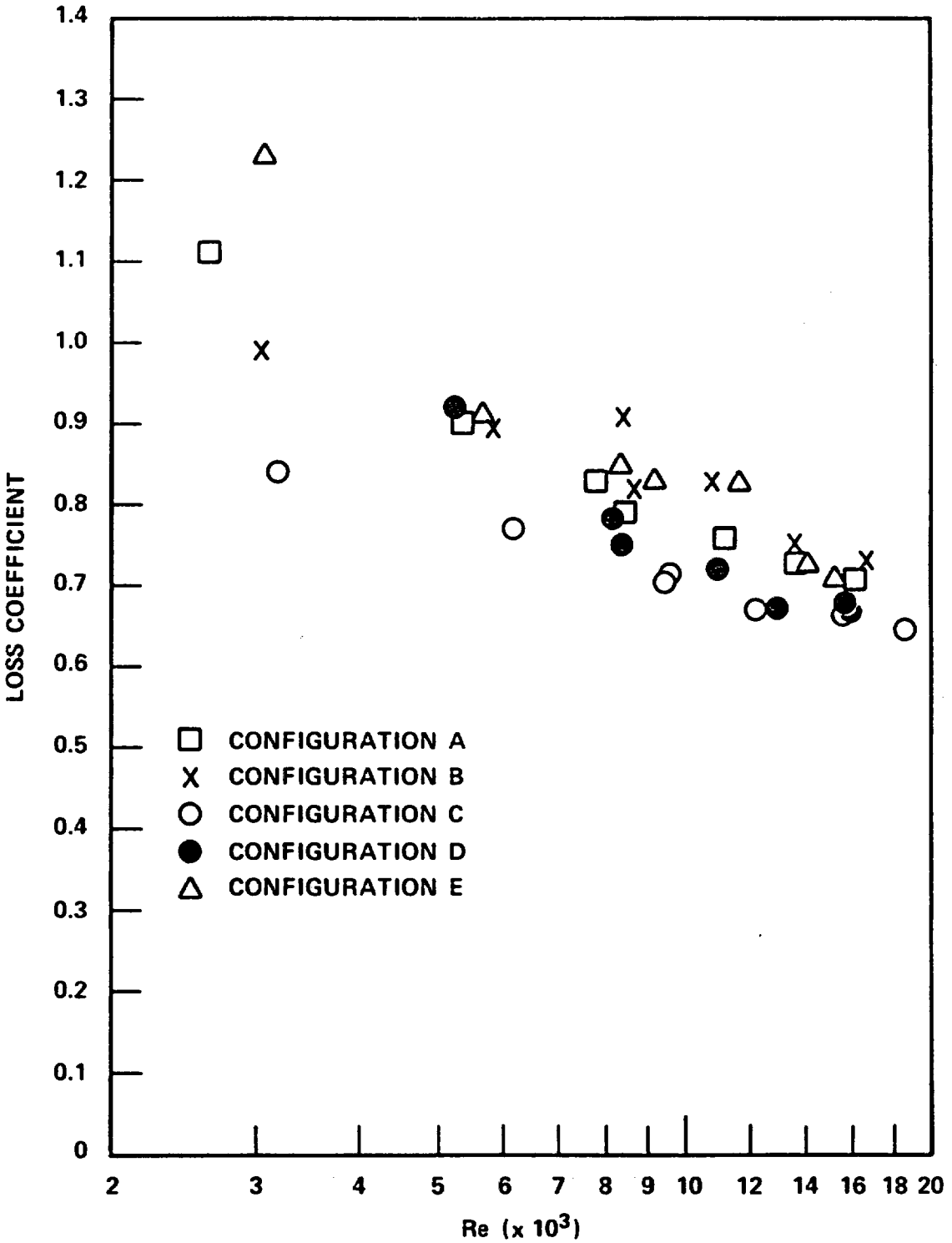

Figure 5-10. 0.53 m (21 in.) Grid Loss Coefficient Versus Reynolds Number

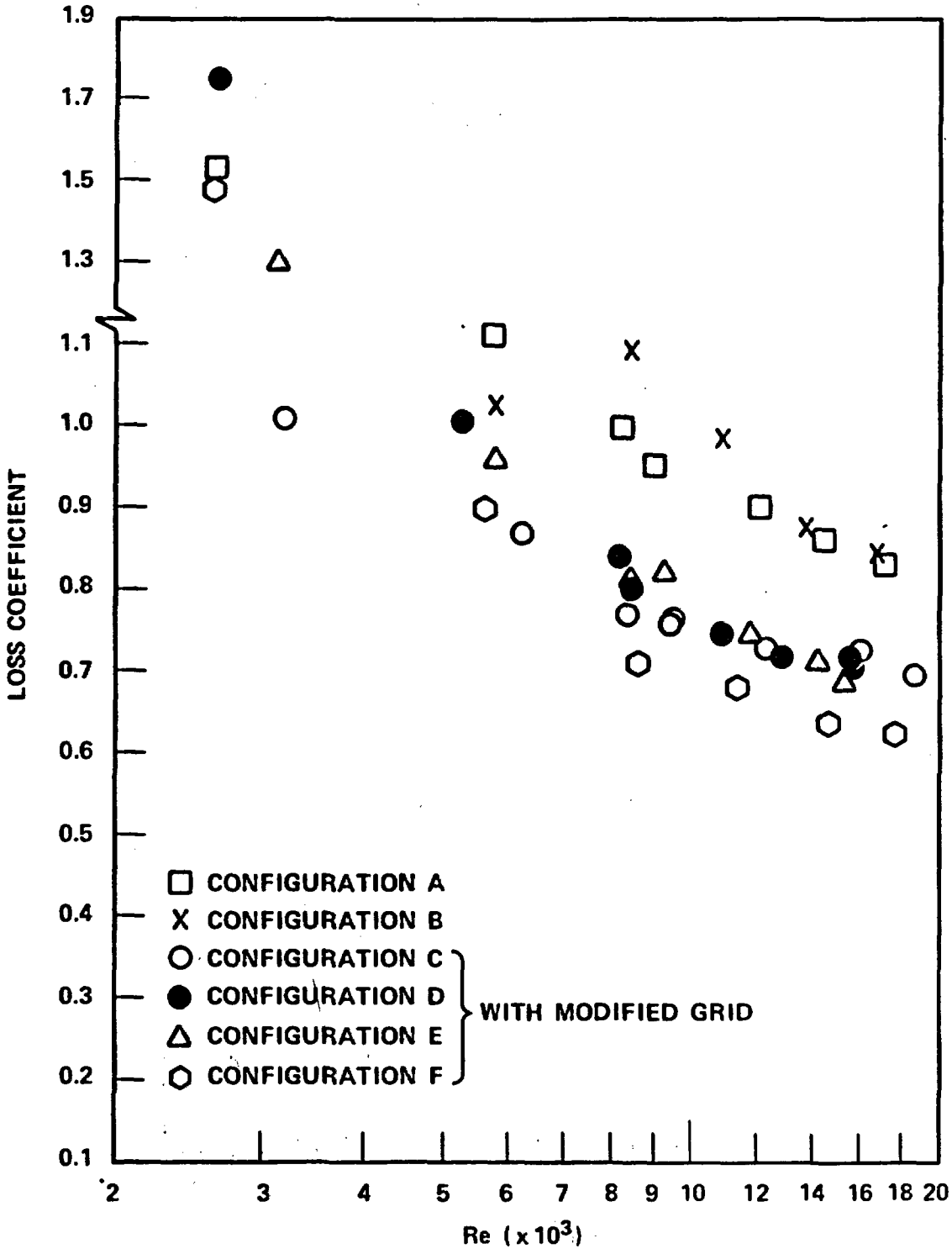

Figure 5-11. 1.07 m (42 in.) Grid Loss Coefficient Versus Reynolds Number

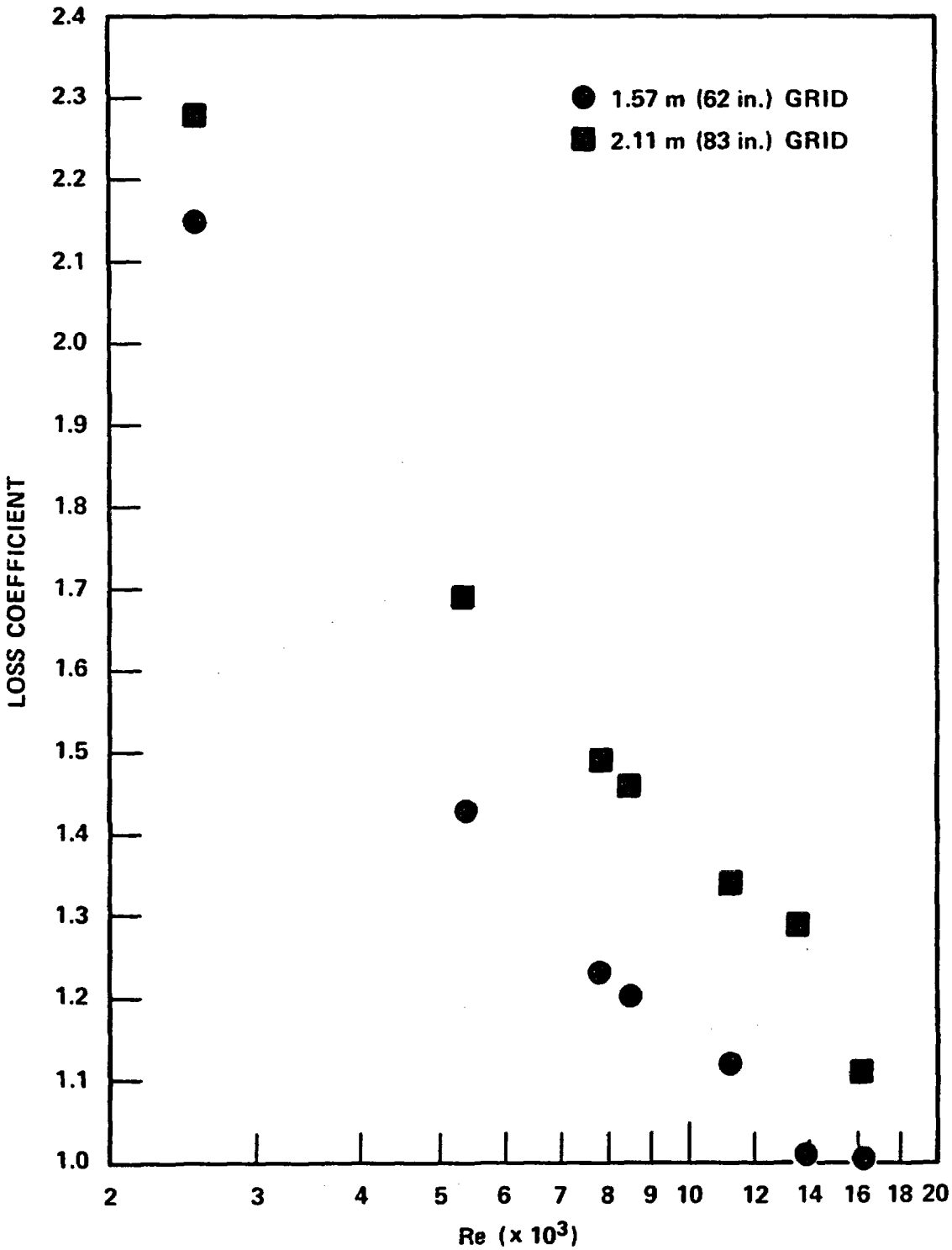

Figure 5-12. 1.57 and 2.11 m (62 and 83 in.) Grid Loss Coefficients Versus Reynolds Number, Configuration A

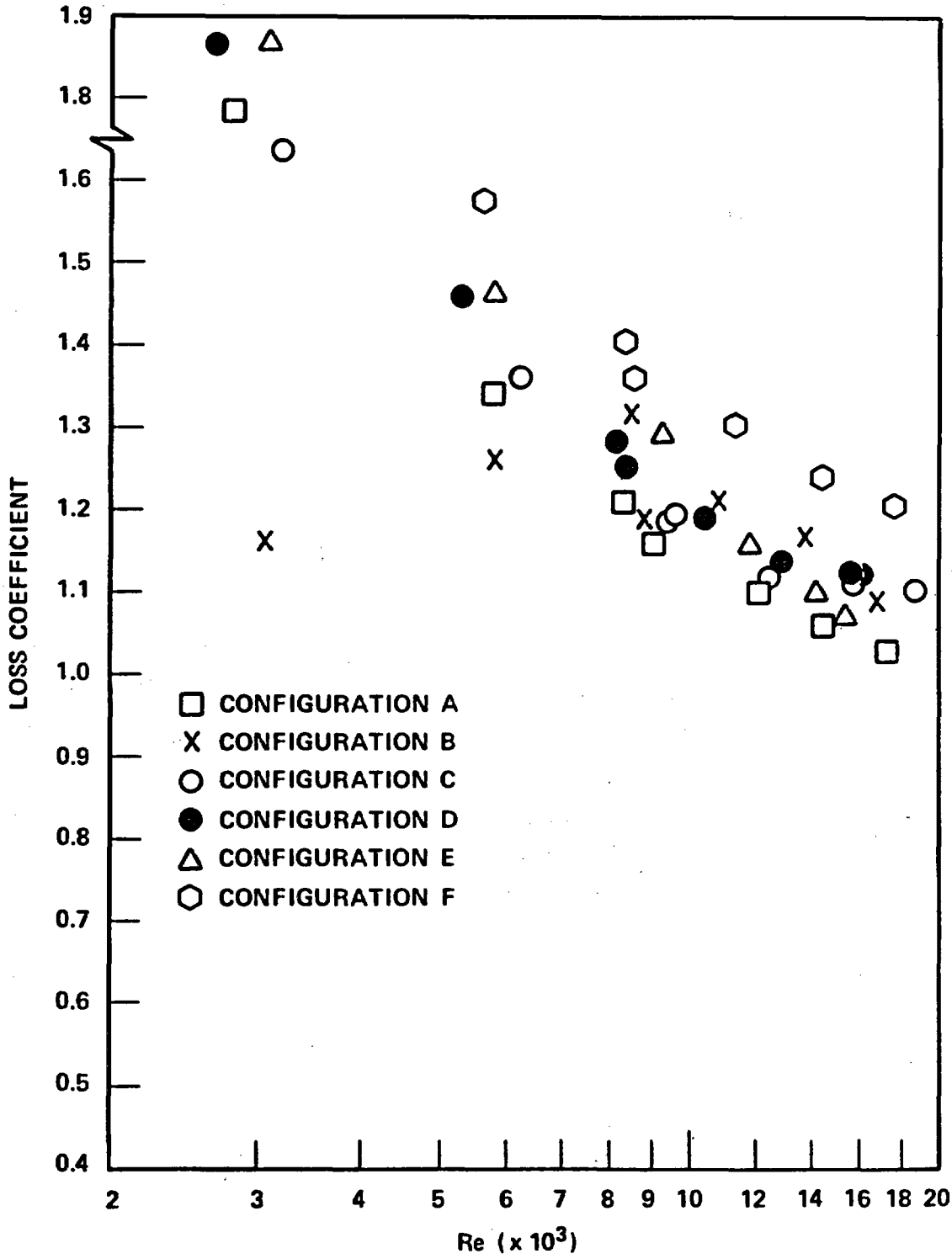

Figure 5-13. 2.59 m (102 in.) Grid Loss Coefficient Versus Reynolds Number

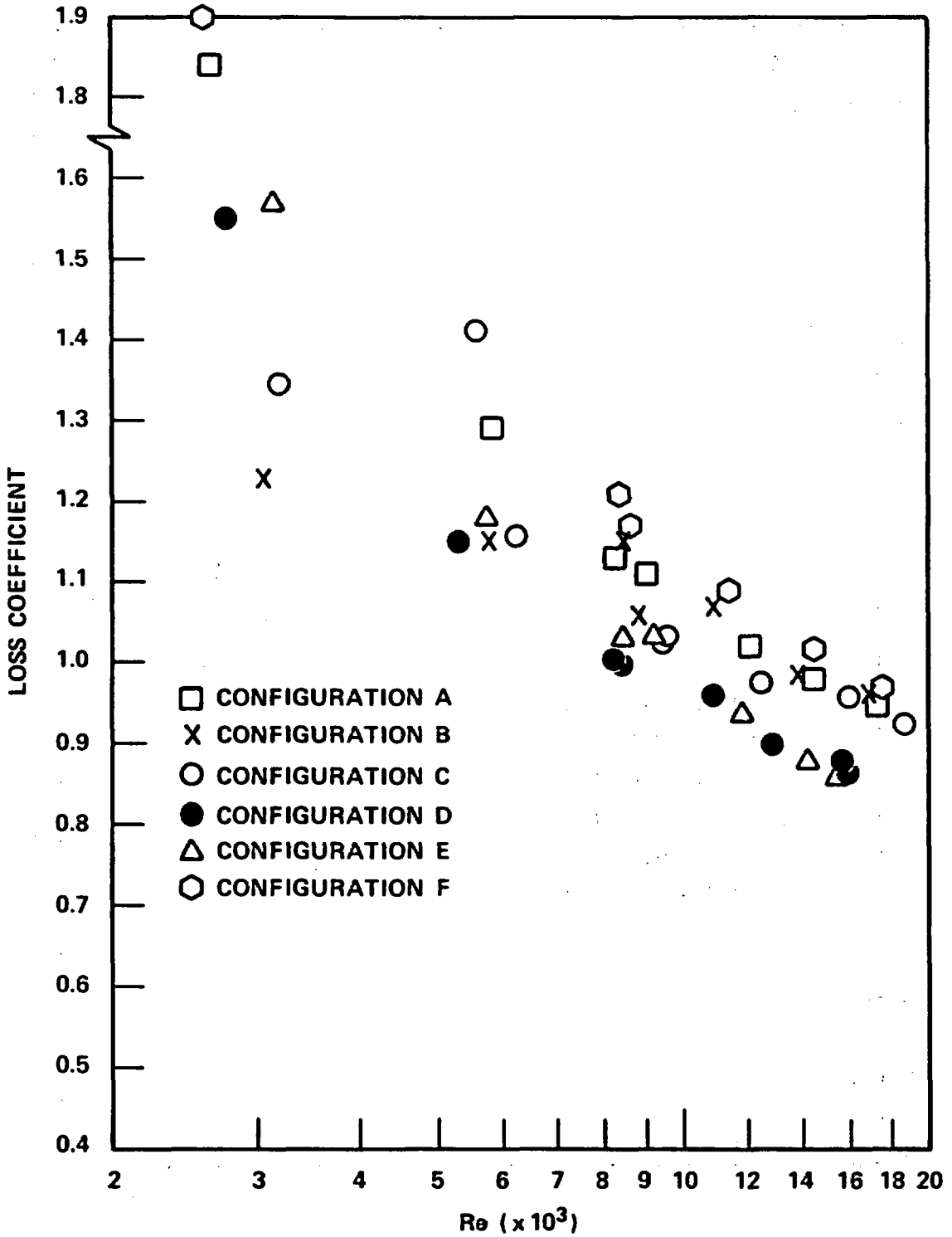

Figure 5-14. 3.15 m (124 in.) Grid Loss Coefficient Versus Reynolds Number

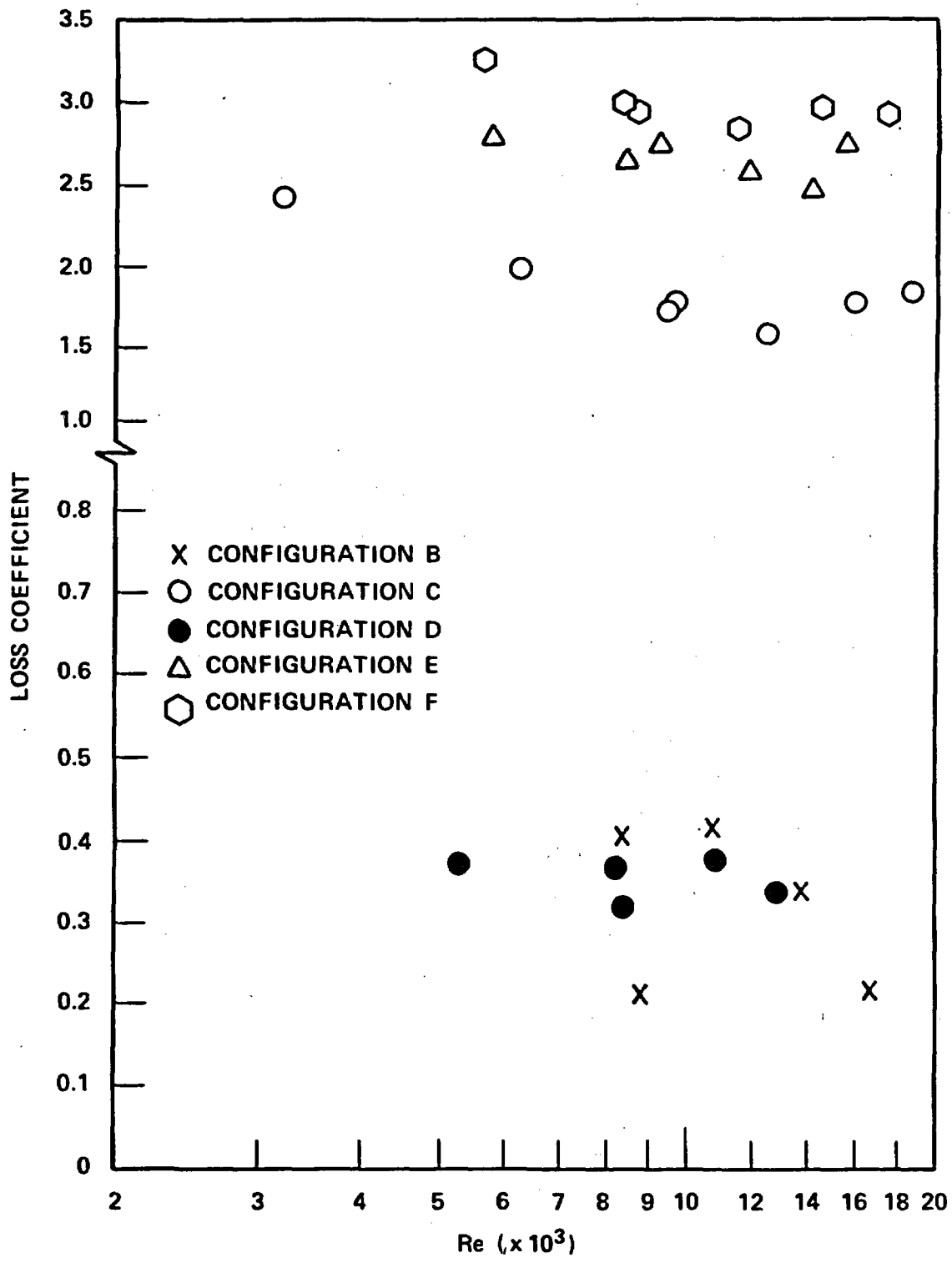

Figure 5-15. Blockage Loss Coefficient Versus Reynolds Number

1.85 m (73 in.). The 2.59 m (102 in.) and the 3.15 m (124 in.) grid loss coefficients for all six test series are shown in figures 5-13 and 5-14, respectively. The blockage loss coefficients for the five blocked bundles are shown in figure 5-15.

The difference in loss coefficients between grids was attributed to the number of steam temperature instruments which were attached to each grid. A complete analysis of these hydraulic characteristics test results is provided in section 6.

5-9. STEAM COOLING TEST RESULTS

The data from the steam cooling tests were reduced using the STMCOOL program. The STMCOOL program calculated the heat transfer coefficient based upon the vapor temperature and subchannel flow as calculated from the COBRA-IV-I code (appendix A), and the measured heater rod temperatures and power. The details of the STMCOOL program and results are presented in section 6.

5-10. GRAVITY REFLOOD TEST RESULTS

Sample gravity reflood test results are shown in figures 5-16 and 5-17. Figure 5-16 shows the bundle flooding rate as calculated from a mass balance on the downcomer for configuration A (unblocked) and configuration E, with the long nonconcentric 36-percent peak strain sleeves. This figure shows that the bundle flooding rates are approximately the same for the unblocked and blocked configurations. Figure 5-17, which shows the clad temperature immediately downstream of the blockage for configurations A and E, indicates a lower clad temperature for the blocked configuration. These results are consistent for all the blocked configurations.

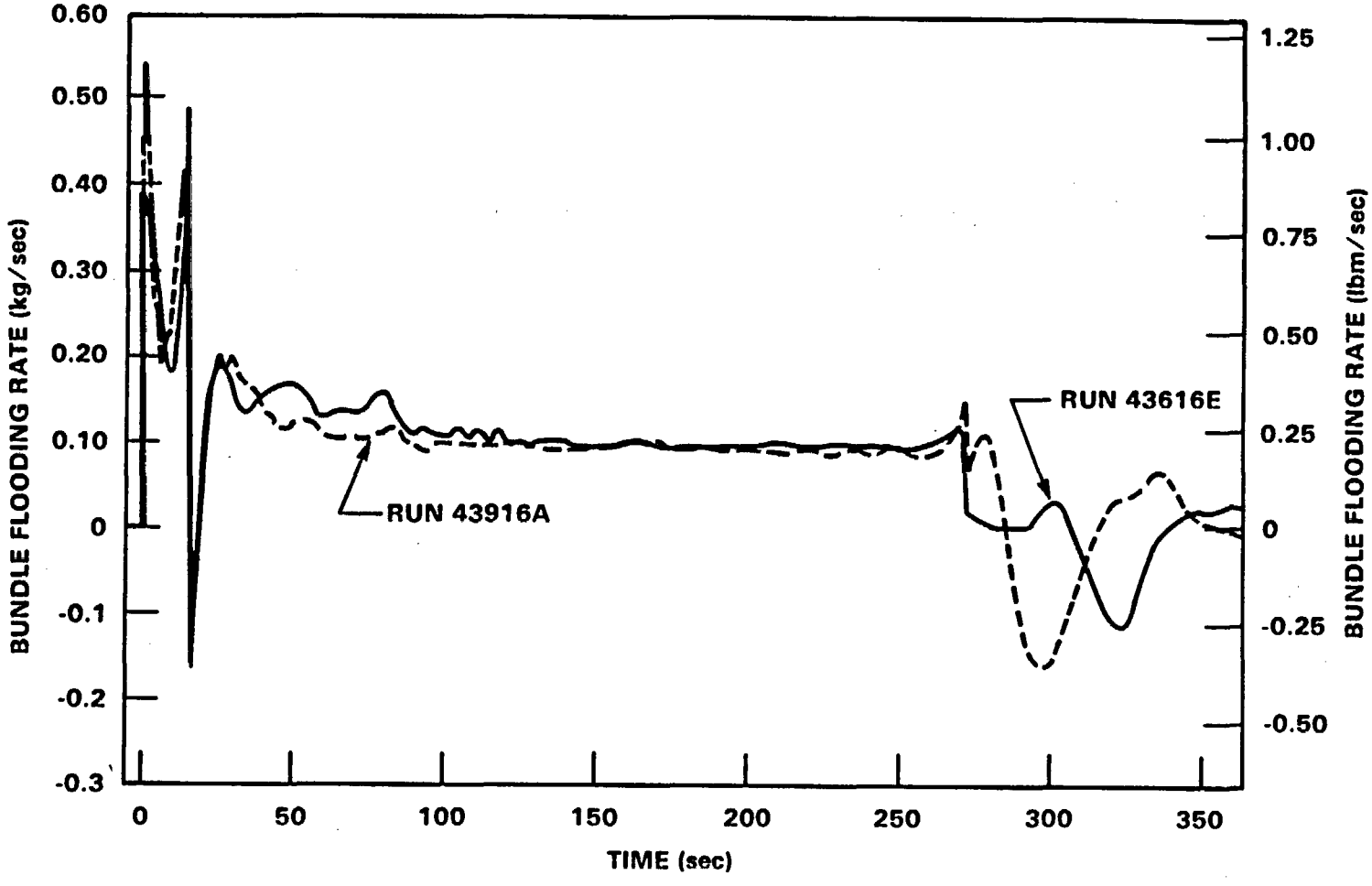

Figure 5-16. Bundle Flooding Rate in Gravity Reflood Tests

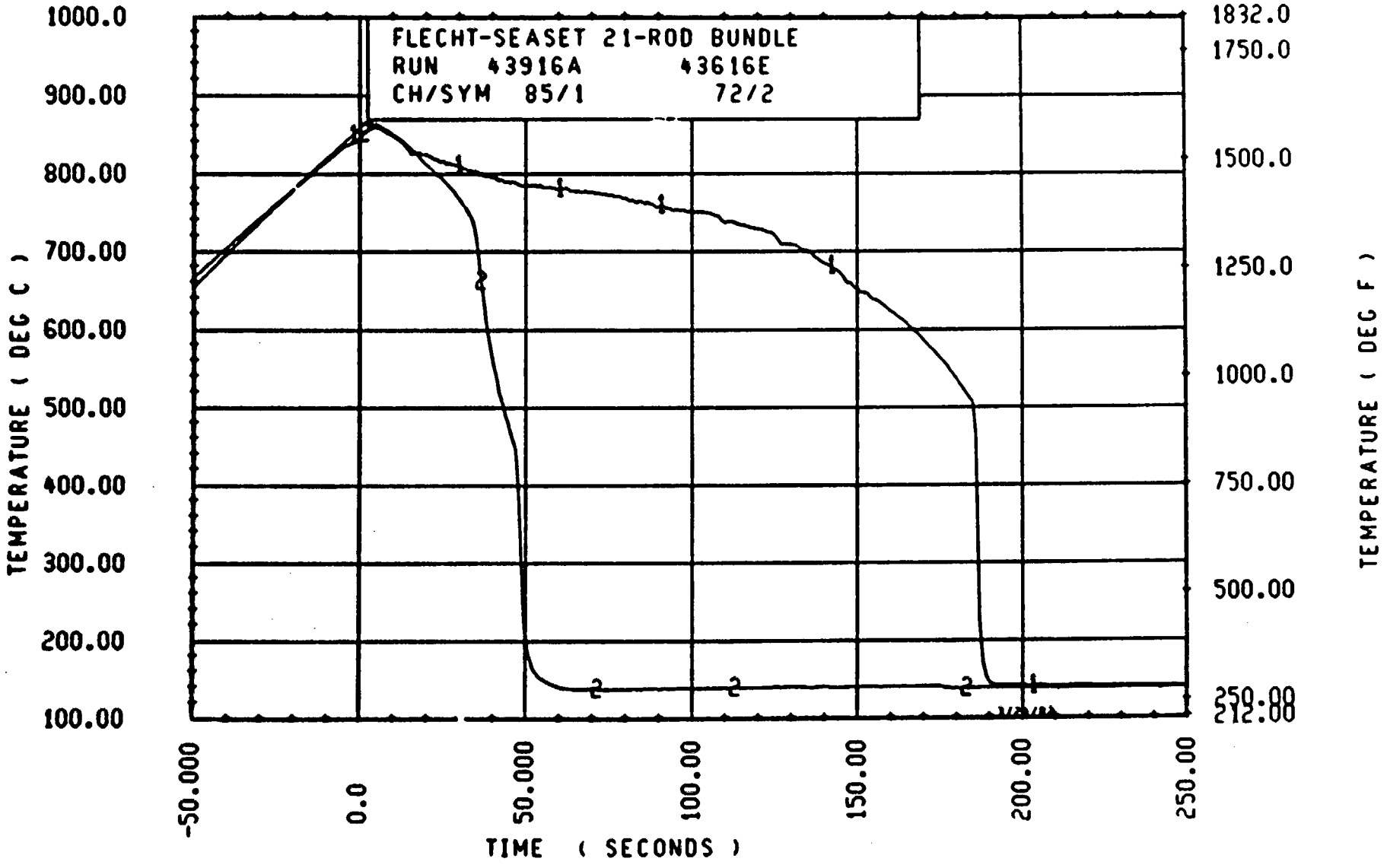

Figure 5-17. Clad Temperature at 2.01 m (79 in.) Elevation in Gravity Reflood Tests

SECTION 6
DATA ANALYSIS

6-1. INTRODUCTION

The data from the hydraulic characteristics tests, the steam cooling tests, and the forced reflood tests were analyzed to the extent necessary to calculate the single-phase and two-phase flow enhancement factors.

The analysis of the hydraulic characteristics test data includes a comparison to available friction factor and grid loss coefficient correlations, and explanations of the differences. The measured blockage pressure loss coefficient was compared to the calculated pressure loss coefficient of the COBRA-IV-I code simulation of the blockage.

The analysis of the steam cooling test data encompassed the analysis of the unblocked data below the 1.52 m (60 in.) elevation for all six test configurations, and the analysis of the data above the 1.52 m (60 in.) elevation for each configuration individually. The steam cooling unblocked test data below 1.52 m (60 in.) were correlated as a function of Reynolds number as previously done for the 161-rod unblocked bundle. The steam cooling test data above 1.52 m (60 in.) were combined with the calculated flow redistribution from the COBRA-IV-I code to calculate the enhancement factor, Ne, as described in section 3.

Similarly, the enhancement factors for the forced reflood tests were calculated for thermocouples in and downstream of the blockage zone as a function of time. The basis for selecting the blockage sleeve shape projected to provide the least favorable heat transfer characteristics in the large 163-rod blocked bundle is also presented.

6-2. HYDRAULIC CHARACTERISTICS TEST DATA ANALYSIS

The data from the hydraulic characteristics tests were analyzed using a simple hydraulics model and the COBRA code. The calculation of the friction factor and grid loss coefficients utilized superheated steam in the COBRA code, and calculations using water properties were also performed. In some cases, data correlations are proposed.

6-3. Bundle Friction Factor

The friction factor data for the 21-rod bundle and housing have been correlated as follows:

-- $f = 1.691\ Re^{-0.43}$ for $3 \times 10^3 < Re < 10^4$

-- $f = 0.117\ Re^{-0.14}$ for $10^4 < Re < 2 \times 10^4$

The correlation is plotted with the data in figure 6-1. The data are always higher than the Moody friction factor for smooth pipes. The COBRA calculation with steam flow for the 21-rod bundle using the Moody friction factor in flow subchannels provides a prediction of bundle friction factor, which is also shown in figure 6-1. The predicted friction factor is 5 to 30 percent higher than the measured friction factor for approximately the same Reynolds number range. This predicted bundle friction factor is generally higher than the Moody friction factor for smooth tubes, since the irregular geometry of the subchannels in the bundle causes nonuniform velocities in different subchannels, and therefore induces higher pressure drop. If the data correlation had been utilized in COBRA, the predicted bundle friction factor would have been much higher; therefore the Moody friction factor was used in this analysis.

The measured and COBRA-calculated (with water) friction factors are shown for two Reynolds numbers in table 6-1. The calculated friction factor is only 10 to 15 percent lower than the measured friction factor.

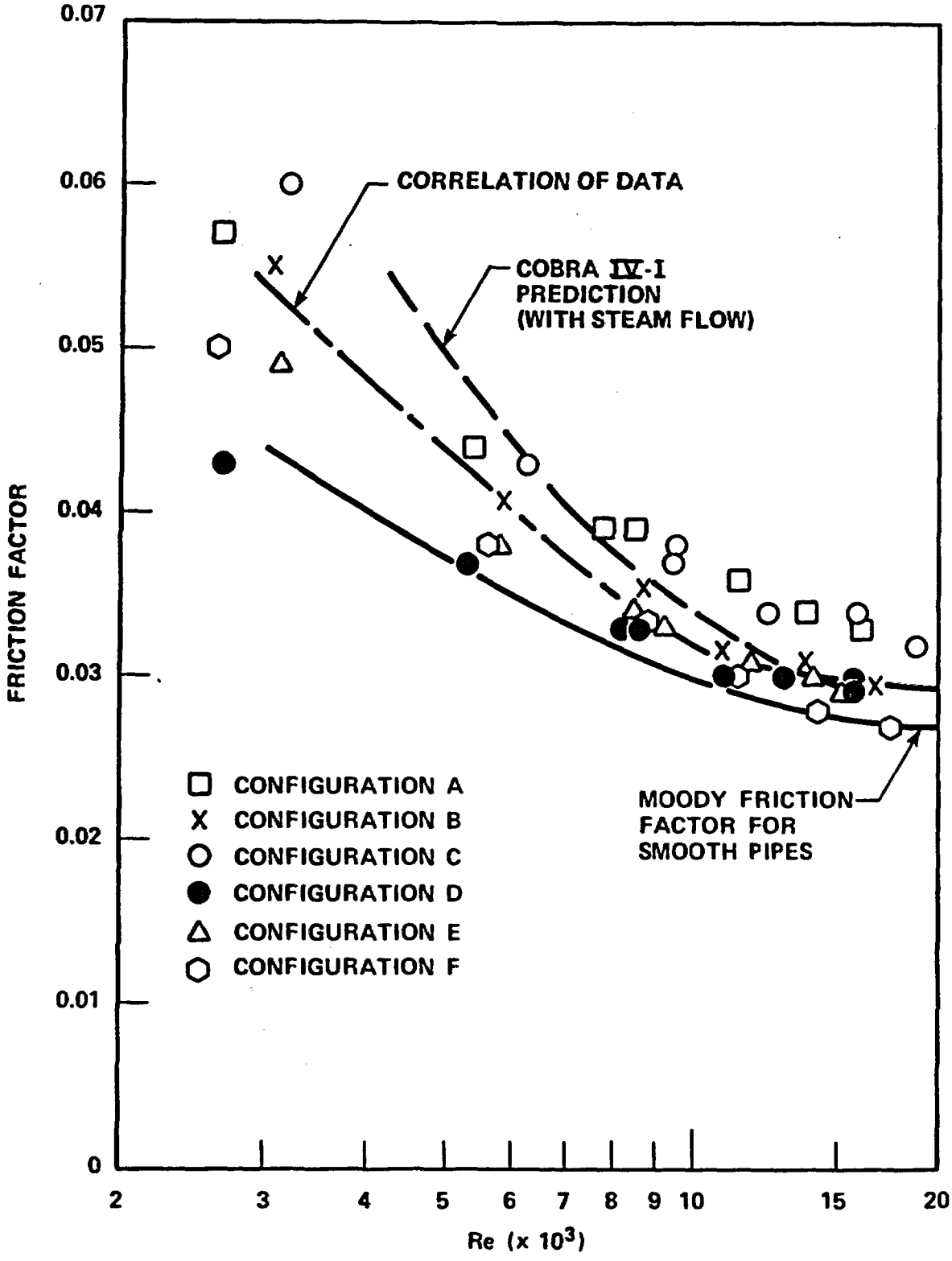

Figure 6-1. Average Bundle Friction Factor Versus Reynolds Number

TABLE 6-1

CONFIGURATION D CALCULATED AND MEASURED HYDRAULIC CHARACTERISTICS

Re	Friction Factor		Grid Loss Coefficient	
	Calculated[a]	Measured	Calculated	Measured
5.3×10^3	0.03355	0.037	1.1574	1.46
1.5×10^4	0.0248	0.0293	0.8195	1.121

a. By COBRA-IV-I code using Moody friction factor with water flow

6-4. Grid Loss Coefficient

The loss coefficient of non-mixing-vane grids in bundles has been correlated by Rehme[1] as

$$K_r = C_v \epsilon^2$$

for high Reynolds numbers, where ϵ is the blockage ratio of the grid projected cross-sectional area to the flow area. Through a detailed review of Rehme's data at lower Reynolds numbers, a more complete correlation has been formulated:

-- $K_r = 196 \times Re^{-0.33} \epsilon^2$ for $10^3 < Re < 10^4$

-- $K_r = 41 \times Re^{-0.16} \epsilon^2$ for $10^4 < Re < 10^5$

-- $K_r = 6.5 \epsilon^2$ for $10^5 < Re$

1. Rehme, K., "Pressure Drop Correlation for Fuel Element Spacers," Nucl.Technol. 17, 15-23 (1973).

Comparison of the above correlation with many other data sets indicates that it should be increased by a factor of about 40 percent. The data from the 21-rod tests can be generally predicted well by the above correlation when it is increased by 40 percent. Thus

$$K = 1.4\, K_r$$

The comparisons of data with the present prediction (based upon bundle-averaged ϵ^2 and configuration A geometry) are shown in figures 6-2 through 6-5. For bundles with a reduced number of dimples (configurations C, D, E, and F), the comparisons are also favorable.

The grid behind the blockage [2.44-2.74 m (96-108 in.)] may be correlated better by

$$K = 1.6\, K_r$$

The increase of loss coefficient may be attributed to the fact that the generated wake behind the blockage has not decayed completely.

The COBRA code was modified to include the above formulation for grid loss coefficient for each subchannel. Although the above formulation is derived from the bundle averaged condition, the comparisons between the data and the COBRA subchannel analysis are in good agreement for some sample cases. Therefore, the present formulation could be used in subchannel analysis as well.

The measured and COBRA-calculated grid loss coefficients with water flow are shown for two Reynolds numbers in table 6-1. The calculated grid loss coefficient is 17 to 26 percent lower than the measured grid loss coefficient. In a steam flow COBRA calculation, the calculated grid loss coefficient was only 10 percent lower than the measured grid loss coefficient (in water flow) at a Reynolds number of 12,000.

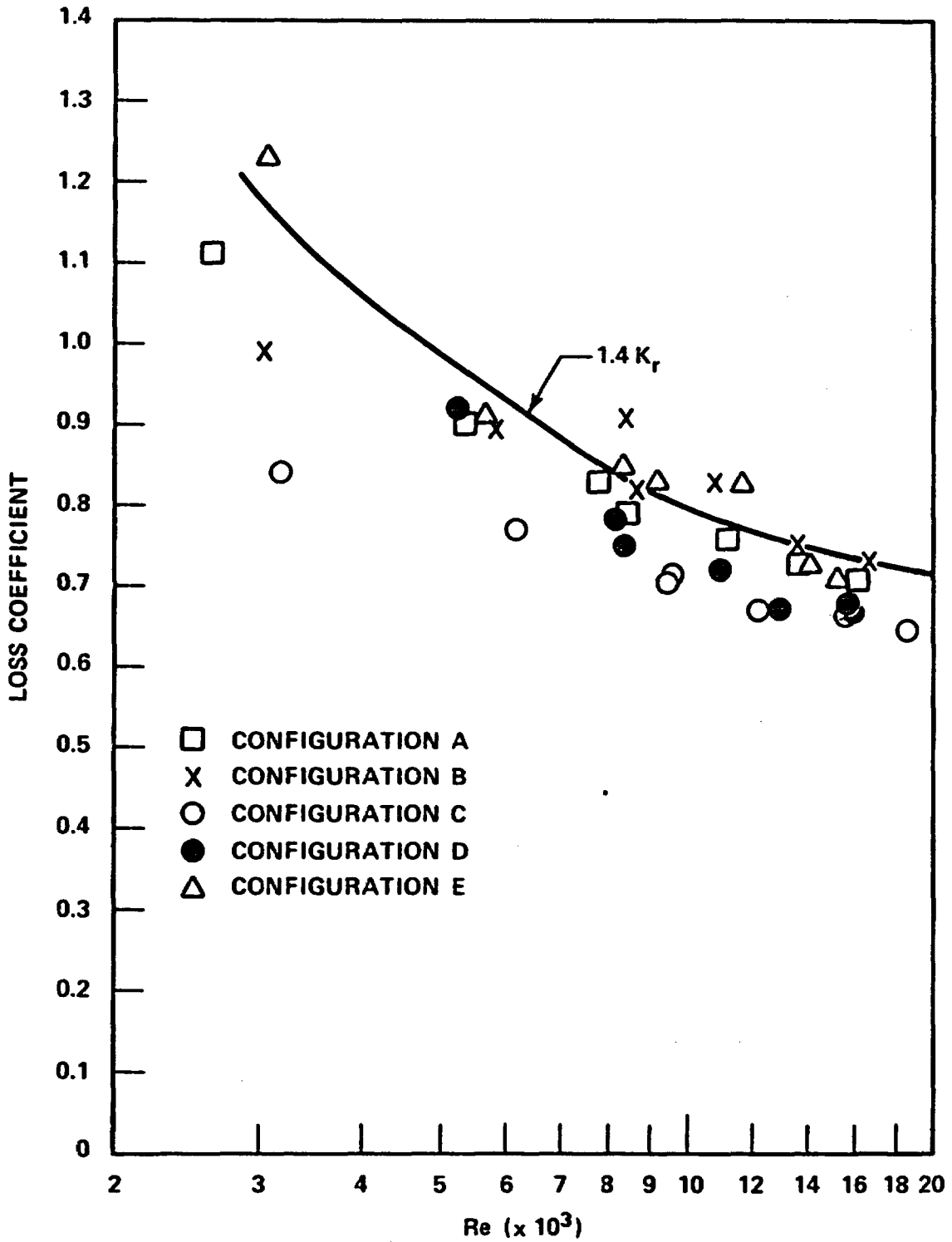

Figure 6-2. Grid Loss Coefficient Correlation Versus Reynolds Number, 0.30-0.61 m (12-24 in.) Grid

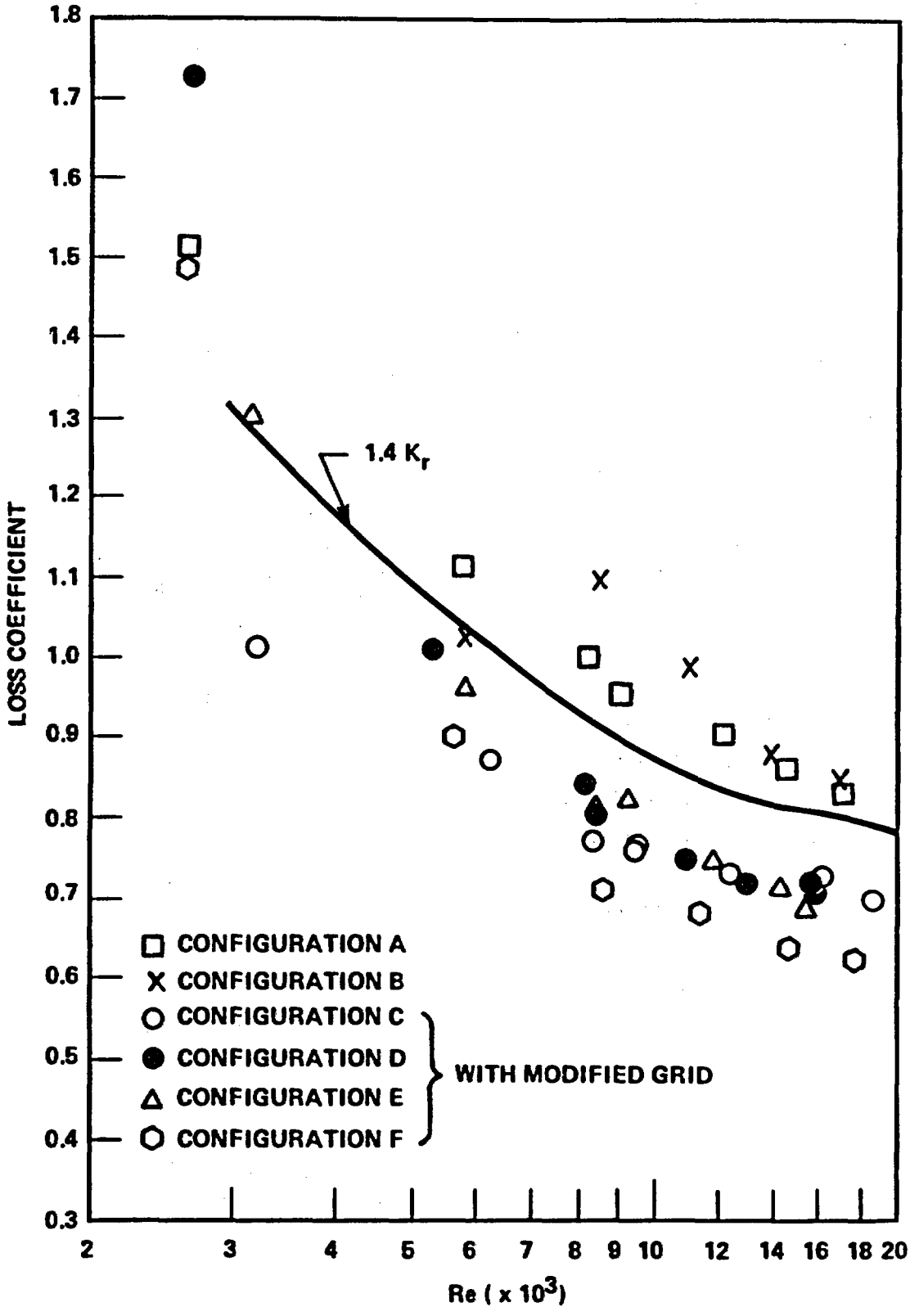

Figure 6-3. Grid Loss Coefficient Correlation Versus Reynolds Number, 0.91-1.22 m (36-48 in.) Grid

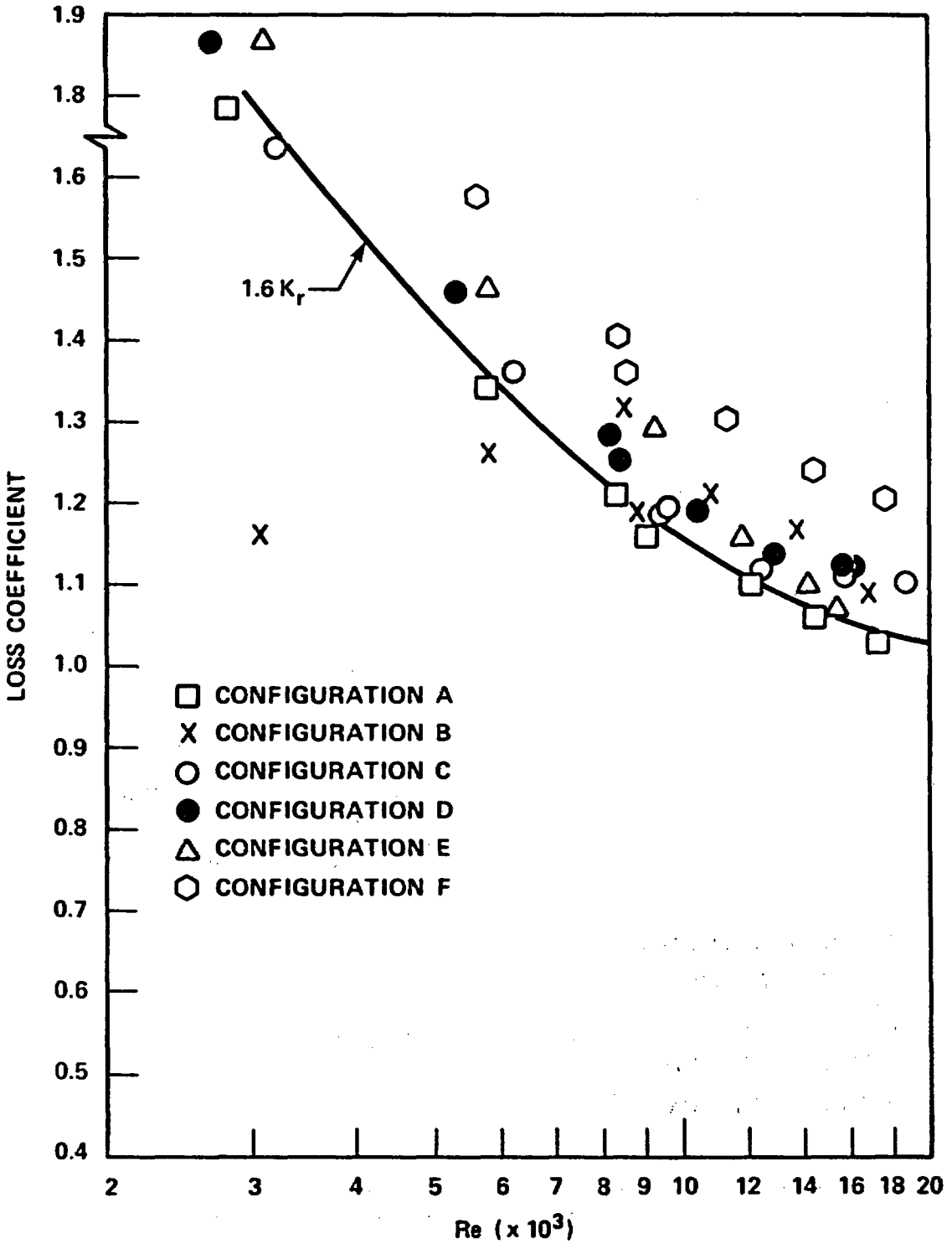

Figure 6-4. Grid Loss Coefficient Correlation Versus Reynolds Number, 2.44-2.74 m (96-108 in.) Grid

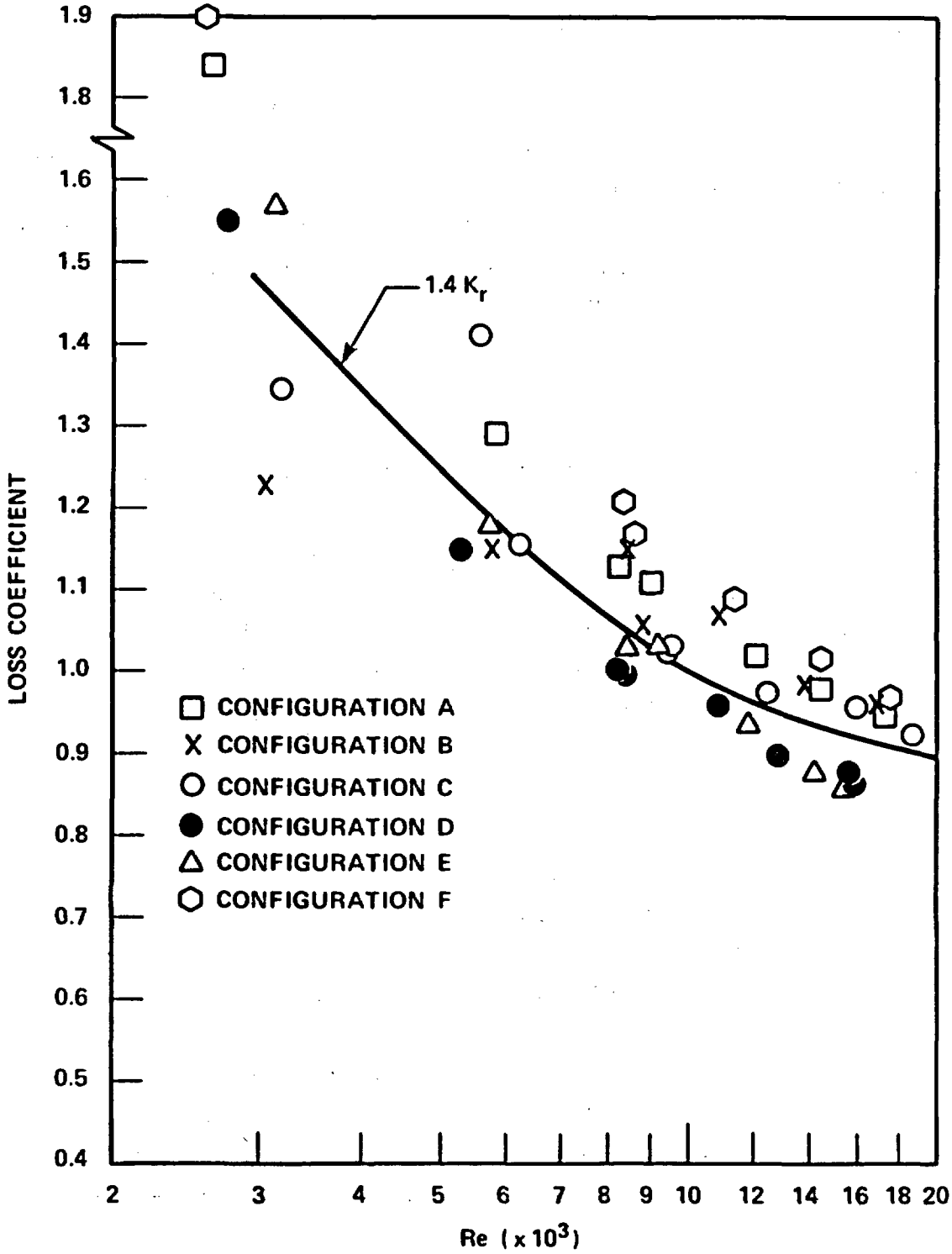

Figure 6-5. Grid Loss Coefficient Correlation Versus Reynolds Number, 3.15 m (124 in.) Grid

6-5. Coplanar Blockage Loss Coefficient

Configuration C contained short concentric blockage sleeves on all 21 rods at the same elevation. The data for this test are shown in figure 6-6. This type of blockage is similar to the grid, except that the geometry resembles a venturi rather than an orifice. Therefore, the loss coefficient of this type of coplanar blockage was correlated following the previous grid loss coefficient formulas. In fact, the data of configuration C in figure 6-6 can be correlated well by

$$K = 0.7\ K_r$$

Configuration B contained short concentric blockage sleeves on nine central rods at the same elevation. Flow bypassed the blockage similar to the flow in two parallel tubes with different flow resistances. The same pressure drop was assumed in the blocked and the unblocked zones. The overall loss coefficient was calculated in terms of the friction factor in the unblocked zone and the loss coefficient in the blocked zone. Since both sets of information are available, as discussed previously, the overall loss coefficient can be calculated. For the typical case of configuration B, the calculated result is

$$K = 0.54\ K_r$$

As shown in figure 6-6, the comparison with data is very favorable.

6-6. Noncoplanar, Concentric Blockage Loss Coefficient

Configuration D contained a noncoplanar distribution of short concentric blockage sleeves on all 21 rods. Since the sleeves were smooth, the flow separation was not expected to be very severe. The loss coefficient has been calculated by COBRA using the Moody friction factor for the rods and blockage surfaces (which are increased because of blockage geometry). The calculated loss coefficient is very close to the data, as shown in figure 6-6 for all Reynolds number ranges. For this type of smooth noncoplanar blockage, it was concluded that the loss coefficient was due to the increase of the skin friction in the blockage zone.

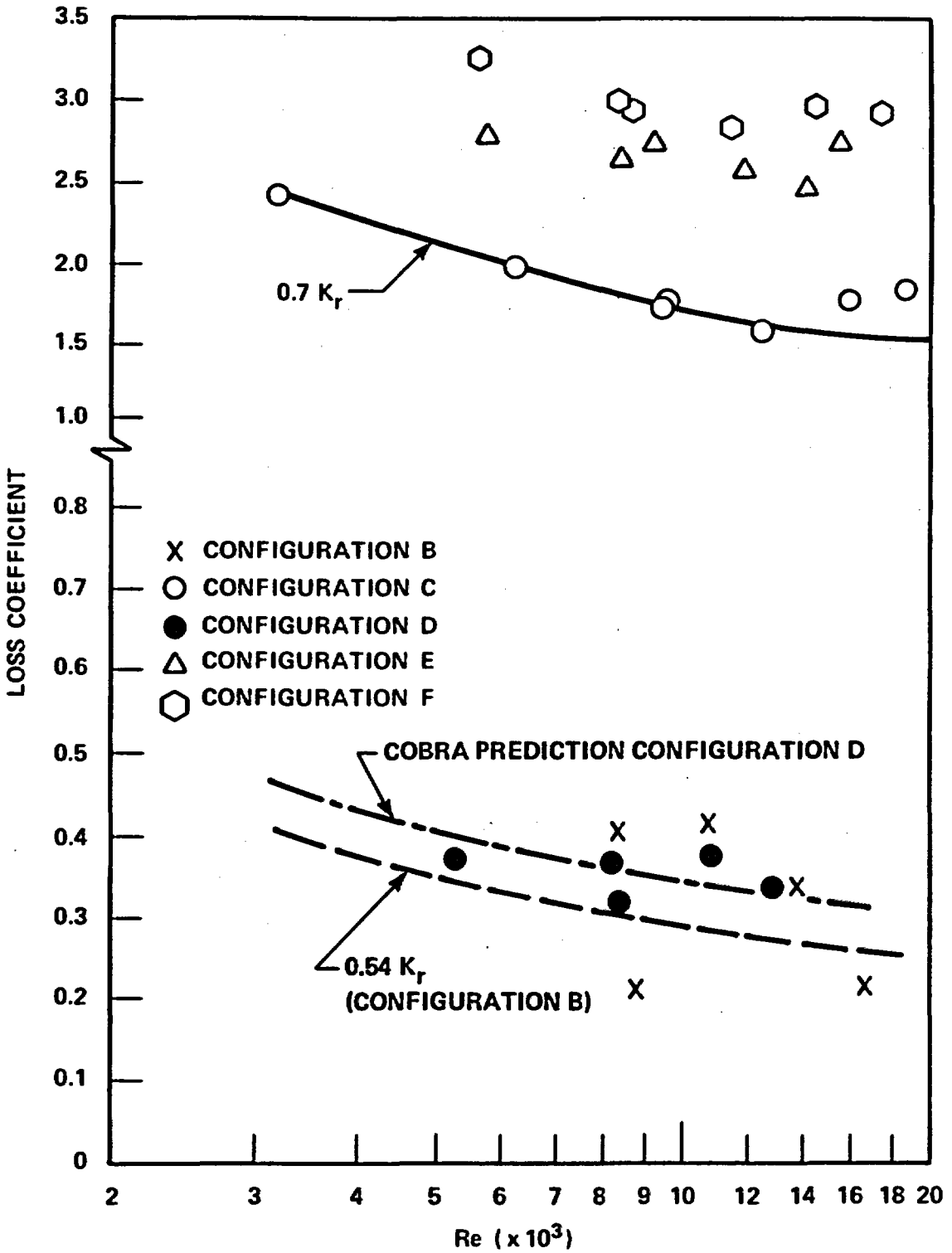

Figure 6-6. Blockage Loss Coefficient Versus Reynolds Number

6-7. Noncoplanar, Nonconcentric Blockage Loss Coefficient

A similar calculation was performed for the nonconcentric blockage in configurations E and F; however, the calculated loss coefficient was approximately 25 percent and 50 percent, respectively, of the experimental results. This difference between the calculated and measured blockage loss coefficients was attributed to the flow separation which occurs downstream of the bulge. To provide an accurate simulation of the nonconcentric flow blockage in configurations E and F, the COBRA-IV-I code was modified to provide a pressure loss coefficient for each nonconcentric bulge. It was assumed that the pressure loss due to the bulge was a function of distance downstream from the bulge similar to the heat transfer exponential decay downstream of the grid.[1] This is mainly because both the pressure loss and the heat transfer augmentation are directly related to the gradual decay of the turbulence in the wakes along the stream.

The modeling of the blockage in COBRA-IV-I utilized the modified Rehme correlation, as previously described in paragraph 6-4. This pressure loss coefficient was then distributed downstream of the bulge utilizing the relationship

$$K \alpha e^{-0.13\,(Z/D)}$$

such that the local loss coefficient becomes

$$K_i = C \int_{(Z/D)i}^{(Z/D)i+1} e^{-0.13(Z/D)}\, d\left(\frac{Z}{D}\right)$$

and the overall loss coefficient is

$$K = C \int_{0}^{(L/D)} e^{-0.13(Z/D)}\, d\left(\frac{Z}{D}\right)$$

---

1. Yao, S. C., et al., "Heat Transfer Augmentation in Rod Bundles Near Grid Spacers," presented at Winter Annual Meeting, American Society of Mechanical Engineers, Chicago, IL, November 16-21, 1980.

Therefore,

$$C = \frac{K}{\int_0^{L/D} e^{-0.13(Z/D)}\, d\left(\frac{Z}{D}\right)}$$

Substituting the above relationship for C into the relationship for the local loss coefficient, K_j, the local loss coefficient becomes

$$K(Z) = 1.4\,K \left[\frac{\int_{(Z/D)_i}^{(Z/D)_{i+1}} e^{-0.13(Z/D)}\, d\left(\frac{Z}{D}\right)}{\int_0^{(L/D)} e^{-0.13(Z/D)}\, d\left(\frac{Z}{D}\right)} \right]$$

The Reynolds number and blockage factor were calculated at the elevation of maximum blockage. The axial distribution also includes a simulated entrance loss effect with 50 percent of the magnitude of the highest value. The general representation of the term within the brackets in the above equation is shown below:

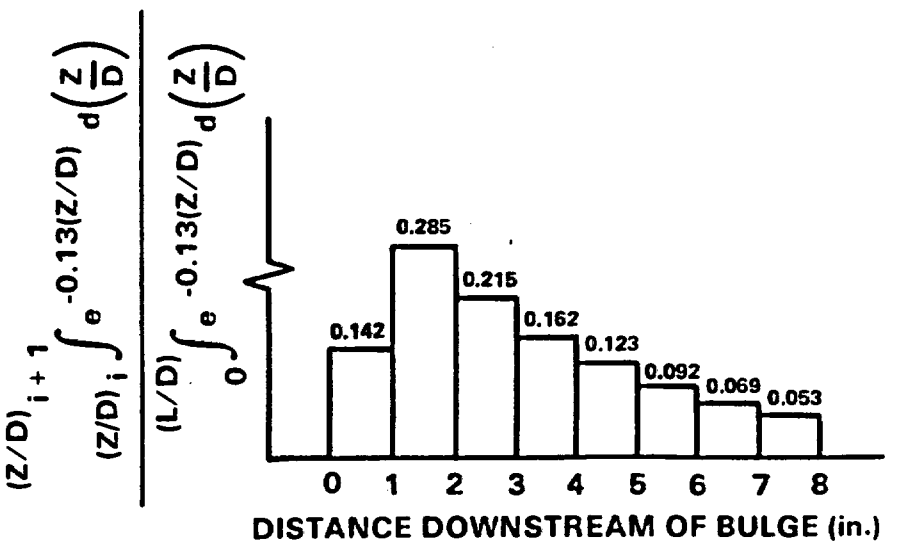

The results from the COBRA calculation (with steam) and the hydraulic characteristics tests are shown in table 6-2 for a Reynolds number of 14,000.

TABLE 6-2

CALCULATED[a] AND MEASURED HYDRAULIC CHARACTERISTICS FOR CONFIGURATIONS E AND F AT Re = 14000

Configuration	Friction Factor[b]		Grid Loss Coefficient		Blockage Loss Coefficient	
	Calculated	Measured	Calculated	Measured	Calculated	Measured
E	0.026	0.028	1.04	1.1	2.16	2.47
F	0.026	0.028	1.03	1.1	3.07	2.9

a. Using steam in COBRA-IV-I code
b. COBRA-IV-I code using Moody friction factor

Because these results were fairly reasonable, the COBRA blockage modeling described above can be utilized in other similar cases.

6-8. STEAM COOLING TEST DATA ANALYSIS

The 21-rod bundle steam cooling test data were reduced and analyzed in the same manner as the data from the 161-rod unblocked bundle.[1] The COBRA-IV-I computer code was utilized to calculate the subchannel vapor temperatures and the mass flows. In this fashion, the effects of the housing, the filler rods, and subsequent subchannel mixing could be taken into account. The measured heater rod temperatures and bundle power were subsequently coupled with the calculated vapor temperatures and mass flows to calculate the corresponding heat transfer coefficients.

1. Wong, S., and Hochreiter, L. E., "Analysis of the FLECHT SEASET Unblocked Bundle Steam Cooling and Boiloff Tests," NRC/EPRI/Westinghouse-8, January 1981. NUREG/CR-1533.

The steam cooling test data were reduced and analyzed in the following two steps:

-- The data below the 1.52 m (60 in.) elevation for all six bundles were analyzed together.

-- The data between the 1.52 and 2.44 m (60 and 96 in.) elevations were analyzed for each configuration individually.

It was possible to use the above two steps because the data for all six configurations represented the unblocked condition below 1.52 m (60 in.) and could therefore be reduced and analyzed together. Also, the COBRA-IV-I model of the blockage zone required small nodes [25 mm (1 in.)] to accurately calculate the flow redistribution around the blockage sleeves. Since the data below 1.52 m (60 in.) were measured in approximately 0.30 m (12 in.) increments, a much larger node [1.52 mm (6 in.)] could be utilized. The data above 2.44 m (96 in.) were not analyzed, since reverse heat transfer occurred as a result of the low power at these elevations. The subchannel vapor temperatures and mass flow rates calculated from the 0 to 1.52 m (0 to 60 in.) models were utilized as boundary conditions for the respective 1.52 to 2.44 m (60 to 96 in.) models.

6-9. Data Reduction Method

The STMCOOL code (described in paragraph 6-10) was written to calculate the local Nusselt and Reynolds numbers in the 21-rod bundle test section, based on the calculated COBRA-IV-I results and the measured data as shown in figure 6-7.

The unblocked data were correlated as a function of Reynolds numbers in the same way as the 161-rod unblocked bundle data. The enhancement factor (described in section 3) was calculated for the blockage data. The data correlation as a function of elevation, blockage, and Reynolds number will be provided in a later evaluation report.

6-10. COBRA-IV-I Models

The COBRA-IV-I code was set up and run with the assistance of Battelle Northwest Laboratory to calculate subchannel vapor temperatures and mass flows. Figure 6-8

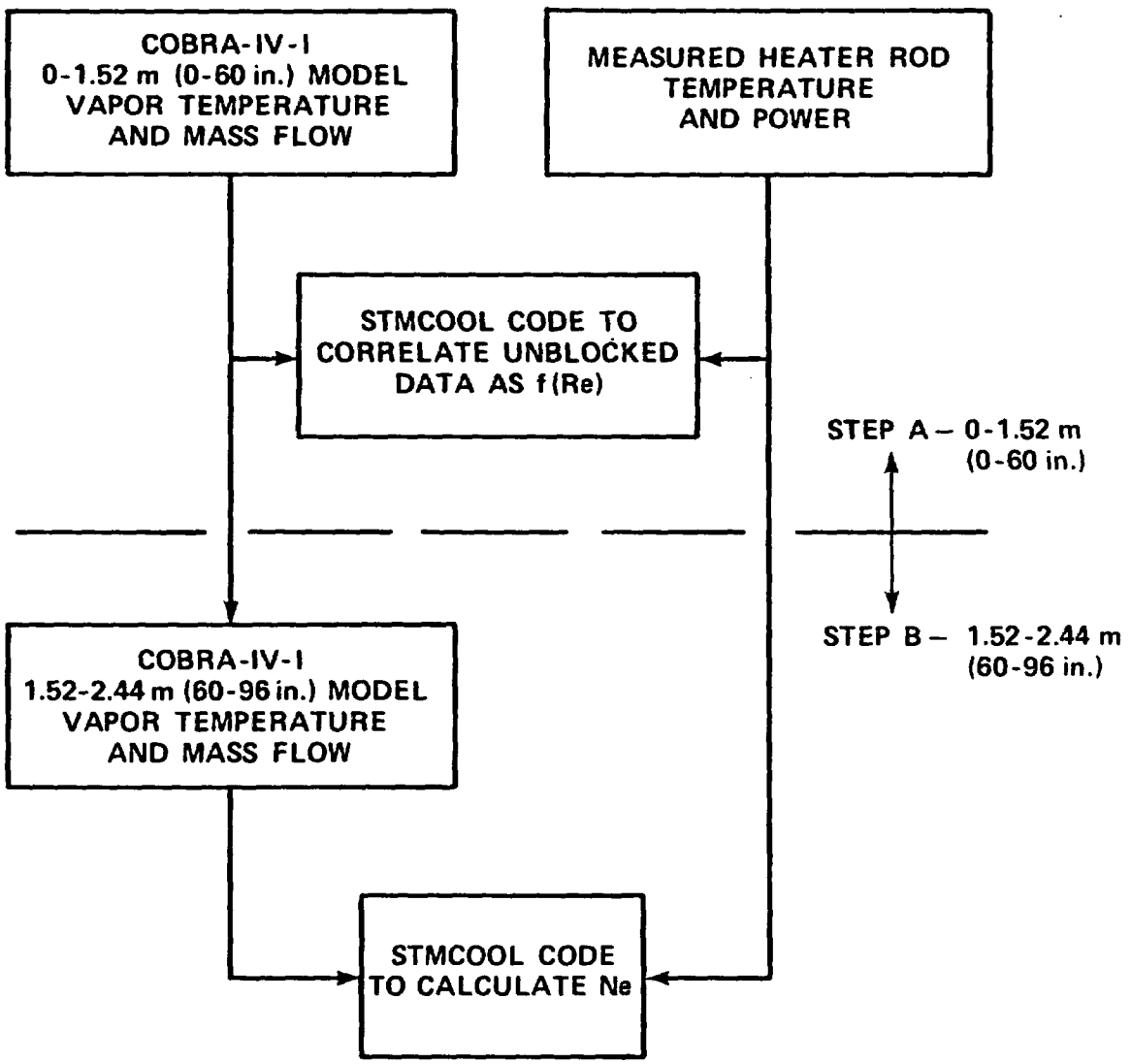

Figure 6-7. Calculation of Nusselt and Reynolds Numbers by STMCOOL Code

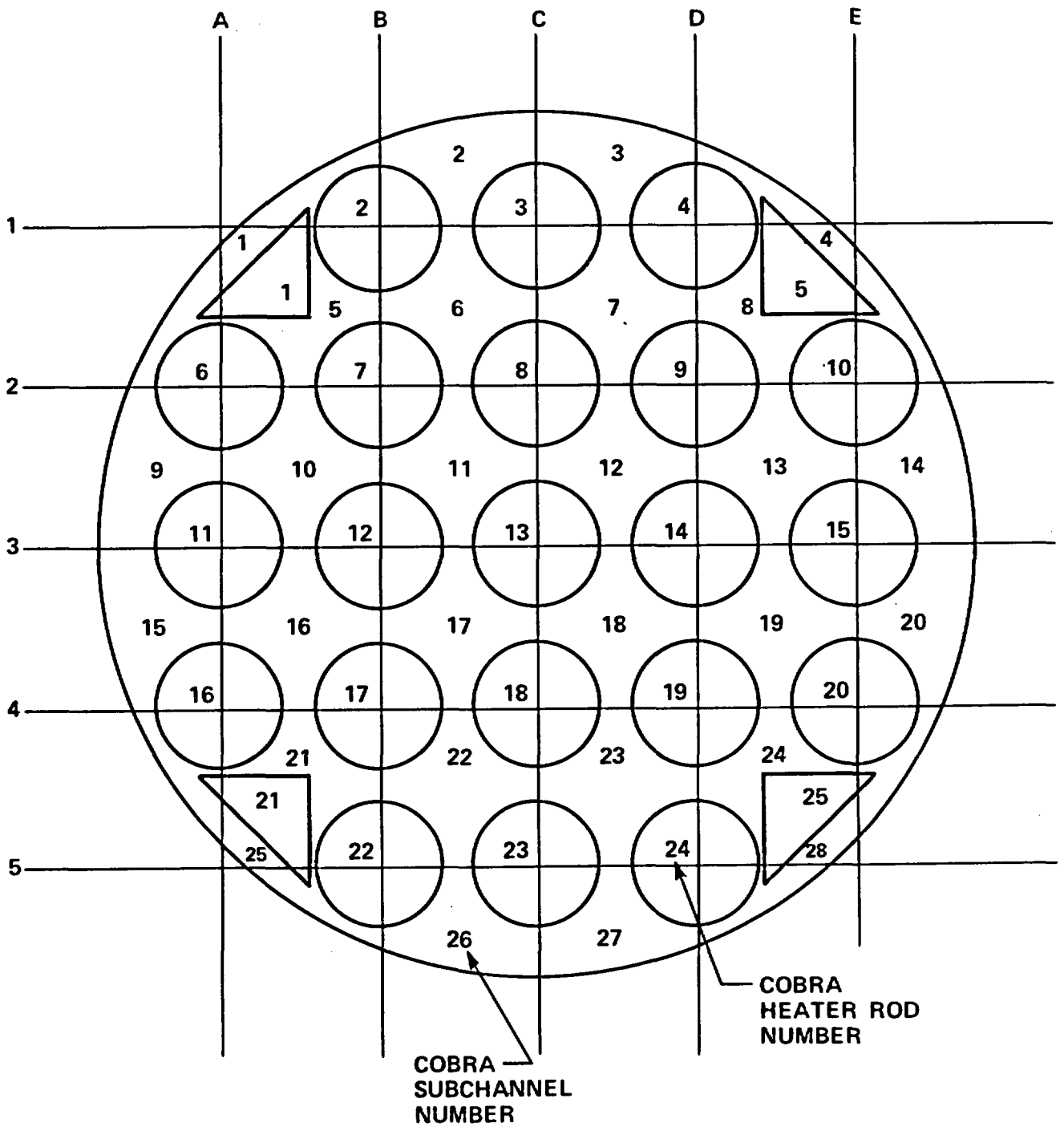

Figure 6-8. COBRA Model of 21-Rod Bundle

shows the subchannel simulation of the unblocked 21-rod bundle test section for the COBRA-IV-I code. The measured pressure, inlet steam temperature, inlet mass flow rate, and power were utilized as boundary conditions. The heater rod radial power factors based on the measured heater element resistances, and bundle-averaged axial power profiles, as calculated from the heater rod quality assurance data, were incorporated into the COBRA model for each of the six test configurations.

Since the steam cooling tests were conducted at steady state, low power, and low temperature, the energy loss through the housing and insulation was not negligible. This energy loss was simulated in COBRA by appropriately reducing the rod heat flux into the 12 peripheral subchannels. The energy loss was a function of bundle power and elevation, as shown in figure 6-9.

6-11. STMCOOL Code

The STMCOOL code was written to calculate the local Nusselt and Reynolds numbers as follows:

$$Re = \frac{G D_h}{\mu}$$

$$Nu = \frac{h D_h}{K}$$

where

Re = vapor Reynolds number
G = vapor mass flux
μ = vapor viscosity
D_h = hydraulic diameter
Nu = Nusselt number
h = heat transfer coefficient
K = vapor conductivity

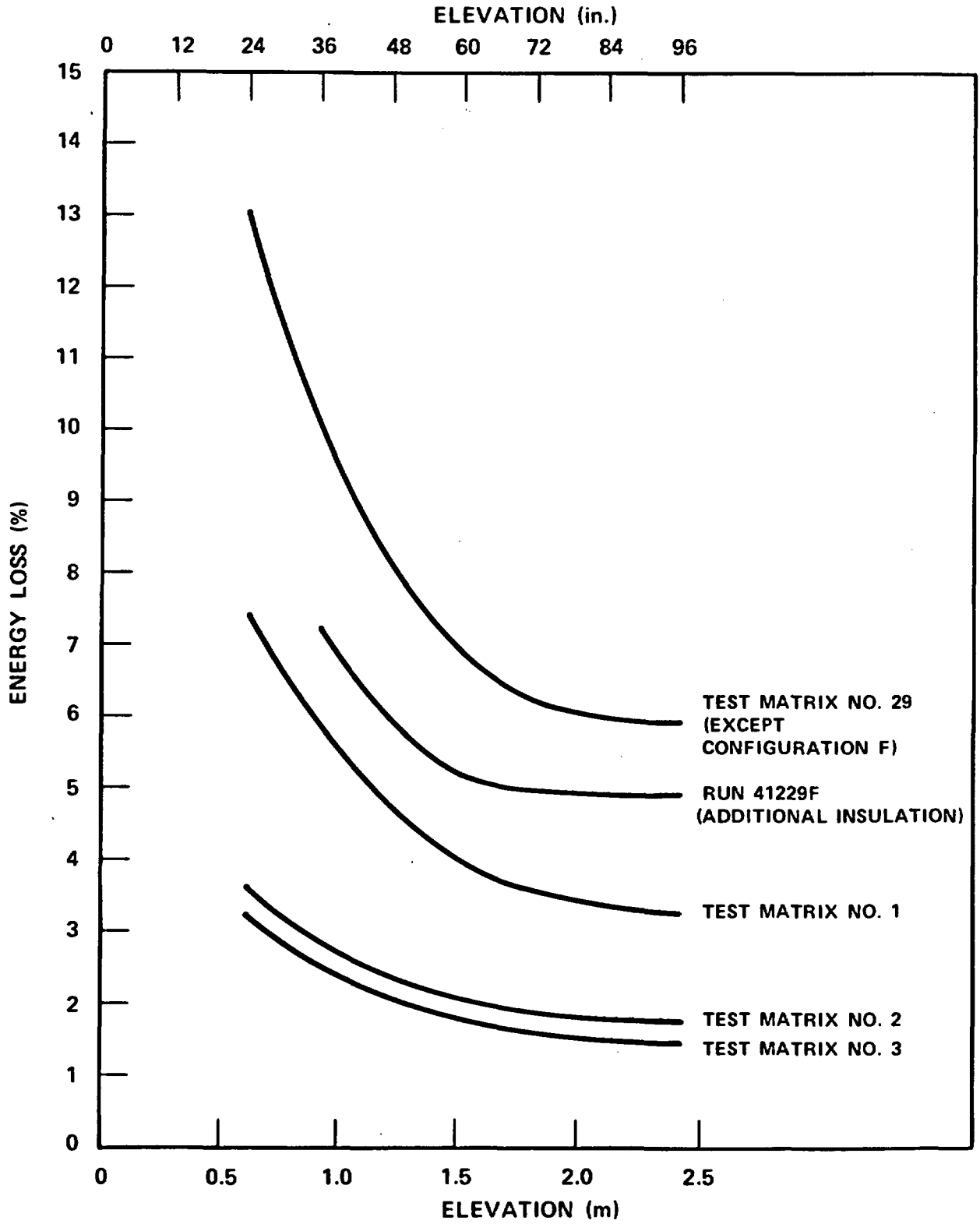

Figure 6-9. Bundle Energy Losses for Steam Cooling Tests

The heat transfer coefficient was given by

$$h = \frac{q''_w}{T_c - T_v}$$

where

q''_w = wall heat flux
T_c = clad temperature
T_v = vapor temperature

The vapor mass flux, G, was calculated by the COBRA-IV-I code. The measured bundle inlet steam flow was distributed among the 28 subchannels to maintain an equal pressure gradient. The mass flux used in the STMCOOL code was the average of the mass fluxes in the four COBRA code subchannels surrounding the particular heater rod.

The hydraulic diameter, D_h, was defined by a rod-centered subchannel and in the STMCOOL code was the average of the hydraulic diameters in the four COBRA code subchannels surrounding the particular heater rod. The vapor properties μ and K were evaluated at the film temperature, since the wall-to-vapor temperature difference was small [between 6°C and 28°C (10°F and 50°F)].

The wall heat flux was calculated from the measured power as follows:

$$q''_w \text{ (i-th rod, Z)} = R_i \, F_{iZ} \frac{\overline{q''}}{\pi d}$$

where

R_i = ratio of the power of the i-th rod to the average rod power
F_{iZ} = axial power factor of the i-th rod at elevation Z

$\overline{q''}$ = average linear power = $\frac{\text{measured power (kw)}}{21 \times 12}$

d = diameter of heater rod

The clad temperature, T_c, utilized in the above formulation was the measured rod temperature. The difference between using the measured rod temperature at the inside surface of the clad and the outside surface temperature as calculated by the DATAR code was less than 1 percent of the rod-to-vapor temperature differential. All of the measured rod temperatures were reviewed to ensure that steady-state conditions had been achieved. It was assumed that no more than 0.6°C (1°F) change in heater rod temperature in approximately 300 seconds represented steady-state conditions.

The vapor temperature, T_v, as previously discussed, was calculated by the COBRA-IV-I code. The vapor temperature used in the STMCOOL code was the average of the vapor temperatures in the four COBRA code subchannels surrounding the particular heater rod. Vapor temperature measurements were made at various elevations and radial positions in the bundle, but in insufficient quantities for detailed heat transfer calculations. However, comparisons of calculated and measured vapor temperatures from 0.89 to 2.46 m (35 to 97 in.) generally showed good agreement, as shown in figures 6-10 through 6-12 for configuration C. The subchannel locations for the measured vapor temperatures in these figures are identified in figure 6-8.

In the lowest-flow steam cooling tests, the measured vapor temperatures were consistently higher than the COBRA-code calculated vapor temperatures. It was believed that condensation in the injection between the flow measurement location and the bundle inlet reduced the steam flow through the bundle, and thereby provided higher measurements of the vapor temperature than would have been expected. The steam flow was subsequently reduced in the COBRA code such that the calculated vapor temperature was approximately the same as the measured vapor temperature. The measured and calculated vapor temperatures (for both measured and reduced flows) are shown in figure 6-13 for run 41329C. Similar flow reductions were required in the low-flow steam cooling tests for the other five configurations, although the percentage reduction varied for each configuration as shown below:

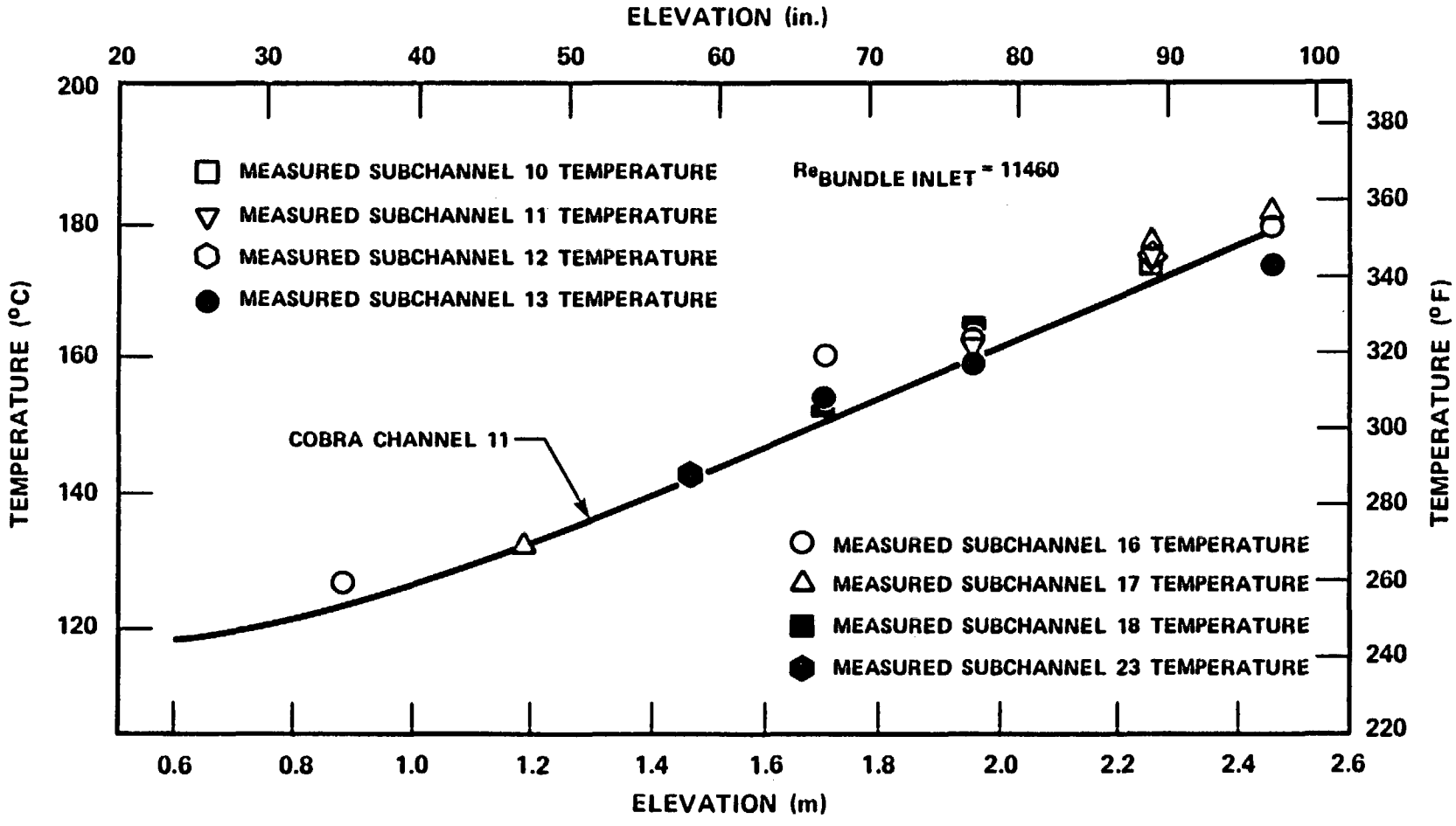

Figure 6-10. Calculated and Measured Vapor Temperatures, Run 41003C

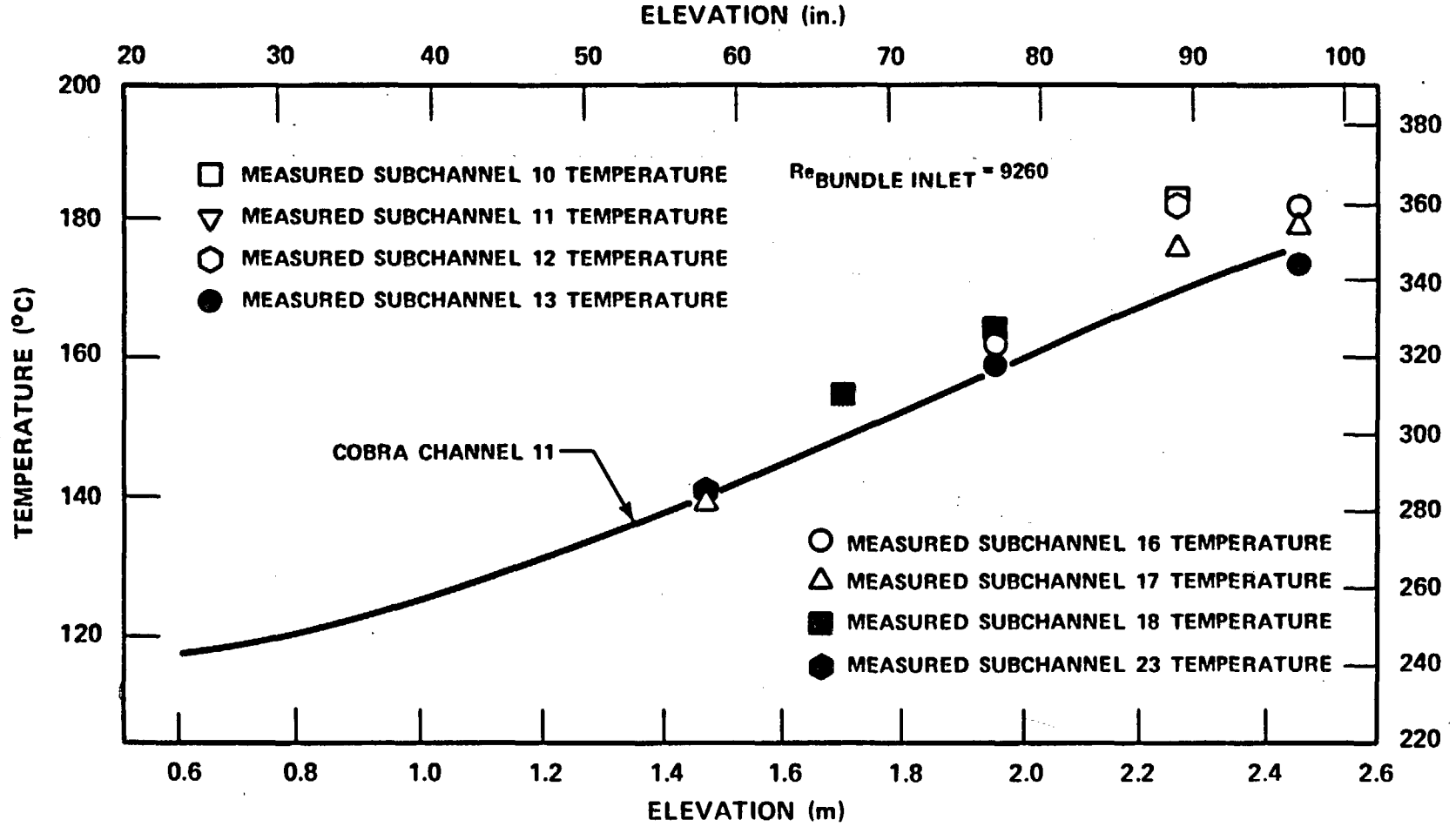

Figure 6-11. Calculated and Measured Vapor Temperatures, Run 43902C

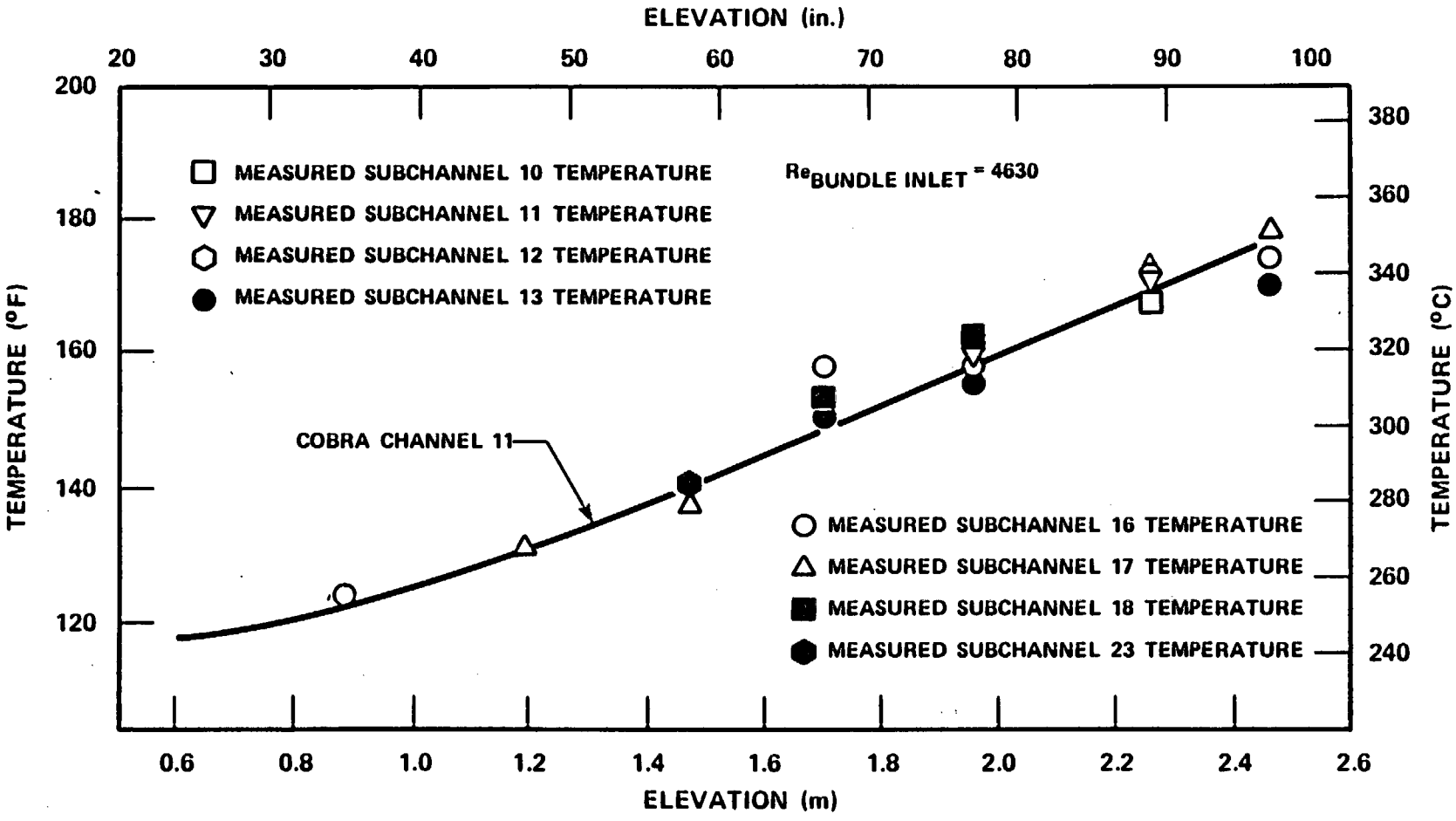

Figure 6-12. Calculated and Measured Vapor Temperatures, Run 41201C

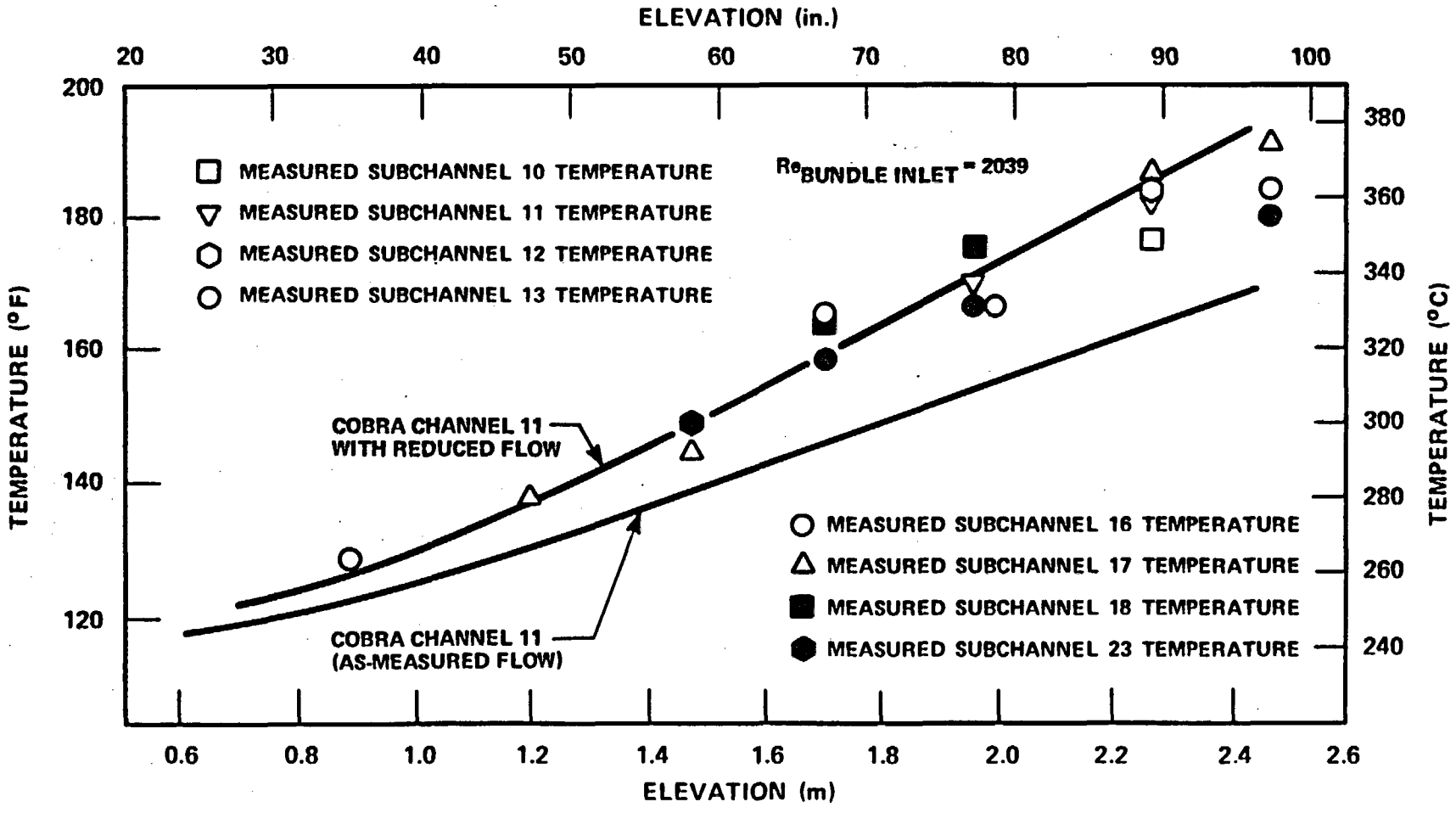

Figure 6-13. Calculated and Measured Vapor Temperatures, Run 41329C

Configuration	Run	Flow Reduction (%)	Corrected Bundle Inlet Reynolds Number
A	44529A	30.9	1907
B	43129B	10.6	2396
C	41329C	23.9	2039
D	41529D	20.6	2053
E	43929E	31.8	1879
	44029E	34.5	1802
F	41229F	32.6	1836

In each of the above tests, the flow was reduced approximately 29 percent except for run 43129B, which was reduced 10.6 percent. The measured vapor temperatures and the calculated vapor temperatures for run 43129B are shown in figure 6-14. The measured vapor temperatures for run 43129B at the upper elevations were found to be approximately 11°C to 17°C (20°F to 30°F) lower than the other six low-flow-test measured vapor temperatures. It was therefore concluded that this test should not and would not be considered for further analysis.

6-12. Unblocked Region Model Results

For the unblocked region [0 to 1.52 m (0 to 60 in.)], the 21-rod bundle steam cooling data (Nusselt number versus Reynolds number) are shown in figure 6-15 for all 23 valid steam cooling tests. These results are generally greater than the results of the Dittus-Boelter turbulent flow heat transfer correlation,[1] and the results for fully developed laminar flow in a rod bundle where the Nusselt number equals 7.86.[2] However, the heat transfer results obtained in these tests are approximately the same as the 161-rod unblocked bundle results at Reynolds numbers greater than 3000. Data at the lower

1. Dittus, F. W., and Boelter, L. M. K., "Heat Transfer in Automobile Radiators of the Tubular Type," Univ. Calif., Berkeley Publ. Eng. 2, 13, 443-462 (1930).

2. Kim, J. H., "Heat Transfer in Longitudinal Laminar Flow Along Cylinders in Square Array," in Fluid Flow and Heat Transfer Over Rod or Tube Bundles, ASME, New York, 1979, pp 155-161.

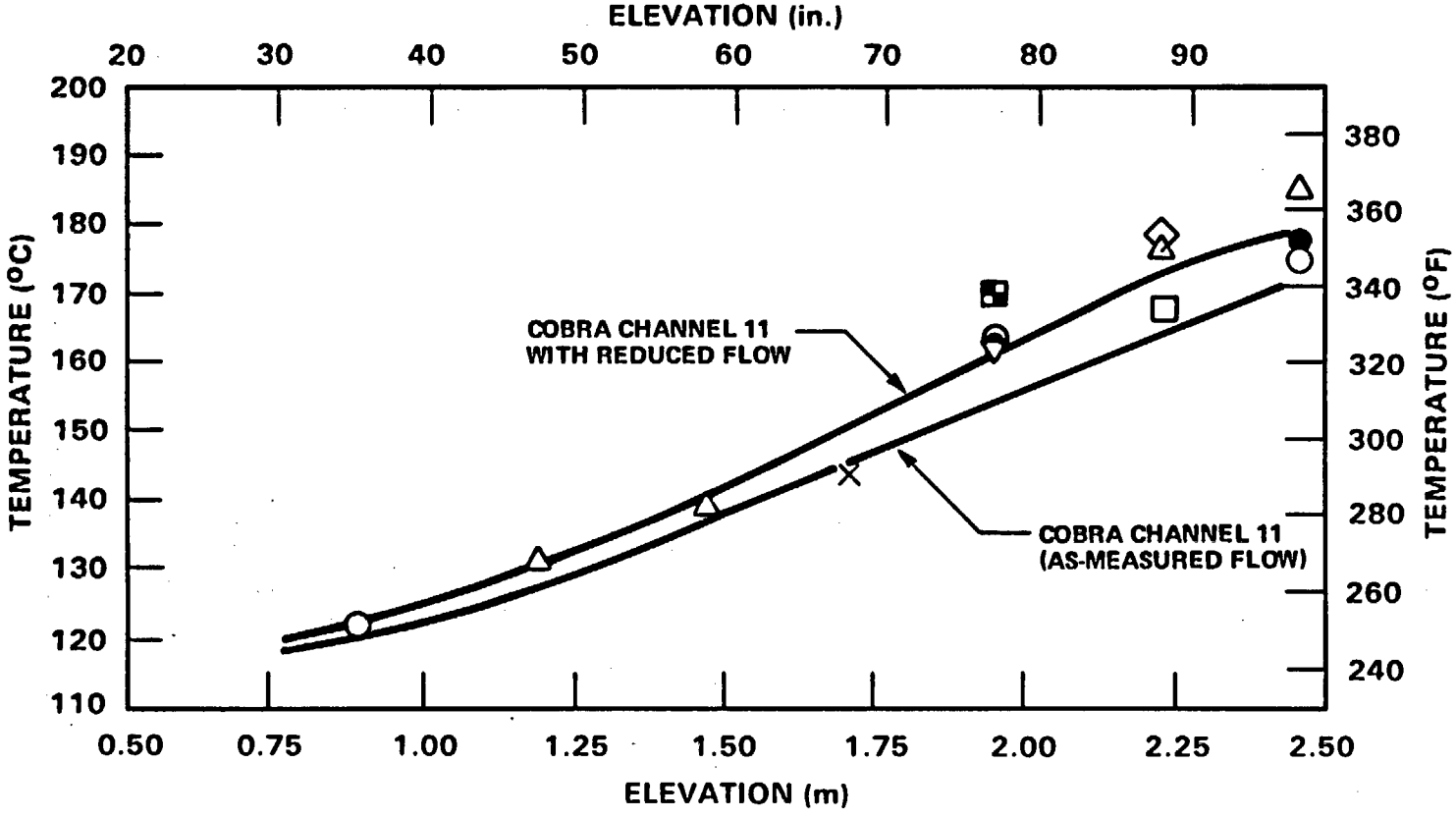

Figure 6-14. Calculated and Measured Vapor Temperatures, Run 43129B

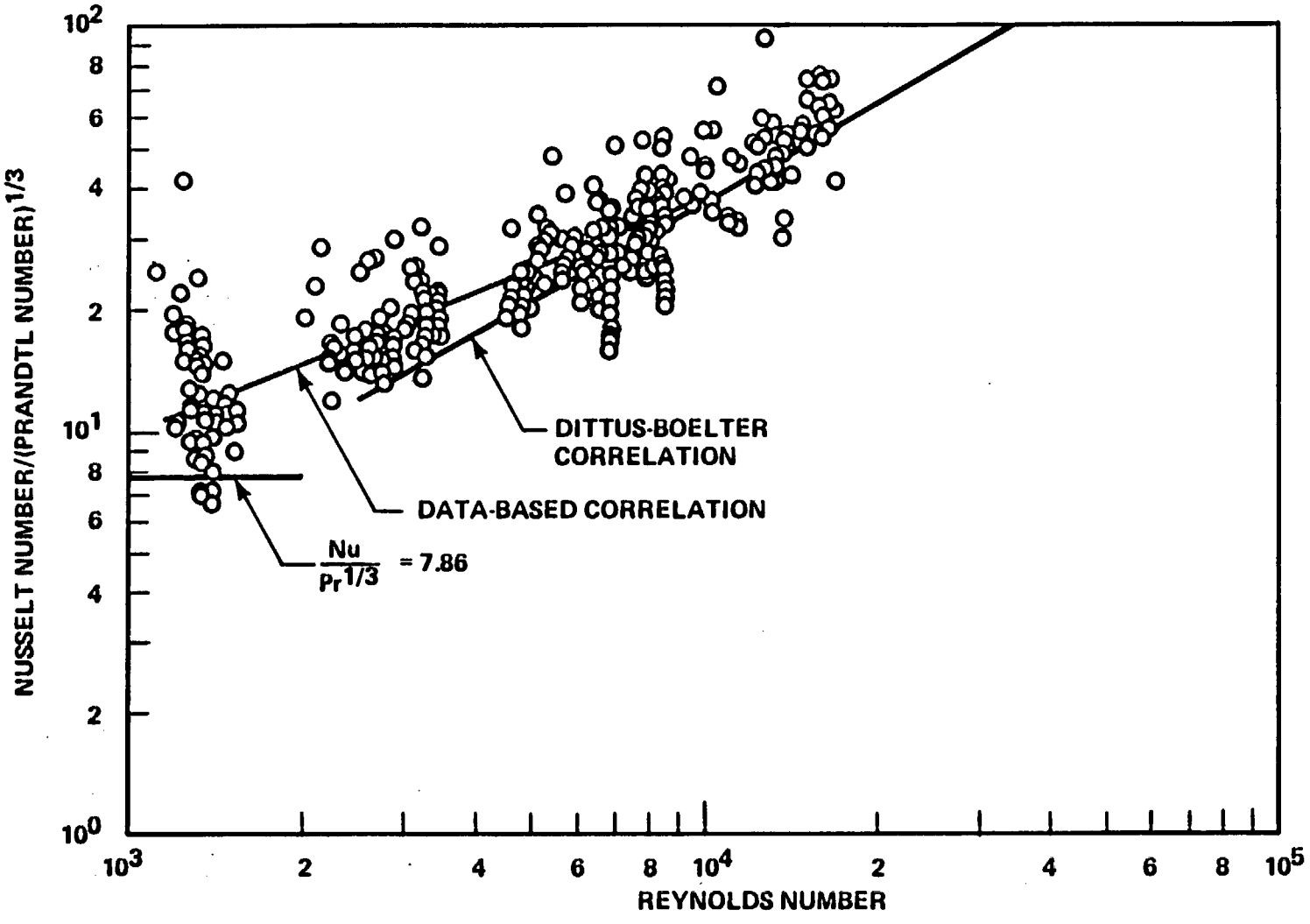

Figure 6-15. Nusselt Number Versus Reynolds Number, Unblocked Region, All Tests

Reynolds numbers, however, were not obtained in the 161-rod unblocked bundle. The 21-rod bundle correlation, developed from a linear regression fit using 375 data points, is represented by

$$\frac{Nu}{Pr^{1/3}} = 0.1805\ Re^{0.5788} \qquad \text{for } 1115 \leq Re \leq 11075$$

A comparison of 21-rod bundle, 161-rod bundle, and Dittus-Boelter heat transfer correlations is shown in table 6-3.

TABLE 6-3

COMPARISON OF HEAT TRANSER CORRELATIONS

	Ratio of Nusselt Numbers		
Re	$\frac{Nu\ (21\text{-}Rod)^{(a)}}{Nu\ (161\text{-}Rod)^{(b)}}$	$\frac{Nu\ (21\text{-}Rod)}{Nu\ (DB)^{(c)}}$	$\frac{Nu\ (161\text{-}Rod)}{Nu\ (DB)}$
2,500	1.047	1.390	1.330
10,000	0.913	1.023	1.122

a. $Nu\ (21\text{-rod}) = 0.1805\ Re^{0.5788}$
b. $Nu\ (161\text{-rod}) = 0.0797\ Re^{0.6774}$
c. $Nu\ (Dittus\text{-}Boelter) = 0.023\ Re^{0.8}$

The Nusselt number, as normalized to the following correlations with the same Prandtl number, is shown in figures 6-16 through 6-38 as a function of elevation:

$$Re \geq 2500,\ \frac{Nu}{Pr^{1/3}} = 0.023\ Re^{0.8}\ \text{(Dittus-Boelter)}$$

$$Re \leq 2000,\ \frac{Nu}{Pr^{1/3}} = 7.86$$

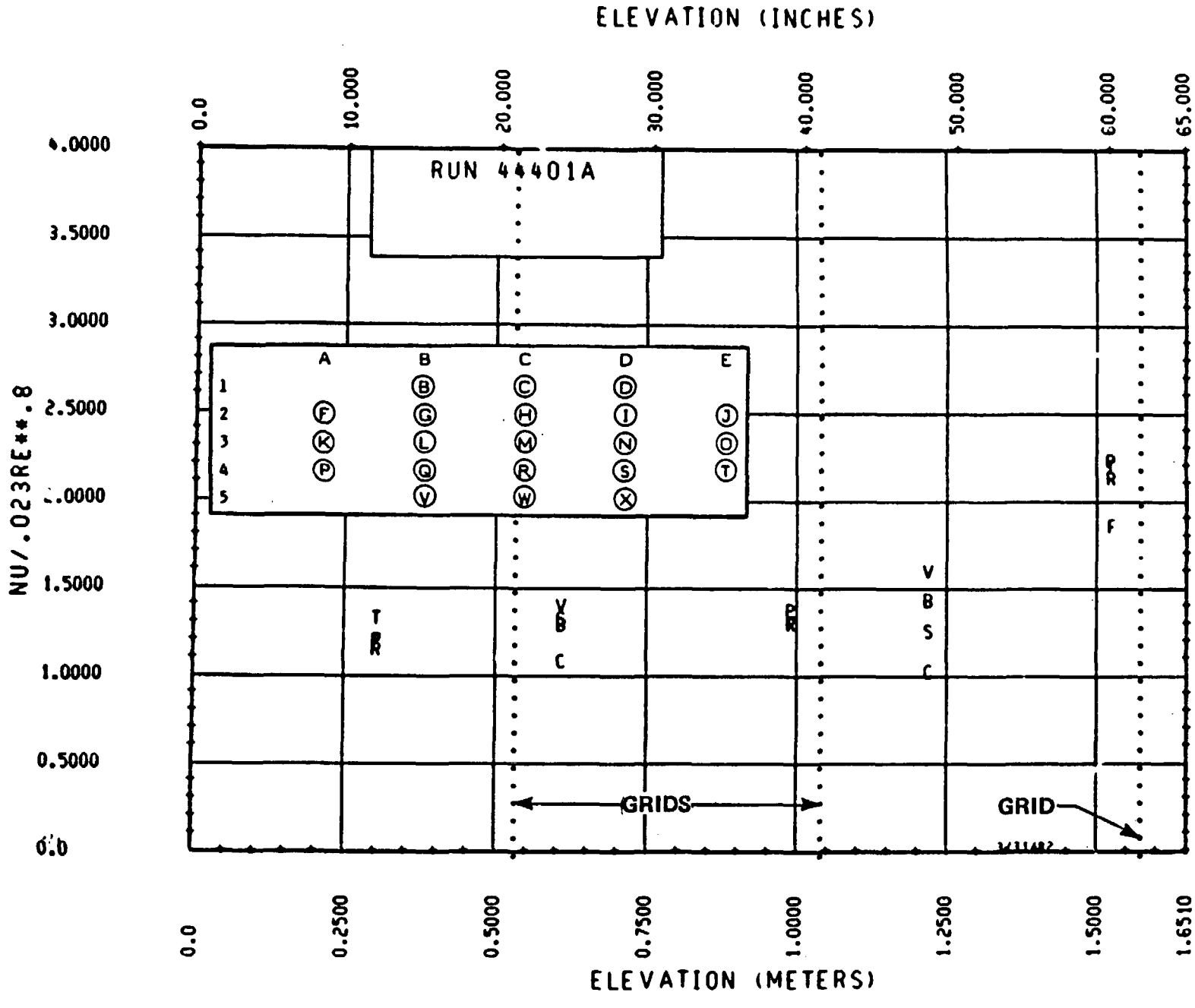

Figure 6-16. Heat Transfer From 0 to 1.52 m (0 to 60 in.), Run 44401A

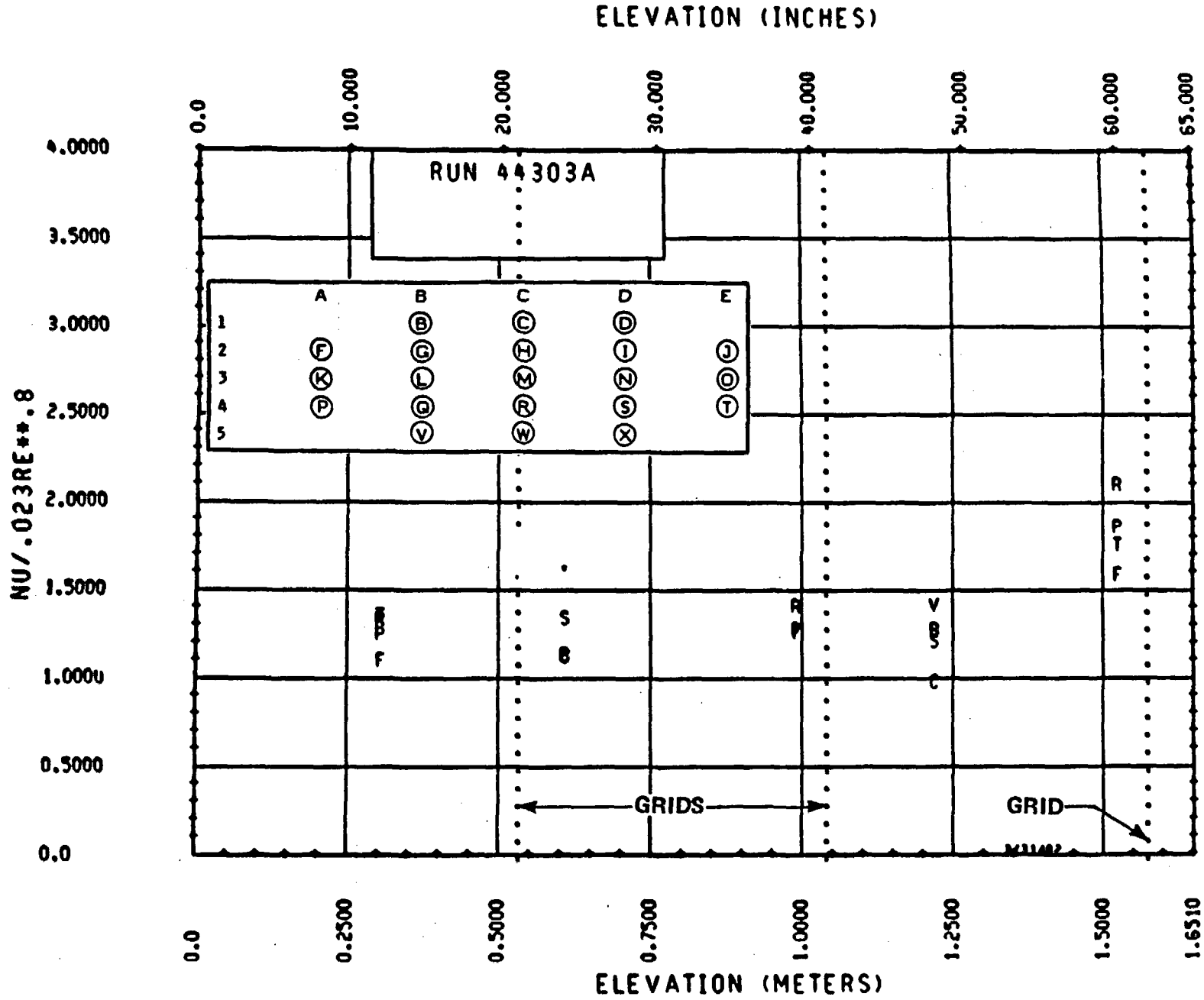

Figure 6-17. Heat Transfer From 0 to 1.52 m (0 to 60 in.), Run 44303A

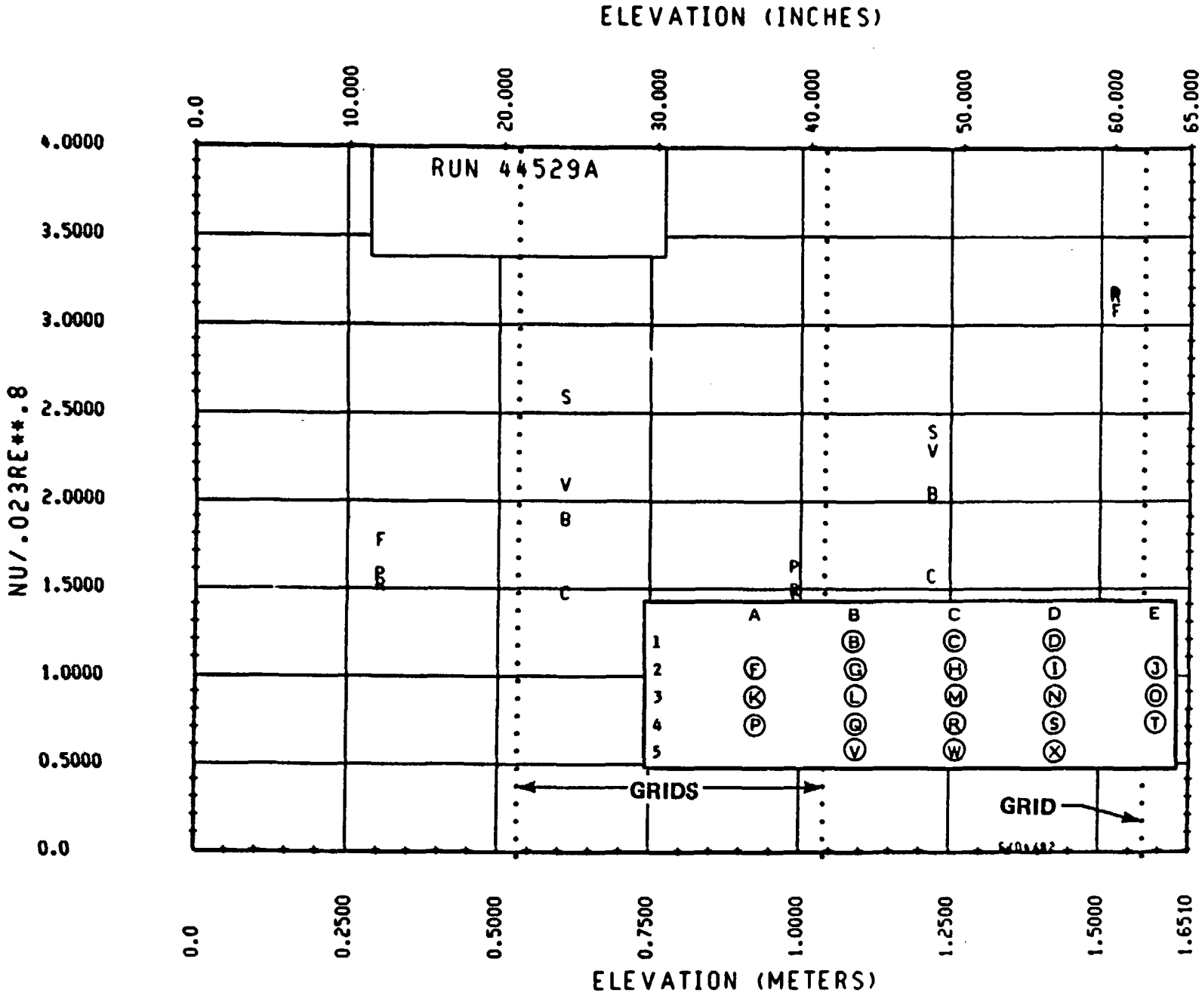

Figure 6-18. Heat Transfer From 0 to 1.52 m (0 to 60 in.), Run 44529A

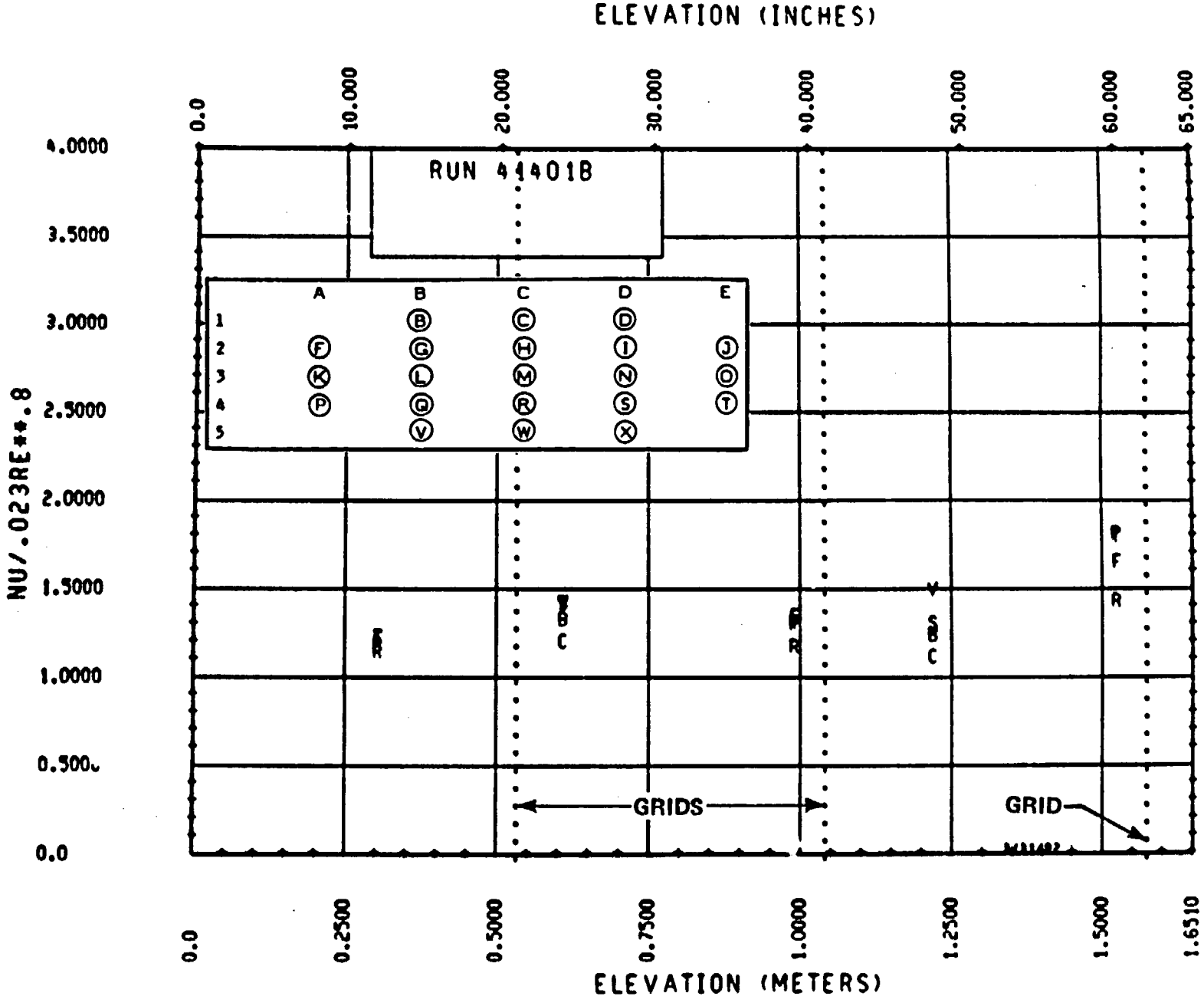

Figure 6-19. Heat Transfer From 0 to 1.52 m (0 to 60 in.), Run 41401B

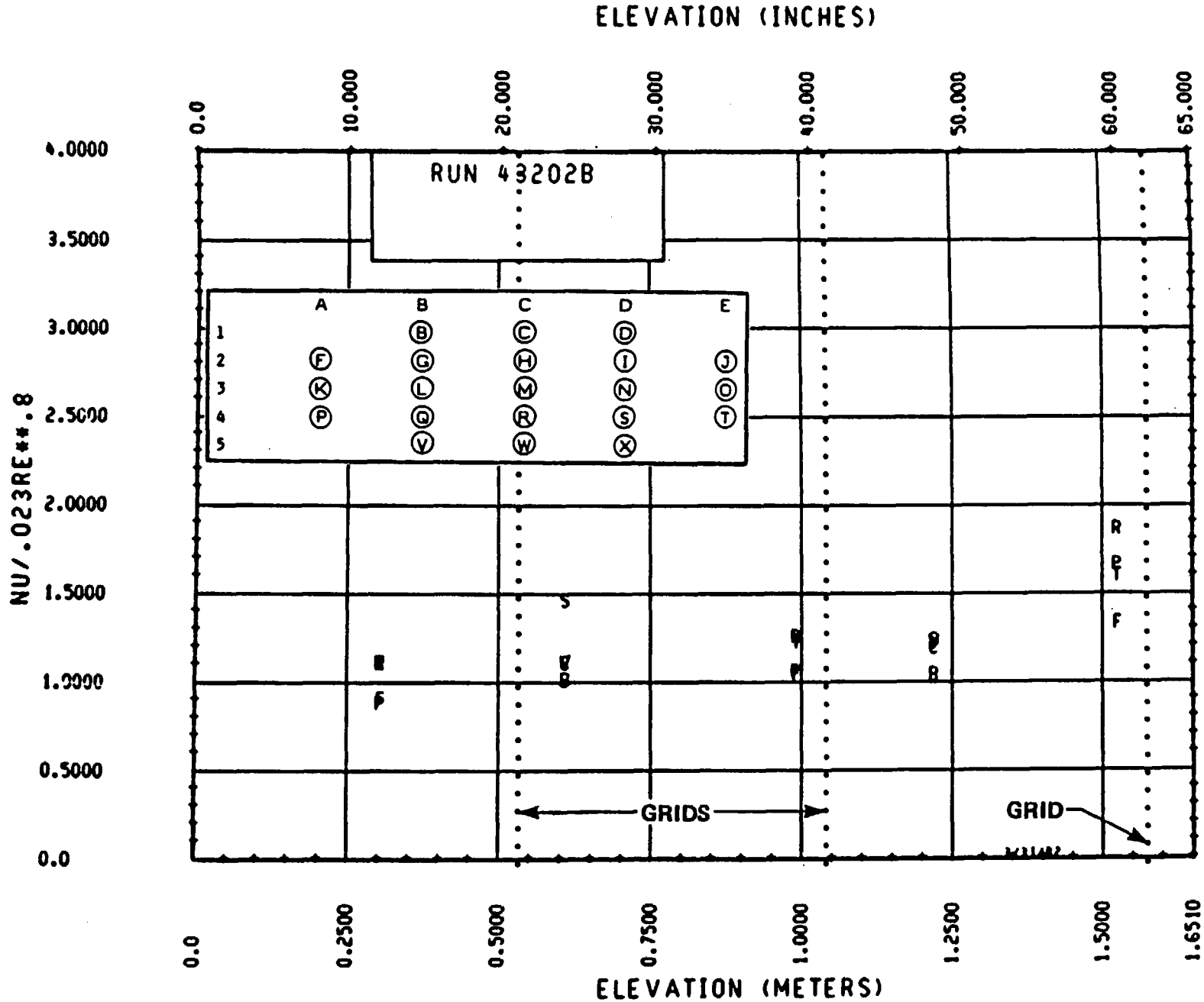

Figure 6-20. Heat Transfer From 0 to 1.52 m (0 to 60 in.), Run 43202B

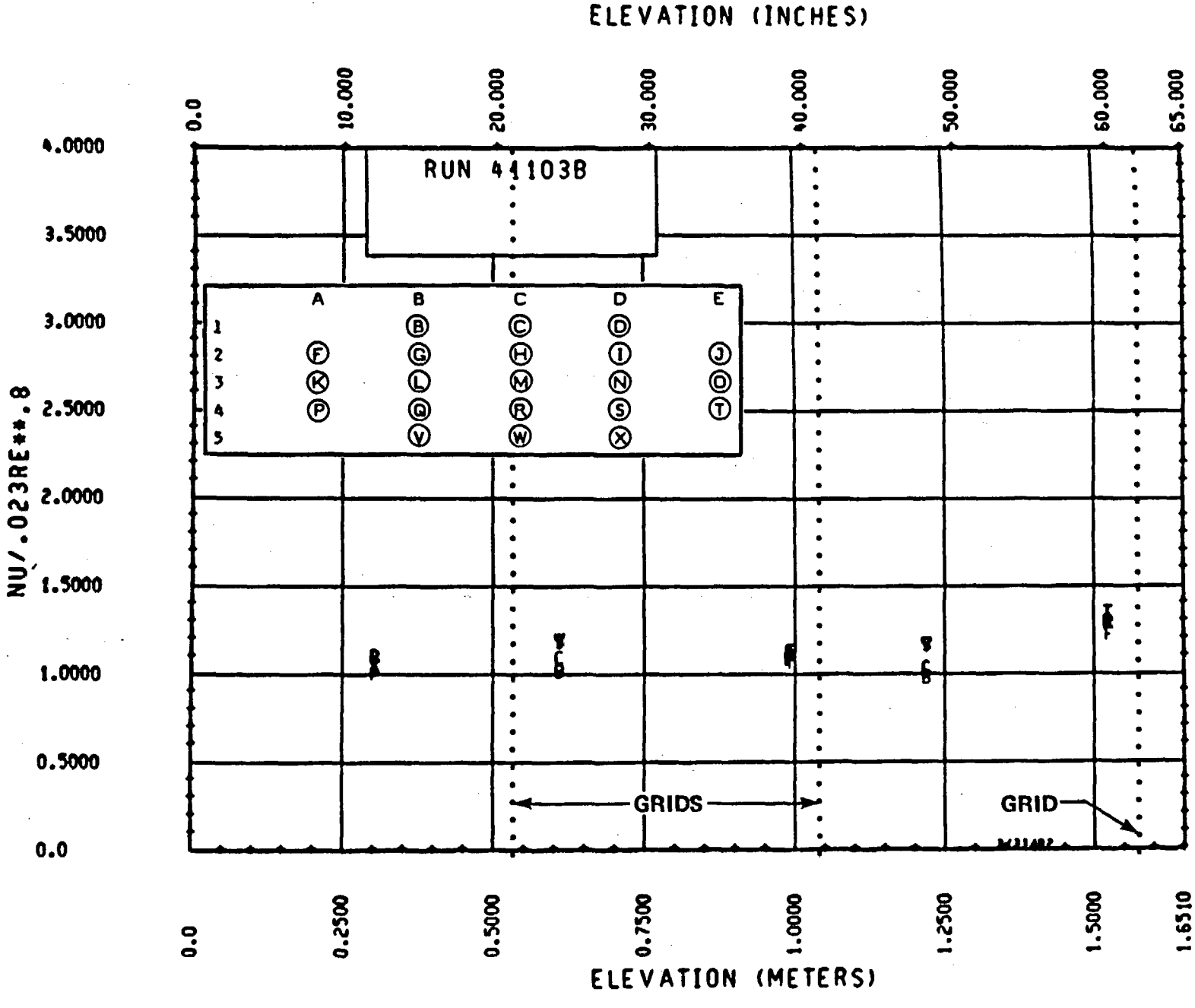

Figure 6-21. Heat Transfer From 0 to 1.52 m (0 to 60 in.), Run 41103B

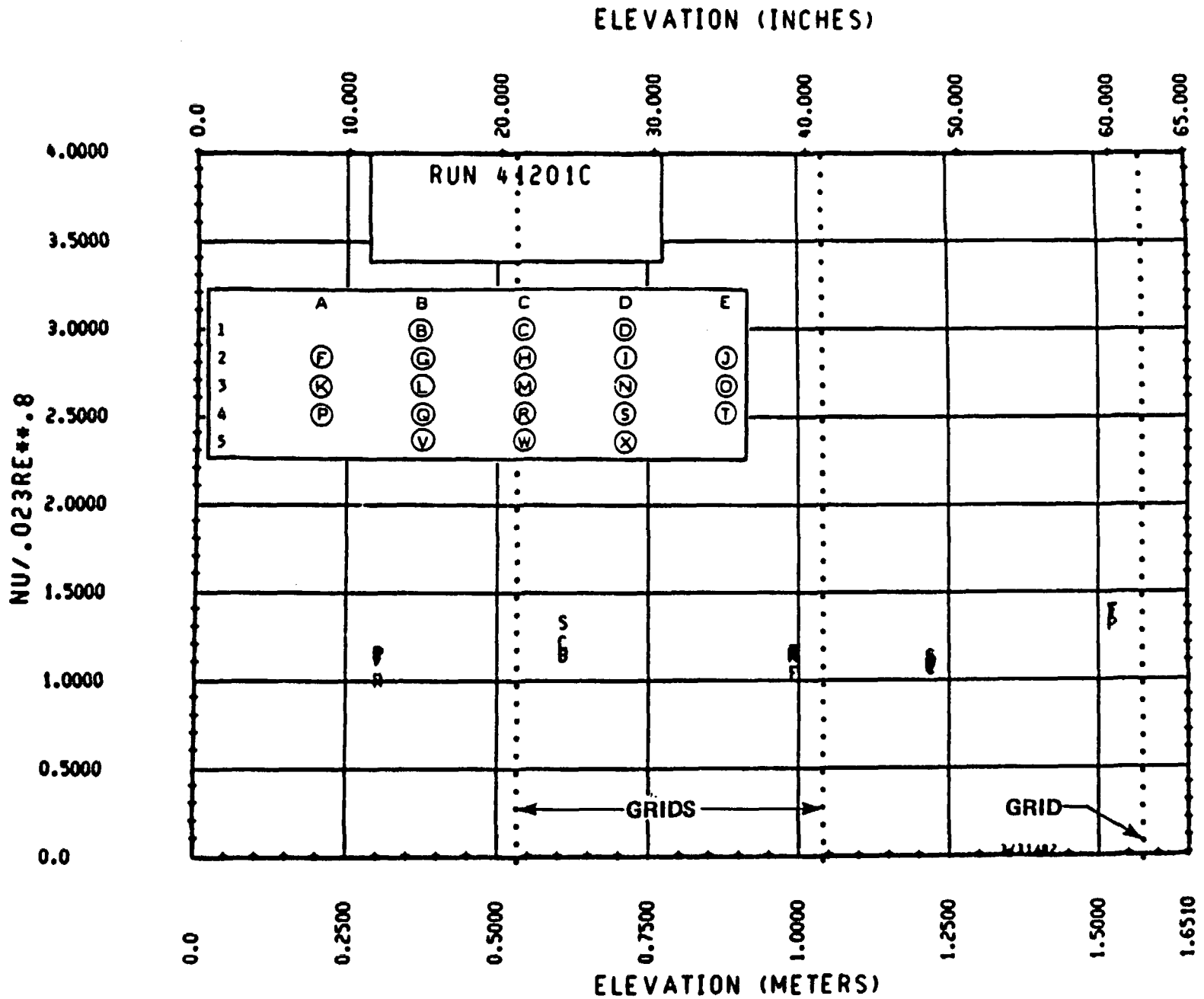

Figure 6-22. Heat Transfer From 0 to 1.52 m (0 to 60 in.), Run 41201C

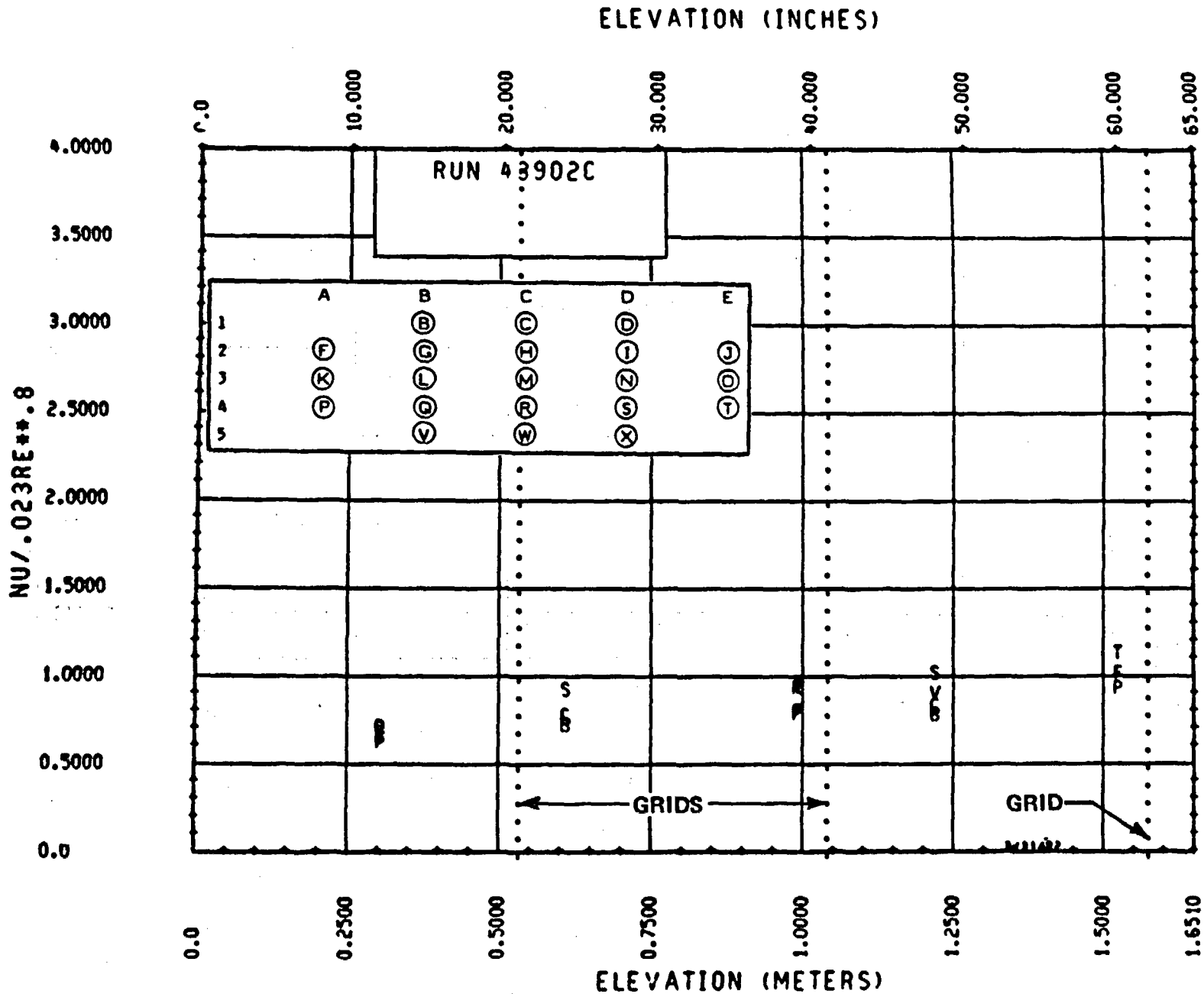

Figure 6-23. Heat Transfer From 0 to 1.52 m (0 to 60 in.), Run 43902C

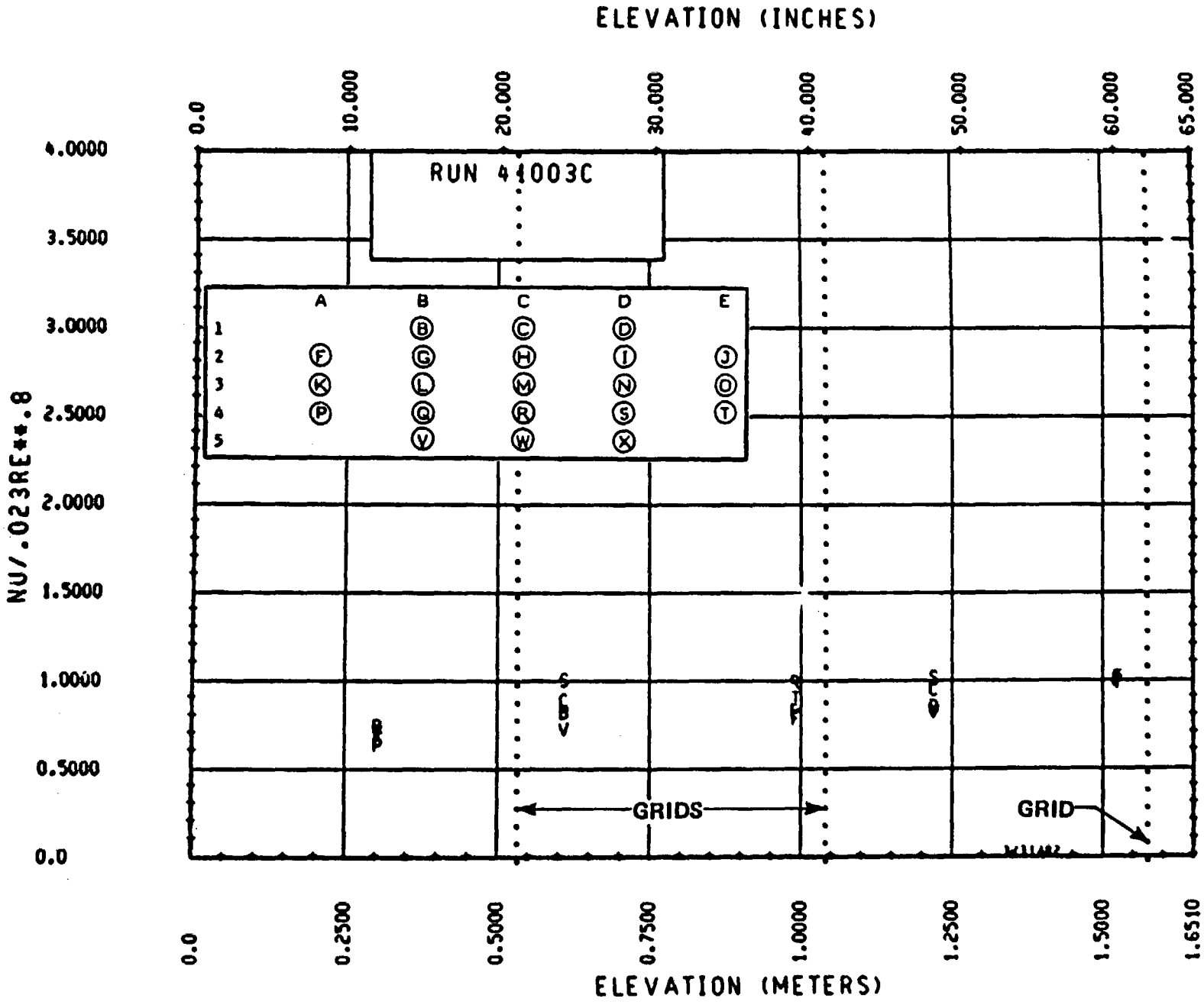

Figure 6-24. Heat Transfer From 0 to 1.52 m (0 to 60 in.), Run 41003C

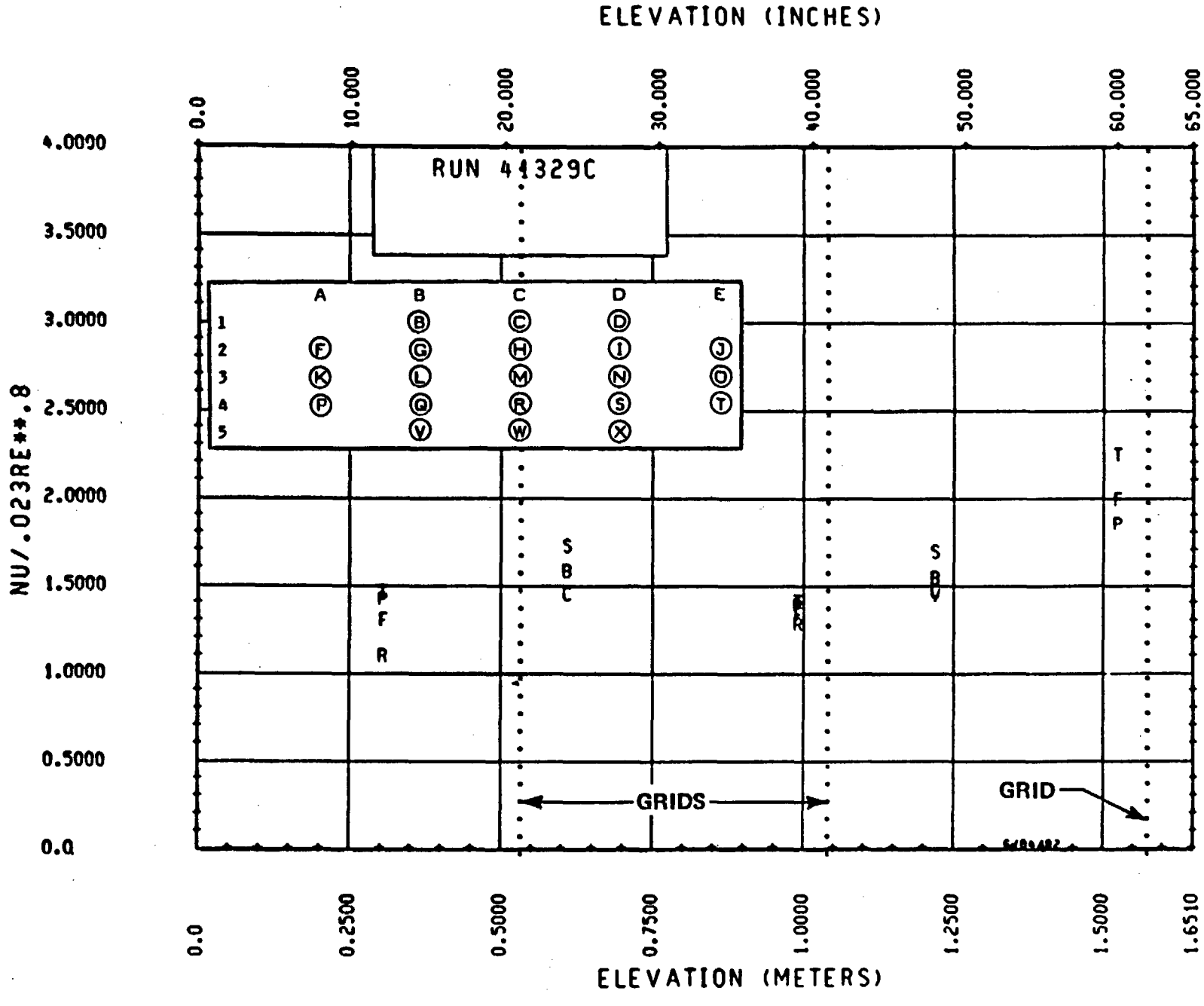

Figure 6-25. Heat Transfer From 0 to 1.52 m (0 to 60 in.), Run 41329C

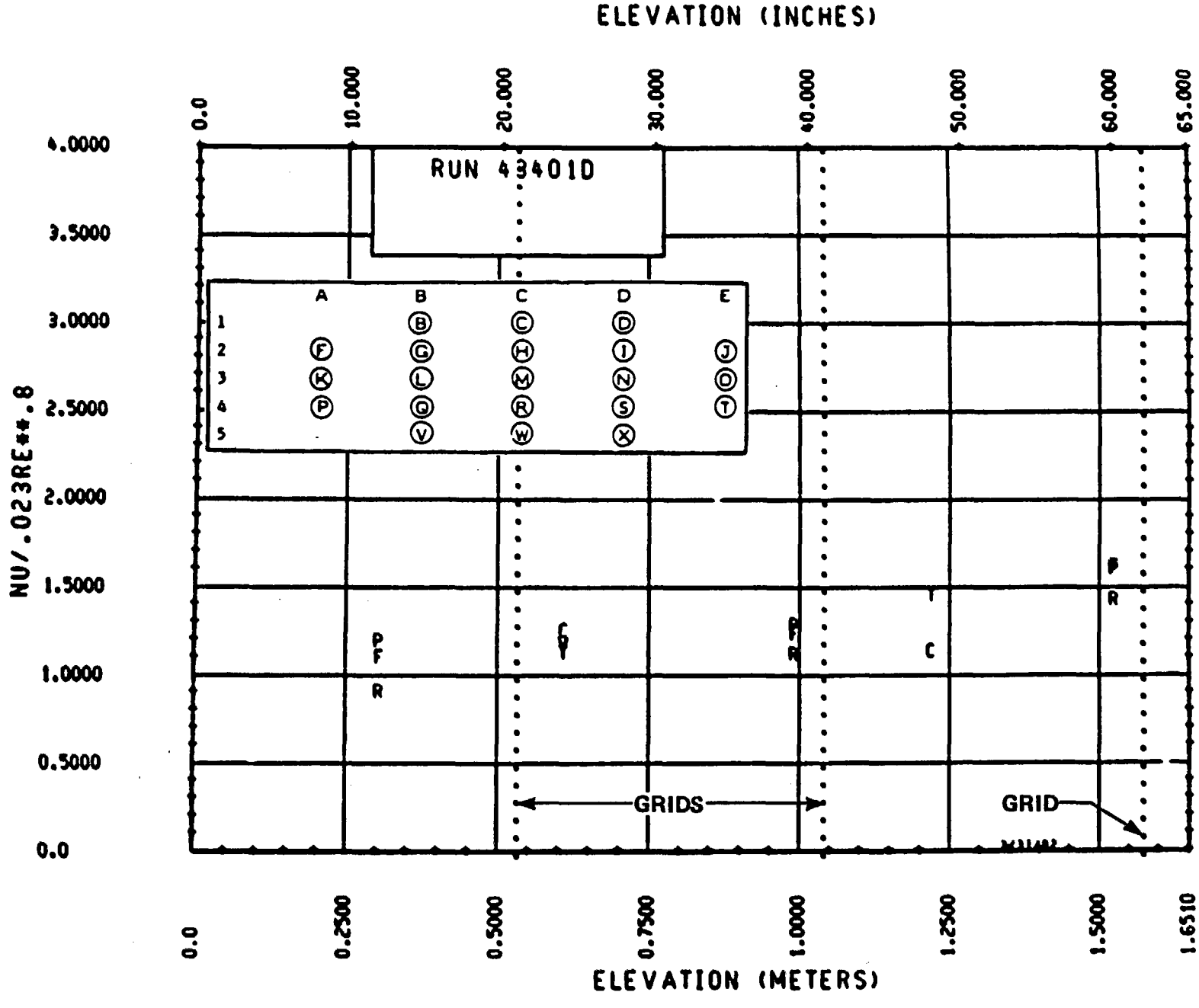

Figure 6-26. Heat Transfer From 0 to 1.52 m (0 to 60 in.), Run 43401D

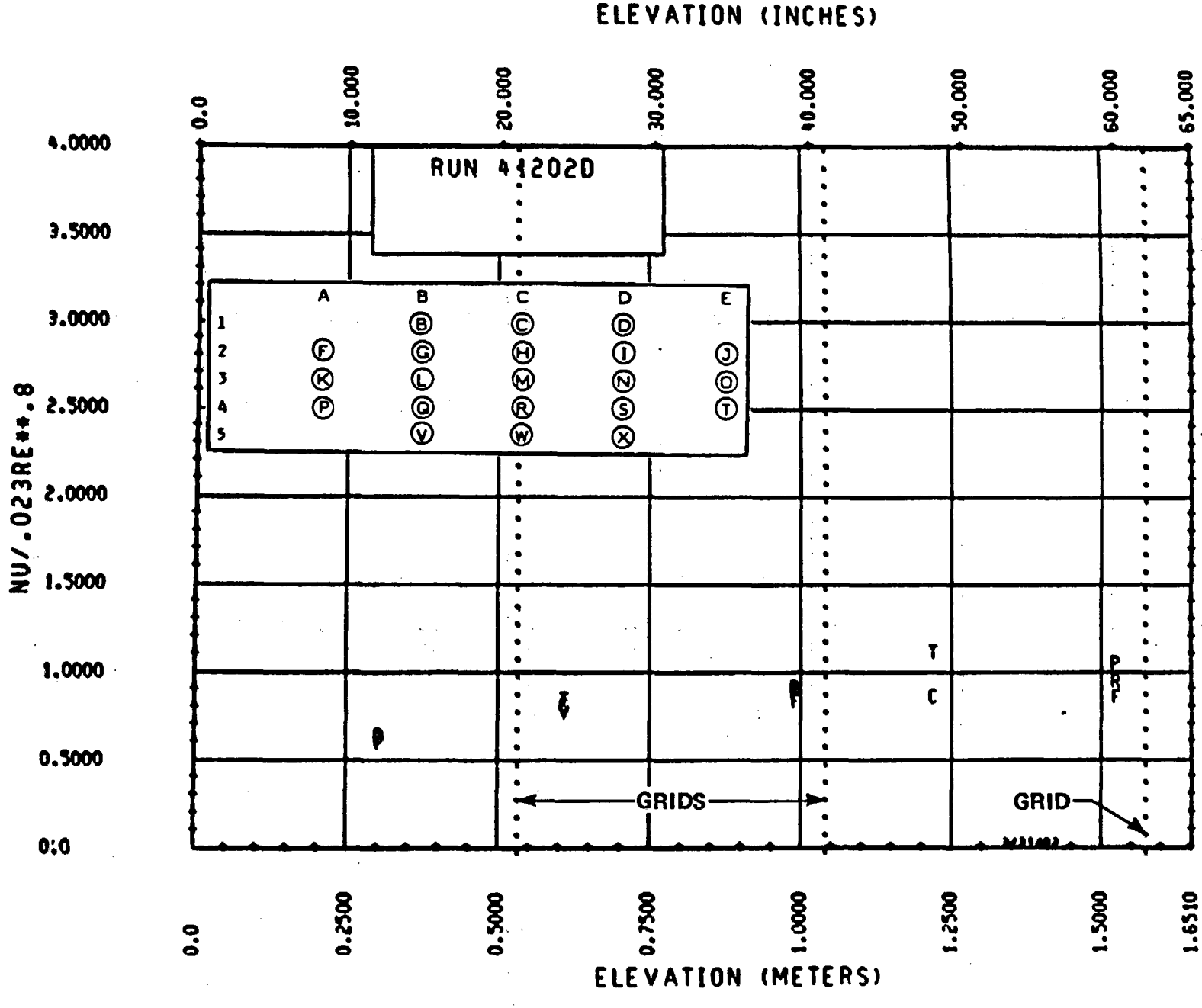

Figure 6-27. Heat Transfer From 0 to 1.52 m (0 to 60 in.), Run 41202D

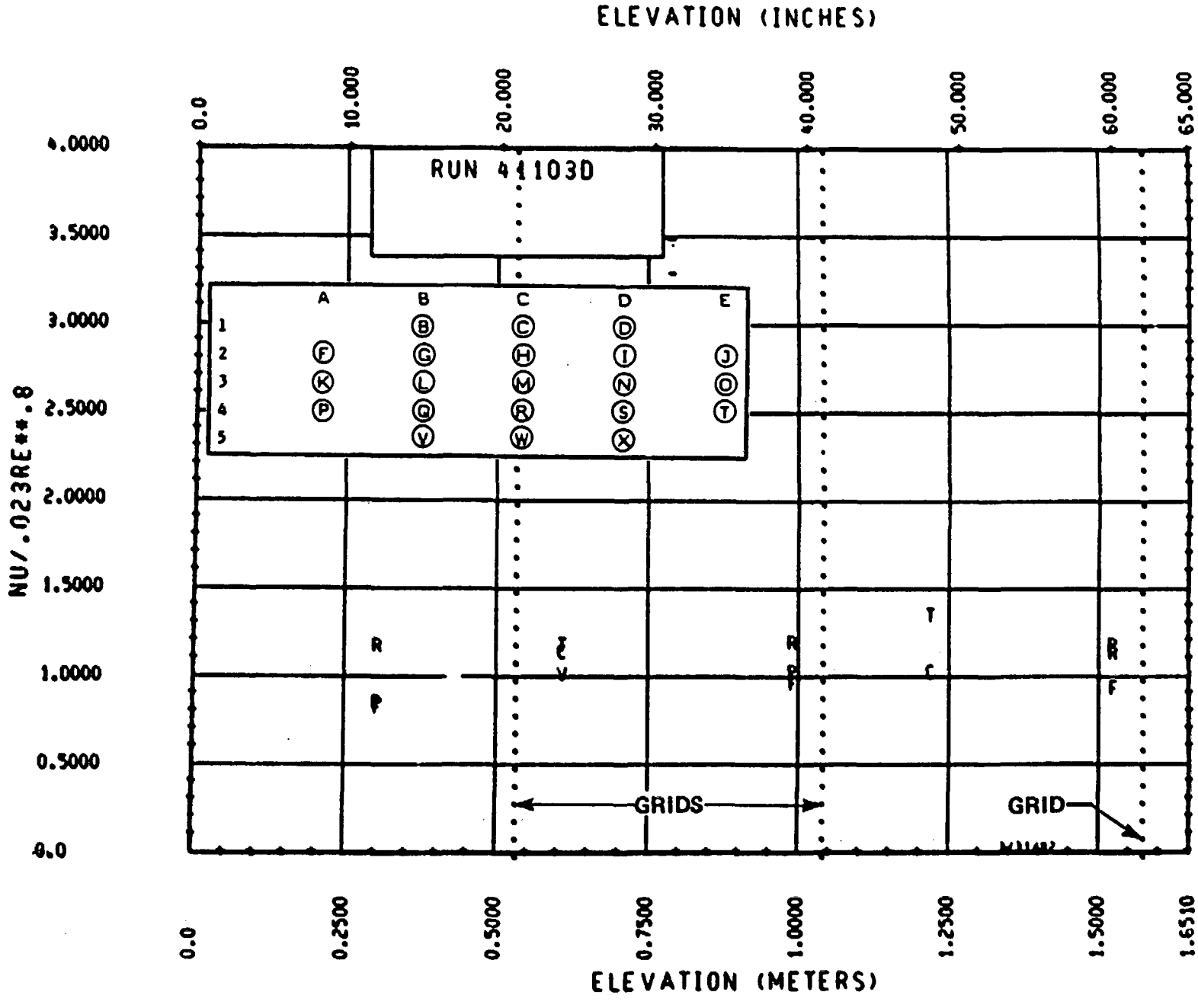

Figure 6-28. Heat Transfer From 0 to 1.52 m (0 to 60 in.), Run 41103D

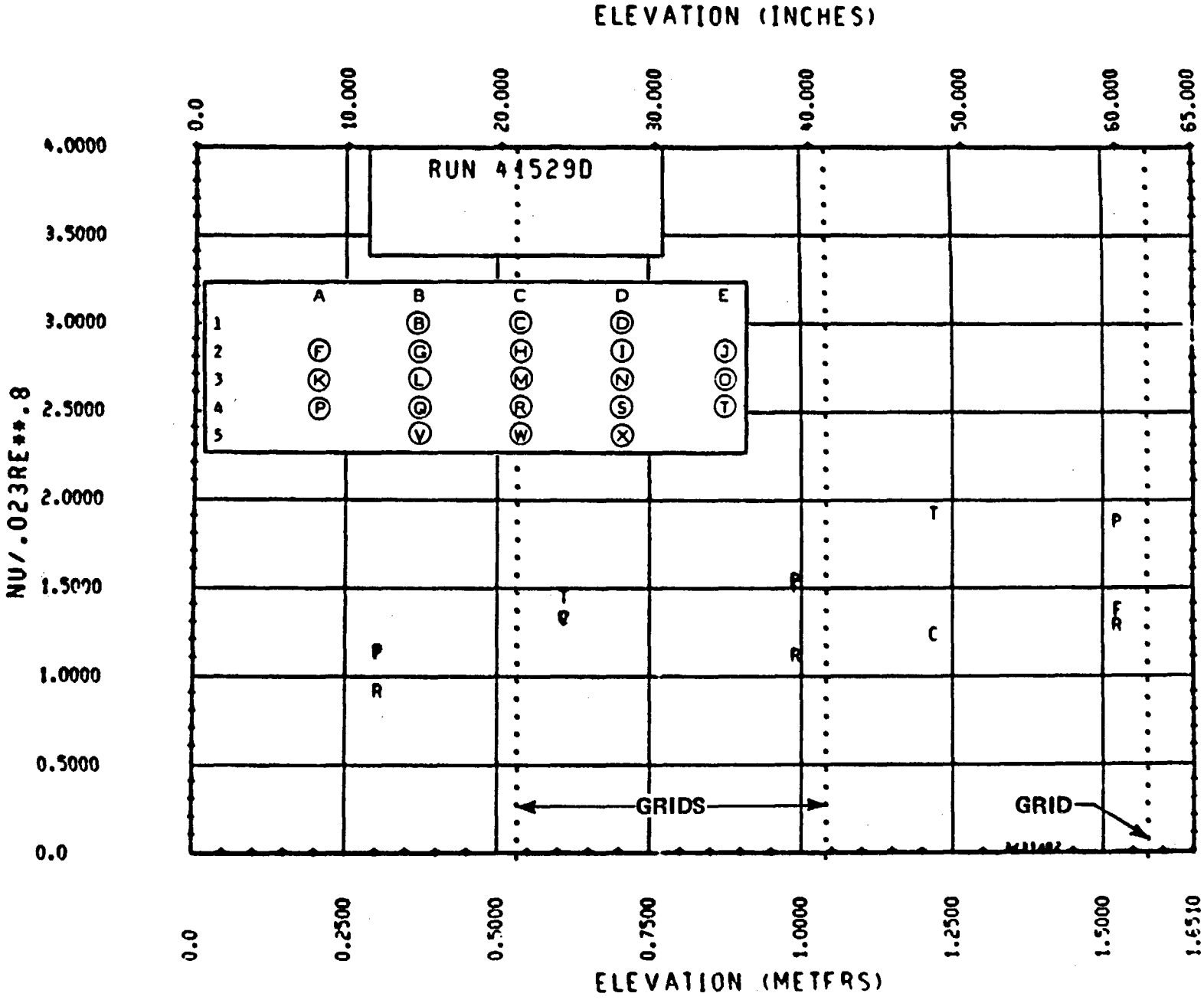

Figure 6-29. Heat Transfer From 0 to 1.52 m (0 to 60 in.), Run 41529D

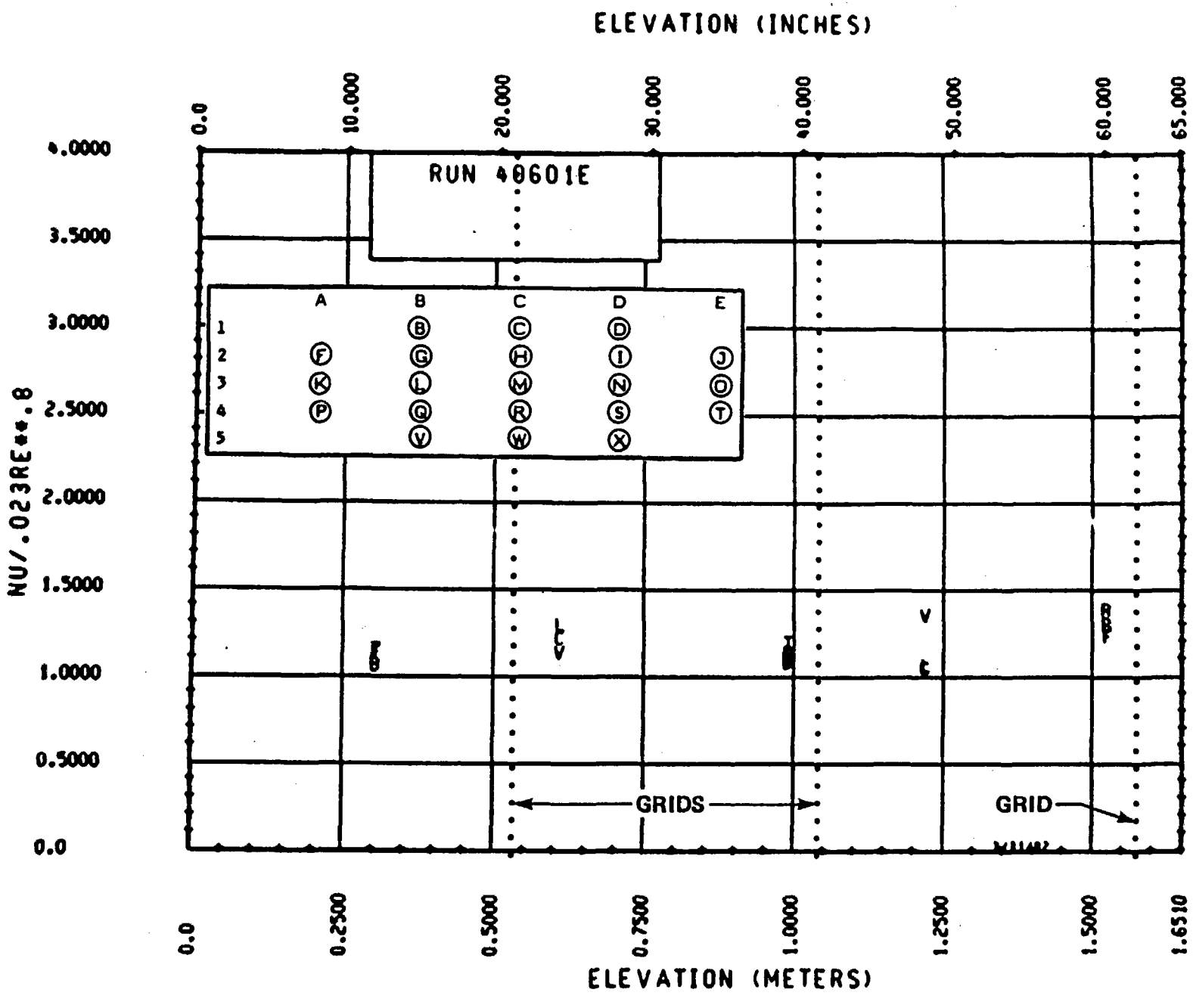

Figure 6-30. Heat Transfer From 0 to 1.52 m (0 to 60 in.), Run 40601E

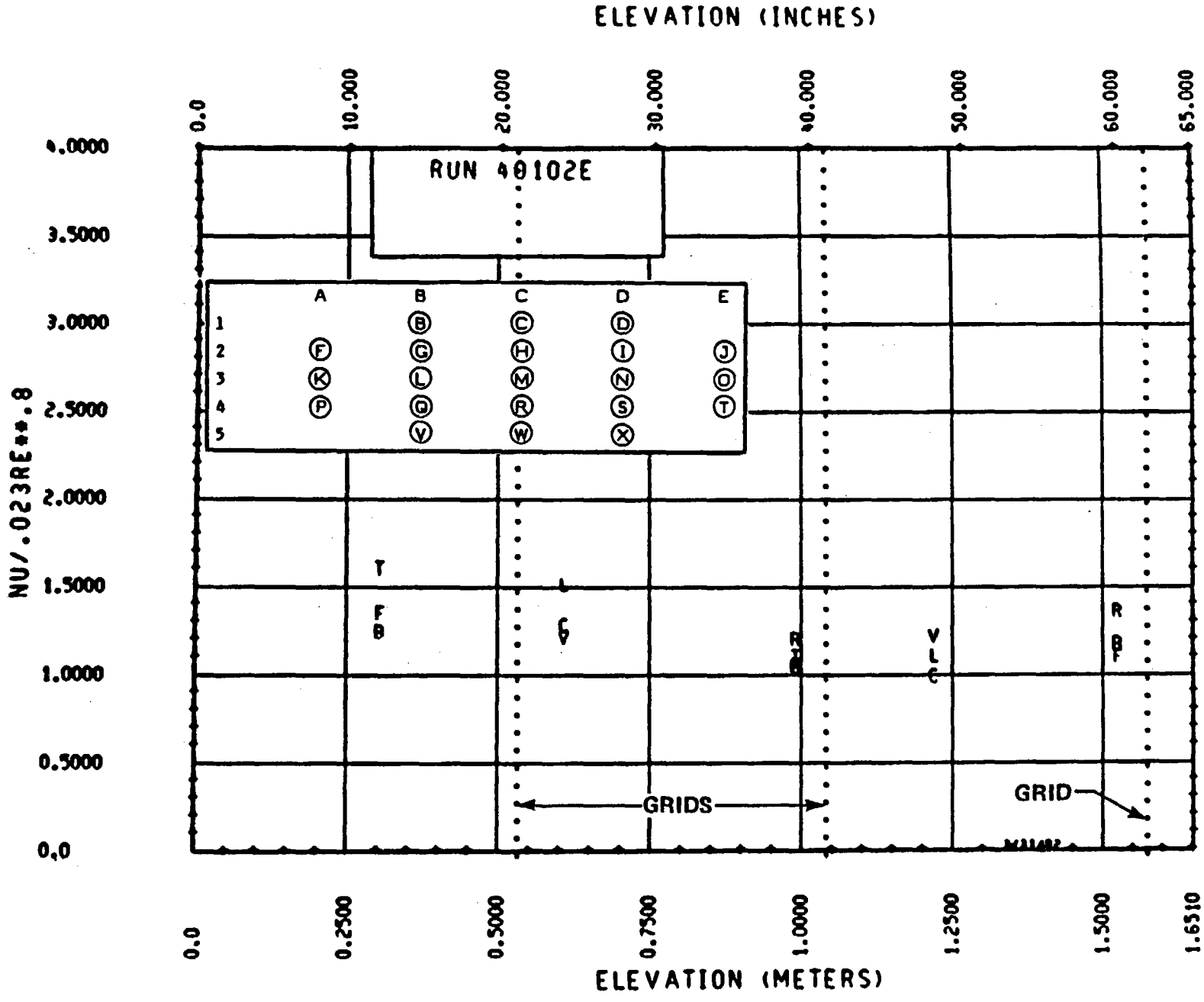

Figure 6-31. Heat Transfer From 0 to 1.52 m (0 to 60 in.), Run 40102E

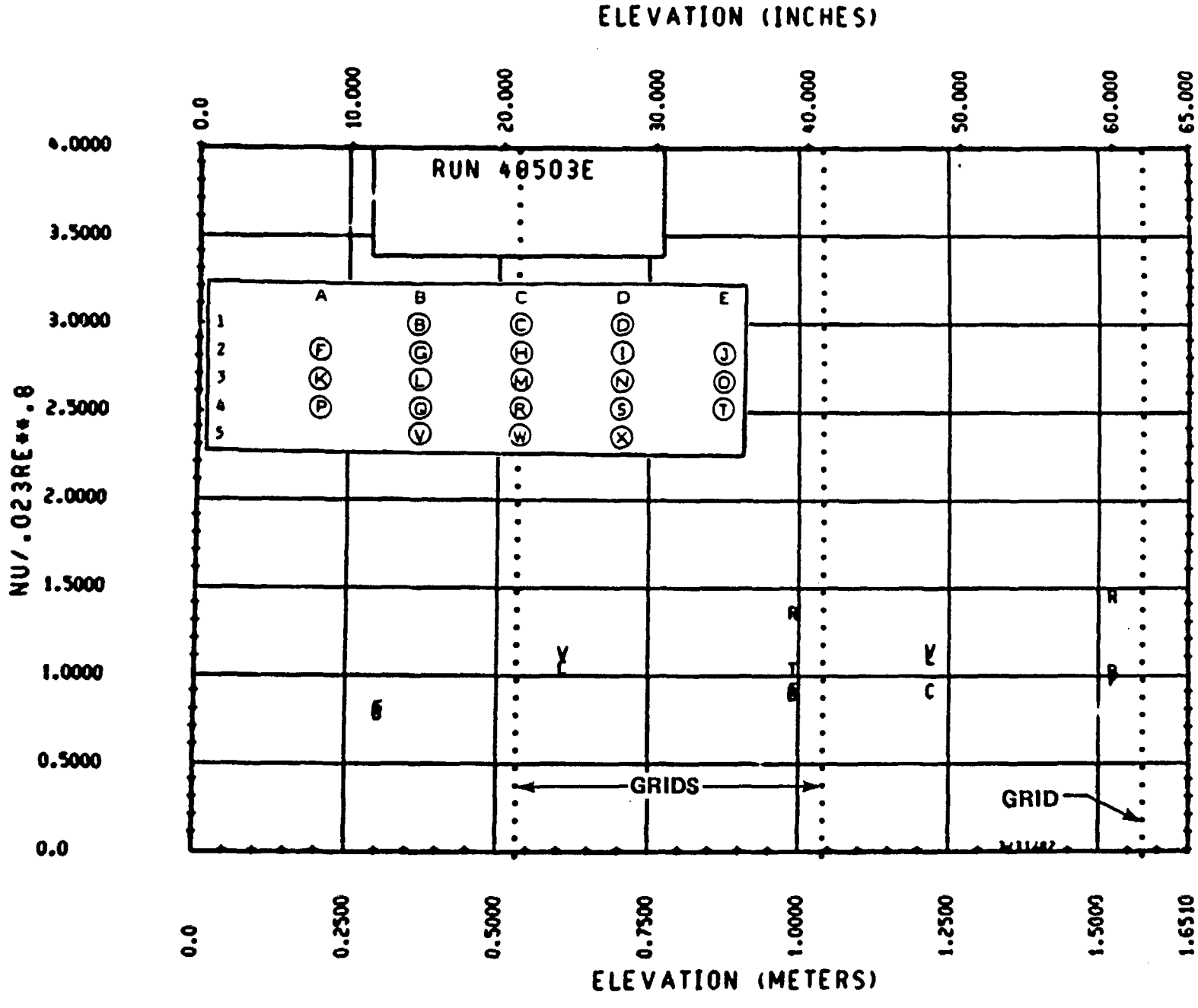

Figure 6-32. Heat Transfer From 0 to 1.52 m (0 to 60 in.), Run 40503E

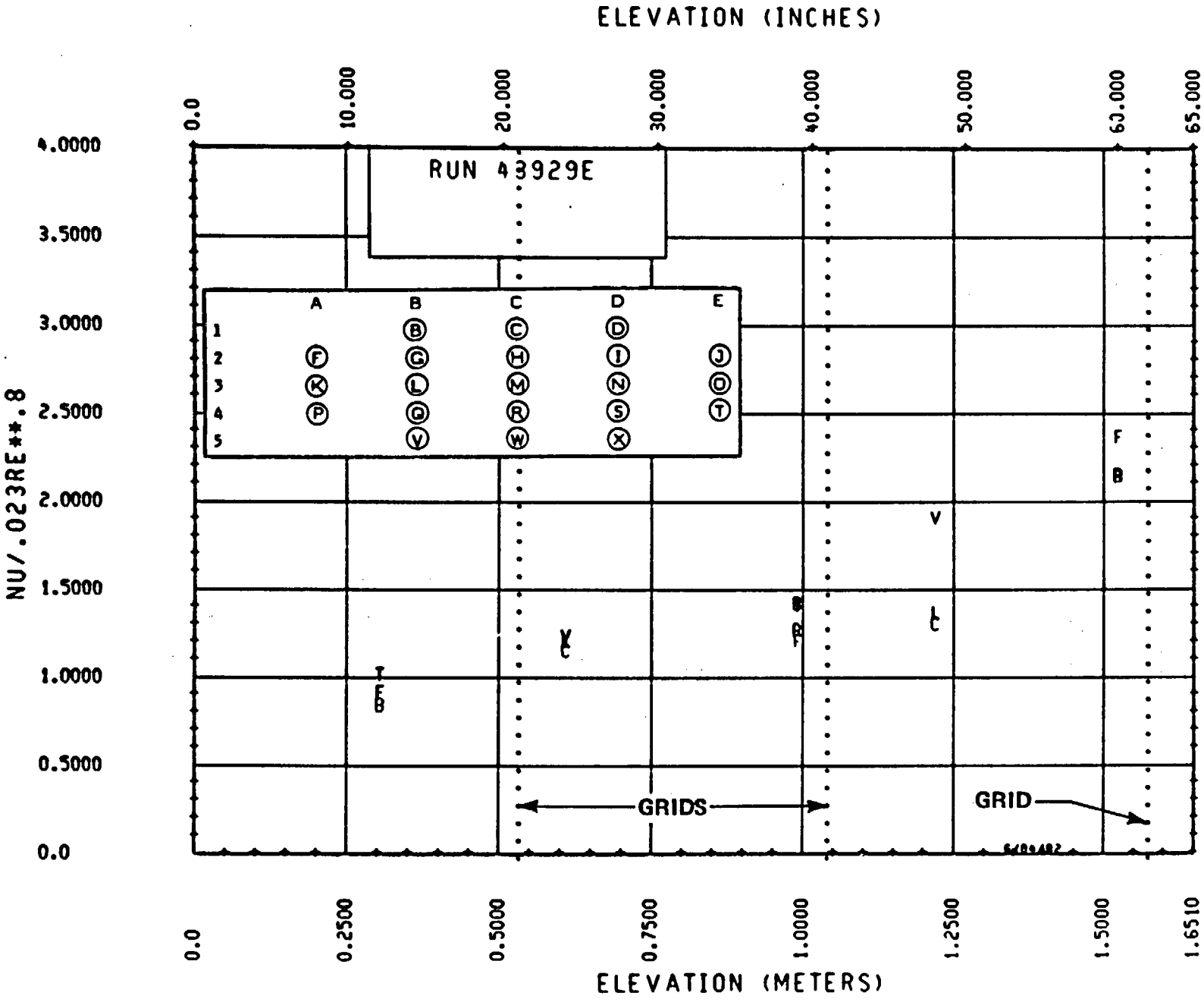

Figure 6-33. Heat Transfer From 0 to 1.52 m (0 to 60 in.), Run 43929E

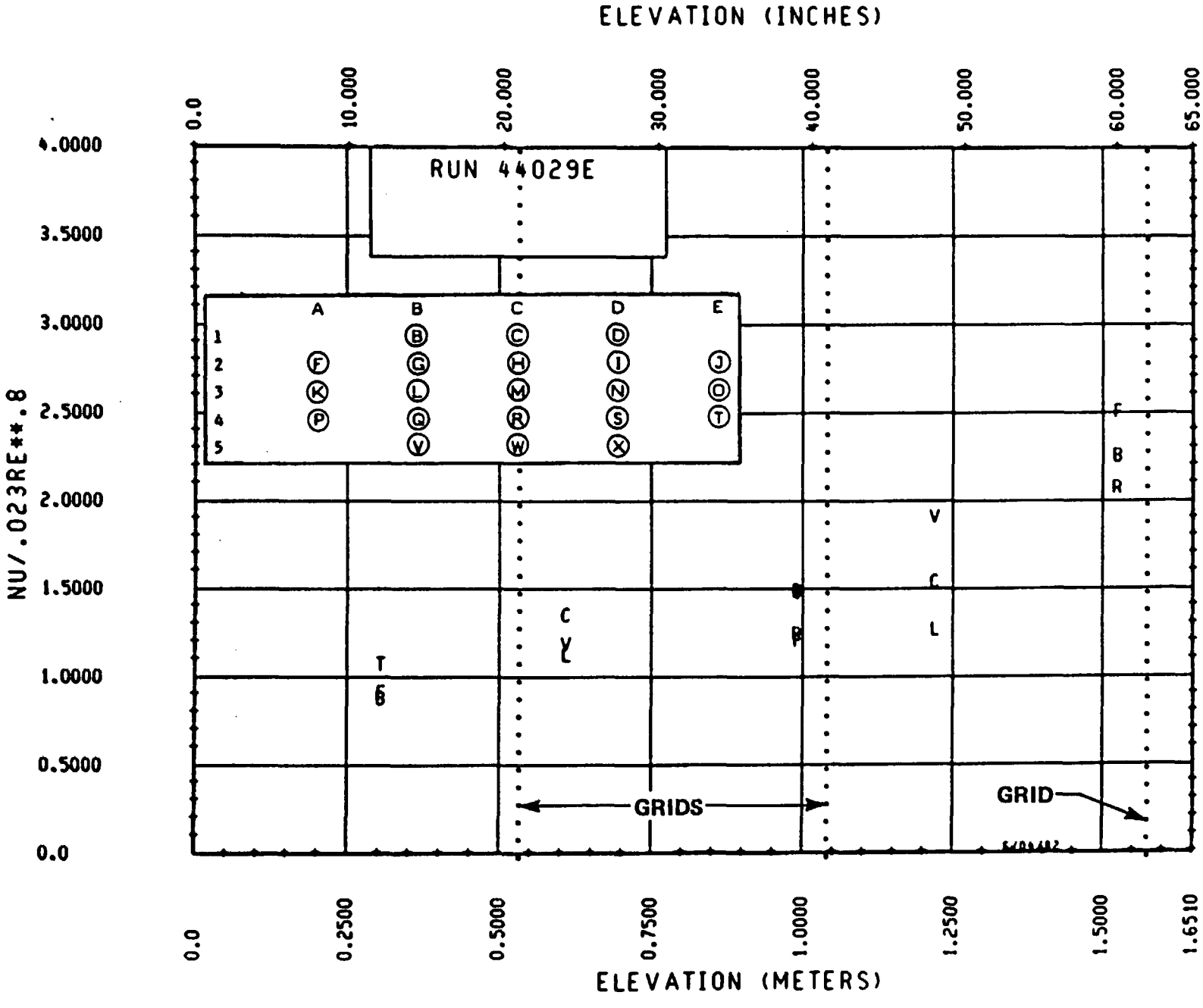

Figure 6-34. Heat Transfer From 0 to 1.52 m (0 to 60 in.), Run 44029E

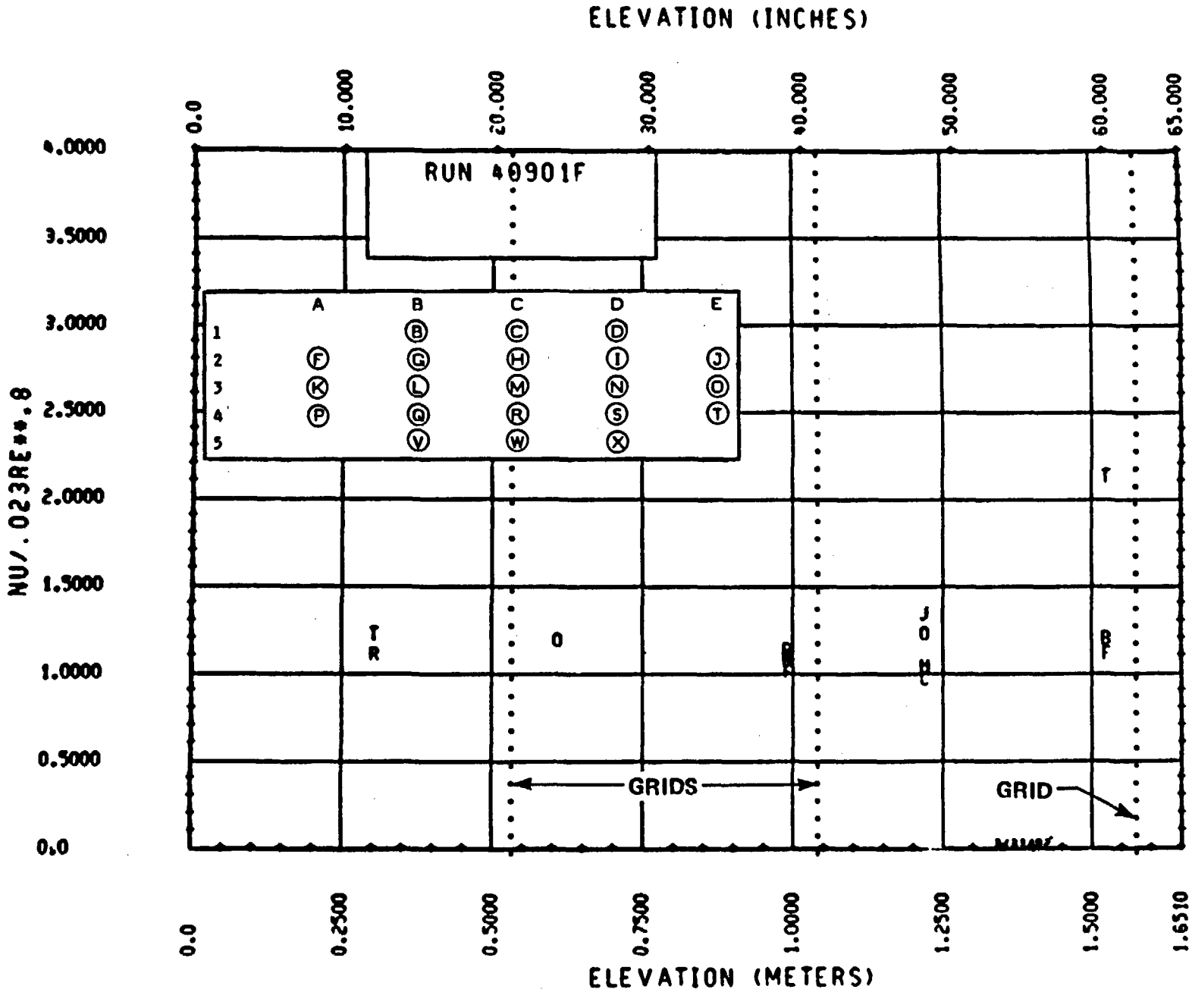

Figure 6-35. Heat Transfer From 0 to 1.52 m (0 to 60 in.), Run 40901F

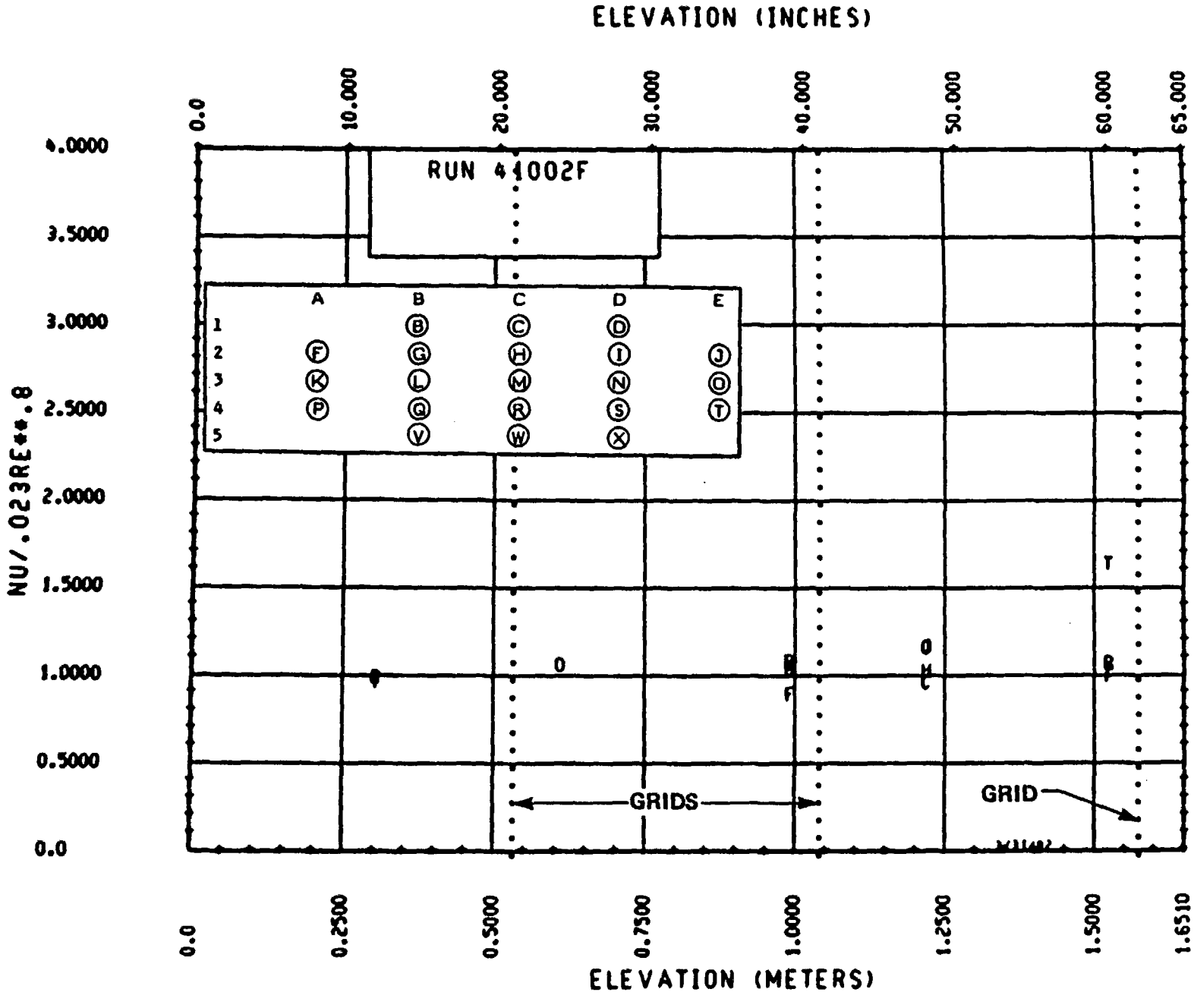

Figure 6-36. Heat Transfer From 0 to 1.52 m (0 to 60 in.), Run 41002F

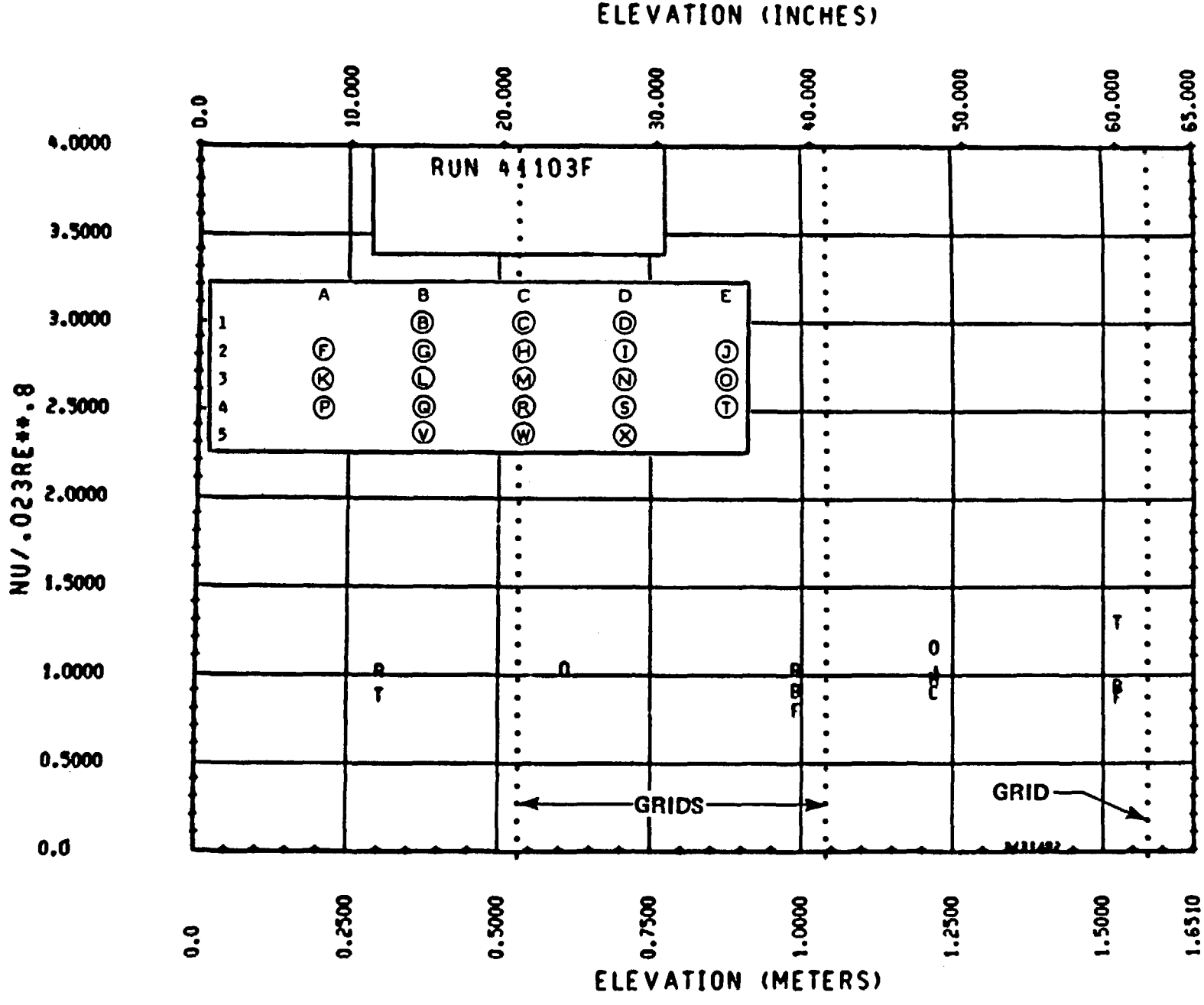

Figure 6-37. Heat Transfer From 0 to 1.52 m (0 to 60 in.), Run 41103F

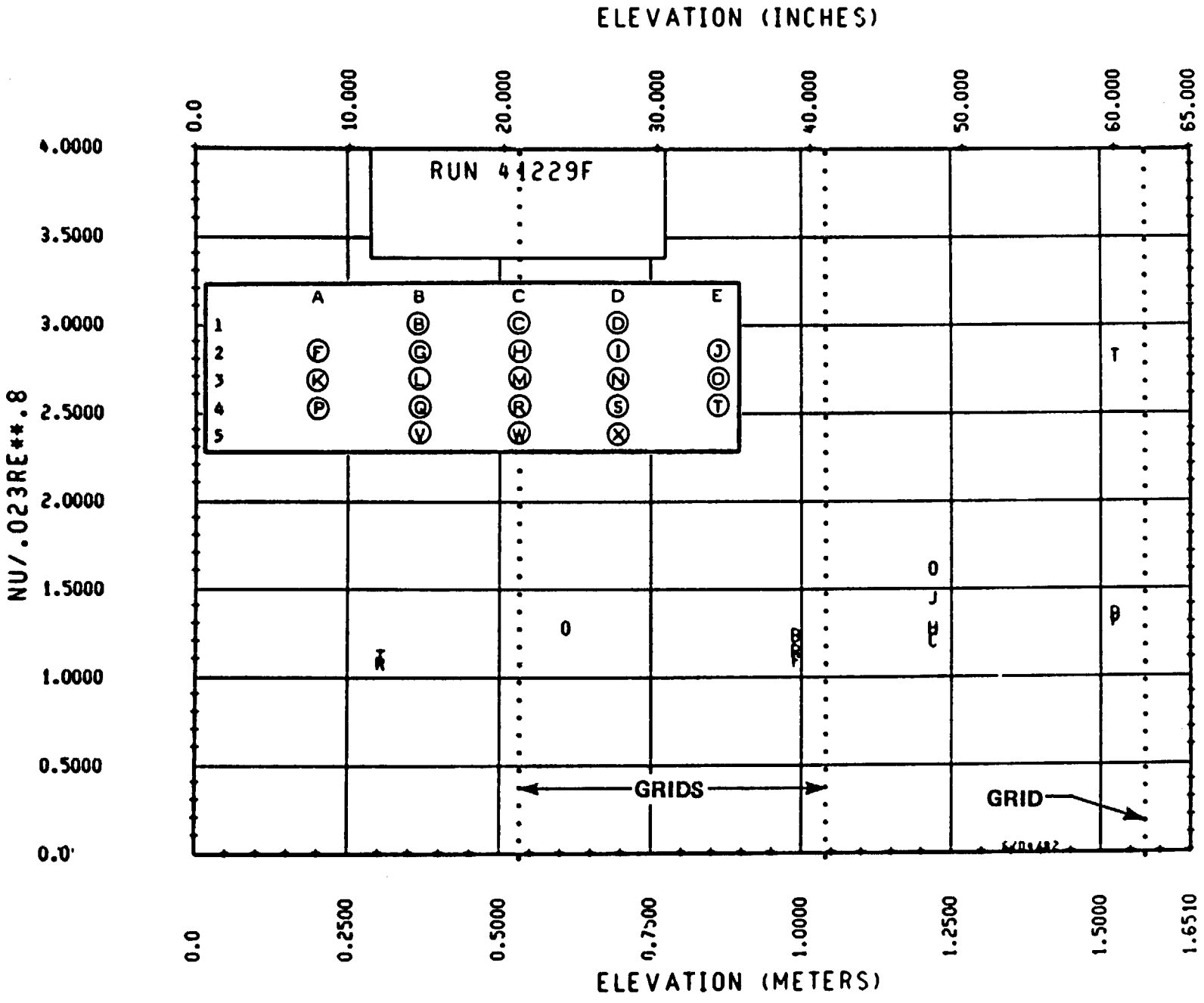

Figure 6-38. Heat Transfer From 0 to 1.52 m (0 to 60 in.), Run 41229F

$$2000 < Re < 2500, \frac{Nu}{Pr^{1/3}} = -8.799 + 0.00833\ Re$$ (linear interpolation between above two correlations)

Each individual 21-rod bundle heater rod is designated by a letter as shown in the figures.

As shown in these figures, the data for both corner and inside rods generally "collapse" to similar values which are usually greater than the reference correlation utilizing the COBRA-code-calculated Reynolds number. The heat transfer data below 1.52 m (60 in.) are generally independent of elevation, although the data at the 1.52 m (60 in.) elevation are typically greater than data at the lower elevations for all tests. This increased heat transfer at the 1.52 m (60 in.) elevation may be attributed to the large quantity of steam temperature instruments (six) attached to the 1.57 m (62 in.) grid which is immediately downstream of the rod temperature measurements. Most of the tests (20 out of 23) provided a normalized heat transfer equal to or greater than 1.0.

The measured heat flux and rod temperature, the calculated vapor temperature, the Nusselt number, and the Reynolds number at each instrumentation location below 1.52 m (60 in.) for all valid steam cooling tests are given in appendix K.

6-13. Blocked Region Model Results

To determine the effects of flow blockage on rod bundle heat transfer, it was desired that the data in and above the blockage region be referenced to the corresponding unblocked data. The unblocked heat transfer data above the 1.52 m (60 in.) elevation, calculated in the same manner as that below the 1.52 m (60 in.) elevation, are plotted in figure 6-39 as a function of the Reynolds number. The Nusselt numbers above the 1.52 m (60 in.) elevation are generally higher than those below the 1.52 m (60 in.) elevation. It is believed that several factors contribute to the results above 1.52 m (60 in.), which are different from those below 1.52 m (60 in.). The COBRA-IV-I code does not allow for incorporation of individual rod axial power distribution and the heat loss from the 12 peripheral subchannels would have an integrated effect on both the vapor temperatures and the velocities, thereby affecting the results at the midplane elevations more than at the lower elevations. The COBRA-calculated flow conditions

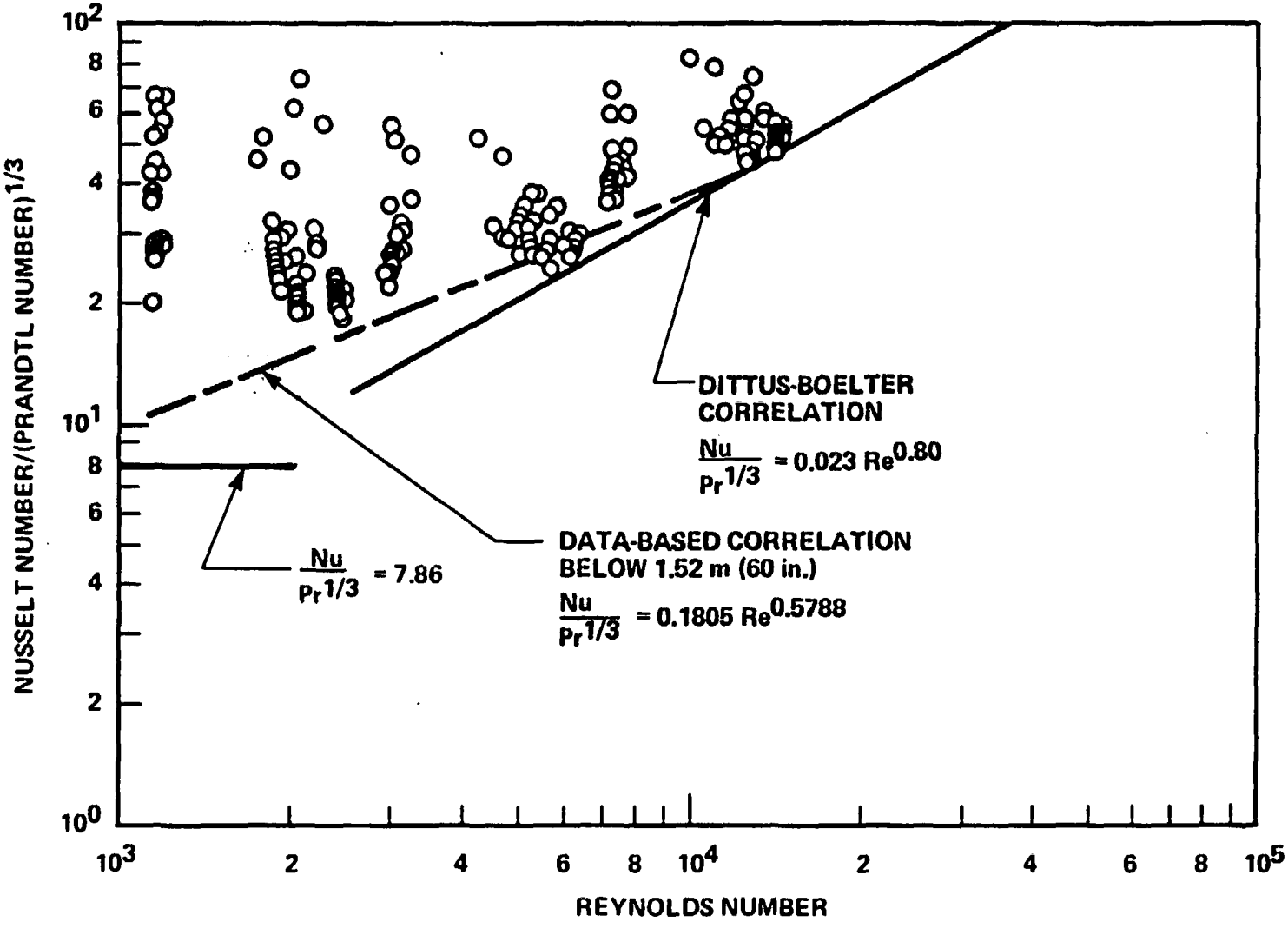

Figure 6-39. Nusselt Number Versus Reynolds Number for Configuration A, Above 1.52 m (60 in.)

for each of the different subchannels, as shown in figure 6-40 for run 44401A at 1.80 m (71 in.), indicate a significant variation in both the Reynolds number and the vapor temperature from subchannel to subchannel. The corner subchannel is in laminar flow while the center subchannel is in transition flow. However, in the process of averaging the flow conditions to obtain a rod-centered subchannel, the differences among the subchannels becomes much less significant, as shown in figure 6-41.

The Nusselt numbers as normalized to the previous correlations for all the valid steam cooling tests are plotted as a function of elevation in figures 6-42 through 6-64.

As shown in figure 6-42 for run 44401A, the corner heater rods have a greater normalized heat transfer than the inside rods. However, by increasing the bundle Reynolds number from 4790 for run 44401A to 11590 for run 44303A, the differences between the corner rods and the inside rods become much less significant, as shown in figure 6-43. This result may be attributed to the flow associated with each heater rod. In run 44401A, the corner rod is calculated by COBRA to be in laminar flow ($Re < 2000$) while the inside rod is in transition flow ($Re > 2000$); however, in run 44303A, the corner rod is in transition flow while the inside rod is in turbulent flow ($Re > 10000$). If this situation actually exists in the bundle, the thermal response of the heater rods could be affected more by the combination of laminar and transition flows than by the combination of transition and turbulent flows. In runs 44401A and 44303A, the normalized heat transfer is independent of elevation between the grids at 1.57 and 2.11 m (62 and 83 in.). The heat transfer does increase downstream of the grid located at 2.11 m (83 in.).

In the coplanar blockage tests of configurations B and C, the normalized heat transfer data downstream of the blockage were generally greater than data upstream of the blockage, as shown in figures 6-45 through 6-51. The heat transfer data downstream of the coplanar blockage without flow bypass (configuration C) were greater than data with the flow bypass (configuration B). The improvement in the heat transfer behind the coplanar blockage decreases with increased distance downstream of the blockage and also decreases with increased Reynolds number.

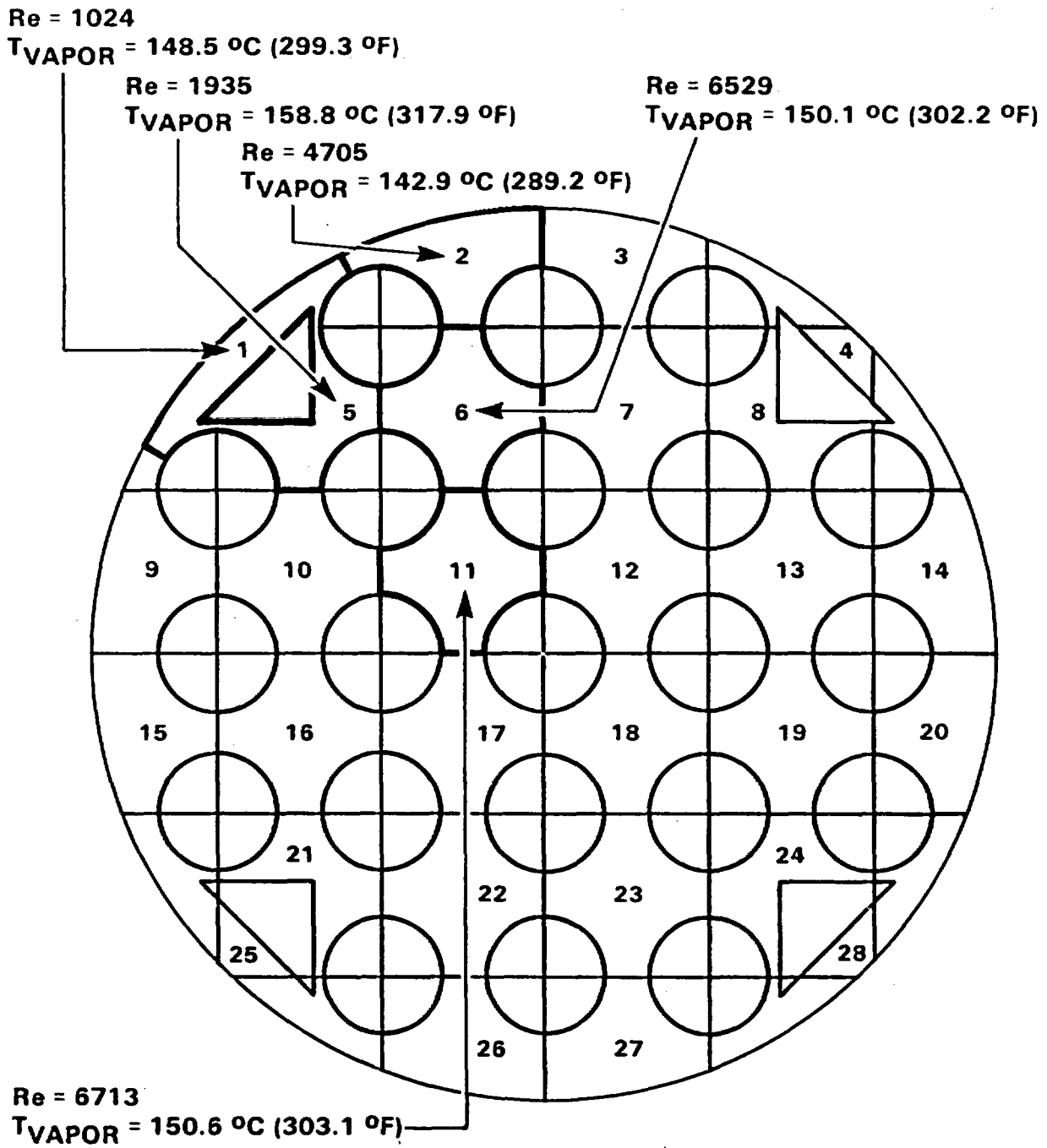

Figure 6-40. COBRA Subchannel Reynolds Number and Vapor Temperature at 1.80 m (71 in.), Run 44401A

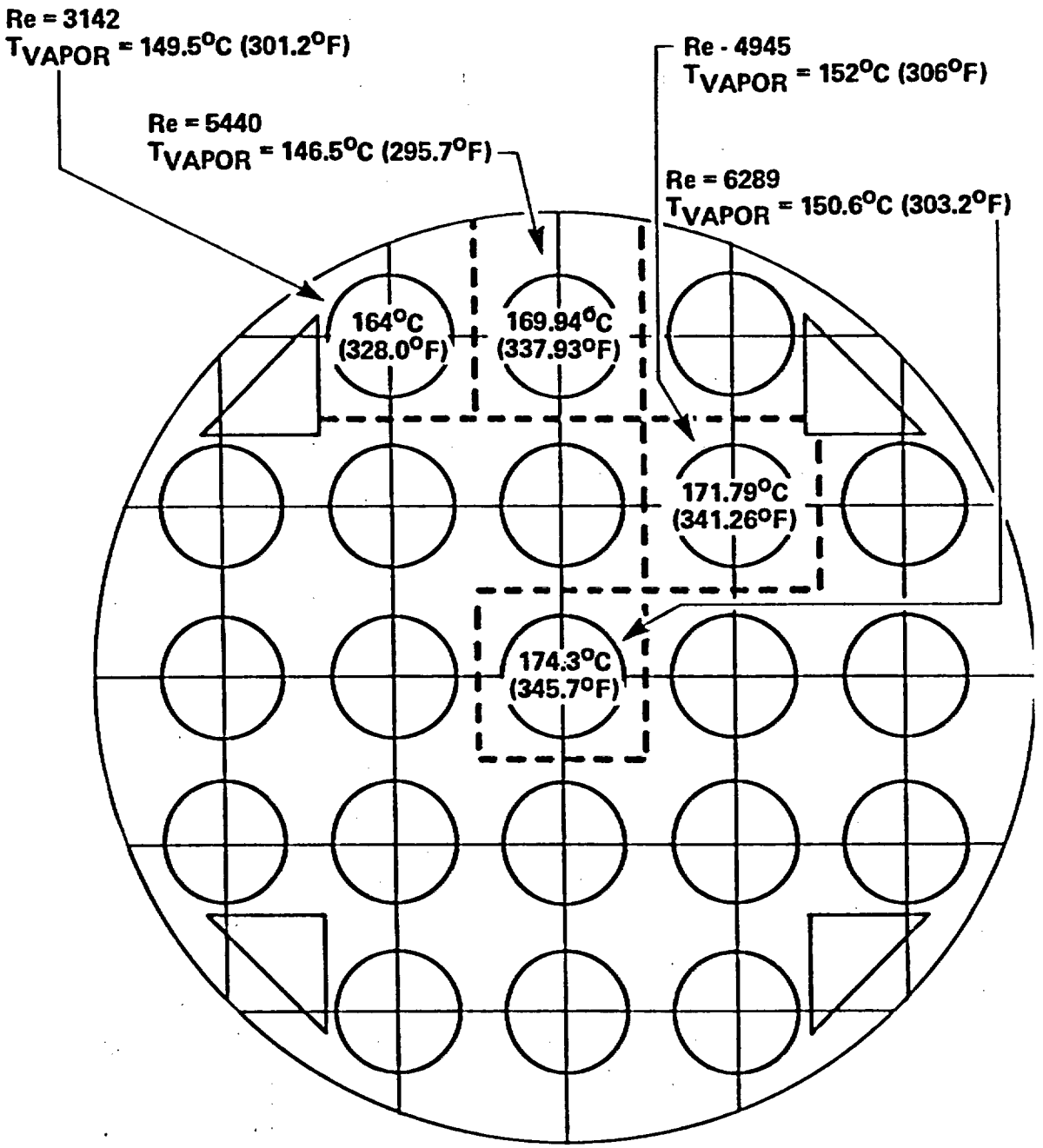

Figure 6-41. COBRA Averaged Subchannel Vapor and Measured Heater Rod Temperatures at 1.80 m (71 in.), Run 44401A

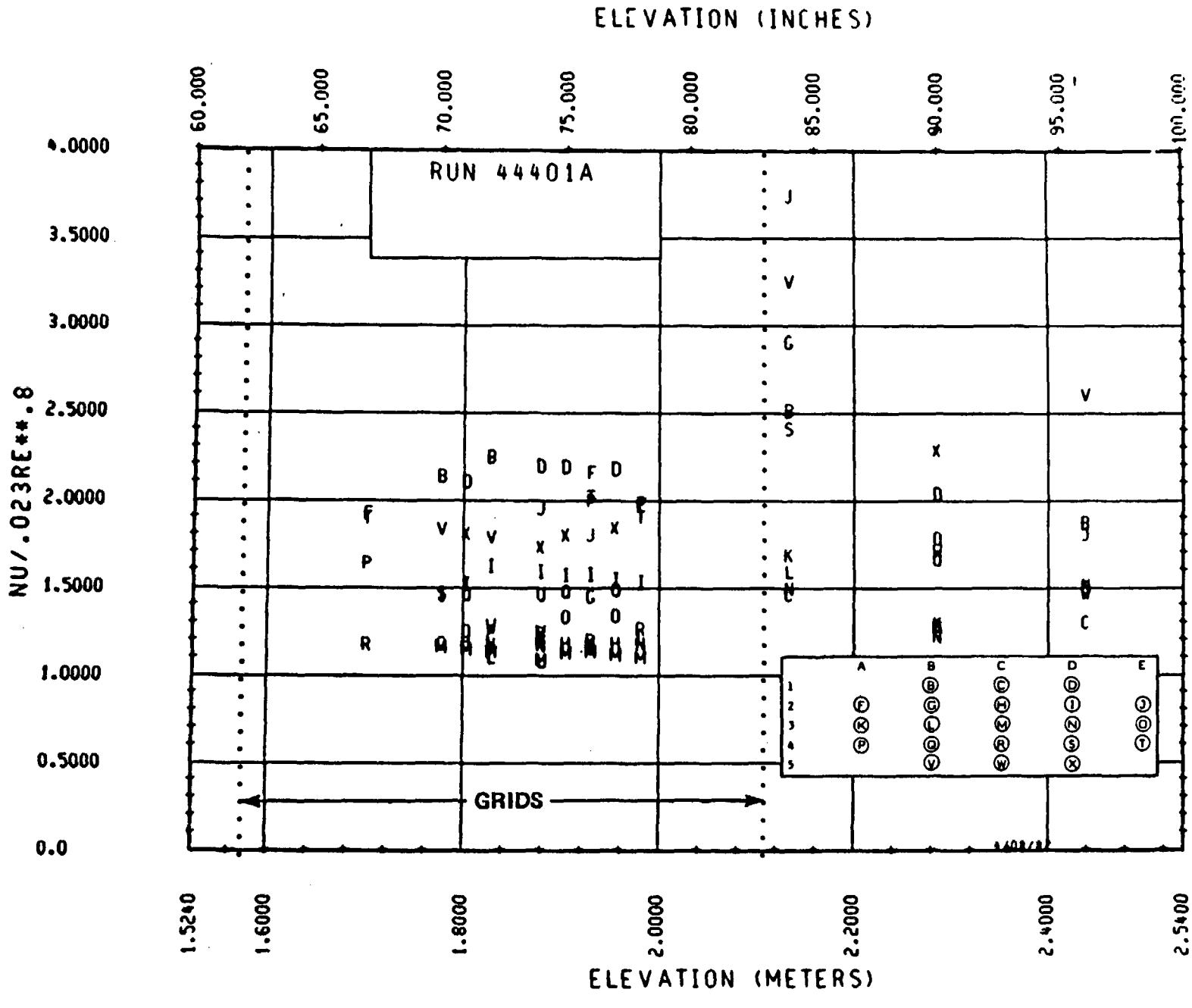

Figure 6-42. Heat Transfer From 1.52 to 2.44 m (60 to 96 in.) Run 44401A

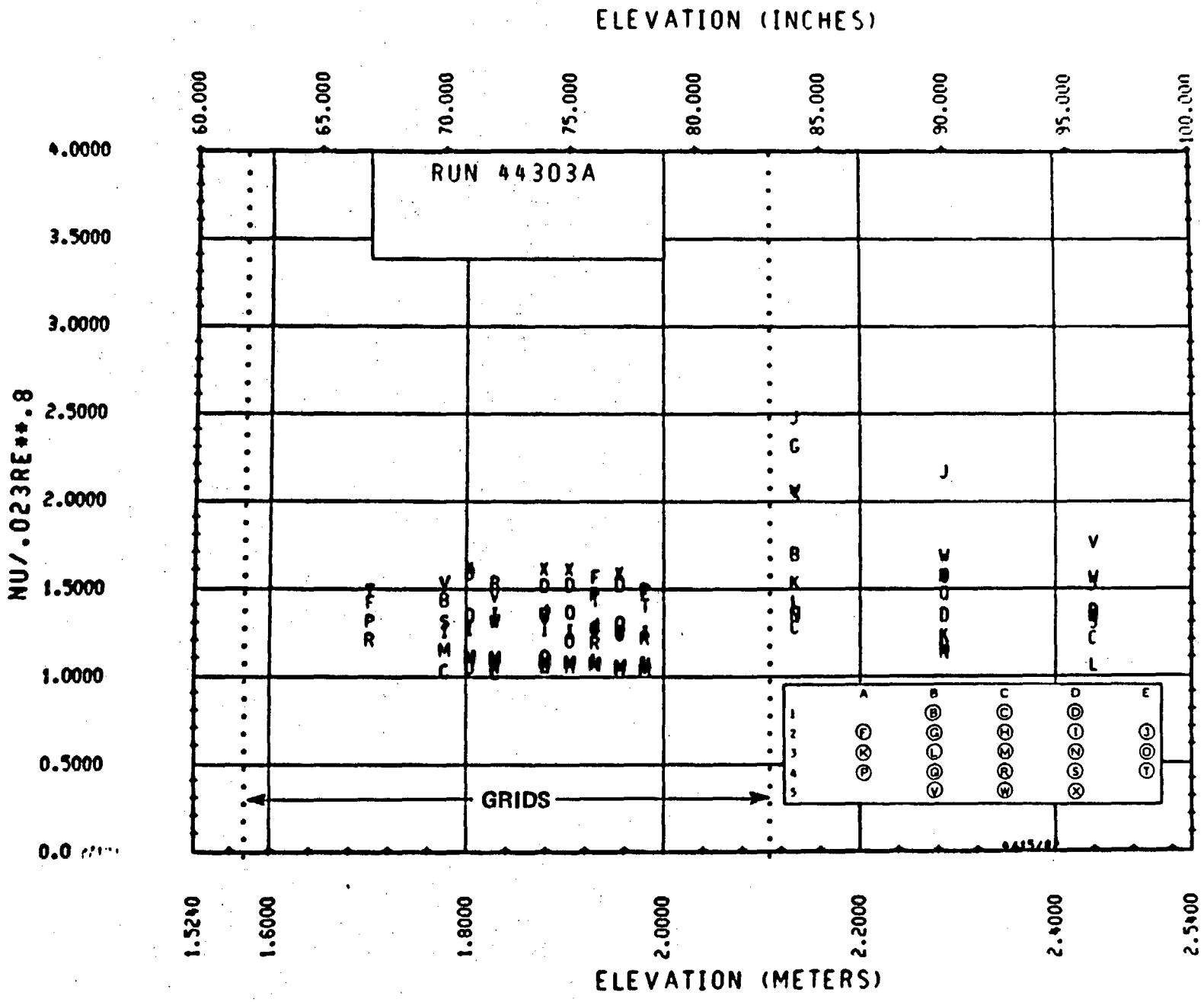

Figure 6-43. Heat Transfer From 1.52 to 2.44 m (60 to 96 in.) Run 44303A

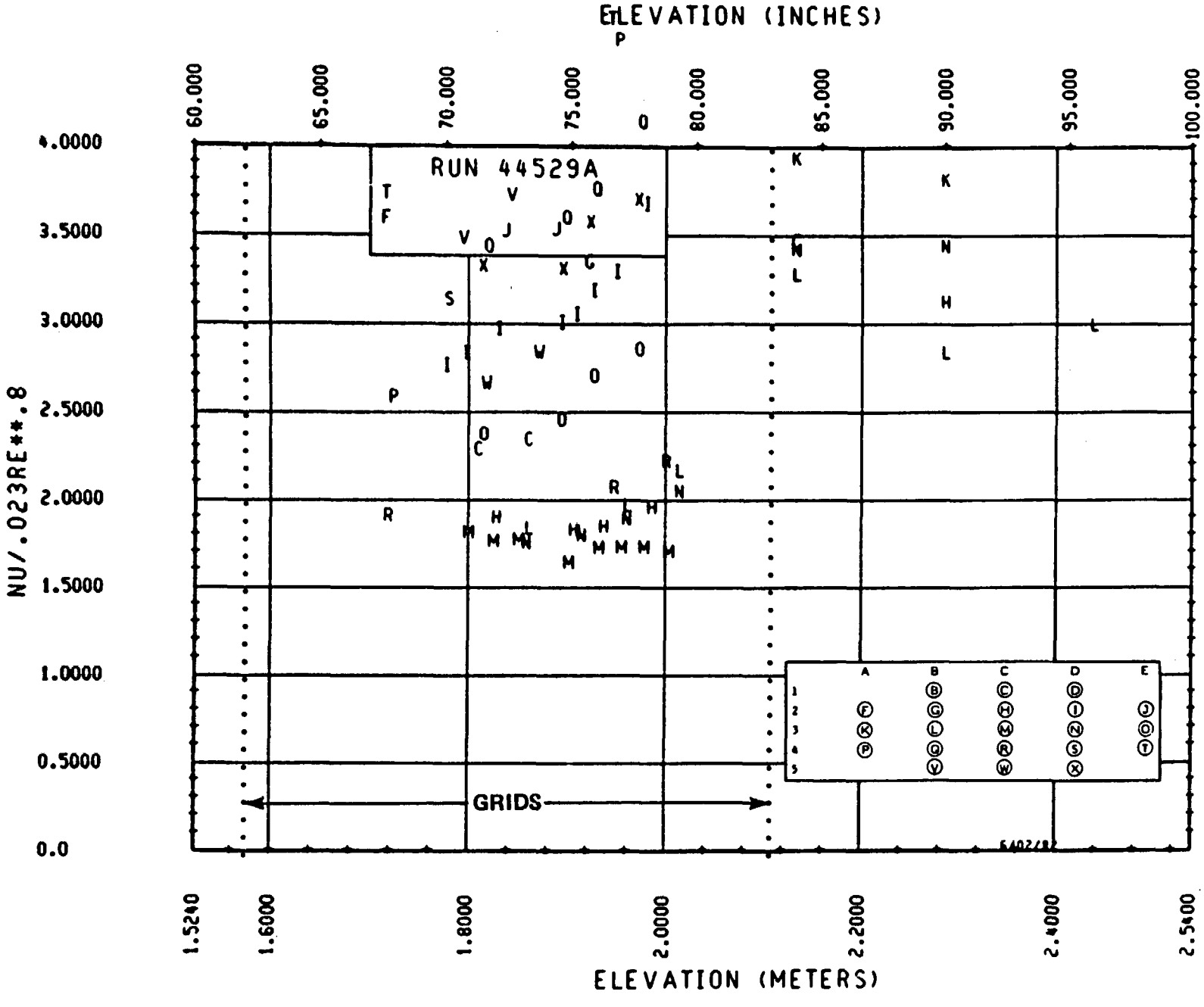

Figure 6-44. Heat Transfer From 1.52 to 2.44 m (60 to 96 in.) Run 44529A

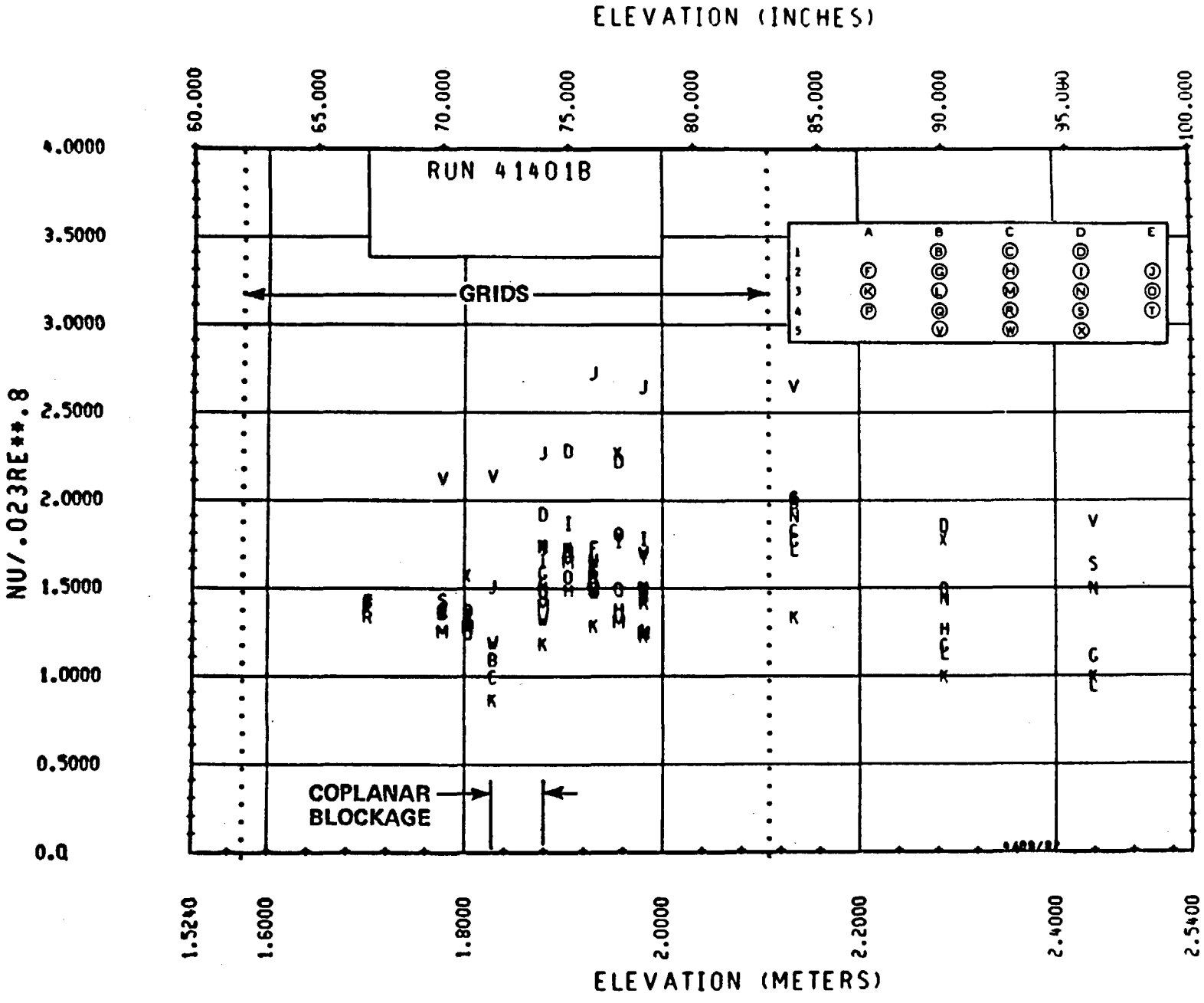

Figure 6-45. Heat Transfer From 1.52 to 2.44 m (60 to 96 in.) Run 41401B

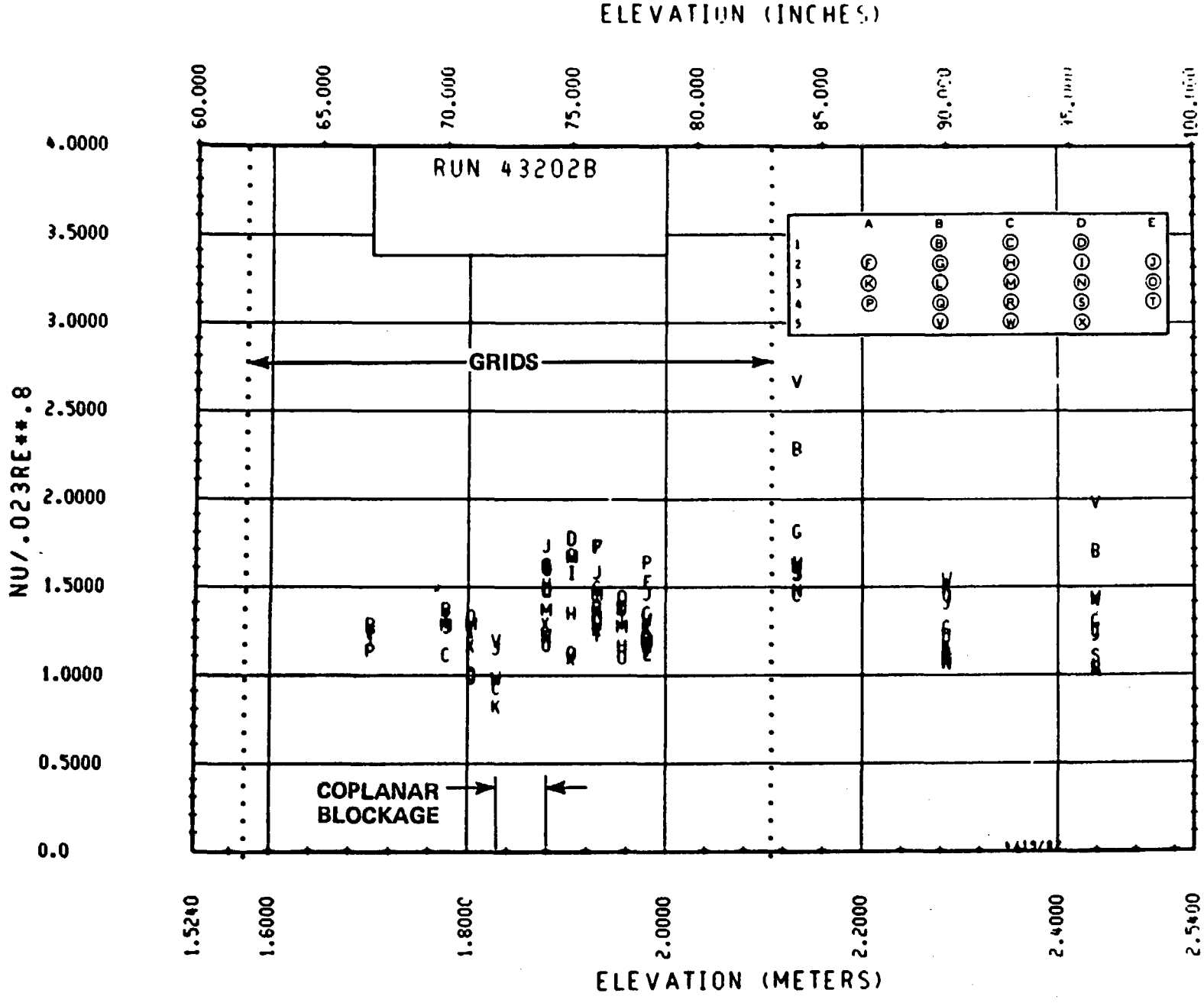

Figure 6-46. Heat Transfer From 1.52 to 2.44 m (60 to 96 in.) Run 43202B

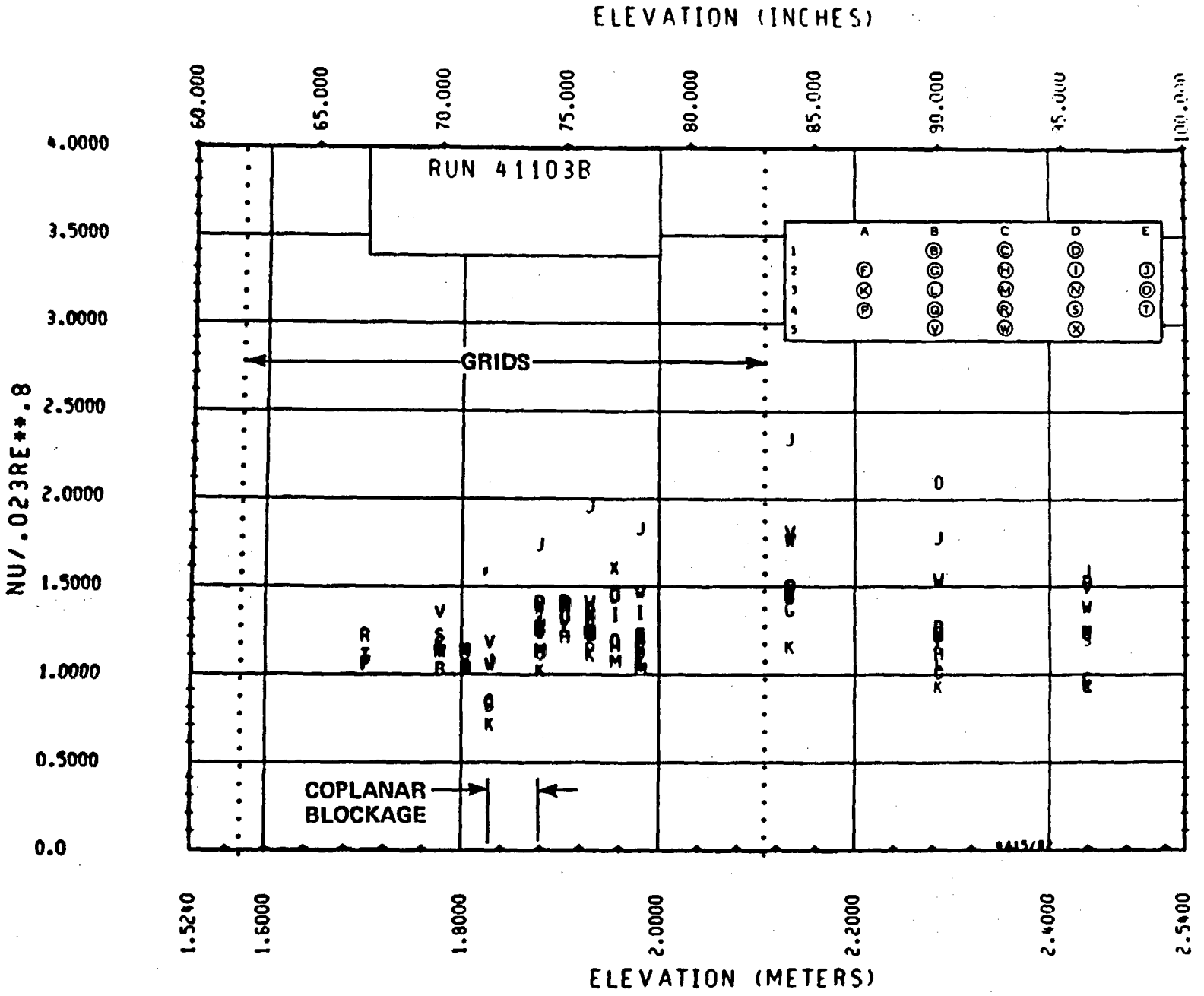

Figure 6-47. Heat Transfer From 1.52 to 2.44 m (60 to 96 in.) Run 41103B

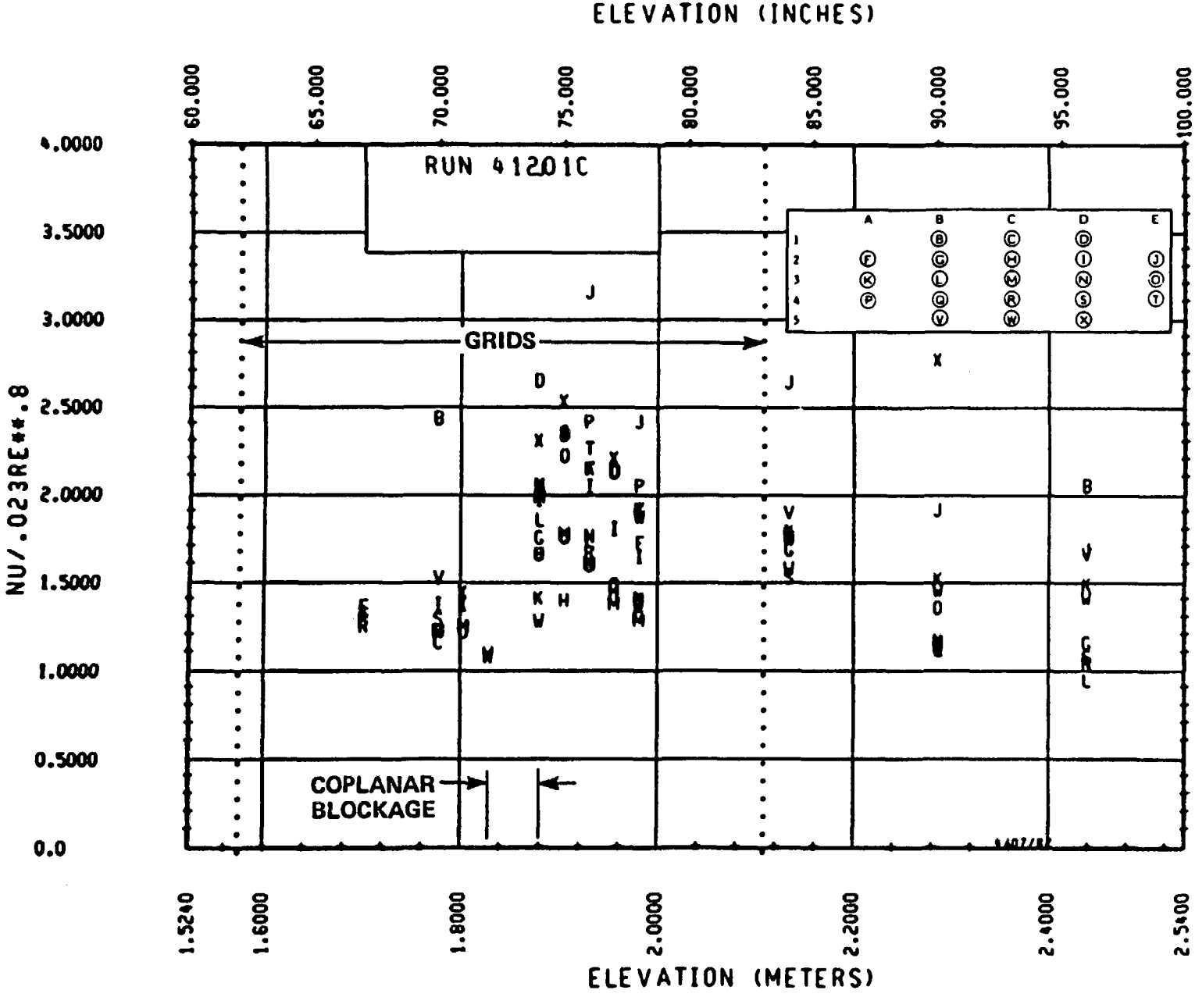

Figure 6-48. Heat Transfer From 1.52 to 2.44 m (60 to 96 in.) Run 41201C

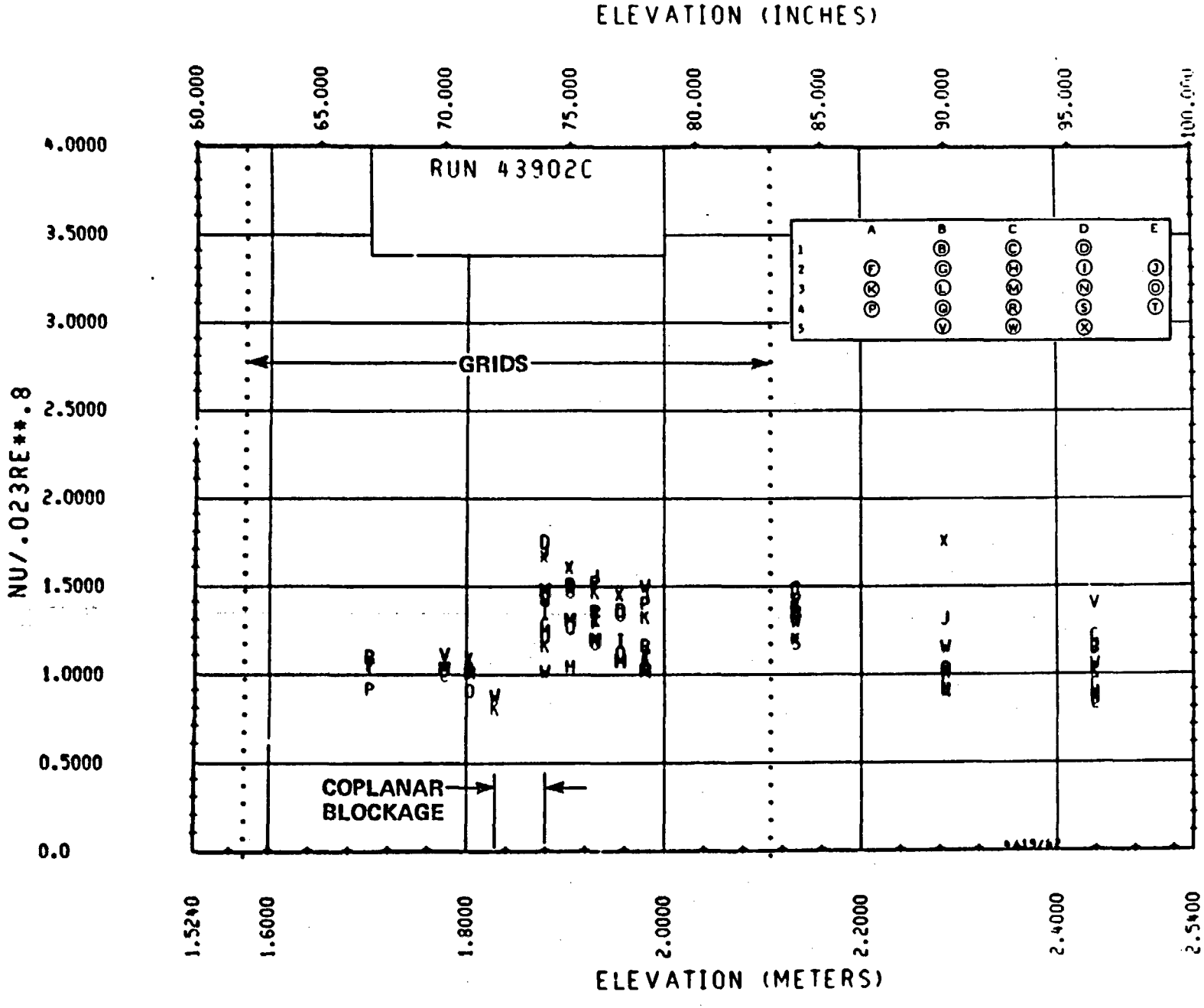

Figure 6-49. Heat Transfer From 1.52 to 2.44 m (60 to 96 in.) Run 43902C

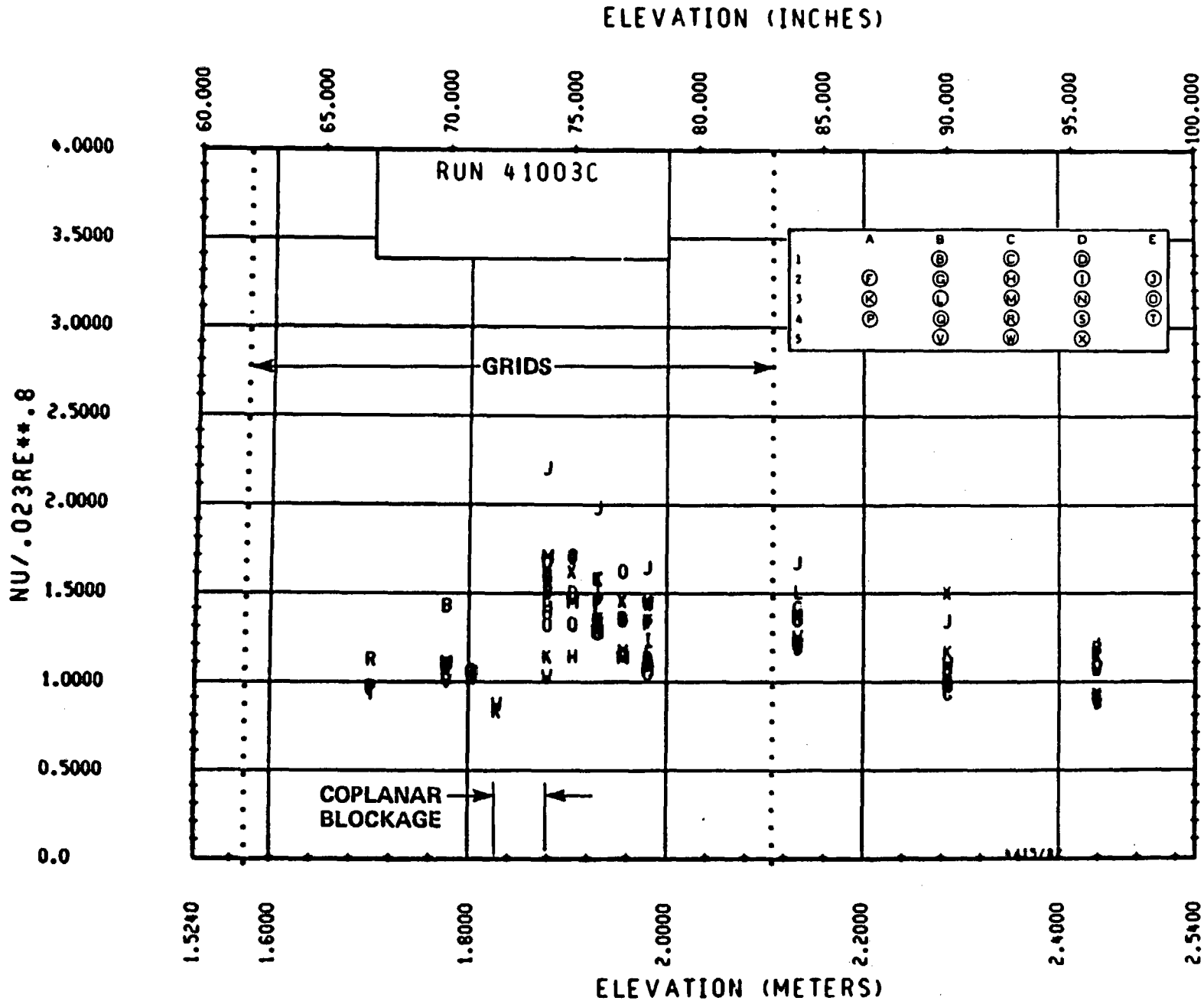

Figure 6-50. Heat Transfer From 1.52 to 2.44 m (60 to 96 in.) Run 41003C

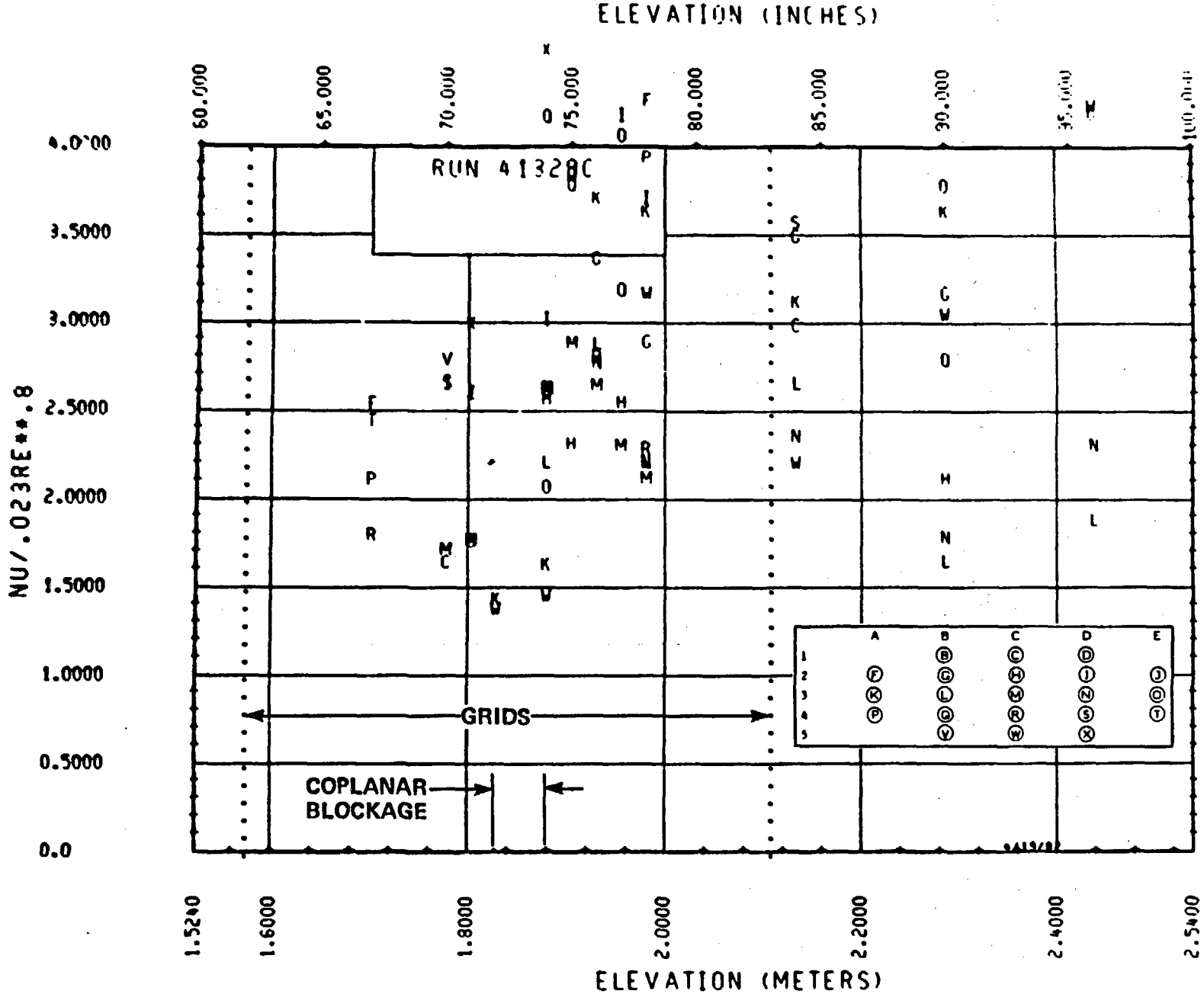

Figure 6-51. Heat Transfer From 1.52 to 2.44 m (60 to 96 in.) Run 41329C

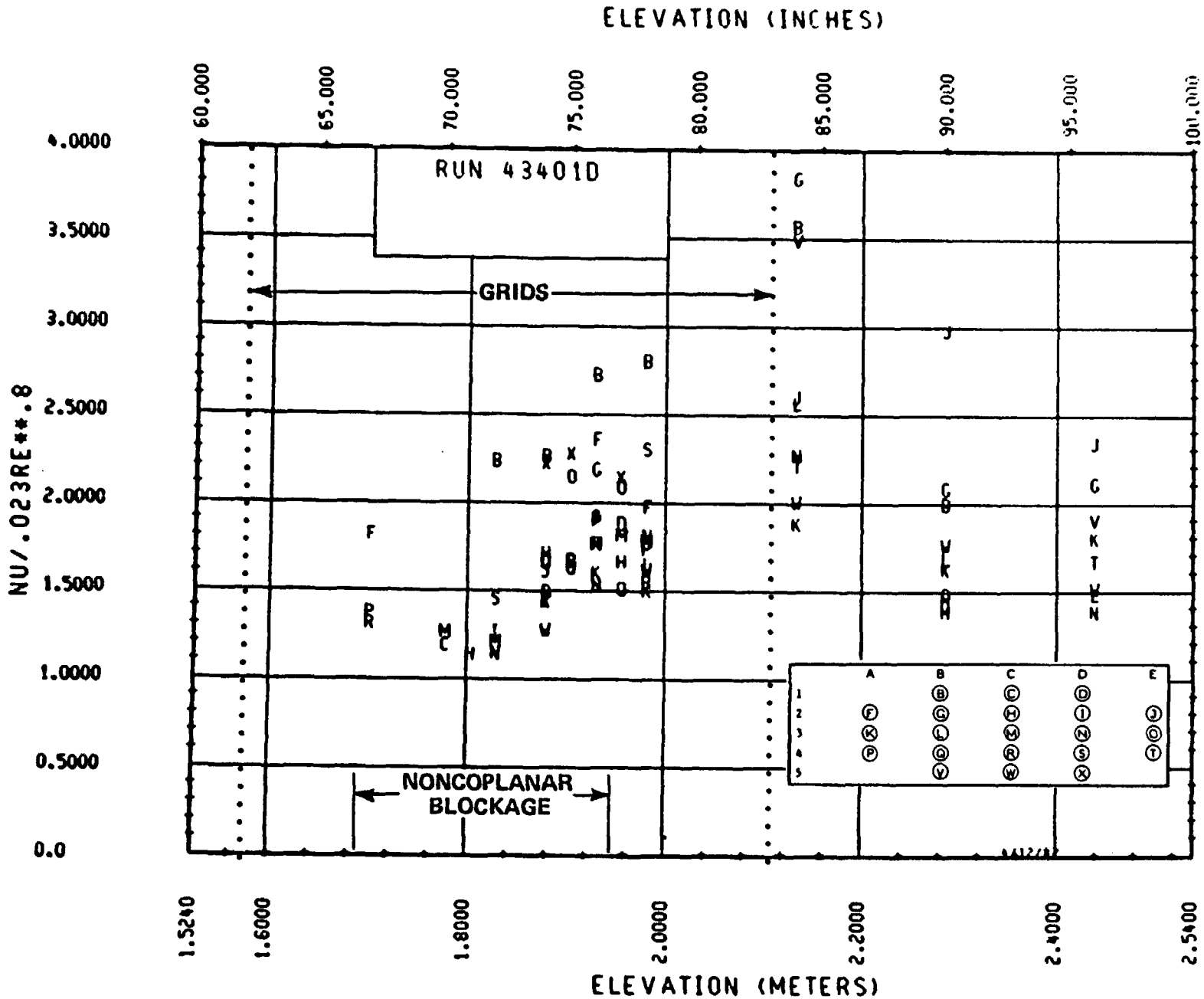

Figure 6-52. Heat Transfer From 1.52 to 2.44 m (60 to 96 in.) Run 43401D

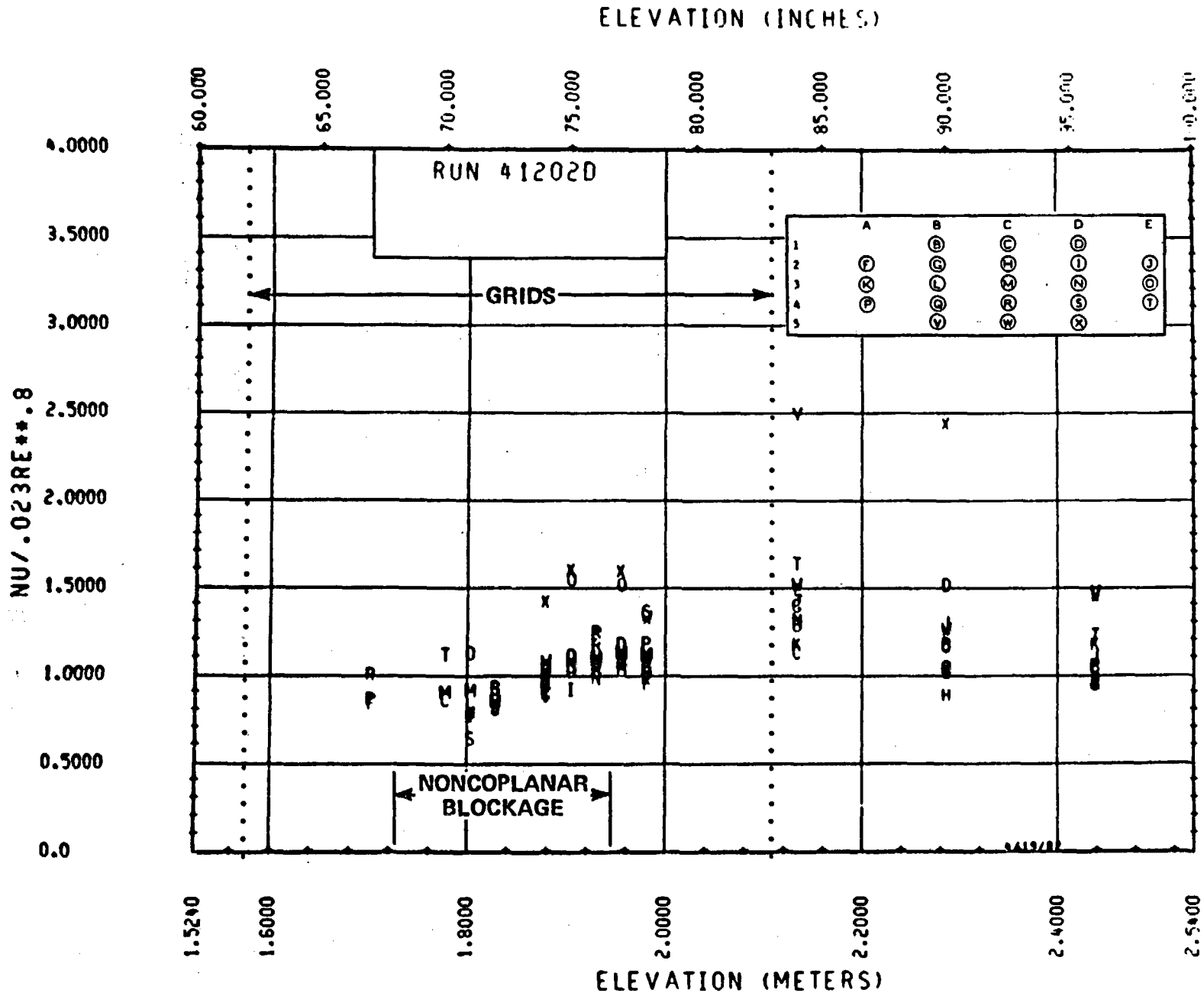

Figure 6-53. Heat Transfer From 1.52 to 2.44 m (60 to 96 in.) Run 41202D

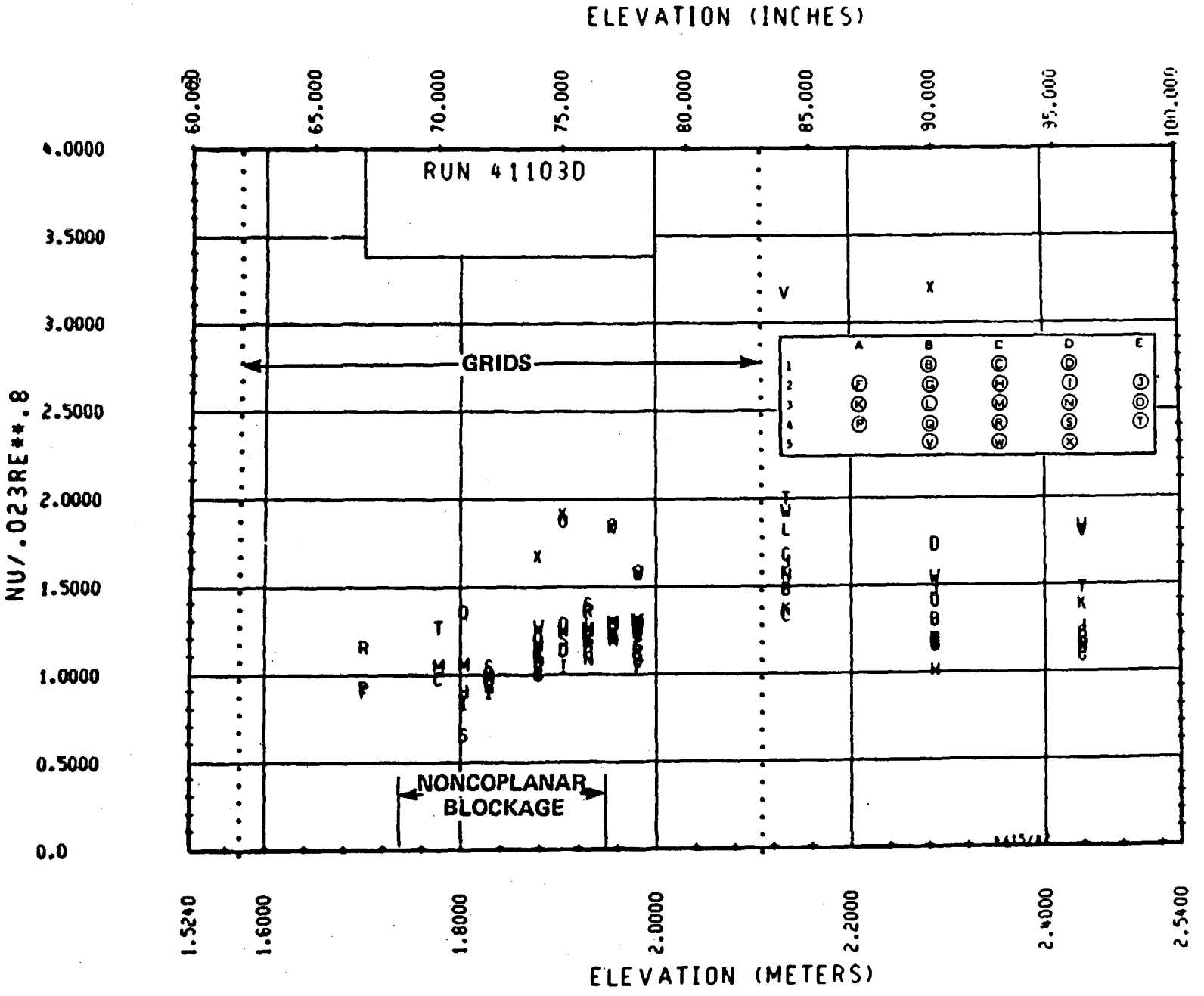

Figure 6-54. Heat Transfer From 1.52 to 2.44 m (60 to 96 in.) Run 41103D

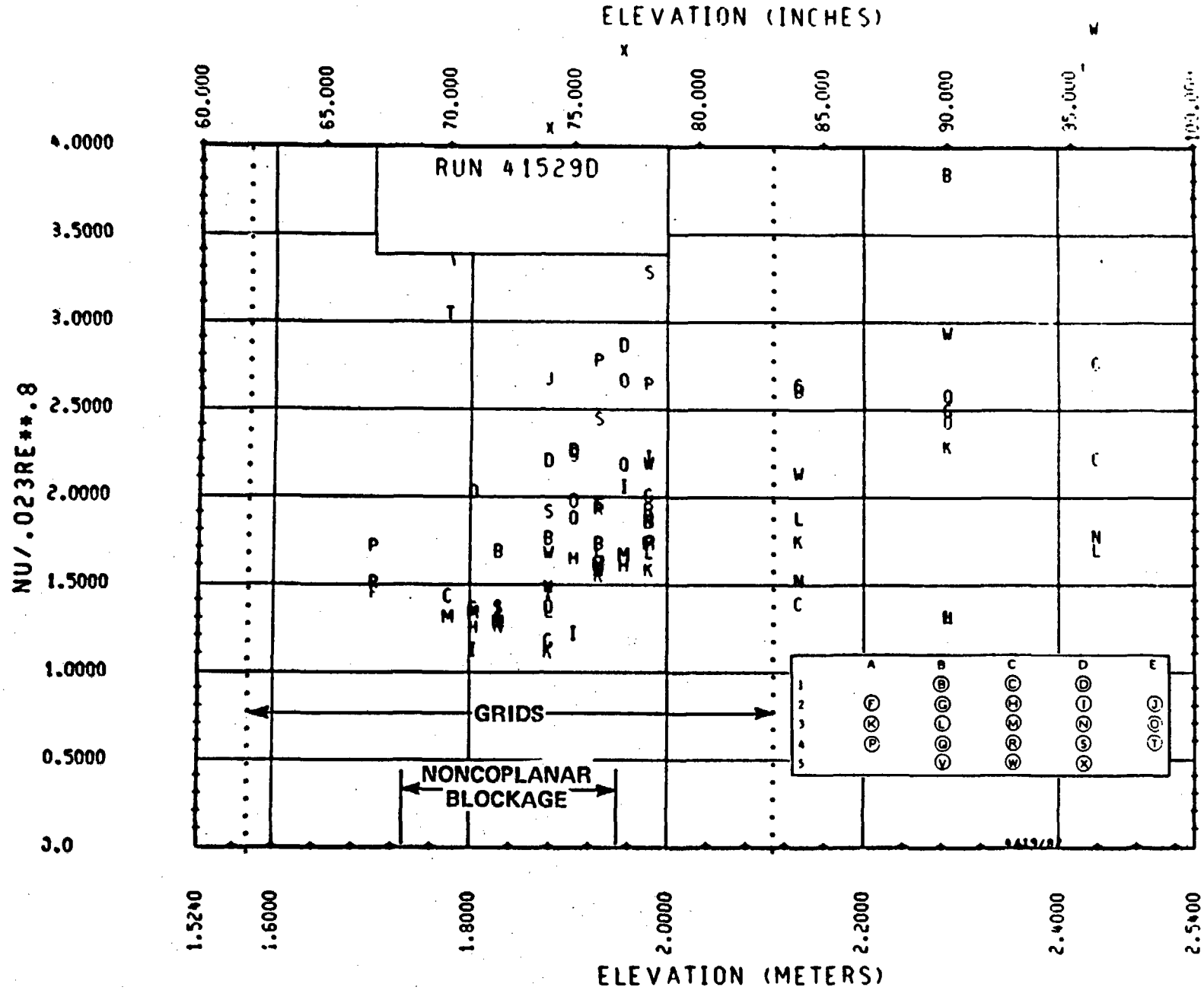

Figure 6-55. Heat Transfer From 1.52 to 2.44 m (60 to 96 in.) Run 41529D

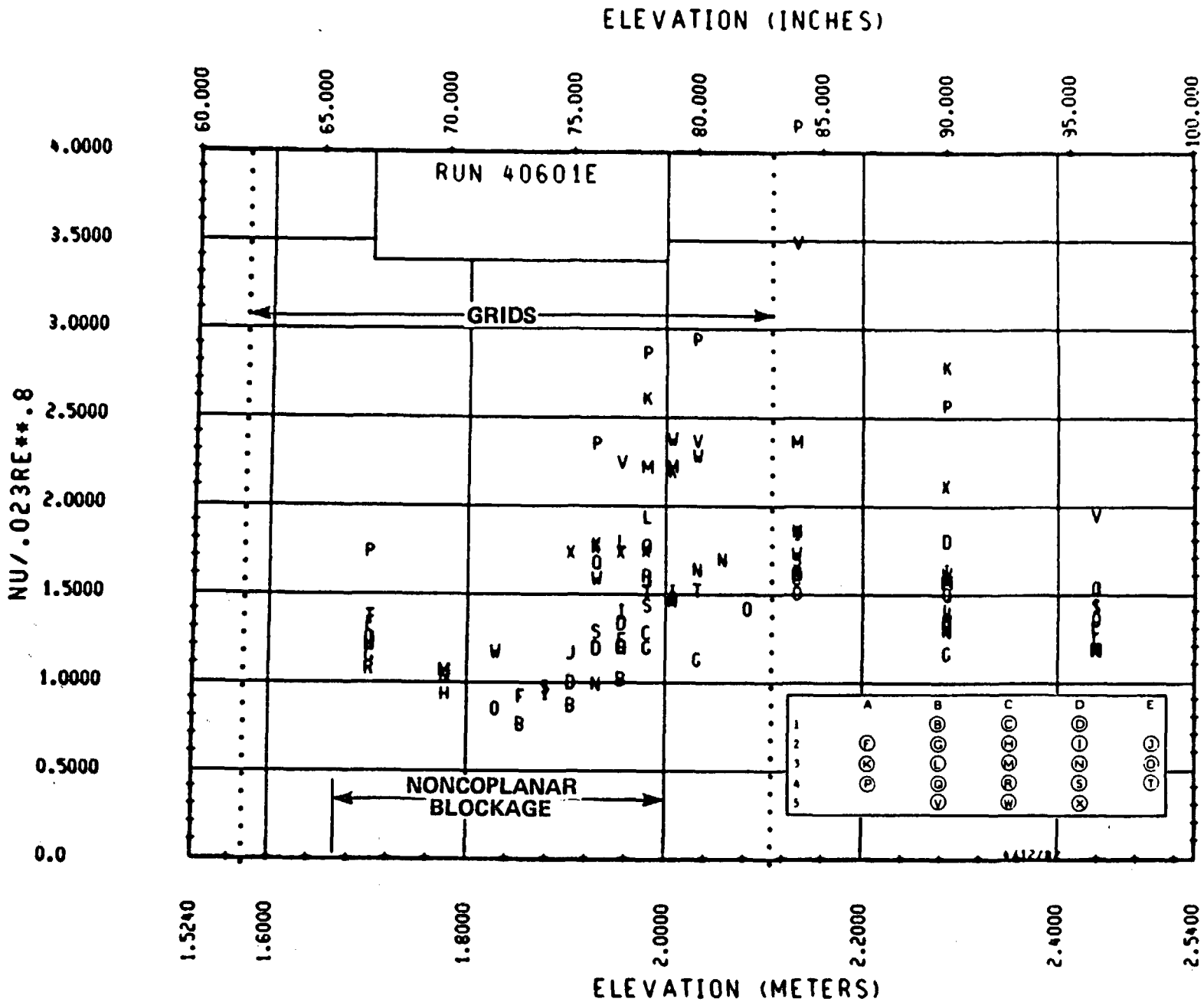

Figure 6-56. Heat Transfer From 1.52 to 2.44 m (60 to 96 in.) Run 40601E

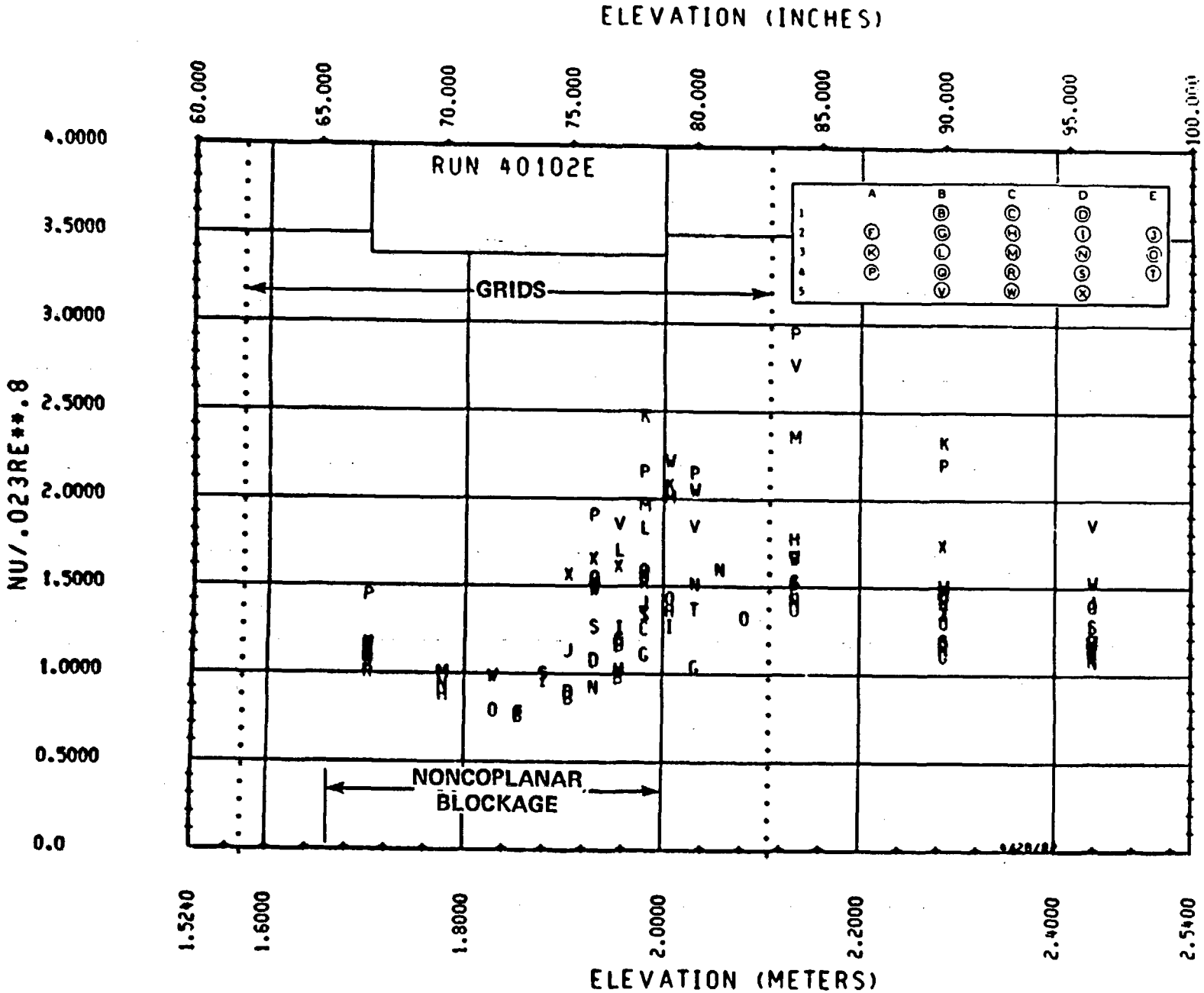

Figure 6-57. Heat Transfer From 1.52 to 2.44 m (60 to 96 in.) Run 40102E

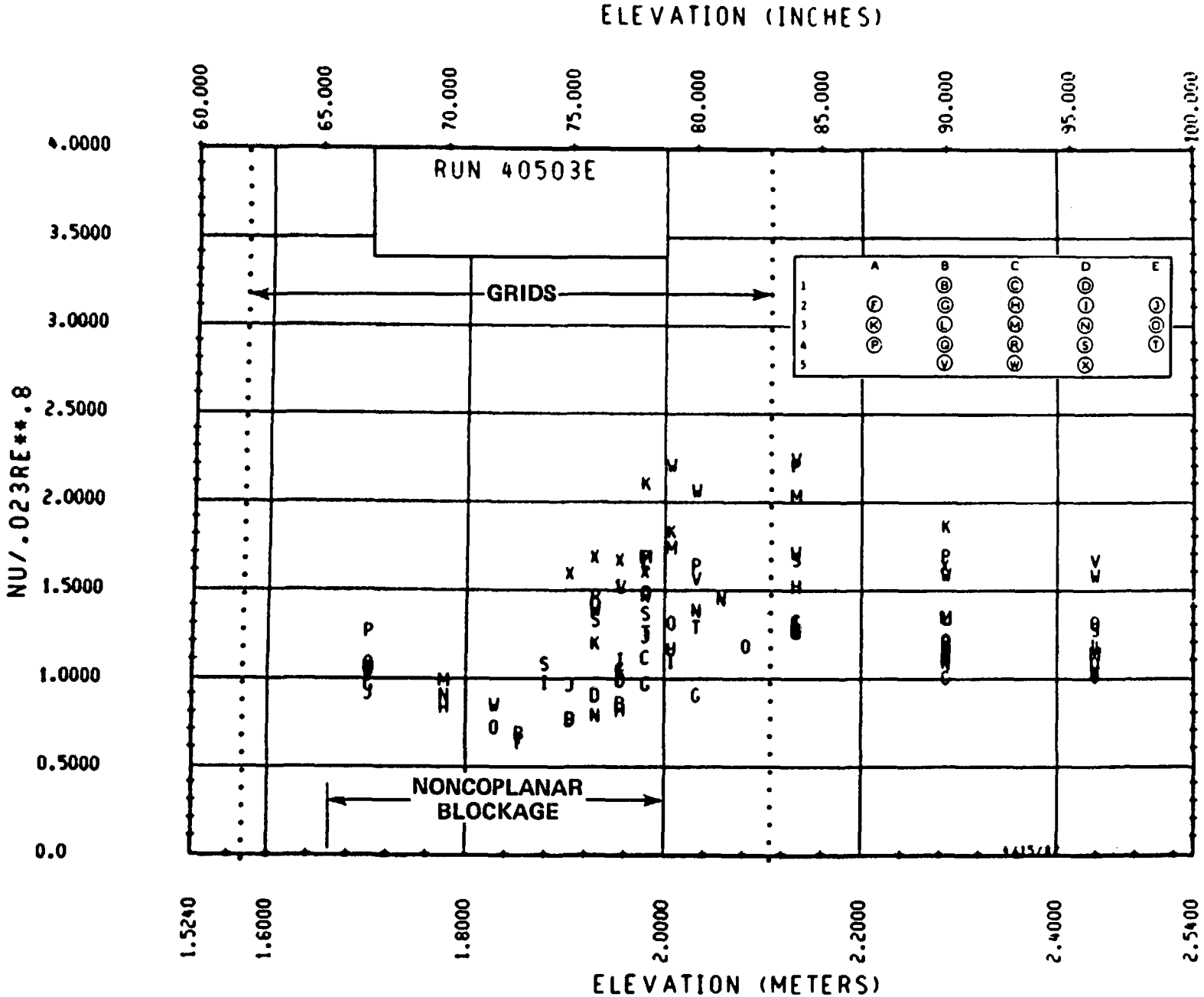

Figure 6-58. Heat Transfer From 1.52 to 2.44 m (60 to 96 in.) Run 40503E

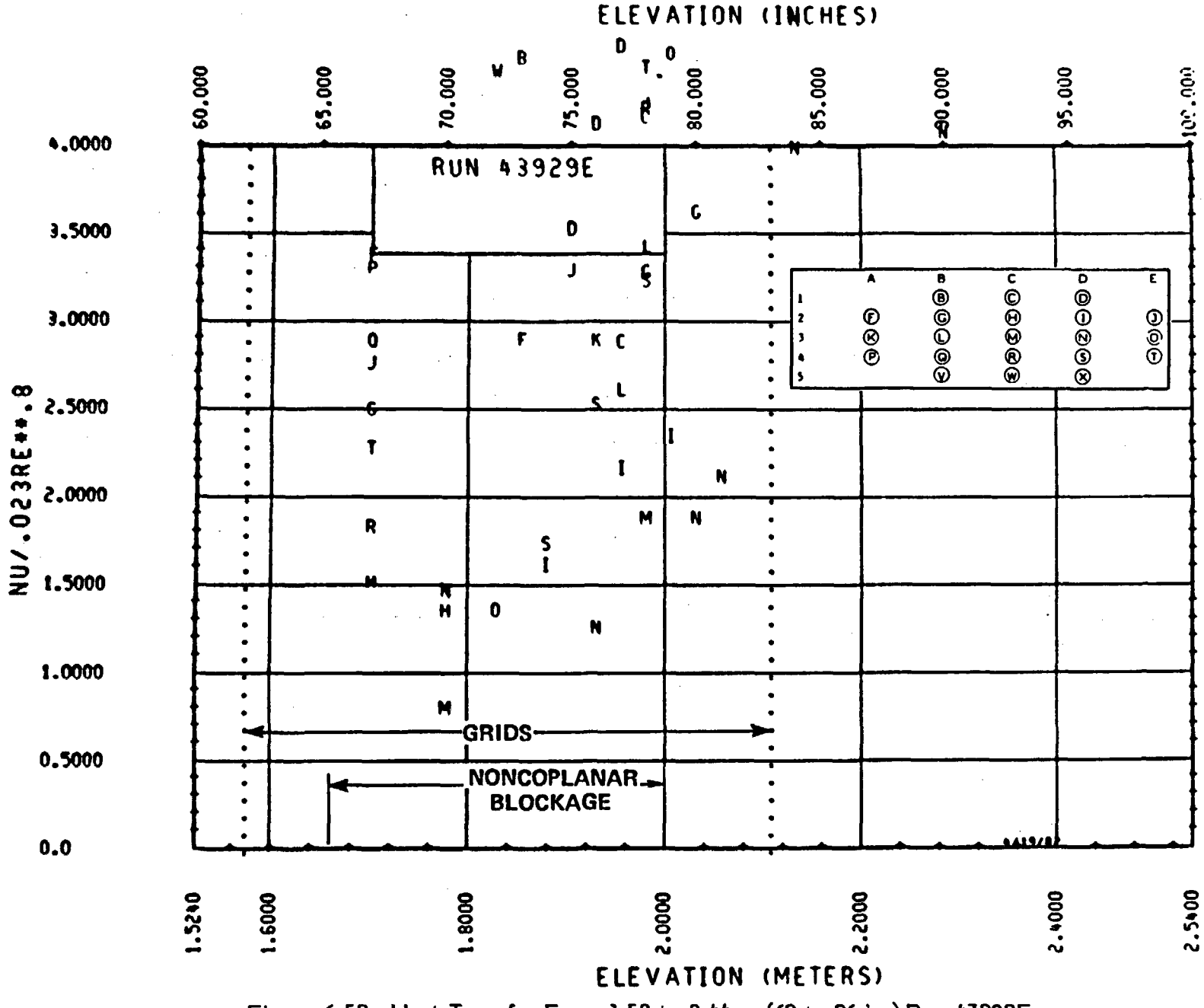

Figure 6-59. Heat Transfer From 1.52 to 2.44 m (60 to 96 in.) Run 43929E

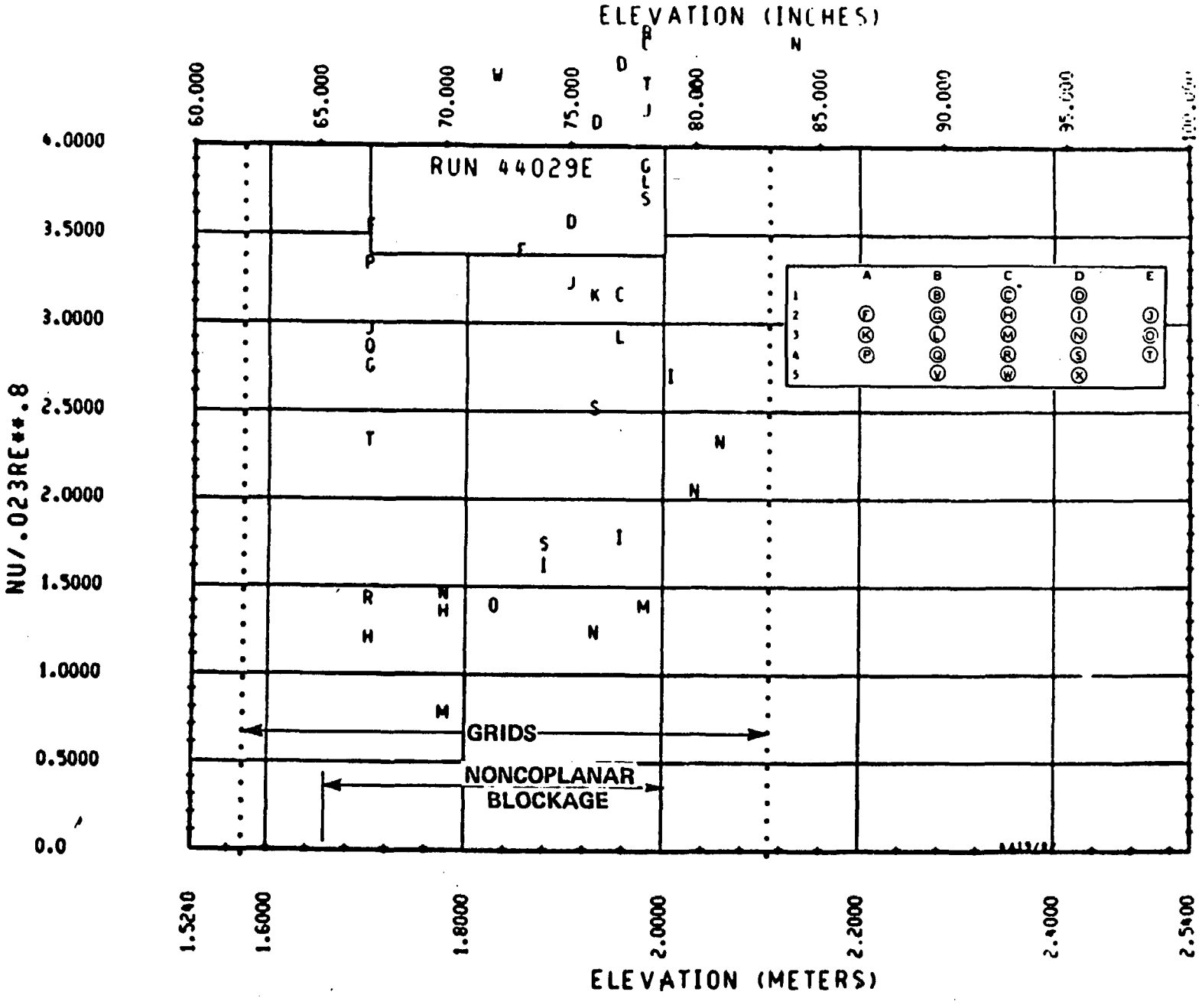

Figure 6-60. Heat Transfer From 1.52 to 2.44 m (60 to 96 in.) Run 44029E

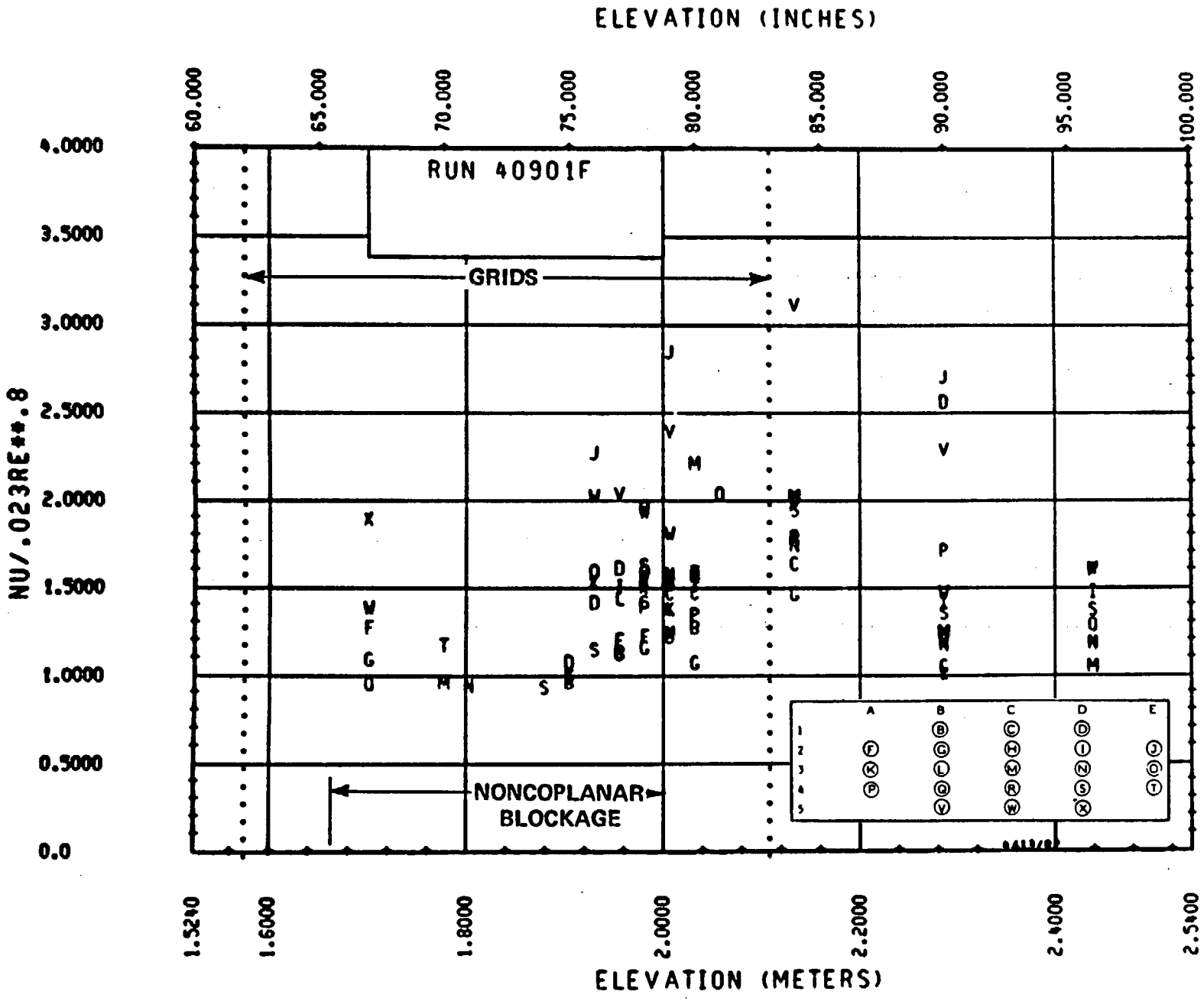

Figure 6-61. Heat Transfer From 1.52 to 2.44 m (60 to 96 in.) Run 40901F

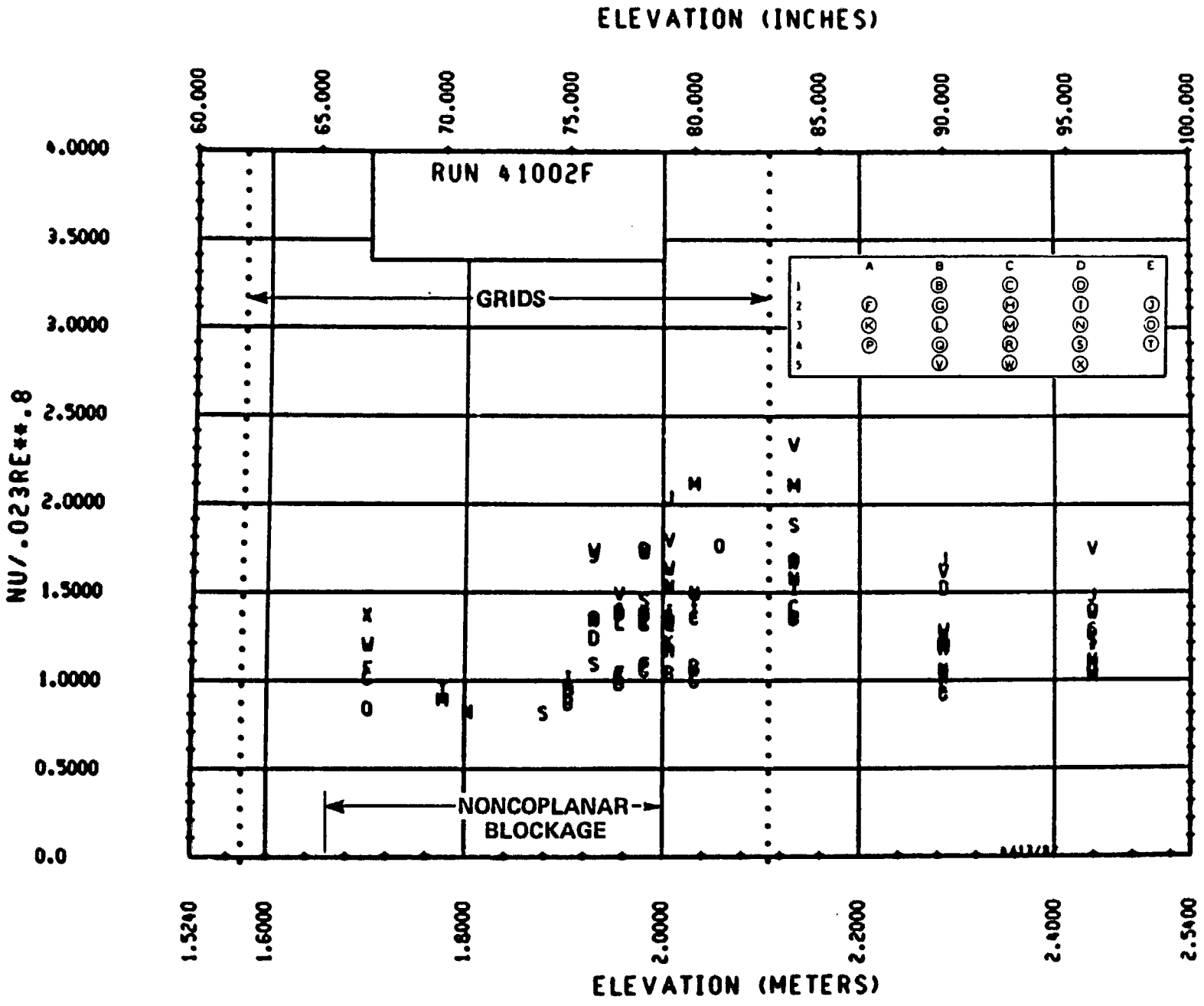

Figure 6-62. Heat Transfer From 1.52 to 2.44 m (60 to 96 in.) Run 41002F

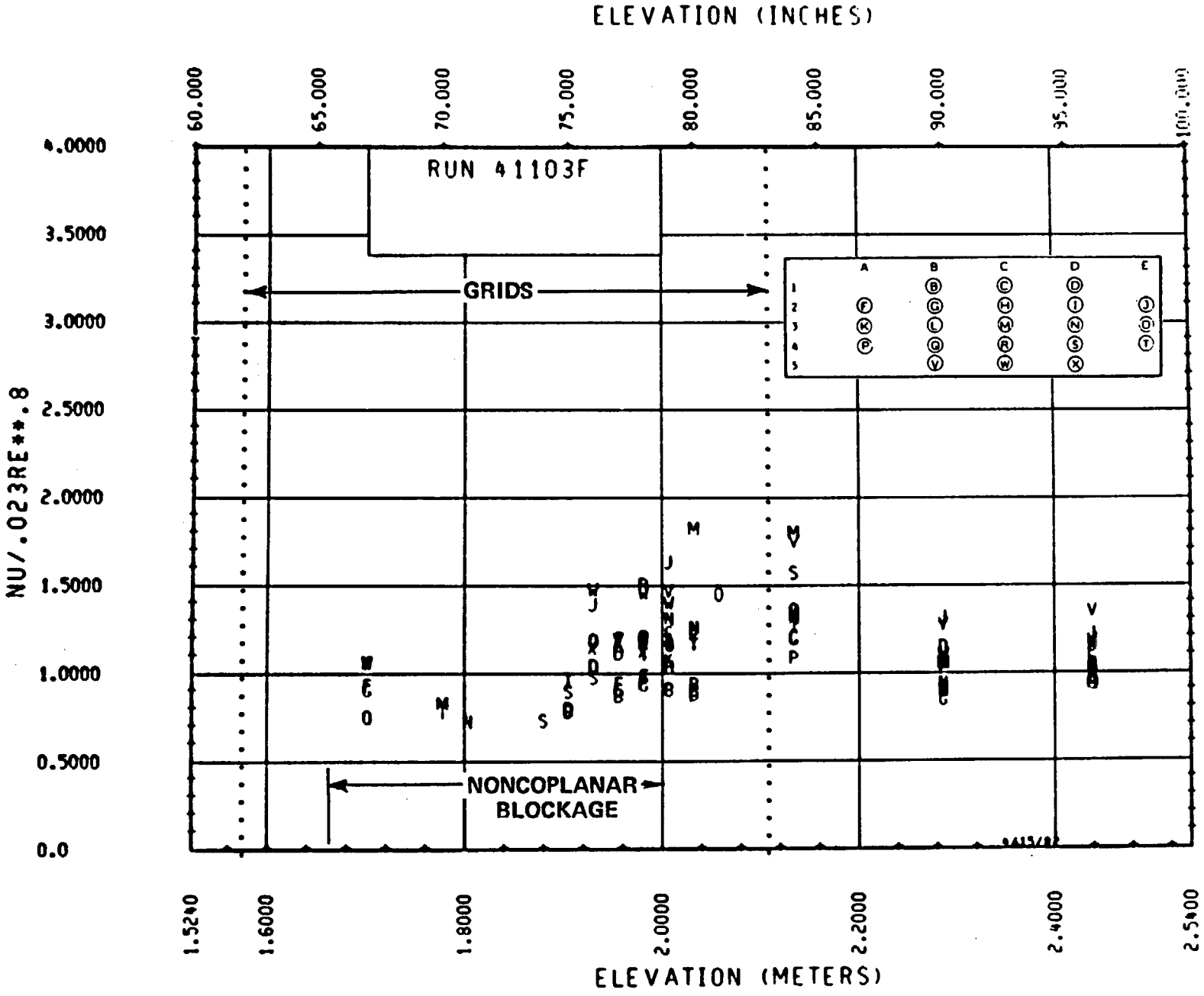

Figure 6-63. Heat Transfer From 1.52 to 2.44 m (60 to 96 in.) Run 41103F

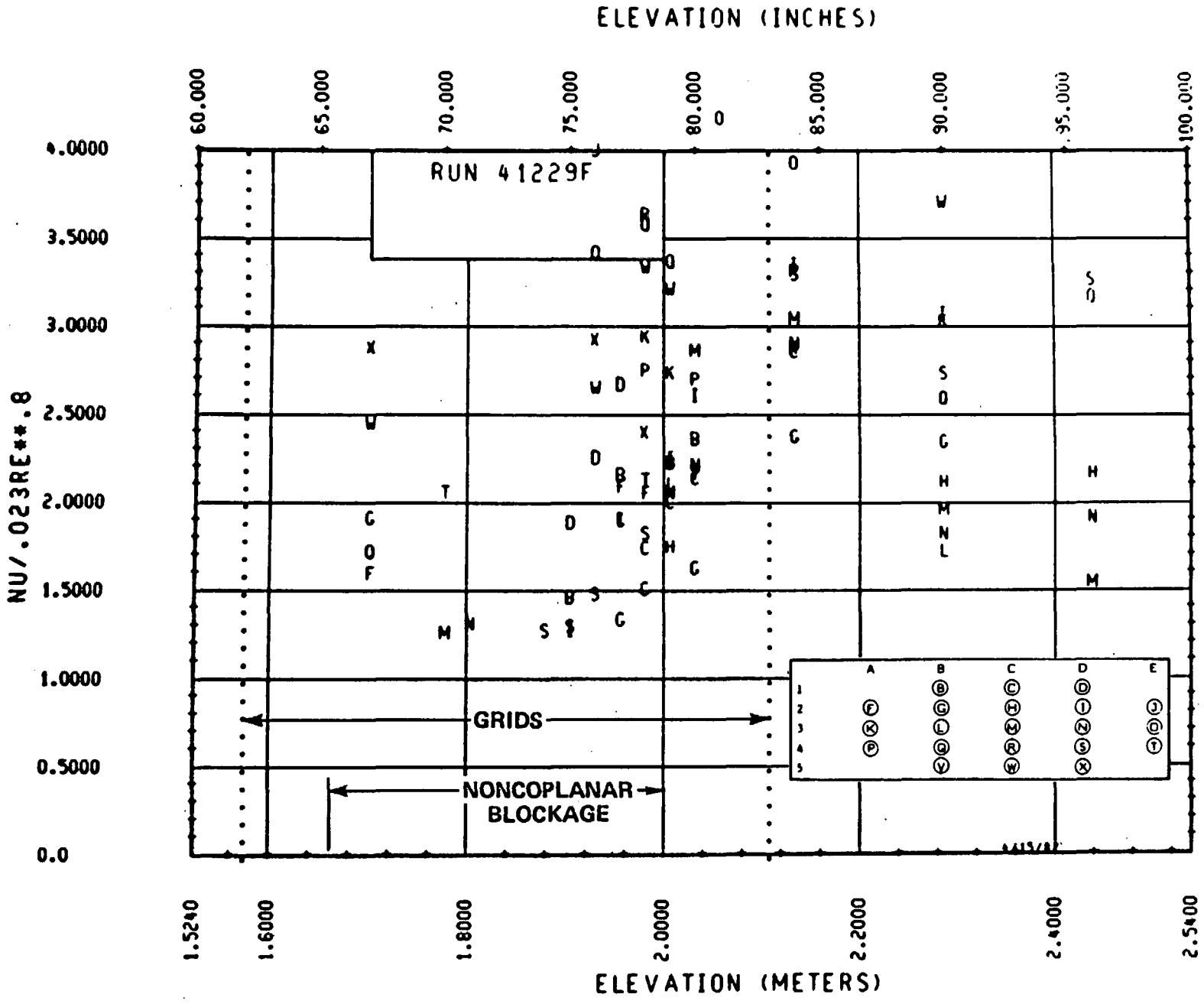

Figure 6-64. Heat Transfer From 1.52 to 2.44 m (60 to 96 in.) Run 41229F

In the noncoplanar blockage tests of configurations D, E, and F, the normalized heat transfer tended to have a minimum value near the center of the blockage, that is, at approximately 1.85 m (73 in.), as shown in figures 6-52 through 6-64. This could simply be a result of the limited amount of data available at this elevation, or it could be symptomatic of the COBRA code flow redistribution calculations. For example, the subchannel velocity as calculated by COBRA could be greater than the actual velocity, a fact which would consequently increase the Reynolds number and decrease the vapor temperature, and thereby provide a lower normalized heat transfer. The heat transfer data also tended to have greater rod-to-rod variations as the distance increased downstream from the blockage centerline. Within this "envelope" of data, no apparent trends were observed.

The measured heat flux and heater rod temperature, the calculated vapor temperature, the Nusselt number, and the Reynolds number are tabulated for each of the steam cooling tests in appendix K. The actual thermocouple locations are shown in parentheses for the blockage zone thermocouples in appendix K.

The enhancement factor, as previously discussed in section 3 and defined as follows:

$$Ne = \frac{h_b}{h_o}\left(\frac{G_b}{G_o}\right)^{-m}$$

was calculated for the five blockage configurations utilizing the STMCOOL code. Since the as-built thermocouple locations varied from bundle to bundle as described in appendix N, the unblocked measured heat transfer, h_o, and the calculated mass flux, G_o, were interpolated to provide data at locations comparable with the blocked configurations.

Review of the measured heater rod temperatures for each of the steam cooling tests showed that, accounting for both inlet steam temperatures and power-to-flow differences, 11 of the 20 blocked configuration tests had axial rod temperature distributions below the blockage zone which were different from those of the corresponding unblocked configuration tests. Also, of the nine tests which had comparable axial temperature distributions, four were conducted at Reynolds numbers which were more than 26 percent different from those of the corresponding unblocked configuration

tests. Therefore, in order to avoid introducing bundle-to-bundle and Reynolds number effects, the heat transfer data upstream of the blockage region were utilized to calculate the enhancement factor. The upstream heat transfer data for these 15 tests were simply averaged, as listed below:

Run	$(Nu/0.023\ Re^{0.8})_{upstream}$
41201C	1.20
40601E	1.20
40901F	1.17
43202B	1.25
43902C	0.90
41202D	0.90
40102E	1.25
41002F	1.05
41003C	0.90
41103D	1.10
40503E	1.10
41103F	1.0
43929E	1.4
44029E	1.4
41229F	1.25

For run 41401B, which could utilize the unblocked configuration data, a comparison with the enhancement factor based on the upstream data indicated fairly good results for the 13 noncorner heater rods, as shown in table 6-4. The eight corner heater rods did not provide a good comparison between the two methods of calculating enhancement factor. The enhancement factors for each of the blocked configuration tests are shown in figures 6-65 through 6-84 as a function of elevation with the actual thermocouple elevation. The enhancement factor based on the upstream heat transfer data is denoted on the vertical axis for the above figures. The enhancement factors for the coplanar blockage configurations (configurations B and C) for the inside heater rods were between values of 1 and 1.95 immediately downstream of the blockage and subsequently decreased to values of 0.85 to 1.30 with increasing distance downstream of the

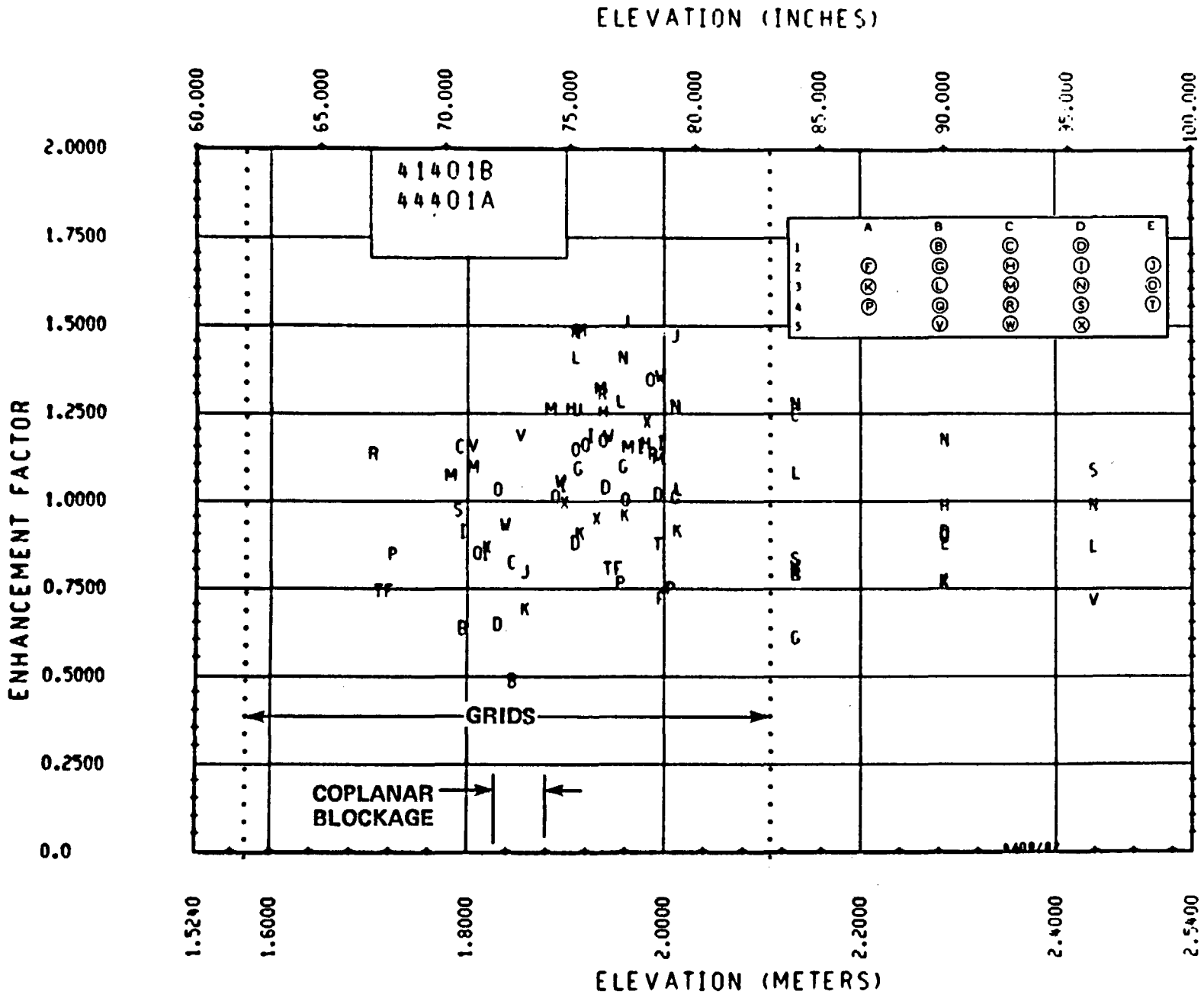

Figure 6-65. Enhancement Factor for Run 41401B

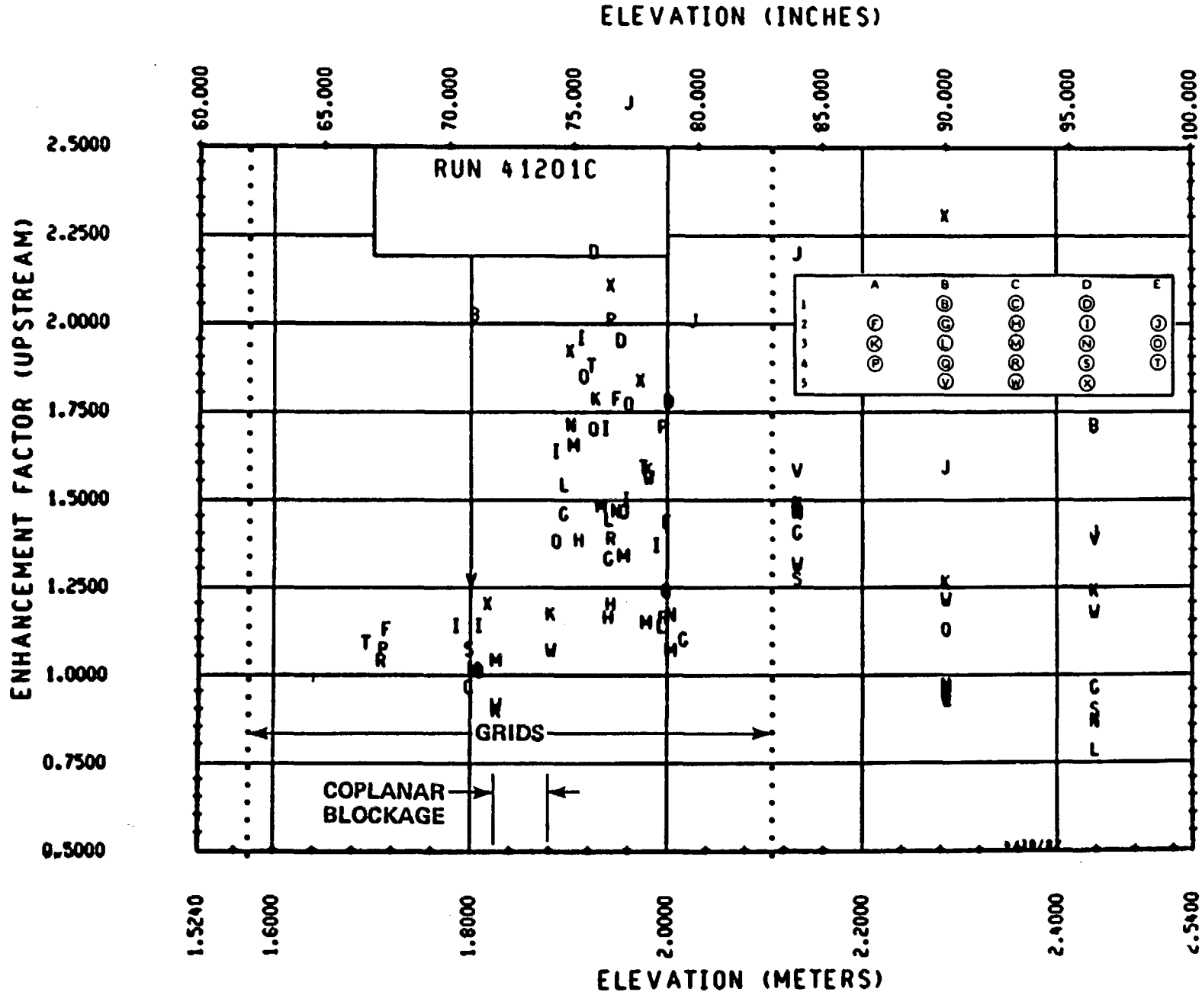

Figure 6-66. Enhancement Factor for Run 41201C

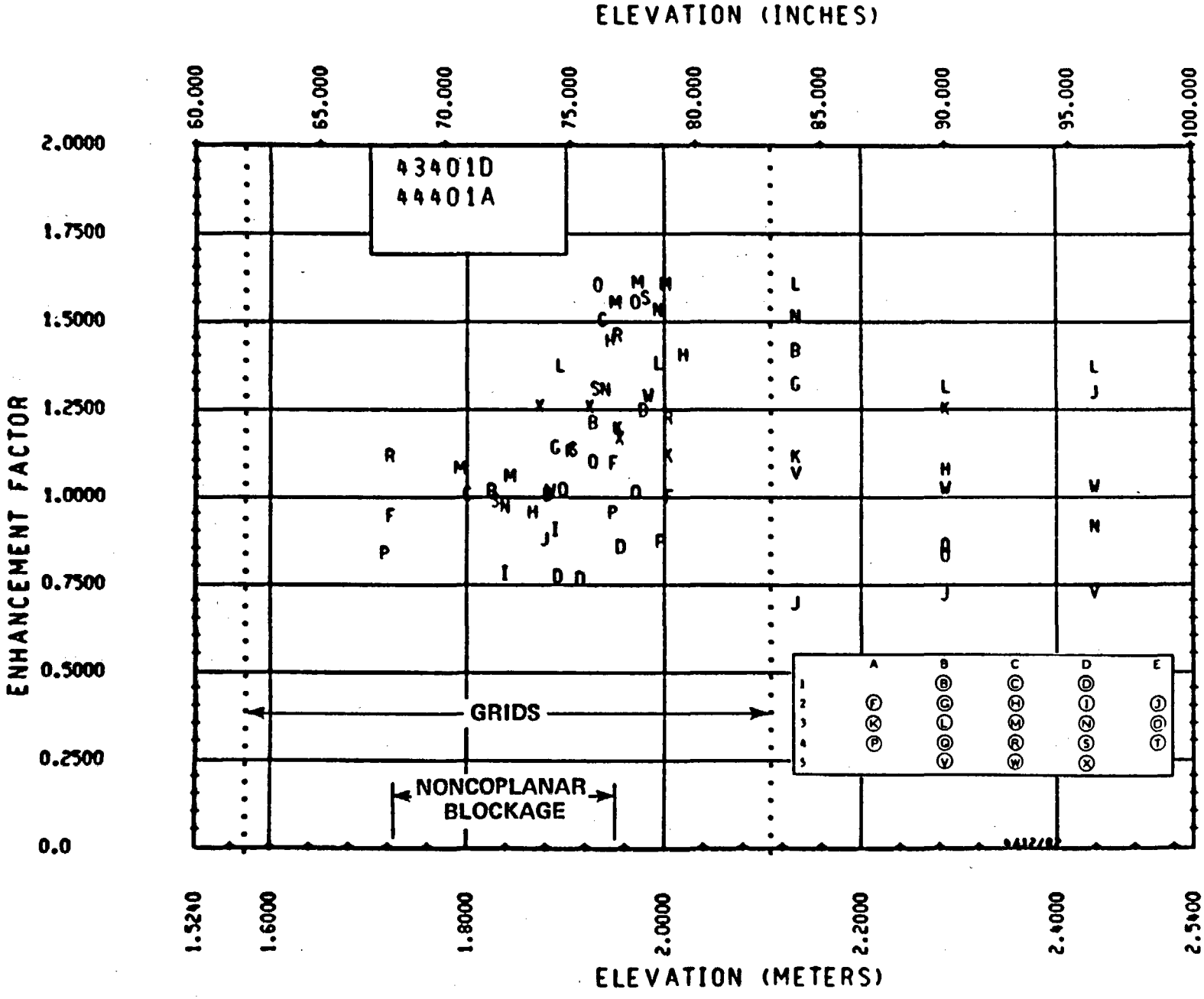

Figure 6-67. Enhancement Factor for Run 43401D

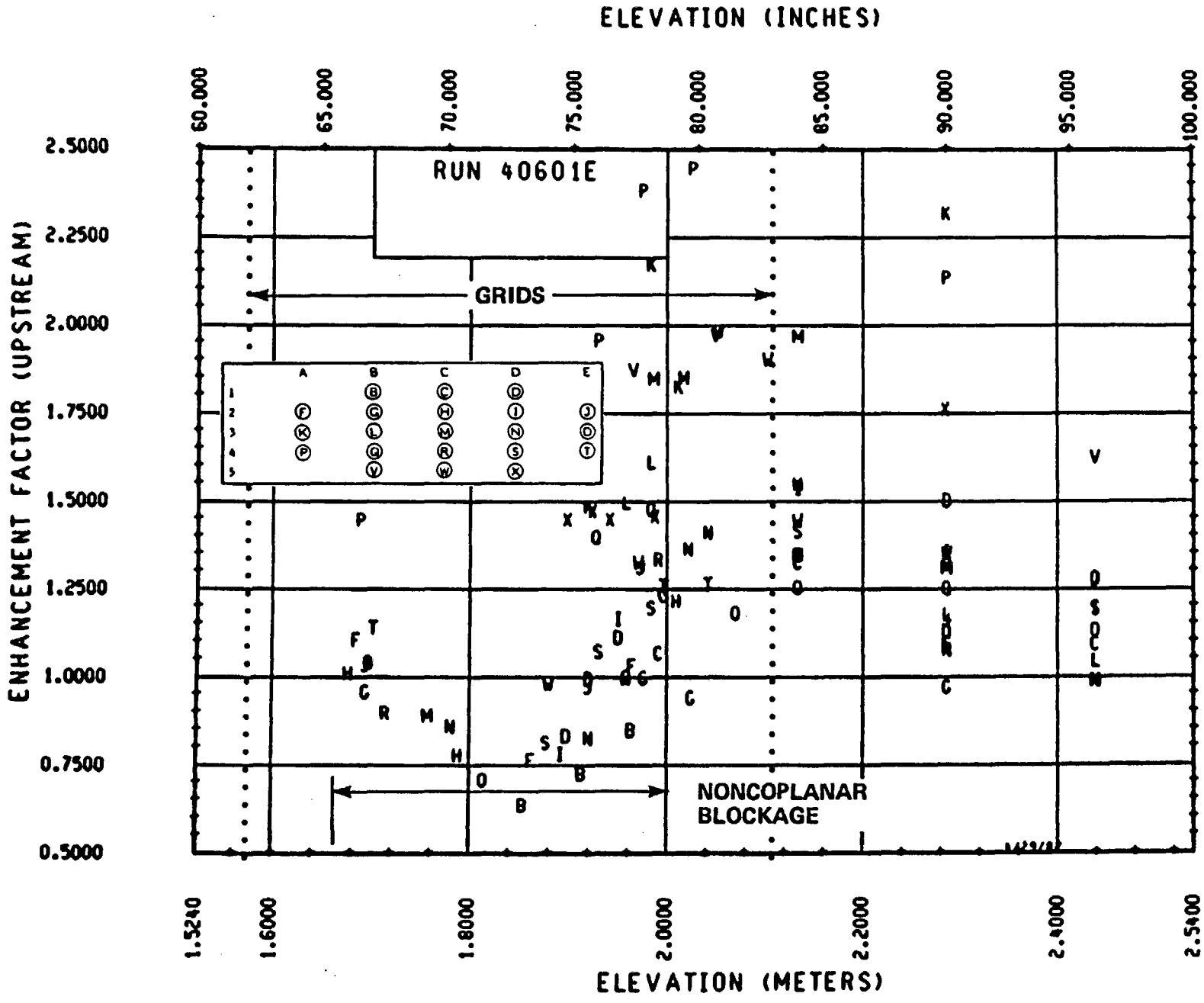

Figure 6-68. Enhancement Factor for Run 40601E

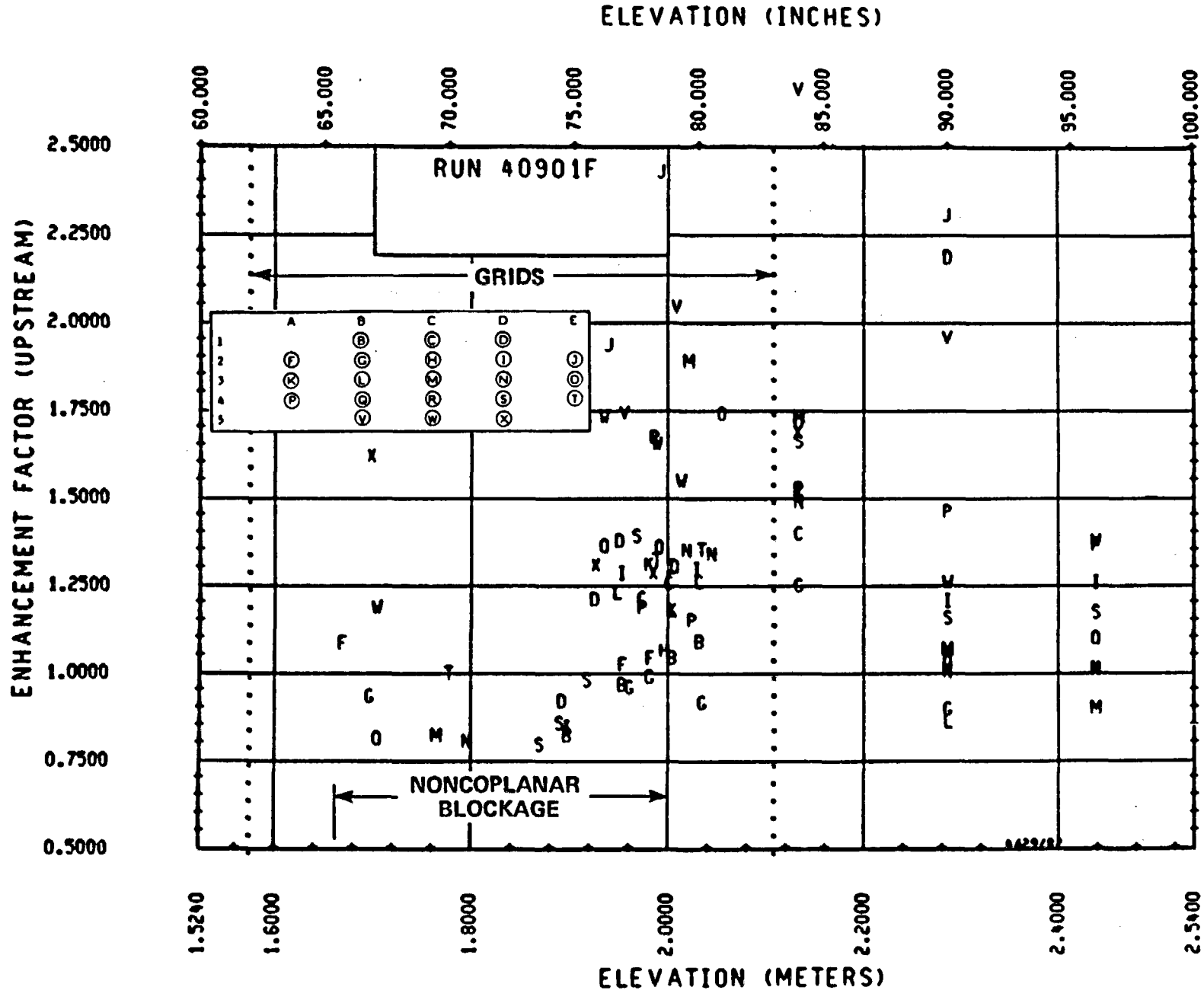

Figure 6-69. Enhancement Factor for Run 40901F

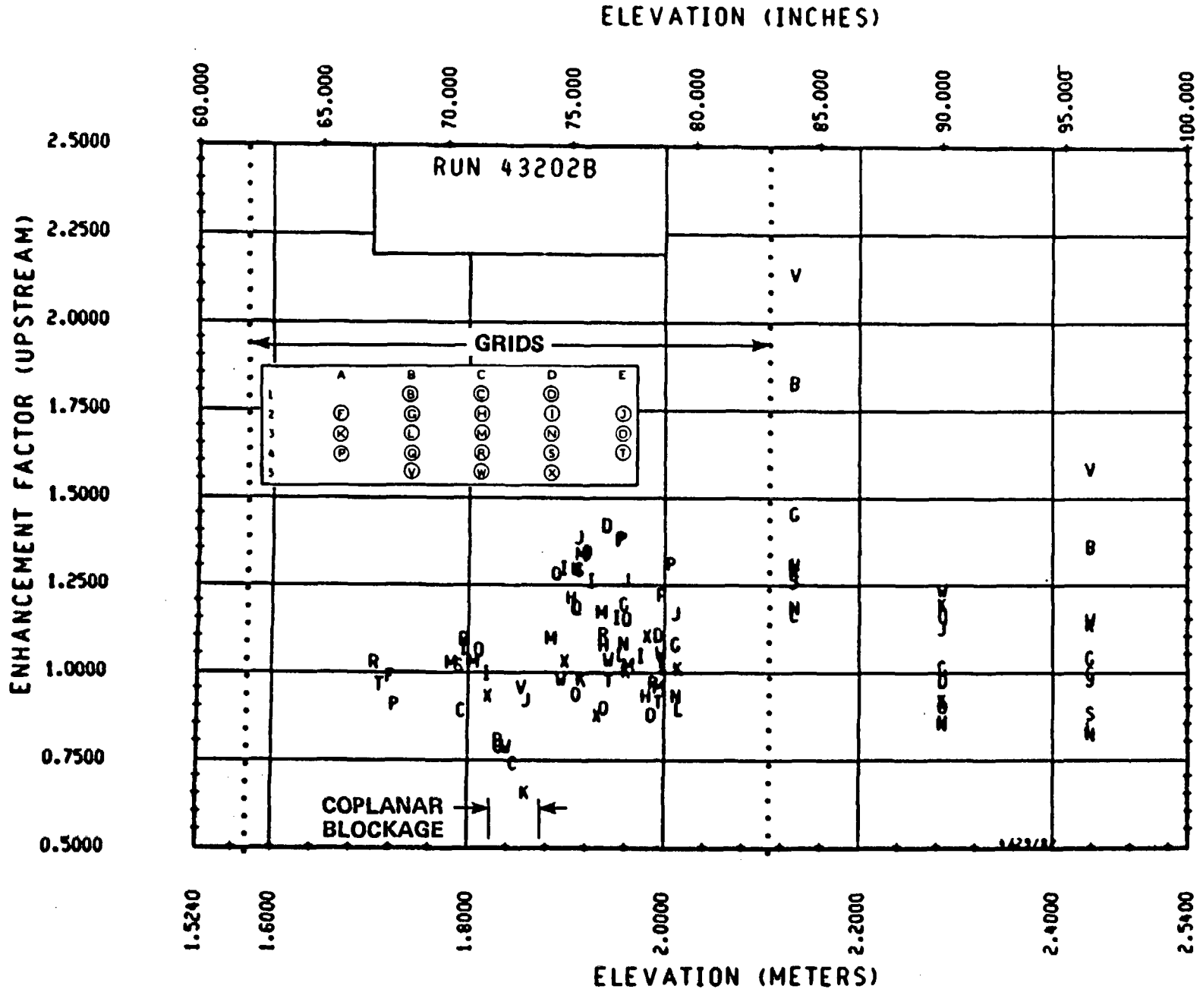

Figure 6-70. Enhancement Factor for Run 43202B

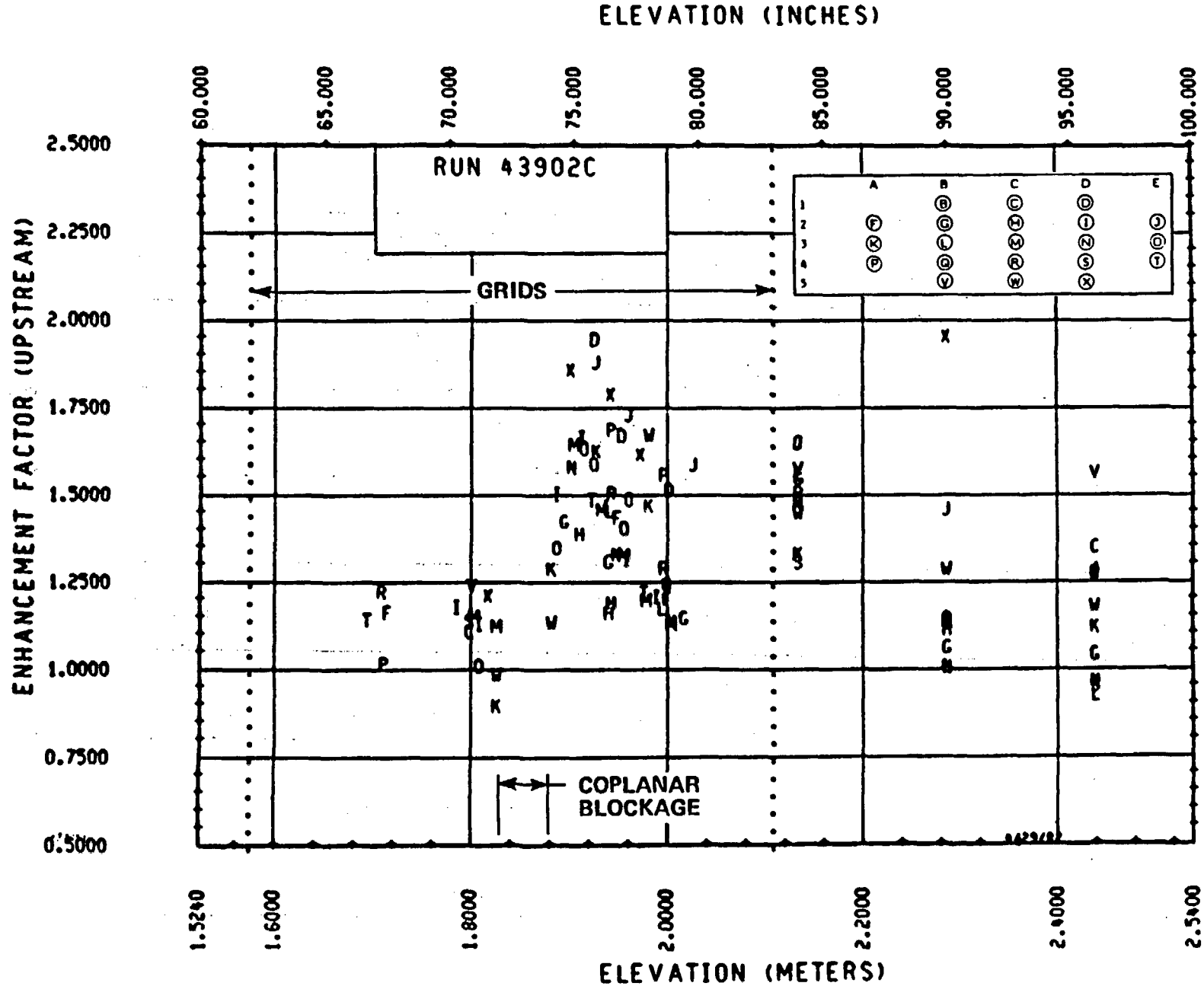

Figure 6-71. Enhancement Factor for Run 43902C

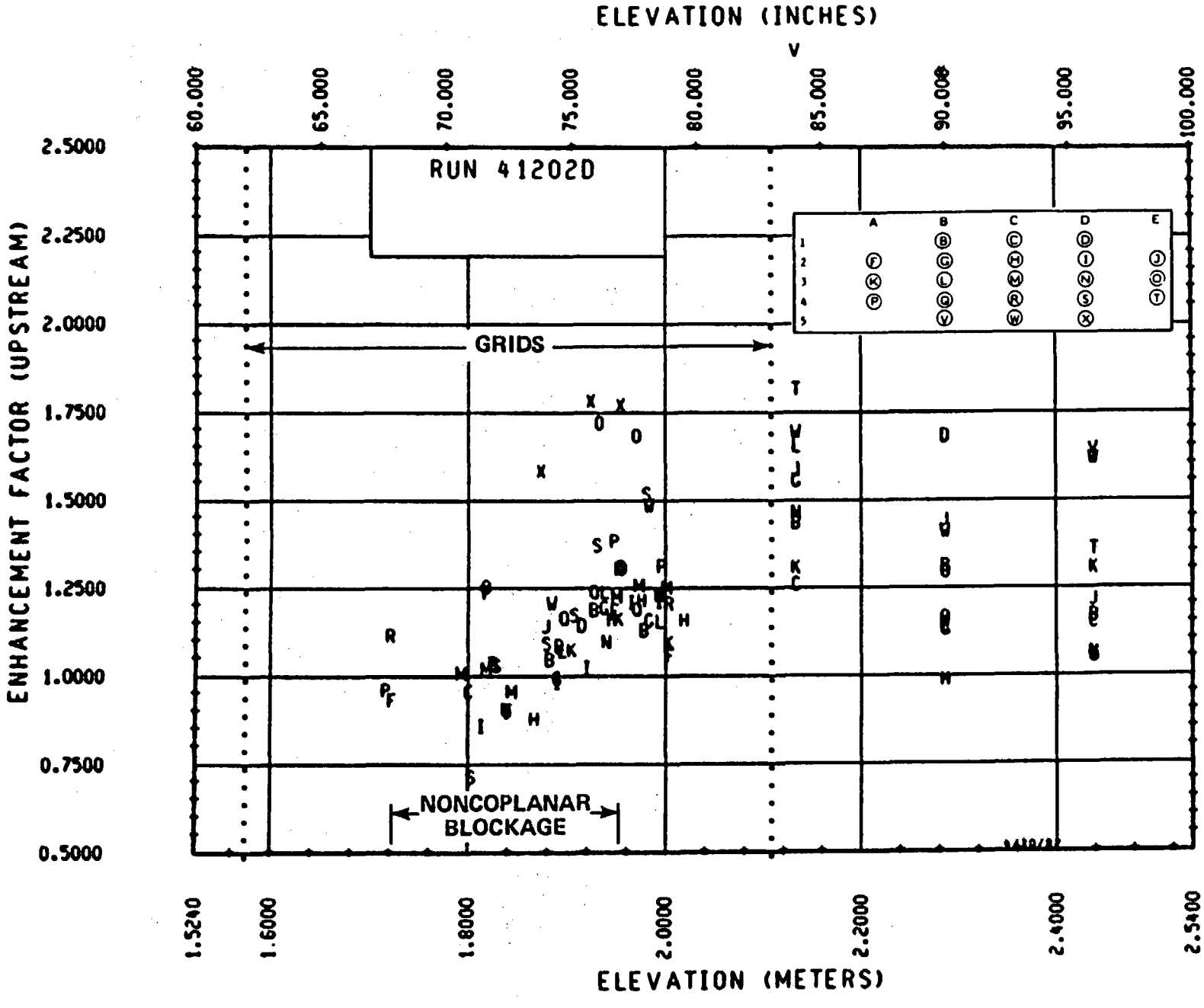

Figure 6-72. Enhancement Factor for Run 41202D

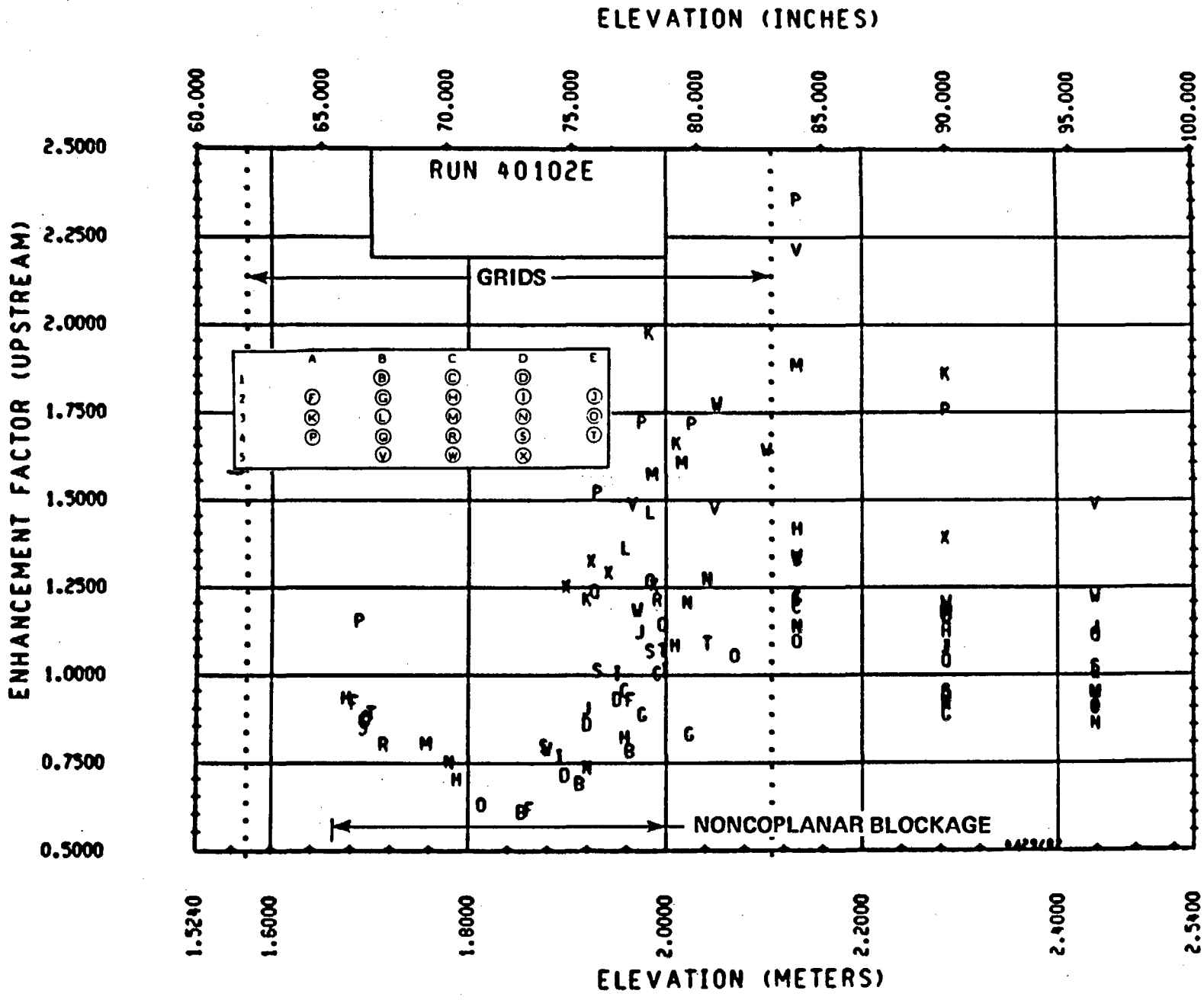

Figure 6-73. Enhancement Factor for Run 40102E

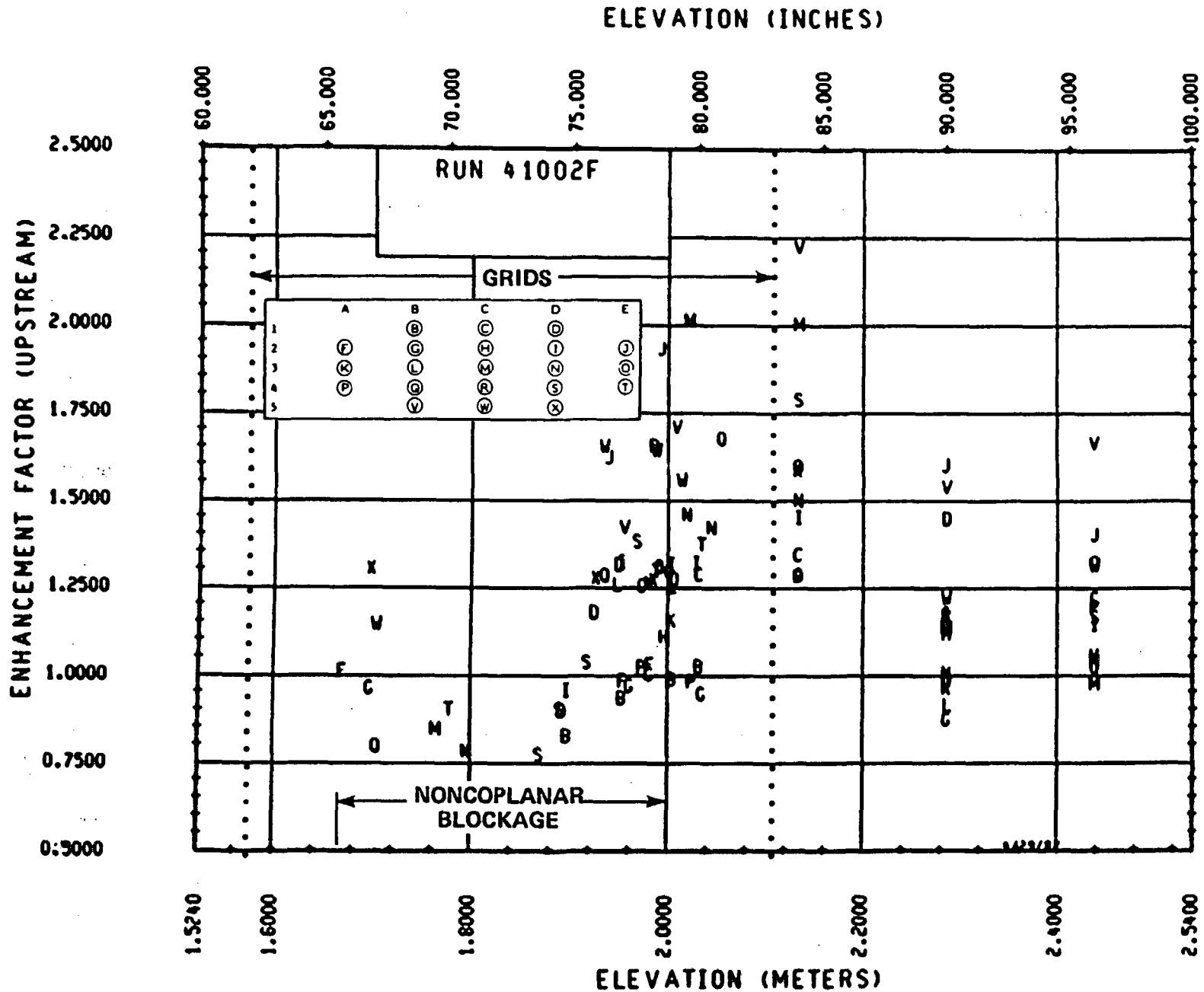

Figure 6-74. Enhancement Factor for Run 41002F

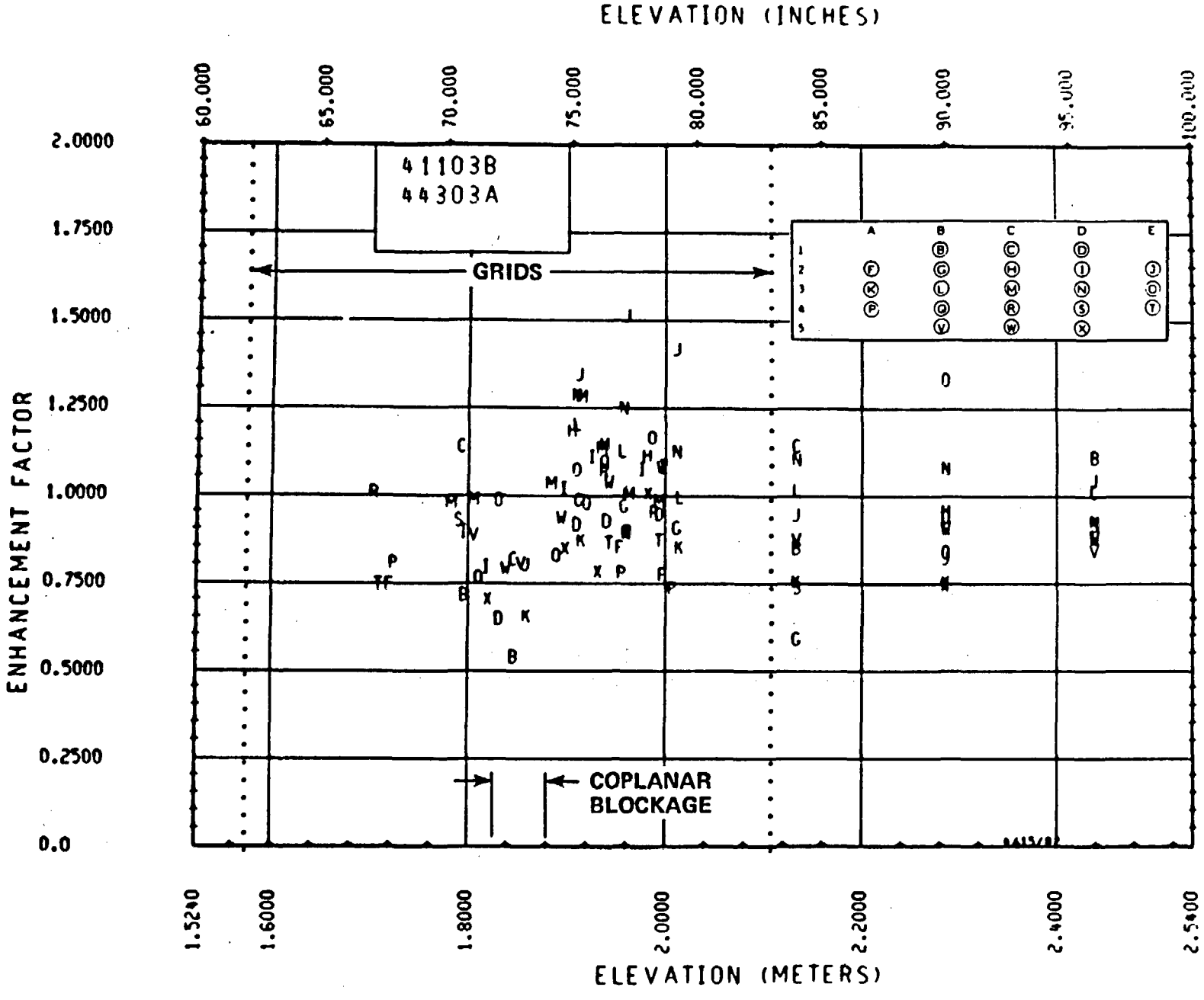

Figure 6-75. Enhancement Factor for Run 41103B

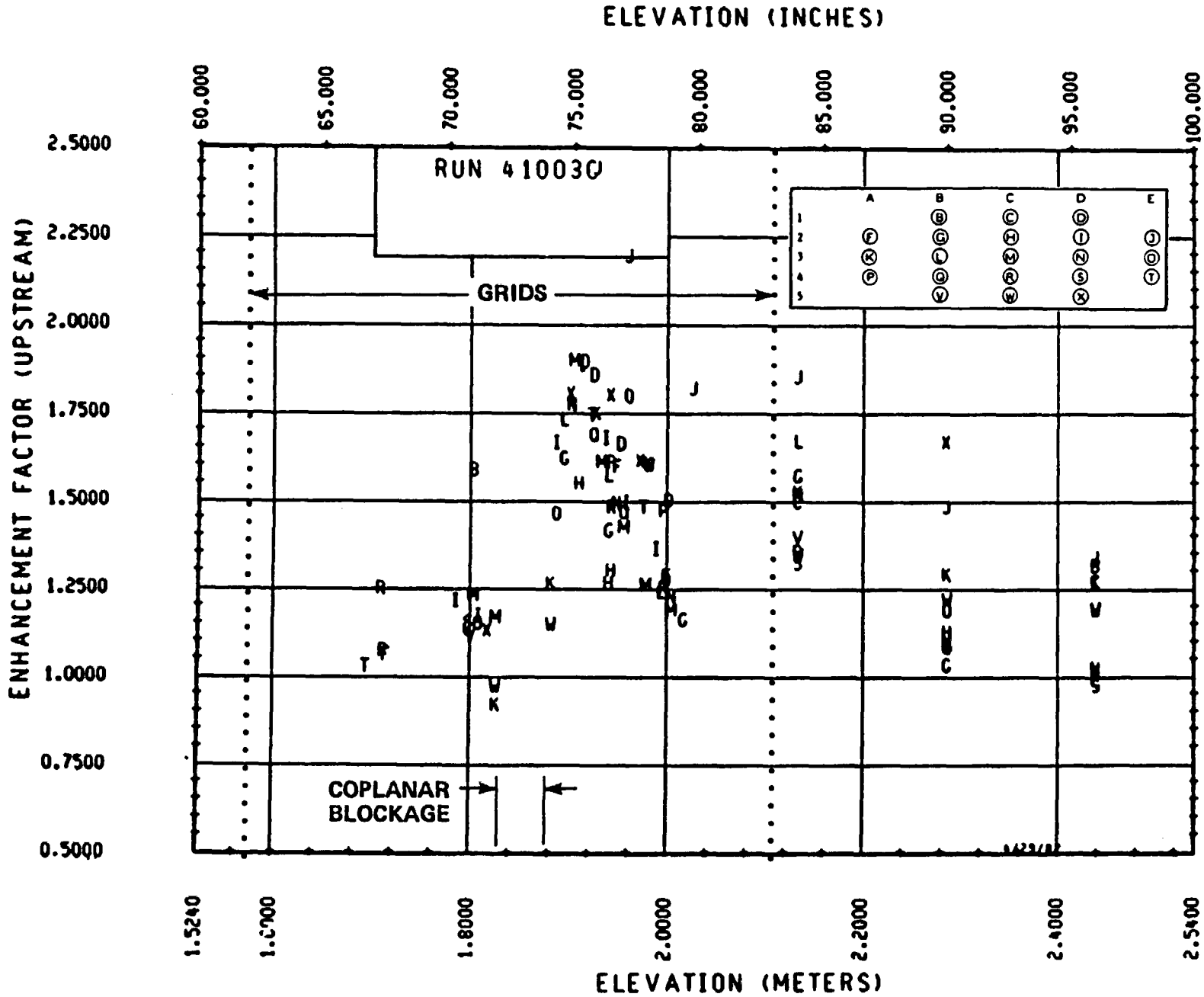

Figure 6-76. Enhancement Factor for Run 41003C

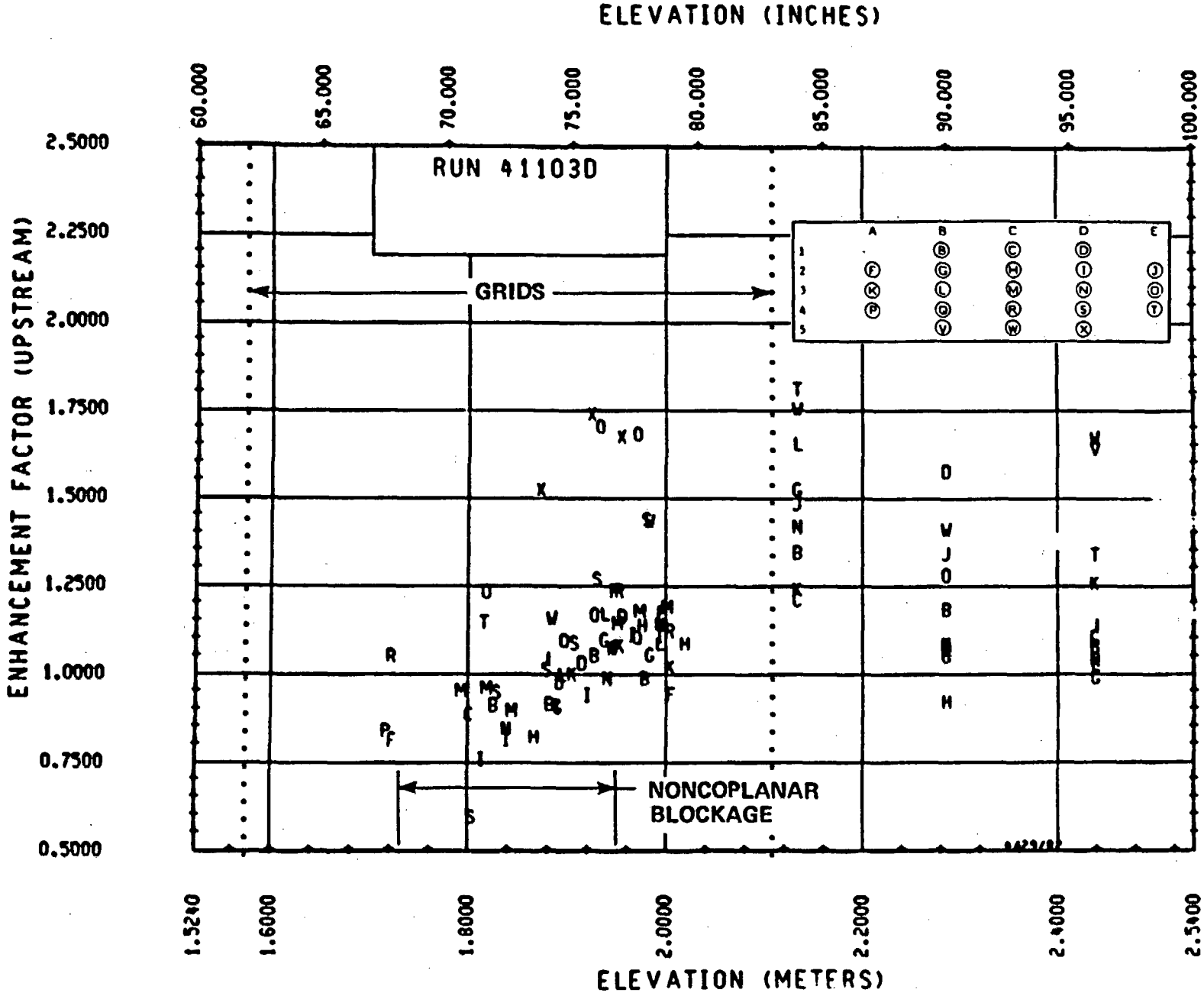

Figure 6-77. Enhancement Factor for Run 41103D

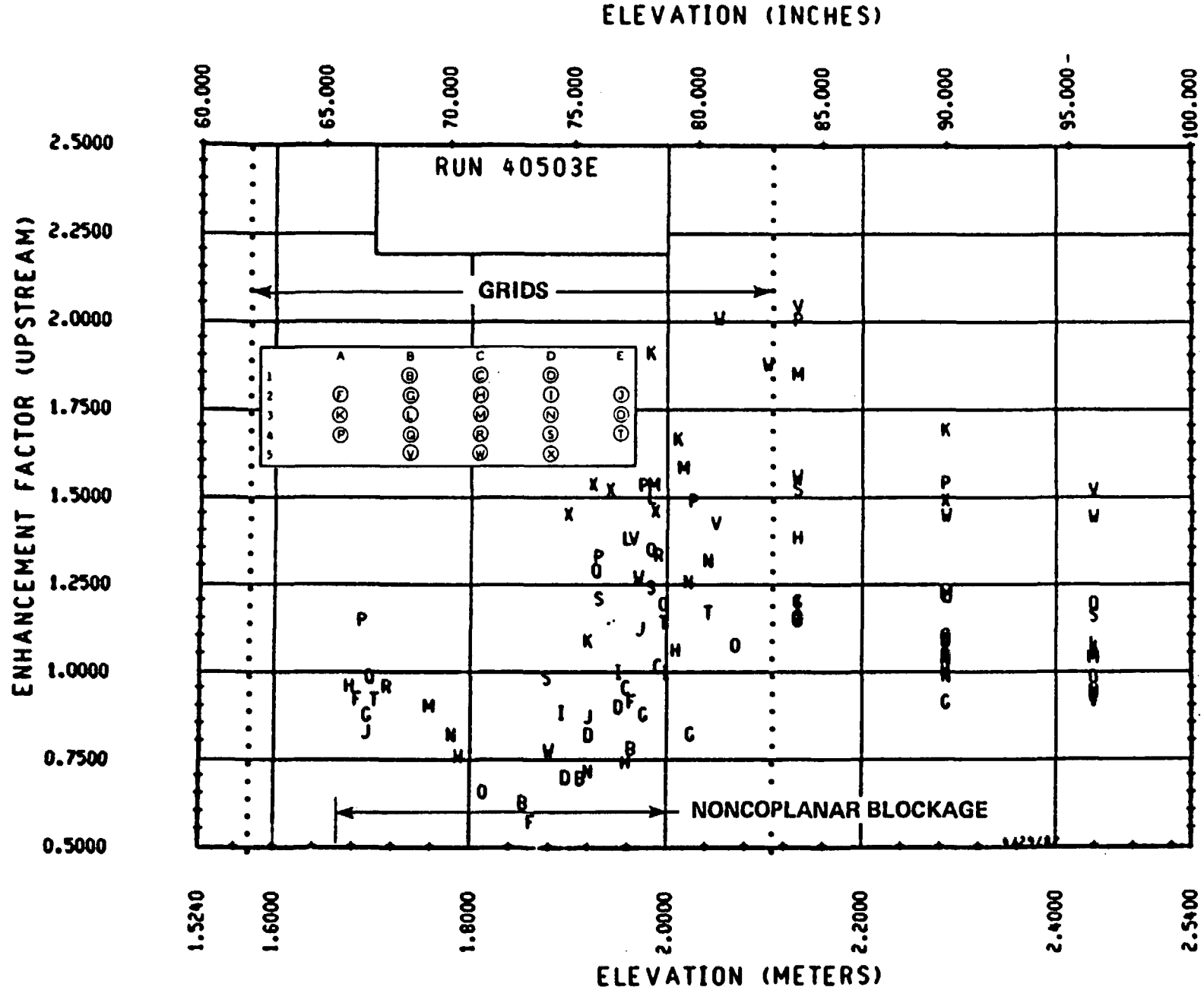

Figure 6-78. Enhancement Factor for Run 40503E

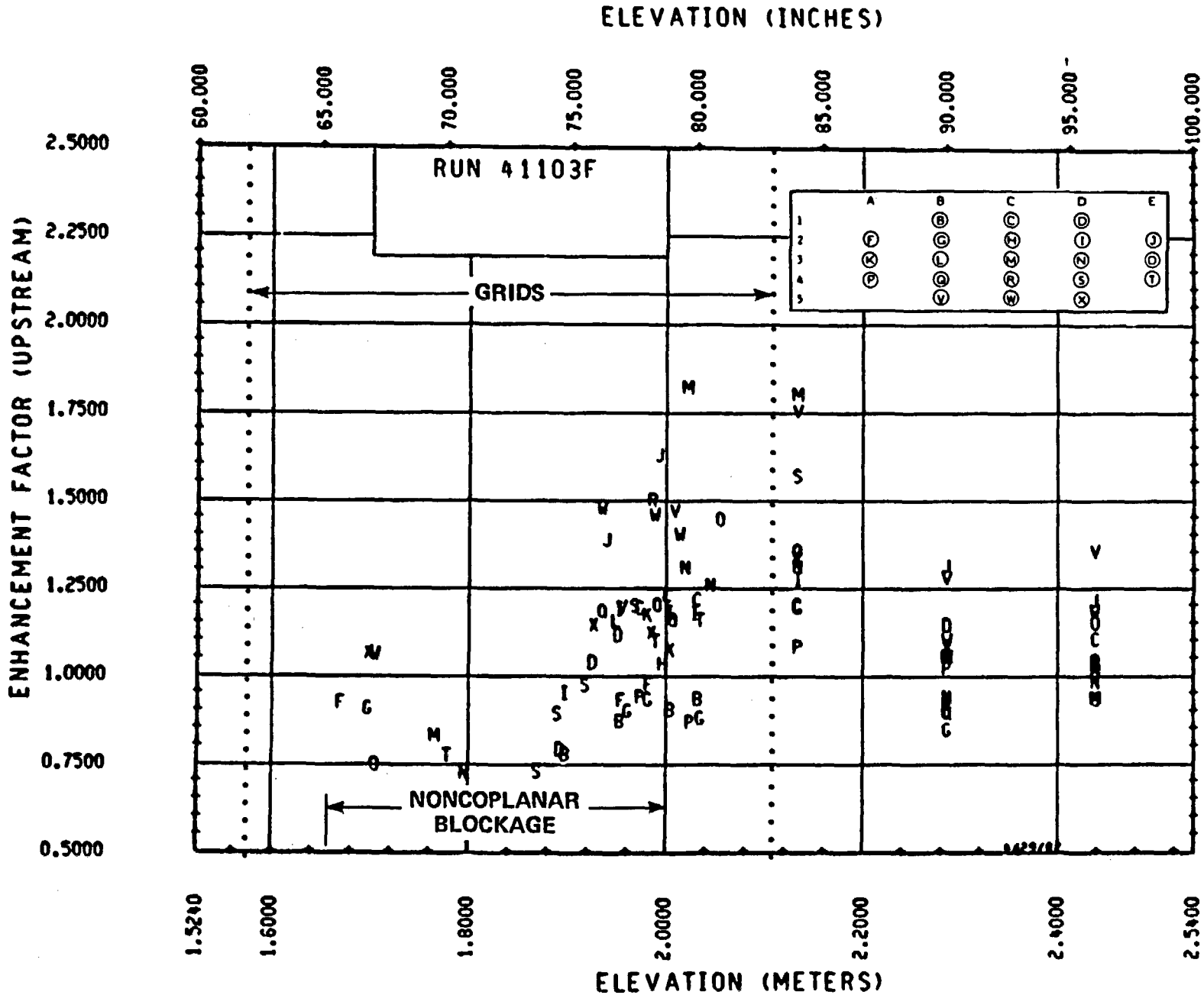

Figure 6-79. Enhancement Factor for Run 41103F

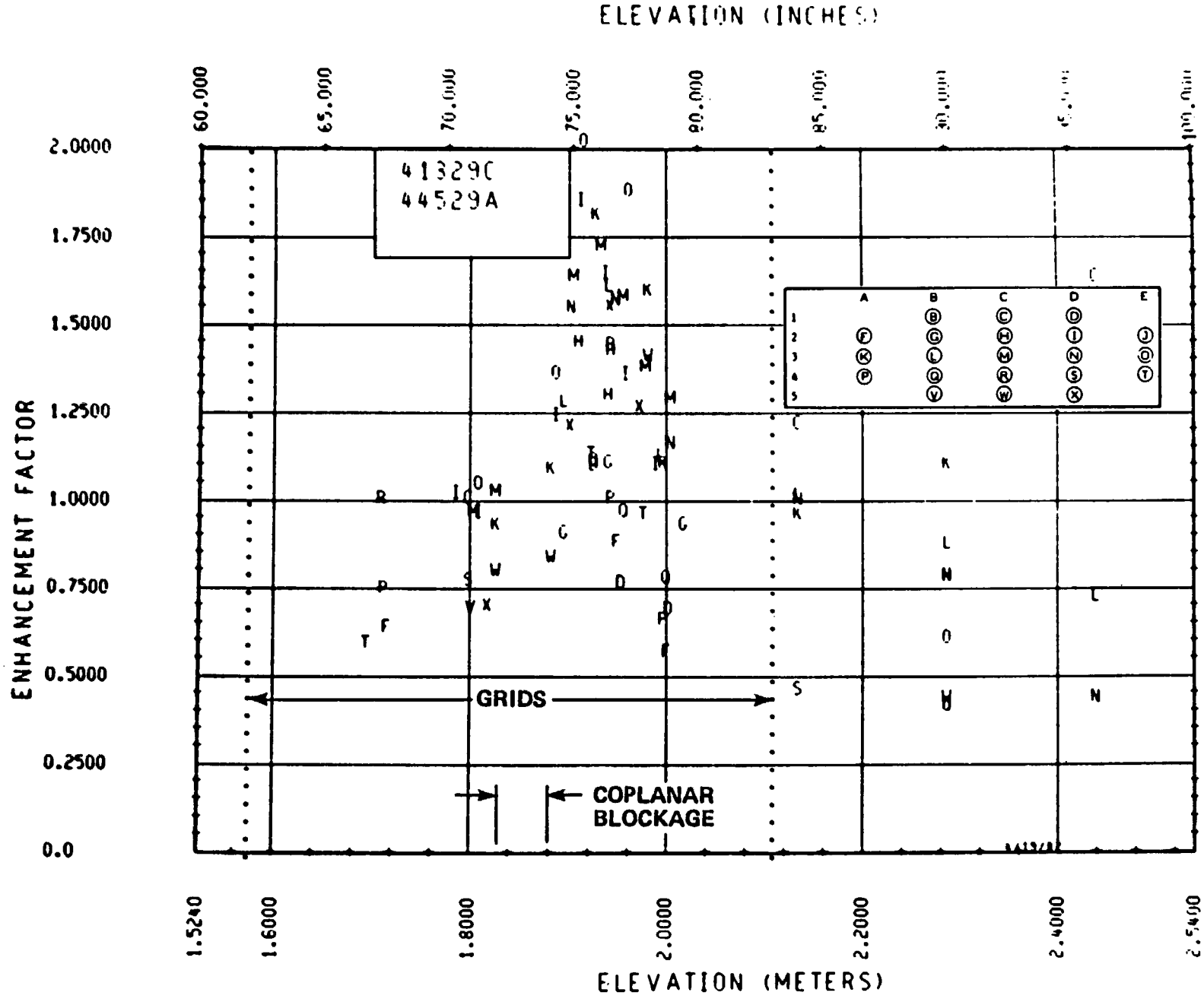

Figure 6-80. Enhancement Factor for Run 41329C

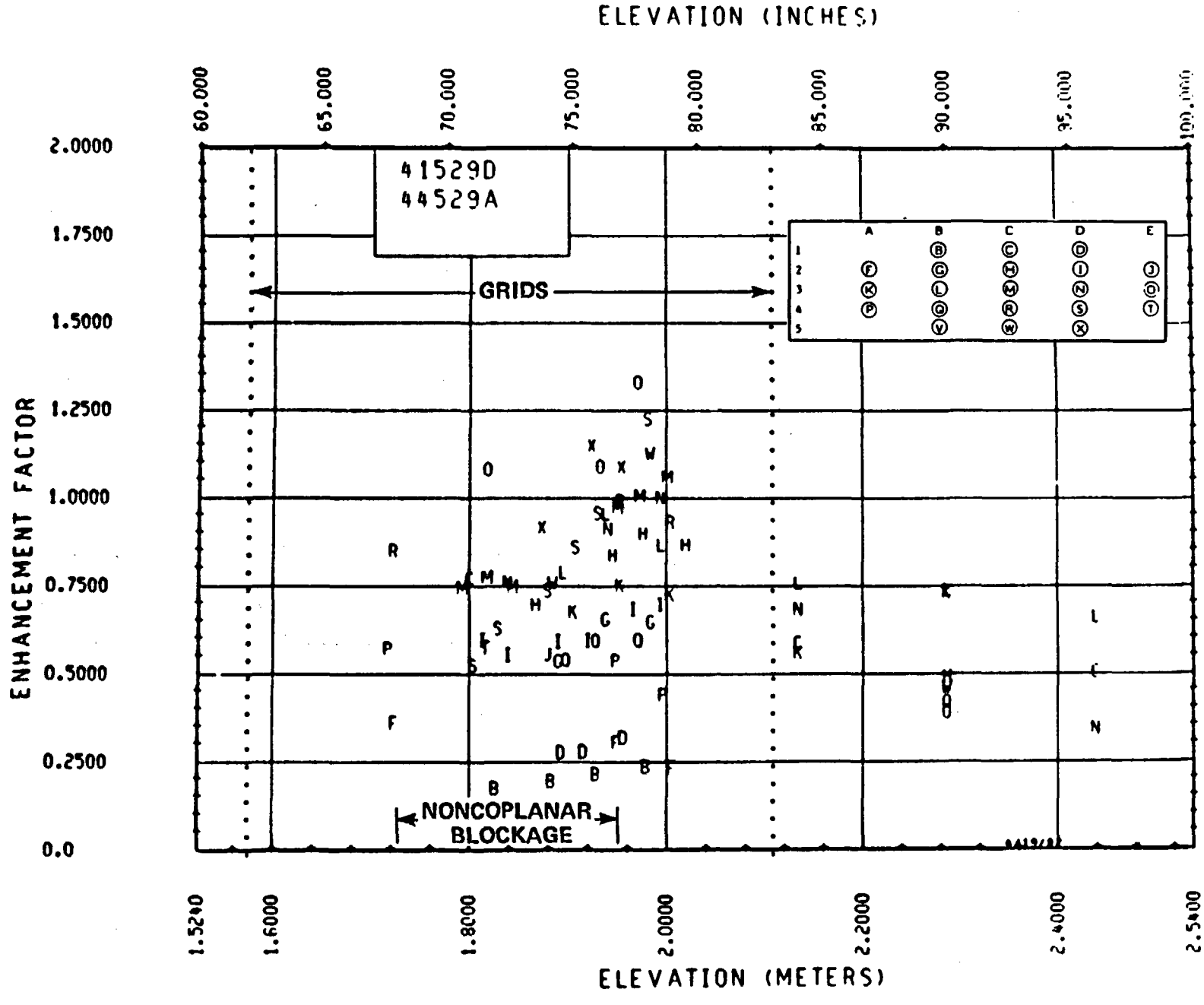

Figure 6-81. Enhancement Factor for Run 41529D

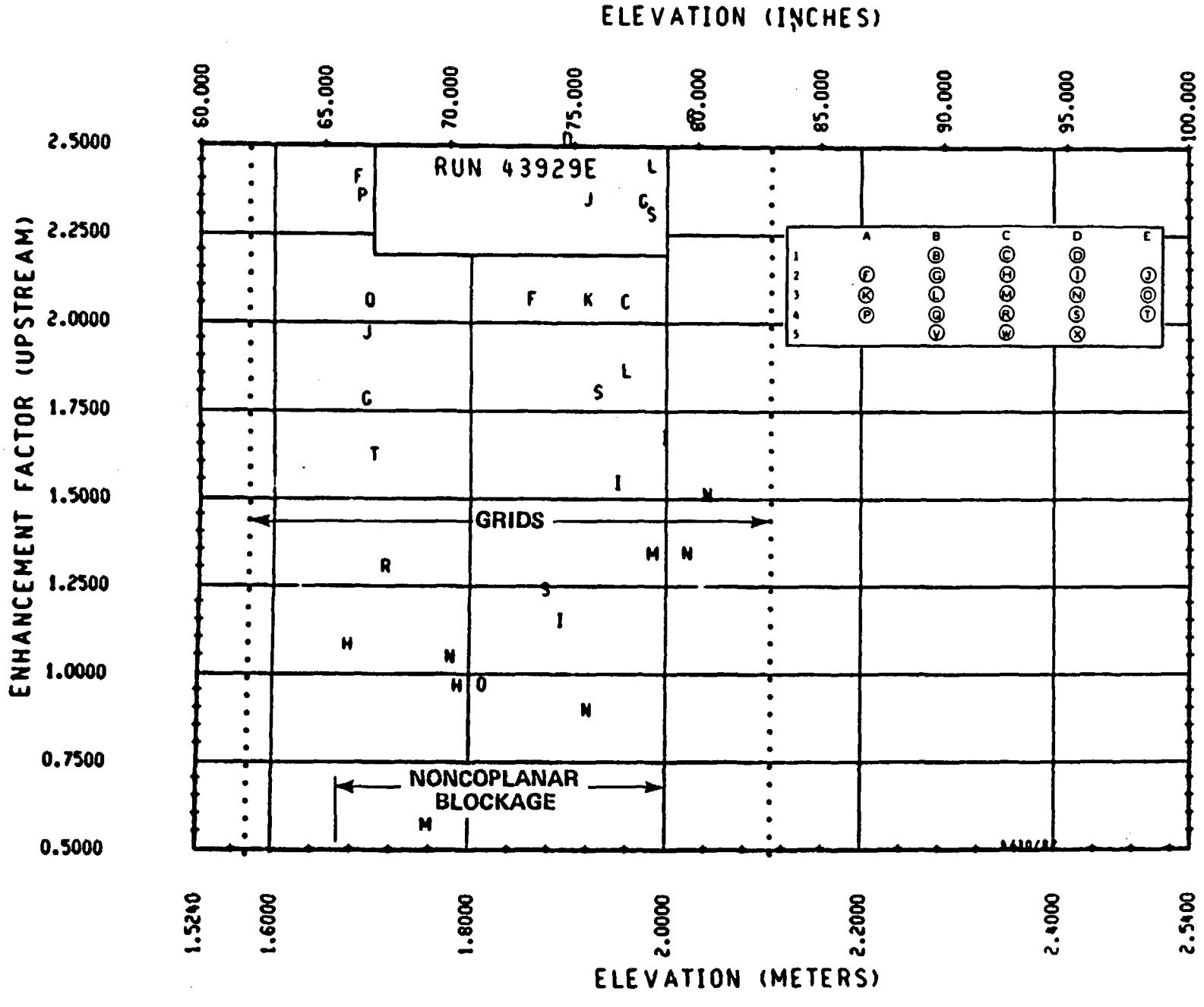

Figure 6-82. Enhancement Factor for Run 43929E

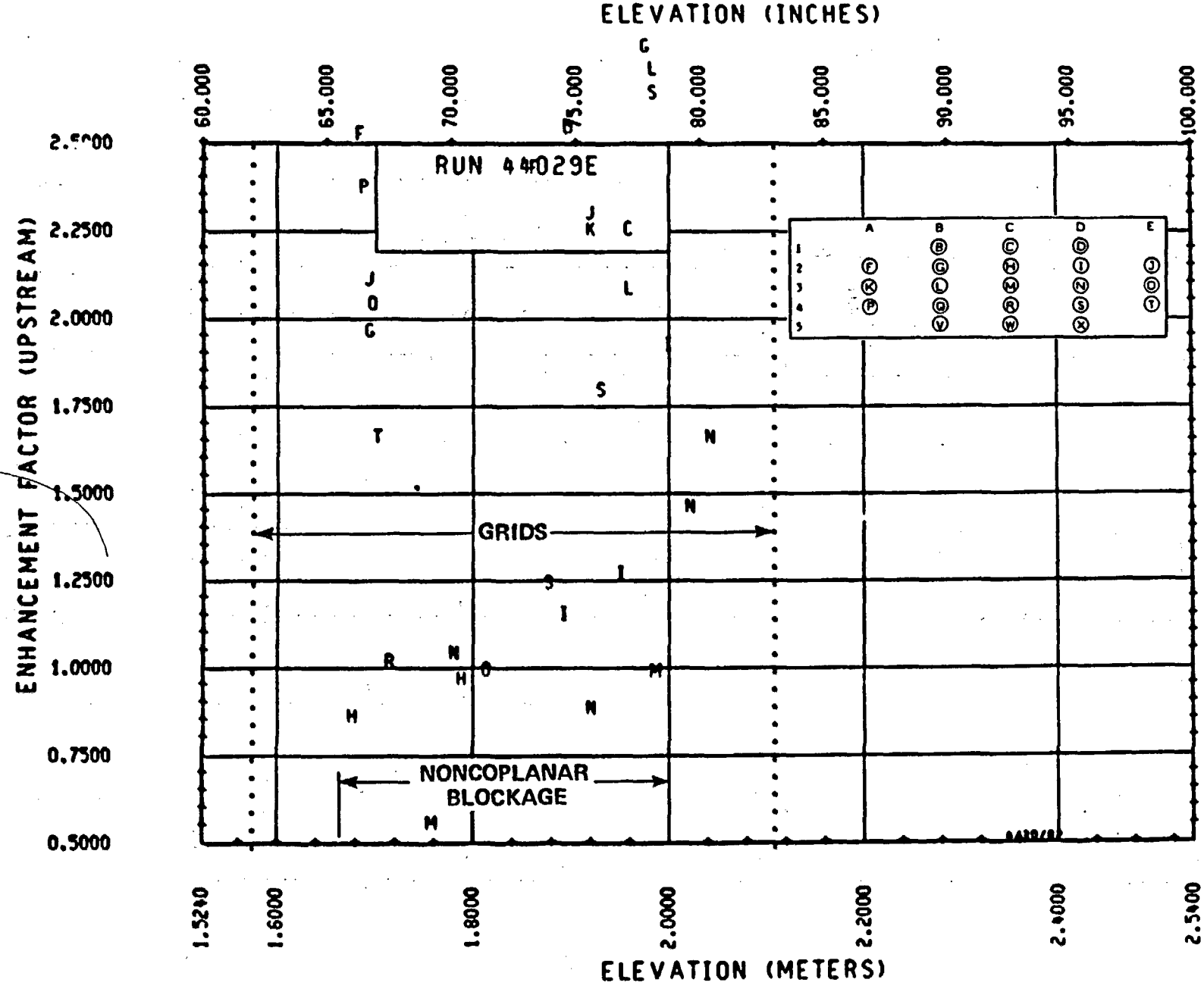

Figure 6-83. Enhancement Factor for Run 44029E

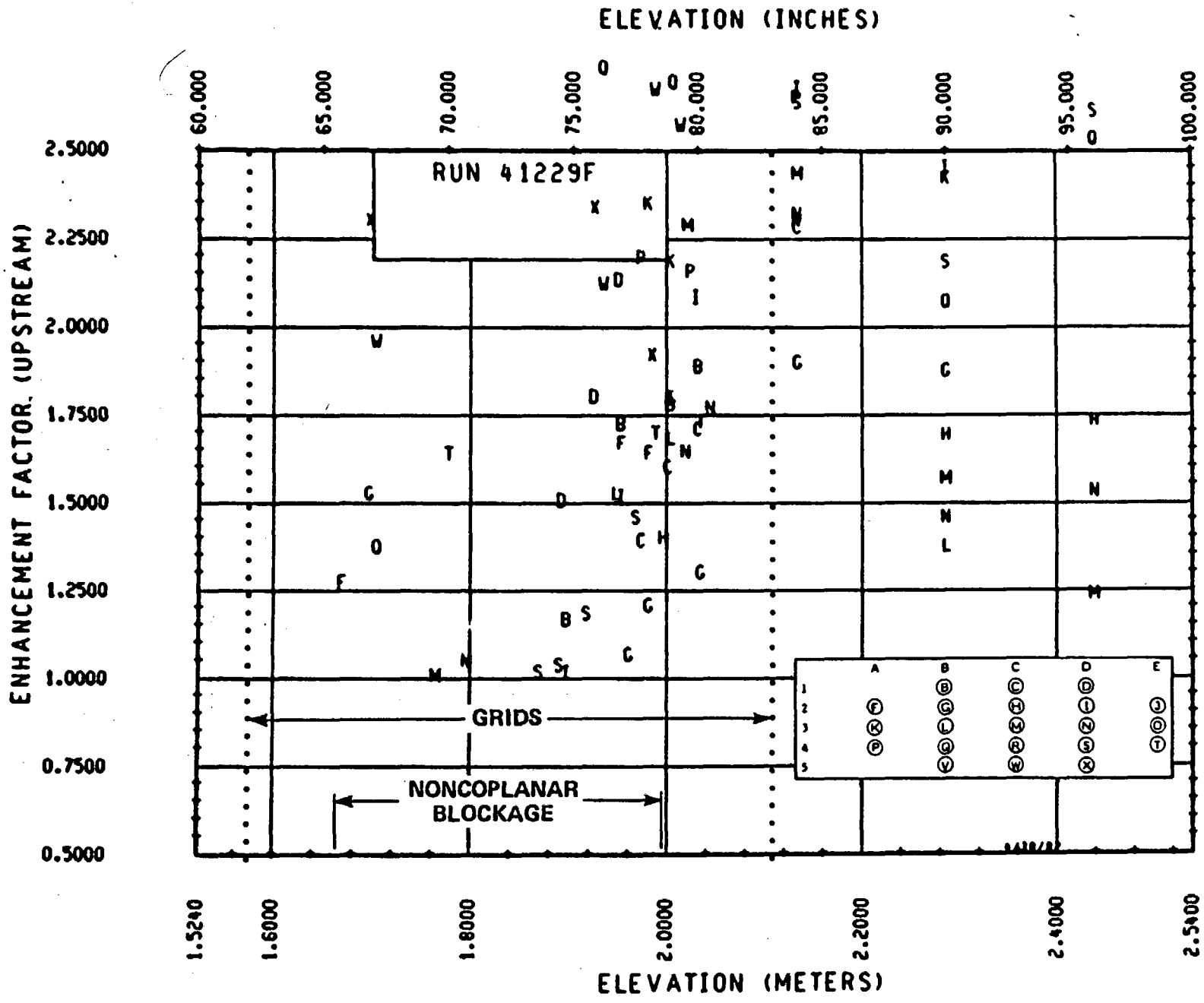

Figure 6-84. Enhancement Factor for Run 41229F

TABLE 6-4

COMPARISON OF ENHANCEMENT FACTORS, RUN 41401B

Noncorner Rod and Elevation	Enhancement Factor	
	Bundle A Data	Upstream Data[a]
4C 1.70 m (67.1 in.)	1.15	1.075
3C 1.78 m (70.2 in.)	1.09	1.01
4D 1.79 m (70.5 in.)	0.99	1.15
3C 1.81 m (71.1 in.)	1.11	1.03
3E 1.83 m (72.1 in.)	1.05	1.04
3C 1.88 m (74.2 in.)	1.28	1.13
2C 1.90 m (75.0 in.)	1.29	1.21
3D 1.91 m (75.2 in.)	1.50	1.40
2B 1.96 m (77.1 in.)	1.12	1.27
3D 1.96 m (77.1 in.)	1.43	1.35
2C 1.98 m (78 in.)	1.18	1.10
3B 2.01 m (79.3 in.)	1.05	1.0
3D 2.01 m (79.2 in.)	1.29	1.21
3A 2.01 m (79.3 in.)	0.93	0.98

a. $Nu/0.023\ Re^{0.8} = 1.25$

blockage. However, the enhancement factors for the corner heater rods were generally less than a value of 1 if the blocked data were normalized by the corresponding unblocked data, and conversely, were generally greater than that of the inside rods if the blocked data were normalized by the upstream data. The enhancement factors for the inside heater rods were consistently greater for the coplanar blockage configuration without flow bypass than for the configuration with flow bypass.

The enhancement factors for the noncoplanar blockage configurations (configurations D, E, and F) for both the inside and corner heater rods varied significantly in

magnitude within and downstream of the blockage. In reviewing the data, there appeared to be no consistent relationship between the enhancement factor and the blockage sleeve location. The noncoplanar blockage distribution would cause the thermal response of the heater rods to be affected by adjacent blockage sleeves. However, a fairly consistent trend observed was the relationship between the local COBRA-calculated Reynolds number and the enhancement factor. As the local Reynolds number decreased, the enhancement factor increased, although not necessarily proportionally. This is quite similar to the coplanar blockage cases, in which the improvement in the heat transfer generally decreases with Reynolds number. These enhancement factors will be correlated as a function of elevation, Reynolds number, and blockage for publication in the data evaluation report.

6-14. FORCED REFLOOD TEST DATA ANALYSIS

The following paragraphs discuss COBRA simulation of the tests and calculation of the enhancement factor.

The enhancement factor (Ne) was defined in section 3 as

$$\frac{h_b}{h_o} = \left(\frac{G_b}{G_o}\right)^m Ne \qquad (6\text{-}1)$$

according to the Hall and Duffey approach. The subscripts b and o represent the blocked and unblocked bundles, respectively. The heat transfer coefficient (h) is obtained from DATAR code results, G is mass flux, and m is a constant exponent, which could be 0.8 if the Dittus-Boelter correlation is used as a basis.

6-15. COBRA-IV-I Simulation

The fluid flow condition above the quench front during a reflood test is a dispersed nonequilibrium flow. The local mass flow rate and quality are also changing with time. Even though an ideal simulation of the flow above the quench front should

include all these effects, some of them may be second-order for the present purpose and the problem can be simplified significantly.

Since the dispersed droplet flow usually has a high void fraction, the flow can be reasonably assumed to be single phase. Since droplets resist flow diversion at blockages, this assumption will give conservative results in the enhancement factor calculation.

The mass flow and heat addition effect have been studied by Westinghouse,[1] EG&G,[2] and Prelewicz,[3] with the following results:

-- Mass flow rate change does not affect flow redistribution at the blockage in any significant way.

-- Heat addition can change flow redistribution to some extent, but the ratio between the blocked bundle and unblocked bundle (G_b/G_o) is not affected significantly.

Based on the above observations, it was decided to simulate the reflood test as a single-phase steam flow test with a constant flow rate and isothermal condition. For this case, equation (6-1) can be written as

$$\frac{h_b}{h_o} = \left(\frac{v_b}{v_o}\right)^m Ne \qquad (6\text{-}2)$$

where v = velocity.

---

1. Presentation at FLECHT SEASET PMG meeting, Washington, DC, November 6-7, 1980.

2. Ogden, D., "Evaluation of FLECHT SEASET COBRA IV-I Flow Blockage Model", EG&G-CAAD-5376, March 1981.

3. Prelewicz, D. A., and Caruso, M. A., "Evaluation of Flow Redistribution due to Flow Blockage in Rod Bundles Using COBRA Code Simulation," ERPI-NP-1662, January 1981.

The simulated flow conditions are summarized in table 6-5. Because of the noncoplanar blockage distribution, the entire cross section of the bundle was simulated as indicated by channel and rod numbers in figure 6-85. The simulated axial length was 1.75 m (69 in.) between the 1.30 and 3.05 m (51 and 120 in.) elevations, as indicated in figure 6-85. The axial node length was taken to be 25 mm (1 in.)

TABLE 6-5

COBRA SIMULATION FLOW CONDITIONS

Pressure	0.28 MPa (40 psia)
Fluid temperature	Slightly superheated steam
Flow rate	453 kg/m^2-sec (1000 lb/ft^2-hr
Linear velocity	~ 9.1 m/sec (30 ft/sec)
Re	≈ 12,500
Power	Isothermal

This node length should provide reasonable simulation.[1] Flow blockage was simulated by flow area variation only in configurations B through D, and with both flow area variation and pressure loss coefficient for configurations E and F, as previously described in paragraph 6-7. The grid loss coefficients were estimated based on Rehme's method. The input parameters for the COBRA simulation, including area, gap variation, and pressure loss coefficient tables, are provided in appendix A.

6-16. Determination of Enhancement Factor

It was found that the circumferential temperature variation on rods was not significant (see appendix I) and the temperature on a rod was affected by the fluid flow in the four adjacent subchannels. Therefore it is logical to use the average fluid flow rate in the four channels surrounding a rod. That is, rod-centered subchannels (figure 6-86) should

1. Letter to R. E. Tiller from J. A. Dearien, January 12, 1981.

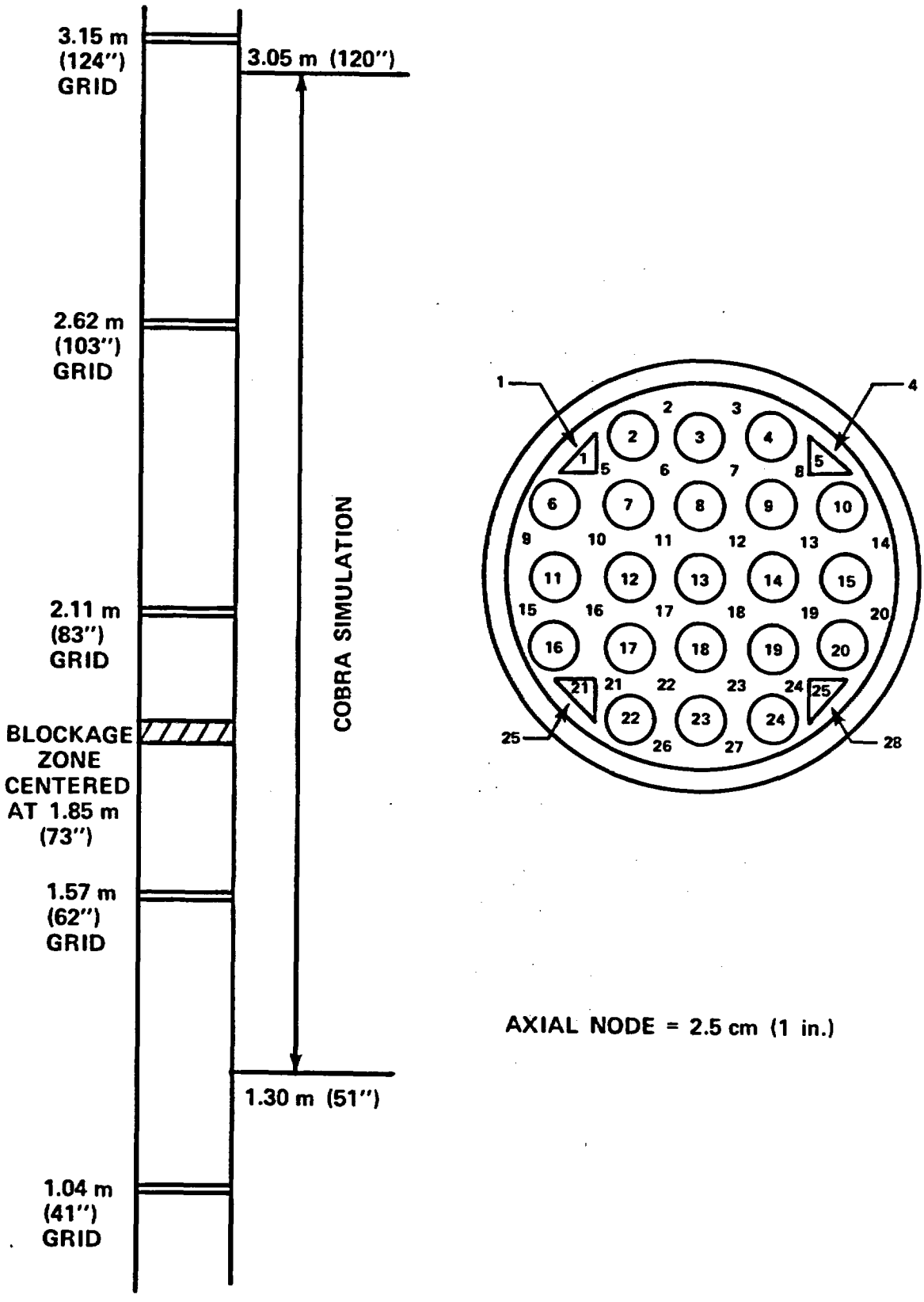

Figure 6-85. COBRA Simulation of 21-Rod Bundle

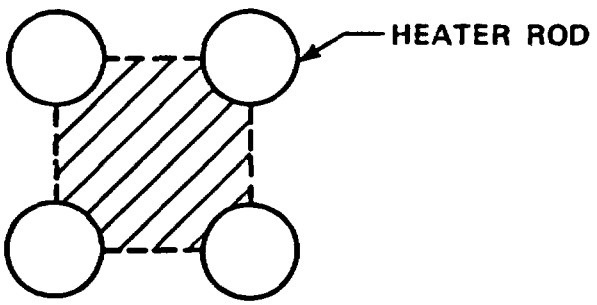

(a) FLOW-CENTERED SUBCHANNEL

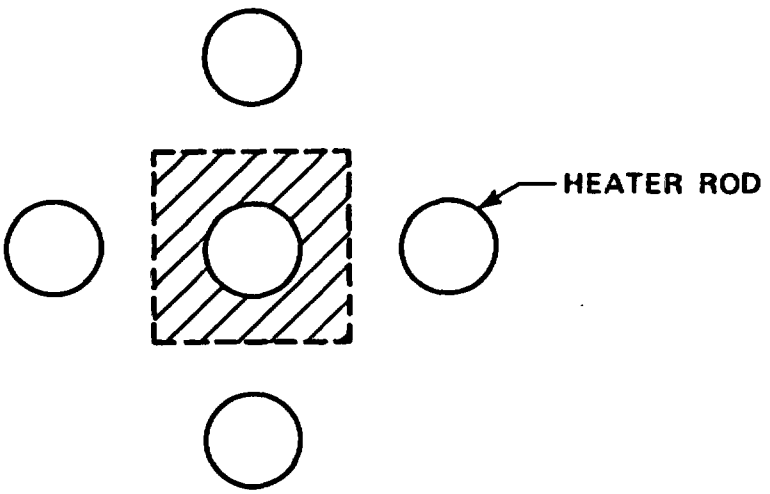

(b) ROD-CENTERED SUBCHANNEL

Figure 6-86. Subchannel Definitions

be considered in calculating the enhancement factors. The flow rate in the rod-centered subchannels are calculated by the COBROD code, which reads the COBRA results and obtains rod-centered subchannel average flows.

The computer program COMPARE has been modified to calculate the enhancement factor according to equation (6-1). A schematic diagram of the logic used to calculate the enhancement factor is shown in figure 6-87. The resulting enhancement factors using m=0.8 for the reference tests [28 mm/sec and 0.28 MPa (1.1 in./sec and 40 psia)] are presented in figures 6-88 through 6-132 for configurations C through E.

The enhancement factors for configurations B and F for the reference tests and configurations B through F for other test conditions [23 mm/sec and 0.28 MPa (0.9 in./sec and 40 psia)] are presented in appendix O.

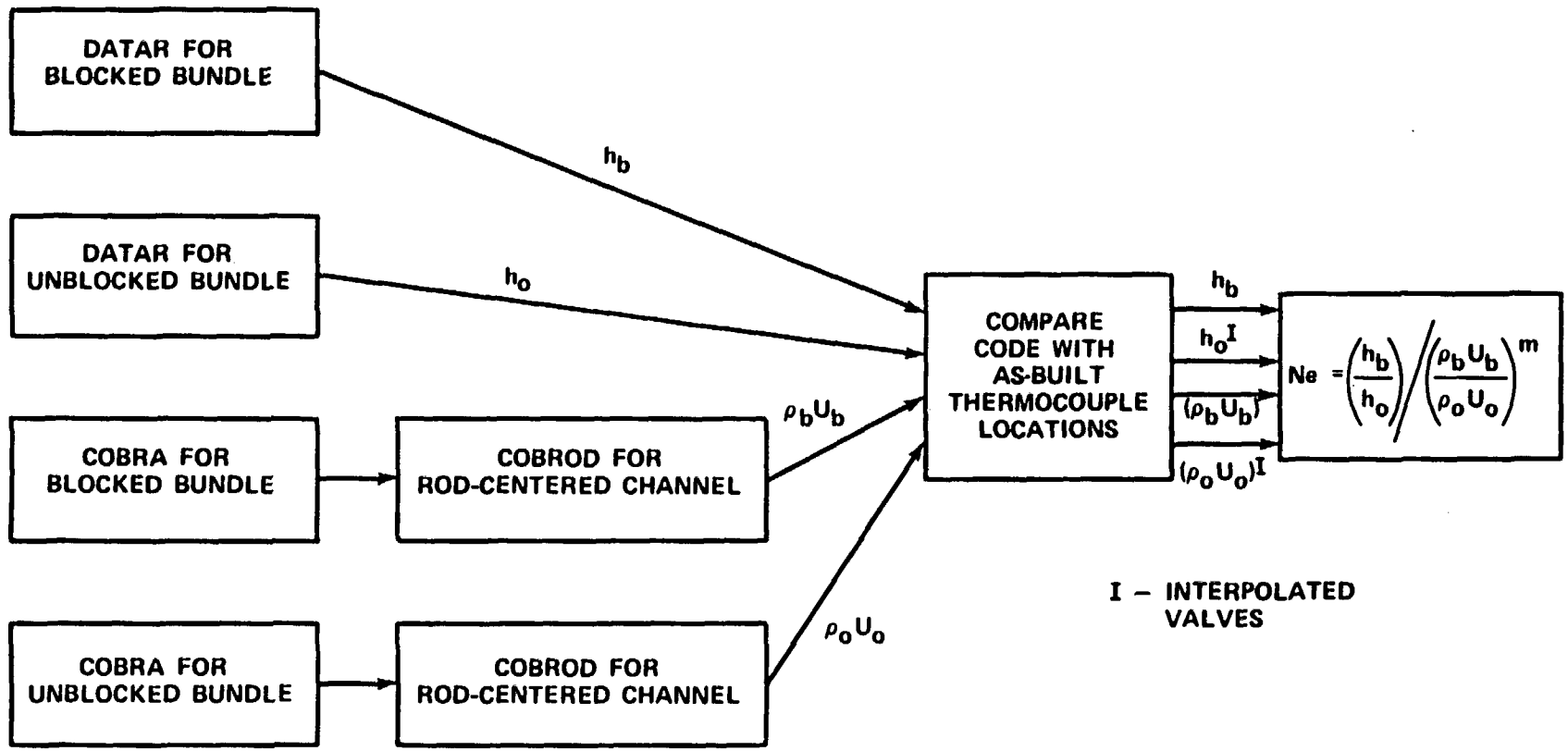

Figure 6-87. Estimation of Enhancement Factor

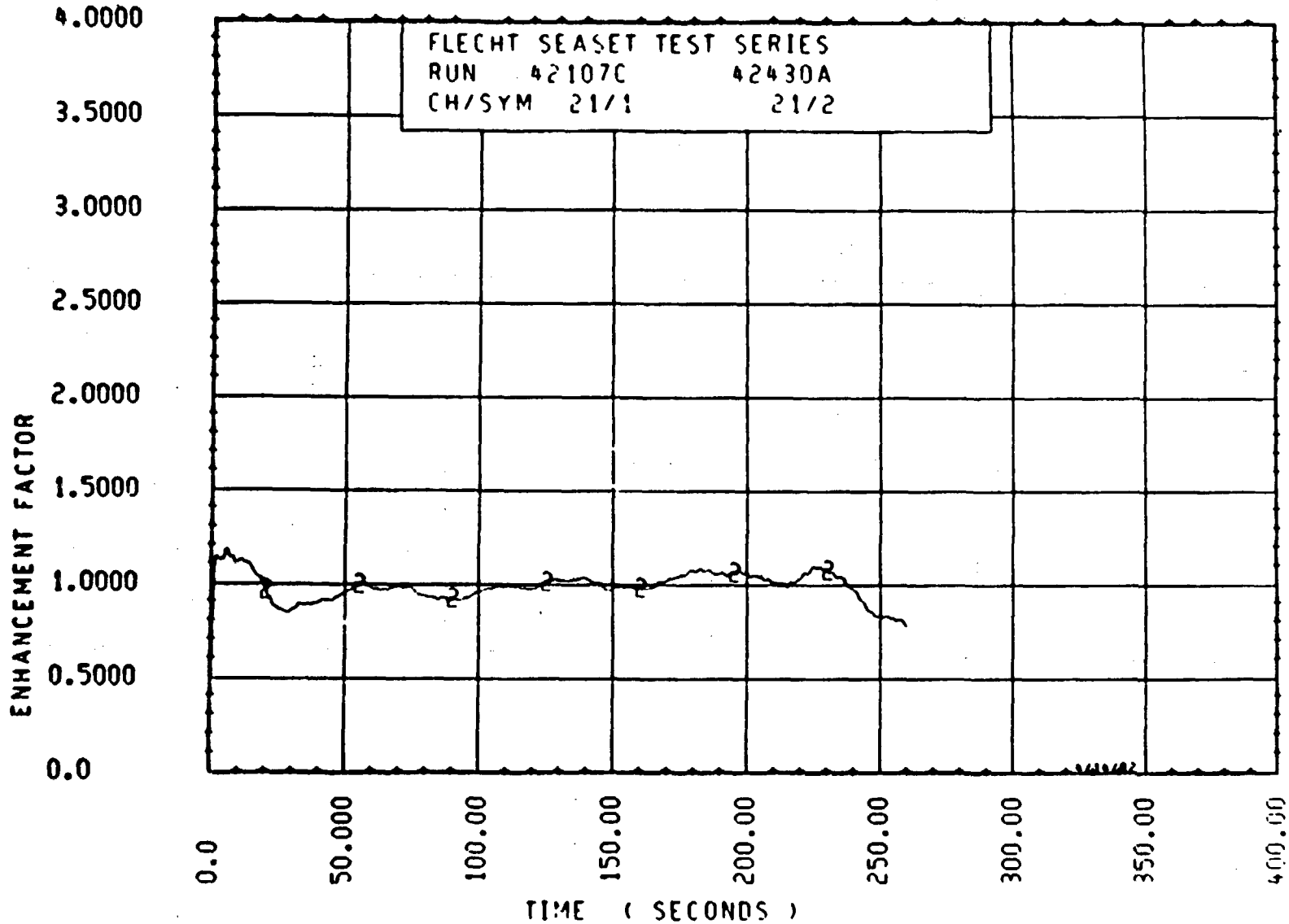

Figure 6-88. Enhancement Factor for Run 42107C, Rod 2A, 1.71 m (67.5 in.) Elevation

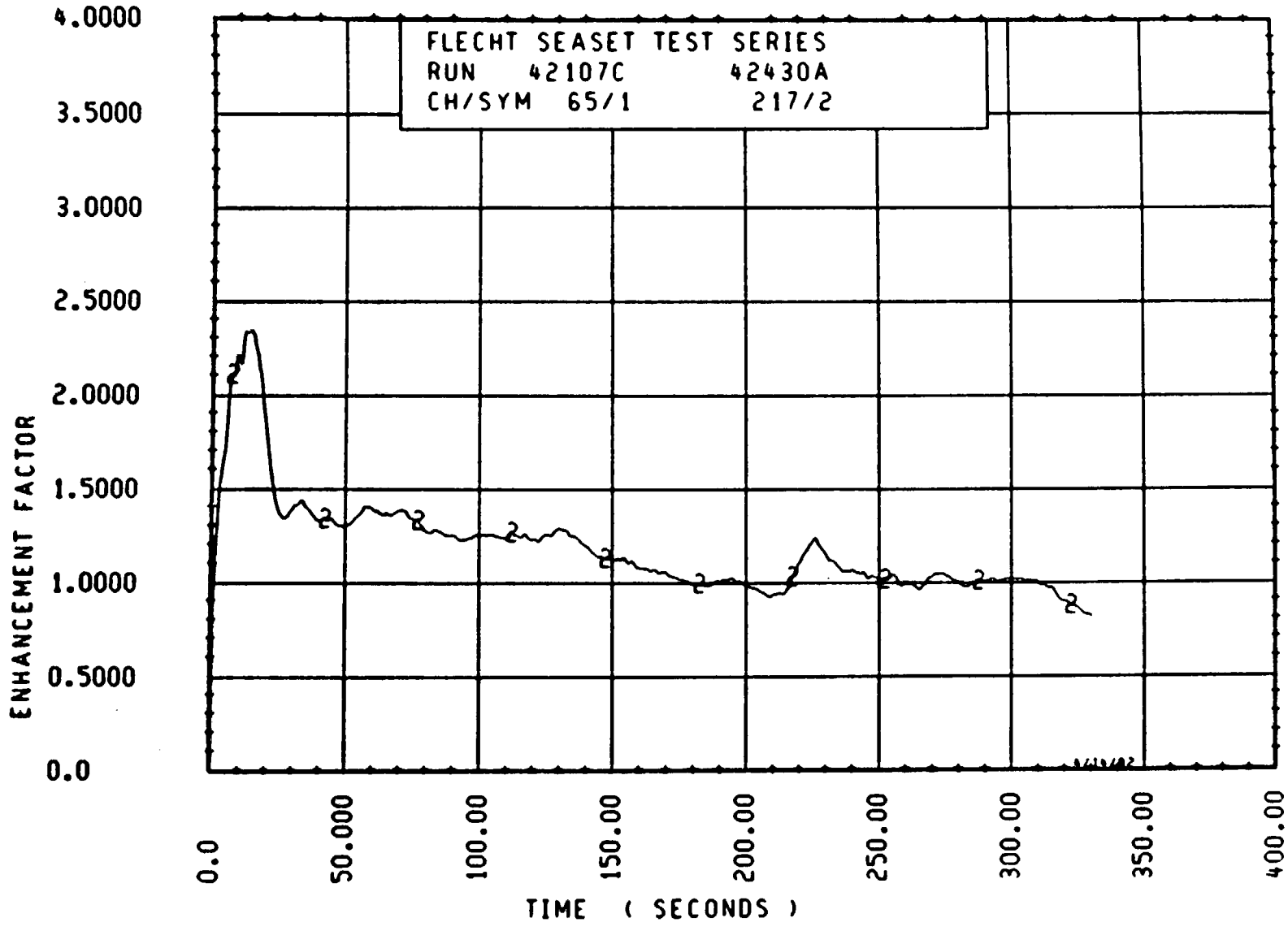

Figure 6-89. Enhancement Factor for Run 42107C, Rod 2D, 1.91 m (75.3 in.) Elevation

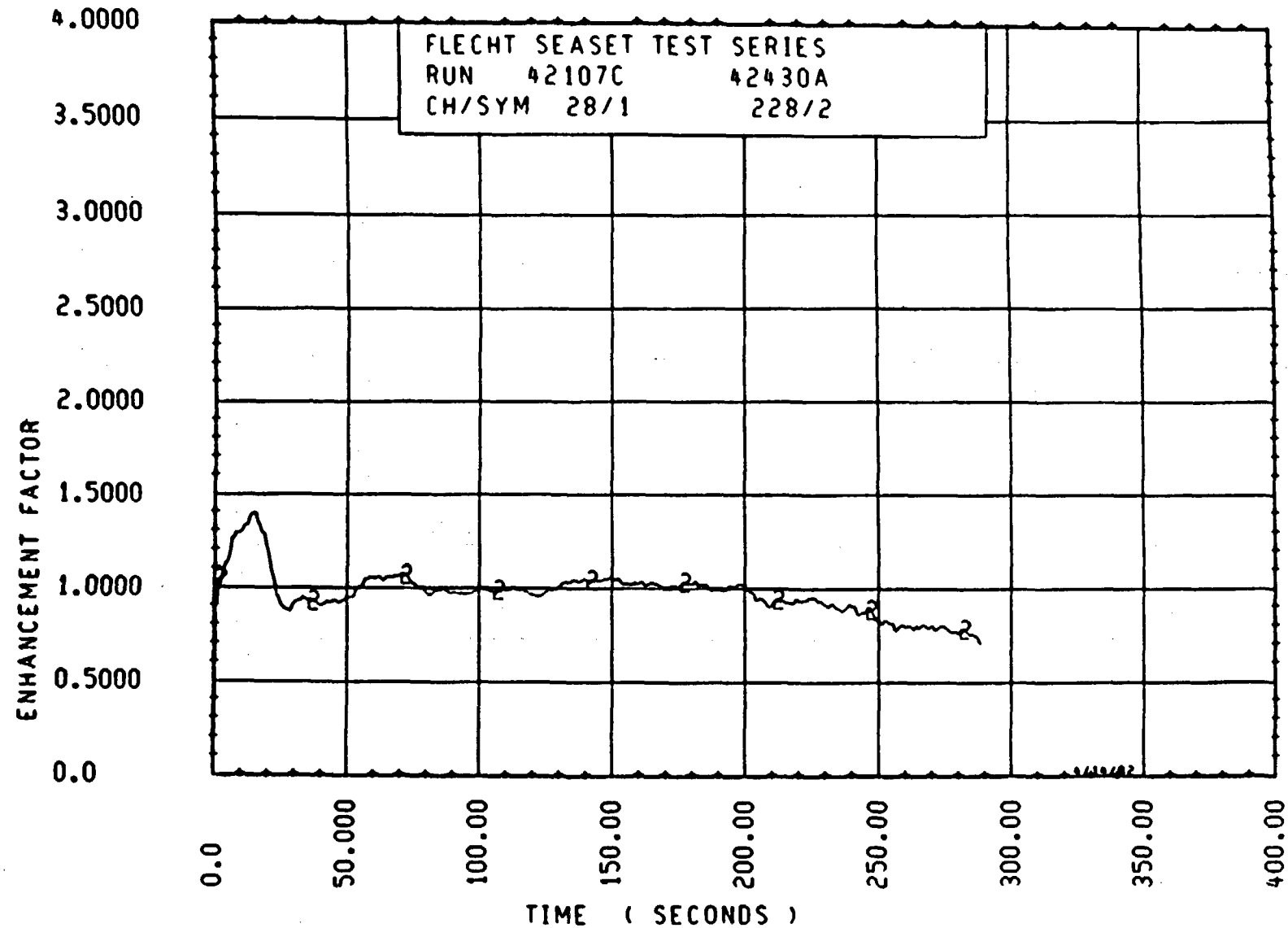

Figure 6-90. Enhancement Factor for Run 42107C, Rod 3C, 1.80 m (71 in.) Elevation

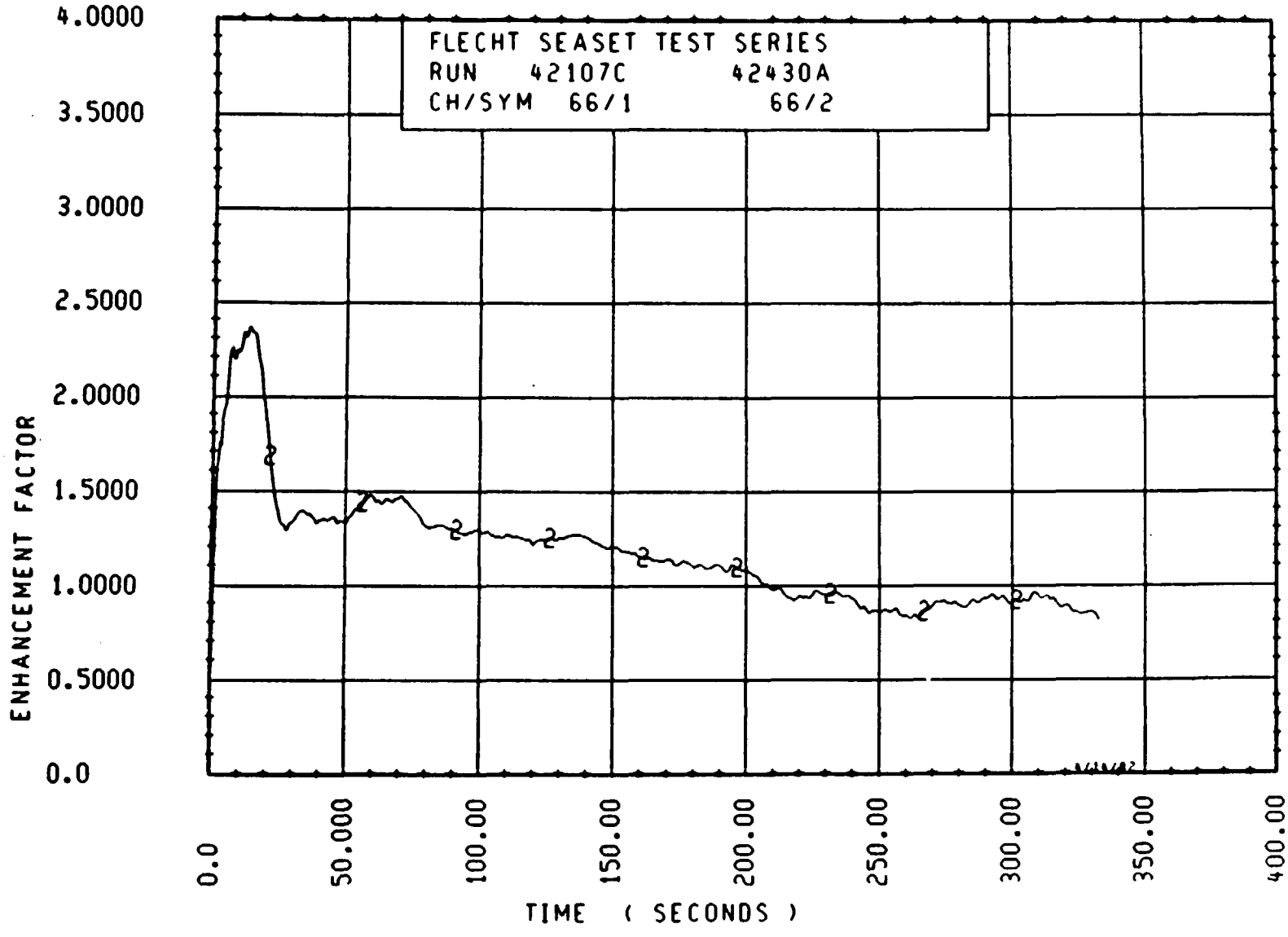

Figure 6-91. Enhancement Factor for Run 42107C, Rod 3C, 1.93 m (76.1 in.) Elevation

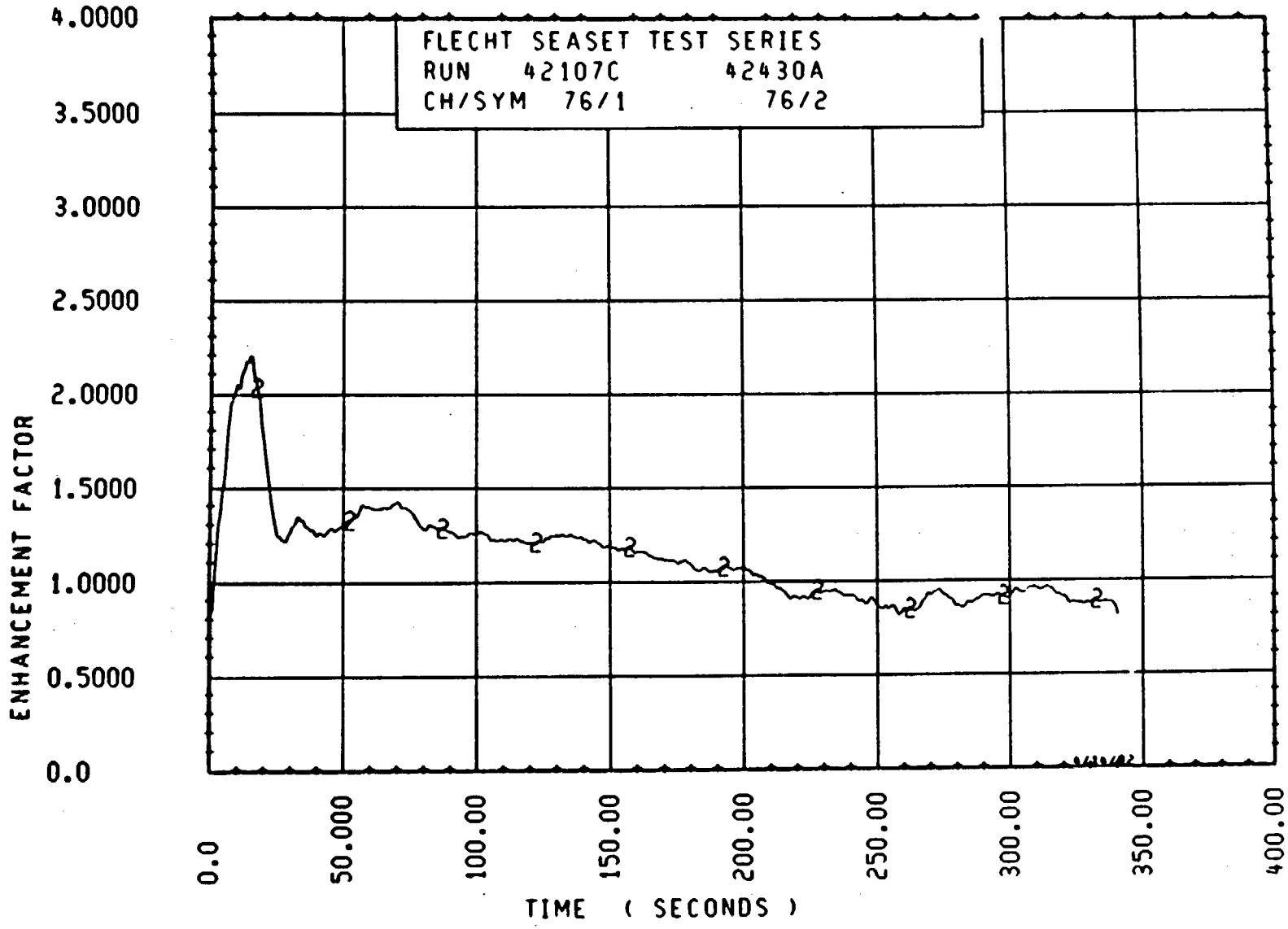

Figure 6-92. Enhancement Factor for Run 42107C, Rod 3C, 1.96 m (77 in.) Elevation

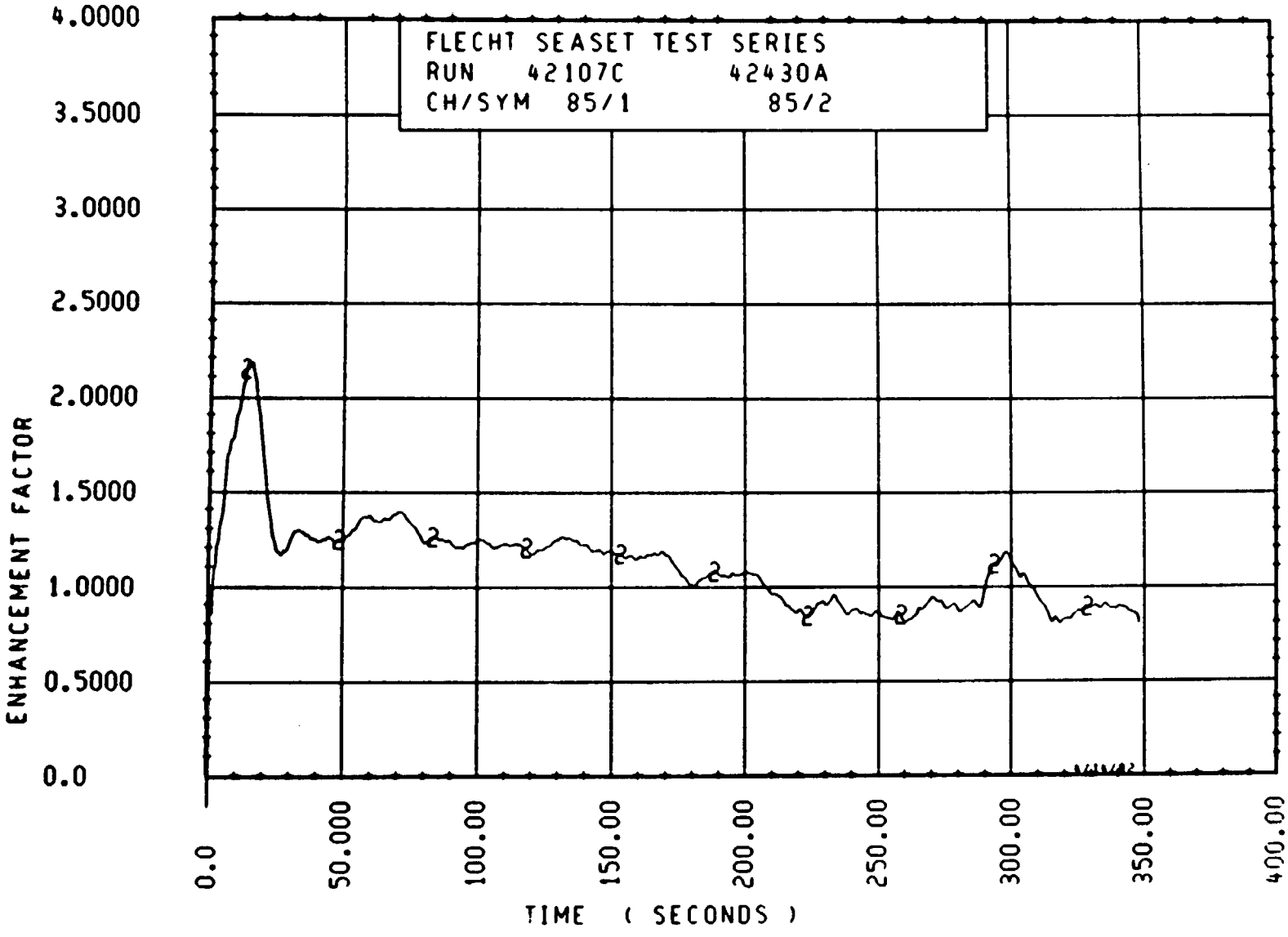

Figure 6-93. Enhancement Factor for Run 42107C, Rod 3C, 1.98 m (77.9 in.) Elevation

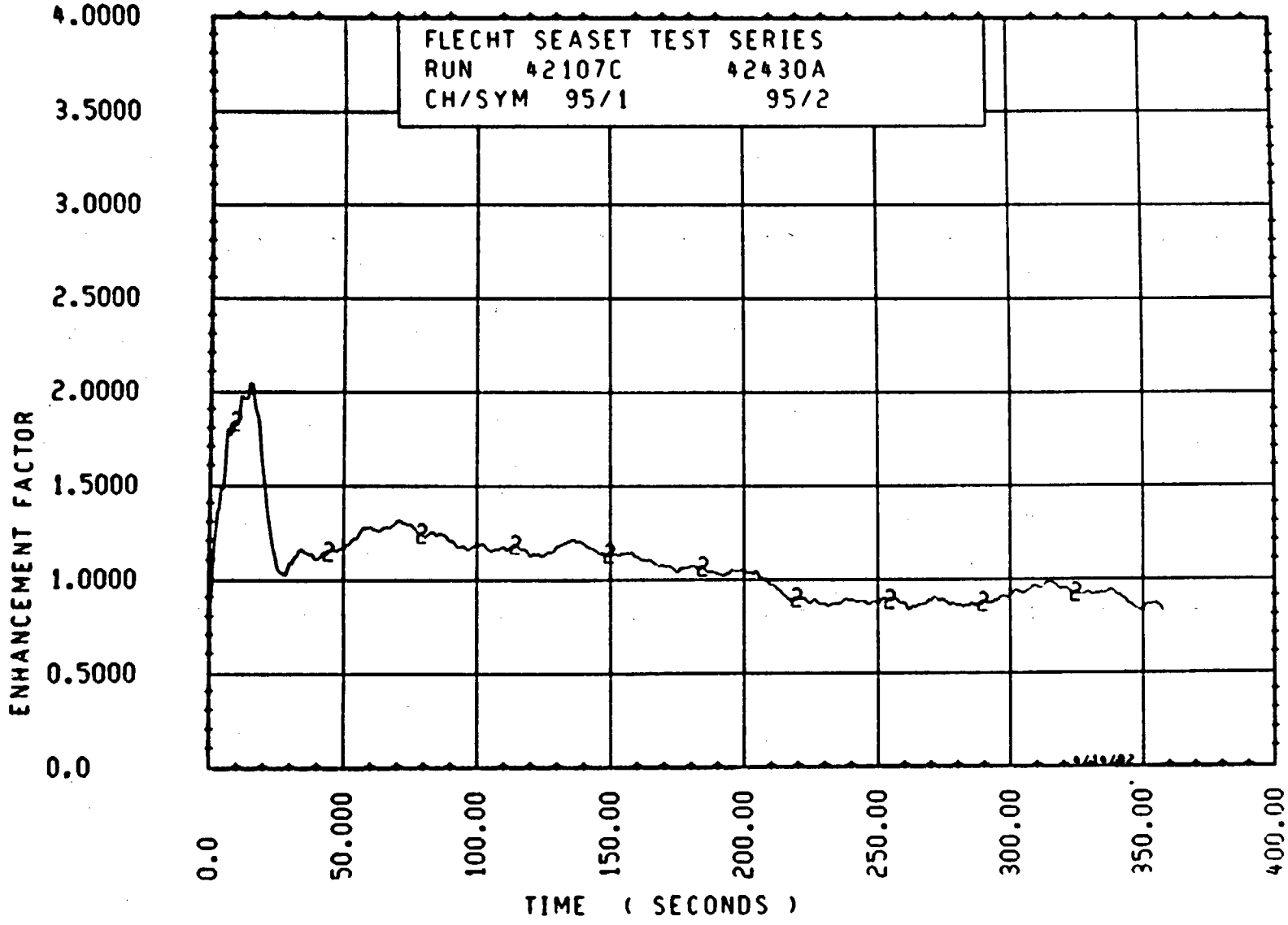

Figure 6-94. Enhancement Factor for Run 42107C, Rod 3C, 2.00 m (78.9 in.) Elevation

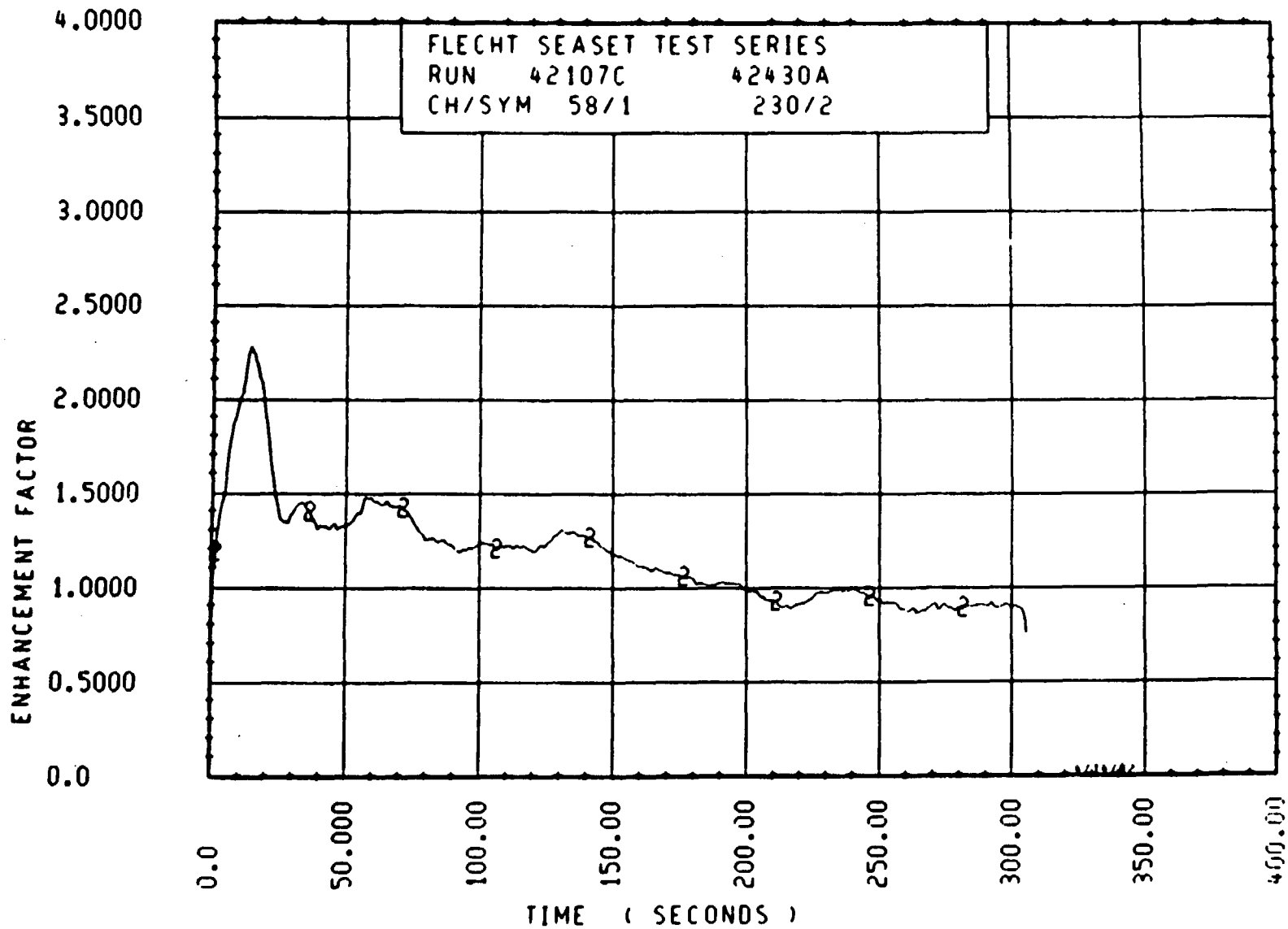

Figure 6-95. Enhancement Factor for Run 42107C, Rod 3D, 1.90 m (74.9 in.) Elevation

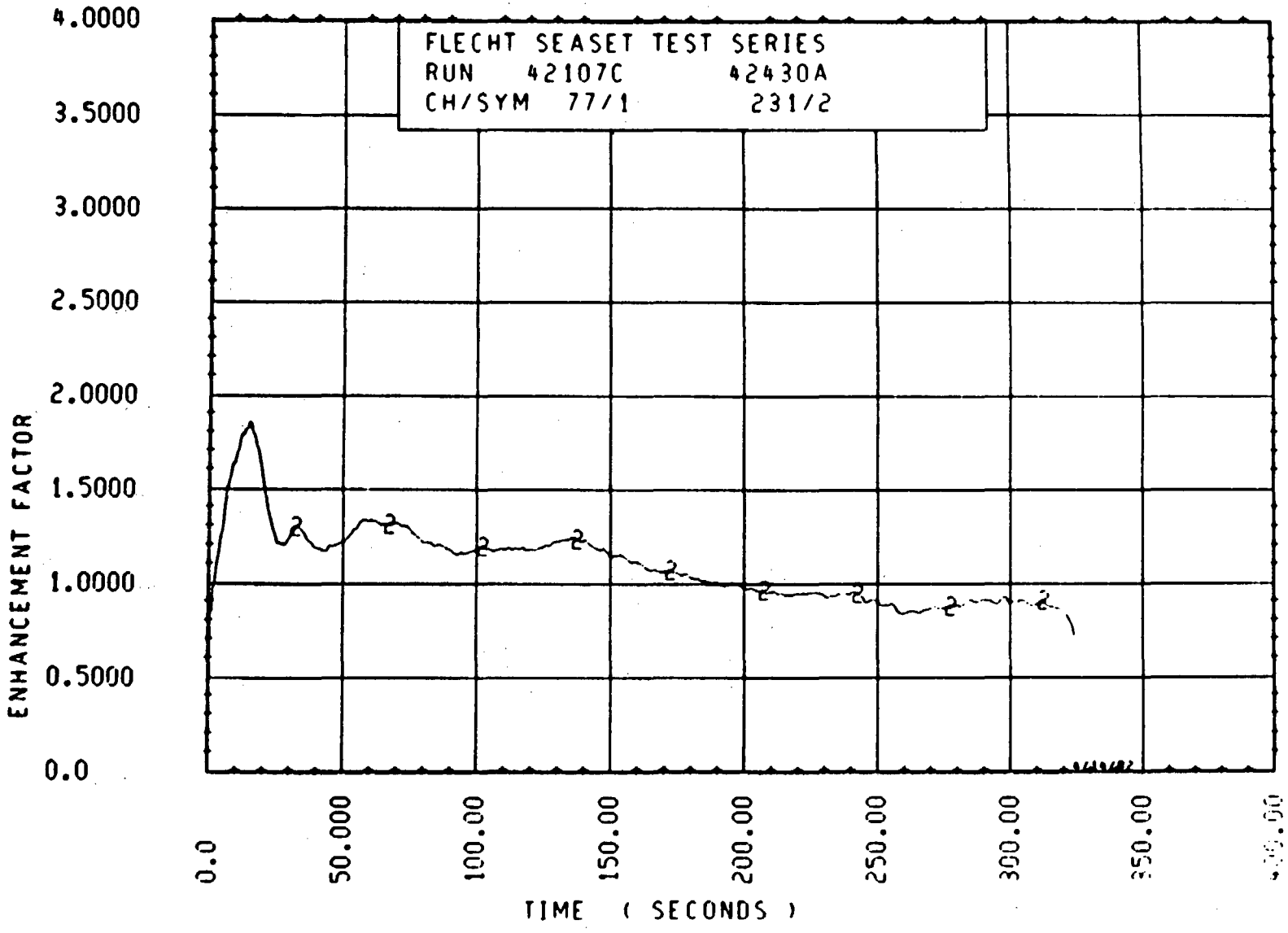

Figure 6-96. Enhancement Factor for Run 42107C, Rod 3D, 1.95 m (76.7 in.) Elevation

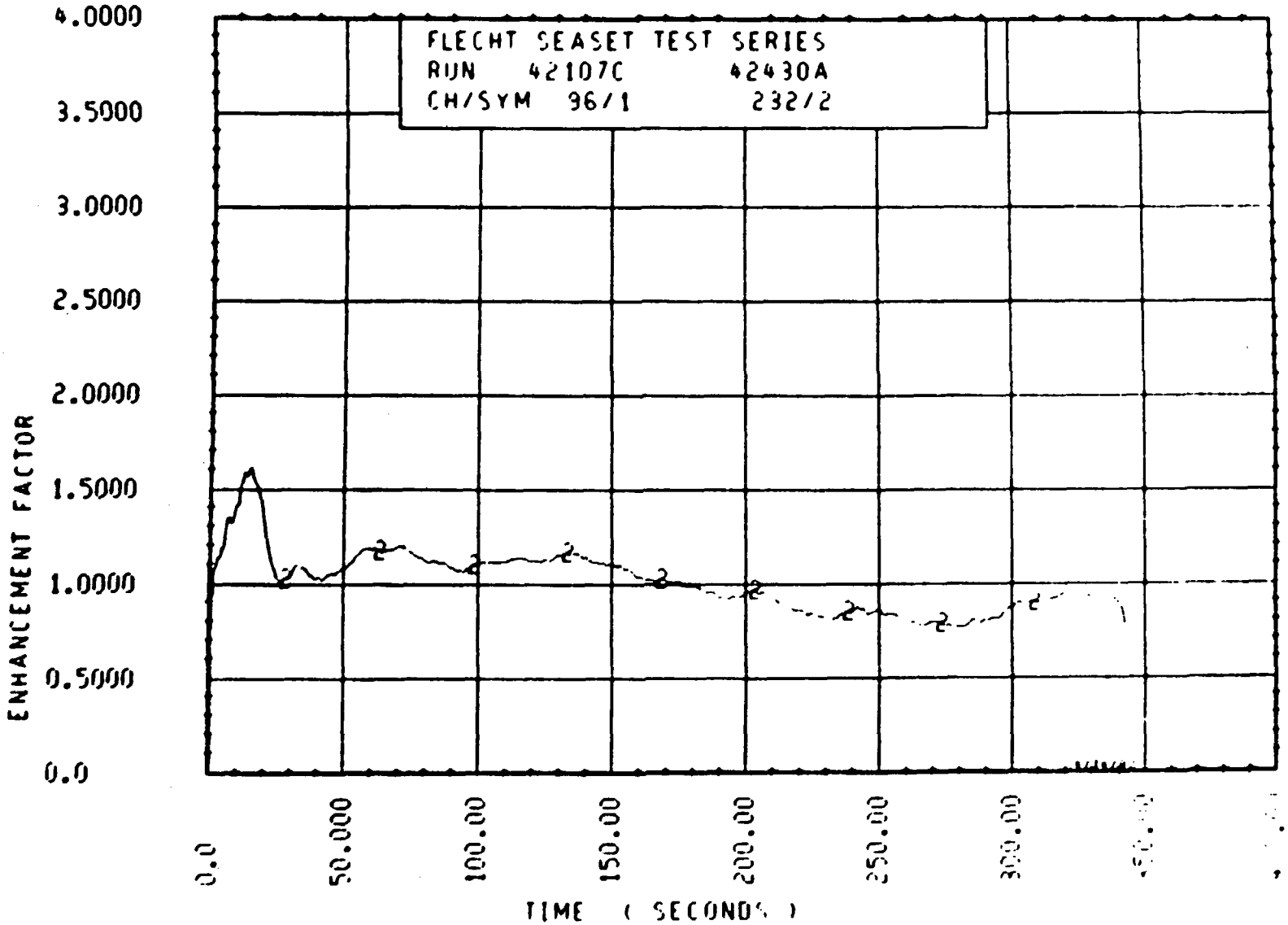

Figure 6-97. Enhancement Factor for Run 42107C, Rod 3D, 2.00 m (78.9 in.) Elevation

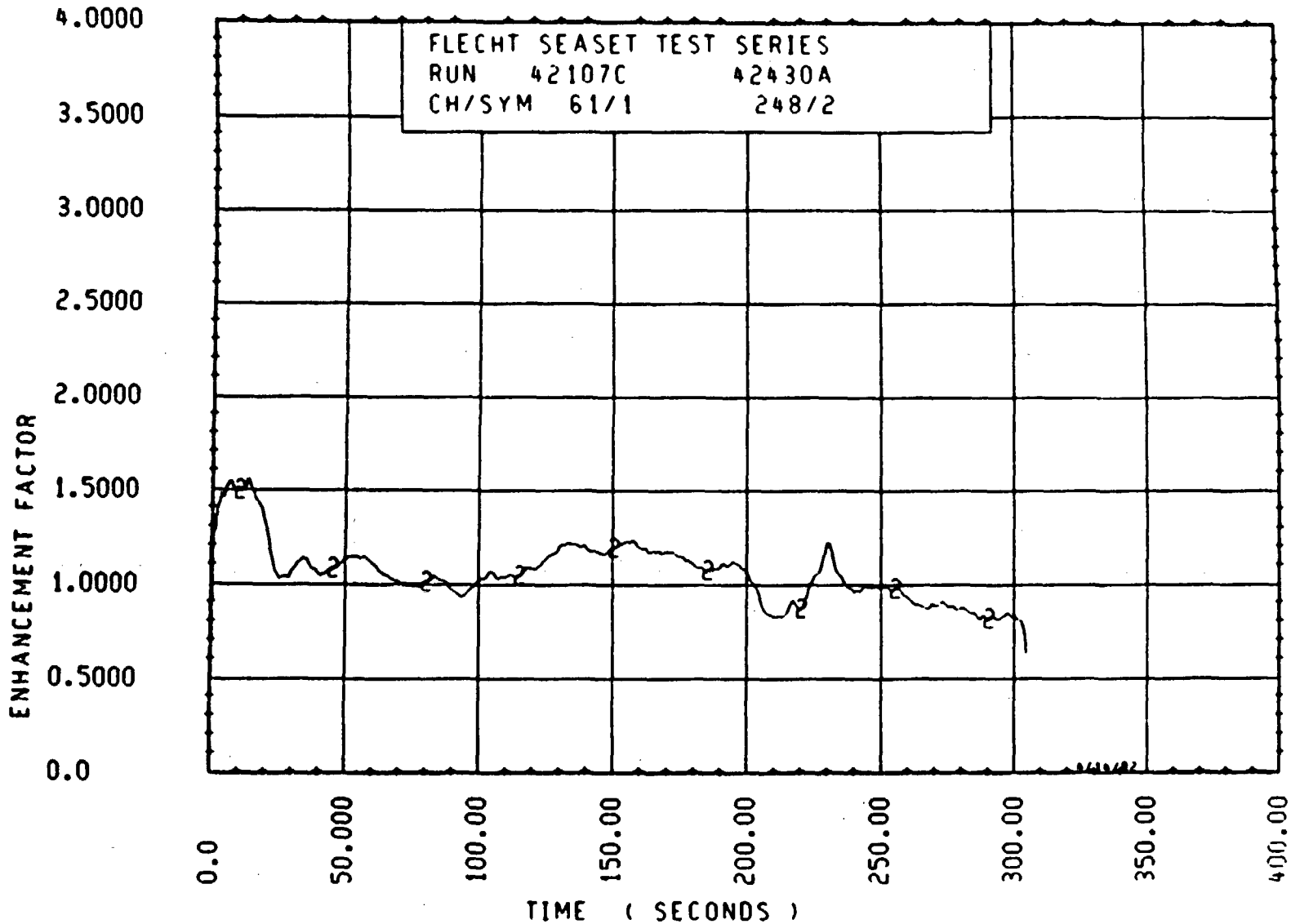

Figure 6-98. Enhancement Factor for Run 42107C, Rod 5C, 1.88 m (74.1 in.) Elevation

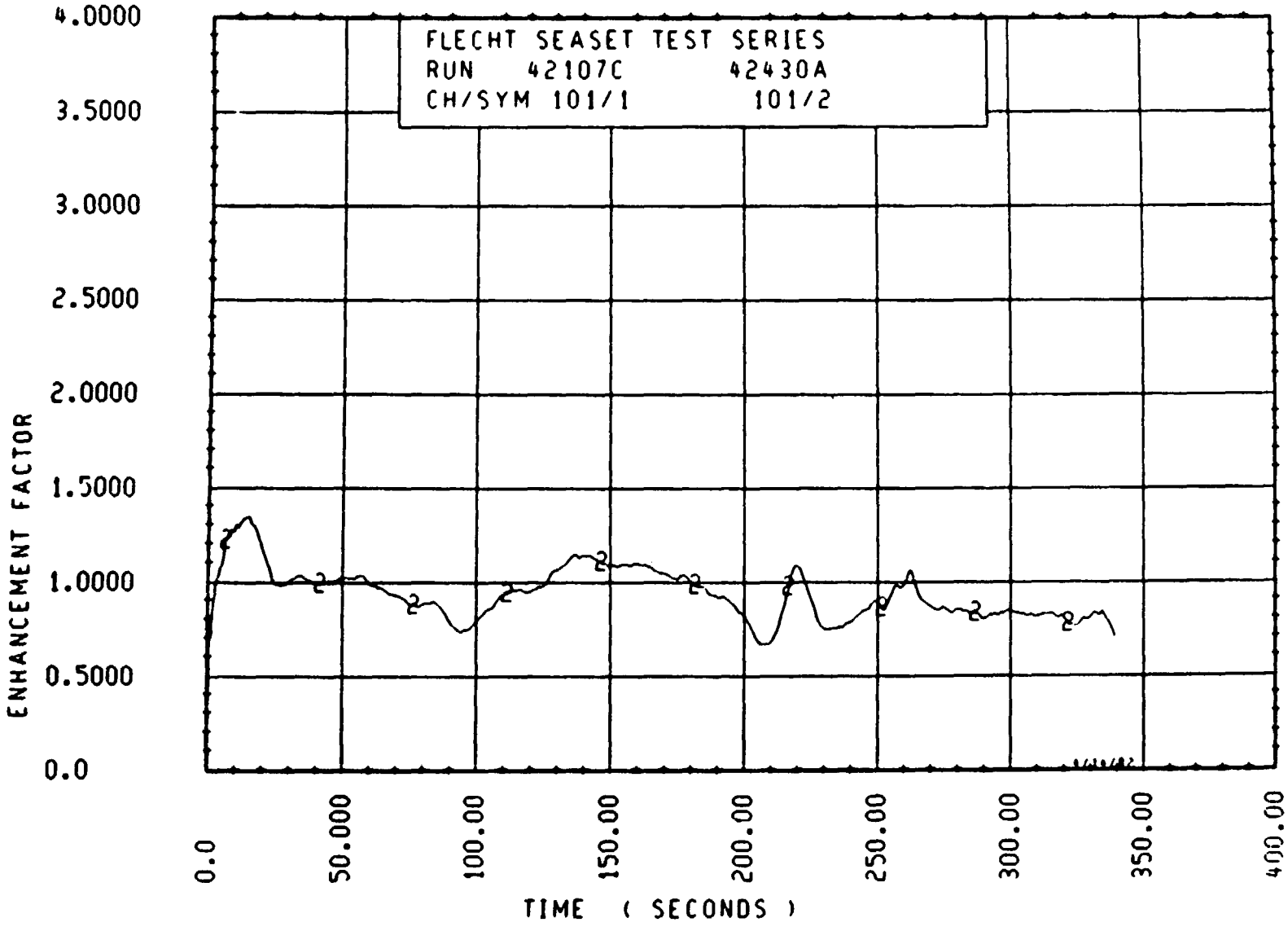

Figure 6-99. Enhancement Factor for Run 42107C, Rod 5C, 1.98 m (78 in.) Elevation

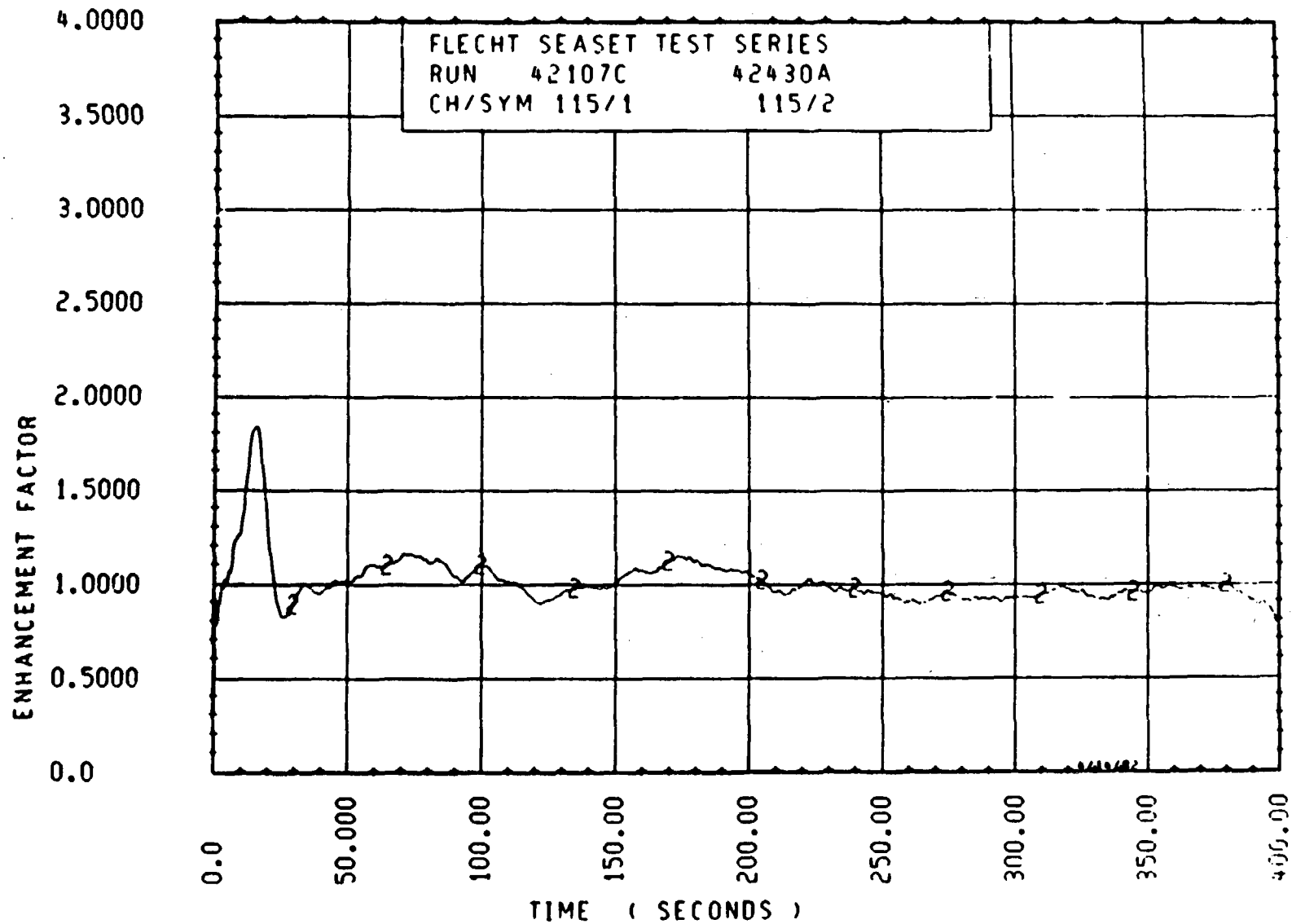

Figure 6-100. Enhancement Factor for Run 42107C, Rod 3D, 2.13 m (84 in.) Elevation

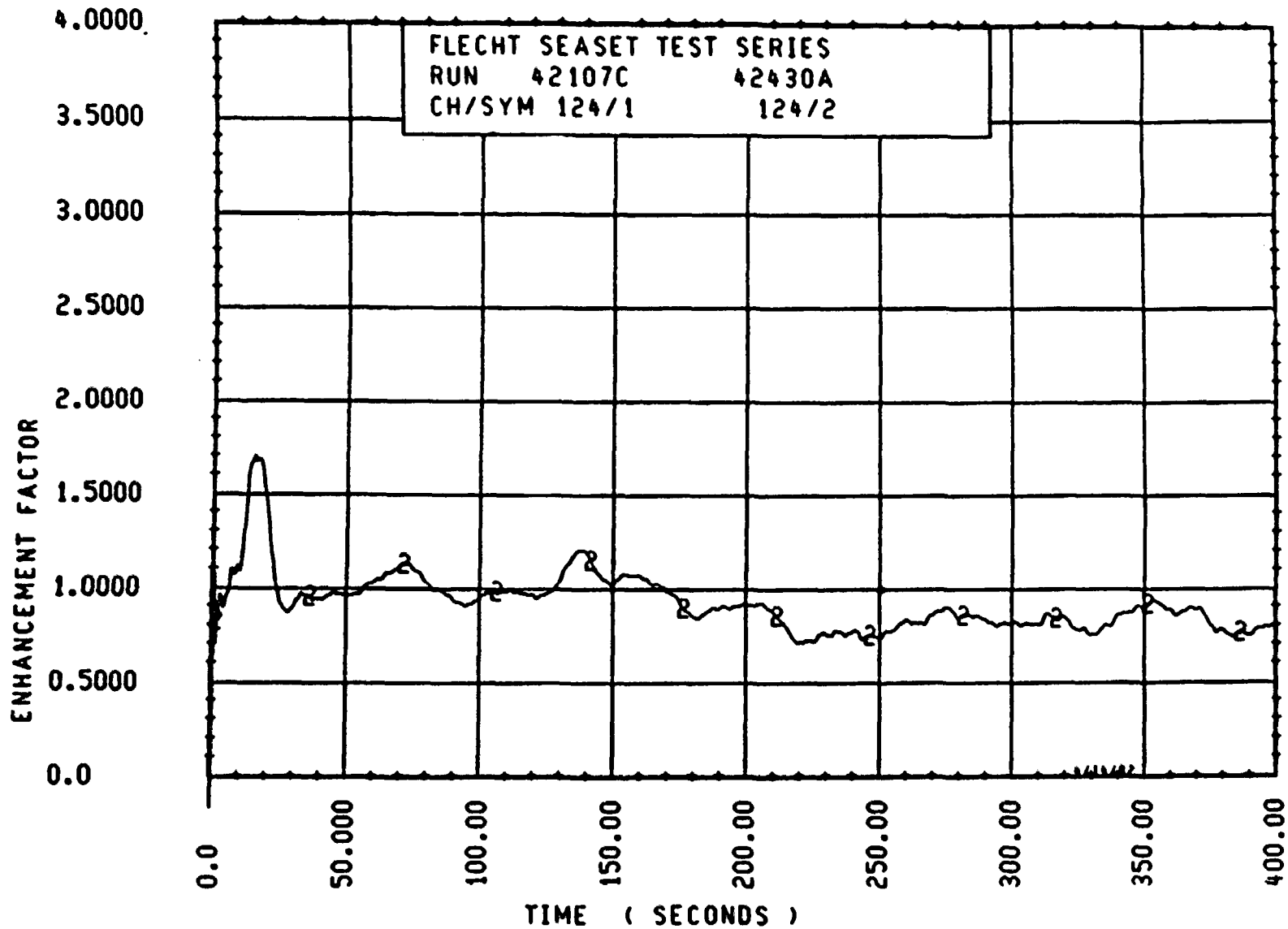

Figure 6-101. Enhancement Factor for Run 42107C, Rod 3B, 2.29 m (90 in.) Elevation

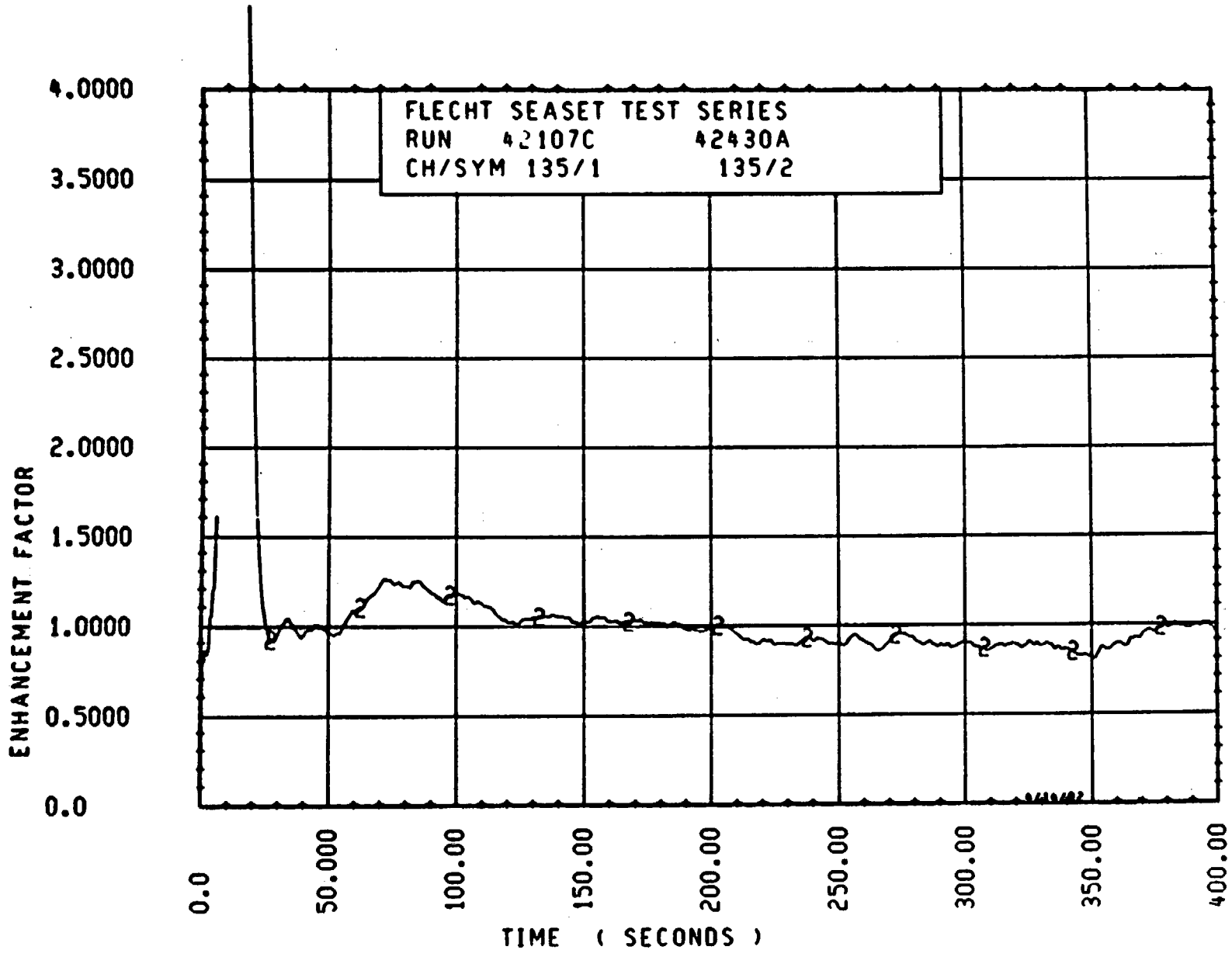

Figure 6-102. Enhancement Factor for Run 42107C, Rod 3B, 2.44 m (96 in.) Elevation

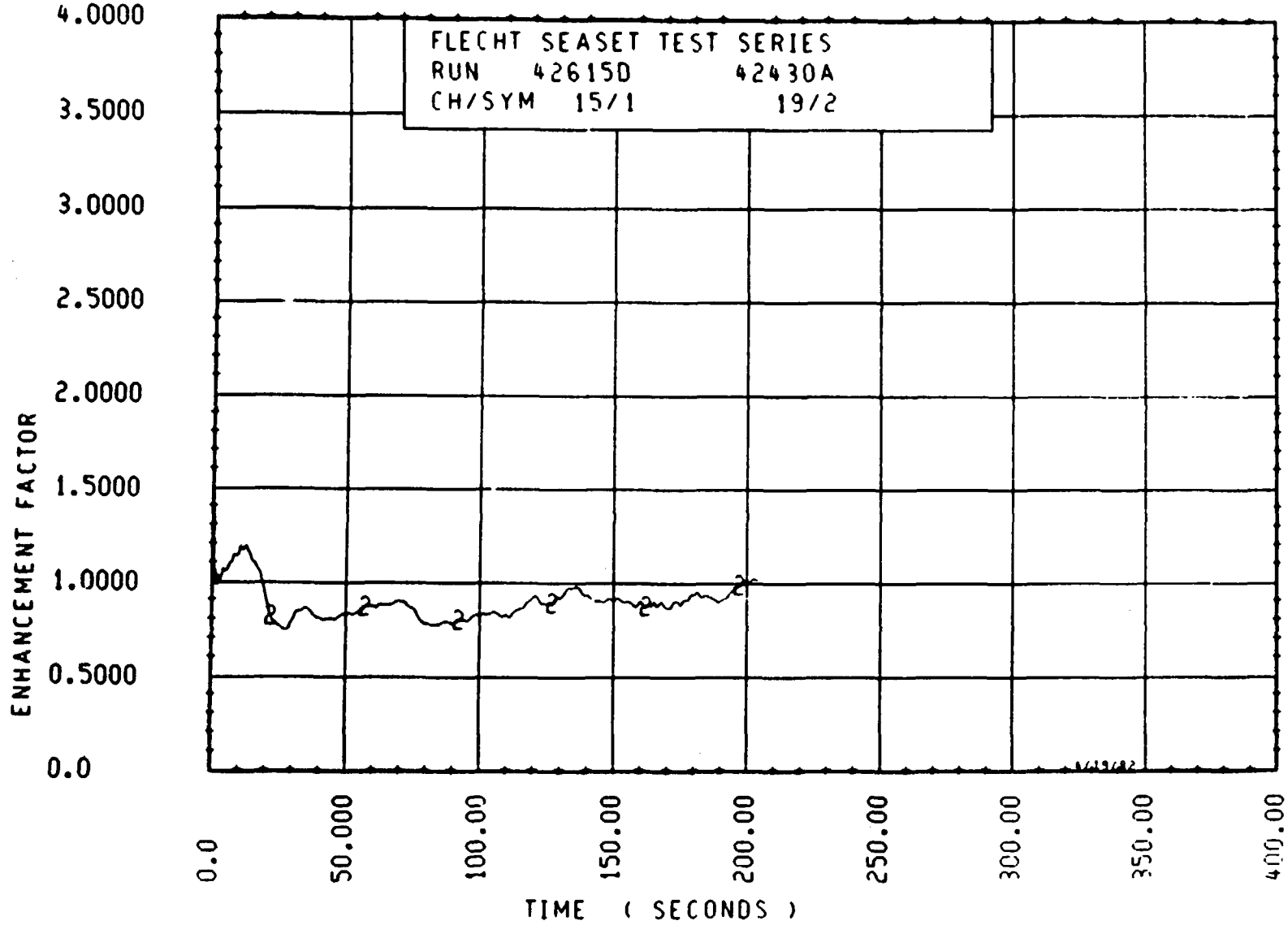

Figure 6-103. Enhancement Factor for Run 42615D, Rod 4C, 1.52 m (60 in.) Elevation

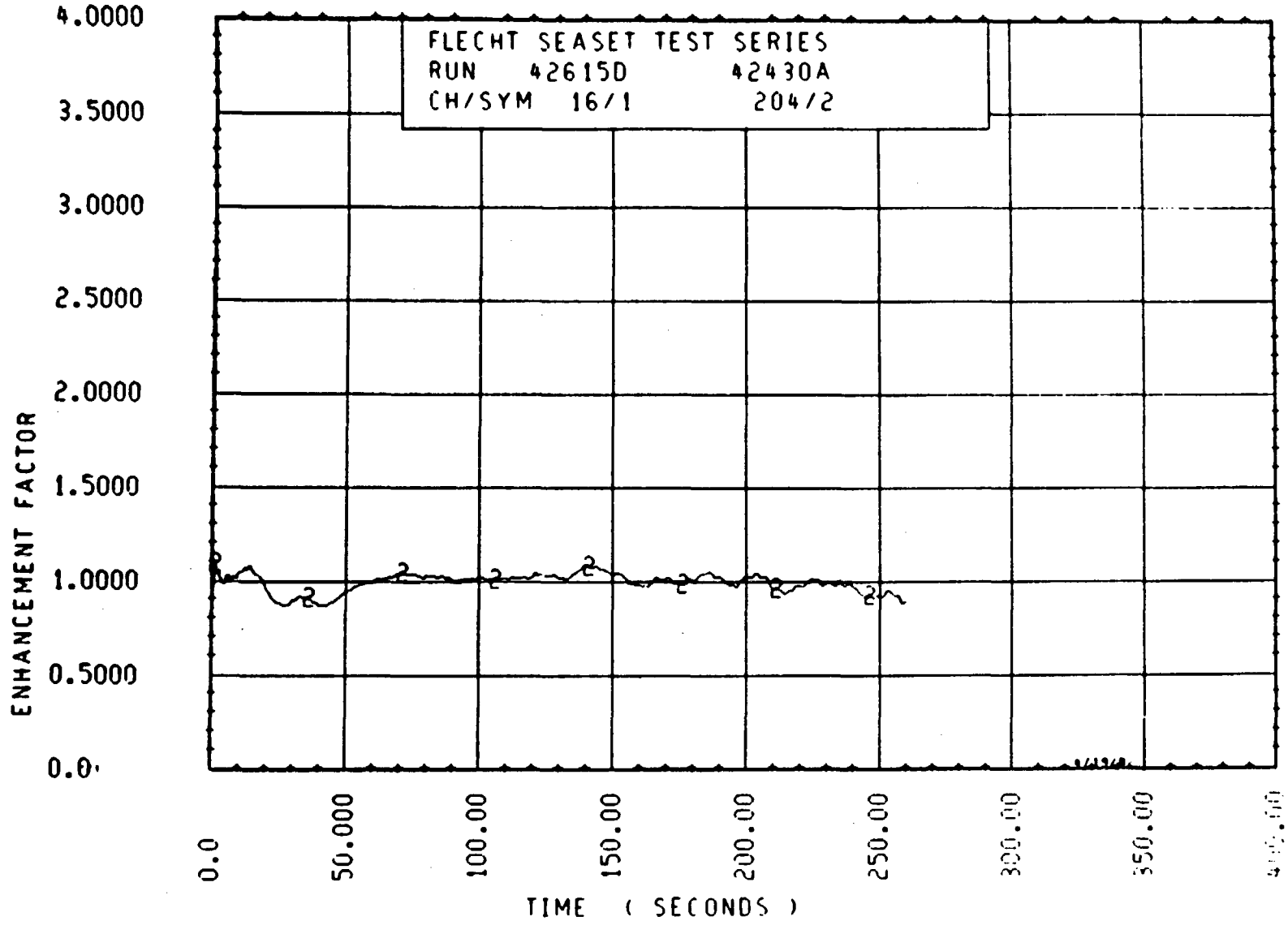

Figure 6-104. Enhancement Factor for Run 42615D, Rod 2A, 1.72 m (67.8 in.) Elevation

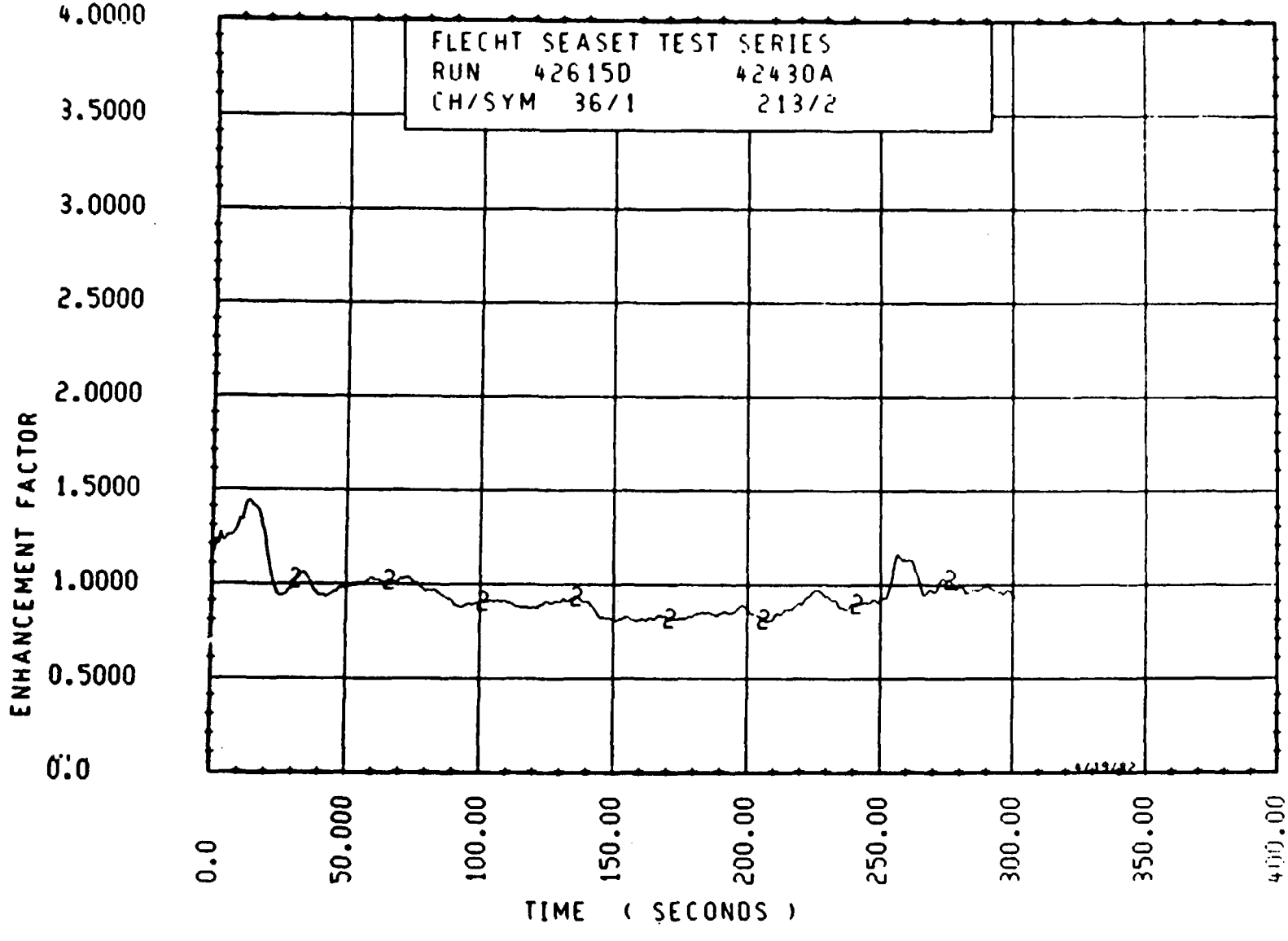

Figure 6-105. Enhancement Factor for Run 42615D, Rod 2D, 1.84 m (72.4 in.) Elevation

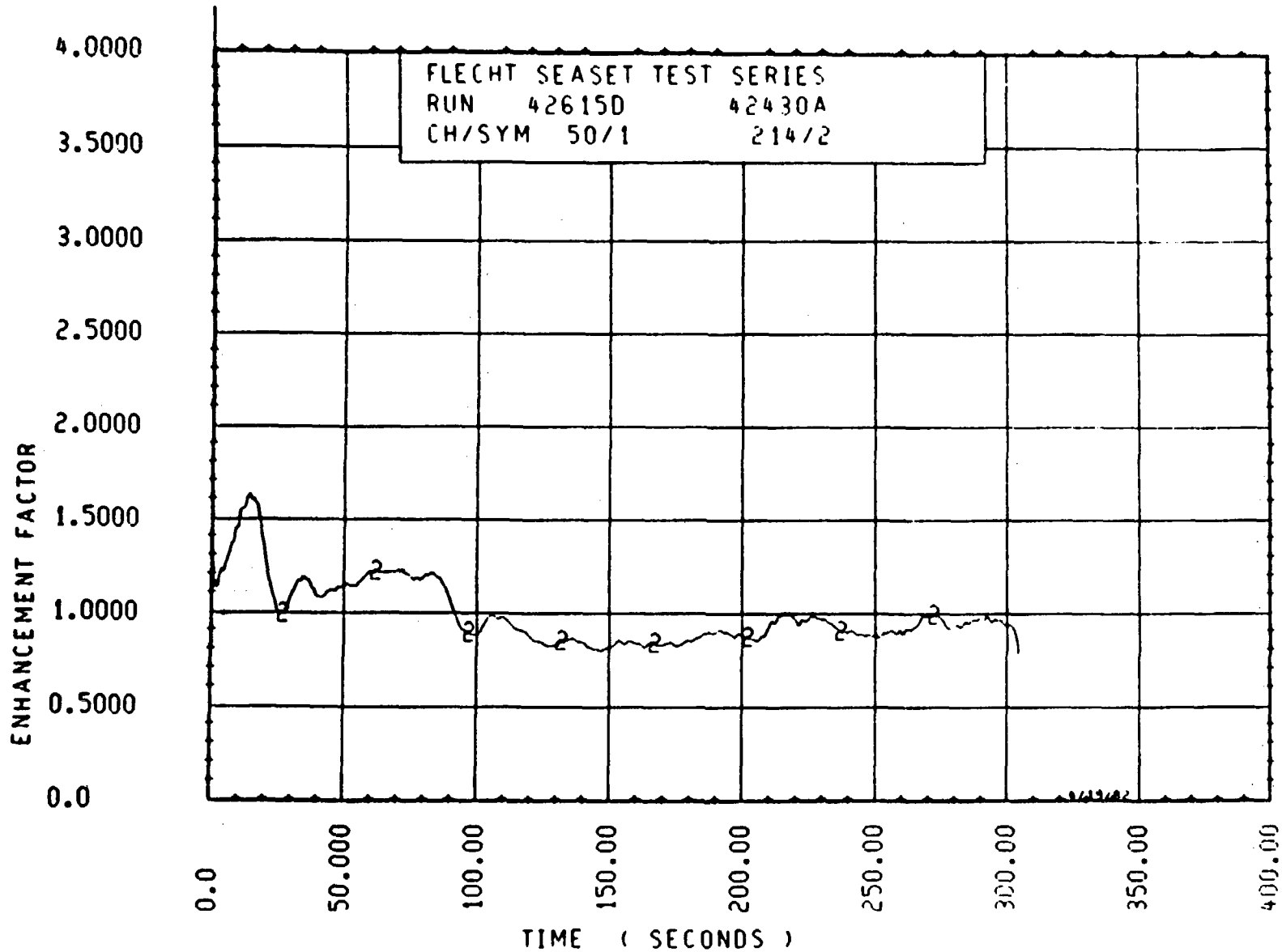

Figure 6-106. Enhancement Factor for Run 42615D, Rod 2D, 1.89 m (74.4 in.) Elevation

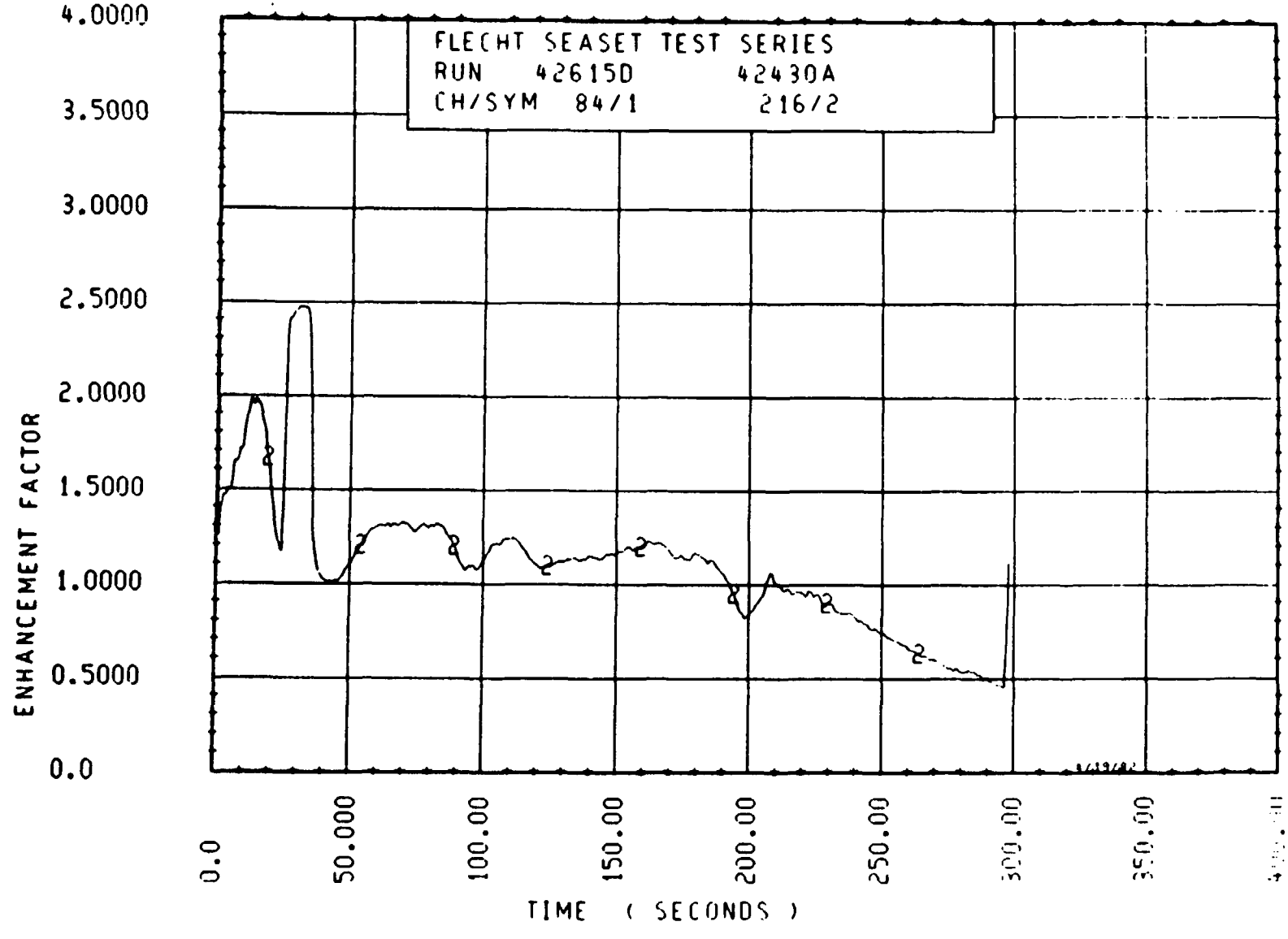

Figure 6-107. Enhancement Factor for Run 42615D, Rod 2D, 1.97 m (77.4 in.) Elevation

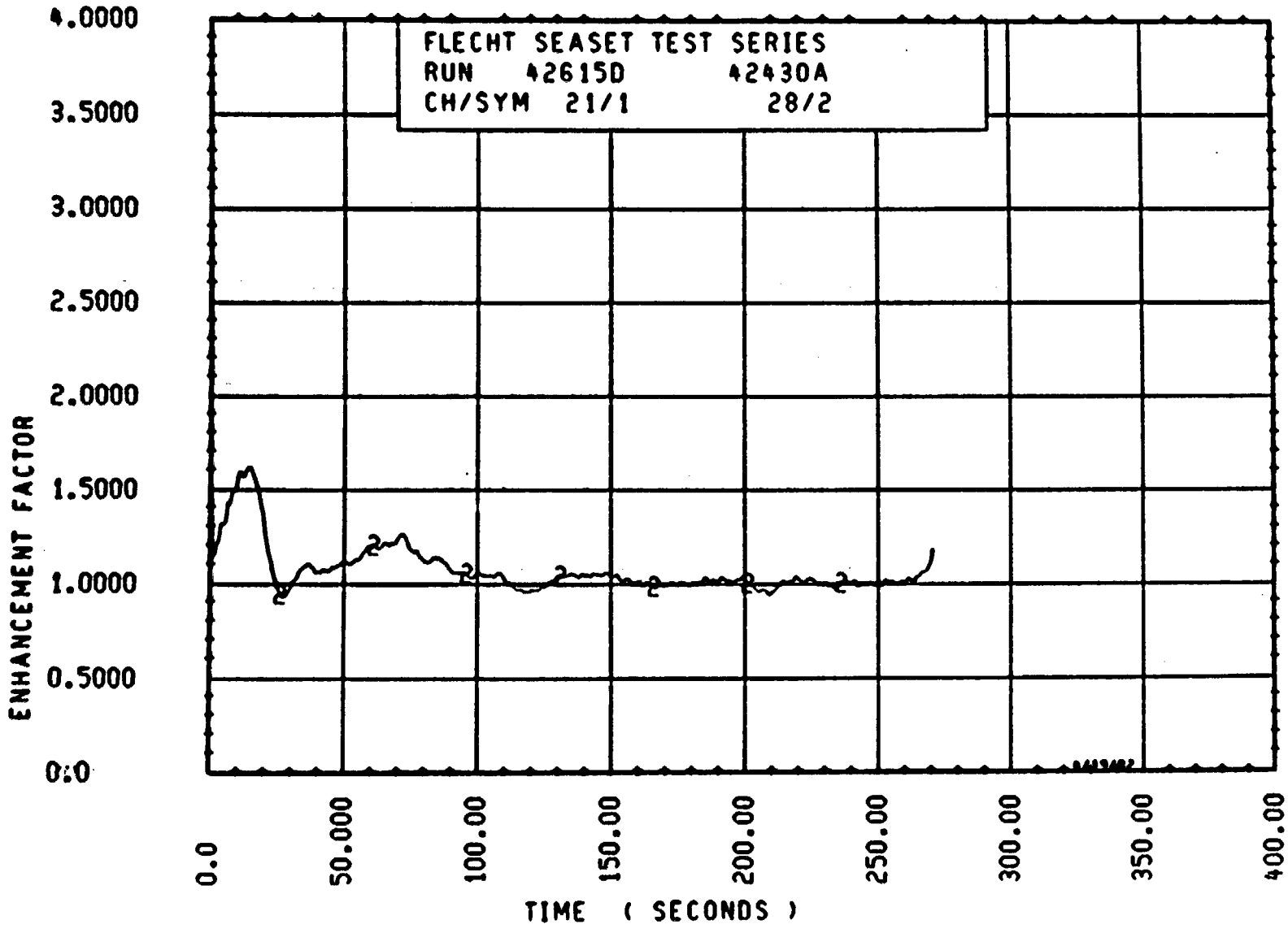

Figure 6-108. Enhancement Factor for Run 42615D, Rod 3C, 1.79 m (70.6 in.) Elevation

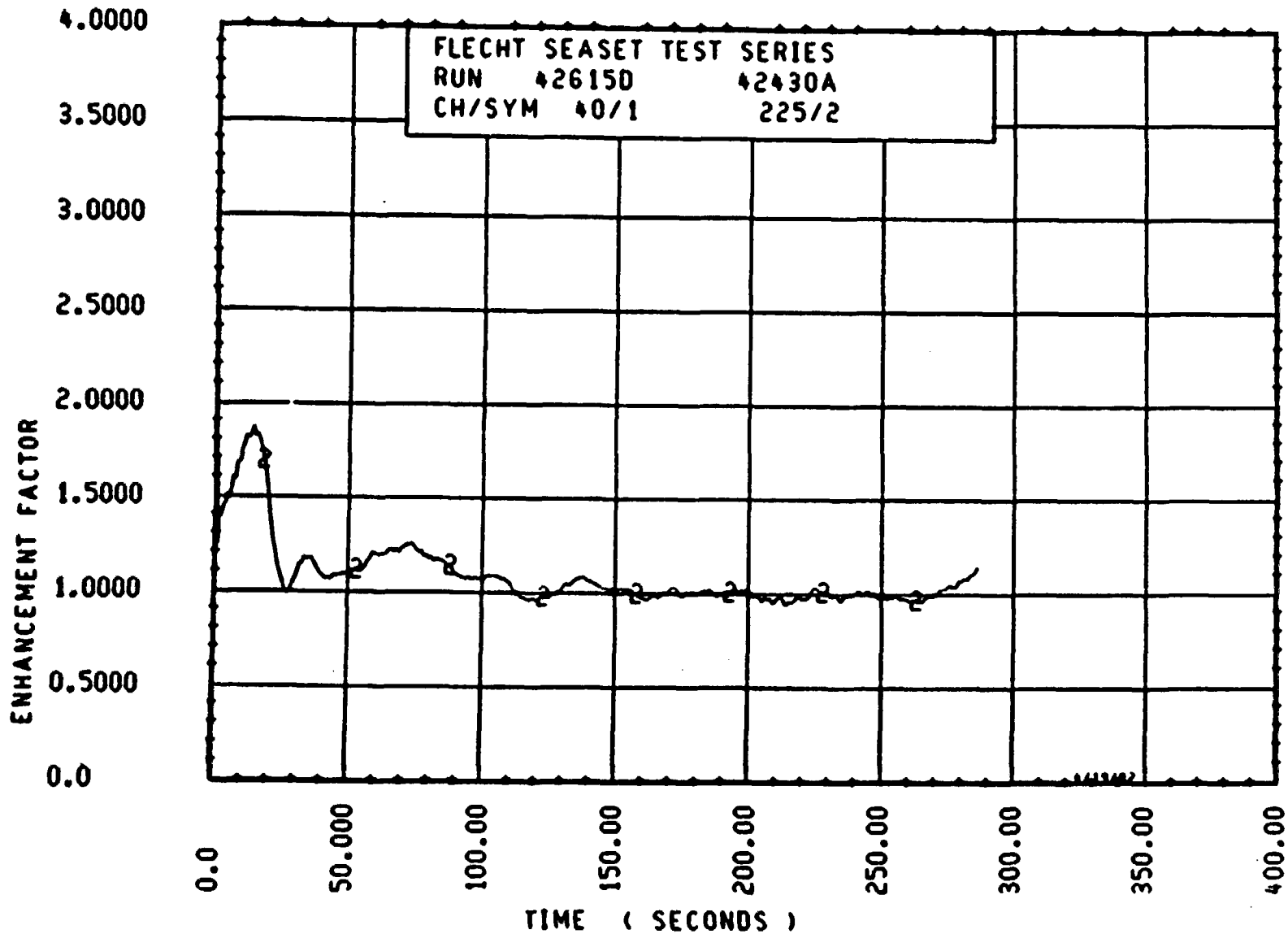

Figure 6-109. Enhancement Factor for Run 42615D, Rod 3C, 1.84 m (72.6 in.) Elevation

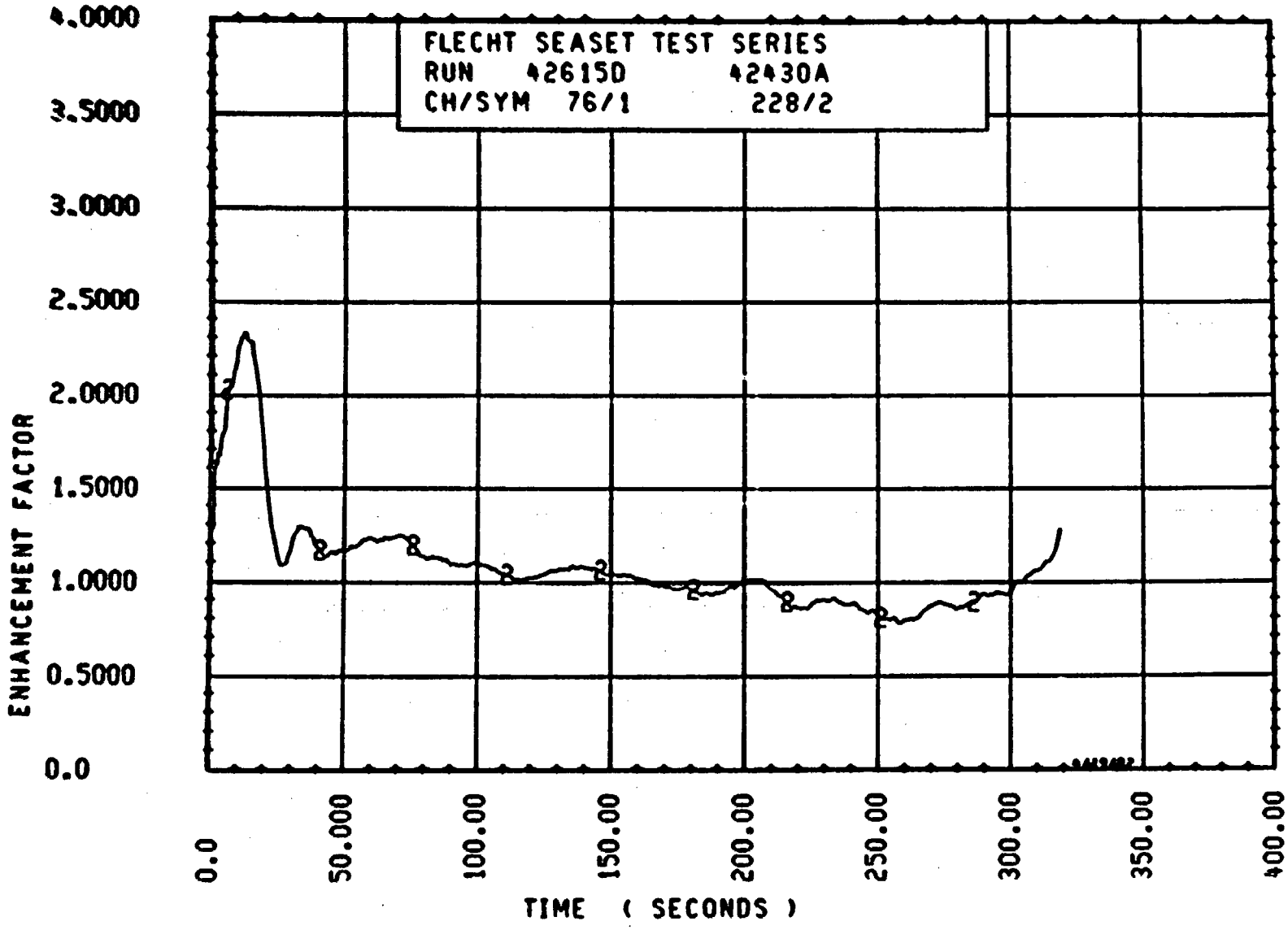

Figure 6-110. Enhancement Factor for Run 42615D, Rod 3C, 1.95 m (76.8 in.) Elevation

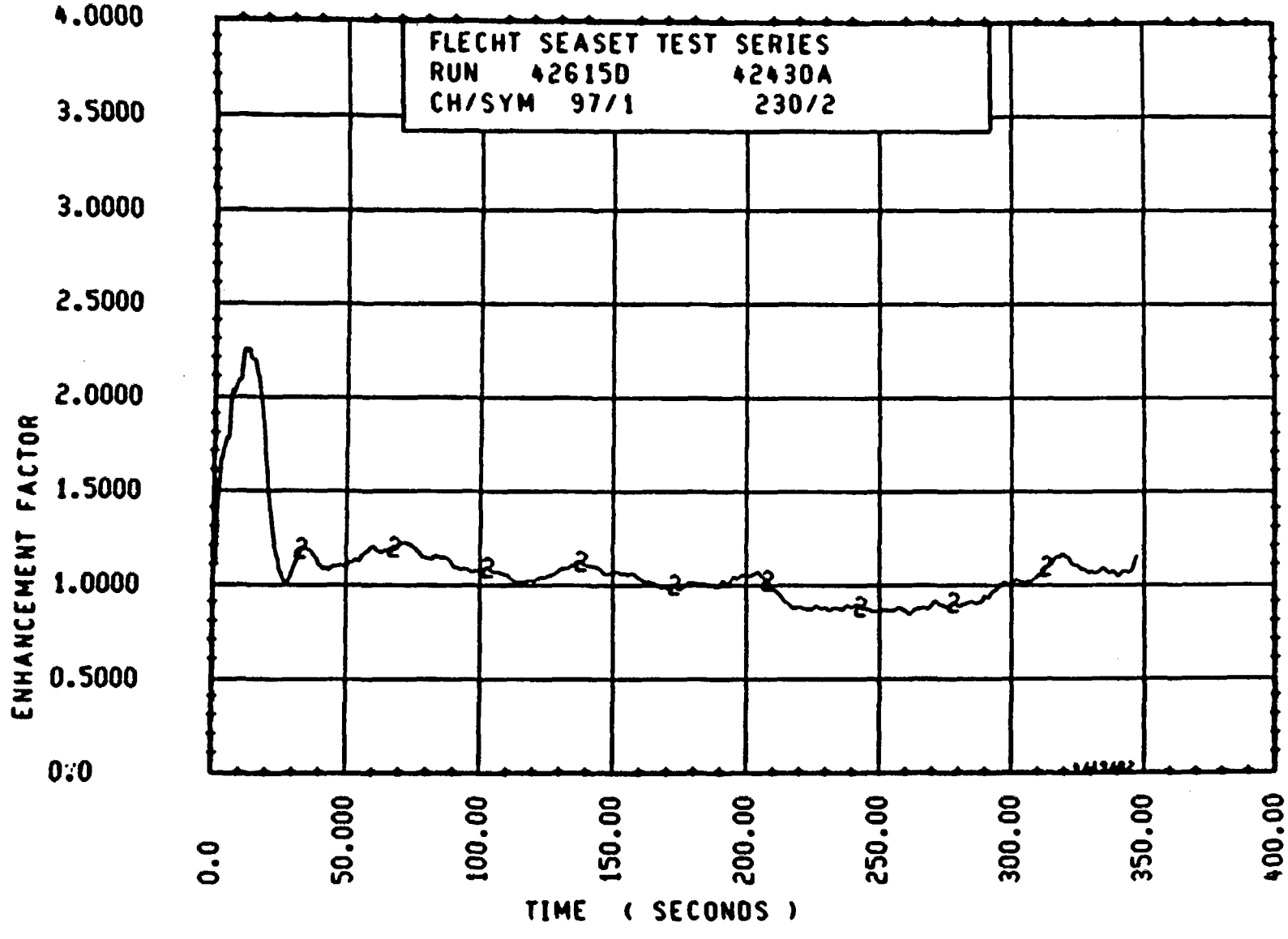

Figure 6-111. Enhancement Factor for Run 42615D, Rod 3C, 2.00 m (78.8 in.) Elevation

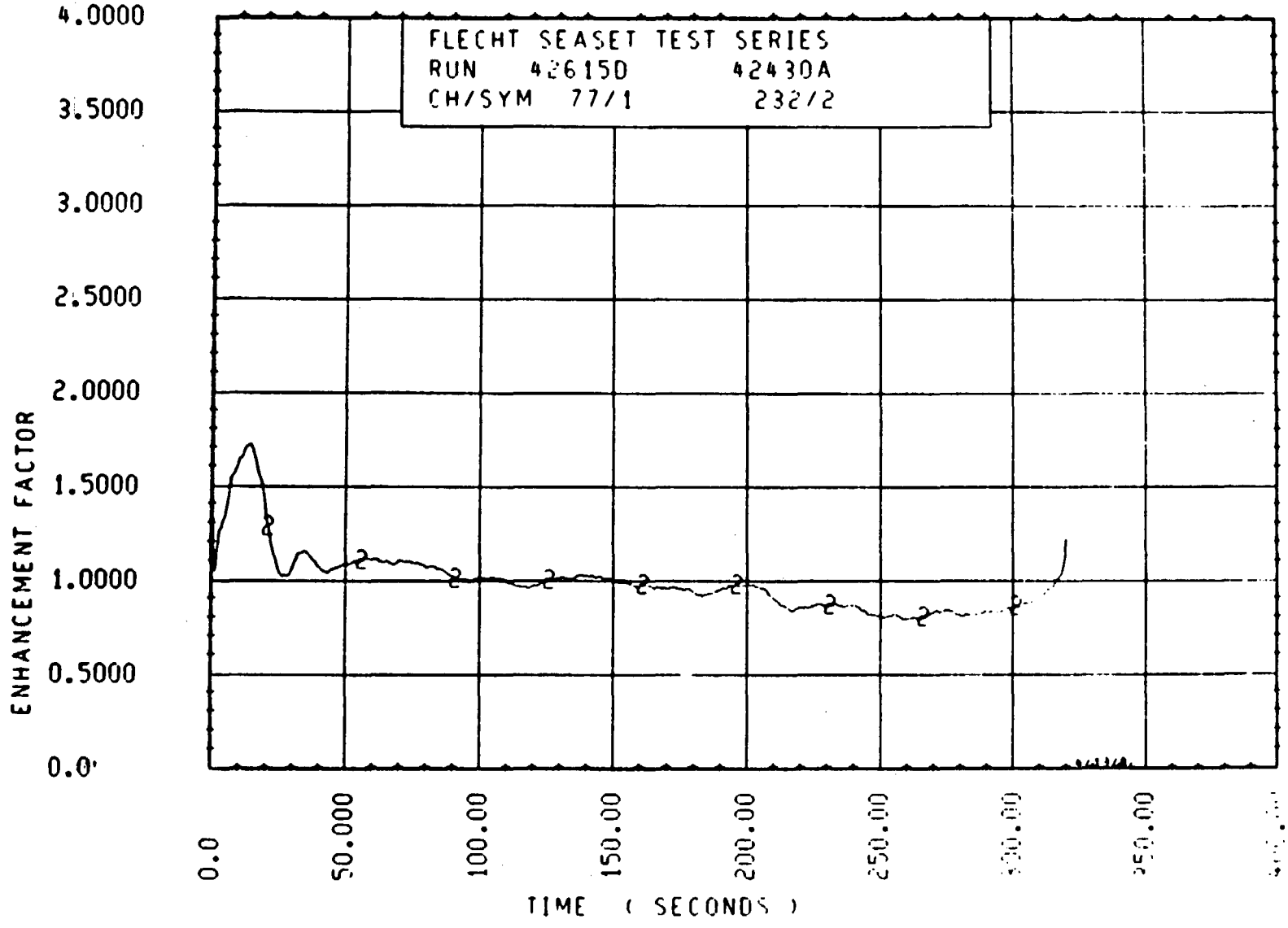

Figure 6-112. Enhancement Factor for Run 42615D, Rod 3D, 1.94 m (76.4 in.) Elevation

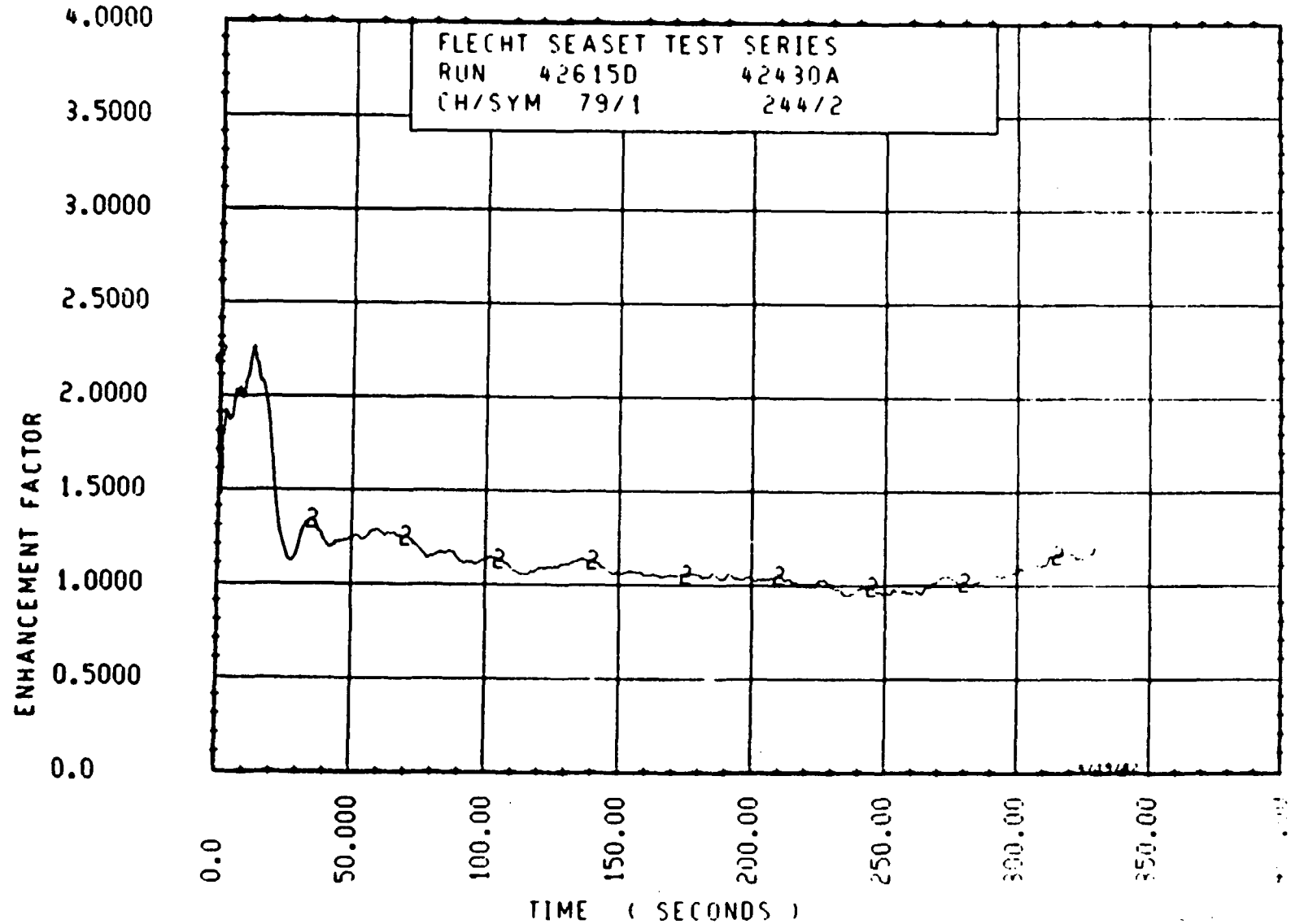

Figure 6-113. Enhancement Factor for Run 42615D, Rod 4C, 1.95 m (76.9 in.) Elevation

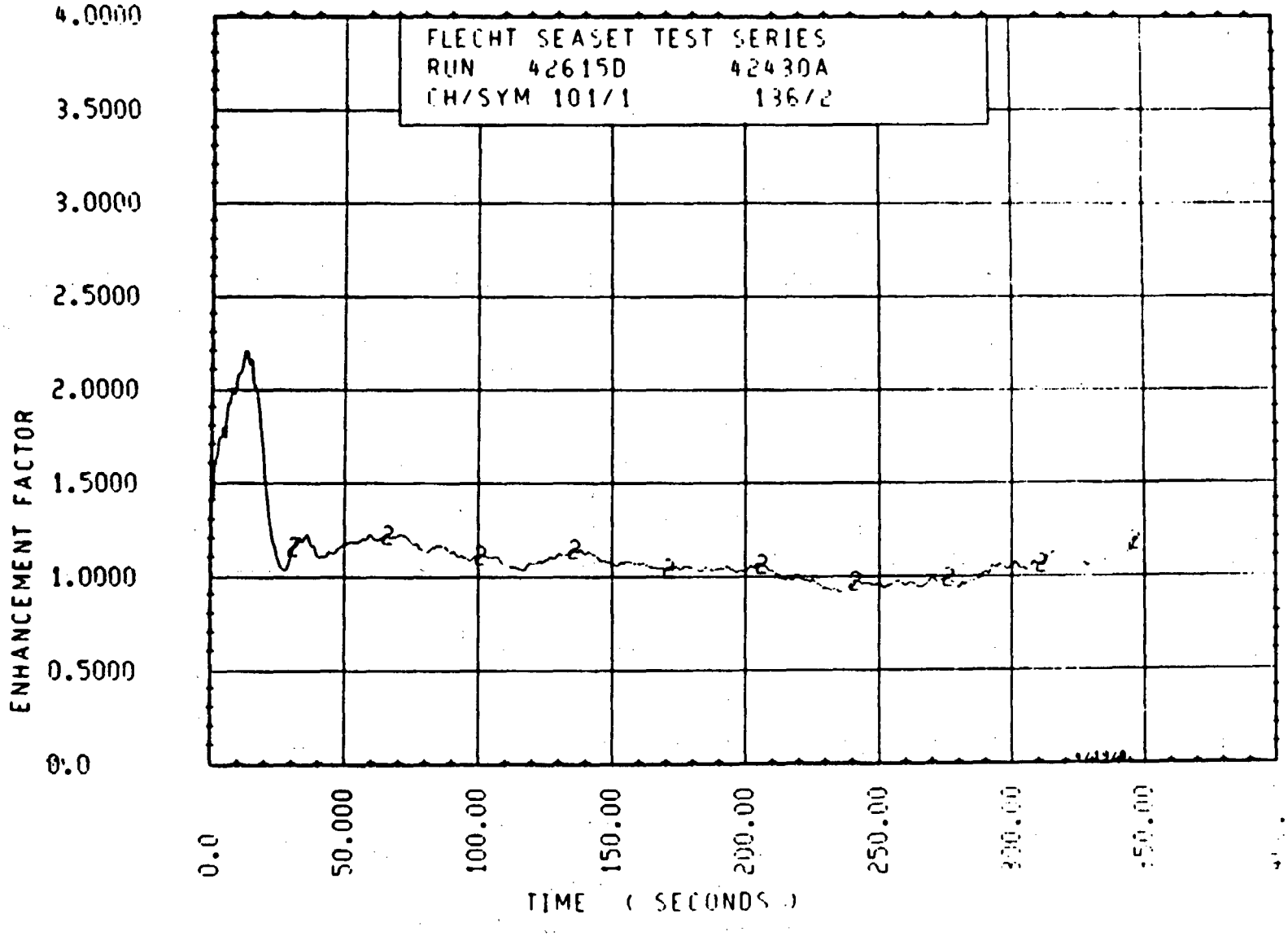

Figure 6-114. Enhancement Factor for Run 42615D, Rod 4C, 2.00 m (78.9 in.) Elevation

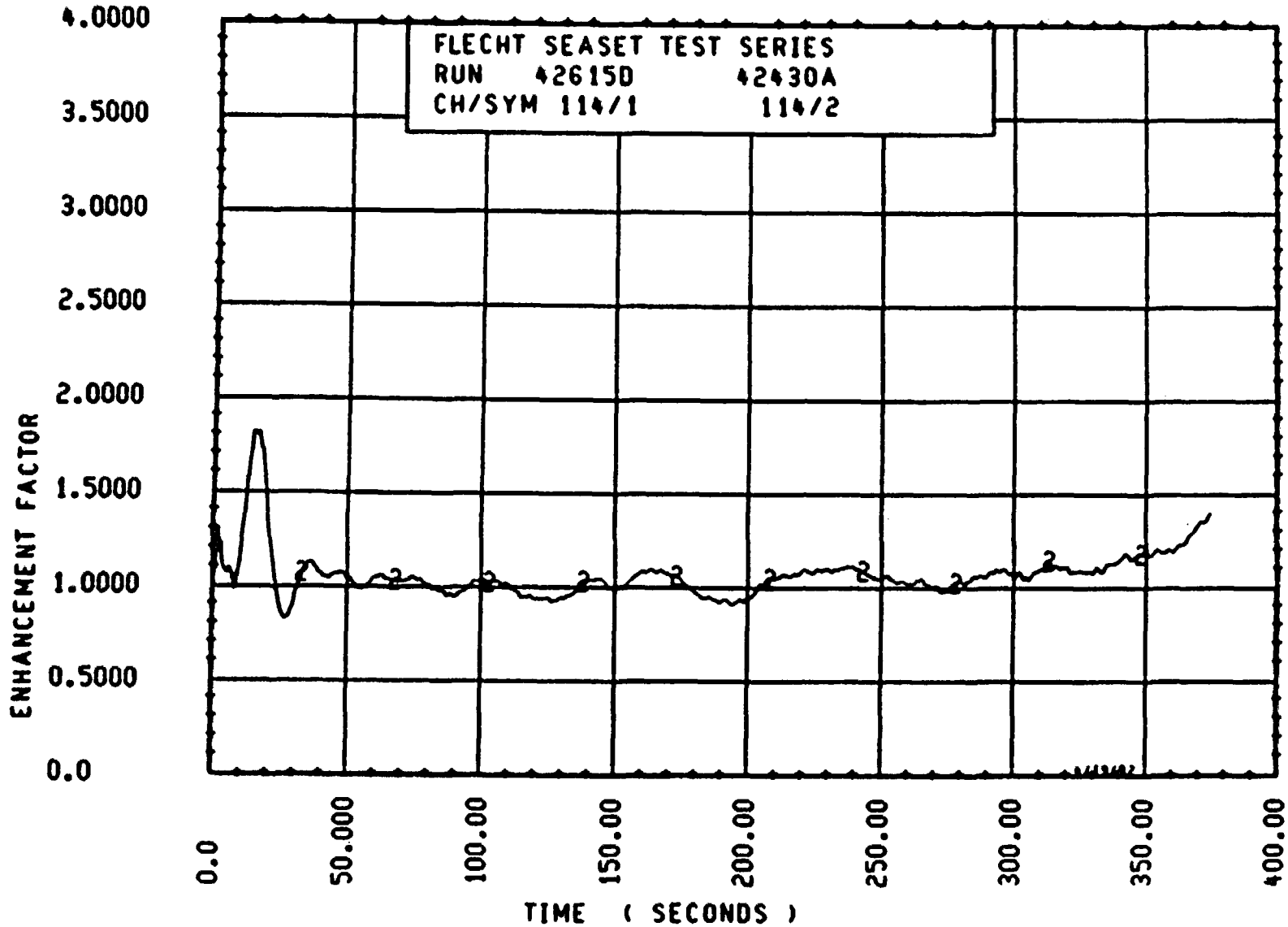

Figure 6-115. Enhancement Factor for Run 42615D, Rod 3B, 2.13 m (84 in.) Elevation

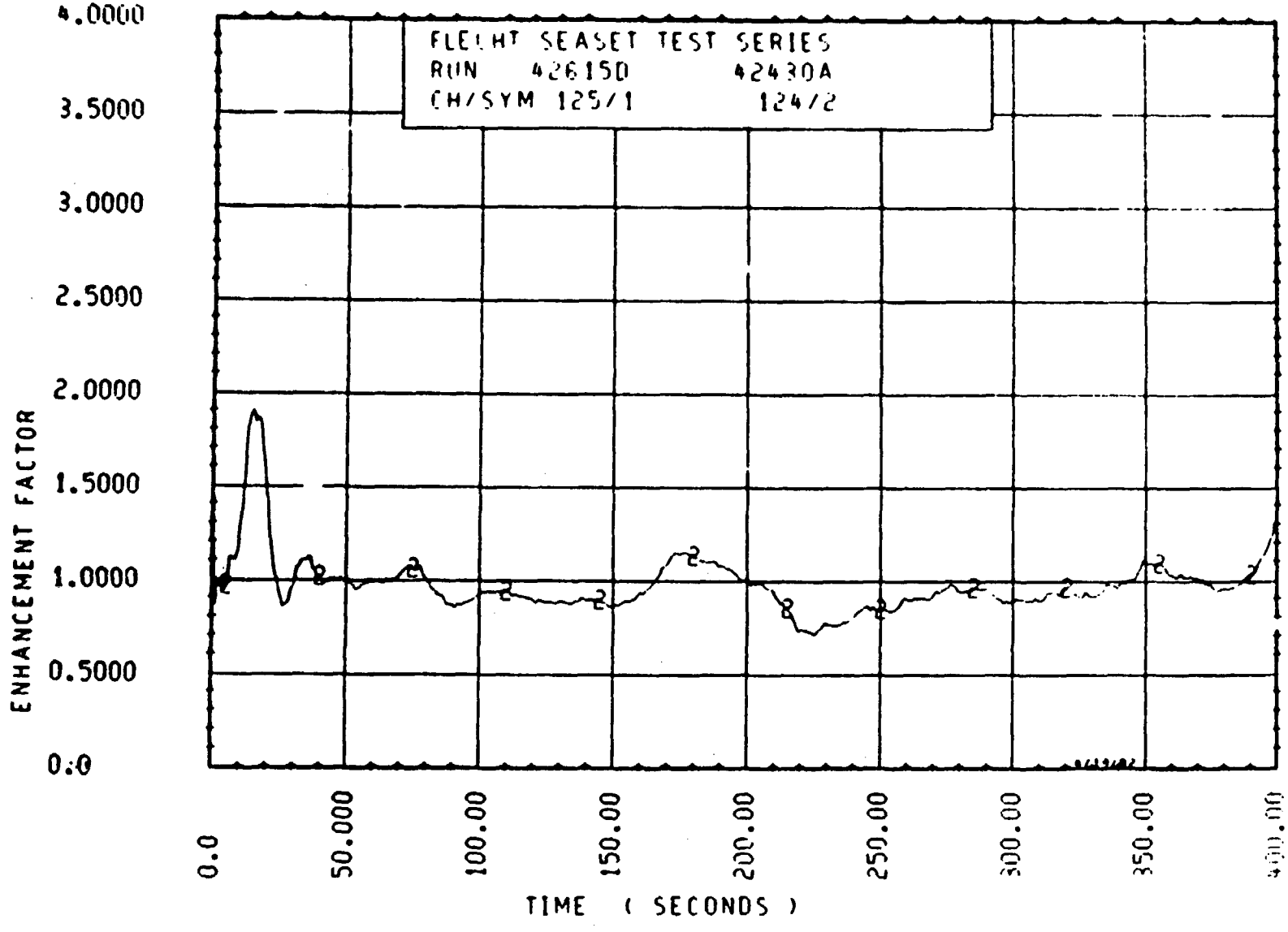

Figure 6-116. Enhancement Factor for Run 42615D, Rod 3B, 2.29 m (90 in.) Elevation

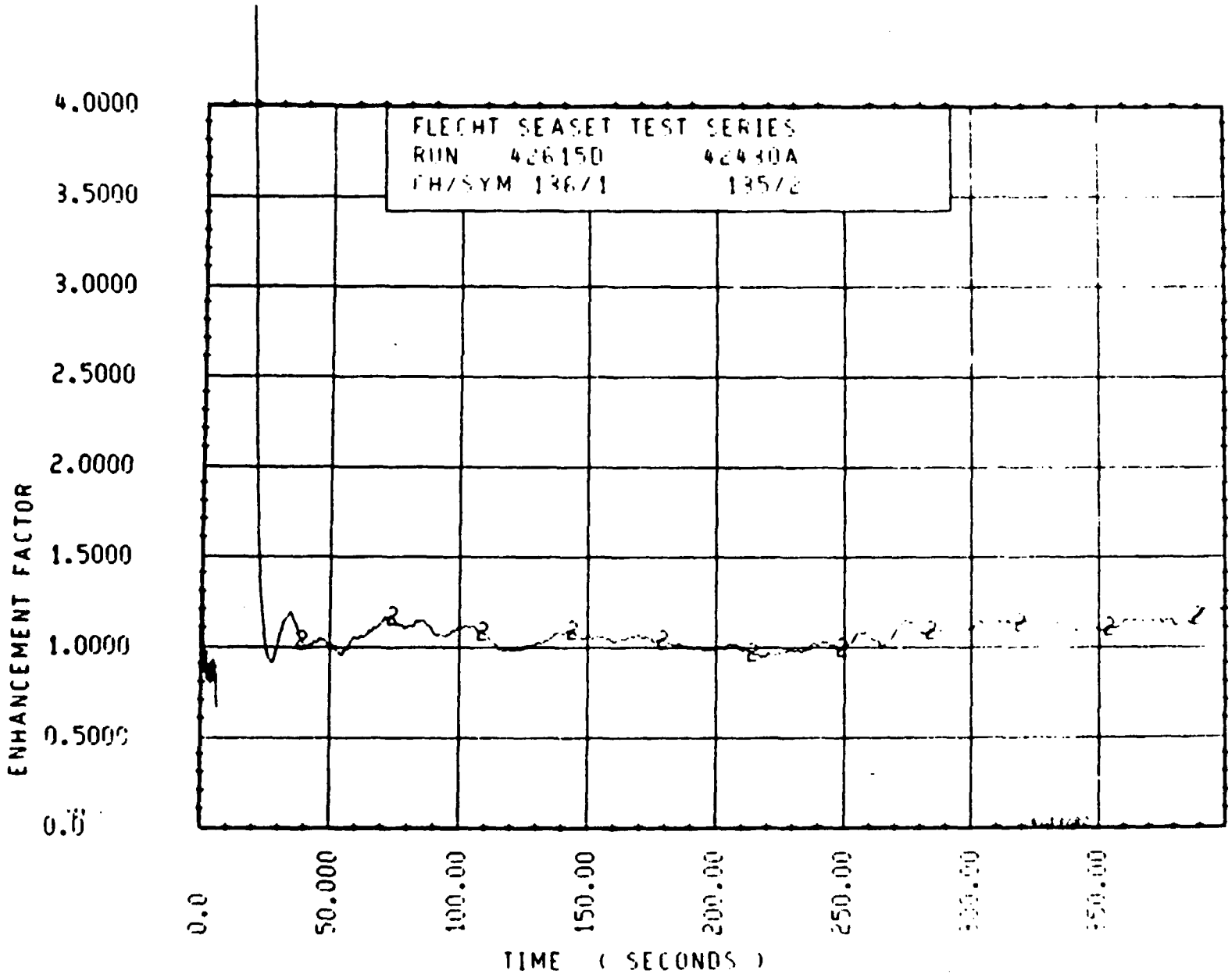

Figure 6-117. Enhancement Factor for Run 42615D, Rod 3B, 2.44 m (96 in.) Elevation

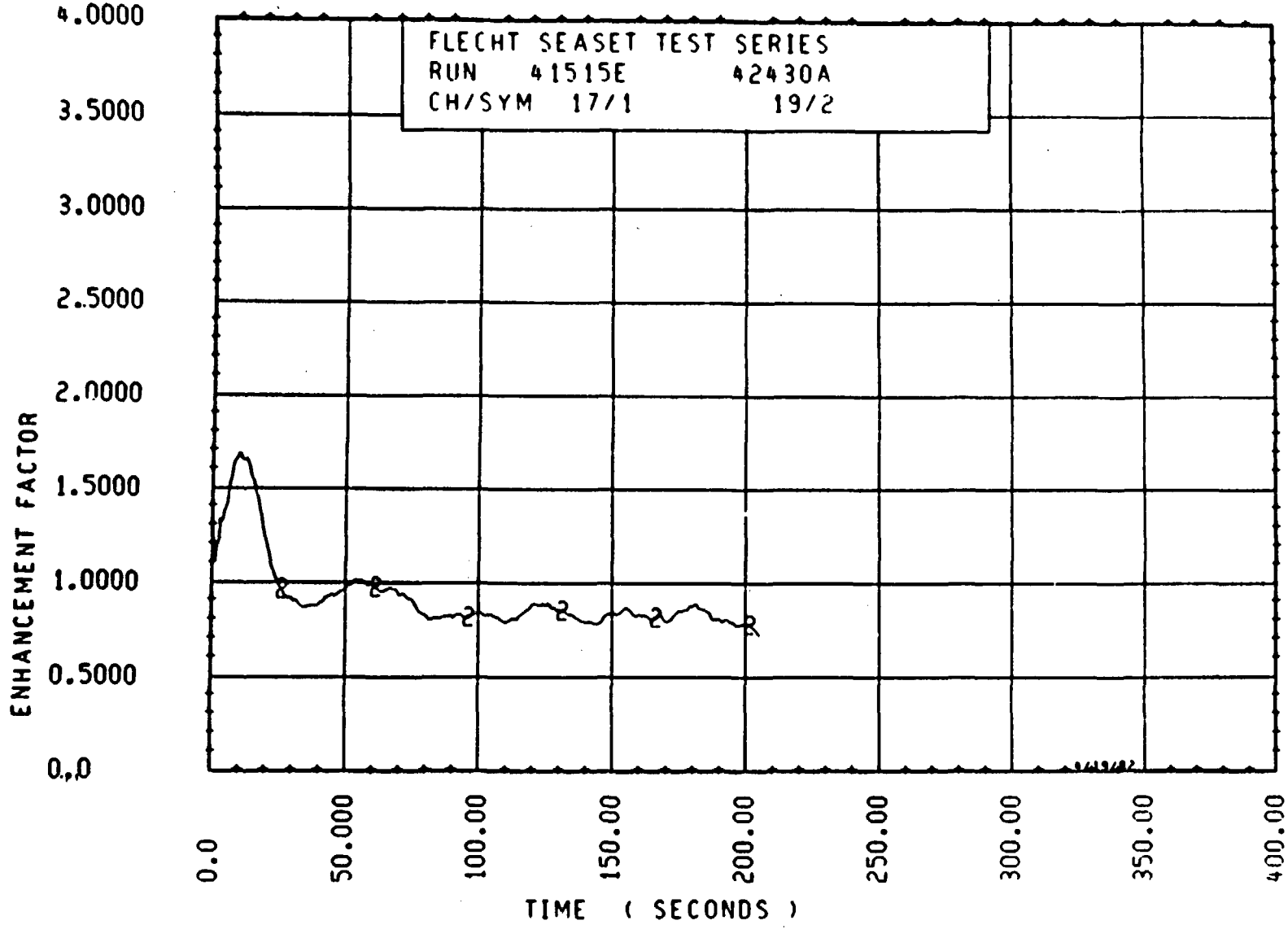

Figure 6-118. Enhancement Factor for Run 41515E, Rod 4C, 1.52 m (60 in.) Elevation

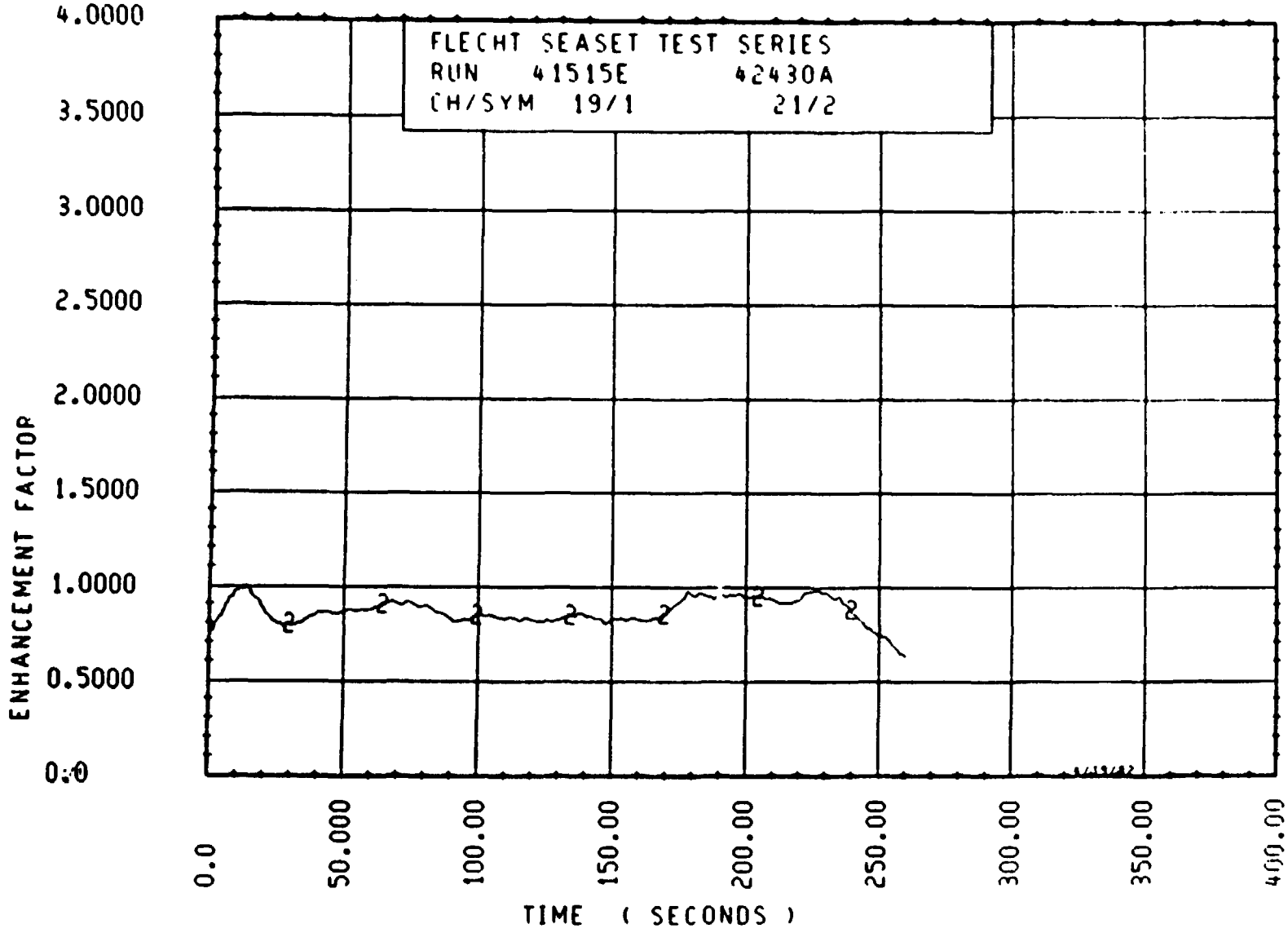

Figure 6-119. Enhancement Factor for Run 41515E, Rod 2A, 1.68 m (66.3 in.) Elevation

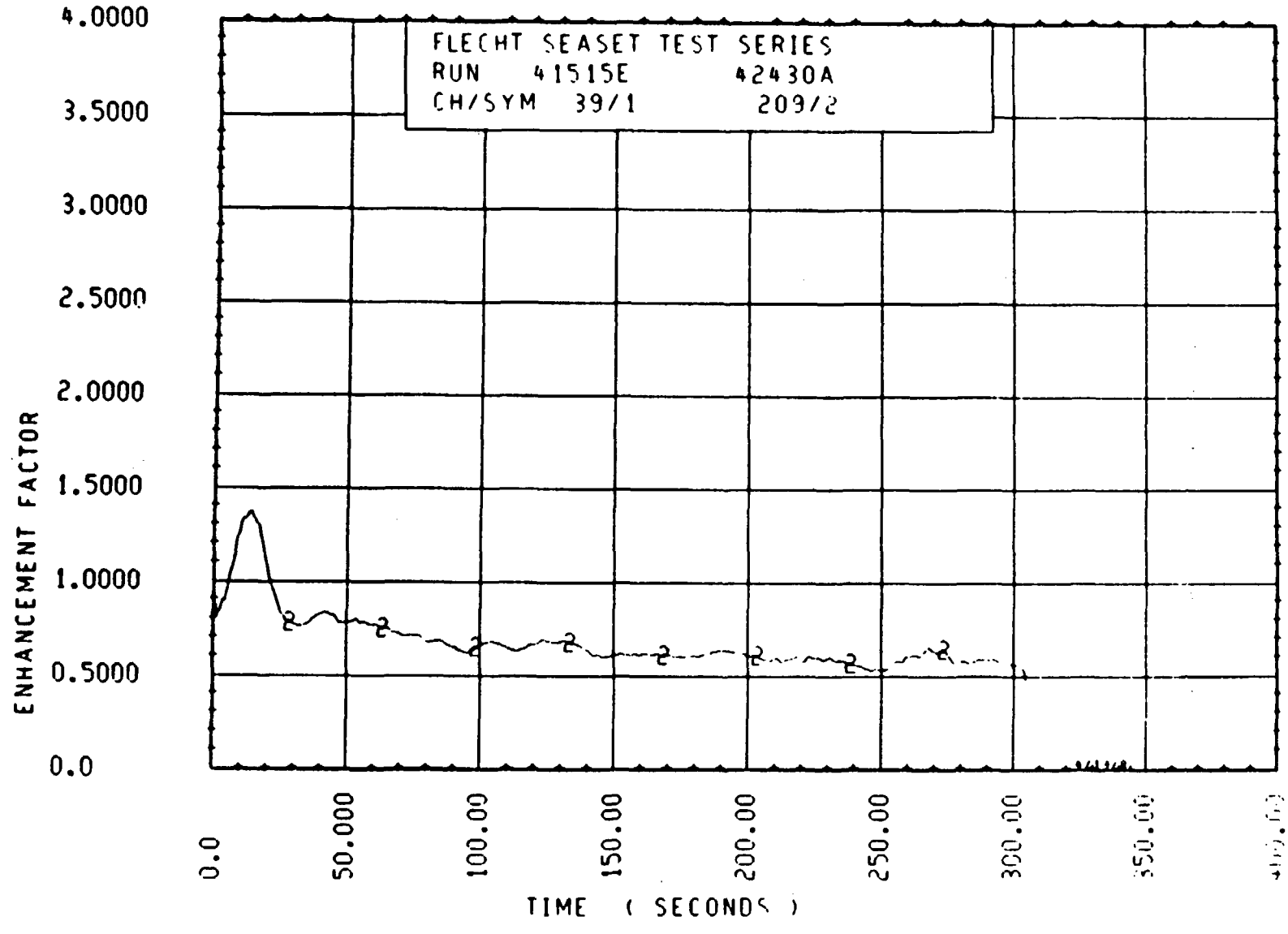

Figure 6-120. Enhancement Factor for Run 41515E, Rod 2D, 1.89 m (74.5 in.) Elevation

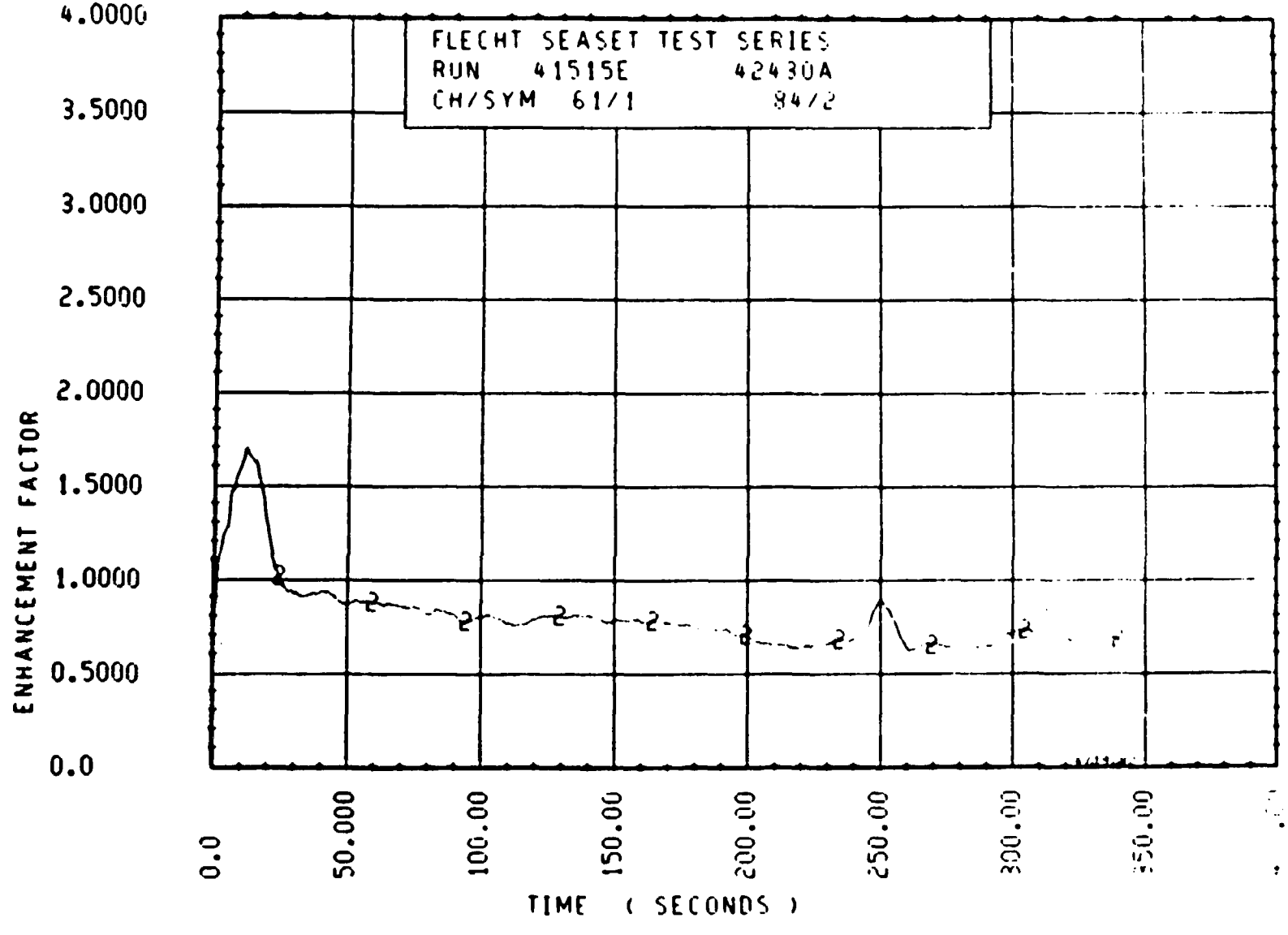

Figure 6-121. Enhancement Factor for Run 41515E, Rod 2D, 1.95 m (76.8 in.) Elevation

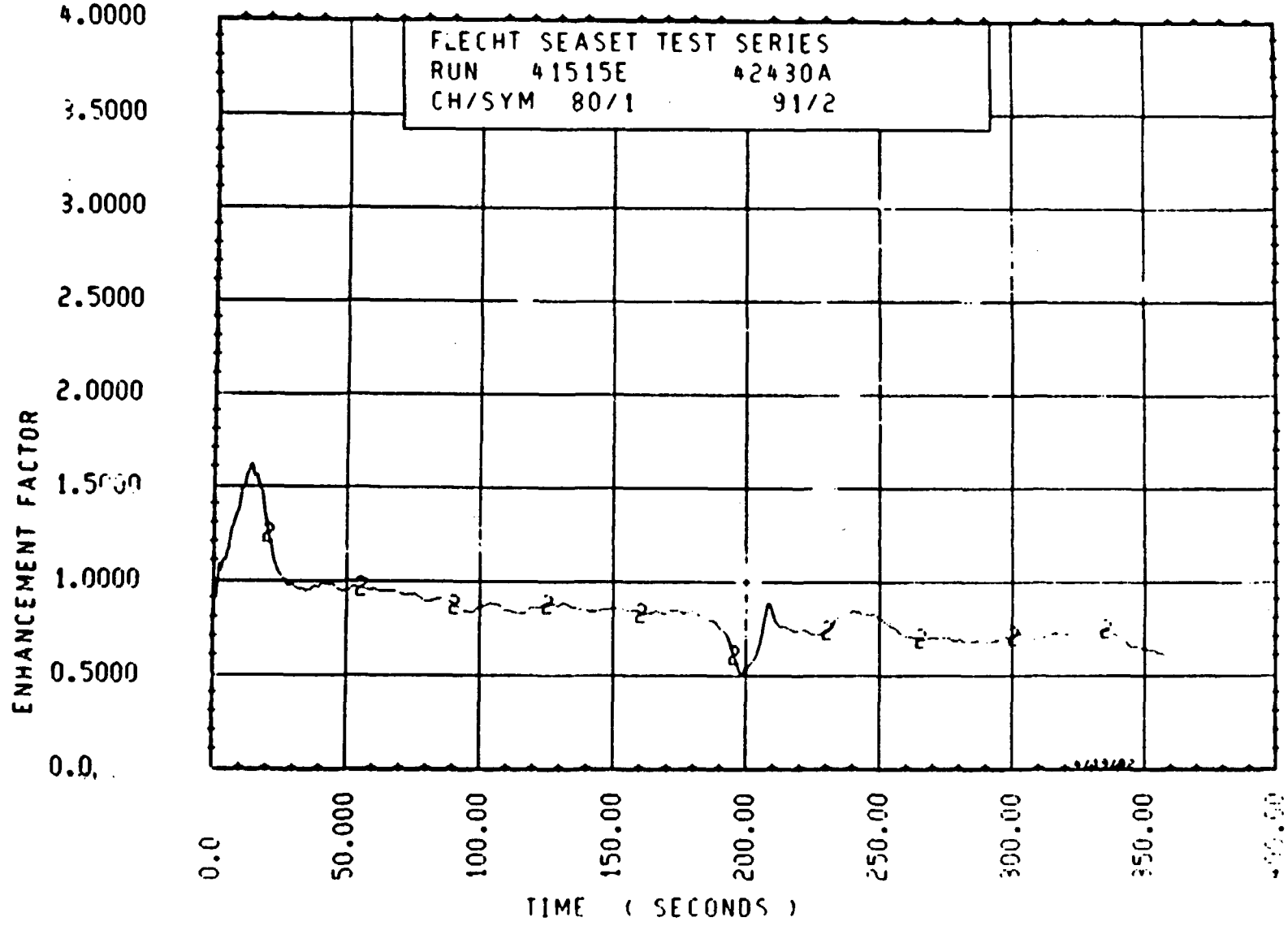

Figure 6-122. Enhancement Factor for Run 41515E, Rod 2D, 2.00 m (78.7 in.) Elevation

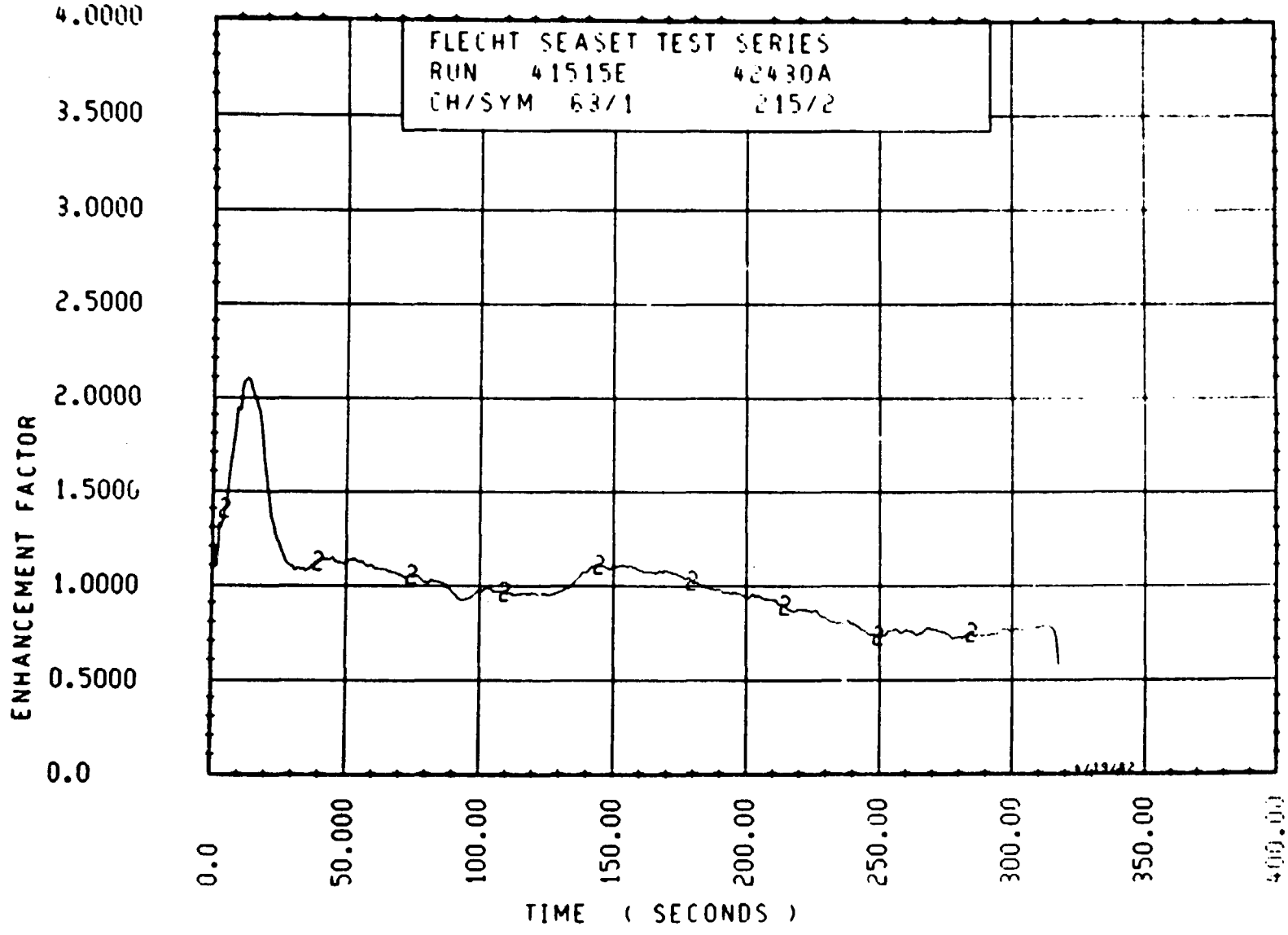

Figure 6-123. Enhancement Factor for Run 41515E, Rod 3B, 1.96 m (77.1 in.) Elevation

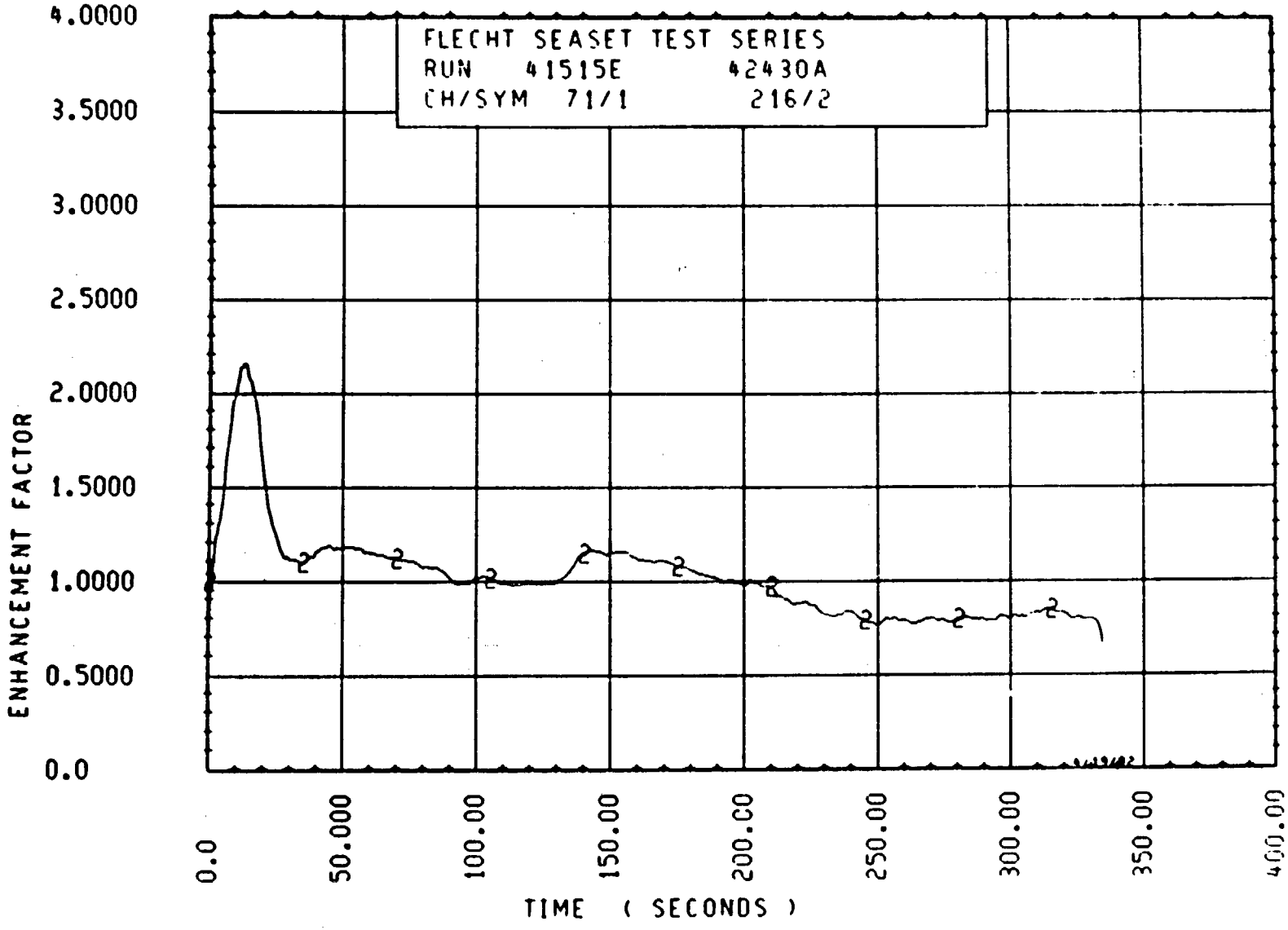

Figure 6-124. Enhancement Factor for Run 41515E, Rod 3B, 1.98 m (78.1 in.) Elevation

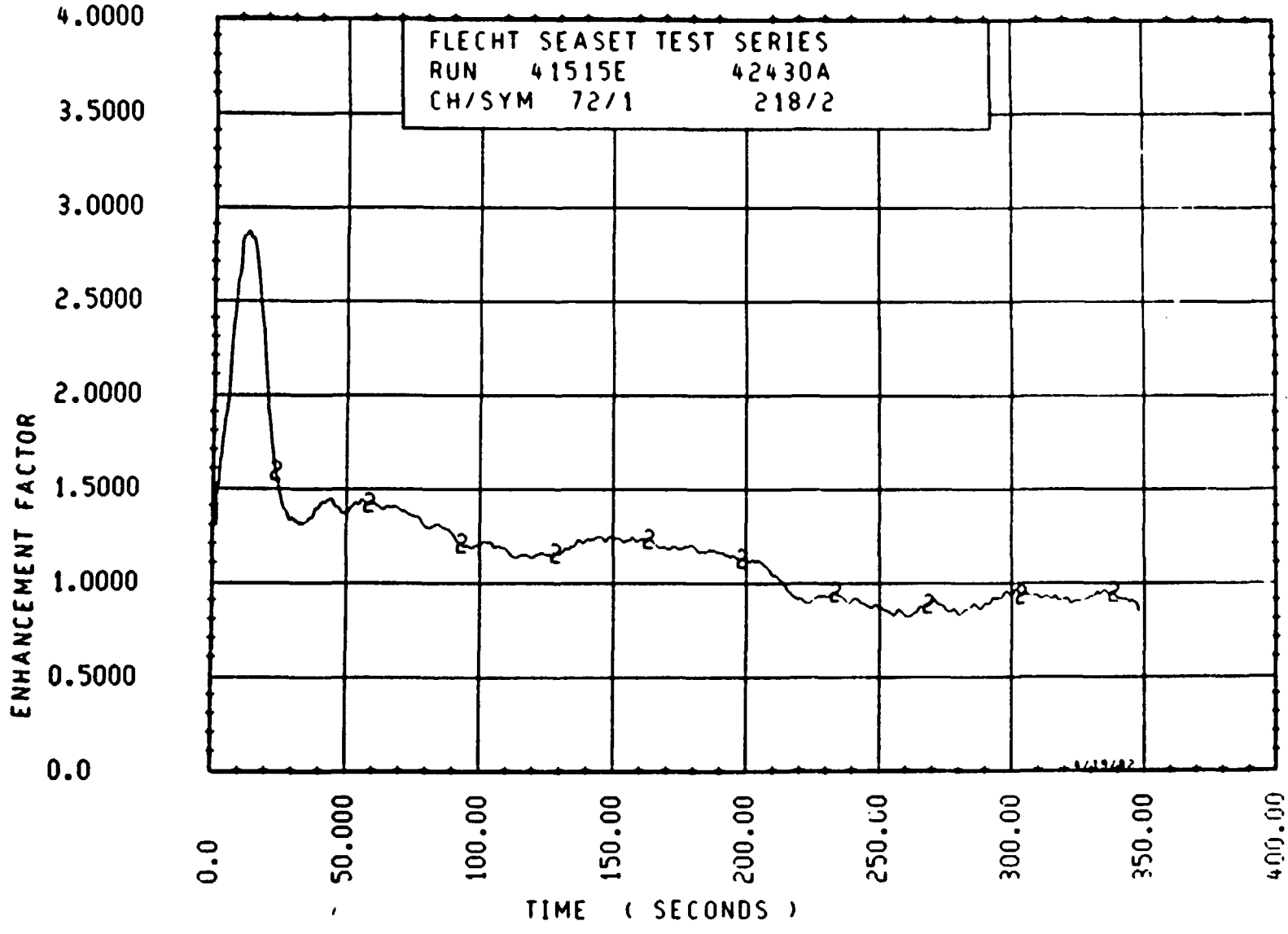

Figure 6-125. Enhancement Factor for Run 41515E, Rod 3C, 1.99 m (78.2 in.) Elevation

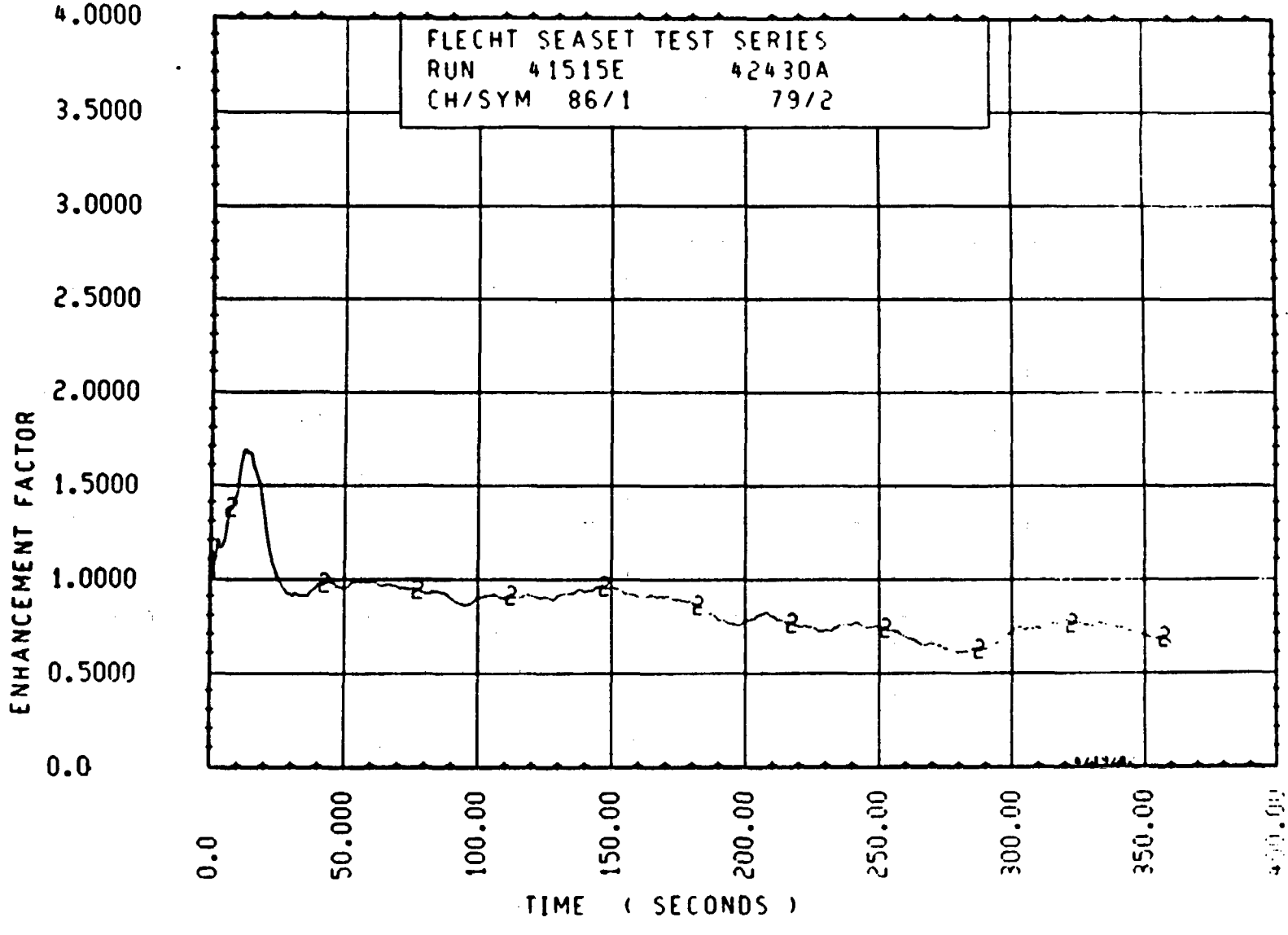

Figure 6-126. Enhancement Factor for Run 41515E, Rod 3D, 2.02 m (79.6 in.) Elevation

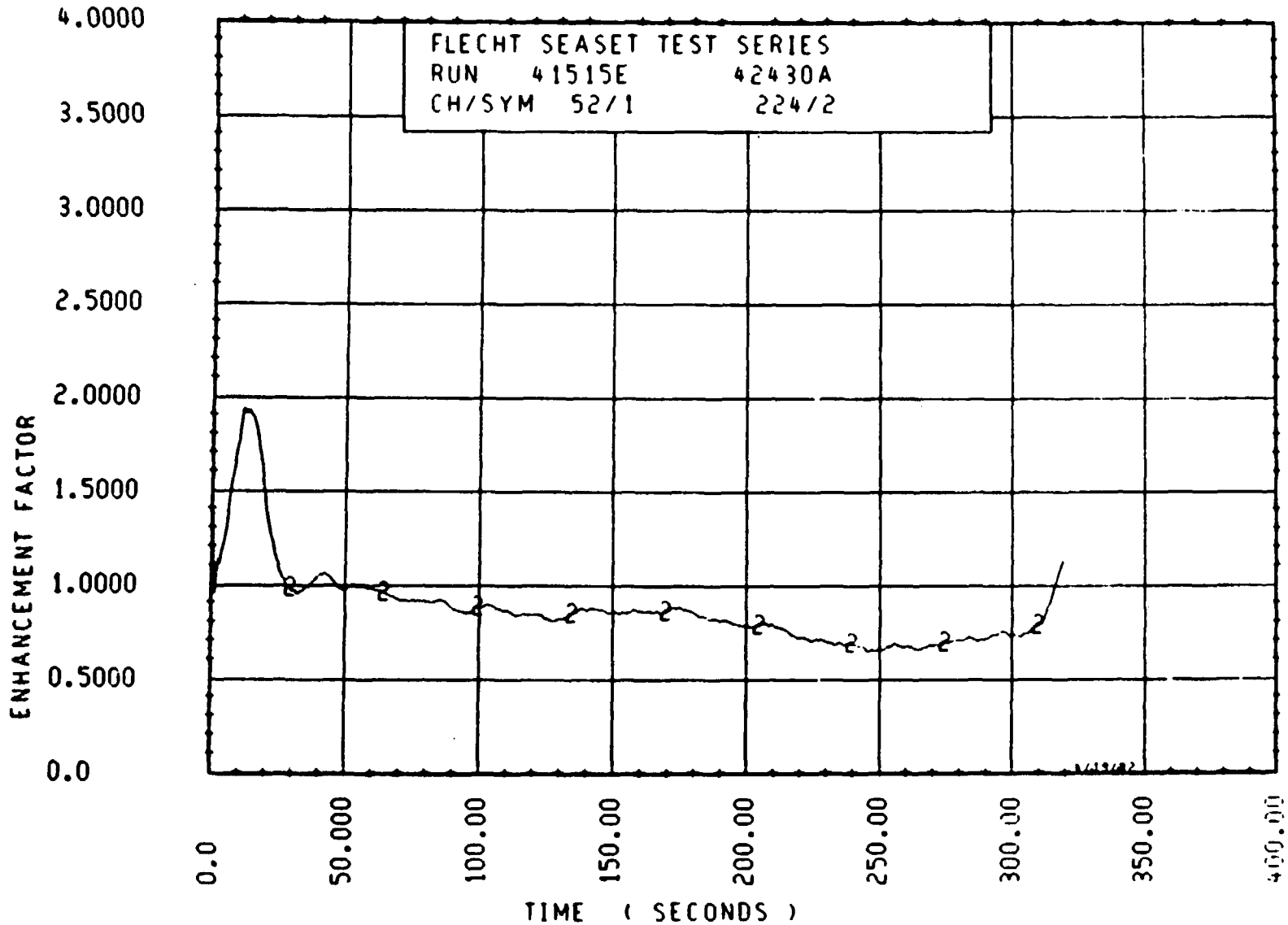

Figure 6-127. Enhancement Factor for Run 41515E, Rod 4B, 1.93 m (75.9 in.) Elevation

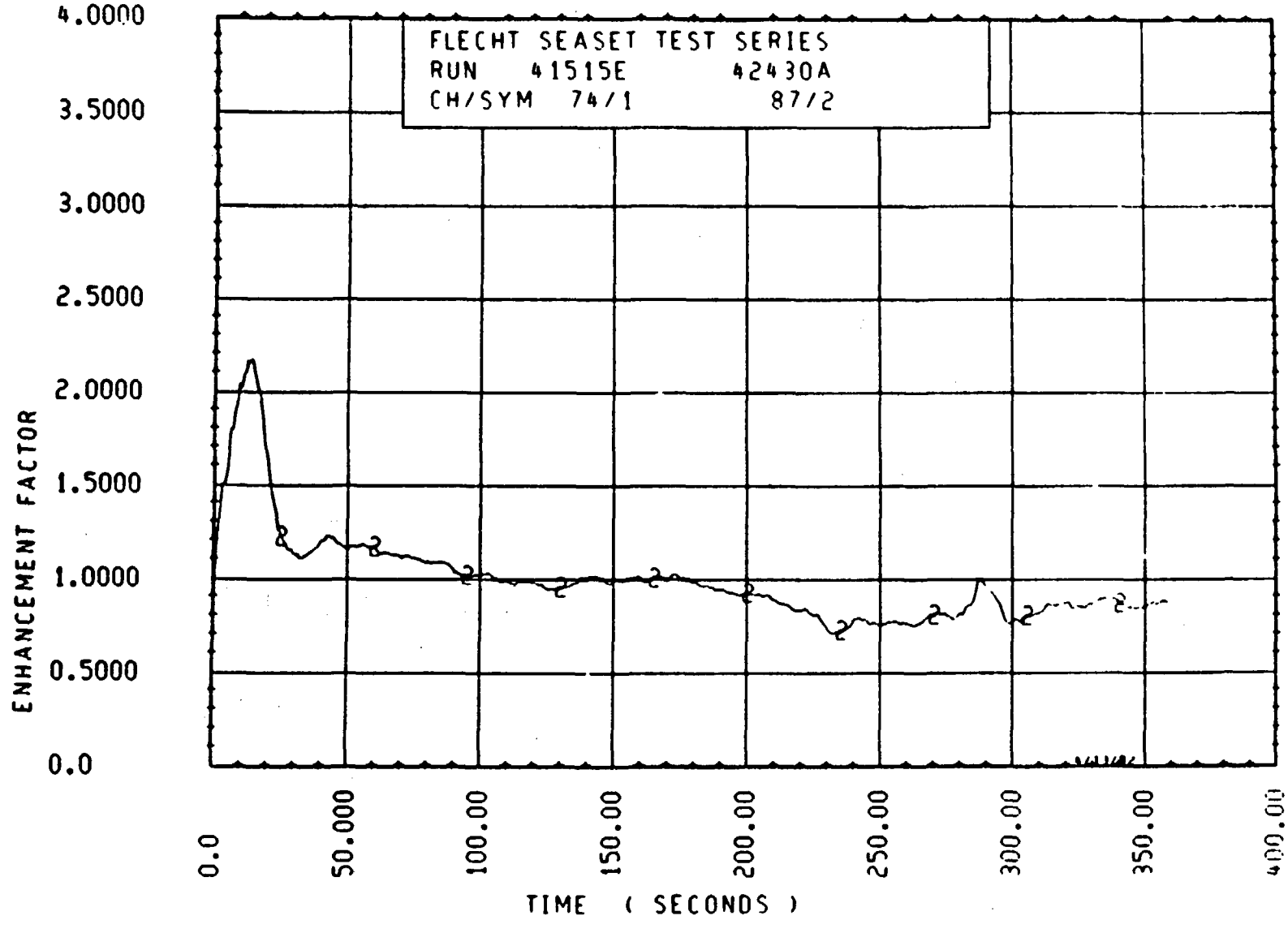

Figure 6-128. Enhancement Factor for Run 41515E, Rod 4B, 1.98 m (78.1 in.) Elevation

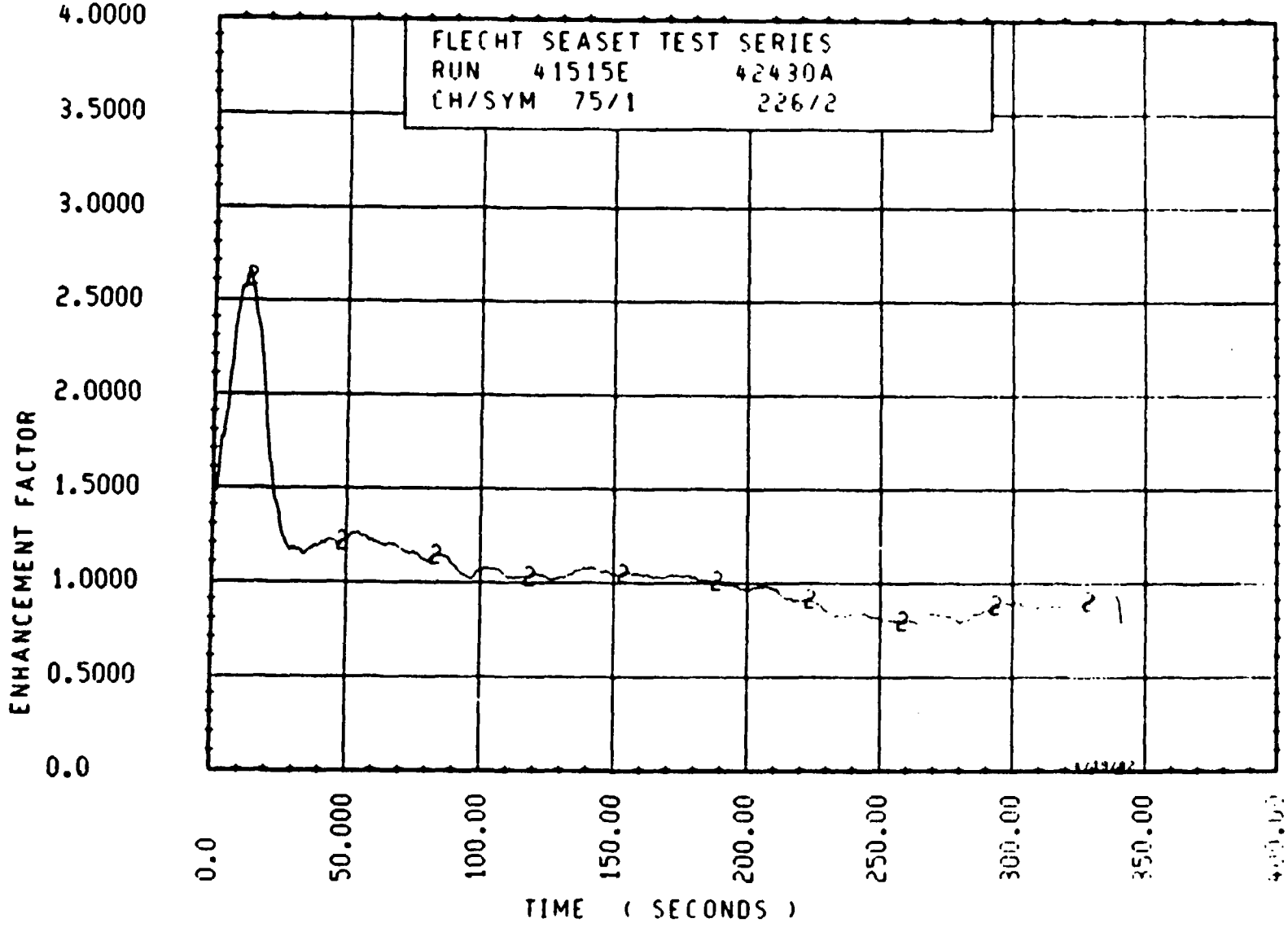

Figure 6-129. Enhancement Factor for Run 41515E, Rod 4C, 1.99 m (78.4 in.) Elevation

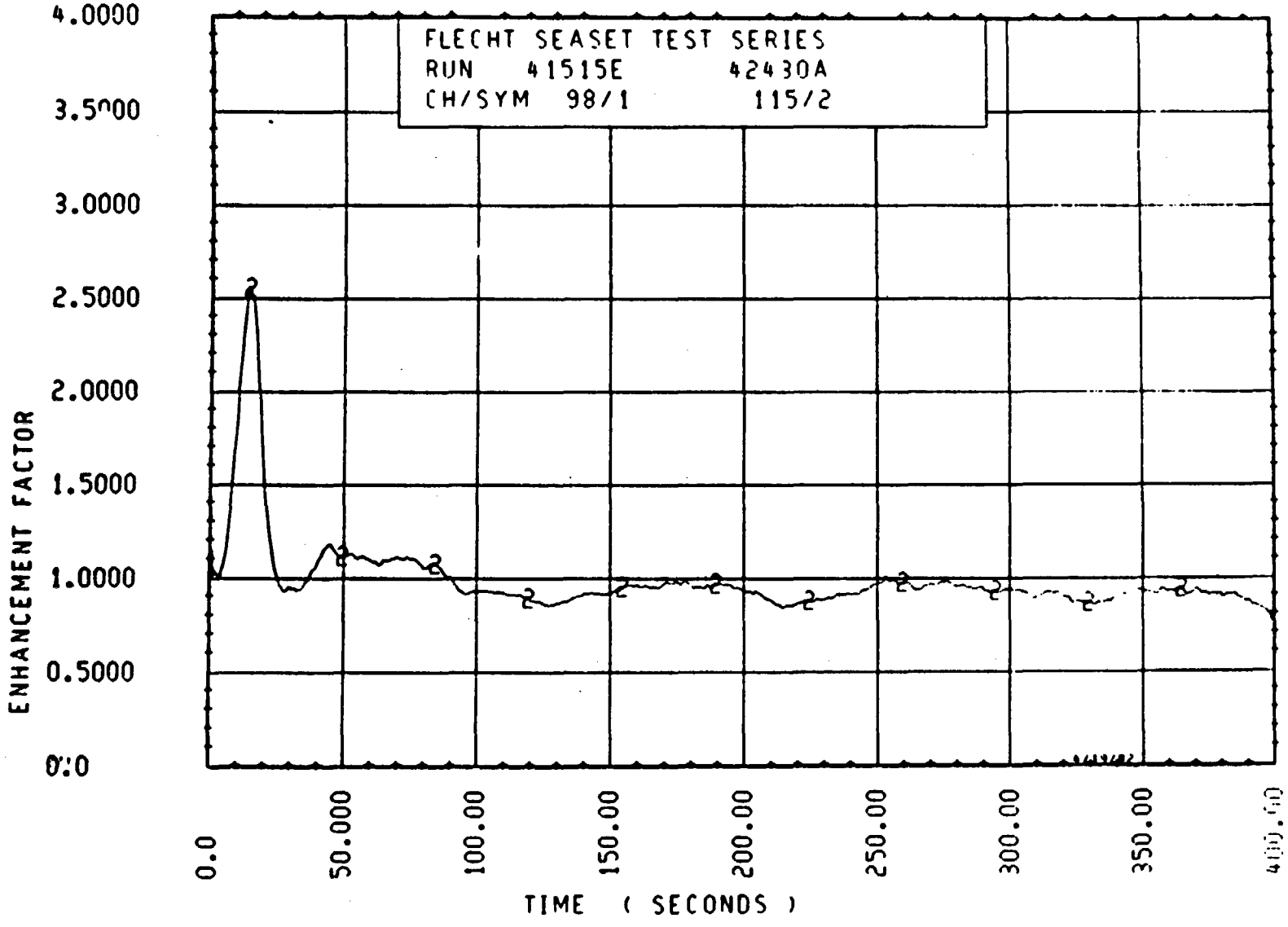

Figure 6-130. Enhancement Factor for Run 41515E, Rod 3D, 2.13 m (84 in.) Elevation

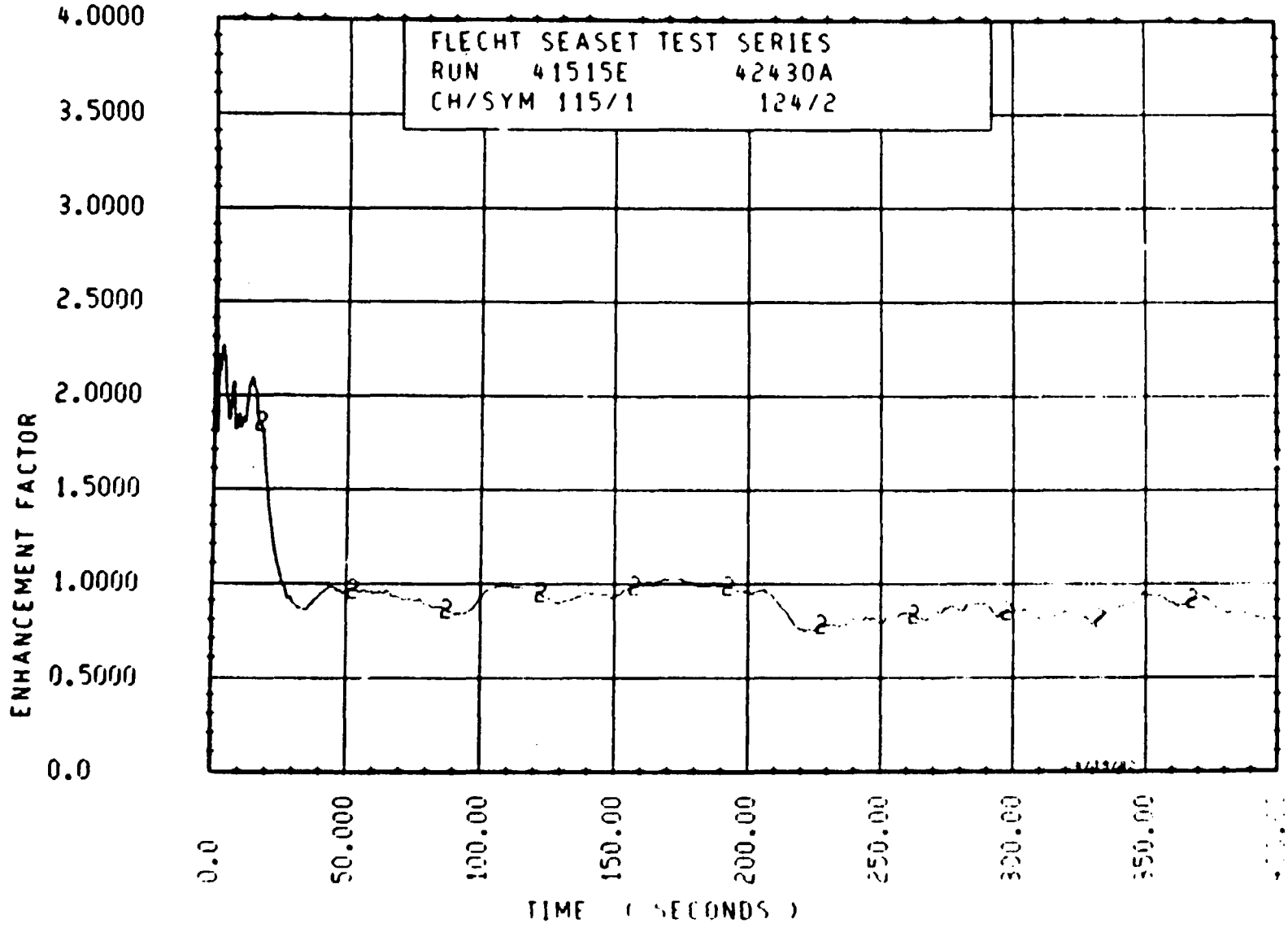

Figure 6-131. Enhancement Factor for Run 41515E, Rod 3B, 2.29 m (90 in.) Elevation

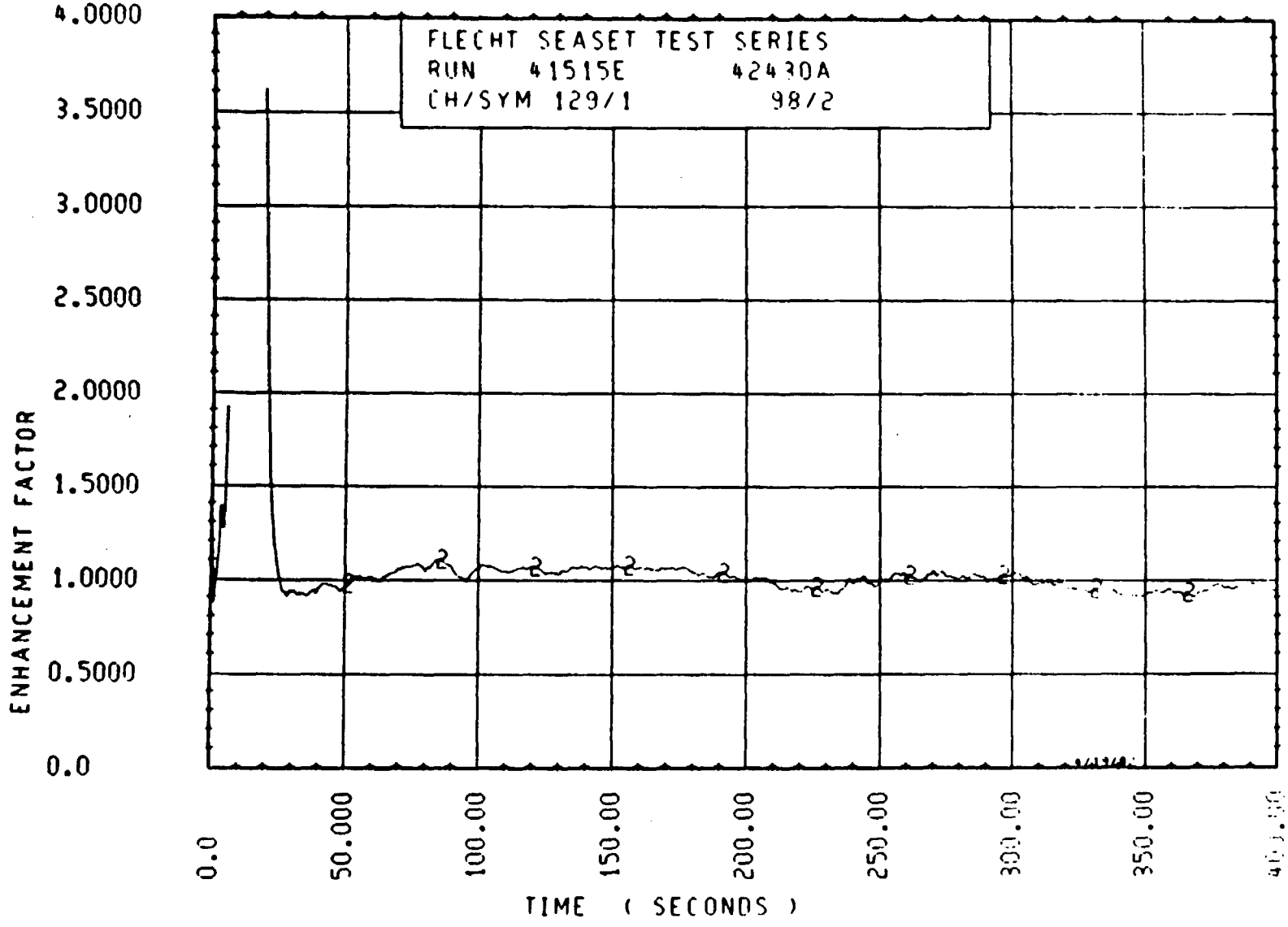

Figure 6-132. Enhancement Factor for Run 41515E, Rod 3D, 2.44 m (96 in.) Elevation

SECTION 7
CONCLUSIONS

The objectives of the 21-rod bundle flow blockage test program were judged to have been successfully met. Thermal-hydraulic data from one unblocked 21-rod bundle configuration and five blocked 21-rod bundle configurations, including both coplanar and noncoplanar blockage distribution, were obtained and analyzed. The selection of the long nonconcentric blockage sleeve for use in the large 163-rod blocked bundle was based on the measured 21-rod bundle reflood heat transfer data and the calculated COBRA-IV-I code flow redistribution. The long nonconcentric blockage sleeve was projected to provide the least favorable heat transfer characteristics in the large 163-rod blocked bundle.

In addition, isothermal characteristics tests and low-power, low-temperature steam cooling tests were successfully conducted on all six bundle configurations. The results from the hydraulic characteristics tests were utilized to provide a good simulation of the 21-rod bundle in the COBRA-IV-I code. The single-phase steam cooling tests will provide the basis for evaluating the two-phase reflood data and developing a blockage heat transfer model.

As with all experimental programs, some factors which are not typical of PWR behavior do exist in the 21-rod bundle data; however, they are not believed to limit the usefulness of the data. The small size of the 21-rod bundle test facility tends to enhance the housing or wall effects. The wall, although heated, still provides a radiation heat sink to the heater rods. The radiation effects were minimized for the central nine rods by heating the housing and having the 12 remaining rods acting as guard heater rods.

Since the test philosophy was to obtain very repeatable test conditions, the blocked data can be normalized by the unblocked data. In this fashion, the additional radiation

effect of the housing would become a second-order effect for the normalized heat transfer data for the outer rods and an even smaller effect for the central nine rods.

Normalization of the data is perhaps the simplest method for examination of the flow blockage effects on the resulting heat transfer. If the 21-rod bundle were to be modeled with a best-estimate computer code, then the additional radiation heat sink effect would have to be modeled in that code. Again, since the test philosophy was to repeat test conditions exactly from configuration to configuration, the computer code could be normalized to the unblocked data, and then used to analyze the blocked data. The housing effects in each test are essentially the same.

The gravity reflood scoping tests apparently have higher flooding rates than expected. The result is a masking of the effects of flow blockage. Approximate scaling of the loop resistance and estimation of the steam binding effect were apparently insufficient to compensate for the large flooding rates into the bundle. However, the 21-rod bundle gravity reflood data are still valuable and can be used as a code assessment tool for gravity reflood situations.

APPENDIX A
COBRA MODEL

COBRA-IV-I was utilized extensively in determining the sleeve type for the use in the large bundle test. This code is well summarized in the 21-rod bundle task plan.[1] In this appendix, pertinent information is provided for all blockage configurations tested in this program.

The input for configuration A is shown in table A-1, which includes all parameters of bundle geometry and thermal hydraulic variables. The simulation of the bundle was performed by the implicit method with inlet flows specified, and the results were written on a catalog tape. This catalog tape was used to provide initial conditions for the simulations of configurations B through F. These bundles were simulated by the explicit method with the initial conditions using a pseudo-flow transient case. The input for the area and gap variations for the bundles are provided in tables A-2 through A-6. The input for the pressure loss coefficients for the grids and the blockage sleeves are provided in tables A-7 and A-8 for configurations E and F, respectively.

1. Hochreiter, L.E., et al., "PWR FLECHT SEASET 21-Rod Bundle Flow Blockage Task: Task Plan Report," NRC/EPRI/Westinghouse-5, March 1980. NUREG/CR-1370.

TABLE A-1

INPUTS FOR CONFIGURATION A

SUMMARY OF INPUT OPTIONS

GROUP	H1	H2	H3	H4	H5	H6	H7	H8	H9
1	7	1	1	0	0	0	0	0	0
2	0	0	0	1	1	0	0	0	0
3	2	0	0	0	0	0	0	0	0
4	28	28	0	0	0	0	0	0	0
7	2	0	3	3	5	0	0	0	0
8	25	25	0	0	0	0	0	0	0
9	0	0	0	0	0	0	0	0	0
10	0	0	0	0	0	0	0	0	0
11	0	1	0	0	0	0	0	0	0
12	0	0	0	0	0	0	0	0	0

FLUID PROPERTY TABLE

P	T	VF	VG	HF	HG	VISC.	KF	SIGMA
15.0	213.00	.01670	26.29000	181.19	1150.90	.07900	.04780	.08000
20.0	228.00	.01680	20.09000	196.26	1156.40	.07900	.04780	.08000
25.0	240.10	.01690	16.30600	208.52	1160.70	.07900	.04780	.08000
30.0	250.30	.01700	13.74800	218.93	1164.30	.07900	.04780	.08000
35.0	259.30	.01710	11.90000	228.04	1167.40	.07900	.04780	.08000
40.0	267.30	.01710	10.50100	236.16	1169.70	.07900	.04780	.08000
45.0	274.50	.01720	9.40300	243.51	1172.30	.07900	.04780	.08000

SUPERHEATED STEAM PROPERTIES AT 40.00 PSI

T	H	CP	V	VISC	K	PR
DEG F	BTU/LBM	BTU/LBM-R	CU FT/LBM	LBM/FT-HR	BTU/HR-FT-F	
267.3	1169.7	.530	10.4992	.0319	.0161	1.05
278.4	1175.4	.522	10.6840	.0325	.0165	1.04
269.4	1181.4	.516	10.8688	.0332	.0165	1.03
300.5	1187.1	.505	11.0478	.0338	.0168	1.02
333.7	1203.8	.495	11.5827	.0357	.0177	1.00
366.8	1220.2	.489	12.1084	.0375	.0185	.99
400.0	1236.5	.489	12.6274	.0394	.0196	.98

FRICTION FACTOR CORRELATION

CHANNEL TYPE 1 FRICT = MAXIMUM OF (.340*RE**(-.250) + 0.0000 OR 64.0000*RE**(-1.0000) + 0.0000)
CHANNEL TYPE 2 FRICT = MAXIMUM OF (.340*RE**(-.250) + 0.0000 OR 64.0000*RE**(-1.0000) + 0.0000)
CHANNEL TYPE 3 FRICT = MAXIMUM OF (.340*RE**(-.250) + 0.0000 OR 64.0000*RE**(-1.0000) + 0.0000)
CHANNEL TYPE 4 FRICT = MAXIMUM OF (.340*RE**(-.250) + 0.0000 OR 64.0000*RE**(-1.0000) + 0.0000)
WALL VISCOSITY CORRECTION TO FRICTION FACTOR IS INCLUDED

SINGLE PHASE HEAT TRANSFER CORRELATION

HFILM = K/D(.023*RE**(.800)*PR**(.400) + 0.000)

TWO-PHASE FLOW CORRELATIONS

NO SUBCOOLED VOID CORRELATION
HOMOGENEOUS BULK VOID MODEL
HOMOGENEOUS MODEL FRICTION MULTIPLIER

TABLE A-1 (cont)

INPUTS FOR CONFIGURATION A

HEAT FLUX DISTRIBUTION

X/L	RELATIVE FLUX
0.000	1.000
1.000	1.000

SUBCHANNEL INPUT DATA

CHANNEL NO.	TYPE	AREA (SQ-IN)	WETTED PERIM. (IN)	HEATED PERIM. (IN)	HYDRAULIC DIAMETER (IN)	(ADJACENT CHANNEL NO., SPACING, CENTROID DISTANCE)			
1	4	.079000	2.062000	.414000	.153249	(2, .059,0.000)	(5, .030,0.000)	(9, .059,0.000)	(0,0.000,0.000)
2	3	.117000	1.302000	.674000	.359447	(3, .176,0.000)	(6, .122,0.000)	(0,0.000,0.000)	(0,0.000,0.000)
3	3	.117000	1.302000	.674000	.359447	(4, .059,0.000)	(7, .122,0.000)	(0,0.000,0.000)	(0,0.000,0.000)
4	4	.079000	2.062000	.414000	.153249	(8, .030,0.000)	(14, .059,0.000)	(0,0.000,0.000)	(0,0.000,0.000)
5	2	.078000	1.444000	.881000	.216066	(6, .122,0.000)	(10, .122,0.000)	(0,0.000,0.000)	(0,0.000,0.000)
6	1	.136000	1.175000	1.175000	.462979	(7, .122,0.000)	(11, .122,0.000)	(0,0.000,0.000)	(0,0.000,0.000)
7	1	.136000	1.175000	1.175000	.462979	(8, .122,0.000)	(12, .122,0.000)	(0,0.000,0.000)	(0,0.000,0.000)
8	2	.078000	1.444000	.881000	.216066	(13, .122,0.000)	(0,0.000,0.000)	(0,0.000,0.000)	(0,0.000,0.000)
9	3	.117000	1.302000	.674000	.359447	(10, .122,0.000)	(15, .176,0.000)	(0,0.000,0.000)	(0,0.000,0.000)
10	1	.136000	1.175000	1.175000	.462979	(11, .122,0.000)	(16, .122,0.000)	(0,0.000,0.000)	(0,0.000,0.000)
11	1	.136000	1.175000	1.175000	.462979	(12, .122,0.000)	(17, .122,0.000)	(0,0.000,0.000)	(0,0.000,0.000)
12	1	.136000	1.175000	1.175000	.462979	(13, .122,0.000)	(18, .122,0.000)	(0,0.000,0.000)	(0,0.000,0.000)
13	1	.136000	1.175000	1.175000	.462979	(14, .122,0.000)	(19, .122,0.000)	(0,0.000,0.000)	(0,0.000,0.000)
14	3	.117000	1.302000	.674000	.359447	(20, .176,0.000)	(0,0.000,0.000)	(0,0.000,0.000)	(0,0.000,0.000)
15	3	.117000	1.302000	.674000	.359447	(16, .122,0.000)	(25, .059,0.000)	(0,0.000,0.000)	(0,0.000,0.000)
16	1	.136000	1.175000	1.175000	.462979	(17, .122,0.000)	(21, .122,0.000)	(0,0.000,0.000)	(0,0.000,0.000)
17	1	.136000	1.175000	1.175000	.462979	(18, .122,0.000)	(22, .122,0.000)	(0,0.000,0.000)	(0,0.000,0.000)
18	1	.136000	1.175000	1.175000	.462979	(19, .122,0.000)	(23, .122,0.000)	(0,0.000,0.000)	(0,0.000,0.000)
19	1	.136000	1.175000	1.175000	.462979	(20, .122,0.000)	(24, .122,0.000)	(0,0.000,0.000)	(0,0.000,0.000)
20	3	.117000	1.302000	.674000	.359447	(28, .059,0.000)	(0,0.000,0.000)	(0,0.000,0.000)	(0,0.000,0.000)
21	2	.078000	1.444000	.881000	.216066	(22, .122,0.000)	(25, .030,0.000)	(0,0.000,0.000)	(0,0.000,0.000)
22	1	.136000	1.175000	1.175000	.462979	(23, .122,0.000)	(26, .122,0.000)	(0,0.000,0.000)	(0,0.000,0.000)
23	1	.136000	1.175000	1.175000	.462979	(24, .122,0.000)	(27, .122,0.000)	(0,0.000,0.000)	(0,0.000,0.000)
24	2	.078000	1.444000	.881000	.216066	(28, .030,0.000)	(0,0.000,0.000)	(0,0.000,0.000)	(0,0.000,0.000)
25	4	.079000	2.062000	.414000	.153249	(26, .059,0.000)	(0,0.000,0.000)	(0,0.000,0.000)	(0,0.000,0.000)
26	3	.117000	1.302000	.674000	.359447	(27, .176,0.000)	(0,0.000,0.000)	(0,0.000,0.000)	(0,0.000,0.000)
27	3	.117000	1.302000	.674000	.359447	(28, .059,0.000)	(0,0.000,0.000)	(0,0.000,0.000)	(0,0.000,0.000)
28	4	.079000	2.062000	.414000	.153249	(0,0.000,0.000)	(0,0.000,0.000)	(0,0.000,0.000)	(0,0.000,0.000)

SPACER DATA

SPACER TYPE NO.	1	2	3
LOCATION (X/L)	.159	.464	.754

SPACER TYPE 1

CHANNEL NO.	DRAG COEFF.	CHANNEL NO.	DRAG COEFF.	CHANNEL NO.	DRAG COEFF.	CHANNEL NO.	DRAG COEFF.
1	.884	2	.313	3	.313	4	.744
5	1.008	6	.450	7	.490	8	1.372
9	.313	10	.450	11	.446	12	.446
13	.884	14	.313	15	.794	16	1.398
17	1.195	18	1.196	19	.696	20	.313
21	1.369	22	.674	23	.884	24	1.792
25	.805	26	.313	27	.313	28	.829

TABLE A-1 (cont)

INPUTS FOR CONFIGURATION A

SPACER TYPE 2

CHANNEL NO.	DRAG COEFF.	CHANNEL NO.	DRAG COEFF.	CHANNEL NO.	DRAG COEFF.	CHANNEL NO.	DRAG COEFF.
1	.858	2	.313	3	.313	4	.805
5	1.792	6	.694	7	.450	8	1.372
9	.313	10	.883	11	1.253	12	.853
13	1.042	14	.313	15	.313	16	.[illegible]
17	.871	18	.871	19	.450	20	.313
21	1.792	22	.694	23	.[illegible]	24	1.372
25	.805	26	.313	27	.313	28	.724

SPACER TYPE 3

CHANNEL NO.	DRAG COEFF.	CHANNEL NO.	DRAG COEFF.	CHANNEL NO.	DRAG COEFF.	CHANNEL NO.	DRAG COEFF.
1	.744	2	.313	3	.313	4	.744
5	1.372	6	.450	7	.450	8	1.372
9	.313	10	.884	11	.444	12	.444
13	.884	14	.313	15	.313	16	.884
17	1.254	18	.444	19	.450	20	.313
21	1.792	22	.694	23	.450	24	1.008
25	.869	26	.313	27	.313	28	.684

ROD INPUT DATA

ROD NO.	TYPE NO.	DIA (in)	RADIAL POWER FACTOR	FRACTION OF POWER TO ADJACENT CHANNELS (ADJ. CHANNEL NO.)					
1	1	.2200	0.0000	.5000(1)	.5000(5)	0.0000(0)	0.0000(0)	0.0000(0)	0.0000(0)
2	1	.3740	1.0000	.1600(1)	.3200(2)	.2500(5)	.2500(6)	0.0000(0)	0.0000(0)
3	1	.3740	1.0000	.2500(2)	.2500(3)	.2500(6)	.2500(7)	0.0000(0)	0.0000(0)
4	1	.3740	1.0000	.3200(3)	.1600(4)	.2500(7)	.2500(8)	0.0000(0)	0.0000(0)
5	1	.2200	0.0000	.5000(4)	.5000(8)	0.0000(0)	0.0000(0)	0.0000(0)	0.0000(0)
6	1	.3740	1.0000	.1600(1)	.2500(5)	.3200(9)	.2500(10)	0.0000(0)	0.0000(0)
7	1	.3740	1.0000	.2500(5)	.2500(6)	.2500(10)	.2500(11)	0.0000(0)	0.0000(0)
8	1	.3740	1.0000	.2500(6)	.2500(7)	.2500(11)	.2500(12)	0.0000(0)	0.0000(0)
9	1	.3740	1.0000	.2500(7)	.2500(8)	.2500(12)	.2500(13)	0.0000(0)	0.0000(0)
10	1	.3740	1.0000	.1600(6)	.2500(8)	.2500(13)	.3200(14)	0.0000(0)	0.0000(0)
11	1	.3740	1.0000	.2500(9)	.2500(10)	.2500(15)	.2500(16)	0.0000(0)	0.0000(0)
12	1	.3740	1.0000	.2500(10)	.2500(11)	.2500(16)	.2500(17)	0.0000(0)	0.0000(0)
13	1	.3740	1.0000	.2500(11)	.2500(12)	.2500(17)	.2500(18)	0.0000(0)	0.0000(0)
14	1	.3740	1.0000	.2500(12)	.2500(13)	.2500(18)	.2500(19)	0.0000(0)	0.0000(0)
15	1	.3740	1.0000	.2500(13)	.2500(14)	.2500(19)	.2500(20)	0.0000(0)	0.0000(0)
16	1	.3740	1.0000	.3200(15)	.2500(17)	.2500(21)	.1600(25)	0.0000(0)	0.0000(0)
17	1	.3740	1.0000	.2500(16)	.2500(17)	.2500(21)	.2500(22)	0.0000(0)	0.0000(0)
18	1	.3740	1.0000	.2500(17)	.2500(18)	.2500(22)	.2500(23)	0.0000(0)	0.0000(0)
19	1	.3740	1.0000	.2500(18)	.2500(19)	.2500(23)	.2500(24)	0.0000(0)	0.0000(0)
20	1	.3740	1.0000	.2500(19)	.3200(20)	.2500(24)	.1600(28)	0.0000(0)	0.0000(0)
21	1	.2200	0.0000	.5000(21)	.5000(25)	0.0000(0)	0.0000(0)	0.0000(0)	0.0000(0)
22	1	.3740	1.0000	.2500(21)	.2500(22)	.1600(26)	.3200(27)	0.0000(0)	0.0000(0)
23	1	.3740	1.0000	.2500(22)	.2500(23)	.2500(27)	.2500(28)	0.0000(0)	0.0000(0)
24	1	.3740	1.0000	.2500(23)	.2500(24)	.3200(28)	.1600(32)	0.0000(0)	0.0000(0)
25	1	.2200	0.0000	.5000(25)	.5000(29)	0.0000(0)	0.0000(0)	0.0000(0)	0.0000(0)

TABLE A-1 (cont)

INPUTS FOR CONFIGURATION A

IMPLICIT SOLUTION WITH INLET FLOWS SPECIFIED

CALCULATION PARAMETERS

LATERAL RESISTANCE FACTOR	.1500		CHANNEL LENGTH	69.0000 INCHES
(S/L) PARAMETER	.2500		NUMBER OF AXIAL NODES	29
TURBULENT MOMENTUM FACTOR	1.0000		AXIAL NODE LENGTH	1.0000 INCHES
CHANNEL ORIENTATION	0.0000 DEGREES		TOTAL TRANSIENT TIME	0.0000 SECONDS
ROLL OPTION (0 = NO ROLL)	0		NUMBER OF TIME STEPS	0
			NOMINAL TIME STEP	********* SECONDS

DATA FOR IMPLICIT SOLUTION

EXTERNAL ITERATION LIMIT	20	MINIMUM INTERNAL ITERATIONS	5
INTERNAL ITERATION LIMIT	96	FRACTION DONOR CELL USTAR	1.0000
CONVERGENCE FACTORS		ACCELERATION FACTORS	
EXTERNAL (DW/W)	.1000	CROSSFLOW SOLUTION	1.4000
INTERNAL (DW/W)	.0010	LATERAL DELTA-P	.6000
FLOW (DF/F)	.0010	FLOW	.6000

MIXING CORRELATIONS

SUBCOOLED MIXING, BETA = .0200

BOILING MIXING, BETA IS ASSUMED SAME AS SUBCOOLED

OPERATING CONDITIONS

SYSTEM PRESSURE	=	40.0 PSIA
INLET ENTHALPY	=	1171.0 BTU/LB
AVG. MASS VELOCITY	=	.010 MILLION LB/(HR-SQFT)
INLET TEMPERATURE	=	269.7 DEGREES F
AVG. HEAT FLUX	=	0.000000 MILLION BTU/(HR-SQFT)

UNIFORM INLET ENTHALPY

FLOWS SPLIT FOR EQUAL PRESSURE GRADIENT (CHANNEL-FLOW)

(1 = 9.531E-04)	(2 = 2.251E-03)	(3 = 2.251E-03)	(4 = 9.531E-04)	(5 = 1.224E-03)	(6 = 2.868E-03)
(7 = 2.868E-03)	(8 = 1.224E-03)	(9 = 2.251E-03)	(10 = 2.868E-03)	(11 = 2.644E-03)	(12 = 2.644E-03)
(13 = 2.868E-03)	(14 = 2.251E-03)	(15 = 2.251E-03)	(16 = 2.868E-03)	(17 = 2.644E-03)	(18 = 2.644E-03)
(19 = 2.868E-03)	(20 = 2.251E-03)	(21 = 1.224E-03)	(22 = 2.868E-03)	(23 = 2.644E-03)	(24 = 1.224E-03)
(25 = 9.531E-04)	(26 = 2.251E-03)	(27 = 2.251E-03)	(28 = 9.531E-04)		

TABLE A-2

AREA AND GAP VARIATIONS OF CONFIGURATION B

X/L	AREA VARIATION FACTORS FOR SUBCHANNEL (I)									
	(5)	(6)	(7)	(8)	(10)	(11)	(12)	(13)	(16)	(17)
0.000	1.000	1.000	1.000	1.000	1.000	1.000	1.000	1.000	1.000	1.000
.301	1.000	1.000	1.000	1.000	1.000	1.000	1.000	1.000	1.000	1.000
.304	.954	.949	.949	.954	.949	.897	.897	.949	.949	.897
.312	.791	.760	.760	.791	.760	.521	.521	.760	.760	.521
.319	.731	.691	.691	.731	.691	.388	.388	.691	.691	.388
.326	.791	.760	.760	.791	.760	.521	.521	.760	.760	.521
.333	.954	.949	.949	.954	.949	.897	.897	.949	.949	.897
.335	1.000	1.000	1.000	1.000	1.000	1.000	1.000	1.000	1.000	1.000
1.000	1.000	1.000	1.000	1.000	1.000	1.000	1.000	1.000	1.000	1.000

X/L	AREA VARIATION FACTORS FOR SUBCHANNEL (I)					
	(18)	(19)	(21)	(22)	(23)	(24)
0.000	1.000	1.000	1.000	1.000	1.000	1.000
.301	1.000	1.000	1.000	1.000	1.000	1.000
.304	.897	.949	.954	.949	.949	.954
.312	.521	.760	.791	.760	.760	.791
.319	.388	.691	.731	.691	.691	.731
.326	.521	.760	.791	.760	.760	.791
.333	.897	.949	.954	.949	.949	.954
.335	1.000	1.000	1.000	1.000	1.000	1.000
1.000	1.000	1.000	1.000	1.000	1.000	1.000

X/L	GAP SPACING VARIATION FACTORS FOR ADJACENT SUBCHANNELS (I,J)											
	(5, 6)	(5,10)	(6, 7)	(6,11)	(7, 8)	(7,12)	(8,13)	(10,11)	(10,16)	(11,12)	(11,17)	(12,13)
0.000	1.000	1.000	1.000	1.000	1.000	1.000	1.000	1.000	1.000	1.000	1.000	1.000
.301	1.000	1.000	1.000	1.000	1.000	1.000	1.000	1.000	1.000	1.000	1.000	1.000
.304	.902	.902	.902	.802	.902	.802	.902	.802	.902	.802	.802	.802
.312	.598	.598	.598	.197	.598	.197	.598	.197	.598	.197	.197	.197
.319	.500	.500	.500	0.000	.500	0.000	.500	0.000	.500	0.000	0.000	0.000
.326	.598	.598	.598	.197	.598	.197	.598	.197	.598	.197	.197	.197
.333	.902	.902	.902	.802	.902	.802	.902	.802	.902	.802	.802	.802
.336	1.000	1.000	1.000	1.000	1.000	1.000	1.000	1.000	1.000	1.000	1.000	1.000
1.000	1.000	1.000	1.000	1.000	1.000	1.000	1.000	1.000	1.000	1.000	1.000	1.000

X/L	GAP SPACING VARIATION FACTORS FOR ADJACENT SUBCHANNELS (I,J)											
	(12,18)	(13,19)	(16,17)	(16,21)	17,18)	(17,22)	(18,19)	(18,23)	(19,24)	(21,22)	(22,23)	(23,24)
0.000	1.000	1.000	1.000	1.000	1.000	1.000	1.000	1.000	1.000	1.000	1.000	1.000
.301	1.000	1.000	1.000	1.000	1.000	1.000	1.000	1.000	1.000	1.000	1.000	1.000
.304	.802	.902	.802	.902	.802	.802	.802	.802	.902	.902	.902	.902
.312	.197	.598	.197	.598	.197	.197	.197	.197	.598	.598	.598	.598
.319	0.000	.500	0.000	.500	0.000	0.000	0.000	0.000	.500	.500	.500	.500
.326	.197	.598	.197	.598	.197	.197	.197	.197	.598	.598	.598	.598
.333	.802	.902	.802	.902	.802	.802	.802	.802	.902	.902	.902	.902
.335	1.000	1.000	1.000	1.000	1.000	1.000	1.000	1.000	1.000	1.000	1.000	1.000
1.000	1.000	1.000	1.000	1.000	1.000	1.000	1.000	1.000	1.000	1.000	1.000	1.000

TABLE A-3

AREA AND GAP VARIATIONS OF CONFIGURATION C

X/L	AREA VARIATION FACTORS FOR SUBCHANNEL (I)									
	(1)	(2)	(3)	(4)	(5)	(6)	(7)	(8)	(9)	(10)
0.000	1.000	1.000	1.000	1.000	1.000	1.000	1.000	1.000	1.000	1.000
.301	1.000	1.000	1.000	1.000	1.000	1.000	1.000	1.000	1.000	1.000
.304	.873	.908	.908	.873	.859	.897	.897	.859	.908	.897
.312	.873	.708	.708	.873	.665	.521	.521	.665	.708	.521
.319	.873	.624	.624	.873	.585	.388	.388	.585	.624	.388
.326	.873	.708	.708	.873	.665	.521	.521	.665	.708	.521
.333	.873	.908	.908	.873	.859	.897	.897	.859	.908	.897
.336	1.000	1.000	1.000	1.000	1.000	1.000	1.000	1.000	1.000	1.000
1.000	1.000	1.000	1.000	1.000	1.000	1.000	1.000	1.000	1.000	1.000

X/L	AREA VARIATION FACTORS FOR SUBCHANNEL (I)									
	(11)	(12)	(13)	(14)	(15)	(16)	(17)	(18)	(19)	(20)
0.000	1.000	1.000	1.000	1.000	1.000	1.000	1.000	1.000	1.000	1.000
.301	1.000	1.000	1.000	1.000	1.000	1.000	1.000	1.000	1.000	1.000
.304	.897	.897	.897	.908	.908	.897	.897	.897	.897	.908
.312	.521	.521	.521	.708	.708	.521	.521	.521	.521	.708
.319	.388	.388	.388	.624	.624	.388	.388	.388	.388	.624
.326	.521	.521	.521	.708	.708	.521	.521	.521	.521	.708
.333	.897	.897	.897	.908	.908	.897	.897	.897	.897	.908
.336	1.000	1.000	1.000	1.000	1.000	1.000	1.000	1.000	1.000	1.000
1.000	1.000	1.000	1.000	1.000	1.000	1.000	1.000	1.000	1.000	1.000

X/L	AREA VARIATION FACTORS FOR SUBCHANNEL (I)							
	(21)	(22)	(23)	(24)	(25)	(26)	(27)	(28)
0.000	1.000	1.000	1.000	1.000	1.000	1.000	1.000	1.000
.301	1.000	1.000	1.000	1.000	1.000	1.000	1.000	1.000
.304	.859	.897	.897	.859	.873	.908	.908	.873
.312	.665	.521	.521	.665	.873	.708	.708	.873
.319	.585	.388	.388	.585	.873	.624	.624	.873
.326	.665	.521	.521	.665	.873	.708	.708	.873
.333	.859	.897	.897	.859	.873	.908	.908	.873
.336	1.000	1.000	1.000	1.000	1.000	1.000	1.000	1.000
1.000	1.000	1.000	1.000	1.000	1.000	1.000	1.000	1.000

X/L	GAP SPACING VARIATION FACTORS FOR ADJACENT SUBCHANNELS (I,J)									
	(1, 2)	(1, 5)	(1, 9)	(2, 3)	(2, 6)	(3, 4)	(3, 7)	(4, 8)	(4,14)	(5, 6)
0.000	1.000	1.000	1.000	1.000	1.000	1.000	1.000	1.000	1.000	1.000
.301	1.000	1.000	1.000	1.000	1.000	1.000	1.000	1.000	1.000	1.000
.304	.780	0.000	.780	.932	.802	.780	.802	0.000	.780	.802
.312	.780	0.000	.780	.724	.197	.780	.197	0.000	.780	.197
.319	.780	0.000	.780	.653	0.000	.780	0.000	0.000	.780	0.000
.326	.780	0.000	.780	.724	.197	.780	.197	0.000	.780	.197
.333	.780	0.000	.780	.932	.802	.780	.802	0.000	.780	.802
.336	1.000	1.000	1.000	1.000	1.000	1.000	1.000	1.000	1.000	1.000
1.000	1.000	1.000	1.000	1.000	1.000	1.000	1.000	1.000	1.000	1.000

TABLE A-3 (cont)

AREA AND GAP VARIATIONS OF CONFIGURATION C

GAP SPACING VARIATION FACTORS FOR ADJACENT SUBCHANNELS (I,J)

X/L	(5,10)	(6,7)	(6,11)	(7,8)	(7,12)	(8,13)	(9,10)	(9,14)	(10,11)	(10,15)
0.000	1.000	1.000	1.000	1.000	1.000	1.000	1.000	1.000	1.000	1.000
.301	1.000	1.000	1.000	1.000	1.000	1.000	1.000	1.000	1.000	1.000
.305	.802	.802	.802	.802	.802	.802	.802	.932	.802	.802
.312	.197	.197	.197	.197	.197	.197	.197	.724	.197	.197
.319	0.000	0.000	0.000	0.000	0.000	0.000	0.000	.653	0.000	0.000
.325	.197	.197	.197	.197	.197	.197	.197	.724	.197	.197
.333	.802	.802	.802	.802	.802	.802	.802	.932	.802	.802
.335	1.000	1.000	1.000	1.000	1.000	1.000	1.000	1.000	1.000	1.000
1.000	1.000	1.000	1.000	1.000	1.000	1.000	1.000	1.000	1.000	1.000

X/L	(11,12)	(11,17)	(12,13)	(12,18)	(13,14)	(13,19)	(14,20)	(15,16)	(15,25)	(16,17)
0.000	1.000	1.000	1.000	1.000	1.000	1.000	1.000	1.000	1.000	1.000
.301	1.000	1.000	1.000	1.000	1.000	1.000	1.000	1.000	1.000	1.000
.305	.802	.802	.802	.802	.802	.802	.932	.802	.700	.802
.312	.197	.197	.197	.197	.197	.197	.724	.197	.700	.197
.319	0.000	0.000	0.000	0.000	0.000	0.000	.653	0.000	.700	0.000
.325	.197	.197	.197	.197	.197	.197	.724	.197	.700	.197
.333	.802	.802	.802	.802	.802	.802	.932	.802	.700	.802
.335	1.000	1.000	1.000	1.000	1.000	1.000	1.000	1.000	1.000	1.000
1.000	1.000	1.000	1.000	1.000	1.000	1.000	1.000	1.000	1.000	1.000

X/L	(16,21)	(17,18)	(17,22)	(18,19)	(18,23)	(19,20)	(19,24)	(20,[illegible])	(21,22)	(21,25)
0.000	1.000	1.000	1.000	1.000	1.000	1.000	1.000	1.000	1.000	1.000
.301	1.000	1.000	1.000	1.000	1.000	1.000	1.000	1.000	1.000	1.000
.305	.802	.802	.802	.802	.802	.802	.802	.700	.802	0.000
.312	.197	.197	.197	.197	.197	.197	.197	.700	.197	0.000
.319	0.000	0.000	0.000	0.000	0.000	0.000	0.000	.700	0.000	0.000
.325	.197	.197	.197	.197	.197	.197	.197	.700	.197	0.000
.333	.802	.802	.802	.802	.802	.802	.802	.700	.802	0.000
.335	1.000	1.000	1.000	1.000	1.000	1.000	1.000	1.000	1.000	1.000
1.000	1.000	1.000	1.000	1.000	1.000	1.000	1.000	1.000	1.000	1.000

X/L	(22,23)	(22,2[illegible])	(23,24)	(23,27)	(24,2[illegible])	(25,2[illegible])	(26,2[illegible])	(27,[illegible])
0.000	1.000	1.000	1.000	1.000	1.000	1.000	1.000	1.000
[illegible]	1.000	1.000	1.000	1.000	1.000	1.000	1.000	1.000
[illegible]	.802	.802	.802	.802	[illegible]	[illegible]	[illegible]	[illegible]
.312	.197	.197	.197	.197	[illegible]	[illegible]	[illegible]	[illegible]
.319	0.000	0.000	0.000	0.000	[illegible]	[illegible]	[illegible]	[illegible]
[illegible]	.197	.197	.197	.197	[illegible]	[illegible]	[illegible]	[illegible]
[illegible]	.802	.802	.802	.802	[illegible]	[illegible]	[illegible]	[illegible]
[illegible]	1.000	1.000	1.000	1.000	1.000	1.000	1.000	1.000
1.000	1.000	1.000	1.000	1.000	1.000	1.000	1.000	1.000

TABLE A-4

AREA AND GAP VARIATIONS OF CONFIGURATION D

X/L	AREA VARIATION FACTORS FOR SUBCHANNEL (I)									
	(1)	(2)	(3)	(4)	(5)	(6)	(7)	(8)	(9)	(10)
0.000	1.000	1.000	1.000	1.000	1.000	1.000	1.000	1.000	1.000	1.000
.232	1.000	1.000	1.000	1.000	1.000	1.000	1.000	1.000	1.000	1.000
.238	1.000	1.000	1.000	1.000	1.000	1.000	1.000	1.000	1.000	1.000
.243	1.000	1.000	1.000	1.000	1.000	1.000	1.000	1.000	1.000	1.000
.249	.937	.856	1.000	1.000	.881	.926	1.000	1.000	1.000	1.000
.255	.937	.791	1.000	1.000	.819	.870	1.000	1.000	1.000	1.000
.261	.937	.764	1.000	1.000	.794	.847	.973	.954	1.000	1.000
.267	.937	.791	1.000	1.000	.794	.870	.894	.814	1.000	1.000
.272	.937	.856	1.000	1.000	.881	.926	.853	.744	1.000	1.000
.278	1.000	1.000	.856	.937	1.000	1.000	.779	.625	1.000	1.000
.284	1.000	1.000	.791	.937	1.000	1.000	.764	.633	1.000	1.000
.290	1.000	1.000	.764	.873	1.000	1.000	.820	.681	1.000	1.000
.296	1.000	1.000	.791	.873	1.000	1.000	.870	.664	1.000	1.000
.301	1.000	1.000	.856	.873	1.000	1.000	.926	.682	1.000	1.000
.307	1.000	.856	.856	.937	.872	.853	.926	.801	.770	.779
.313	1.000	.791	.791	.937	.773	.740	.870	.845	.639	.610
.319	.937	.764	.764	.937	.666	.694	.847	.933	.555	.515
.325	.937	.791	.791	1.000	.618	.740	.870	1.000	.515	.503
.330	.937	.856	.856	1.000	.672	.853	.926	1.000	.599	.632
.336	.937	1.000	1.000	1.000	.801	.926	.926	1.000	.771	.853
.342	.937	1.000	1.000	1.000	.845	.870	.870	1.000	.818	.894
.348	.937	1.000	1.000	1.000	.933	.847	.847	1.000	.911	.973
.354	.937	1.000	1.000	1.000	1.000	.870	.870	1.000	1.000	1.000
.359	1.000	1.000	1.000	1.000	1.000	.926	.926	1.000	1.000	1.000
.365	1.000	1.000	1.000	1.000	1.000	1.000	1.000	1.000	1.000	1.000
.371	1.000	1.000	1.000	1.000	1.000	1.000	1.000	1.000	1.000	1.000
.377	1.000	1.000	1.000	1.000	1.000	1.000	1.000	1.000	1.000	1.000
.383	1.000	1.000	1.000	1.000	1.000	1.000	1.000	1.000	1.000	1.000
1.000	1.000	1.000	1.000	1.000	1.000	1.000	1.000	1.000	1.000	1.000

X/L	AREA VARIATION FACTORS FOR SUBCHANNEL (I)									
	(11)	(12)	(13)	(14)	(15)	(16)	(17)	(18)	(19)	(20)
0.000	1.000	1.000	1.000	1.000	1.000	1.000	1.000	1.000	1.000	1.000
.232	1.000	1.000	1.000	1.000	1.000	1.000	1.000	1.000	1.000	1.000
.238	1.000	1.000	1.000	1.000	1.000	1.000	1.000	1.000	1.000	1.000
.243	1.000	1.000	1.000	1.000	1.000	1.000	1.000	1.000	1.000	1.000
.249	1.000	1.000	1.000	1.000	1.000	1.000	1.000	1.000	1.000	1.000
.255	1.000	1.000	1.000	1.000	1.000	1.000	1.000	1.000	1.000	1.000
.261	1.000	.973	.973	1.000	1.000	1.000	1.000	.973	.973	1.000
.267	1.000	.894	.894	1.000	1.000	1.000	1.000	.894	.894	1.000
.272	1.000	.853	.853	1.000	1.000	1.000	1.000	.853	.853	1.000
.278	1.000	.853	.853	1.000	1.000	1.000	1.000	.853	.853	1.000
.284	1.000	.894	.894	1.000	1.000	1.000	1.000	.894	.894	1.000
.290	1.000	.973	.947	.911	.911	.947	.973	.973	.973	1.000
.296	1.000	1.000	.894	.818	.818	.788	.894	1.000	1.000	1.000
.301	1.000	1.000	.853	.771	.771	.706	.853	1.000	1.000	1.000
.307	.853	1.000	.853	.771	.686	.559	.779	1.000	1.000	1.000
.313	.740	1.000	.894	.818	.667	.527	.764	1.000	1.000	1.000
.319	.694	1.000	.947	.880	.733	.641	.794	.973	.947	.973
.325	.740	1.000	.894	.818	.791	.740	.764	.894	.773	.894
.330	.853	1.000	.853	.771	.856	.853	.779	.853	.706	.600
.336	.853	.779	.779	.771	1.000	1.000	.779	.706	.633	.600
.342	.740	.610	.764	.818	1.000	1.000	.764	.634	.657	.695
.348	.694	.541	.820	.911	1.000	1.000	.820	.668	.794	.880
.354	.740	.610	.870	1.000	1.000	1.000	.870	.740	.870	1.000
.359	.853	.779	.926	1.000	1.000	1.000	.926	.853	.926	1.000
.365	1.000	1.000	1.000	1.000	1.000	1.000	1.000	1.000	1.000	1.000
.371	1.000	1.000	1.000	1.000	1.000	1.000	1.000	1.000	1.000	1.000
.377	1.000	1.000	1.000	1.000	1.000	1.000	1.000	1.000	1.000	1.000
.383	1.000	1.000	1.000	1.000	1.000	1.000	1.000	1.000	1.000	1.000
1.000	1.000	1.000	1.000	1.000	1.000	1.000	1.000	1.000	1.000	1.000

TABLE A-4 (cont)

AREA AND GAP VARIATIONS OF CONFIGURATION D

X/L	AREA VARIATION FACTORS FOR SUBCHANNEL (I)							
	(21)	(22)	(23)	(24)	(25)	(26)	(27)	(28)
0.000	1.000	1.000	1.000	1.000	1.000	1.000	1.000	1.000
.232	1.000	1.000	1.000	1.000	1.000	1.000	1.000	1.000
.238	1.000	1.000	1.000	1.000	1.000	1.000	1.000	1.000
.243	1.000	1.000	1.000	1.000	1.000	1.000	1.000	1.000
.249	1.000	1.000	1.000	1.000	1.000	1.000	1.000	1.000
.255	1.000	1.000	1.000	1.000	1.000	1.000	1.000	1.000
.261	1.000	1.000	.973	.954	1.000	1.000	1.000	1.000
.267	1.000	1.000	.894	.814	1.000	1.000	1.000	1.000
.272	1.000	1.000	.853	.744	1.000	1.000	1.000	1.000
.278	1.000	.926	.706	.625	1.000	.856	.770	.937
.284	1.000	.870	.634	.633	1.000	.791	.639	.937
.290	.886	.820	.668	.748	.937	.764	.586	.937
.296	.660	.764	.740	.819	.937	.791	.639	.937
.301	.544	.779	.853	.881	.937	.856	.770	.937
.307	.425	.779	1.000	1.000	.873	.856	1.000	1.000
.313	.479	.764	1.000	1.000	.873	.791	1.000	1.000
.319	.680	.794	.973	.901	.873	.764	1.000	.937
.325	.819	.764	.894	.845	.937	.791	1.000	.937
.330	.881	.779	.853	.801	.937	.856	1.000	.937
.336	1.000	.853	.853	.801	1.000	1.000	1.000	.937
.342	1.000	.894	.894	.845	1.000	1.000	1.000	.937
.348	1.000	.973	.973	.901	1.000	1.000	1.000	.937
.354	1.000	1.000	1.000	1.000	1.000	1.000	1.000	1.000
.359	1.000	1.000	1.000	1.000	1.000	1.000	1.000	1.000
.365	1.000	1.000	1.000	1.000	1.000	1.000	1.000	1.000
.371	1.000	1.000	1.000	1.000	1.000	1.000	1.000	1.000
.377	1.000	1.000	1.000	1.000	1.000	1.000	1.000	1.000
.383	1.000	1.000	1.000	1.000	1.000	1.000	1.000	1.000
1.000	1.000	1.000	1.000	1.000	1.000	1.000	1.000	1.000

X/L	GAP SPACING VARIATION FACTORS FOR ADJACENT SUBCHANNELS (I,J)									
	(1, 2)	(1, 5)	(1, 9)	(2, 3)	(2, 6)	(3, 4)	(3, 7)	(4, 8)	(4,14)	(5, 6)
0.000	1.000	1.000	1.000	1.000	1.000	1.000	1.000	1.000	1.000	1.000
.232	1.000	1.000	1.000	1.000	1.000	1.000	1.000	1.000	1.000	1.000
.238	1.000	1.000	1.000	1.000	1.000	1.000	1.000	1.000	1.000	1.000
.243	1.000	1.000	1.000	1.000	1.000	1.000	1.000	1.000	1.000	1.000
.249	.050	.050	1.000	1.000	.742	1.000	1.000	1.000	1.000	.742
.255	.050	.050	1.000	1.000	.567	1.000	1.000	1.000	1.000	.567
.261	.050	.050	1.000	1.000	.500	1.000	1.000	1.000	1.000	.500
.267	.050	.050	1.000	1.000	.567	1.000	1.000	1.000	1.000	.567
.272	.050	.050	1.000	1.000	.742	1.000	1.000	1.000	1.000	.742
.278	1.000	1.000	1.000	1.000	1.000	.050	.742	.050	1.000	1.000
.284	1.000	1.000	1.000	1.000	1.000	.050	.567	.050	1.000	1.000
.290	1.000	1.000	1.000	1.000	1.000	.050	.500	0.000	.050	1.000
.296	1.000	1.000	1.000	1.000	1.000	.050	.567	0.000	.050	1.000
.301	1.000	1.000	1.000	1.000	1.000	.050	.742	0.000	.050	1.000
.307	1.000	1.000	1.000	.821	.742	1.000	.742	.050	.050	.742
.313	1.000	1.000	1.000	.699	.567	1.000	.567	.050	.050	.567
.319	1.000	.050	.050	.653	.500	1.000	.500	.050	.050	.500
.325	1.000	.050	.050	.699	.567	1.000	.567	1.000	1.000	.567
.330	1.000	.050	.050	.821	.742	1.000	.742	1.000	1.000	.742
.336	1.000	.050	.050	1.000	1.000	1.000	1.000	1.000	1.000	1.000
.342	1.000	.050	.050	1.000	1.000	1.000	1.000	1.000	1.000	1.000
.348	1.000	.050	.050	1.000	1.000	1.000	1.000	1.000	1.000	1.000
.354	1.000	1.000	1.000	1.000	1.000	1.000	1.000	1.000	1.000	1.000
.359	1.000	1.000	1.000	1.000	1.000	1.000	1.000	1.000	1.000	1.000
.365	1.000	1.000	1.000	1.000	1.000	1.000	1.000	1.000	1.000	1.000
.371	1.000	1.000	1.000	1.000	1.000	1.000	1.000	1.000	1.000	1.000
.377	1.000	1.000	1.000	1.000	1.000	1.000	1.000	1.000	1.000	1.000
.383	1.000	1.000	1.000	1.000	1.000	1.000	1.000	1.000	1.000	1.000
1.000	1.000	1.000	1.000	1.000	1.000	1.000	1.000	1.000	1.000	1.000

TABLE A-4 (cont)

AREA AND GAP VARIATIONS OF CONFIGURATION D

X/L	GAP SPACING VARIATION FACTORS FOR ADJACENT SUBCHANNELS (I,J)									
	(5,10)	(6, 7)	(6,11)	(7, 8)	(7,12)	(8,13)	(9,10)	(9,15)	(10,11)	(10,16)
0.000	1.000	1.000	1.000	1.000	1.000	1.000	1.000	1.000	1.000	1.000
.232	1.000	1.000	1.000	1.000	1.000	1.000	1.000	1.000	1.000	1.000
.238	1.000	1.000	1.000	1.000	1.000	1.000	1.000	1.000	1.000	1.000
.243	1.000	1.000	1.000	1.000	1.000	1.000	1.000	1.000	1.000	1.000
.249	1.000	1.000	1.000	1.000	1.000	1.000	1.000	1.000	1.000	1.000
.255	1.000	1.000	1.000	1.000	1.000	1.000	1.000	1.000	1.000	1.000
.261	1.000	1.000	1.000	.902	.902	.902	1.000	1.000	1.000	1.000
.267	1.000	1.000	1.000	.639	.639	.639	1.000	1.000	1.000	1.000
.272	1.000	1.000	1.000	.518	.518	.518	1.000	1.000	1.000	1.000
.278	1.000	1.000	1.000	.260	.518	.518	1.000	1.000	1.000	1.000
.284	1.000	1.000	1.000	.206	.639	.639	1.000	1.000	1.000	1.000
.290	1.000	1.000	1.000	.403	.902	.804	1.000	1.000	1.000	1.000
.296	1.000	1.000	1.000	.567	1.000	.639	1.000	1.000	1.000	1.000
.301	1.000	1.000	1.000	.742	1.000	.518	1.000	1.000	1.000	1.000
.307	.742	.742	.742	1.000	1.000	.518	.742	.821	.484	.484
.313	.567	.567	.567	1.000	1.000	.639	.567	.699	.134	.134
.319	.403	.500	.500	1.000	1.000	.902	.403	.653	.001	.001
.325	.206	.567	.567	1.000	1.000	1.000	.206	.699	.134	.134
.330	.260	.742	.742	1.000	1.000	1.000	.260	.821	.484	.484
.336	.518	.742	.742	1.000	.742	1.000	.518	1.000	1.000	1.000
.342	.639	.567	.567	1.000	.567	1.000	.639	1.000	1.000	1.000
.348	.902	.500	.500	1.000	.500	1.000	.902	1.000	1.000	1.000
.354	1.000	.567	.567	1.000	.567	1.000	1.000	1.000	1.000	1.000
.359	1.000	.742	.742	1.000	.742	1.000	1.000	1.000	1.000	1.000
.365	1.000	1.000	1.000	1.000	1.000	1.000	1.000	1.000	1.000	1.000
.371	1.000	1.000	1.000	1.000	1.000	1.000	1.000	1.000	1.000	1.000
.377	1.000	1.000	1.000	1.000	1.000	1.000	1.000	1.000	1.000	1.000
.383	1.000	1.000	1.000	1.000	1.000	1.000	1.000	1.000	1.000	1.000
1.000	1.000	1.000	1.000	1.000	1.000	1.000	1.000	1.000	1.000	1.000

X/L	GAP SPACING VARIATION FACTORS FOR ADJACENT SUBCHANNELS (I,J)									
	(11,12)	(11,17)	(12,13)	(12,18)	(13,14)	(13,19)	(14,20)	(15,16)	(15,25)	(16,17)
0.000	1.000	1.000	1.000	1.000	1.000	1.000	1.000	1.000	1.000	1.000
.232	1.000	1.000	1.000	1.000	1.000	1.000	1.000	1.000	1.000	1.000
.238	1.000	1.000	1.000	1.000	1.000	1.000	1.000	1.000	1.000	1.000
.243	1.000	1.000	1.000	1.000	1.000	1.000	1.000	1.000	1.000	1.000
.249	1.000	1.000	1.000	1.000	1.000	1.000	1.000	1.000	1.000	1.000
.255	1.000	1.000	1.000	1.000	1.000	1.000	1.000	1.000	1.000	1.000
.261	1.000	1.000	.902	1.000	1.000	1.000	1.000	1.000	1.000	1.000
.267	1.000	1.000	.639	1.000	1.000	1.000	1.000	1.000	1.000	1.000
.272	1.000	1.000	.518	1.000	1.000	1.000	1.000	1.000	1.000	1.000
.278	1.000	1.000	.518	1.000	1.000	1.000	1.000	1.000	1.000	1.000
.284	1.000	1.000	.639	1.000	1.000	1.000	1.000	1.000	1.000	1.000
.290	1.000	1.000	.902	1.000	.902	1.000	1.000	.902	.050	.902
.296	1.000	1.000	1.000	1.000	.639	1.000	1.000	.639	.050	.639
.301	1.000	1.000	1.000	1.000	.518	1.000	1.000	.518	.050	.518
.307	1.000	.742	1.000	1.000	.518	1.000	1.000	.260	.050	.260
.313	1.000	.567	1.000	1.000	.639	1.000	1.000	.206	.050	.206
.319	1.000	.500	1.000	1.000	.804	.902	.932	.403	.050	.403
.325	1.000	.567	1.000	1.000	.639	.639	.750	.567	1.000	.567
.330	1.000	.742	1.000	1.000	.518	.518	.666	.742	1.000	.742
.336	.484	.742	.742	.484	.518	.260	.666	1.000	1.000	1.000
.342	.134	.567	.567	.134	.639	.206	.750	1.000	1.000	1.000
.348	.001	.500	.500	.001	.902	.403	.932	1.000	1.000	1.000
.354	.134	.567	.567	.134	1.000	.567	1.000	1.000	1.000	1.000
.359	.484	.742	.742	.484	1.000	.742	1.000	1.000	1.000	1.000
.365	1.000	1.000	1.000	1.000	1.000	1.000	1.000	1.000	1.000	1.000
.371	1.000	1.000	1.000	1.000	1.000	1.000	1.000	1.000	1.000	1.000
.377	1.000	1.000	1.000	1.000	1.000	1.000	1.000	1.000	1.000	1.000
.383	1.000	1.000	1.000	1.000	1.000	1.000	1.000	1.000	1.000	1.000
1.000	1.000	1.000	1.000	1.000	1.000	1.000	1.000	1.000	1.000	1.000

TABLE A-4 (cont)

AREA AND GAP VARIATIONS OF CONFIGURATION D

X/L	GAP SPACING VARIATION FACTORS FOR ADJACENT SUBCHANNELS (I,J)									
	(16,21)	(17,18)	(17,22)	(18,19)	(18,23)	(19,20)	(19,24)	(20,28)	(21,22)	(21,25)
0.000	1.000	1.000	1.000	1.000	1.000	1.000	1.000	1.000	1.000	1.000
.232	1.000	1.000	1.000	1.000	1.000	1.000	1.000	1.000	1.000	1.000
.238	1.000	1.000	1.000	1.000	1.000	1.000	1.000	1.000	1.000	1.000
.243	1.000	1.000	1.000	1.000	1.000	1.000	1.000	1.000	1.000	1.000
.249	1.000	1.000	1.000	1.000	1.000	1.000	1.000	1.000	1.000	1.000
.255	1.000	1.000	1.000	1.000	1.000	1.000	1.000	1.000	1.000	1.000
.261	1.000	1.000	1.000	.902	.902	1.000	.902	1.000	1.000	1.000
.267	1.000	1.000	1.000	.639	.639	1.000	.639	1.000	1.000	1.000
.272	1.000	1.000	1.000	.518	.518	1.000	.518	1.000	1.000	1.000
.278	1.000	1.000	1.000	.518	.518	1.000	.518	1.000	1.000	1.000
.284	1.000	1.000	1.000	.639	.639	1.000	.639	1.000	1.000	1.000
.290	.804	1.000	.902	.902	.902	1.000	.902	1.000	.902	.050
.296	.278	1.000	.639	1.000	1.000	1.000	1.000	1.000	.639	.050
.301	.035	1.000	.518	1.000	1.000	1.000	1.000	1.000	.518	.050
.307	.035	1.000	.518	1.000	1.000	1.000	1.000	1.000	.260	0.000
.313	.278	1.000	.639	1.000	1.000	1.000	1.000	1.000	.206	0.000
.319	.804	.902	.804	1.000	.902	.804	.902	.050	.403	0.000
.325	1.000	.639	.639	1.000	.639	.278	.639	.050	.567	.050
.330	1.000	.518	.518	1.000	.518	.035	.518	.050	.742	.050
.336	1.000	.260	.518	.742	.518	.035	.518	.050	1.000	1.000
.342	1.000	.206	.639	.567	.639	.278	.639	.050	1.000	1.000
.348	1.000	.403	.902	.500	.902	.804	.902	.050	1.000	1.000
.354	1.000	.567	1.000	.567	1.000	1.000	1.000	1.000	1.000	1.000
.359	1.000	.742	1.000	.742	1.000	1.000	1.000	1.000	1.000	1.000
.365	1.000	1.000	1.000	1.000	1.000	1.000	1.000	1.000	1.000	1.000
.371	1.000	1.000	1.000	1.000	1.000	1.000	1.000	1.000	1.000	1.000
.377	1.000	1.000	1.000	1.000	1.000	1.000	1.000	1.000	1.000	1.000
.383	1.000	1.000	1.000	1.000	1.000	1.000	1.000	1.000	1.000	1.000
1.000	1.000	1.000	1.000	1.000	1.000	1.000	1.000	1.000	1.000	1.000

X/L	GAP SPACING VARIATION FACTORS FOR ADJACENT SUBCHANNELS (I,J)							
	(22,23)	(22,26)	(23,24)	(23,27)	(24,28)	(25,26)	(26,27)	(27,28)
0.000	1.000	1.000	1.000	1.000	1.000	1.000	1.000	1.000
.232	1.000	1.000	1.000	1.000	1.000	1.000	1.000	1.000
.238	1.000	1.000	1.000	1.000	1.000	1.000	1.000	1.000
.243	1.000	1.000	1.000	1.000	1.000	1.000	1.000	1.000
.249	1.000	1.000	1.000	1.000	1.000	1.000	1.000	1.000
.255	1.000	1.000	1.000	1.000	1.000	1.000	1.000	1.000
.261	1.000	1.000	.902	1.000	1.000	1.000	1.000	1.000
.267	1.000	1.000	.639	1.000	1.000	1.000	1.000	1.000
.272	1.000	1.000	.518	1.000	1.000	1.000	1.000	1.000
.278	.742	.742	.260	.484	.050	1.000	.821	.050
.284	.567	.567	.206	.134	.050	1.000	.699	.050
.290	.500	.500	.403	.001	.050	1.000	.653	.050
.296	.567	.567	.567	.134	.050	1.000	.699	.050
.301	.742	.742	.742	.484	.050	1.000	.821	.050
.307	1.000	.742	1.000	1.000	1.000	.050	1.000	1.000
.313	1.000	.567	1.000	1.000	1.000	.050	1.000	1.000
.319	.902	.500	1.000	1.000	.050	.050	1.000	1.000
.325	.639	.567	1.000	1.000	.050	.050	1.000	1.000
.330	.518	.742	1.000	1.000	.050	.050	1.000	1.000
.336	.518	1.000	1.000	1.000	.050	1.000	1.000	1.000
.342	.639	1.000	1.000	1.000	.050	1.000	1.000	1.000
.348	.902	1.000	1.000	1.000	.050	1.000	1.000	1.000
.354	1.000	1.000	1.000	1.000	1.000	1.000	1.000	1.000
.359	1.000	1.000	1.000	1.000	1.000	1.000	1.000	1.000
.365	1.000	1.000	1.000	1.000	1.000	1.000	1.000	1.000
.371	1.000	1.000	1.000	1.000	1.000	1.000	1.000	1.000
.377	1.000	1.000	1.000	1.000	1.000	1.000	1.000	1.000
.383	1.000	1.000	1.000	1.000	1.000	1.000	1.000	1.000
1.000	1.000	1.000	1.000	1.000	1.000	1.000	1.000	1.000

TABLE A-5

AREA AND GAP VARIATIONS OF CONFIGURATION E

X/L	AREA VARIATION FACTORS FOR SUBCHANNEL (I)													
	(1)	(2)	(3)	(4)	(5)	(6)	(7)	(8)	(9)	(10)	(11)	(12)	(13)	(14)
0.000	1.000	1.000	1.000	1.000	1.000	1.000	1.000	1.000	1.000	1.000	1.000	1.000	1.000	1.000
.206	1.000	1.000	1.000	1.000	1.000	1.000	1.000	1.000	1.000	1.000	1.000	1.000	1.000	1.000
.212	.937	.928	1.000	1.000	.985	.988	1.000	1.000	1.000	1.000	1.000	1.000	1.000	1.000
.217	.937	.912	1.000	1.000	.933	.975	1.000	1.000	1.000	1.000	1.000	1.000	1.000	1.000
.223	.937	.896	1.000	1.000	.918	.960	.995	.992	1.000	1.000	1.000	.995	.995	1.000
.229	.937	.879	1.000	1.000	.902	.945	.982	.968	1.000	1.000	1.000	.982	.982	1.000
.235	.937	.853	1.000	1.000	.887	.931	.967	.944	1.000	1.000	1.000	.967	.967	1.000
.241	.937	.788	.928	.937	.878	.924	.941	.867	1.000	1.000	1.000	.953	.953	1.000
.246	.937	.717	.912	.937	.869	.916	.912	.825	1.000	1.000	1.000	.938	.938	1.000
.252	.937	.643	.896	.873	.860	.908	.888	.748	1.000	1.000	1.000	.896	.923	.937
.258	.937	.600	.879	.873	.851	.899	.865	.703	1.000	1.000	1.000	.838	.901	.921
.264	.937	.600	.853	.873	.851	.899	.843	.658	1.000	1.000	1.000	.772	.879	.904
.270	.937	.615	.775	.873	.840	.885	.816	.619	.915	.965	.977	.720	.856	.887
.275	.937	.657	.687	.873	.824	.865	.786	.580	.883	.924	.949	.700	.833	.869
.281	.873	.696	.597	.873	.765	.844	.771	.574	.844	.876	.920	.720	.826	.816
.287	.873	.726	.536	.873	.732	.822	.756	.570	.793	.817	.891	.772	.813	.732
.293	.873	.719	.511	.873	.709	.808	.750	.576	.744	.761	.855	.838	.799	.639
.299	.873	.718	.489	.873	.695	.796	.747	.589	.709	.723	.769	.862	.772	.562
.304	.873	.716	.492	.873	.679	.780	.744	.607	.673	.685	.671	.861	.745	.521
.310	.873	.714	.489	.873	.669	.764	.744	.635	.606	.650	.571	.833	.744	.496
.316	.937	.708	.511	.873	.698	.744	.744	.715	.520	.618	.496	.803	.744	.489
.322	.937	.708	.536	.873	.689	.730	.758	.755	.443	.610	.468	.768	.744	.489
.328	.937	.727	.597	.873	.695	.739	.787	.795	.402	.626	.498	.710	.750	.496
.333	.937	.745	.687	.873	.700	.747	.806	.827	.397	.642	.554	.638	.749	.521
.339	.937	.764	.775	.873	.723	.755	.820	.859	.439	.674	.607	.558	.764	.562
.345	.937	.782	.853	.937	.746	.762	.831	.926	.517	.706	.654	.505	.778	.639
.351	.937	.815	.879	.937	.779	.790	.845	.941	.627	.755	.690	.505	.801	.732
.357	.937	.849	.896	.937	.813	.828	.868	.957	.728	.808	.735	.558	.830	.816
.362	.937	.883	.912	1.000	.848	.865	.890	1.000	.810	.861	.780	.638	.853	.869
.368	.937	.915	.928	1.000	.890	.901	.912	1.000	.860	.918	.824	.715	.876	.887
.374	.937	1.000	1.000	1.000	.926	.931	.931	1.000	.904	.967	.863	.786	.899	.904
.380	.937	1.000	1.000	1.000	.941	.945	.945	1.000	.921	.982	.891	.836	.927	.921
.386	.937	1.000	1.000	1.000	.957	.960	.960	1.000	.937	.995	.920	.880	.955	.937
.391	11000	1.000	1.000	1.000	1.000	.975	.975	1.000	1.000	1.000	.949	.924	.975	1.000
.397	1.000	1.000	1.000	1.000	1.000	.988	.988	1.000	1.000	1.000	.977	.965	.988	1.000
.403	1.000	1.000	1.000	1.000	1.000	1.000	1.000	1.000	1.000	1.000	1.000	1.000	1.000	1.000
1.000	1.000	1.000	1.000	1.000	1.000	1.000	1.000	1.000	1.000	1.000	1.000	1.000	1.000	1.000

TABLE A-5 (cont)

AREA AND GAP VARIATIONS OF CONFIGURATION E

X/L	AREA VARIATION FACTORS FOR SUBCHANNEL (I)													
	(15)	(16)	(17)	(18)	(19)	(20)	(21)	(22)	(23)	(24)	(25)	(26)	(27)	(28)
0.000	1.000	1.000	1.000	1.000	1.000	1.000	1.000	1.000	1.000	1.000	1.000	1.000	1.000	1.000
.206	1.000	1.000	1.000	1.000	1.000	1.000	1.000	1.000	1.000	1.000	1.000	1.000	1.000	1.000
.212	1.000	1.000	1.000	1.000	1.000	1.000	1.000	1.000	1.000	1.000	1.000	1.000	1.000	1.000
.217	1.000	1.000	1.000	1.000	1.000	1.000	1.000	1.000	1.000	1.000	1.000	1.000	1.000	1.000
.223	1.000	1.000	1.000	.995	.995	1.000	1.000	1.000	.995	.992	1.000	1.000	1.000	1.000
.229	1.000	1.000	1.000	.982	.982	1.000	1.000	1.000	.982	.968	1.000	1.000	1.000	1.000
.235	1.000	1.000	1.000	.967	.967	1.000	1.000	1.000	.967	.944	1.000	1.000	1.000	1.000
.241	1.000	1.000	1.000	.953	.953	1.000	1.000	.988	.930	.867	1.000	.928	.915	.937
.246	1.000	1.000	1.000	.938	.938	1.000	1.000	.975	.887	.825	1.000	.912	.883	.937
.252	.937	.991	.995	.896	.927	1.000	.949	.955	.848	.791	.937	.896	.849	.937
.258	.921	.963	.982	.838	.920	1.000	.909	.927	.810	.762	.937	.879	.815	.937
.266	.904	.935	.967	.772	.912	1.000	.870	.899	.774	.733	.937	.853	.773	.937
.270	.874	.883	.941	.720	.904	1.000	.777	.865	.751	.710	.873	.775	.699	.937
.275	.840	.824	.912	.700	.895	1.000	.718	.828	.727	.687	.873	.687	.619	.937
.281	.775	.775	.852	.716	.894	.931	.673	.791	.714	.648	.873	.597	.535	.873
.287	.690	.730	.765	.754	.875	.899	.635	.746	.692	.639	.873	.536	.483	.873
.293	.588	.686	.663	.806	.854	.866	.597	.710	.686	.637	.873	.511	.483	.873
.299	.463	.654	.530	.826	.821	.832	.565	.687	.695	.643	.873	.489	.535	.873
.304	.368	.622	.419	.824	.788	.797	.533	.664	.707	.654	.873	.492	.619	.873
.310	.317	.622	.320	.801	.768	.737	.548	.662	.727	.678	.873	.489	.699	.873
.316	.335	.622	.262	.778	.752	.660	.562	.662	.750	.703	.873	.511	.773	.873
.322	.411	.638	.240	.748	.736	.574	.585	.676	.784	.734	.873	.556	.815	.873
.328	.522	.670	.228	.690	.726	.504	.616	.699	.819	.766	.873	.597	.849	.873
.333	.644	.707	.251	.618	.706	.471	.654	.723	.844	.781	.873	.687	.883	.873
.339	.733	.753	.284	.554	.715	.504	.705	.768	.881	.805	.873	.775	.915	.873
.345	.815	.797	.370	.517	.723	.574	.756	.810	.912	.865	.873	.853	1.000	.937
.351	.856	.854	.471	.525	.739	.660	.811	.846	.920	.874	.873	.879	1.000	.937
.357	.890	.911	.595	.578	.763	.737	.866	.883	.927	.882	.873	.896	1.000	.937
.362	.912	.949	.719	.660	.791	.797	.933	.912	.938	.893	.937	.912	1.000	.937
.368	.928	.977	.809	.744	.829	.832	.949	.941	.953	.910	.937	.928	1.000	.937
.374	1.000	1.000	.891	.822	.866	.866	1.000	.967	.967	.926	1.000	1.000	1.000	.937
.380	1.000	1.000	.927	.872	.908	.899	1.000	.982	.982	.941	1.000	1.000	1.000	.937
.386	1.000	1.000	.955	.916	.951	.931	1.000	.995	.995	.957	1.000	1.000	1.000	.937
.391	1.000	1.000	.975	.949	.975	1.000	1.000	1.000	1.000	1.000	1.000	1.000	1.000	1.000
.397	1.000	1.000	.988	.977	.988	1.000	1.000	1.000	1.000	1.000	1.000	1.000	1.000	1.000
.403	1.000	1.000	1.000	1.000	1.000	1.000	1.000	1.000	1.000	1.000	1.000	1.000	1.000	1.000
1.000	1.000	1.000	1.000	1.000	1.000	1.000	1.000	1.000	1.000	1.000	1.000	1.000	1.000	1.000

TABLE A-5 (cont)

AREA AND GAP VARIATIONS OF CONFIGURATION E

X/L	GAP SPACING VARIATION FACTORS FOR ADJACENT SUBCHANNELS (I,J)											
	(1, 2)	(1, 5)	(1, 9)	(2, 3)	(2, 6)	(3, 4)	(3, 7)	(4, 8)	(4,14)	(5, 6)	(5,10)	(6, 7
0.000	1.000	1.000	1.000	1.000	1.000	1.000	1.000	1.000	1.000	1.000	1.000	1.000
.206	1.000	1.000	1.000	1.000	1.000	1.000	1.000	1.000	1.000	1.000	1.000	1.000
.212	.050	.050	1.000	1.000	.957	1.000	1.000	1.000	1.000	.957	1.000	1.000
.217	.050	.050	1.000	1.000	.906	1.000	1.000	1.000	1.000	.906	1.000	1.000
.223	.050	.050	1.000	1.000	.855	1.000	1.000	1.000	1.000	.855	1.000	1.000
.229	.050	.050	1.000	1.000	.805	1.000	1.000	1.000	1.000	.805	1.000	1.000
.235	.050	.050	1.000	1.000	.758	1.000	1.000	1.000	1.000	.758	1.000	1.000
.241	.050	.050	1.000	1.000	.733	.050	.957	.050	1.000	.733	1.000	1.000
.246	.050	.050	1.000	1.000	.707	.050	.906	.050	1.000	.707	1.000	1.000
.252	.050	.050	1.000	1.000	.682	.050	.855	0.000	.050	.682	1.000	1.000
.258	.050	.050	1.000	1.000	.657	.050	.805	0.000	.050	.657	1.000	1.000
.264	.050	.050	1.000	1.000	.657	.050	.758	0.000	.050	.657	1.000	1.000
.270	.050	.050	1.000	.970	.639	.050	.690	0.000	.050	.639	.957	.957
.275	.050	.050	1.000	.935	.614	.050	.614	0.000	.050	.614	.906	.906
.281	.050	0.000	.050	.900	.588	.050	.537	0.000	.050	.588	.838	.855
.287	.050	0.000	.050	.865	.563	.050	.461	0.000	.050	.563	.736	.805
.293	.050	0.000	.050	.832	.563	.050	.415	0.000	.050	.563	.639	.758
.299	.050	0.000	.050	.815	.588	.050	.415	0.000	.050	.588	.563	.690
.304	.050	0.000	.050	.797	.614	.050	.415	0.000	.050	.614	.487	.614
.310	.050	0.000	.050	.780	.639	.050	.415	0.000	.050	.639	.428	.537
.316	1.000	.050	.050	.762	.657	.050	.415	0.000	.050	.657	.377	.461
.322	1.000	.050	.050	.762	.657	.050	.461	0.000	.050	.657	.351	.415
.328	1.000	.050	.050	.780	.682	.050	.537	0.000	.050	.682	.351	.415
.333	1.000	.050	.050	.797	.707	.050	.614	0.000	.050	.707	.351	.415
.339	1.000	.050	.050	.815	.733	.050	.690	0.000	.050	.733	.402	.415
.345	1.000	.050	.050	.832	.758	1.000	.758	.050	.050	.758	.453	.415
.351	1.000	.050	.050	.865	.805	1.000	.805	.050	.050	.805	.525	.461
.357	1.000	.050	.050	.900	.855	1.000	.855	.050	.050	.855	.601	.537
.362	1.000	.050	.050	.935	.906	1.000	.906	1.000	1.000	.906	.685	.614
.368	1.000	.050	.050	.970	.957	1.000	.957	1.000	1.000	.957	.787	.690
.374	1.000	.050	.050	1.000	1.000	1.000	1.000	1.000	1.000	1.000	.881	.758
.380	1.000	.050	.050	1.000	1.000	1.000	1.000	1.000	1.000	1.000	.931	.805
.386	1.000	.050	.050	1.000	1.000	1.000	1.000	1.000	1.000	1.000	.982	.855
.391	1.000	1.000	1.000	1.000	1.000	1.000	1.000	1.000	1.000	1.000	1.000	.906
.397	1.000	1.000	1.000	1.000	1.000	1.000	1.000	1.000	1.000	1.000	1.000	.957
.403	1.000	1.000	1.000	1.000	1.000	1.000	1.000	1.000	1.000	1.000	1.000	1.000
1.000	1.000	1.000	1.000	1.000	1.000	1.000	1.000	1.000	1.000	1.000	1.000	1.000

TABLE A-5 (cont)

AREA AND GAP VARIATIONS OF CONFIGURATION E

X/L	GAP SPACING VARIATION FACTORS FOR ADJACENT SUBCHANNELS (I,J)											
	(6,11)	(7, 8)	(7,12)	(8,13)	(9,10)	(9,15)	(10,11)	(10,16)	(11,12)	(11,17)	(12,13)	(12,18)
0.000	1.000	1.000	1.000	1.000	1.000	1.000	1.000	1.000	1.000	1.000	1.000	1.000
.206	1.000	1.000	1.000	1.000	1.000	1.000	1.000	1.000	1.000	1.000	1.000	1.000
.212	1.000	1.000	1.000	1.000	1.000	1.000	1.000	1.000	1.000	1.000	1.000	1.000
.217	1.000	1.000	1.000	1.000	1.000	1.000	1.000	1.000	1.000	1.000	1.000	1.000
.223	1.000	.982	.982	.982	1.000	1.000	1.000	1.000	1.000	1.000	.982	1.000
.229	1.000	.931	.931	.931	1.000	1.000	1.000	1.000	1.000	1.000	.931	1.000
.235	1.000	.881	.881	.881	1.000	1.000	1.000	1.000	1.000	1.000	.881	1.000
.241	1.000	.787	.830	.830	1.000	1.000	1.000	1.000	1.000	1.000	.830	1.000
.246	1.000	.685	.779	.779	1.000	1.000	1.000	1.000	1.000	1.000	.779	1.000
.252	1.000	.601	.746	.728	1.000	1.000	1.000	1.000	1.000	1.000	.746	1.000
.258	1.000	.525	.720	.652	1.000	1.000	1.000	1.000	1.000	1.000	.720	1.000
.264	1.000	.453	.695	.575	1.000	1.000	1.000	1.000	1.000	1.000	.695	1.000
.270	.957	.402	.669	.499	.957	.970	.914	.914	1.000	.957	.669	1.000
.275	.906	.351	.644	.423	.906	.935	.812	.812	1.000	.906	.644	1.000
.281	.855	.351	.669	.415	.838	.900	.711	.711	1.000	.855	.669	1.000
.287	.805	.351	.695	.415	.736	.865	.609	.609	1.000	.805	.695	1.000
.293	.758	.377	.720	.415	.639	.832	.517	.517	1.000	.758	.720	1.000
.299	.690	.428	.702	.415	.563	.815	.466	.466	.914	.690	.702	.914
.304	.614	.487	.685	.423	.487	.797	.415	.415	.812	.614	.685	.812
.310	.537	.563	.685	.499	.428	.780	.364	.364	.711	.537	.685	.711
.316	.461	.639	.685	.575	.377	.762	.313	.313	.609	.461	.685	.609
.322	.415	.736	.690	.652	.351	.762	.313	.313	.517	.415	.690	.517
.328	.415	.838	.715	.728	.351	.780	.364	.364	.466	.415	.715	.466
.333	.415	.906	.707	.779	.351	.797	.415	.415	.415	.415	.707	.415
.339	.415	.957	.682	.830	.402	.815	.466	.466	.364	.415	.682	.364
.345	.415	1.000	.657	.881	.453	.832	.517	.517	.313	.415	.657	.313
.351	.461	1.000	.657	.931	.525	.865	.609	.609	.313	.461	.657	.313
.357	.537	1.000	.682	.982	.601	.900	.711	.711	.364	.537	.682	.364
.362	.614	1.000	.707	1.000	.685	.935	.812	.812	.415	.614	.707	.415
.368	.690	1.000	.733	1.000	.787	.970	.914	.914	.466	.690	.733	.466
.374	.758	1.000	.758	1.000	.881	1.000	1.000	1.000	.517	.758	.758	.517
.380	.805	1.000	.805	1.000	.931	1.000	1.000	1.000	.609	.805	.805	.609
.386	.855	1.000	.855	1.000	.982	1.000	1.000	1.000	.711	.855	.855	.711
.391	.906	1.000	.906	1.000	1.000	1.000	1.000	1.000	.812	.906	.906	.812
.397	.957	1.000	.957	1.000	1.000	1.000	1.000	1.000	.914	.957	.957	.914
.403	1.000	1.000	1.000	1.000	1.000	1.000	1.000	1.000	1.000	1.000	1.000	1.000
1.000	1.000	1.000	1.000	1.000	1.000	1.000	1.000	1.000	1.000	1.000	1.000	1.000

TABLE A-5 (cont)

AREA AND GAP VARIATIONS OF CONFIGURATION E

X/L	GAP SPACING VARIATION FACTORS FOR ADJACENT SUBCHANNELS (I,J)											
	(13,14)	(13,19)	(14,20)	(15,16)	(15,25)	(16,17)	(16,21)	(17,18)	(17,22)	(18,19)	(18,23)	(19,20)
0.000	1.000	1.000	1.000	1.000	1.000	1.000	1.000	1.000	1.000	1.000	1.000	1.000
.206	1.000	1.000	1.000	1.000	1.000	1.000	1.000	1.000	1.000	1.000	1.000	1.000
.212	1.000	1.000	1.000	1.000	1.000	1.000	1.000	1.000	1.000	1.000	1.000	1.000
.217	1.000	1.000	1.000	1.000	1.000	1.000	1.000	1.000	1.000	1.000	1.000	1.000
.223	1.000	1.000	1.000	1.000	1.000	1.000	1.000	1.000	1.000	.982	.982	1.000
.229	1.000	1.000	1.000	1.000	1.000	1.000	1.000	1.000	1.000	.931	.931	1.000
.235	1.000	1.000	1.000	1.000	1.000	1.000	1.000	1.000	1.000	.881	.881	1.000
.241	1.000	1.000	1.000	1.000	1.000	1.000	1.000	1.000	1.000	.830	.830	1.000
.246	1.000	1.000	1.000	1.000	1.000	1.000	1.000	1.000	1.000	.779	.779	1.000
.252	.982	1.000	1.000	.982	.050	.982	.964	1.000	.982	.746	.746	1.000
.258	.931	1.000	1.000	.931	.050	.931	.863	1.000	.931	.720	.720	1.000
.264	.881	1.000	1.000	.881	.050	.881	.761	1.000	.881	.695	.695	1.000
.270	.830	1.000	1.000	.787	.050	.787	.660	1.000	.830	.669	.669	1.000
.275	.779	1.000	1.000	.685	.050	.685	.558	1.000	.779	.644	.644	1.000
.281	.728	.982	.988	.601	.050	.601	.491	.982	.728	.669	.651	.964
.287	.652	.931	.952	.525	.050	.525	.440	.931	.652	.695	.626	.863
.293	.575	.881	.917	.453	.050	.453	.389	.881	.575	.720	.601	.761
.299	.499	.787	.882	.402	.050	.402	.338	.787	.499	.702	.576	.660
.304	.423	.685	.847	.351	.050	.351	.208	.685	.423	.685	.558	.558
.310	.415	.601	.824	.351	.050	.351	.338	.601	.415	.685	.576	.491
.316	.415	.525	.806	.351	.050	.351	.389	.525	.415	.685	.601	.440
.322	.415	.453	.789	.377	.050	.377	.440	.453	.415	.690	.626	.389
.328	.415	.402	.771	.428	.050	.428	.491	.402	.415	.715	.651	.338
.333	.423	.351	.753	.487	.050	.487	.558	.351	.423	.707	.644	.288
.339	.499	.351	.771	.563	.050	.563	.660	.351	.499	.682	.669	.338
.345	.575	.351	.789	.639	.050	.639	.761	.351	.575	.657	.695	.389
.351	.652	.377	.806	.736	.050	.736	.863	.377	.652	.657	.720	.440
.357	.728	.428	.824	.838	.050	.838	.964	.428	.728	.682	.746	.491
.362	.779	.487	.847	.906	1.000	.906	1.000	.487	.779	.707	.779	.558
.368	.830	.563	.882	.957	1.000	.957	1.000	.563	.830	.733	.830	.660
.374	.881	.639	.917	1.000	1.000	1.000	1.000	.639	.881	.758	.881	.761
.380	.931	.736	.952	1.000	1.000	1.000	1.000	.736	.931	.805	.931	.863
.386	.982	.838	.988	1.000	1.000	1.000	1.000	.838	.982	.855	.982	.964
.391	1.000	.906	1.000	1.000	1.000	1.000	1.000	.906	1.000	.906	1.000	1.000
.397	1.000	.957	1.000	1.000	1.000	1.000	1.000	.957	1.000	.957	1.000	1.000
.403	1.000	1.000	1.000	1.000	1.000	1.000	1.000	1.000	1.000	1.000	1.000	1.000
1.000	1.000	1.000	1.000	1.000	1.000	1.000	1.000	1.000	1.000	1.000	1.000	1.000

TABLE A-5 (cont)

AREA AND GAP VARIATIONS OF CONFIGURATION E

X/L	GAP SPACING VARIATION FACTORS FOR ADJACENT SUBCHANNELS (I,J)											
	(19,24)	(20,28)	(21,22)	(21,25)	(22,23)	(22,26)	(23,24)	(23,27)	(24,28)	(25,26)	(26,27)	(27,28)
0.000	1.000	1.000	1.000	1.000	1.000	1.000	1.000	1.000	1.000	1.000	1.000	1.000
.206	1.000	1.000	1.000	1.000	1.000	1.000	1.000	1.000	1.000	1.000	1.000	1.000
.212	1.000	1.000	1.000	1.000	1.000	1.000	1.000	1.000	1.000	1.000	1.000	1.000
.217	1.000	1.000	1.000	1.000	1.000	1.000	1.000	1.000	1.000	1.000	1.000	1.000
.223	.982	1.000	1.000	1.000	1.000	1.000	.982	1.000	1.000	1.000	1.000	1.000
.229	.931	1.000	1.000	1.000	1.000	1.000	.931	1.000	1.000	1.000	1.000	1.000
.235	.881	1.000	1.000	1.000	1.000	1.000	.881	1.000	1.000	1.000	1.000	1.000
.241	.830	1.000	1.000	1.000	.957	.957	.787	.914	.050	1.000	.970	.050
.246	.779	1.000	1.000	1.000	.906	.906	.685	.812	.050	1.000	.935	.050
.252	.746	1.000	.982	.050	.855	.855	.601	.711	.050	1.000	.900	.050
.258	.720	1.000	.931	.050	.805	.805	.525	.609	.050	1.000	.865	.050
.264	.695	1.000	.881	.050	.758	.758	.453	.517	.050	1.000	.832	.050
.270	.669	1.000	.787	0.000	.733	.690	.402	.466	.050	.050	.815	.050
.275	.644	1.000	.685	0.000	.707	.614	.351	.415	.050	.050	.797	.050
.281	.651	.050	.601	0.000	.664	.537	.351	.364	0.000	.050	.780	.050
.287	.626	.050	.525	0.000	.588	.461	.351	.313	0.000	.050	.762	.050
.293	.601	.050	.453	0.000	.537	.415	.377	.313	0.000	.050	.762	.050
.299	.576	.050	.402	0.000	.512	.415	.428	.364	0.000	.050	.780	.050
.304	.558	.050	.351	0.000	.487	.415	.487	.415	0.000	.050	.797	.050
.310	.576	.050	.351	0.000	.478	.415	.563	.466	0.000	.050	.815	.050
.316	.601	.050	.351	0.000	.478	.415	.639	.517	0.000	.050	.832	.050
.322	.626	.050	.377	0.000	.499	.461	.736	.609	0.000	.050	.865	.050
.328	.651	.050	.428	0.000	.525	.537	.838	.711	0.000	.050	.900	.050
.333	.644	.050	.487	0.000	.550	.614	.906	.812	0.000	.050	.935	.050
.339	.669	.050	.563	0.000	.626	.690	.957	.914	0.000	.050	.970	.050
.345	.695	.050	.639	0.000	.695	.758	1.000	1.000	.050	.050	1.000	1.000
.351	.720	.050	.736	0.000	.720	.805	1.000	1.000	.050	.050	1.000	1.000
.357	.746	.050	.838	0.000	.746	.855	1.000	1.000	.050	.050	1.000	1.000
.362	.779	.050	.906	.050	.779	.906	1.000	1.000	.050	.050	1.000	1.000
.368	.830	.050	.957	.050	.830	.957	1.000	1.000	.050	.050	1.000	1.000
.374	.881	.050	1.000	1.000	.881	1.000	1.000	1.000	.050	1.000	1.000	1.000
.380	.931	.050	1.000	1.000	.931	1.000	1.000	1.000	.050	1.000	1.000	1.000
.386	.982	.050	1.000	1.000	.982	1.000	1.000	1.000	.050	1.000	1.000	1.000
.391	1.000	1.000	1.000	1.000	1.000	1.000	1.000	1.000	1.000	1.000	1.000	1.000
.397	1.000	1.000	1.000	1.000	1.000	1.000	1.000	1.000	1.000	1.000	1.000	1.000
.403	1.000	1.000	1.000	1.000	1.000	1.000	1.000	1.000	1.000	1.000	1.000	1.000
1.000	1.000	1.000	1.000	1.000	1.000	1.000	1.000	1.000	1.000	1.000	1.000	1.000

TABLE A-6

AREA AND GAP VARIATIONS OF CONFIGURATION F

X/L	AREA VARIATION FACTORS FOR SUBCHANNEL (I)													
	(1)	(2)	(3)	(4)	(5)	(6)	(7)	(8)	(9)	(10)	(11)	(12)	(13)	(14)
0.000	1.000	1.000	1.000	1.000	1.000	1.000	1.000	1.000	1.000	1.000	1.000	1.000	1.000	1.000
.206	1.000	1.000	1.000	1.000	1.000	1.000	1.000	1.000	1.000	1.000	1.000	1.000	1.000	1.000
.212	.937	.926	1.000	1.000	.946	.986	1.000	1.000	1.000	1.000	1.000	1.000	1.000	1.000
.217	.937	.905	1.000	1.000	.927	.969	1.000	1.000	1.000	1.000	1.000	1.000	1.000	1.000
.223	.937	.885	1.000	1.000	.908	.951	.994	.990	1.000	1.000	1.000	.994	.994	1.000
.229	.937	.863	1.000	1.000	.888	.932	.977	.960	1.000	1.000	1.000	.977	.977	1.000
.235	.937	.833	1.000	1.000	.867	.914	.960	.930	1.000	1.000	1.000	.960	.960	1.000
.241	.937	.756	.926	.937	.855	.902	.927	.844	1.000	1.000	1.000	.942	.942	1.000
.246	.937	.671	.905	.937	.841	.890	.891	.792	1.000	1.000	1.000	.923	.923	1.000
.252	.937	.582	.885	.873	.827	.878	.859	.703	1.000	1.000	1.000	.874	.903	.935
.258	.937	.531	.863	.873	.813	.865	.828	.643	1.000	1.000	1.000	.805	.874	.915
.264	.937	.531	.833	.873	.813	.865	.798	.582	1.000	1.000	1.000	.726	.844	.895
.270	.937	.550	.739	.873	.803	.849	.759	.527	.909	.958	.972	.664	.813	.874
.275	.937	.597	.634	.873	.786	.827	.717	.470	.869	.906	.937	.640	.781	.852
.281	.873	.641	.525	.873	.724	.804	.699	.464	.821	.847	.902	.664	.774	.778
.287	.873	.674	.452	.873	.686	.779	.681	.459	.758	.774	.864	.726	.757	.688
.293	.873	.644	.421	.873	.655	.761	.675	.467	.696	.703	.820	.805	.740	.577
.299	.873	.657	.397	.873	.634	.741	.674	.488	.647	.649	.714	.831	.707	.484
.304	.873	.660	.399	.873	.612	.717	.671	.512	.596	.593	.594	.829	.672	.433
.310	.873	.640	.397	.873	.593	.692	.672	.573	.510	.541	.470	.794	.672	.404
.316	.937	.627	.421	.873	.612	.662	.671	.631	.400	.490	.376	.757	.672	.396
.322	.937	.627	.452	.873	.599	.644	.689	.696	.309	.478	.341	.712	.672	.396
.328	.937	.656	.525	.873	.607	.657	.725	.758	.267	.504	.373	.639	.676	.404
.333	.937	.686	.634	.873	.614	.670	.749	.804	.267	.528	.437	.547	.671	.433
.339	.937	.715	.739	.873	.650	.682	.766	.843	.324	.578	.497	.446	.690	.484
.345	.937	.743	.833	.937	.684	.693	.779	.917	.424	.627	.550	.377	.708	.577
.351	.937	.784	.863	.937	.730	.729	.797	.937	.553	.693	.594	.377	.738	.688
.357	.937	.827	.885	.937	.775	.779	.828	.955	.680	.751	.657	.446	.780	.778
.362	.937	.869	.905	1.000	.822	.827	.859	1.000	.779	.829	.717	.547	.813	.852
.368	.937	.909	.926	1.000	.873	.874	.888	1.000	.841	.899	.776	.645	.844	.874
.376	.937	1.000	1.000	1.000	.917	.914	.916	1.000	.895	.950	.829	.736	.876	.895
.380	.937	1.000	1.000	1.000	.937	.932	.932	1.000	.915	.977	.854	.797	.910	.915
.386	.937	1.000	1.000	1.000	.955	.951	.951	1.000	.935	.994	.902	.852	.945	.935
.391	1.000	1.000	1.000	1.000	1.000	.969	.969	1.000	1.000	1.000	.937	.906	.969	1.000
.397	1.000	1.000	1.000	1.000	1.000	.986	.986	1.000	1.000	1.000	.972	.958	.986	1.000
.403	1.000	1.000	1.000	1.000	1.000	1.000	1.000	1.000	1.000	1.000	1.000	1.000	1.000	1.000
1.000	1.000	1.000	1.000	1.000	1.000	1.000	1.000	1.000	1.000	1.000	1.000	1.000	1.000	1.000

TABLE A-6 (cont)

AREA AND GAP VARIATIONS OF CONFIGURATION F

X/L	AREA VARIATION FACTORS FOR SUBCHANNEL (I)													
	(15)	(16)	(17)	(18)	(19)	(20)	(21)	(22)	(23)	(24)	(25)	(26)	(27)	(28)
0.000	1.000	1.000	1.000	1.000	1.000	1.000	1.000	1.000	1.000	1.000	1.000	1.000	1.000	1.000
.206	1.000	1.000	1.000	1.000	1.000	1.000	1.000	1.000	1.000	1.000	1.000	1.000	1.000	1.000
.212	1.000	1.000	1.000	1.000	1.000	1.000	1.000	1.000	1.000	1.000	1.000	1.000	1.000	1.000
.217	1.000	1.000	1.000	1.000	1.000	1.000	1.000	1.000	1.000	1.000	1.000	1.000	1.000	1.000
.223	1.000	1.000	1.000	.994	.994	1.000	1.000	1.000	.994	.990	1.000	1.000	1.000	1.000
.229	1.000	1.000	1.000	.977	.977	1.000	1.000	1.000	.977	.920	1.000	1.000	1.000	1.000
.235	1.000	1.000	1.000	.960	.960	1.000	1.000	1.000	.960	.930	1.000	1.000	1.000	1.000
.241	1.000	1.000	1.000	.942	.942	1.000	1.000	.984	.913	.835	1.000	.926	.909	.937
.246	1.000	1.000	1.000	.923	.923	1.000	1.000	.939	.850	.792	1.000	.905	.859	.937
.252	.935	.908	.994	.874	.908	1.000	.945	.945	.810	.747	.937	.885	.827	.937
.258	.915	.955	.977	.805	.896	1.000	.897	.910	.761	.707	.937	.853	.784	.937
.264	.895	.920	.960	.726	.884	1.000	.847	.874	.713	.665	.937	.833	.735	.937
.270	.857	.855	.927	.664	.871	1.000	.741	.830	.676	.630	.873	.739	.615	.937
.275	.815	.783	.891	.640	.858	1.000	.669	.781	.638	.593	.873	.634	.543	.937
.281	.738	.718	.819	.659	.860	.928	.608	.731	.620	.558	.873	.525	.440	.873
.287	.636	.657	.714	.704	.839	.889	.555	.671	.591	.548	.873	.452	.374	.873
.293	.515	.596	.592	.764	.816	.849	.499	.623	.586	.550	.873	.421	.374	.873
.299	.365	.547	.432	.787	.777	.806	.451	.593	.605	.564	.873	.397	.440	.873
.304	.251	.497	.298	.783	.737	.762	.400	.561	.626	.583	.873	.399	.543	.873
.310	.192	.497	.180	.752	.709	.688	.424	.559	.655	.613	.873	.397	.642	.873
.316	.213	.497	.110	.721	.684	.594	.445	.559	.685	.645	.873	.421	.733	.873
.322	.303	.522	.084	.681	.659	.488	.481	.577	.726	.682	.873	.452	.784	.873
.328	.436	.572	.069	.608	.639	.402	.528	.608	.767	.718	.873	.525	.827	.873
.333	.580	.626	.096	.515	.607	.357	.583	.640	.796	.733	.873	.634	.859	.873
.339	.688	.688	.137	.440	.620	.402	.649	.701	.843	.767	.873	.739	.909	.873
.345	.785	.748	.239	.396	.632	.488	.714	.758	.884	.834	.873	.833	1.000	.937
.351	.837	.819	.361	.408	.657	.594	.784	.806	.896	.848	.873	.883	1.000	.937
.357	.878	.890	.510	.477	.694	.688	.853	.853	.908	.861	.873	.885	1.000	.937
.362	.905	.937	.658	.580	.736	.762	.927	.891	.923	.877	.937	.905	1.000	.937
.368	.926	.972	.768	.684	.786	.806	.946	.927	.942	.897	.937	.925	1.000	.937
.374	1.000	1.000	.865	.780	.834	.849	1.000	.960	.960	.917	1.000	1.000	1.000	.937
.380	1.000	1.000	.910	.842	.887	.889	1.000	.977	.977	.937	1.000	1.000	1.000	.937
.386	1.000	1.000	.945	.896	.939	.928	1.000	.995	.994	.955	1.000	1.000	1.000	.937
.391	1.000	1.000	.959	.937	.969	1.000	1.000	1.000	1.000	1.000	1.000	1.000	1.000	1.000
.397	1.000	1.000	.985	.972	.986	1.000	1.000	1.000	1.000	1.000	1.000	1.000	1.000	1.000
.403	1.000	1.000	1.000	1.000	1.000	1.000	1.000	1.000	1.000	1.000	1.000	1.000	1.000	1.000
1.000	1.000	1.000	1.000	1.000	1.000	1.000	1.000	1.000	1.000	1.000	1.000	1.000	1.000	1.000

TABLE A-6 (cont)

AREA AND GAP VARIATIONS OF CONFIGURATION F

X/L	GAP SPACING VARIATION FACTORS FOR ADJACENT SUBCHANNELS (I,J)											
	(1, 2)	(1, 5)	(1, 9)	(2, 3)	(2, 6)	(3, 4)	(3, 7)	(4, 8)	(4,14)	(5, 6)	(5,10)	(6, 7)
0.000	1.000	1.000	1.000	1.000	1.000	1.000	1.000	1.000	1.000	1.000	1.000	1.000
.206	1.000	1.000	1.000	1.000	1.000	1.000	1.000	1.000	1.000	1.000	1.000	1.000
.212	.050	.050	1.000	1.000	.947	1.000	1.000	1.000	1.000	.947	1.000	1.000
.217	.050	.050	1.000	1.000	.885	1.000	1.000	1.000	1.000	.885	1.000	1.000
.223	.050	.050	1.000	1.000	.823	1.000	1.000	1.000	1.000	.823	1.000	1.000
.229	.050	.050	1.000	1.000	.761	1.000	1.000	1.000	1.000	.761	1.000	1.000
.235	.050	.050	1.000	1.000	.703	1.000	1.000	1.000	1.000	.703	1.000	1.000
.241	.050	.050	1.000	1.000	.665	.050	.947	.050	1.000	.665	1.000	1.000
.246	.050	.050	1.000	1.000	.628	.050	.885	.050	1.000	.628	1.000	1.000
.252	.050	.050	1.000	1.000	.590	.050	.823	0.000	.050	.590	1.000	1.000
.258	.050	.050	1.000	1.000	.552	.050	.761	0.000	.050	.552	1.000	1.000
.264	.050	.050	1.000	1.000	.552	.050	.703	0.000	.050	.552	1.000	1.000
.270	.050	.050	1.000	.964	.537	.050	.613	0.000	.050	.537	.947	.947
.275	.050	.050	1.000	.921	.513	.050	.513	0.000	.050	.513	.885	.885
.281	.050	0.000	.050	.877	.489	.050	.413	0.000	.050	.489	.801	.823
.287	.050	0.000	.050	.835	.465	.050	.313	0.000	.050	.465	.677	.761
.293	.050	0.000	.050	.794	.465	.050	.255	0.000	.050	.465	.558	.703
.299	.050	0.000	.050	.768	.489	.050	.255	0.000	.050	.489	.458	.613
.304	.050	0.000	.050	.742	.513	.050	.255	0.000	.050	.513	.358	.513
.310	.050	0.000	.050	.715	.537	.050	.255	0.000	.050	.537	.274	.413
.316	1.000	.050	.050	.689	.552	.050	.255	0.000	.050	.552	.198	.313
.322	1.000	.050	.050	.689	.552	.050	.313	0.000	.050	.552	.140	.255
.328	1.000	.050	.050	.715	.590	.050	.413	0.000	.050	.590	.140	.255
.333	1.000	.050	.050	.742	.628	.050	.513	0.000	.050	.628	.140	.255
.339	1.000	.050	.050	.768	.665	.050	.613	0.000	.050	.665	.236	.255
.345	1.000	.050	.050	.794	.703	1.000	.703	.050	.050	.703	.312	.255
.351	1.000	.050	.050	.835	.761	1.000	.761	.050	.050	.761	.408	.313
.357	1.000	.050	.050	.877	.823	1.000	.823	.050	.050	.823	.508	.413
.362	1.000	.050	.050	.921	.885	1.000	.885	1.000	1.000	.885	.615	.513
.368	1.000	.050	.050	.964	.947	1.000	.947	1.000	1.000	.947	.739	.613
.374	1.000	.050	.050	1.000	1.000	1.000	1.000	1.000	1.000	1.000	.854	.703
.380	1.000	.050	.050	1.000	1.000	1.000	1.000	1.000	1.000	1.000	.916	.761
.385	1.000	.050	.050	1.000	1.000	1.000	1.000	1.000	1.000	1.000	.978	.823
.391	1.000	1.000	1.000	1.000	1.000	1.000	1.000	1.000	1.000	1.000	1.000	.885
.397	1.000	1.000	1.000	1.000	1.000	1.000	1.000	1.000	1.000	1.000	1.000	.947
.403	1.000	1.000	1.000	1.000	1.000	1.000	1.000	1.000	1.000	1.000	1.000	1.000
1.000	1.000	1.000	1.000	1.000	1.000	1.000	1.000	1.000	1.000	1.000	1.000	1.000

TABLE A-6 (cont)

AREA AND GAP VARIATIONS OF CONFIGURATION F

X/L	GAP SPACING VARIATION FACTORS FOR ADJACENT SUBCHANNELS (I,J)											
	(6,11)	(7, 6)	(7,12)	(8,13)	(9,10)	(9,15)	(10,11)	(10,16)	(11,12)	(11,17)	(12,13)	(12,18)
0.000	1.000	1.000	1.000	1.000	1.000	1.000	1.000	1.000	1.000	1.000	1.000	1.000
.206	1.000	1.000	1.000	1.000	1.000	1.000	1.000	1.000	1.000	1.000	1.000	1.000
.212	1.000	1.000	1.000	1.000	1.000	1.000	1.000	1.000	1.000	1.000	1.000	1.000
.217	1.000	1.000	1.000	1.000	1.000	1.000	1.000	1.000	1.000	1.000	1.000	1.000
.223	1.000	.978	.978	.978	1.000	1.000	1.000	1.000	1.000	1.000	.978	1.000
.229	1.000	.916	.916	.916	1.000	1.000	1.000	1.000	1.000	1.000	.916	1.000
.235	1.000	.854	.854	.854	1.000	1.000	1.000	1.000	1.000	1.000	.854	1.000
.241	1.000	.739	.792	.792	1.000	1.000	1.000	1.000	1.000	1.000	.792	1.000
.246	1.000	.615	.730	.730	1.000	1.000	1.000	1.000	1.000	1.000	.730	1.000
.252	1.000	.508	.684	.663	1.000	1.000	1.000	1.000	1.000	1.000	.684	1.000
.258	1.000	.408	.646	.563	1.000	1.000	1.000	1.000	1.000	1.000	.646	1.000
.264	1.000	.312	.609	.463	1.000	1.000	1.000	1.000	1.000	1.000	.609	1.000
.270	.947	.236	.571	.363	.947	.984	.895	.895	1.000	.947	.571	1.000
.275	.885	.160	.533	.263	.885	.921	.770	.770	1.000	.885	.533	1.000
.281	.823	.160	.571	.255	.801	.877	.646	.646	1.000	.823	.571	1.000
.287	.761	.160	.609	.255	.677	.835	.522	.522	1.000	.761	.609	1.000
.293	.703	.198	.646	.255	.558	.794	.407	.407	1.000	.703	.646	1.000
.299	.613	.274	.632	.255	.458	.768	.331	.331	.895	.613	.632	.895
.304	.513	.358	.615	.263	.358	.742	.255	.255	.770	.513	.615	.770
.310	.413	.458	.615	.363	.274	.715	.179	.179	.646	.413	.615	.646
.316	.313	.558	.615	.463	.198	.689	.103	.103	.522	.313	.615	.522
.322	.255	.677	.620	.563	.160	.689	.103	.103	.407	.255	.620	.407
.328	.255	.801	.644	.663	.160	.715	.179	.179	.331	.255	.644	.331
.333	.255	.885	.628	.730	.160	.742	.255	.255	.255	.255	.628	.255
.339	.255	.947	.590	.792	.236	.768	.331	.331	.179	.255	.590	.179
.345	.255	1.000	.552	.854	.312	.794	.407	.407	.103	.255	.552	.103
.351	.313	1.000	.552	.916	.408	.835	.522	.522	.103	.313	.552	.103
.357	.413	1.000	.590	.978	.508	.877	.646	.646	.179	.413	.590	.179
.362	.513	1.000	.628	1.000	.615	.921	.770	.770	.255	.513	.628	.255
.368	.613	1.000	.665	1.000	.739	.964	.895	.895	.331	.613	.665	.331
.374	.703	1.000	.703	1.000	.854	1.000	1.000	1.000	.407	.703	.703	.407
.380	.761	1.000	.761	1.000	.916	1.000	1.000	1.000	.522	.761	.761	.522
.386	.823	1.000	.823	1.000	.978	1.000	1.000	1.000	.646	.823	.823	.646
.391	.885	1.000	.885	1.000	1.000	1.000	1.000	1.000	.770	.885	.885	.770
.397	.947	1.000	.947	1.000	1.000	1.000	1.000	1.000	.895	.947	.947	.895
.403	1.000	1.000	1.000	1.000	1.000	1.000	1.000	1.000	1.000	1.000	1.000	1.000
1.000	1.000	1.000	1.000	1.000	1.000	1.000	1.000	1.000	1.000	1.000	1.000	1.000

TABLE A-6 (cont)

AREA AND GAP VARIATIONS OF CONFIGURATION F

X/L	GAP SPACING VARIATION FACTORS FOR ADJACENT SUBCHANNELS (I,J)											
	(13,14)	(13,19)	(14,20)	(15,16)	(15,25)	(16,17)	(16,21)	(17,18)	(17,22)	(18,19)	(18,23)	(19,20)
0.000	1.000	1.000	1.000	1.000	1.000	1.000	1.000	1.000	1.000	1.000	1.000	1.000
.206	1.000	1.000	1.000	1.000	1.000	1.000	1.000	1.000	1.000	1.000	1.000	1.000
.212	1.000	1.000	1.000	1.000	1.000	1.000	1.000	1.000	1.000	1.000	1.000	1.000
.217	1.000	1.000	1.000	1.000	1.000	1.000	1.000	1.000	1.000	1.000	1.000	1.000
.223	1.000	1.000	1.000	1.000	1.000	1.000	1.000	1.000	1.000	.978	.978	1.000
.229	1.000	1.000	1.000	1.000	1.000	1.000	1.000	1.000	1.000	.916	.916	1.000
.235	1.000	1.000	1.000	1.000	1.000	1.000	1.000	1.000	1.000	.854	.854	1.000
.241	1.000	1.000	1.000	1.000	1.000	1.000	1.000	1.000	1.000	.792	.792	1.000
.246	1.000	1.000	1.000	1.000	1.000	1.000	1.000	1.000	1.000	.730	.730	1.000
.252	.978	1.000	1.000	.978	.050	.978	.957	1.000	.978	.684	.684	1.000
.258	.916	1.000	1.000	.916	.050	.916	.833	1.000	.916	.646	.646	1.000
.264	.854	1.000	1.000	.854	.050	.854	.708	1.000	.854	.609	.609	1.000
.270	.792	1.000	1.000	.739	.050	.739	.584	1.000	.792	.571	.571	1.000
.275	.730	1.000	1.000	.615	.050	.615	.460	1.000	.730	.533	.533	1.000
.281	.643	.978	.905	.508	.050	.508	.369	.978	.663	.571	.549	.957
.287	.563	.916	.942	.408	.050	.408	.293	.916	.563	.609	.525	.833
.293	.463	.854	.899	.312	.050	.312	.217	.854	.463	.646	.501	.708
.299	.363	.739	.856	.236	.050	.236	.141	.739	.363	.632	.477	.584
.304	.263	.615	.813	.160	.050	.160	.055	.615	.263	.615	.460	.460
.310	.255	.508	.701	.160	.050	.160	.141	.508	.255	.615	.477	.369
.316	.255	.408	.755	.160	.050	.160	.217	.408	.255	.615	.501	.293
.322	.255	.312	.728	.198	.050	.198	.293	.312	.255	.620	.525	.217
.328	.255	.236	.702	.274	.050	.274	.369	.236	.255	.644	.549	.141
.333	.263	.160	.676	.358	.050	.358	.440	.160	.263	.628	.533	.065
.339	.363	.160	.702	.458	.050	.458	.584	.160	.363	.560	.571	.141
.345	.463	.160	.728	.558	.050	.558	.708	.160	.463	.552	.609	.217
.351	.563	.198	.755	.677	.050	.677	.833	.198	.563	.552	.646	.293
.357	.663	.274	.781	.801	.050	.801	.957	.274	.663	.560	.684	.369
.362	.730	.358	.813	.885	1.000	.885	1.000	.358	.730	.628	.730	.460
.368	.792	.458	.856	.947	1.000	.947	1.000	.458	.792	.695	.792	.584
.374	.854	.558	.899	1.000	1.000	1.000	1.000	.558	.854	.703	.854	.708
.380	.916	.677	.942	1.000	1.000	1.000	1.000	.677	.916	.761	.916	.833
.386	.978	.801	.985	1.000	1.000	1.000	1.000	.801	.978	.823	.978	.957
.391	1.000	.885	1.000	1.000	1.000	1.000	1.000	.885	1.000	.885	1.000	1.000
.397	1.000	.947	1.000	1.000	1.000	1.000	1.000	.947	1.000	.947	1.000	1.000
.403	1.000	1.000	1.000	1.000	1.000	1.000	1.000	1.000	1.000	1.000	1.000	1.000
1.000	1.000	1.000	1.000	1.000	1.000	1.000	1.000	1.000	1.000	1.000	1.000	1.000

TABLE A-6 (cont)

AREA AND GAP VARIATIONS OF CONFIGURATION F

X/L	GAP SPACING VARIATION FACTORS FOR ADJACENT SUBCHANNELS (I,J)											
	(19,24)	(20,26)	(21,22)	(21,25)	(22,23)	(22,26)	(23,24)	(23,27)	(24,28)	(25,26)	(26,27)	(27,28)
0.000	1.000	1.000	1.000	1.000	1.000	1.000	1.000	1.000	1.000	1.000	1.000	1.000
.204	1.000	1.000	1.000	1.000	1.000	1.000	1.000	1.000	1.000	1.000	1.000	1.000
.212	1.000	1.000	1.000	1.000	1.000	1.000	1.000	1.000	1.000	1.000	1.000	1.000
.217	1.000	1.000	1.000	1.000	1.000	1.000	1.000	1.000	1.000	1.000	1.000	1.000
.223	.978	1.000	1.000	1.000	1.000	1.000	.978	1.000	1.000	1.000	1.000	1.000
.229	.916	1.000	1.000	1.000	1.000	1.000	.916	1.000	1.000	1.000	1.000	1.000
.235	.854	1.000	1.000	1.000	1.000	1.000	.854	1.000	1.000	1.000	1.000	1.000
.241	.792	1.000	1.000	1.000	.947	.947	.739	.895	.050	1.000	.921	.050
.246	.730	1.000	1.000	1.000	.885	.885	.615	.770	.050	1.000	.921	.050
.252	.684	1.000	.978	.050	.823	.823	.508	.646	.050	1.000	.877	.050
.258	.646	1.000	.916	.050	.761	.761	.408	.522	.050	1.000	.835	.050
.264	.609	1.000	.854	.050	.703	.703	.312	.407	.050	1.000	.794	.050
.270	.571	1.000	.739	0.000	.665	.613	.256	.331	.050	.050	.768	.050
.275	.533	1.000	.615	0.000	.628	.513	.160	.255	.050	.050	.742	.050
.281	.569	.050	.508	0.000	.568	.413	.160	.179	0.000	.050	.715	.050
.287	.525	.050	.408	0.000	.468	.313	.160	.103	0.000	.050	.689	.050
.293	.501	.050	.312	0.000	.404	.255	.198	.103	0.000	.050	.689	.050
.299	.477	.050	.236	0.000	.342	.255	.274	.179	0.000	.050	.715	.050
.304	.460	.050	.160	0.000	.358	.255	.358	.255	0.000	.050	.742	.050
.310	.477	.050	.160	0.000	.350	.255	.458	.331	0.000	.050	.768	.050
.316	.501	.050	.160	0.000	.350	.255	.558	.407	0.000	.050	.794	.050
.322	.525	.050	.198	0.000	.370	.313	.677	.522	0.000	.050	.835	.050
.328	.549	.050	.274	0.000	.394	.413	.801	.646	0.000	.050	.877	.050
.333	.533	.050	.358	0.000	.416	.513	.885	.770	0.000	.050	.921	.050
.339	.571	.050	.458	0.000	.518	.613	.947	.895	0.000	.050	.964	.050
.345	.609	.050	.558	0.000	.609	.703	1.000	1.000	.050	.050	1.000	1.000
.351	.646	.050	.677	0.000	.646	.761	1.000	1.000	.050	.050	1.000	1.000
.357	.684	.050	.801	0.000	.684	.823	1.000	1.000	.050	.050	1.000	1.000
.362	.730	.050	.885	.050	.730	.885	1.000	1.000	.050	.050	1.000	1.000
.368	.792	.050	.947	.050	.792	.947	1.000	1.000	.050	.050	1.000	1.000
.374	.854	.050	1.000	1.000	.854	1.000	1.000	1.000	.050	1.000	1.000	1.000
.380	.916	.050	1.000	1.000	.916	1.000	1.000	1.000	.050	1.000	1.000	1.000
.385	.978	.050	1.000	1.000	.978	1.000	1.000	1.000	.050	1.000	1.000	1.000
.391	1.000	1.000	1.000	1.000	1.000	1.000	1.000	1.000	1.000	1.000	1.000	1.000
.397	1.000	1.000	1.000	1.000	1.000	1.000	1.000	1.000	1.000	1.000	1.000	1.000
.403	1.000	1.000	1.000	1.000	1.000	1.000	1.000	1.000	1.000	1.000	1.000	1.000
1.000	1.000	1.000	1.000	1.000	1.000	1.000	1.000	1.000	1.000	1.000	1.000	1.000

TABLE A-7

GRID AND BLOCKAGE SLEEVE COBRA INPUT (ϵ^2) AS A FUNCTION OF ELEVATION FOR CONFIGURATION E

SPACER DATA

SPACER TYPE NO.	1	2	3	4	5	6	7	8	9	10

SPACER DATA

SPACER TYPE NO.	11	12	13	14	15					
LOCATION (X/L)	.159	.275	.290	.304	.319	.333	.347	.362	.377	.391
LOCATION (X/L)	.406	.420	.434	.464	.754					

SPACER TYPE 1

CHANNEL NO.	DRAG COEFF.	CHANNEL NO.	DRAG COEFF.	CHANNEL NO.	DRAG COEFF.	CHANNEL NO.	DRAG COEFF.
1	.058	2	.041	3	.041	4	.063
5	.105	6	.066	7	.066	8	.143
9	.041	10	.066	11	.066	12	.066
13	.130	14	.041	15	.104	16	.176
17	.176	18	.153	19	.102	20	.041
21	.187	22	.102	23	.130	24	.187
25	.068	26	.041	27	.041	28	.073

SPACER TYPE 2

CHANNEL NO.	DRAG COEFF.	CHANNEL NO.	DRAG COEFF.	CHANNEL NO.	DRAG COEFF.	CHANNEL NO.	DRAG COEFF.
1	0.000	2	.028	3	0.000	4	0.000
5	0.000	6	0.000	7	0.000	8	0.000
9	0.000	10	0.000	11	0.000	12	.009
13	0.000	14	0.000	15	0.000	16	0.000
17	0.000	18	.009	19	0.000	20	0.000
21	0.000	22	0.000	23	0.000	24	0.000
25	0.000	26	0.000	27	0.000	28	0.000

SPACER TYPE 3

CHANNEL NO.	DRAG COEFF.	CHANNEL NO.	DRAG COEFF.	CHANNEL NO.	DRAG COEFF.	CHANNEL NO.	DRAG COEFF.
1	0.000	2	.021	3	.016	4	0.000
5	0.000	6	0.000	7	0.000	8	0.000
9	0.000	10	0.000	11	0.000	12	.018
13	0.000	14	.010	15	0.000	16	0.000
17	0.000	18	.018	19	0.000	20	0.000
21	0.000	22	0.000	23	0.000	24	0.000
25	0.000	26	.016	27	.018	28	0.000

SPACER TYPE 4

CHANNEL NO.	DRAG COEFF.	CHANNEL NO.	DRAG COEFF.	CHANNEL NO.	DRAG COEFF.	CHANNEL NO.	DRAG COEFF.
1	0.000	2	.016	3	.033	4	0.000
5	0.000	6	0.000	7	0.000	8	0.000
9	0.000	10	0.000	11	0.000	12	.013
13	0.000	14	.021	15	.026	16	0.000
17	.018	18	.013	19	0.000	20	0.000
21	0.000	22	0.000	23	0.000	24	0.000
25	0.000	26	.033	27	.037	28	0.000

SPACER TYPE 5

CHANNEL NO.	DRAG COEFF.	CHANNEL NO.	DRAG COEFF.	CHANNEL NO.	DRAG COEFF.	CHANNEL NO.	DRAG COEFF.
1	0.000	2	.012	3	.042	4	0.000
5	0.000	6	0.000	7	0.000	8	0.000
9	.017	10	0.000	11	.015	12	.010
13	0.000	14	.016	15	.080	16	0.000
17	.068	18	.010	19	0.000	20	0.000

TABLE A-7 (cont)

GRID AND BLOCKAGE SLEEVE COBRA INPUT (ϵ^2) AS A FUNCTION OF ELEVATION FOR CONFIGURATION E

21	0.000	22	0.000	23	0.000	24	0.000
25	0.000	26	.042	27	.028	28	0.000

SPACER TYPE 6

CHANNEL NO.	DRAG COEFF.	CHANNEL NO.	DRAG COEFF.	CHANNEL NO.	DRAG COEFF.	CHANNEL NO.	DRAG COEFF.
1	0.000	2	.009	3	.052	4	0.000
5	0.000	6	0.000	7	0.000	8	0.000
9	.033	10	0.000	11	.029	12	.006
13	0.000	14	.029	15	.096	16	0.000
17	.124	18	.008	19	0.000	20	.019
21	0.000	22	0.000	23	0.000	24	0.000
25	0.000	26	.053	27	.021	28	0.000

SPACER TYPE 7

CHANNEL NO.	DRAG COEFF.	CHANNEL NO.	DRAG COEFF.	CHANNEL NO.	DRAG COEFF.	CHANNEL NO.	DRAG COEFF.
1	0.000	2	.007	3	.040	4	0.000
5	0.000	6	0.000	7	0.000	8	0.000
9	.025	10	0.000	11	.022	12	.020
13	0.000	14	.042	15	.072	16	0.000
17	.139	18	.020	19	0.000	20	.038
21	0.000	22	0.000	23	0.000	24	0.000
25	0.000	26	.040	27	.016	28	0.000

SPACER TYPE 8

CHANNEL NO.	DRAG COEFF.	CHANNEL NO.	DRAG COEFF.	CHANNEL NO.	DRAG COEFF.	CHANNEL NO.	DRAG COEFF.
1	0.000	2	.005	3	.030	4	0.000
5	0.000	6	0.000	7	0.000	8	0.000
9	.019	10	0.000	11	.017	12	.033
13	0.000	14	.032	15	.054	16	0.000
17	.144	18	.032	19	0.000	20	.029
21	0.000	22	0.000	23	0.000	24	0.000
25	0.000	26	.030	27	.012	28	0.000

SPACER TYPE 9

CHANNEL NO.	DRAG COEFF.	CHANNEL NO.	DRAG COEFF.	CHANNEL NO.	DRAG COEFF.	CHANNEL NO.	DRAG COEFF.
1	0.000	2	.023	3	.017	4	0.000
5	0.000	6	0.000	7	0.000	8	0.000
9	.014	10	0.000	11	.013	12	.025
13	0.000	14	.024	15	.041	16	0.000
17	.109	18	.024	19	0.000	20	.022
21	0.000	22	0.000	23	0.000	24	0.000
25	0.000	26	.023	27	.009	28	0.000

SPACER TYPE10

CHANNEL NO.	DRAG COEFF.	CHANNEL NO.	DRAG COEFF.	CHANNEL NO.	DRAG COEFF.	CHANNEL NO.	DRAG COEFF.
1	0.000	2	0.000	3	.017	4	0.000
5	0.000	6	0.000	7	0.000	8	0.000
9	.011	10	0.000	11	.009	12	.018
13	0.000	14	.018	15	.031	16	0.000
17	.082	18	.016	19	0.000	20	.016
21	0.000	22	0.000	23	0.000	24	0.000
25	0.000	26	.017	27	.007	28	0.000

TABLE A-7 (cont)

GRID AND BLOCKAGE SLEEVE COBRA INPUT (ϵ^2) AS A FUNCTION OF ELEVATION FOR CONFIGURATION E

SPACER TYPE11

CHANNEL NO.	DRAG COEFF.	CHANNEL NO.	DRAG COEFF.	CHANNEL NO.	DRAG COEFF.	CHANNEL NO.	DRAG COEFF.
1	0.000	2	0.000	3	.008	4	0.000
5	0.000	6	0.000	7	0.000	8	0.000
9	.008	10	0.000	11	.007	12	.012
13	0.000	14	.011	15	.023	16	0.000
17	.062	18	.012	19	0.000	20	.012
21	0.000	22	0.000	23	0.000	24	0.000
25	0.000	26	.008	27	0.000	28	0.000

SPACER TYPE12

CHANNEL NO.	DRAG COEFF.	CHANNEL NO.	DRAG COEFF.	CHANNEL NO.	DRAG COEFF.	CHANNEL NO.	DRAG COEFF.
1	0.000	2	0.000	3	.006	4	0.000
5	0.000	6	0.000	7	0.000	8	0.000
9	.006	10	0.000	11	.005	12	.009
13	0.000	14	.008	15	.011	16	0.000
17	.042	18	.009	19	0.000	20	.009
21	0.000	22	0.000	23	0.000	24	0.000
25	0.000	26	.006	27	0.000	28	0.000

SPACER TYPE13

CHANNEL NO.	DRAG COEFF.	CHANNEL NO.	DRAG COEFF.	CHANNEL NO.	DRAG COEFF.	CHANNEL NO.	DRAG COEFF.
1	0.000	2	0.000	3	0.000	4	0.000
5	0.000	6	0.000	7	0.000	8	0.000
9	0.000	10	0.000	11	0.000	12	.007
13	0.000	14	.006	15	0.000	16	0.000
17	.023	18	.007	19	0.000	20	.007
21	0.000	22	0.000	23	0.000	24	0.000
25	0.000	26	0.000	27	0.000	28	0.000

SPACER TYPE14

CHANNEL NO.	DRAG COEFF.	CHANNEL NO.	DRAG COEFF.	CHANNEL NO.	DRAG COEFF.	CHANNEL NO.	DRAG COEFF.
1	.073	2	.041	3	.041	4	.073
5	.187	6	.102	7	.102	8	.187
9	.041	10	.153	11	.215	12	.215
13	.153	14	.041	15	.041	16	.130
17	.130	18	.130	19	.066	20	.041
21	.187	22	.102	23	.102	24	.143
25	.068	26	.041	27	.041	28	.063

SPACER TYPE15

CHANNEL NO.	DRAG COEFF.	CHANNEL NO.	DRAG COEFF.	CHANNEL NO.	DRAG COEFF.	CHANNEL NO.	DRAG COEFF.
1	.063	2	.041	3	.041	4	.063
5	.143	6	.066	7	.066	8	.143
9	.041	10	.130	11	.066	12	.066
13	.130	14	.041	15	.041	16	.130
17	.197	18	.066	19	.066	20	.041
21	.187	22	.102	23	.066	24	.105
25	.073	26	.041	27	.041	28	.058

TABLE A-8

GRID AND BLOCKAGE SLEEVE COBRA INPUT (ε^2) AS A FUNCTION OF ELEVATION FOR CONFIGURATION F

SPACER DATA

SPACER TYPE NO.	1	2	3	4	5	6	7	8	9	10

SPACER DATA

SPACER TYPE NO.	11	12	13	14	15					
LOCATION (X/L)	.139	.275	.290	.304	.319	.333	.347	.362	.377	.391
LOCATION (X/L)	.406	.420	.434	.464	.754					

SPACER TYPE 1

CHANNEL NO.	DRAG COEFF.	CHANNEL NO.	DRAG COEFF.	CHANNEL NO.	DRAG COEFF.	CHANNEL NO.	DRAG COEFF.
1	.058	2	.041	3	.041	4	.063
5	.105	6	.066	7	.066	8	.143
9	.041	10	.066	11	.066	12	.066
13	.130	14	.041	15	.104	16	.178
17	.178	18	.153	19	.102	20	.041
21	.187	22	.102	23	.130	24	.187
25	.068	26	.041	27	.041	28	.073

SPACER TYPE 2

CHANNEL NO.	DRAG COEFF.	CHANNEL NO.	DRAG COEFF.	CHANNEL NO.	DRAG COEFF.	CHANNEL NO.	DRAG COEFF.
1	0.000	2	.030	3	0.000	4	0.000
5	0.000	6	0.000	7	0.000	8	0.000
9	0.000	10	0.000	11	0.000	12	.009
13	0.000	14	0.000	15	0.000	16	0.000
17	0.000	18	.009	19	0.000	20	0.000
21	0.000	22	0.000	23	0.000	24	0.000
25	0.000	26	0.000	27	0.000	28	0.000

SPACER TYPE 3

CHANNEL NO.	DRAG COEFF.	CHANNEL NO.	DRAG COEFF.	CHANNEL NO.	DRAG COEFF.	CHANNEL NO.	DRAG COEFF.
1	0.000	2	.023	3	.020	4	0.000
5	0.000	6	0.000	7	0.000	8	0.000
9	0.000	10	0.000	11	0.000	12	.019
13	0.000	14	.012	15	0.000	16	0.000
17	0.000	18	.018	19	0.000	20	0.000
21	0.000	22	0.000	23	0.000	24	0.000
25	0.000	26	.020	27	.024	28	0.000

SPACER TYPE 4

CHANNEL NO.	DRAG COEFF.	CHANNEL NO.	DRAG COEFF.	CHANNEL NO.	DRAG COEFF.	CHANNEL NO.	DRAG COEFF.
1	0.000	2	.017	3	.039	4	0.000
5	0.000	6	0.000	7	0.000	8	0.000
9	0.000	10	0.000	11	0.000	12	.014
13	0.000	14	.024	15	.037	16	0.000
17	.026	18	.014	19	0.000	20	0.000
21	0.000	22	0.000	23	0.000	24	0.000
25	0.000	26	.039	27	.047	28	0.000

SPACER TYPE 5

CHANNEL NO.	DRAG COEFF.	CHANNEL NO.	DRAG COEFF.	CHANNEL NO.	DRAG COEFF.	CHANNEL NO.	DRAG COEFF.
1	0.000	2	.013	3	.050	4	0.000
5	0.000	6	0.000	7	0.000	8	0.000
9	.022	10	0.000	11	.020	12	.011
13	0.000	14	.018	15	.065	16	0.000
17	.116	18	.010	19	0.000	20	0.000

TABLE A-8 (cont)

GRID AND BLOCKAGE SLEEVE COBRA INPUT (ϵ^2) AS A FUNCTION OF ELEVATION FOR CONFIGURATION F

21	0.000	22	0.000	23	0.000	24	0.000
25	0.000	26	.050	27	.036	28	0.000

SPACER TYPE 6

CHANNEL NO.	DRAG COEFF.	CHANNEL NO.	DRAG COEFF.	CHANNEL NO.	DRAG COEFF.	CHANNEL NO.	DRAG COEFF.
1	0.000	2	.010	3	.064	4	0.000
5	0.000	6	0.000	7	0.000	8	0.000
9	.044	10	0.000	11	.040	12	.006
13	0.000	14	.034	15	.141	16	0.000
17	.236	18	.008	19	0.000	20	.025
21	0.000	22	0.000	23	0.000	24	0.000
25	0.000	26	.063	27	.027	28	0.000

SPACER TYPE 7

CHANNEL NO.	DRAG COEFF.	CHANNEL NO.	DRAG COEFF.	CHANNEL NO.	DRAG COEFF.	CHANNEL NO.	DRAG COEFF.
1	0.000	2	.007	3	.048	4	0.000
5	0.000	6	0.000	7	0.000	8	0.000
9	.033	10	0.000	11	.030	12	.026
13	0.000	14	.050	15	.106	16	0.000
17	.298	18	.024	19	0.000	20	.050
21	0.000	22	0.000	23	0.000	24	0.000
25	0.000	26	.048	27	.020	28	0.000

SPACER TYPE 8

CHANNEL NO.	DRAG COEFF.	CHANNEL NO.	DRAG COEFF.	CHANNEL NO.	DRAG COEFF.	CHANNEL NO.	DRAG COEFF.
1	0.000	2	.006	3	.036	4	0.000
5	0.000	6	0.000	7	0.000	8	0.000
9	.025	10	0.000	11	.023	12	.044
13	0.000	14	.038	15	.080	16	0.000
17	.266	18	.041	19	0.000	20	.038
21	0.000	22	0.000	23	0.000	24	0.000
25	0.000	26	.036	27	.015	28	0.000

SPACER TYPE 9

CHANNEL NO.	DRAG COEFF.	CHANNEL NO.	DRAG COEFF.	CHANNEL NO.	DRAG COEFF.	CHANNEL NO.	DRAG COEFF.
1	0.000	2	0.000	3	.027	4	0.000
5	0.000	6	0.000	7	0.000	8	0.000
9	.019	10	0.000	11	.017	12	.033
13	0.000	14	.028	15	.061	16	0.000
17	.201	18	.031	19	0.000	20	.029
21	0.000	22	0.000	23	0.000	24	0.000
25	0.000	26	.027	27	.012	28	0.000

SPACER TYPE10

CHANNEL NO.	DRAG COEFF.	CHANNEL NO.	DRAG COEFF.	CHANNEL NO.	DRAG COEFF.	CHANNEL NO.	DRAG COEFF.
1	0.000	2	0.000	3	.021	4	0.000
5	0.000	6	0.000	7	0.000	8	0.000
9	.014	10	0.000	11	.013	12	.022
13	0.000	14	.021	15	.046	16	0.000
17	.151	18	.021	19	0.000	20	.022
21	0.000	22	0.000	23	0.000	24	0.000
25	0.000	26	.021	27	.009	28	0.000

TABLE A-8 (cont)

GRID AND BLOCKAGE SLEEVE COBRA INPUT (ε^2) AS A FUNCTION OF ELEVATION FOR CONFIGURATION F

SPACER TYPE11

CHANNEL NO.	DRAG COEFF.	CHANNEL NO.	DRAG COEFF.	CHANNEL NO.	DRAG COEFF.	CHANNEL NO.	DRAG COEFF.
1	0.000	2	0.000	3	.010	4	0.000
5	0.000	6	0.000	7	0.000	8	0.000
9	.011	10	0.000	11	.010	12	.016
13	0.000	14	.013	15	.034	16	0.000
17	.114	18	.016	19	0.000	20	.016
21	0.000	22	0.000	23	0.000	24	0.000
25	0.000	26	.010	27	0.000	28	0.000

SPACER TYPE12

CHANNEL NO.	DRAG COEFF.	CHANNEL NO.	DRAG COEFF.	CHANNEL NO.	DRAG COEFF.	CHANNEL NO.	DRAG COEFF.
1	0.000	2	0.000	3	.008	4	0.000
5	0.000	6	0.000	7	0.000	8	0.000
9	.008	10	0.000	11	.007	12	.013
13	0.000	14	.010	15	.016	16	0.000
17	.079	18	.012	19	0.000	20	.012
21	0.000	22	0.000	23	0.000	24	0.000
25	0.000	26	.008	27	0.000	28	0.000

SPACER TYPE13

CHANNEL NO.	DRAG COEFF.	CHANNEL NO.	DRAG COEFF.	CHANNEL NO.	DRAG COEFF.	CHANNEL NO.	DRAG COEFF.
1	0.000	2	0.000	3	0.000	4	0.000
5	0.000	6	0.000	7	0.000	8	0.000
9	0.000	10	0.000	11	0.000	12	.010
13	0.000	14	.007	15	0.000	16	0.000
17	.042	18	.009	19	0.000	20	.009
21	0.000	22	0.000	23	0.000	24	0.000
25	0.000	26	0.000	27	0.000	28	0.000

SPACER TYPE14

CHANNEL NO.	DRAG COEFF.	CHANNEL NO.	DRAG COEFF.	CHANNEL NO.	DRAG COEFF.	CHANNEL NO.	DRAG COEFF.
1	.073	2	.041	3	.041	4	.073
5	.187	6	.102	7	.102	8	.187
9	.041	10	.153	11	.215	12	.215
13	.153	14	.041	15	.041	16	.130
17	.130	18	.130	19	.066	20	.041
21	.187	22	.102	23	.102	24	.143
25	.068	26	.041	27	.041	28	.063

SPACER TYPE15

CHANNEL NO.	DRAG COEFF.	CHANNEL NO.	DRAG COEFF.	CHANNEL NO.	DRAG COEFF.	CHANNEL NO.	DRAG COEFF.
1	.063	2	.041	3	.041	4	.063
5	.143	6	.066	7	.066	8	.143
9	.041	10	.130	11	.066	12	.066
13	.130	14	.041	15	.041	16	.130
17	.187	18	.066	19	.066	20	.041
21	.187	22	.102	23	.066	24	.105
25	.073	26	.041	27	.041	28	.058

APPENDIX B
THERMAL ANALYSIS OF 21-ROD BUNDLE HOUSING

B-1. INTRODUCTION

The 21-rod bundle cylindrical housing was designed with the minimum wall thickness allowed by the ASME Code so that the housing thermal capacitance was minimized and would absorb, and hence release, the minimum amount of energy. The inside diameter of the housing was made as close to the rod bundle outer dimensions as possible to minimize excess flow area. However, the following comparison of housing mass (nominal dimensions) per heater rod for the 21-rod bundle and the 161-rod unblocked bundle indicates simplistically and qualitatively that the housing effect was significant in the 21-rod bundle:

Bundle	Mass/Rod [kg/rod (lb/rod)]
21-rod	0.102 (0.226) for all 21 rods
161-rod	0.0472 (0.104) for all 161 rods
161-rod	0.0925 (0.204) for 82 outside rods

This is true even though other factors, such as housing temperature and radiation heat transfer properties, are equally important.

In the 21-rod bundle, the relatively cold housing provided a heat sink not only for the outer row of heater rods, but also for the center rods. The housing could also quench prior to the bundle; this could cause vapor desuperheating. Therefore, an analysis was performed to determine the effect of the colder housing temperature on the bundle heat transfer data and the extent to which a heated housing would reduce this effect.

B-2. METHOD OF ANALYSIS

The following two methods were utilized to assess the effect of the housing on the heater rod bundle:

-- A calculation of the expected heater rod and housing temperatures for the 21-rod bundle and 161-rod unblocked bundle, utilizing a cylindrical shell model

-- Examination of the measured temperature and quench times of heater rods with and without a heated housing

B-3. ANALYTICAL MODELS

The effect of the housing on the bundle thermal behavior was quantitatively assessed by a simple energy balance on the bundle and the housing. The heater rod bundle was lumped into three concentric cylinders with the housing as the outside cylinder, as shown in figure B-1. Therefore, for the rod bundle,

$$\begin{matrix}\text{change in} \\ \text{internal} \\ \text{energy}\end{matrix} = \begin{matrix}\text{energy} \\ \text{generated}\end{matrix} + \begin{matrix}\text{energy} \\ \text{in}\end{matrix} - \begin{matrix}\text{energy} \\ \text{out}\end{matrix}$$

For the cylinder,

$$\frac{d}{dt}\left(\rho C_p A_n T_n\right) = q'''_n + \left(\dot{q}\ \text{in}\right)_{\text{radiation}} - \left(\dot{q}\ \text{out}\right)_{\text{radiation}} - \left(\dot{q}\ \text{out}\right)_{\text{convection}}$$

$$\rho C_p A_n \frac{dT_n}{dt} = \dot{q}_n + \sigma A_n F_{n-1 \text{ to } n}\left(T^4_{n-1} - T^4_n\right) - \sigma A_{n+1} F_{n \text{ to } n+1}\left(T^4_n - T^4_{n+1}\right) - (C)\pi \frac{D}{12} h \left(T_n - T_{sat}\right)$$

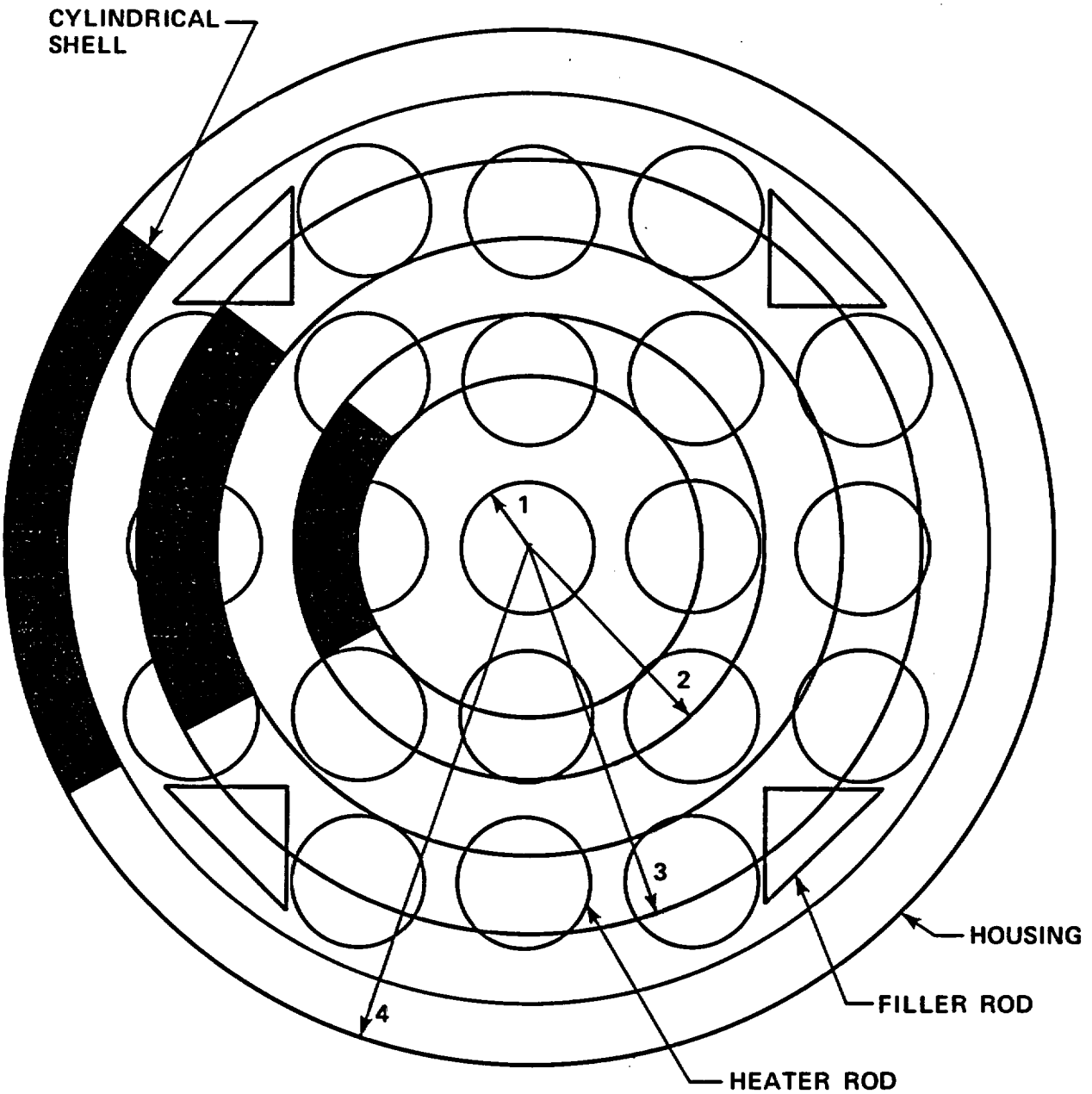

SHELL	OUTSIDE RADIUS	THICKNESS	NUMBER OF HEATER RODS IN SHELL
1	4.75 mm (0.187")	–	1
2	17.3 mm (0.683")	3.91 mm (0.154")	6
3	29.95 mm (1.179")	5.28 mm (0.208")	14
4	38.84 mm (1.529")	4.72 mm (0.186")	0
		TOTAL	21

Figure B-1. 21-Rod Bundle Shell Model

where

$$A_n F_{n-1 \text{ to } n} = P_{n,i} F_{n-1 \text{ to } n}$$

$$= \frac{1}{\frac{\rho}{\varepsilon P_{n-1,0}} + \frac{1}{P_{n-1,0}} + \frac{\rho}{\varepsilon P_{n,i}}}$$

$$= \frac{P_{n,i}}{\left(\frac{\rho}{\varepsilon} + 1\right) \frac{P_{n,i}}{P_{n-1,0}} + \frac{\rho}{\varepsilon}}$$

$$= \frac{2 \pi r_{n,i}}{\left(\frac{\rho}{\varepsilon} + 1\right)\left(\frac{r_{n,i}}{r_{n-1,0}}\right) + \frac{\rho}{\varepsilon}}$$

and

$$A_n F_{n \text{ to } n+1} = P_{n,0} F_{n \text{ to } n+1}$$

$$= \frac{1}{\frac{\rho}{\varepsilon P_{n,0}} + \frac{1}{P_{n,0}} + \frac{\rho}{\varepsilon P_{n+1,i}}}$$

$$= \frac{P_{n,0}}{1 + \frac{\rho}{\varepsilon}\left(1 + \frac{P_{n,0}}{P_{n+1,i}}\right)}$$

$$= \frac{2\pi r_{n,0}}{1 + \frac{\rho}{\varepsilon}\left(1 + \frac{r_{n,0}}{r_{n+1,i}}\right)}$$

C = number of heater rods lumped into cylindrical shell

D = heater rod diameter

$\rho C_p A_n$ = heater rod heat capacity

$= (\rho C_p A)$ boron nitride insulation $+ (\rho C_p A)$ Kanthal heater $+ (\rho C_p A)$ stainless steel clad

$= 195.6$ J/kg-^{o}C (0.04674 Btu/lb-^{o}F)

For the housing, assuming no energy losses to the ambient and neglecting the mass of insulation on the housing, the energy balance is

change in internal energy = energy in by radiation - energy out by convection

$$\frac{d}{dt}\left(\rho C_p A_H T_H\right) = \sigma A_H F_H \left(T_n^4 - T_H^4\right) - \pi \frac{D}{12} h \left(T_H - T_{sat}\right)$$

$$\rho C_p A_H \frac{dT_H}{dt} = \sigma A_H F_H \left(T_n^4 - T_H^4\right) - \pi \frac{D}{12} h \left(T_n - T_{sat}\right)$$

where

$$A_H F_H = P_H F_H$$

$$= \frac{1}{\frac{\rho}{\epsilon P_{n,0}} + \frac{1}{P_{n,0}} + \frac{\rho}{\epsilon P_H}}$$

$$= \frac{P_H}{\left(\frac{\rho}{\epsilon} + 1\right)\frac{P_H}{P_{n,0}} + \frac{\rho}{\epsilon}}$$

$$= \frac{2\pi r_n}{\left(\frac{\rho}{\epsilon} + 1\right)\frac{r_H}{r_n} + \frac{\rho}{\epsilon}}$$

D = nominal housing inside diameter

The mass of the four triangular filler rods, which was 20 percent of the housing mass, was lumped into the housing mass. The emissivities of the heater rods and housing were assumed to be the same, at a value of 0.70. The same transient reflood convective heat transfer coefficient was applied to both the heater rods and the housing. The decay rate was equivalent to the ANS + 20 percent power decay curve.

A similar model was developed for the 161-rod unblocked bundle in order to determine the effect of bundle size on the bundle thermal response. The 161-rod heater rod bundle was lumped into eight concentric cylinders with the housing as the outside cylinder (figure B-2). The same boundary and initial conditions were applied to 161-rod bundle model as to the 21-rod bundle model.

B-4. TEMPERATURE RESULTS

The results of this thermal analysis are shown in figures B-3 through B-6. Figure B-3 shows the initial radial temperature distribution for the following three 21-rod bundle cases:

-- Nominal power and unheated housing

-- Nominal power and heated housing

-- High power and heated housing

Because of the housing design temperature limit of 815°C (1500°F) at the midplane and 538°C (1000°F) at the ends, the housing was heated initially to a maximum of approximately 538°C (1000°F).

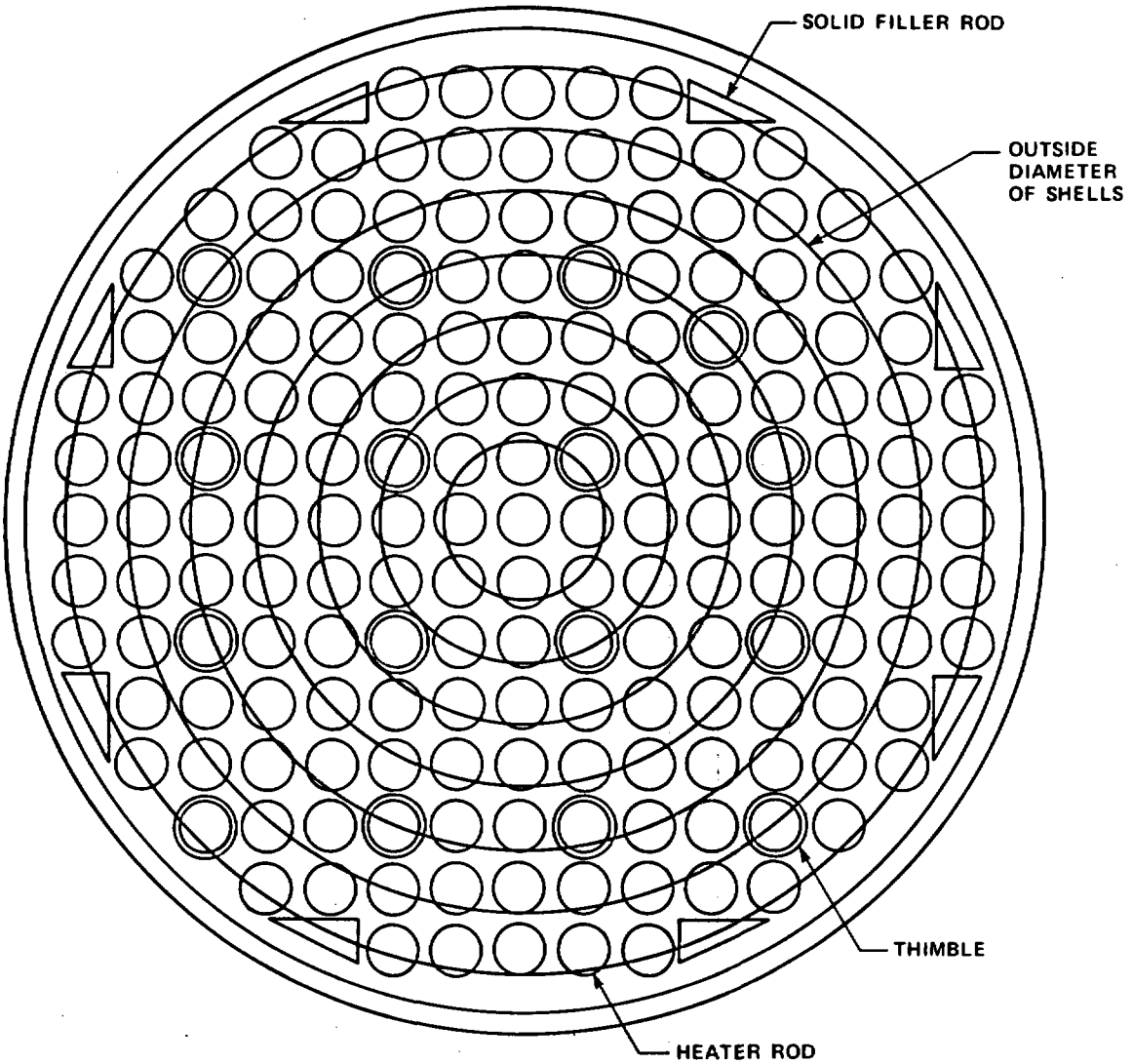

SHELL	NUMBER OF HEATER RODS IN SHELL
1	1
2	5.5
3	10
4	15.75
5	23
6	25.25
7	33.75
8	46.75
9	0
TOTAL	161

Figure B-2. 161-Rod Bundle Nine-Node Model

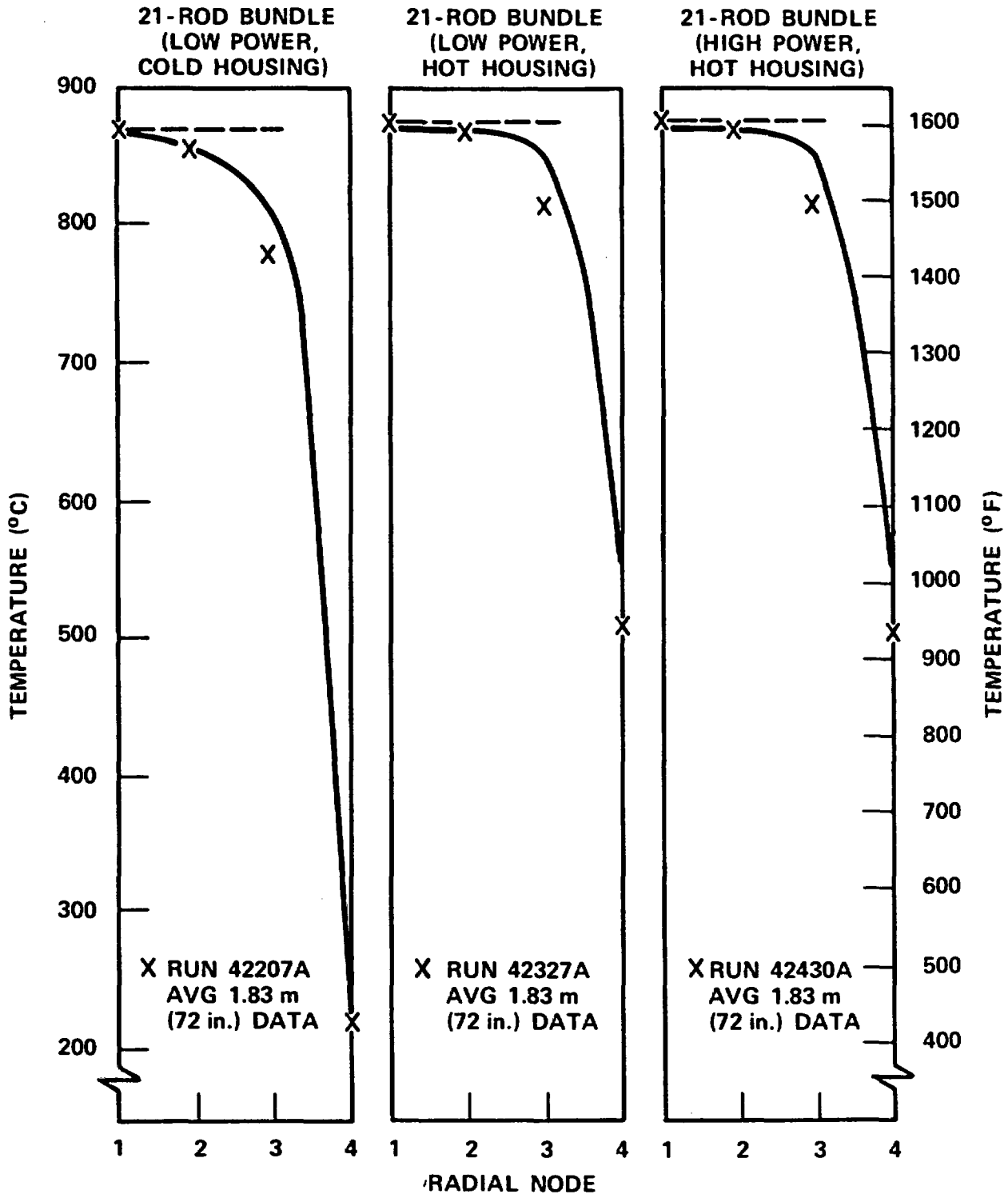

Figure B-3. Measured and Calculated Radial Temperature Distribution for 21-Rod Bundle Configuration A at Flood Time

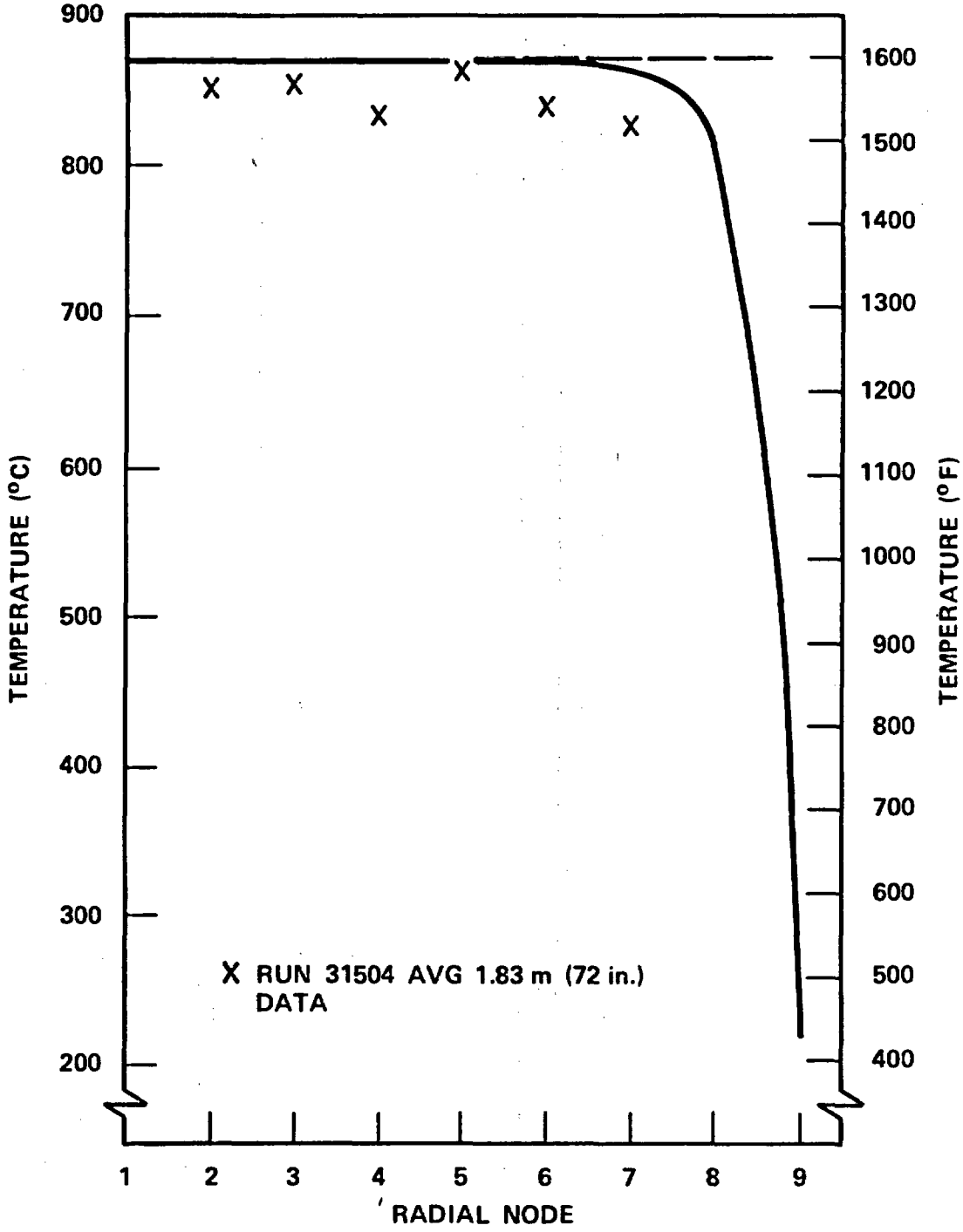

Figure B-4. Measured and Calculated Radial Temperature Distribution for 161-Rod Unblocked Bundle at Flood Time

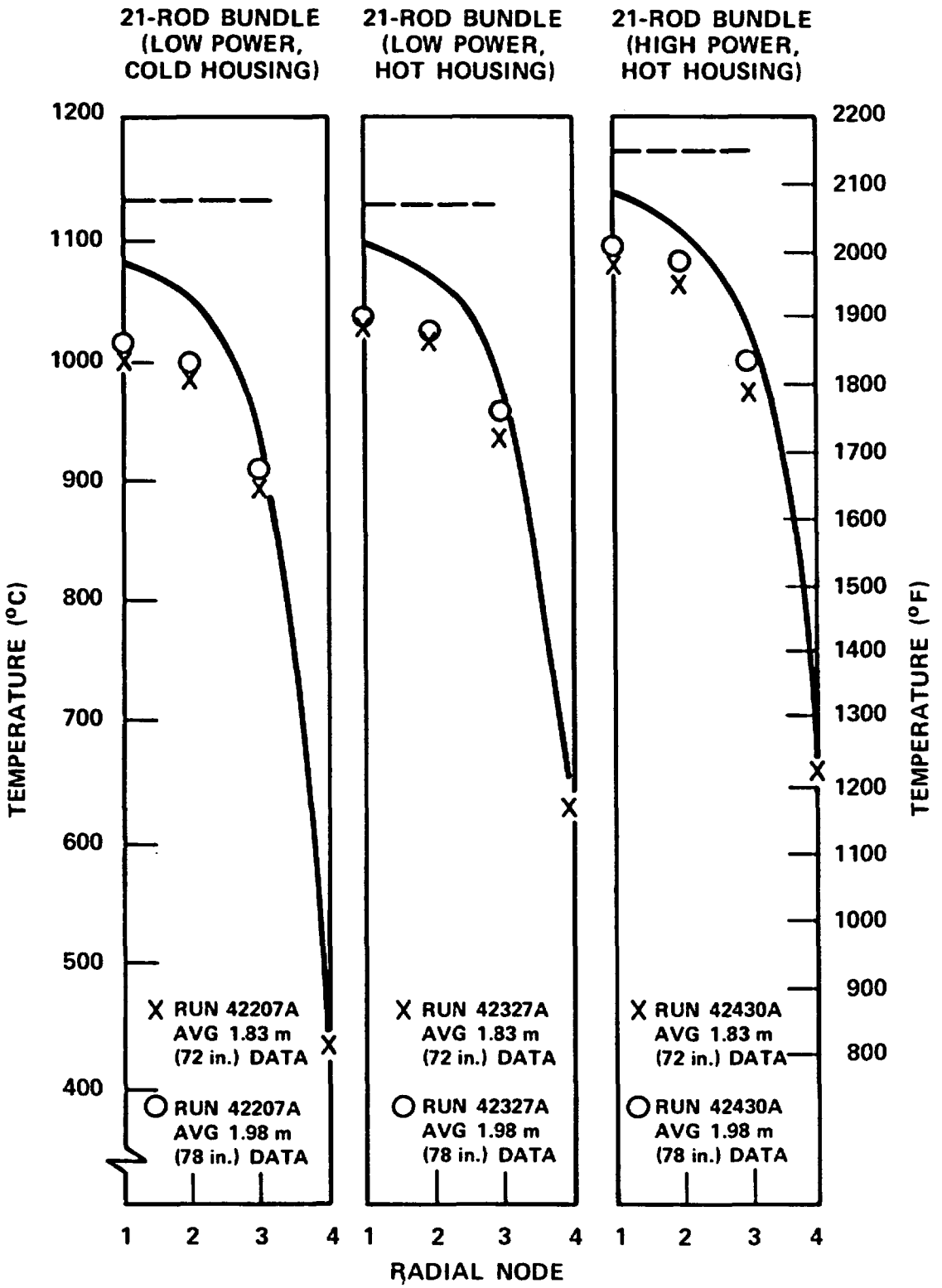

Figure B-5. Measured and Calculated Radial Temperature Distribution for 21-Rod Bundle Configuration A at Turnaround Time

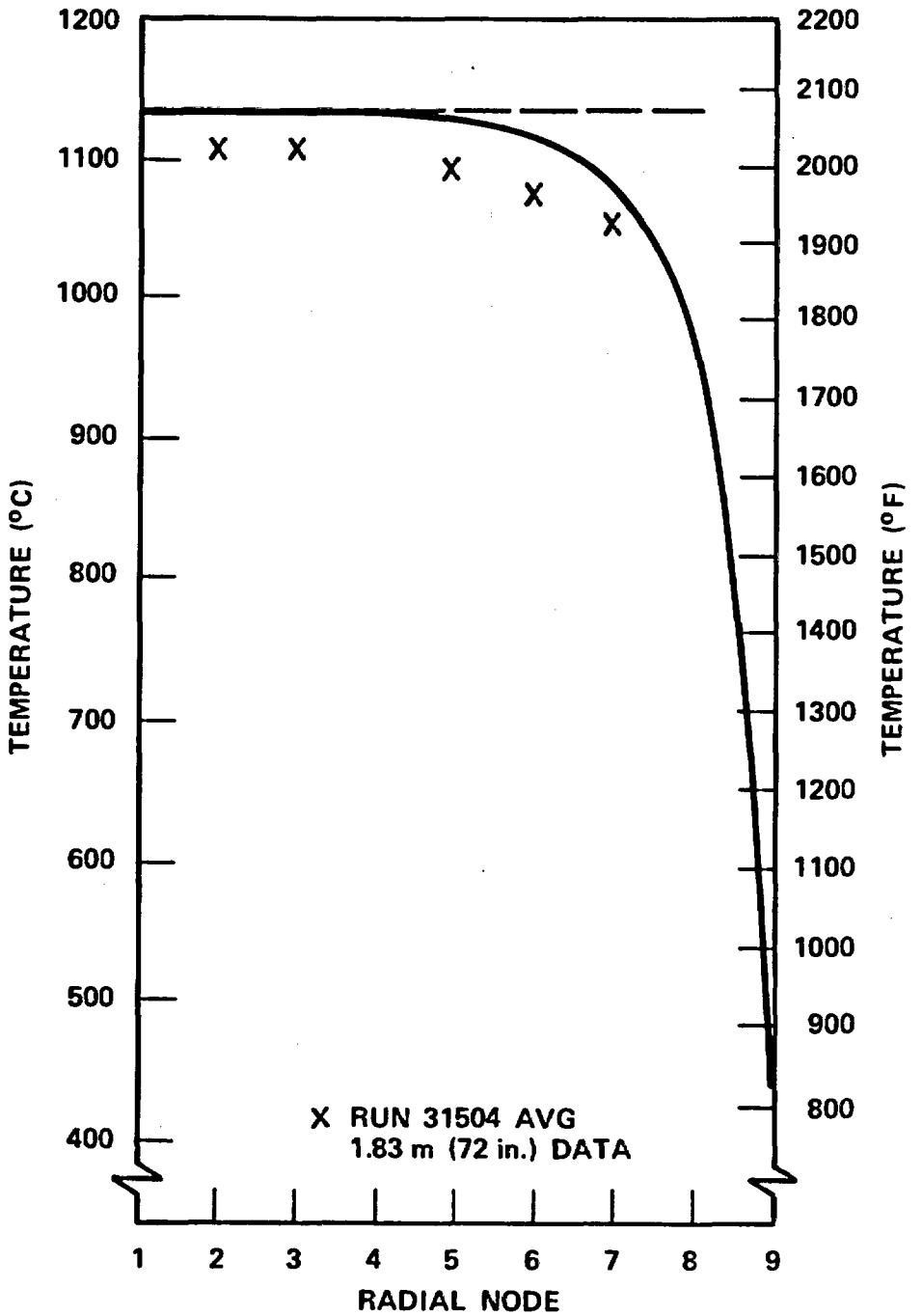

Figure B-6. Measured and Calculated 161-Rod Bundle Radial Temperature Distribution at Turnaround Time

Also shown in figure B-3 is the measured radial temperature distribution for the corresponding 21-rod bundle test conditions. The calculated and measured results should be compared only on a relative basis because of the difference in the respective heat transfer coefficients utilized (as discussed below). These figures indicate that when the 21-rod bundle housing is heated to approximately 538°C (1000°F), the temperatures of the second and third rows of heater rods are increased by approximately 14°C (25°F) and 39°C (70°F), respectively, thereby reducing the radial temperature gradient. The straight line in figure B-3 and all subsequent figures represents the calculated temperature distribution for the case with no housing.

Figure B-4 shows both the calculated and measured initial radial temperature distribution for the 161-rod bundle. The outer three rows of rods are calculated to have a temperature gradient similar to that of the 21-rod bundle with an unheated housing. The outer row of heater rods was not instrumented in the 161-rod bundle; therefore a comparison of the measured and calculated radial temperature gradient was not possible.

Figure B-5 shows the radial temperature distribution at the turnaround time for the previous three 21-rod bundle cases. Figures B-5a and B-5b show that when the housing is heated, the maximum heater rod temperature is increased by approximately 22°C (40°F). Also, the radial temperature gradient across the 21-rod bundle is reduced by approximately 28°C (50°F). However, since there was a large difference, approximately 106°C (190°F), in the hot rod temperature between 21-rod bundle with a heated housing and the 161-rod bundle (figure B-6), the rod power was subsequently increased to 2.6 kw/m (0.78 kw/ft) in order to compensate for (it was believed at the time) the excess flow area. This rod power increase reduced the hot rod temperature difference between the two bundles to approximately 50°C (90°F). It was learned later in the testing that the flooding rate was approximately 10 percent higher than specified.

Comparisons of the measured heat transfer coefficients from the 21-rod bundle and 161-rod bundle tests and the heat transfer coefficient utilized throughout this analysis are shown in figures B-7 and B-8 for heater rods close to housing and away from housing, respectively. The heat transfer coefficient utilized in this analysis was simply a pre-21-rod bundle test estimate of the reflood heat transfer.

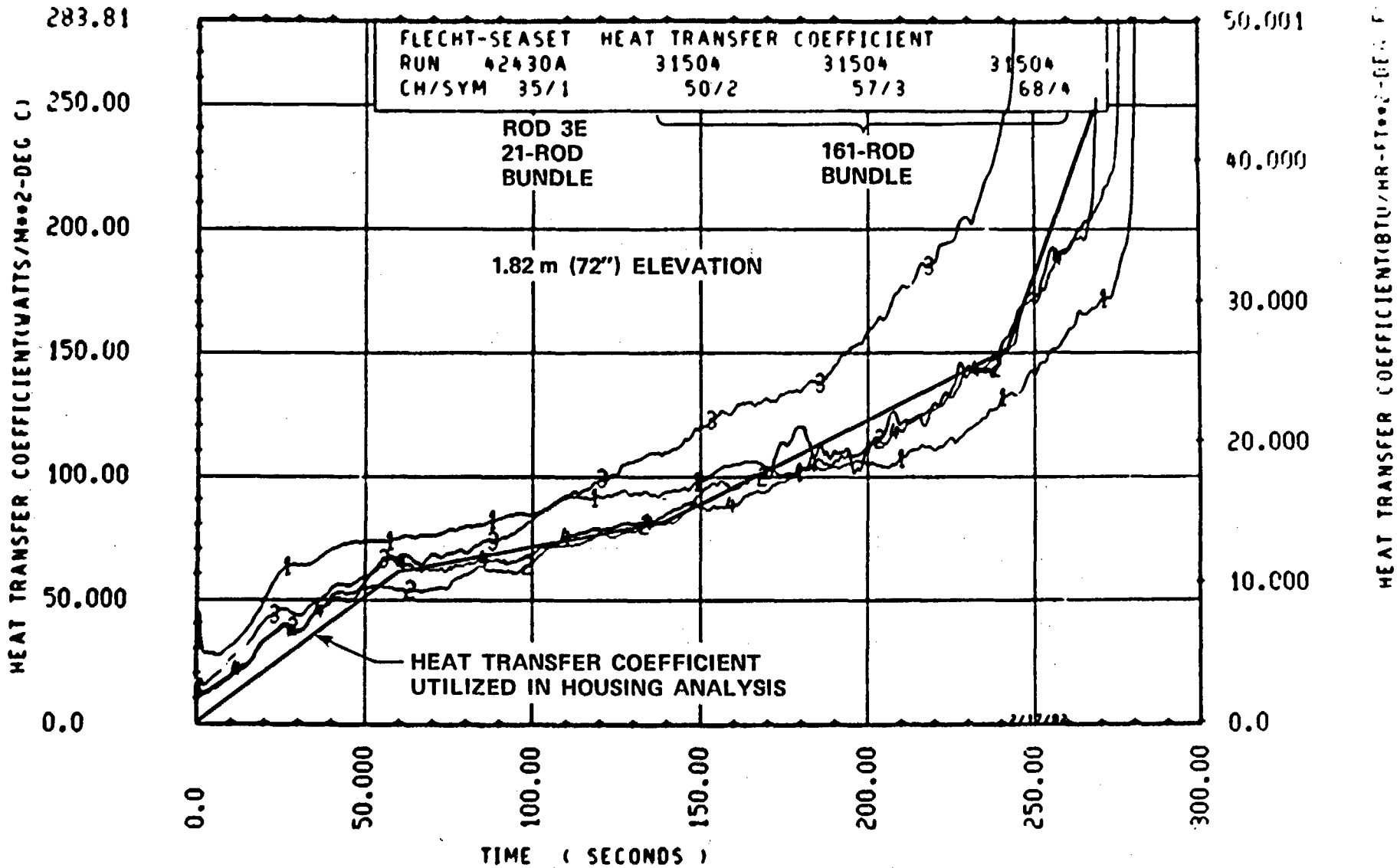

Figure B-7. Heat Transfer Coefficient Comparison, Outside Rods

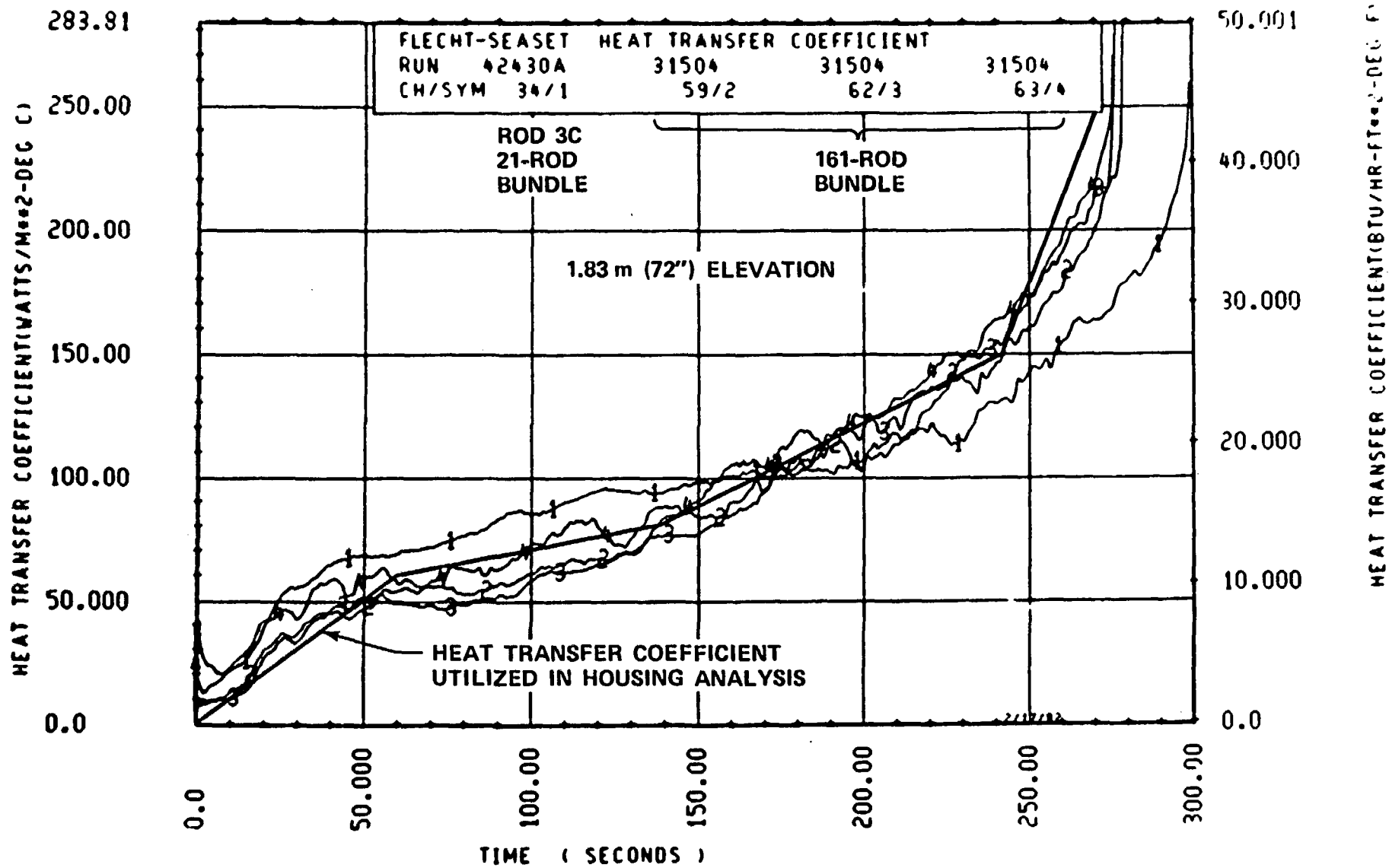

Figure B-8. Heat Transfer Coefficient Comparison, Center Rods

B-5. QUENCH FRONT RESULTS

The quench fronts for the following two 21-rod bundle tests were compared to the quench front for the corresponding 161-rod bundle test (run 31504):

-- Nominal power and unheated housing - run 42207A

-- High power and heated housing - run 42430A

The test with nominal power and heated housing (run 42327A) was terminated after hot rod turnaround because of a computer data acquisition system failure; therefore a quench front comparison was not possible. The quench front comparisons between the two 21-rod bundle tests and the 161-rod bundle test are shown in figures B-9 and B-10. The figures show that the 21-rod bundle heated housing test (run 42430A) provided a better comparison to the 161-rod bundle test. Although the test conditions were not exactly comparable among the three runs, it was believed at the time that to provide a quench front in the 21-rod bundle that was similiar to that of the 161-rod bundle, the rod power should be increased and the housing should be heated. The reflood tests in the first 21-rod bundle were conducted at these conditions until it was learned that the flooding rate was higher than specified, at which point the power was reduced to nominal.

B-6. CONCLUSIONS

As was expected, the housing had a significant effect on the thermal response of the 21-rod bundle. Although this effect was reduced by heating the housing to 538°C (1000°F), the large temperature gradient between the heater rods and housing of approximately 371°C (700°F) still had effects which could not be ignored. However, this housing effect was approximately the same in each of the six bundles; therefore, the measured data can be utilized on a comparative basis. Furthermore, by accounting for the energy stored in the housing and subsequently released by the housing, the measured data can be utilized more generically.

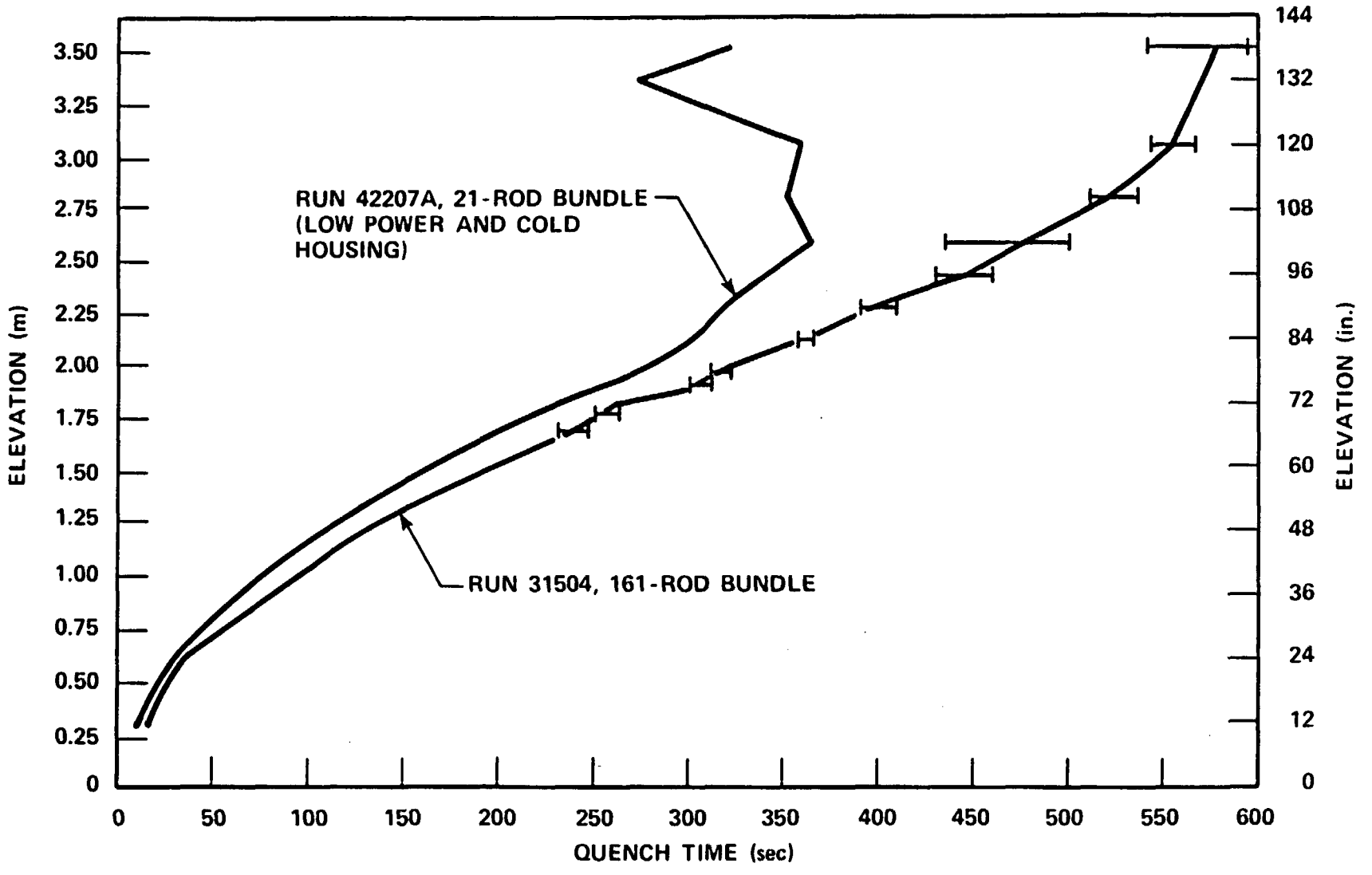

Figure B-9. Quench Front Comparison (161-Rod Test Run 31504 and 21-Rod Test Run 42207A)

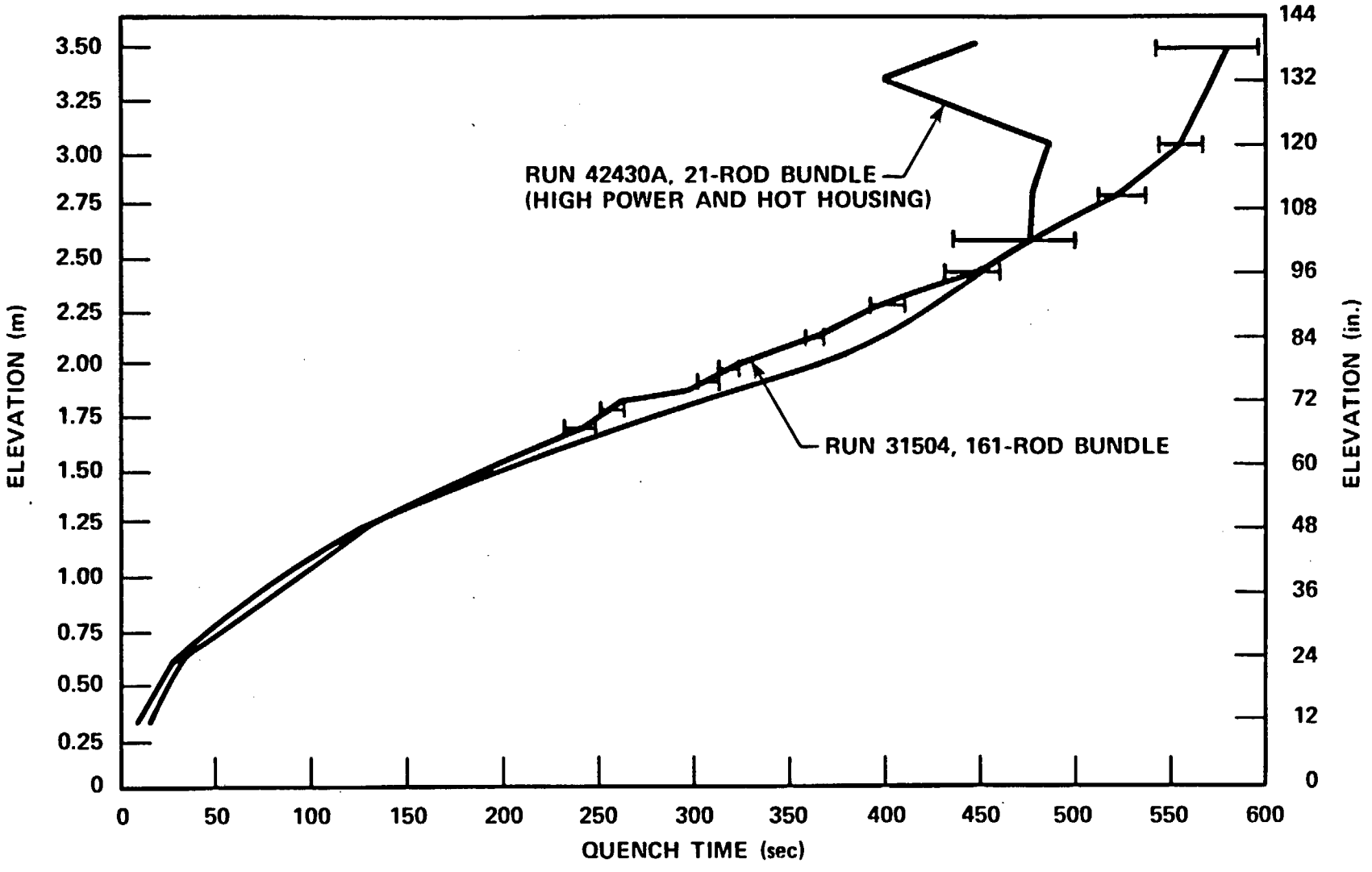

Figure B-10. Quench Front Comparison (161-Rod Test Run 31504 and 21-Rod Test Run 42430A)

APPENDIX C
BLOCKAGE SLEEVE SELECTION

C-1. GENERAL

This appendix discusses the bases of choice between the long and short sleeves, using the test data of configurations A, C, D, and E. This process utilizes the COBRA results discussed in section 6. COBRA simulations of flows in the 163-rod bundle with 21-rod islands (see figure 3-9) were also performed, because the chosen sleeve will be used in the large bundle tests.

C-2. FLOW DIVERSION IN 163-ROD BUNDLE WITH BLOCKAGE

The sleeve choice should be based on resulting heat transfer in tests with enough bypass flow area to allow fluid bypass. The tests of the 21-rod bundle do not provide bypass flow area. Therefore, flow diversions in the large bundle with blockage islands (figure C-1) were calculated using COBRA-IV-I to estimate the heat transfer coefficients in the large bundle as described below. COBRA simulations of this large bundle were performed on half of the bundle to take advantage of bundle symmetry. All the simulation conditions were the same as those of the 21-rod bundle except for the channel and gap addresses. There were also slight changes in flow blockage factors for the peripheral subchannels of the blockage islands, since there was excess flow area in the peripheral subchannels of the 21-rod bundle.

The results, shown in figures C-2 through C-5, show clearly that flow diversion from the blockage islands is important. Figure C-2 shows the total flow rate ratios in the blocked island, figure C-3 the total flow rate ratios just outside the blocked island, and figures C-4 and C-5 show the total flow rate ratios one and two rows away from the blocked islands, respectively.

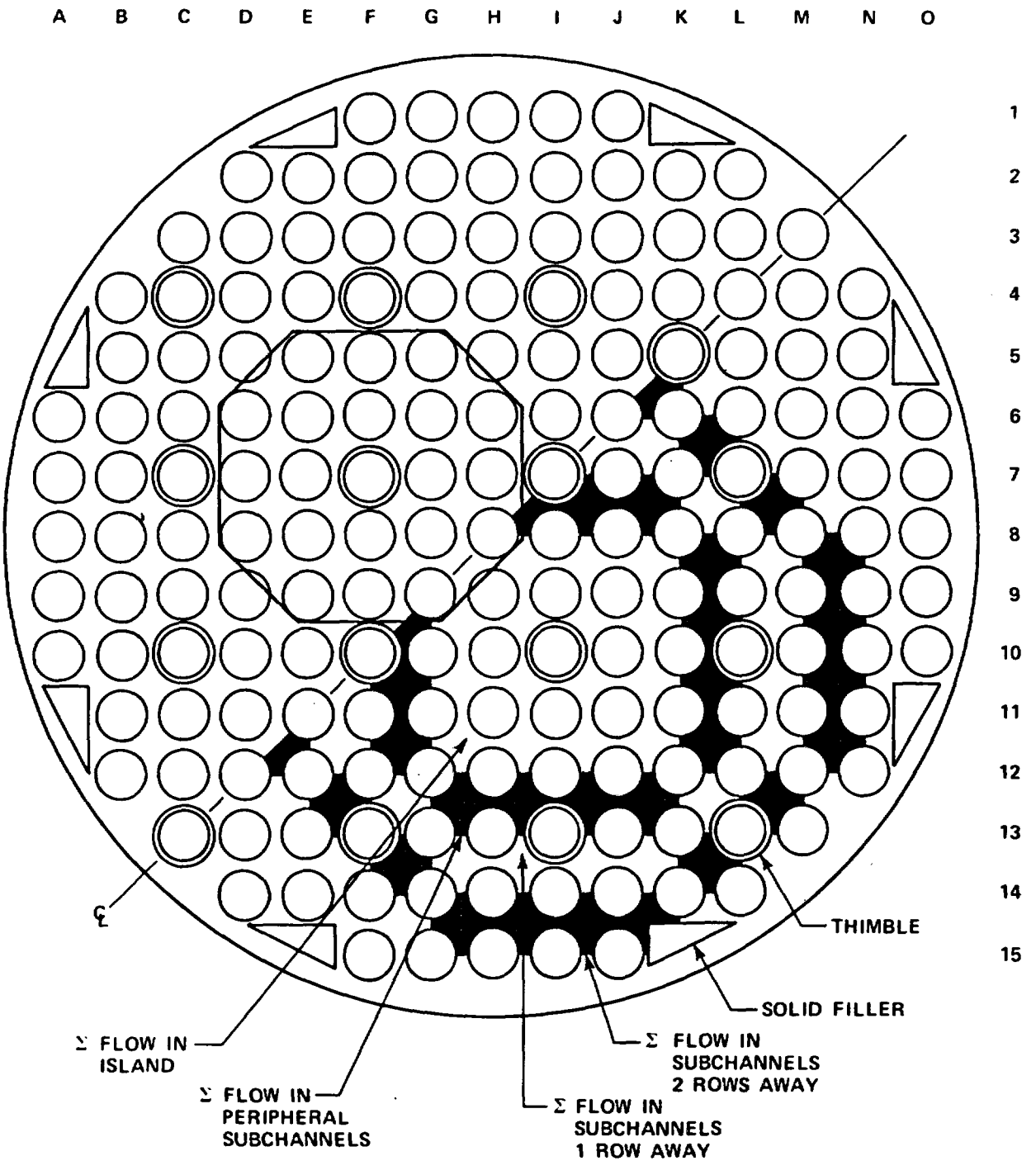

Figure C-1. 21-Rod Island in Large Blocked Bundle

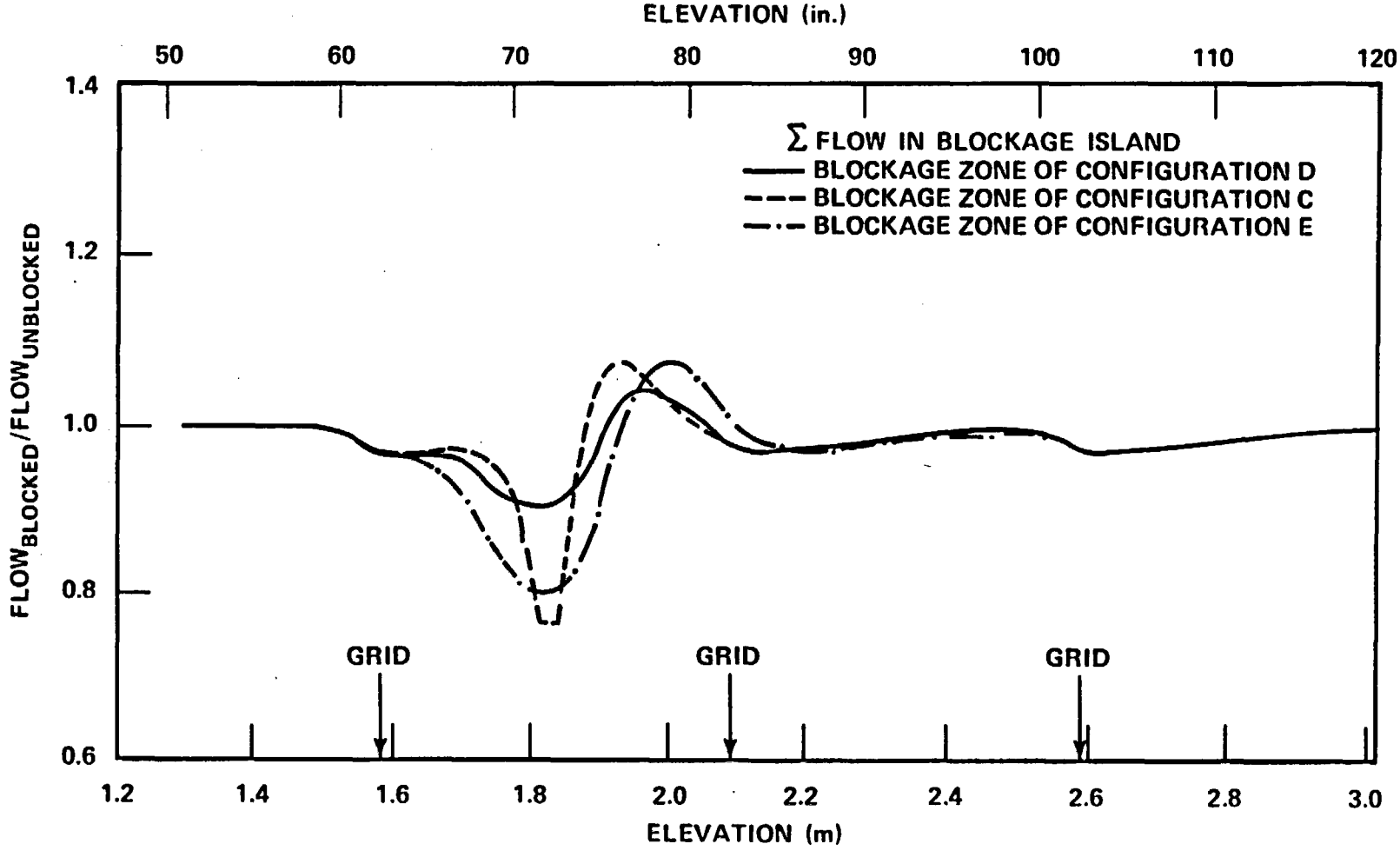

Figure C-2. Integrated Flow Diversion in Blocked Island of Large Bundle

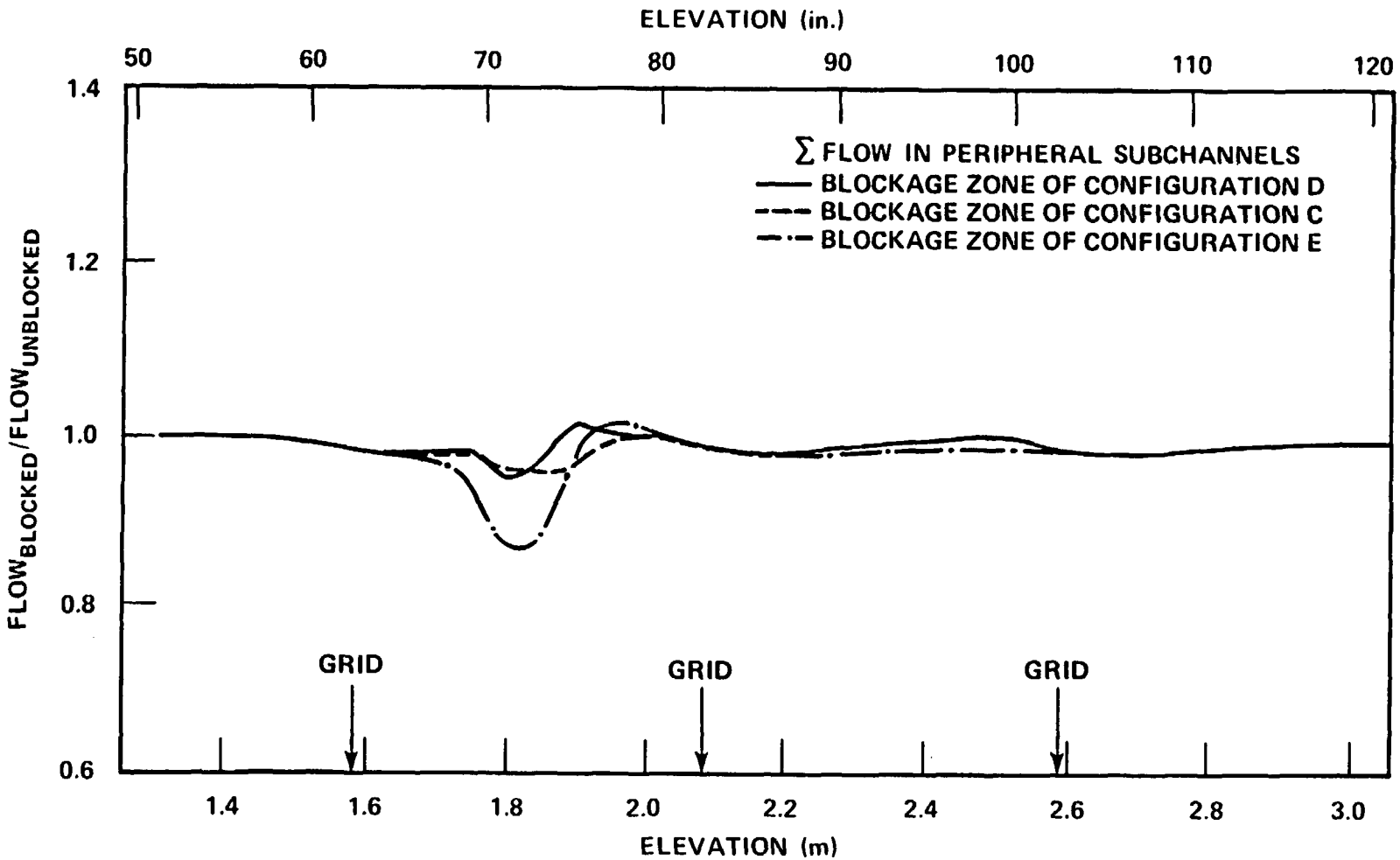

Figure C-3. Integrated Flow Diversion in Peripheral Subchannels of Blocked Island in Large Bundle

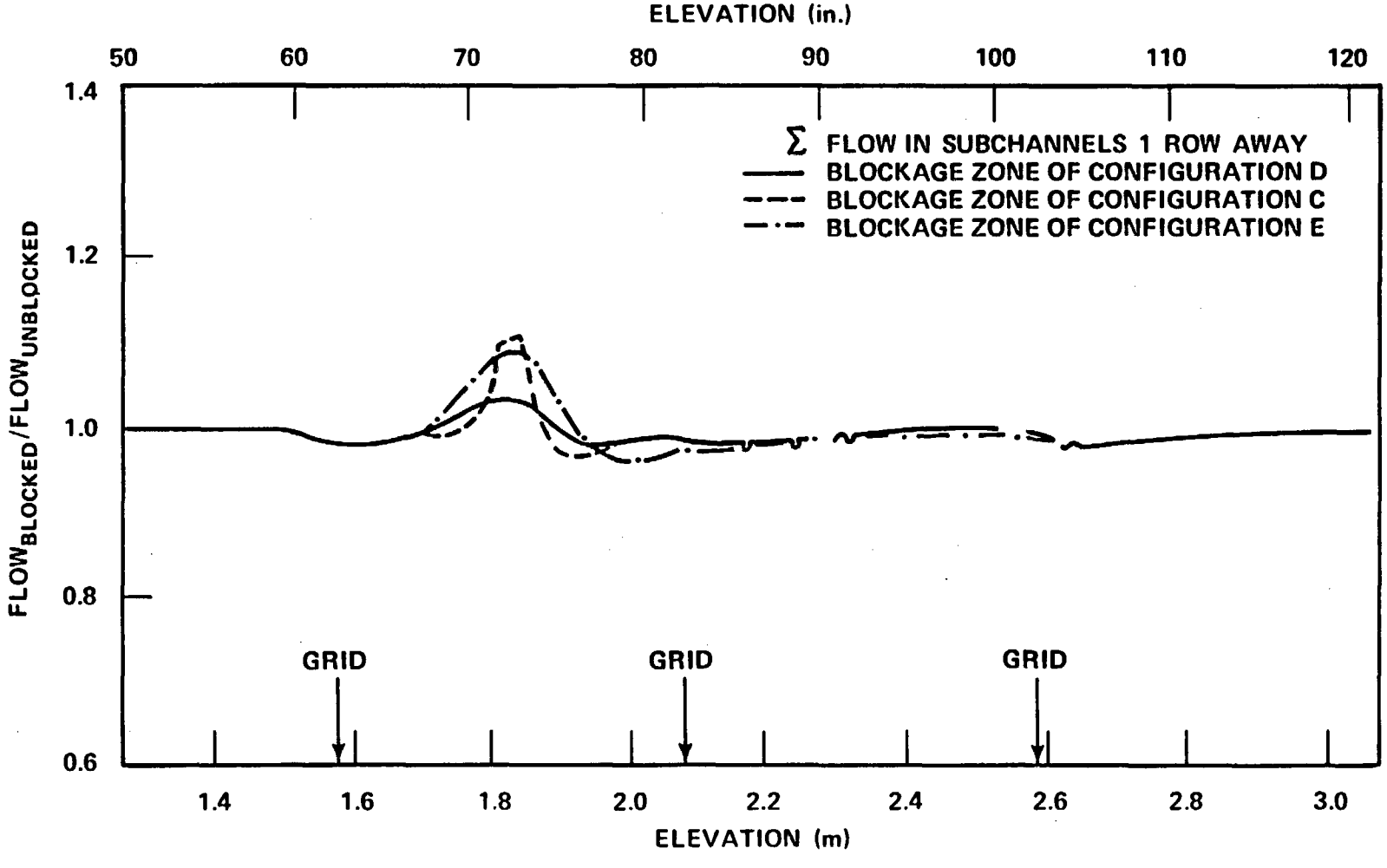

Figure C-4. Integrated Flow Diversion in Channels One Row Away From Blocked Island in Large Bundle

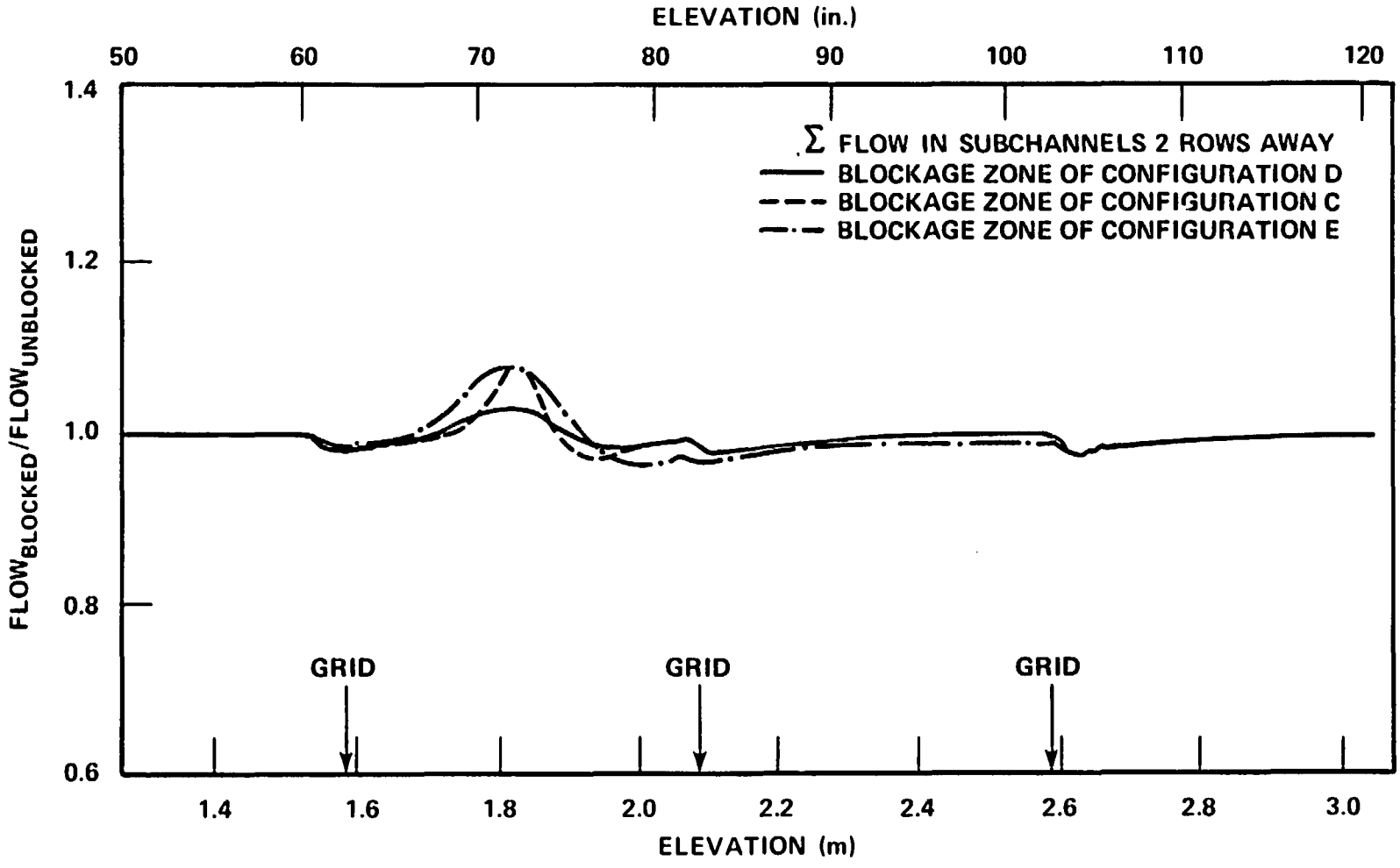

Figure C-5. Integrated Flow Diversion in Channels Two Rows Away From Blocked Island in Large Bundle

C-3. ESTIMATION OF HEAT TRANSFER COEFFICIENTS IN THE LARGE BUNDLE

The heat transfer coefficients in the large bundle with the partial blockages can be estimated using the following relationship:

$$\frac{h_{(i,Z,x,163)}}{h_{(i,Z,A,163)}} = Ne\left(\frac{U_{(i,Z,x,163)}}{U_{(i,Z,A,163)}}\right)^m \qquad \text{(C-1)}$$

where

- i = rod identification
- Z = axial elevation
- x = type of blockage
  - C - coplanar short sleeve
  - D - noncoplanar short sleeve
  - E - noncoplanar long sleeve
- A = unblocked bundle
- 163 = 163-rod bundle
- h = heat transfer coefficient
- Ne = enhancement factor
- U = velocity
- m = exponent (0.6-0.8)

The velocities in equation (C-1) are calculated by COBRA and the enhancement factor can be calculated from the 21-rod bundle test data, assuming that the factor is the same for both bundles. That is,

$$Ne_{(i,Z,x,163)} = Ne_{(i,Z,x,21)} \qquad \text{(C-2)}$$

$$= \left[\frac{h_{(i,Z,x,21)}}{h_{(i,Z,A,21)}} \Big/ \frac{U_{(i,Z,x,21)}}{U_{(i,Z,A,21)}}\right]^m$$

Since the heat transfer coefficients in the unblocked large bundle are available, equation (C-1) permits calculation of the expected heat transfer coefficients in the large bundle with blockages. A schematic diagram of the procedure used to obtain the heat transfer ratios is shown in figure C-6.

Some of the results of the reference tests using the constant 0.8 as the exponent m are shown in figure C-7 for the blockage islands corresponding to bundle configurations C, D, and E. (Configuration C is considered to discern the sleeve distribution effect.) The figures show that the enhancement factors reach a peak during the first 20 to 30 seconds and then decrease to a fairly uniform value. It appears that the blockage effects on heat transfer during these two periods are different from each other. Comparisons of heat transfer among the three bundles at early and late times in the test are shown in table C-1. The comparisons of the heat transfer are summarized as follows:

-- For later times (>30 sec), below 1.98 m (78 in.), configuration E is the lowest for all inner thermocouples (thermocouples on the inner nine rods). Configuration E is generally the lowest for outer thermocouples, in most cases.

-- For early times (<30 seconds), many cases show D<E.

-- At 1.88 m (74 in.), where all cases have blockage, E is the lowest even during the early time.

-- At 1.96 m (77 in.), usually D≃E for the early time period.

-- During the early period above 2.59 m (102 in.), the ratios oscillate. This is possibly due to small-magnitude errors in the heat transfer coefficient.

-- At the later time for 2.59 m (102 in.), E is the lowest except at rod 1D.

-- At 2.82 and 3.05 m (111 and 120 in.), trends are mixed.

Because of the observed contradictory behavior between the two periods, it was not immediately clear which sleeve should be chosen. To resolve this difficulty, it was

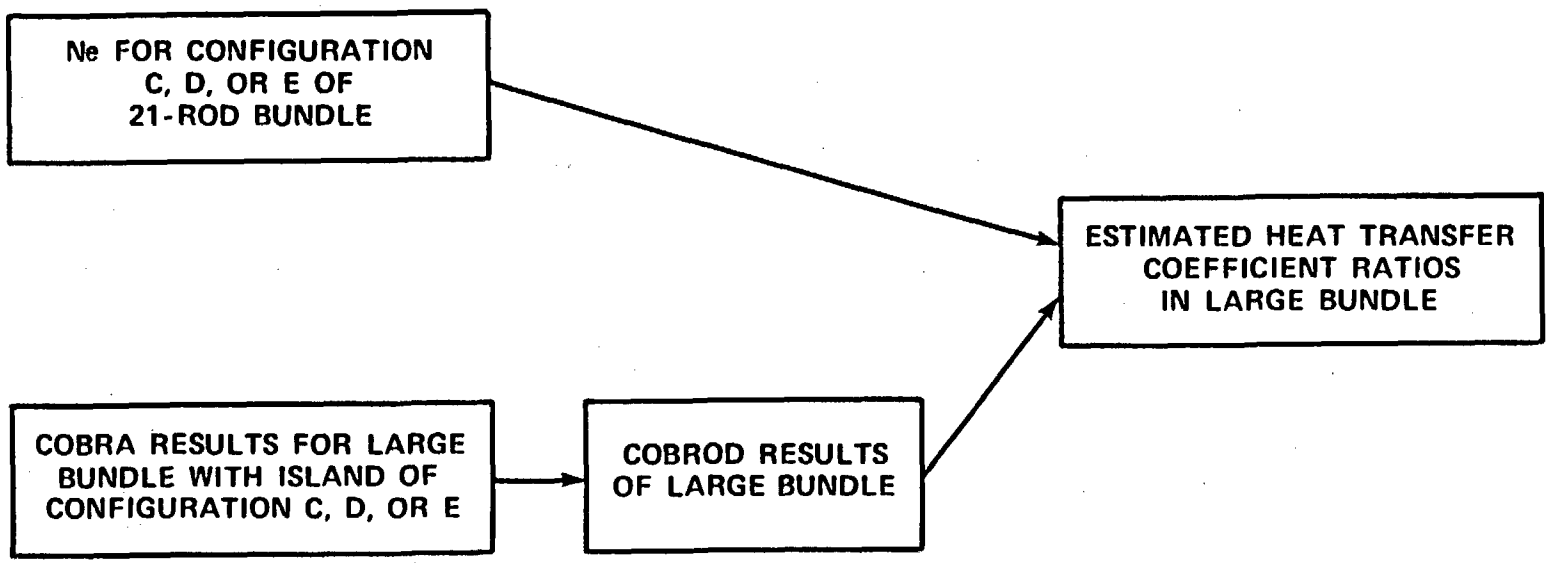

Figure C-6. Estimation of Heat Transfer Coefficient Ratios

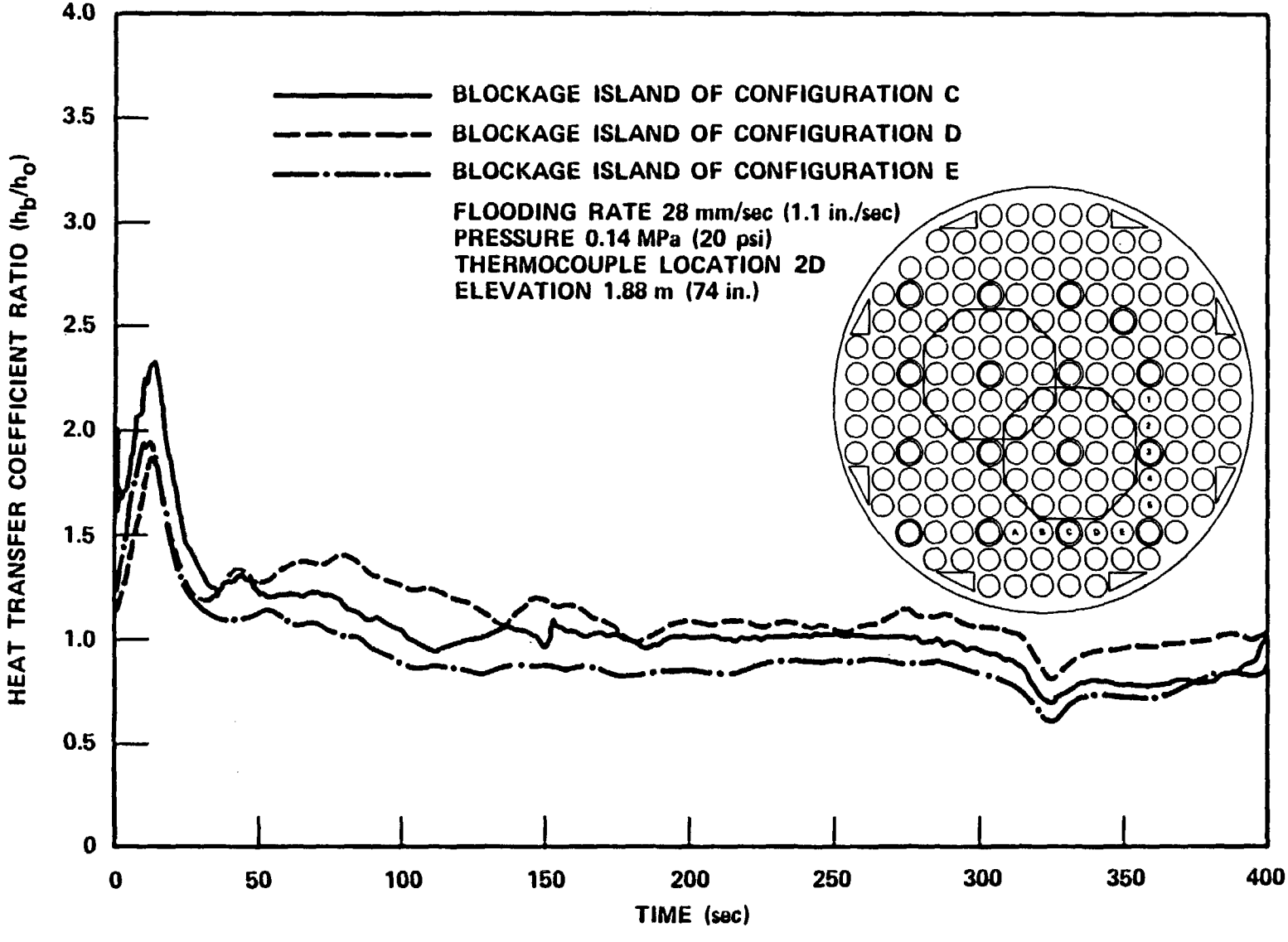

Figure C-7. Estimated Heat Transfer Coefficient Ratios (sheet 1 of 3)

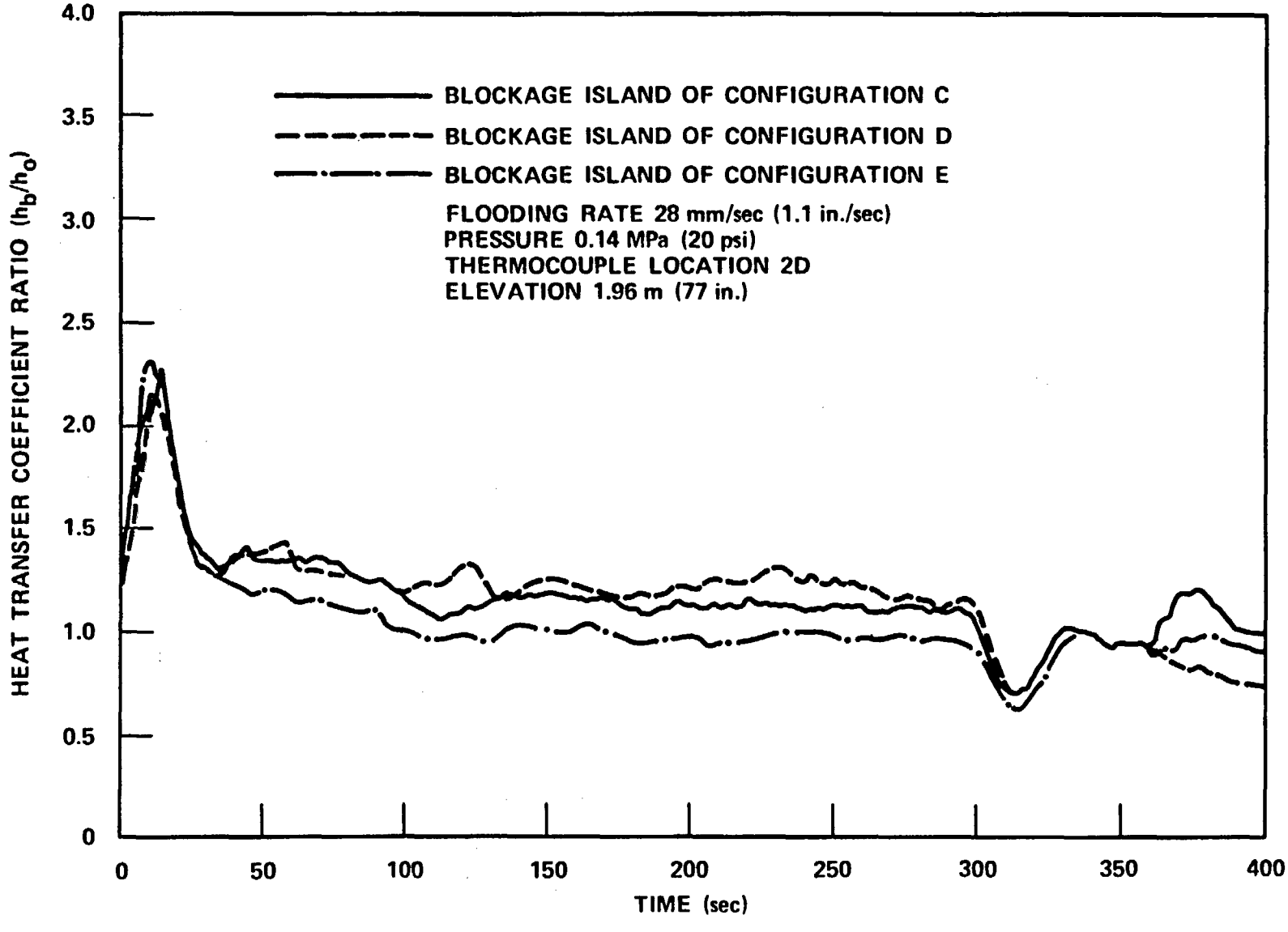

Figure C-7. Estimated Heat Transfer Coefficient Ratios (sheet 2 of 3)

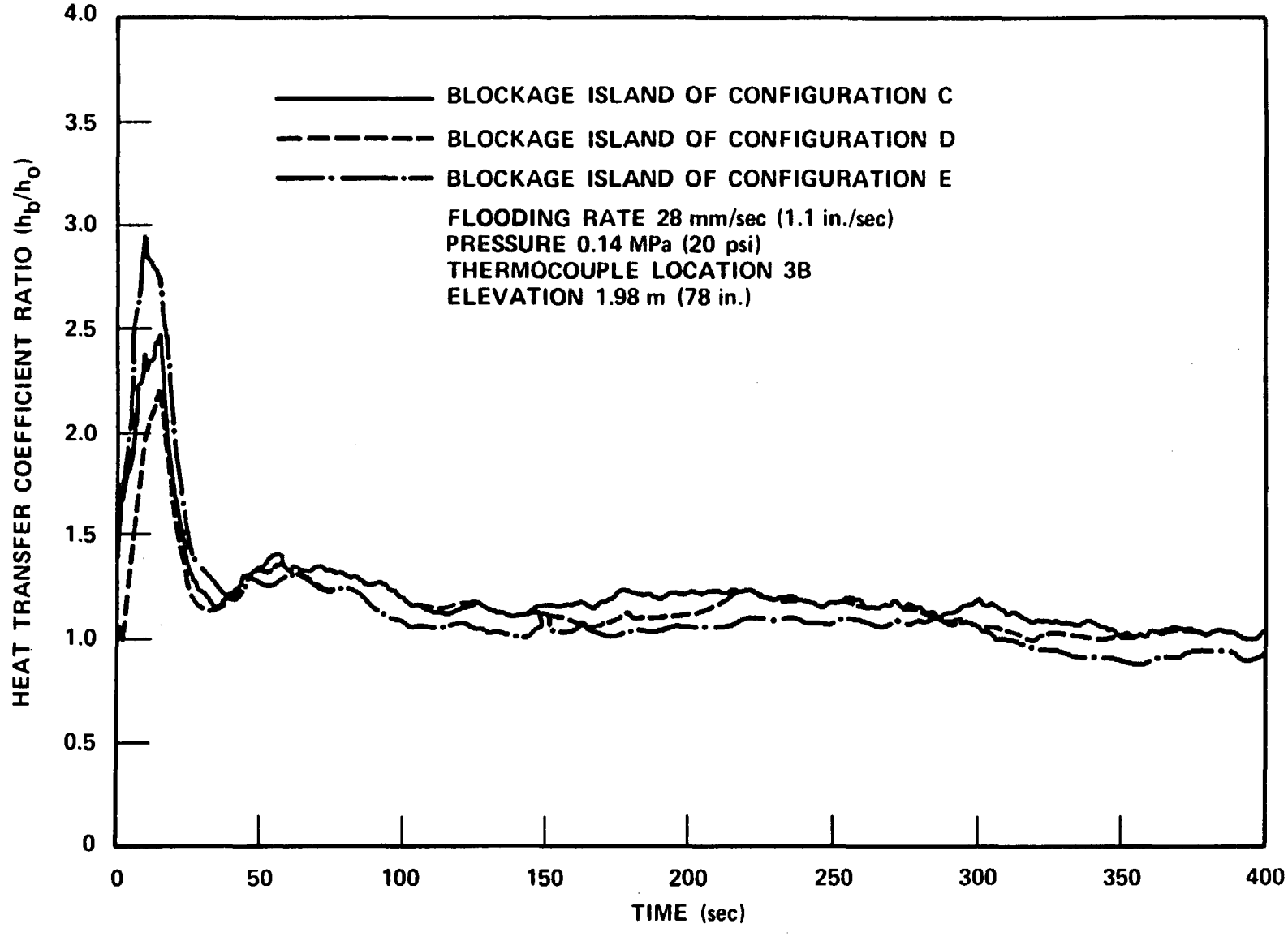

Figure C-7. Estimated Heat Transfer Coefficient Ratios (sheet 3 of 3)

TABLE C-1

CALCULATED HEAT TRANSFER COMPARISONS

Rod	Elevation [m (in.)]	Run 42430A 28 mm/sec (1.1 in./sec) 0.28 MPa (40 psi)		Run 42606A 23 mm/sec (0.91 in./sec) 0.28 MPa (40 psi)		Run 43112A 28 mm/sec (1.1 in./sec) 0.14 MPa (20 psi)		Run 42804A 13 mm/sec (0.52 in./sec) 0.28 MPa (40 psi)	
		Early	Later	Early	Later	Early	Later	Early	Later
2D	1.88(74)	E≈D<C	E<D≈C	E<D<C	E<D<C	D≈E<C	E<C<D	E<D<C	E<C<D
2D	1.96(77)	E≈D≈C	E<D≈C	E≈D≈C	E<D<C	D≈C≈E	E<C<D	E≈D<C	E<D≈C
4C	1.98(78)	-	E<D<C	-	E<D<C	-	E<D<C	-	E<D≈C
3B	1.98(78)	C≈D<E	E<D<C	D<C<E	E<D<C	D<C<E	E<D<C	E≈D≈C	E≈D≈C
3C	1.98(78)	C<D≈E	E<D<C	D≈C≈E	E<D<C	D≈C≈E	E<D<C	C<D≈E	E<C≈D
3D	2.13(84)	C≈D<E	E<D≈C	D<C<E	?	D<C<E	E<C<D	C≈D<E	C<E≈D
2C	2.29(90)	D<C≈E	D≈C≈E	D<E<C	C<E≈D	D<C<E	D≈C≈E	D<C≈E	D<C<E
3B	2.29(90)	C<D≈E	E<D<C	D<C<E	D<E<C	D≈C<E	D≈C≈E	E<D≈C	E<D<C
3B	2.44(96)	-	E<D<C	-	E<D<C	-	E<C<D	-	E=C=D
5C	2.44(96)	C≈D≈E	C≈D≈E	D≈C≈E	D≈C≈E	C≈D<E	E<C<D	-	E≈C≈D
1C	2.59(102)	-	E<C<D	-	E<C<D	-	E<C<D	-	E≈C≈D
3D	2.82(111)	-	D≈C≈E	-	D≈C≈E	-	D≈C≈E	-	C≈E≈D
4C	2.82(111)	-	E≈D<C	-	D<E<C	-	E<D<C	-	C≈E≈D
1D	1.90(75)	E≈D≈C	E<C<D	-	E<D<C	E≈C≈D	E<C<D	E<C<D	E<C<D
5D	1.90(75)	D<C<E	E<C<D	D≈C<E	E<D<C	D<C<E	E<C<D	E<C<D	E<D<C
4A	1.93(76)	C<D<E	E≈C<D	C<D<E	E≈D≈C	C<D<E	E≈C<D	E<C≈D	E<D≈C

TABLE C-1 (cont)

CALCULATED HEAT TRANSFER COMPARISONS

Rod	Elevation [m (in.)]	Run 42430A		Run 42606A		Run 43112A		Run 42804A	
		Early	Later	Early	Later	Early	Later	Early	Later
1D	1.96(77)	C<D<E	E≈C≈D	E<D<C	E≈C≈D	D≈C<E	E≈C<D	C<D≈E	E<D<E
2D	1.96(77)	E≈D≈C	E<D<C	D<E<C	E<D<C	D≈C≈E	E<C<D	D≈E<C	E<D<C
5D	1.96(77)	C<D<E	E≈C<D	C<D<E	E≈D<C	C≈D<E	C≈E≈D	E≈D<C	E≈D≈C
4A	1.98(78)	C<D<E	C<E<D	C<D<E	C≈E≈D	C<D<E	C<E<D	C<D<E	C<D<E
4E	1.98(78)	C<E	E<C	C<E	E<C	C<E	C≈E	C<E	C<E
1C	2.13(84)	C<E<D	D<E<C	E≈C	E≈C	C<E	E≈C	C<E	C<E
2B	2.13(84)	C<E	E≈C	D<C<E	-	D≈C≈E	D<C≈E	D<C<E	D<C<E
4D	2.13(84)	E≈C	E<C	E≈C	E<C	C<E	E<C	-	-
5B	2.13(84)	C≈E≈D	E≈C<D	-	E<D<C	D<C<E	E<C<D	D≈E<C	D≈C≈E
2E	2.29(90)	C<E<D	E≈C≈D	C<D<E	-	C<D<E	C<E<D	C<D≈E	C<E<D
3A	2.29(90)	C≈D	C≈D	-	-	C≈D	C≈D	C<D	D<C
3D	2.29(90)	E≈C	E<C	E≈C	C<E	C<E	C≈E	C<E	C<E
4B	2.29(90)	D<C<E	E<D<C	D<C<E	E≈D<C	D<C<E	E<D≈C	D<C<E	-
5C	2.29(90)	C≈D<E	E<C<D	E≈D≈C	E≈D≈C	C≈D<E	C≈E<D	C<E≈D	C≈E≈D
3E	2.29(90)	C<E<D	C<E<D	E<D	E<D	D<E	E<D	E<D	E<D
1C	2.44(96)	C<D<E	E<C<D	C≈D≈E	C≈D≈E	C≈E≈D	C≈E<D	C<E≈D	C<D<E
2E	2.44(96)	C<E<D	C<E<D	C<E<D	C<E<D	C<D<E	C<E<D	C<D≈E	C≈E<D
3D	2.44(96)	E≈C≈D	E≈C≈D	E≈D≈C	C<D<E	D<C<E	C≈E<D	E<C<D	C<D≈E
4D	2.44(96)	-	-	-	C<E	C≈E	C≈E	-	E≈C

TABLE C-1 (cont)

CALCULATED HEAT TRANSFER COMPARISONS

Rod	Elevation [m (in.)]	Run 42430A		Run 42606A		Run 43112A		Run 42804A	
		Early	Later	Early	Later	Early	Later	Early	Later
5B	2.44(96)	D<E<C	D<E<C	E≈D<C	D≈E<C	D<E<C	E<C<D	D<E<C	D<C<E
1D	2.59(102)	-	D<E<C	-	D<E<C	D<E<C	D≈E<C	-	D<C<E
2C	2.59(102)	-	E<D	-	E<D	-	E<D	-	E≈D
4B	2.59(102)	-	E<D<C	-	E<C≈D	-	E<C<D	-	C≈E≈D
5B	2.59(102)	-	E≈D	-	E<D	-	E<D	-	E<D
5D	2.59(102)	-	-	D<C<E	-	-	E≈C≈D	-	E<C≈D
2A	2.82(111)	E<D	E<D	E<D	E<D	E<D	E<D	-	-
4E	2.82(111)	C<E	C<E	C<E	C<E	C<E	C<E	-	C≈E
1C	3.05(120)	-	D<C<E	-	D<E≈C	-	D≈C≈E	-	-
1D	3.05(120)	-	E<D<C	-	E<D<C	-	D<E<C	-	-
2C	3.05(120)	-	C<E<D	-	C≈D≈E	-	C≈E<D	-	-
4B	3.05(120)	-	-	-	E<D<C	-	E<C<D	-	-
5B	3.05(120)	-	C<D<E	-	-	-	-	-	-
5D	3.05(120)	-	-	-	-	-	C<D<E	-	-

necessary to learn the effect of the early-period behavior on the peak clad temperature up to the turnaround time, because this is the most important period. This can be done by calculation of the clad temperatures or temperature rises by constructing expected temperature histories in the large bundle, as discussed below. In the following discussion, only blockage configurations D and E are considered, since it was found that configuration C blockage usually did not give poorer heat transfer.

C-3. ESTIMATION OF TEMPERATURE HISTORY IN LARGE BUNDLE

Assuming that each rod is homogeneous radially, for simplicity, a one-dimensional heat balance equation can be written as

$$A\rho C_p \frac{dT}{dt} = Q' - hS\ (T - T_{sat}) \qquad \text{(C-3)}$$

where

A = rod cross-sectional area
ρ = rod density
C_p = rod heat capacity
T = temperature
t = time
Q = heat generation rate
h = heat transfer coefficient at rod surface
S = rod peripheral length
T_{sat} = saturation temperature

The terms $A\rho C_p$ and S can be estimated using the rod design information (see appendix P), and Q' from the rod design and power decay factor curve. The heat transfer coefficient can be estimated by

$$h(t) = (h_b)_{163} = \left(\frac{h_b}{h_o}\right)_{161} (h_o) \qquad \text{(C-4)}$$

where h_o is the heat transfer coefficient in an unblocked bundle. In equation (C-4), h_o should ideally be taken from the large unblocked bundle test, but unfortunately there were only two overlapping test conditions at a flooding rate of approximately 25 mm/sec (1 in./sec). For these two cases, h(t) was estimated by using $(h_o)_{161}$. Four other cases were also studied using the heat transfer coefficient obtained from the 21-rod bundle, configuration A test. This procedure was programmed into HEATUP (appendix P). The results are compared in table C-2. Actual temperature rise information is provided in tables C-3 through C-8.

TABLE C-2

SUMMARY OF TEMPERATURE RISE COMPARISONS
FOR LARGE BUNDLE WITH PARTIAL BLOCKAGE

Flooding Rate [mm/sec (in./sec)]	Pressure [MPa (psia)]	Source of h_o (bundle)	No. of Thermocouples Where $\Delta T_E > \Delta T_D$	No. of Thermocouples Where $\Delta T_D > \Delta T_E$	No. of Thermocouples where $\Delta T_D \approx \Delta T_E$[a]
1.1	0.28 (40)	161[b]	11	1	3
1.1	0.14 (20)	161[b]	11	0	1
1.1	0.28 (40)	21	9	3	3
1.1	0.14 (20)	21	4	5	6
0.9	0.28 (40)	21	11	3	1
0.5	0.28 (40)	21	8	3	4

a. Within 11°C (20°F)

b. Considering 21-rod island corresponding to 21-rod bundle tests

These results show that, in most cases, blockage in configuration E will give a higher temperature rise in the large bundle. Therefore, the long nonconcentric sleeve is expected to provide poorer heat transfer than the short concentric sleeve.

Figure C-8 plots the measured turnaround time versus the flooding rates. As expected, the lower the flooding rate, the longer the turnaround time. The longer turnaround time means more significant contribution of the later period effect, in which configuration E consistently showed poorer heat transfer.

Therefore, it is concluded that the long nonconcentric sleeve should be used for the large blocked bundle tests.

TABLE C-3

CALCULATED TEMPERATURE RISES,
CASE 1[a]

Rod	Elevation [m (in.)]	D Island		E Island	
		Channel	ΔT [°C(°F)]	Channel	ΔT [°C(°F)]
2D	1.88 (74)	50	238.1 (428.7)	39	342.6 (616.8)
1D	1.90 (75)	61	305.2 (549.4)	44	353.2 (635.9)
5D	1.90 (75)	68	295.0 (531.1)	46	323.0 (581.4)
4A	1.93 (76)	78	257.6 (463.7)	51	286.4 (515.5)
1D	1.96 (77)	82	268.5 (483.4)	58	297.6 (535.7)
2D	1.96 (77)	84	176.2 (317.2)	61	272.2 (490.0)
5D	1.96 (77)	89	266.5 (479.7)	66	274.8 (494.7)
3B	1.98 (78)	96	210.5 (379.0)	71	234.6 (422.4)
3C	1.98 (78)	97	190.1 (356.6)	72	262.5 (472.6)
4A	1.98 (78)	100	257.1 (462.9)	73	257.4 (463.4)
3D	2.13 (84)	115	266.5 (479.7)	98	292.7 (527.0)
5B	2.13 (84)	117	220.6 (397.2)	103	322.1 (579.9)
2C	2.29 (90)	122	367.4 (661.3)	111	341.1 (614.1)
2E	2.29 (90)	123	375.0 (675.0)	113	395.4 (711.8)
3B	2.29 (90)	125	344.2 (619.6)	115	350.1 (630.3)

SUMMARY

$(\Delta T)_E > (\Delta T)_D$	$(\Delta T)_D > (\Delta T)_E$	$(\Delta T)_D \approx (\Delta T)_E$
11	1	3

a. $(h_o)_{161}$
27.9 mm/sec (1.1 in./sec) flooding rate
0.28 MPa (40 psi) pressure

TABLE C-4

CALCULATED TEMPERATURE RISES,
CASE 2[a]

Rod	Elevation [m (in.)]	D Island		E Island	
		Channel	ΔT [°C(°F)]	Channel	ΔT [°C(°F)]
2D	1.88 (74)	50	179.1 (322.4)	39	317.5 (571.6)
1D	1.90 (75)	61	283.3 (510.0)	44	393.2 (707.9)
5D	1.90 (75)	68	310.4 (558.7)	46	369.4 (664.9)
4A	1.93 (76)	78	262.8 (473.1)	51	291.6 (525.0)
1D	1.96 (77)	82	179.6 (323.4)	58	-
2D	1.96 (77)	84	132.4 (238.4)	61	168.0 (302.4)
5D	1.96 (77)	89	213.2 (416.2)	66	293.0 (527.5)
3B	1.98 (78)	96	148.7 (267.6)	71	-
3C	1.98 (78)	97	129.4 (232.9)	72	-
4A	1.98 (78)	100	210.0 (378.0)	73	240.1 (432.2)
3D	2.13 (84)	115	197.1 (355.9)	98	246.1 (443.0)
5B	2.13 (84)	117	160.2 (288.3)	103	275.5 (499.6)
2C	2.29 (90)	122	250.5 (450.9)	111	262.9 (473.3)
2E	2.29 (90)	123	274.7 (494.5)	113	390.1 (702.3)
3B	2.29 (90)	125	255.1 (405.2)	115	364.2 (655.6)

SUMMARY

$(\Delta T)_E > (\Delta T)_D$	$(\Delta T)_D > (\Delta T)_E$	$(\Delta T)_D \approx (\Delta T)_E$
11	0	1

a. $(h_o)_{161}$
27.9 mm/sec (1.1 in./sec) flooding rate
0.14 MPa (20 psi) pressure

TABLE C-5

CALCULATED TEMPERATURE RISES,
CASE 3[a]

Rod	Elevation [m (in.)]	D Island		E Island	
		Channel	ΔT [°C(°F)]	Channel	ΔT [°C(°F)]
2D	1.88 (74)	50	141.3 (254.3)	39	215.1 (387.2)
1D	1.90 (75)	61	152.8 (275.1)	44	302.4 (364.3)
5D	1.90 (75)	68	164.3 (295.7)	46	189.0 (340.2)
4A	1.93 (76)	78	135.2 (243.3)	51	149.4 (269.0)
1D	1.96 (77)	82	147.9 (266.3)	58	171.3 (308.4)
2D	1.96 (77)	84	109.7 (197.4)	61	171.3 (308.3)
5D	1.96 (77)	89	161.9 (291.5)	66	158.7 (285.7)
3B	1.98 (78)	96	153.9 (277.0)	71	145.7 (262.2)
3C	1.98 (78)	97	161.1 (290.0)	72	188.9 (340.0)
4A	1.98 (78)	100	158.8 (285.8)	73	137.8 (248.0)
3D	2.13 (84)	115	169.0 (304.2)	98	147.8 (266.1)
5B	2.13 (84)	117	135.4 (243.8)	103	157.3 (283.1)
2C	2.29 (90)	122	212.4 (382.3)	111	179.3 (322.7)
2E	2.29 (90)	123	147.7 (265.8)	113	180.5 (324.9)
3B	2.29 (90)	125	184.0 (331.2)	115	189.0 (340.2)

SUMMARY

$(\Delta T)_E > (\Delta T)_D$	$(\Delta T)_D > (\Delta T)_E$	$(\Delta T)_D \approx (\Delta T)_E$
9	3	3

a. $(h_o)_{21}$
27.9 mm/sec (1.1 in./sec) flooding rate
0.28 MPa (40 psi) pressure

TABLE C-6

CALCULATED TEMPERATURE RISES,
CASE 4[a]

Rod	Elevation [m (in.)]	D Island		E Island	
		Channel	ΔT [°C(°F)]	Channel	ΔT [°C(°F)]
2D	1.88 (74)	50	127.6 (229.7)	39	182.9 (329.3)
1D	1.90 (75)	61	143.0 (257.4)	44	188.6 (339.6)
5D	1.90 (75)	68	165.0 (297.0)	46	166.8 (300.2)
4A	1.93 (76)	78	134.5 (242.2)	51	140.9 (253.6)
1D	1.96 (77)	82	139.7 (251.5)	58	148.0 (266.5)
2D	1.96 (77)	84	130.2 (234.4)	61	145.0 (261.0)
5D	1.96 (77)	89	162.7 (292.8)	66	134.4 (242.0)
3B	1.98 (78)	96	148.4 (267.1)	71	118.6 (213.5)
3C	1.98 (78)	97	154.6 (278.3)	72	154.2 (277.5)
4A	1.98 (78)	100	154.9 (278.9)	73	125.0 (225.0)
3D	2.13 (84)	115	135.4 (243.7)	98	91.6 (164.9)
5B	2.13 (84)	117	125.0 (225.1)	103	119.9 (215.8)
2C	2.29 (90)	122	161.0 (289.8)	111	109.8 (197.7)
2E	2.29 (90)	123	126.2 (227.1)	113	126.2 (227.1)
3B	2.29 (90)	125	144.0 (259.3)	115	171.3 (308.4)

SUMMARY

$(\Delta T)_E > (\Delta T)_D$	$(\Delta T)_D > (\Delta T)_E$	$(\Delta T)_D \approx (\Delta T)_E$
4	5	6

a. $(h_o)_{21}$
27.9 mm/sec (1.1 in./sec) flooding rate
0.14 MPa (20 psi) pressure

TABLE C-7

CALCULATED TEMPERATURE RISES,
CASE 5[a]

Rod	Elevation [m (in.)]	D Island		E Island	
		Channel	ΔT [°C(°F)]	Channel	ΔT [°C(°F)]
2D	1.88 (74)	50	200.1 (360.2)	39	305.2 (549.5)
1D	1.90 (75)	61	213.1 (383.7)	44	285.6 (514.2)
5D	1.90 (75)	68	224.4 (400.4)	46	295.1 (531.3)
4A	1.93 (76)	78	188.5 (339.3)	51	224.0 (403.3)
1D	1.96 (77)	82	196.0 (352.8)	58	328.1 (590.6)
2D	1.96 (77)	84	191.6 (344.9)	61	178.9 (322.1)
5D	1.96 (77)	89	215.4 (387.7)	66	288.6 (519.5)
3B	1.98 (78)	96	210.5 (379.0)	71	173.8 (312.9)
3C	1.98 (78)	97	222.2 (400.0)	72	160.8 (289.5)
4A	1.98 (78)	100	215.7 (388.3)	73	238.5 (429.4)
3D	2.13 (84)	115	259.8 (467.6)	98	282.6 (508.8)
5B	2.13 (84)	117	204.3 (367.8)	103	314.7 (566.6)
2C	2.29 (90)	122	309.1 (556.5)	111	218.5 (393.4)
2E	2.29 (90)	123	210.6 (379.2)	113	232.1 (417.9)
3B	2.29 (90)	125	269.3 (484.7)	115	288.2 (518.8)

SUMMARY

$(\Delta T)_E > (\Delta T)_D$	$(\Delta T)_D > (\Delta T)_E$	$(\Delta T)_D \approx (\Delta T)_E$
11	3	1

a. $(h_o)_{21}$
23 mm/sec (0.9 in./sec) flooding rate
0.28 MPa (40 psi) pressure

TABLE C-8

CALCULATED TEMPERATURE RISES,
CASE 6[a]

Rod	Elevation [m (in.)]	D Island		E Island	
		Channel	ΔT [°C(°F)]	Channel	ΔT [°C(°F)]
2D	1.88 (74)	50	80.8 (145.4)	39	131.2 (236.2)
1D	1.90 (75)	61	84.3 (151.7)	44	114.8 (206.7)
5D	1.90 (75)	68	82.3 (148.2)	46	105.2 (189.3)
4A	1.93 (76)	78	63.2 (113.8)	51	82.9 (149.3)
1D	1.96 (77)	82	81.5 (146.7)	58	86.3 (155.3)
2D	1.96 (77)	84	77.1 (138.8)	61	93.3 (168.0)
5D	1.96 (77)	89	76.9 (138.5)	66	78.9 (142.0)
3B	1.98 (78)	96	81.4 (146.5)	71	81.1 (146.0)
3C	1.98 (78)	97	85.8 (154.4)	72	101.2 (182.2)
4A	1.98 (78)	100	85.2 (153.4)	73	69 (125)
3D	2.13 (84)	115	171.3 (308.3)	98	147.1 (264.8)
5B	2.13 (84)	117	136.0 (244.8)	103	136.9 (246.4)
2C	2.29 (90)	122	177.8 (320.0)	111	145.8 (262.4)
2E	2.29 (90)	123	158.5 (285.4)	113	171.1 (308.1)
3B	2.29 (90)	125	155.7 (280.2)	115	219.3 (394.7)

SUMMARY

$(\Delta T)_E > (\Delta T)_D$	$(\Delta T)_D > (\Delta T)_E$	$(\Delta T)_D \approx (\Delta T)_E$
8	3	4

a. $(h_o)_{21}$
13 mm/sec (0.5 in./sec) flooding rate
0.28 MPa (40 psi) pressure

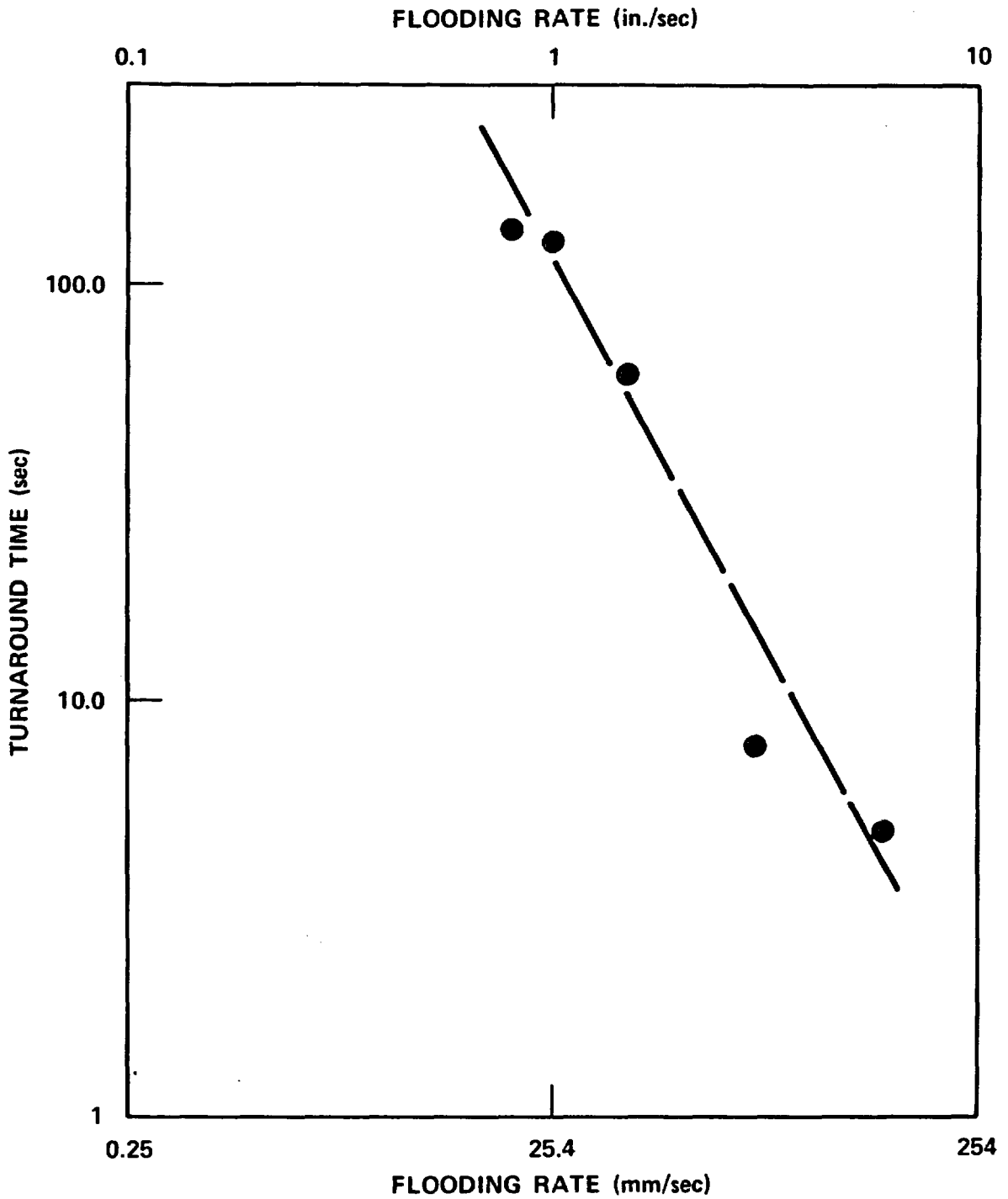

Figure C-8. Relationships Between Turnaround Time and Flooding Rate

APPEND
COFARR PROGRAM AND SELECTION OF NONCOPLANAR DISTRIBUTION

The COFARR program executes the procedure described in paragraph 3-5 to determine sleeve locations on rods and calculates subchannel flow area blockage, given sleeve strain information. A detailed explanation of the program can be found in the 21-rod bundle task plan.[1] A short discussion of the input parameters and a listing of the program are provided therein.

The Westinghouse mean temperature distribution was used with the correction of grid effect as shown by Burman (appendix E). The resultant mean temperature distribution is shown in table D-1. The standard deviation was taken to be 6.7°C (12°F) and a node length of 2.5 cm (1 in.) was used. With these inputs, COFARR calculated the sleeve distribution as indicated in figure 3-8.

TABLE D-1

MEAN TEMPERATURE DISTRIBUTION

Axial Height [m (in.)]	Temperature [°C (°F)]	Axial Height [m (in.)]	Temperature [°C (°F)]
1.57 (62)	914 (1678)	1.83 (72)	949 (1741)
1.60 (63)	920 (1688)	1.85 (73)	948 (1738)
1.63 (64)	925 (1697)	1.88 (74)	946 (1735)
1.65 (65)	930 (1706)	1.90 (75)	938 (1721)
1.68 (66)	934 (1713)	1.93 (76)	933 (1712)
1.70 (67)	938 (1720)	1.96 (77)	929 (1705)
1.73 (68)	942 (1727)	1.98 (78)	927 (1701)
1.75 (69)	944 (1732)	2.01 (79)	925 (1698)
1.78 (70)	947 (1736)	2.03 (80)	923 (1693)
1.80 (71)	947 (1737)	2.06 (81)	918 (1684)

1. Hochreiter, L. E., et al., "PWR FLECHT SEASET 21-Rod Bundle Flow Blockage Task: Task Plan Report," NRC/EPRI/Westinghouse-5, March 1980. NUREG/CR-1370.

APPENDIX E
THIMBLE AND GRID EFFECTS ON BURST

E-1. GENERAL

This appendix provides the analyses of Westinghouse multirod burst tests[1] and the grid effect on the Westinghouse mean temperature calculation.

E-2. EFFECT OF HEATING METHOD ON BURST AND BALLOONING SHAPES IN OUT-OF-PILE LOCA SIMULATIONS

It has been well established by ANL[2] and others that local temperature differences are extremely important in determining the size and shape of rod ballooning and burst under LOCA conditions.

In a reactor, local temperature variations result from many sources, such as pellet enrichment differences, local gap average differences, random cracking and radial redistribution, and pellet radial offset. In addition to these rod internal effects, external heat transfer considerations are also important. Among these are local crud patches and radiant losses to relatively cold sinks, such as control rod thimbles.

To properly simulate these effects out of pile is very difficult and requires compromises. Three principal methods have been used by various investigators:

---

1. Schreiber, R. E., et al., "Performance of Zircaloy-Clad Fuel Rods During a Simulated Loss-of-Coolant Accident -- Multirod Burst Tests," WCAP-7495-L, April 1970.

2. "Light-Water-Reactor Safety Research Program: Quarterly Progress Report -- January-March 1977," ANL-77-34, June 1977.

-- Direct heating of the clad by electrical resistance or induction heating with or without internal mandrels or pellet columns

-- External radiant heating of the clad with internal mandrels or pellet columns

-- Internal electrical heaters with or without annular pellets between the heater and clad

Direct heating of the clad by induction or resistance heating has a temperature smoothing effect not typical of nuclear-heated rods. That is, the local heat deposition is a function of the mass of the clad, whereas heat loss to the environment is a function of surface area. If a hot spot develops in a joule-heated rod and the clad swells locally, the wall thickness decreases, thus increasing local resistance and shunting the electrical current to the cooler, less deformed side of the rod. At the same time, the increased surface area of the bulge is radiating more heat to the environment. The net result is negative feedback function, which produces a more uniform clad temperature distribution and thus larger strains.

The net effect of induction heating is the same as that of joule heating, although the reason for power shifting is different.

External radiant heating does not have the same problems as direct clad heating; however, for this type of heating, the only sink for temperature is the internal mandrel or pellet. These heat sinks are also available to the direct-heated clad and produce the same results. If pellets are used, the random stacking will produce significant and very localized clad temperature differences in both the axial and circumferential directions.[1] This is well illustrated by figure E-1 (taken from ANL-77-34). If an internal mandrel is used and it is slightly nonconcentric to the cladding, the heat loss from the cladding to the mandrel will be greater on the side with minimum clad-to-mandrel gap. This will produce a circumferential temperature gradient in the cladding. Below

1. Motley, F. E., et al., "The Effect of 17 x 17 Fuel Assembly Geometry on Interchannel Thermal Mixing," WCAP-8299, March 1974.

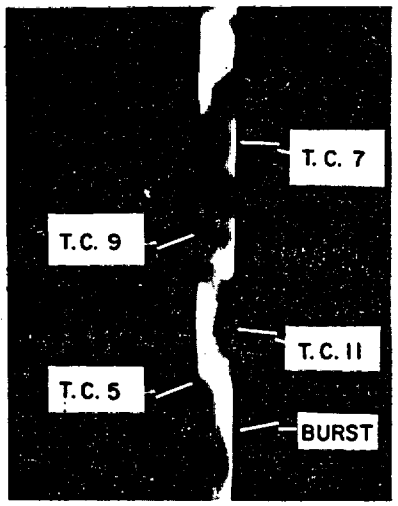

Nonuniform Brightness of Cladding Specimen Containing Al_2O_3 Pellets due to Axial and Circumferential Temperature Variations during Heating at 45°C/s.

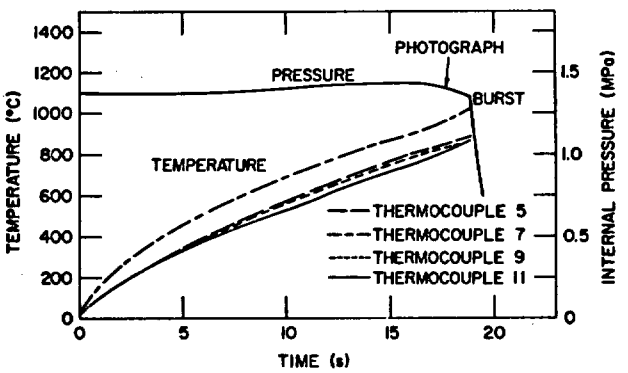

Temperature and Internal Pressure as a Function of Time for Cladding Specimen Described in Fig. III.37.

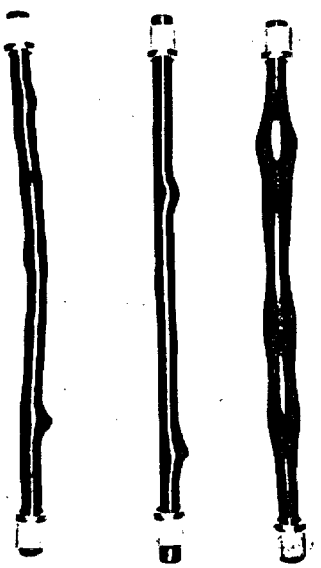

Cladding Constrained by Pellets after Burst. Multiple ballooning regions and irregular bends are a result of temperature nonuniformity.

Figure E-1. Effects of Random Pellet Stacking

about 900°C (1650°F), Zircaloy strains anisotropically and will bow because of the greater strain on the hot side. The direction of the bow will be concave on the hot side. The hot side will thus move toward the mandrel, increasing heat loss on that side. This is a stabilizing mechanism and results in larger strains, at least in the lower temperature range.

The randomness of pellet stacks and thus clad hot spots prevents gross bowing for tests using pellet stacks. Hence, this mechanism is not present to the same degree for those tests with pellet stacks.

If rigid internal heaters are used in burst tests, they act in a manner similar to mandrels except that the heat flow is from mandrel to clad. Clad hot spots will tend to coincide with minimum gaps. The concave bowing of alpha Zircaloy will then reduce the gap on the hot side, creating a self-enhancing reaction.

This results in large circumferential temperature variations and thus low swelling and burst strains; however, the alignment of the hot side close to the heater promotes axial extension of the ballooning, since there is less probability of cold ligaments to localize straining.

Although it is believed that of all the test methods described, the use of internal heaters produces the most prototypical amount of circumferential strain, it tends to produce longer, more gradual axial shapes. From the standpoint of axial shape, the use of externally radiant-heated rods with internal pellets gives the best simulation of nuclear heating.

The effect of radiant losses on localizing strain was examined by reviewing Westinghouse multirod burst test results. The 4x4 test bundles contained two unheated thimbles. The direction of the burst of rods which were laterally or diagonally adjacent to the unheated thimbles was evaluated. Of 68 bursts observed, only three burst in a direction within 45 degrees of the thimbles. For random direction bursting, the expected number would be 17. A frequency this low has a probability of about 7×10^{-6}. This demonstrates that the heat transfer between thimbles and adjacent rods is a

significant factor in determining circumferential temperature distribution in adjacent rods and thus in both the magnitude and direction of the strain.

In a Westinghouse 17x17 assembly, 68 percent of the fuel rods are adjacent to a thimble. In a Westinghouse 15x15 assembly, the ratio is 60 percent.

E-3. EFFECT OF GRID ON AXIAL TEMPERATURE DISTRIBUTION DURING LOCA

The axial temperature distribution for a fuel rod during LOCA determines the location of blockage due to rod bursting. This axial distribution is affected by the presence of spacer grids, because of local power depressions and hydraulic effects.

For Westinghouse Inconel grids, the power depression has been determined near the peak power locations by analysis of gamma scans from irradiated commercial fuel rods.

For a large-break LOCA in which fuel rods are calculated to burst shortly after the end of blowdown, the perturbation in local clad temperature due to a perturbation in local power has been determined to be 6°C (11°F) per percent $\Delta p/p$ for a 17x17 three-loop plant.

The following shows the perturbation in power and the corresponding temperature perturbation as a function of distance from the center of a grid:

Distance from Grid Center [cm (in.)]	% $\Delta p/p$	ΔT [°C (°F)]
0 (0)	8	49 (88)
2.5 (1)	5	31 (55)
5.1 (2)	2	12 (22)
7.6 (3)	0.5	3.1 (5.5)
10 (4)	0	0 (0)

APPENDIX F
FACILITY DRAWINGS

The FLECHT SEASET facility is illustrated in figures F-1 through F-28, as well as figures 4-1 and 4-9.

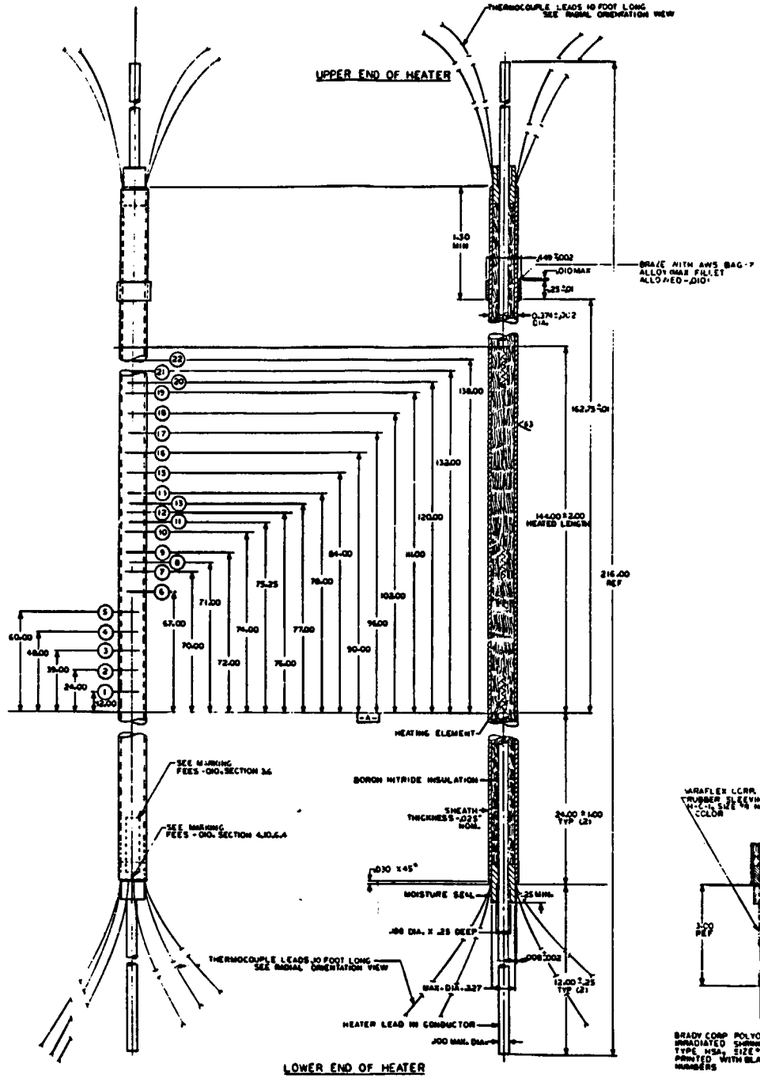

6.20 V - 21 KW		
	DOUBLE ENDED ROD	
GROUP NO	K - THERMOCOUPLE	
	LOWER END	UPPER END
3	2,4,10,11,12,13,14,	
7	1,3,5,6,15,16,	15,16,17,18,
4	1,3,5,6,13,14,	19,21,
13	2,4,7,8,	15,17,18,20,
14	1,6,9,11,	15,16,20,22,

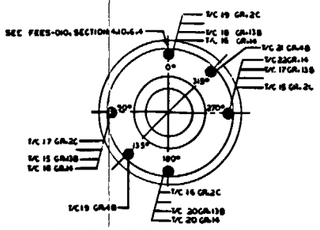

AZIMUTHAL ORIENTATION OF THERMOCOUPLES AS VIEWED FROM BOTTOM END OF ROD

NOTES

1-THIS DWG IS NOT INTENDED TO BE A COMPLETE FABRICATION DWG. THIS DWG IS TO BE USED IN CONJUNCTION WITH ORDERING DATA INCLUDED WITH Ⓝ SPECIFICATION FEES-010.

2-REMOVE ALL BURRS AND SHARP EDGES.

3-SURFACE ROUGHNESS 63 UNLESS OTHERWISE NOTED.

4-ULTRASONIC INSPECT PER ASME BOILER AND PRESSURE VESSEL CODE, SECTION III, CLASS 2 COMPONENTS. CALIBRATION STANDARDS AND DEFECT ACCEPTANCE CRITERIA ARE AS FOLLOWS:

(A) CALIBRATION DEFECT STANDARDS:
DEPTH -.0025 IN.
LENGTH-.050 IN.
WIDTH-.0025 IN.

(B) ACCEPTANCE CRITERIA:
DEFECT IN SHEATH MUST BE LESS THAN THE CALIBRATION DEFECT STANDARDS.

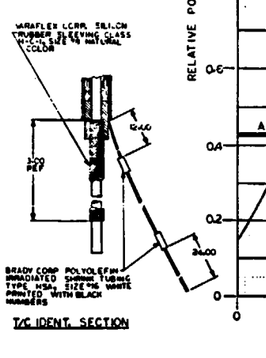

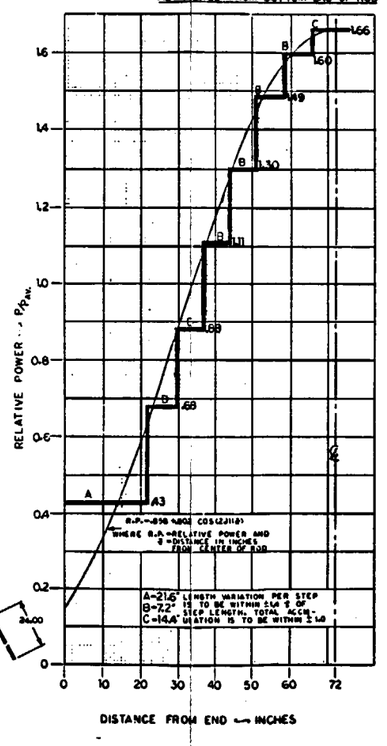

NOTE

1-CIRCLED ① THRU ㉒ ARE THERMOCOUPLES (.040 DIA. 304 STAINLESS STEEL SHEATH TYPE K PREMIUM GRADE INSULATED JUNCTIONS ANNEALED OVER ENTIRE LENGTH) TOLERANCE ON ALL T/C DIMENSIONS TO BE ± 1% AS MEASURED FROM DATUM A.

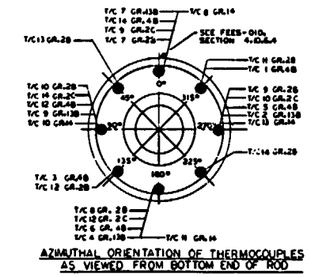

AZIMUTHAL ORIENTATION OF THERMOCOUPLES AS VIEWED FROM BOTTOM END OF ROD

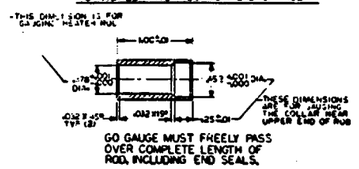

GO GAUGE MUST FREELY PASS OVER COMPLETE LENGTH OF ROD, INCLUDING END SEALS.

Figure F-1. FLECHT SEASET 21-Rod Bundle Heater Rods

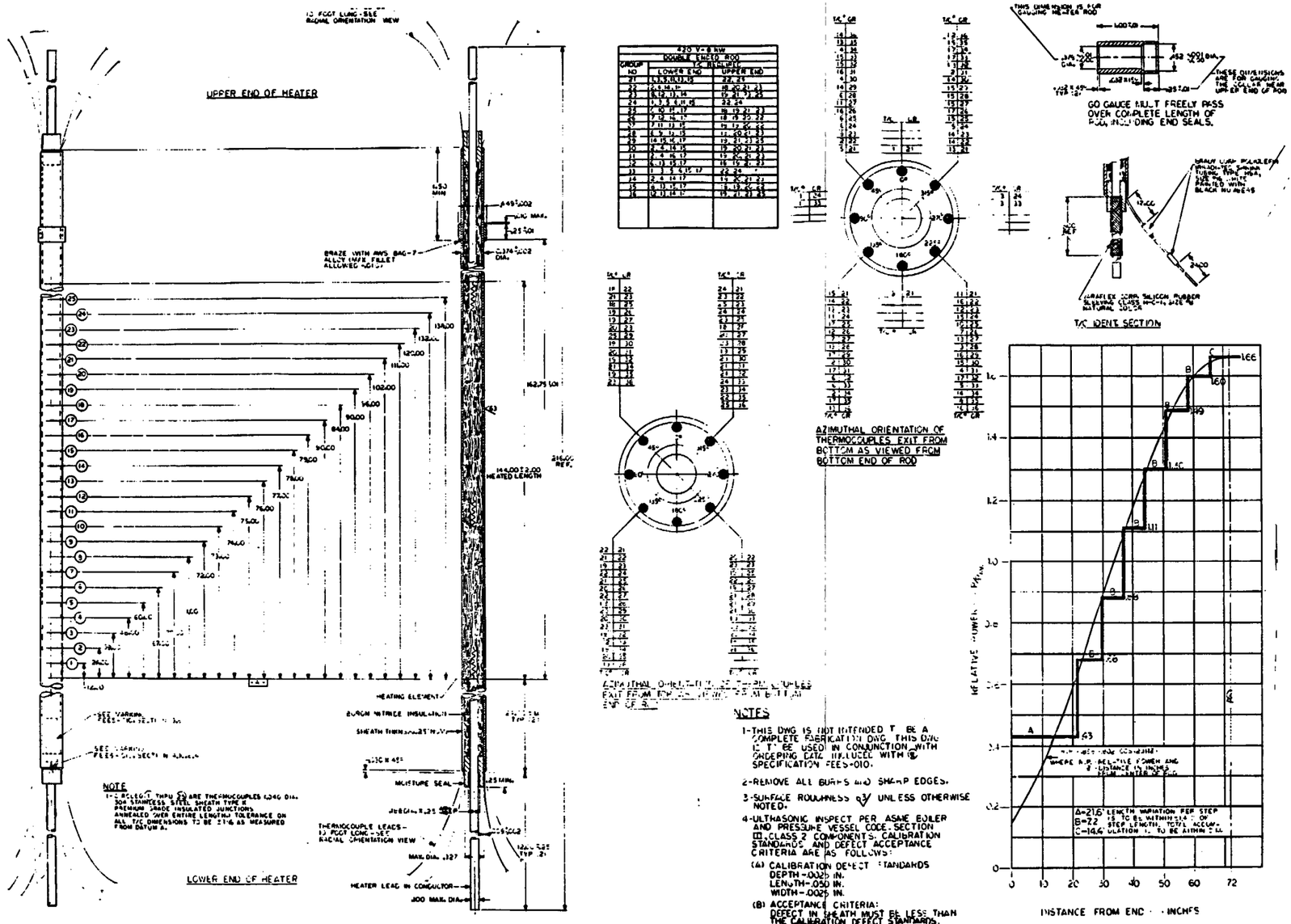

420 V-6 kw DOUBLE ENDED ROD TC RECORD	
GROUP NO	LOWER END / UPPER END
21	1,3,5,10,13,19 / 22,24
22	2,6,14,18 / 18,20,21,23
23	8,12,17,16 / 15,21,23,25
24	1,3,5,6,11,15 / 22,24
25	7,10,17,17 / 18,19,21,23
26	7,12,16,17 / 18,19,21,23
27	7,11,13,15 / 19,17,22,24
28	6,9,12,15 / 11,20,21,23
29	10,15,16,19 / 19,21,23,25
30	2,4,16,19 / 19,20,21,23
31	2,4,16,17 / 19,20,22,23
32	8,13,15,17 / 15,16,18,21
33	1,3,5,6,15,17 / 22,24
34	2,4,14,17 / 19,20,21,23
35	8,13,15,17 / 15,16,18,21
36	9,13,16,17 / 18,19,20,23

Figure F-2. FLECHT SEASET 21-Rod Bundle No. 5 Heater Rods

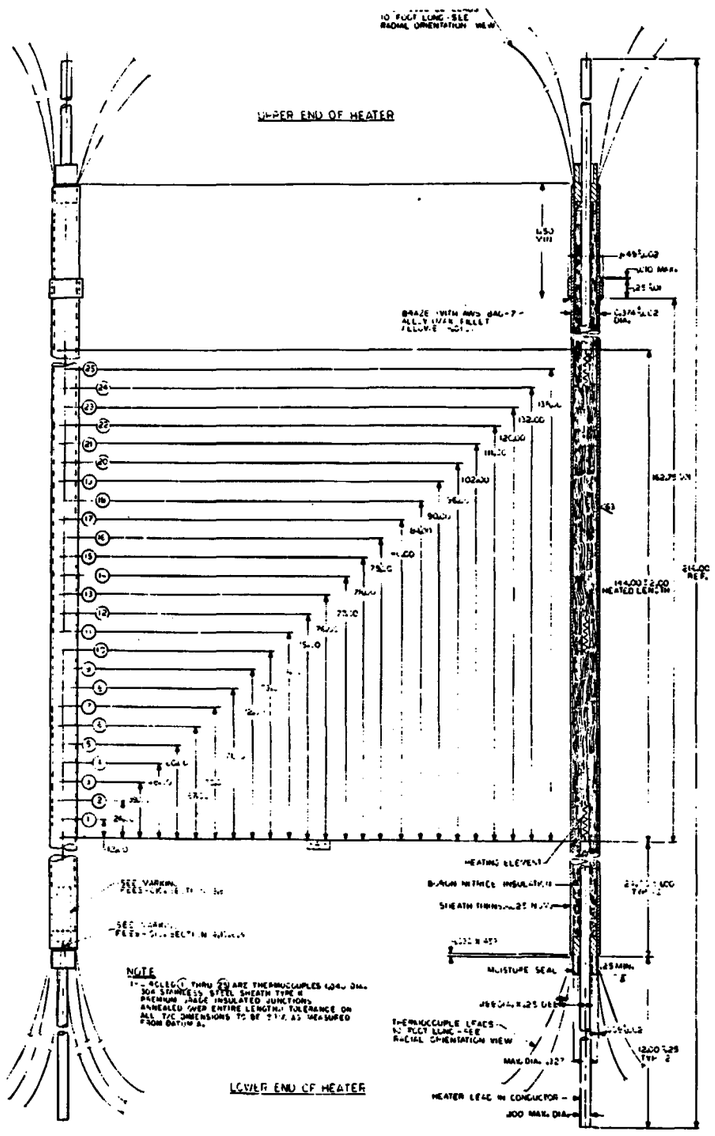

GROUP NO	42C V-6 RW DOUBLE ENDED ROD T/C RECORD LOWER END	UPPER END
26	7,12,16,17	18,19,20,22
39	4,7,8,14,17	18,20,21,23
40	1,3,8,11,0,15	22,24
41	0,10,14,15,16	18,20,24
42	1,2,6,11,14	19,21,23,25
43	3,4,5,9,13,16,	22,24
44	6,12,16,15,17	18,19,21
45	5,11,12,13,18	18,19,20
46	6,11,13,15	19,20,21,23
47	10,14,15,16	19,21,22,23
48	4,5,12,13,16	19,20,24
49	7,9,14,16,17	18,19,20,22
50	2,13,16,17	19,20,21
51	6,13,15	18,19,20,23
52	6,11,13,15,16	19,20,21,23
53	3,5,11,13,15,16	22,24
54	7,11,13,15,16	18,19,20
55	1,5,7,13,15,17	22,24
56	6,10,13,15,17	18,19,20,23
57	12,14,16	19,21,22,23

AZIMUTHAL ORIENTATION OF THERMOCOUPLES EXIT FROM TOP AS VIEWED FROM BOTTOM END OF ROD

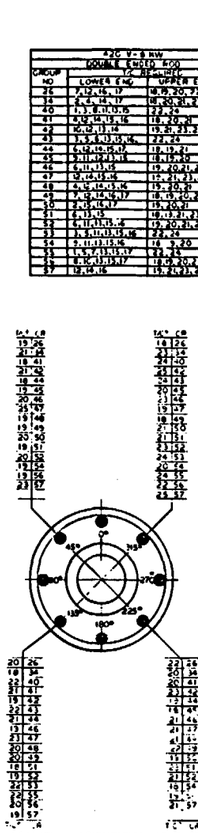

AZIMUTHAL ORIENTATION OF THERMOCOUPLES EXIT FROM BOTTOM AS VIEWED FROM BOTTOM END OF ROD

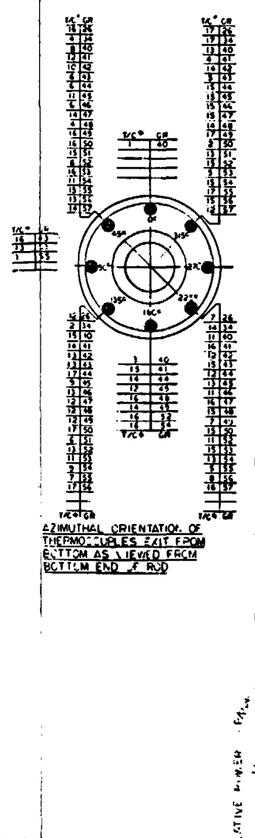

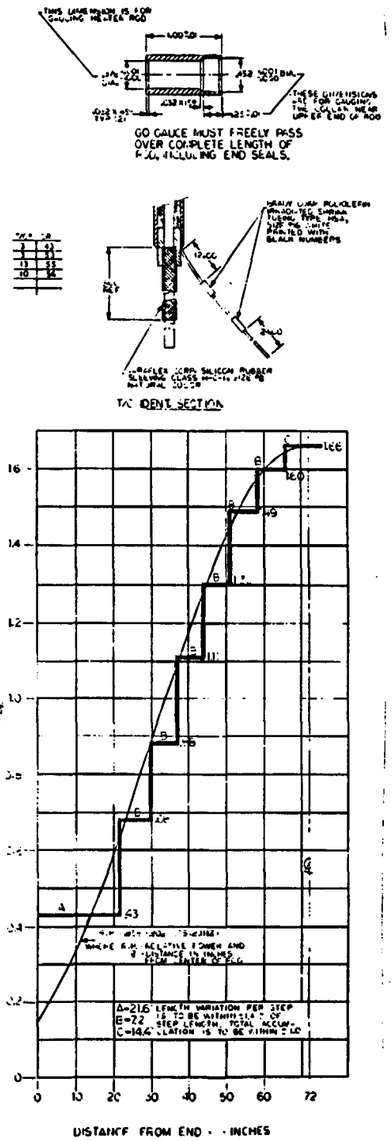

NOTES

1-THIS DWG IS NOT INTENDED TO BE A COMPLETE FABRICATION DWG. THIS DWG IS TO BE USED IN CONJUNCTION WITH SPACERING CAL INCLUDED WITH SPECIFICATION FE65-010.

2-REMOVE ALL BURRS AND SHARP EDGES.

3-SURFACE ROUGHNESS 63 UNLESS OTHERWISE NOTED.

4-ULTRASONIC INSPECT PER ASME BOILER AND PRESSURE VESSEL CODE, SECTION III, CLASS 2 COMPONENTS. CALIBRATION STANDARDS AND DEFECT ACCEPTANCE CRITERIA ARE AS FOLLOWS:

(A) CALIBRATION DEFECT STANDARDS
DEPTH - .0025 IN.
LENGTH - .050 IN.
WIDTH - .0025 IN.

(B) ACCEPTANCE CRITERIA:
DEFECT IN SHEATH MUST BE LESS THAN THE CALIBRATION DEFECT STANDARDS.

Figure F-3. FLECHT SEASET 21-Rod Bundle No. 7 Heater Rods.

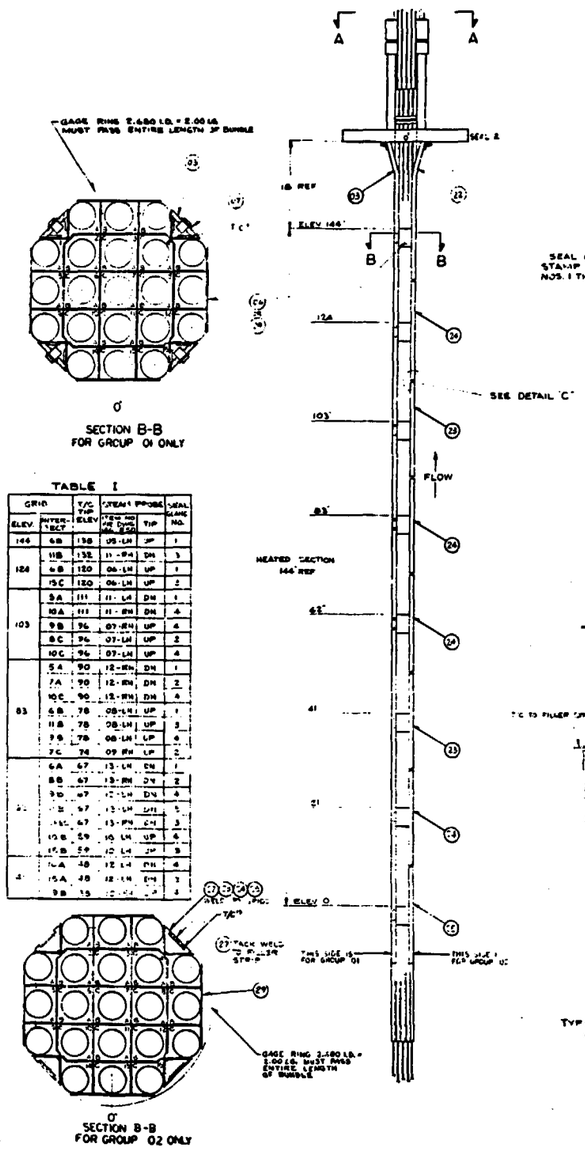

TABLE I

GRID		T/C TYP ELEV	STEAM PROBE		SEAL GLAND NO.
ELEV.	INTERSECT		ITEM NO OF DWG 401-0100	TIP	
144	6B	138	05-LH	2P	1
124	11B	132	11-RH	DN	3
	8B	120	06-LH	UP	1
	9C	120	06-LH	UP	2
103	9A	111	11-LH	DN	1
	10A	111	11-RH	DN	4
	9B	96	07-RH	UP	4
	8C	96	07-LH	UP	2
	10C	96	07-LH	UP	4
83	5A	90	12-RH	DN	1
	7A	90	12-RH	DN	3
	10C	90	12-RH	DN	4
	6B	78	08-LH	UP	1
	11B	78	08-LH	UP	3
	9B	78	08-LH	UP	4
	7C	78	09 RH	UP	2
41	6A	67	13-LH	DN	1
	8B	67	13-RH	DN	3
	9D	67	13-LH	DN	4
	11	67	13-LH	UP	1
	11C	67	13-RH	DN	3
	10B	59	10 LH	UP	4
	11B	59	10 LH	UP	3
21	10A	48	12 LH	DN	4
	11A	48	12 LH	DN	3
	9B	15	12 LH	UP	2

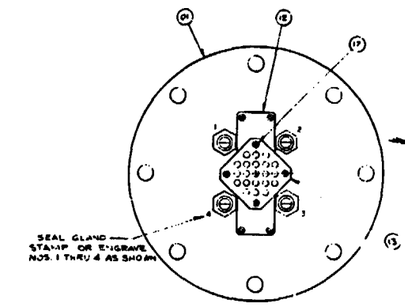

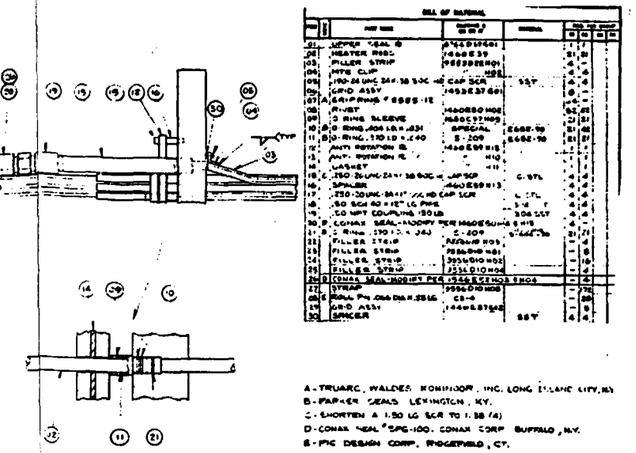

ITEM	PART NAME	PART NO. OR SPEC	MATERIAL	NO. REQ'D PER GROUP		
				01	02	03
01	UPPER SEAL A	6144D39G01		1	1	1
02	HEATER RODS	1484E59		21	21	21
03	FILLER STRIP	9883B88G01		4	4	4
04	PIPE CLIP	H-28		4	4	4
05	1.190-36 UNC-2A x 1.38 LG HEX CAP SCR		SST	4	4	4
06	GRID ASSY	1493E37G01		1	1	1
07	GRIP RING # 6885-12			4	4	4
08	RIVET	MS20600-4H06		42	42	42
09	2 RING SLEEVE	MS90077-H09		4	4	4
10	O RING .606 I.D. x .031	SPECIAL	E6082-70	4	4	4
11	O RING .170 I.D. x .040	S-209	E6082-70	21	21	21
12	ANTI ROTATION BL	1484E99B15		4	4	4
13	ANTI ROTATION PL	- H10		4	4	4
14	WASHER	- H11		4	4	4
15	.250-20 UNC-2A x 1.38 LG HEX CAP SCR		C-1018	4	4	4
16	SPACER	1484E99B13		4	4	4
17	.250-20 UNC-2A x 1" LG HD CAP SCR			4	4	4
18	.50 SCH 80 x 12" LG PIPE		3/4 "	1	1	1
19	.50 NPT COUPLING 1200 LB		304 SST	4	4	4
20	CONAX SEAL-ASSOCIATED PER MODIFICATION # H19			4	4	4
21	O Ring .170 I.D. x .040	S-209	SILICONE RUBBER	21	21	21
22	FILLER STRIP	9884D90H01		1	1	1
23	FILLER STRIP	9884D90H02		1	1	1
24	FILLER STRIP	9884D90H03		1	1	1
25	FILLER STRIP	9884D90H04		1	1	1
26	CONAX SEAL-MODIFY PER MODIFICATION # H26 & H27			4	4	4
27	STRAP	9884D90H05		1	1	1
28	ROLL PIN .066 DIA x .3516	CS-6		4	4	4
29	GRID ASSY	1484E83G02		1	1	1
30	SPACER		SST	4	4	4

A - TRUARC, WALDES KOHINOOR, INC. LONG ISLAND CITY, NY.
B - PARKER SEALS LEXINGTON, KY.
C - SHORTEN A 1.50 LG SCR TO 1.38 (4)
D - CONAX "SEAL" SPG-100. CONAX CORP BUFFALO, N.Y.
E - PIC DESIGN CORP. RIDGEFIELD, CT.

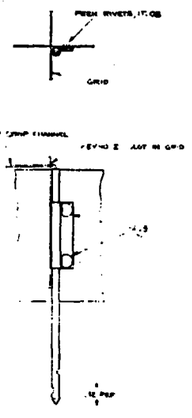

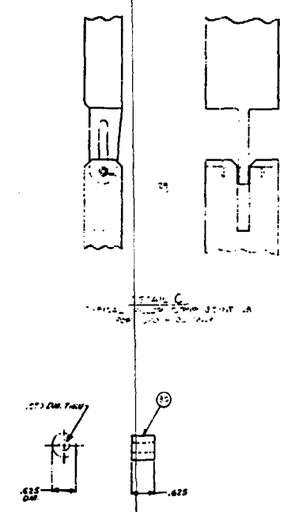

Figure F-4. FLECHT SEASET 21-Rod Bundle Test Assembly

BILL OF MATERIAL

ITEM	QTY	PART NAME	DRAWING & STD NO. IF	MATERIAL	DIM. PER G 01	02	03
01		FILLER STRIP		NOTE - A			
02		FILLER STRIP		NOTE - A			
03		FILLER STRIP		NOTE - A			
04		FILLER STRIP		NOTE - A			
05		STRAP		304 SST			

NOTE:
A - INK.FR, 3/16"-DIA "INVAR 36" - FLEE CUT ROD

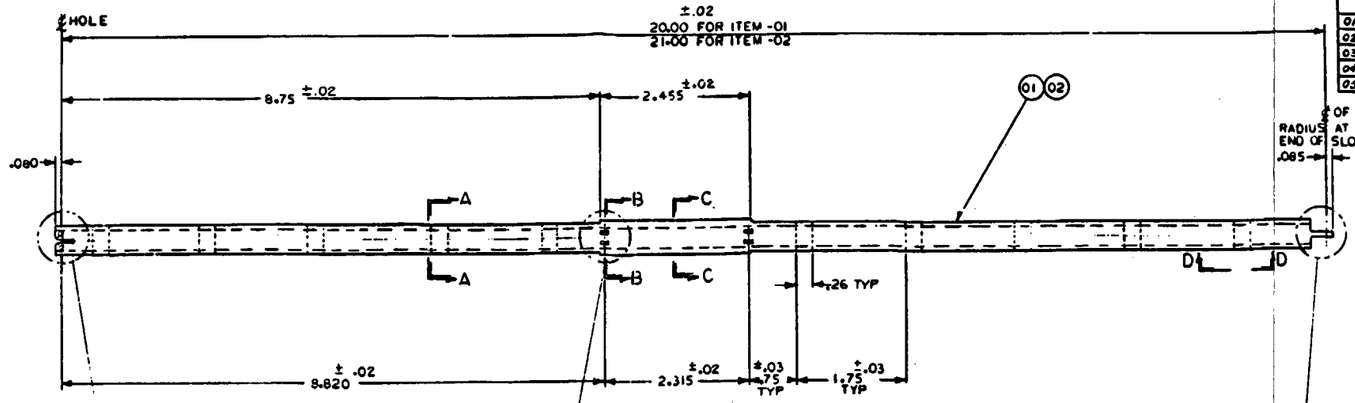

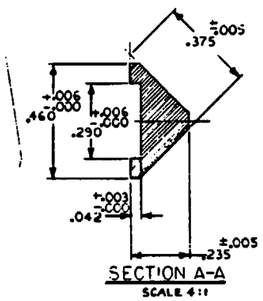

SECTION A-A
SCALE 4:1

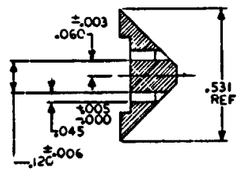

SECTION B-B
SCALE 4:1

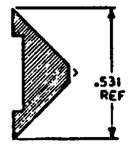

SECTION C-C
SCALE 4:1

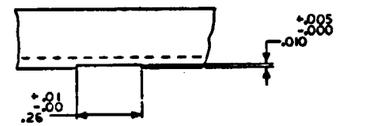

VIEW D-D TYP 10 EA. FOR IT. 01 & 02, 12 FOR IT. 03
SCALE 4:1

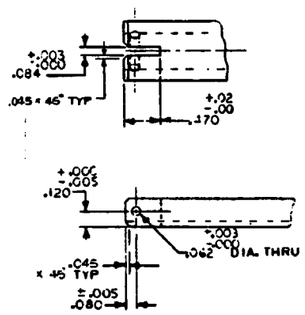

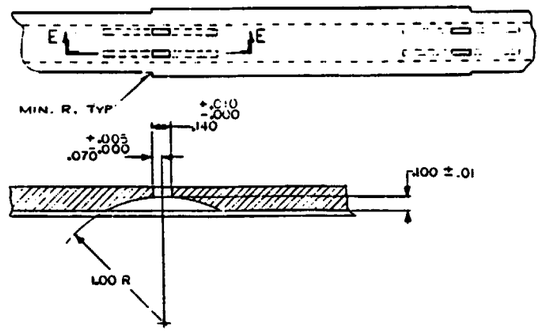

SECTION E-E SCALE 2:1 TYP 4 PLACES

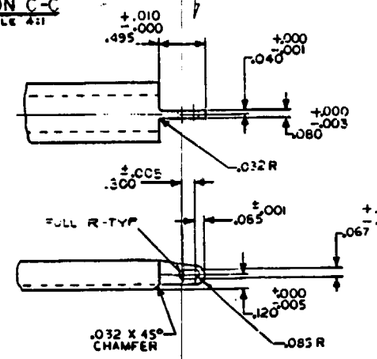

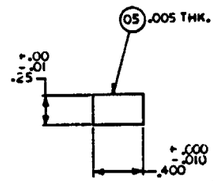

Figure F-5. FLECHT SEASET 21-Rod Bundle Filler Strip (sheet 1 of 2)

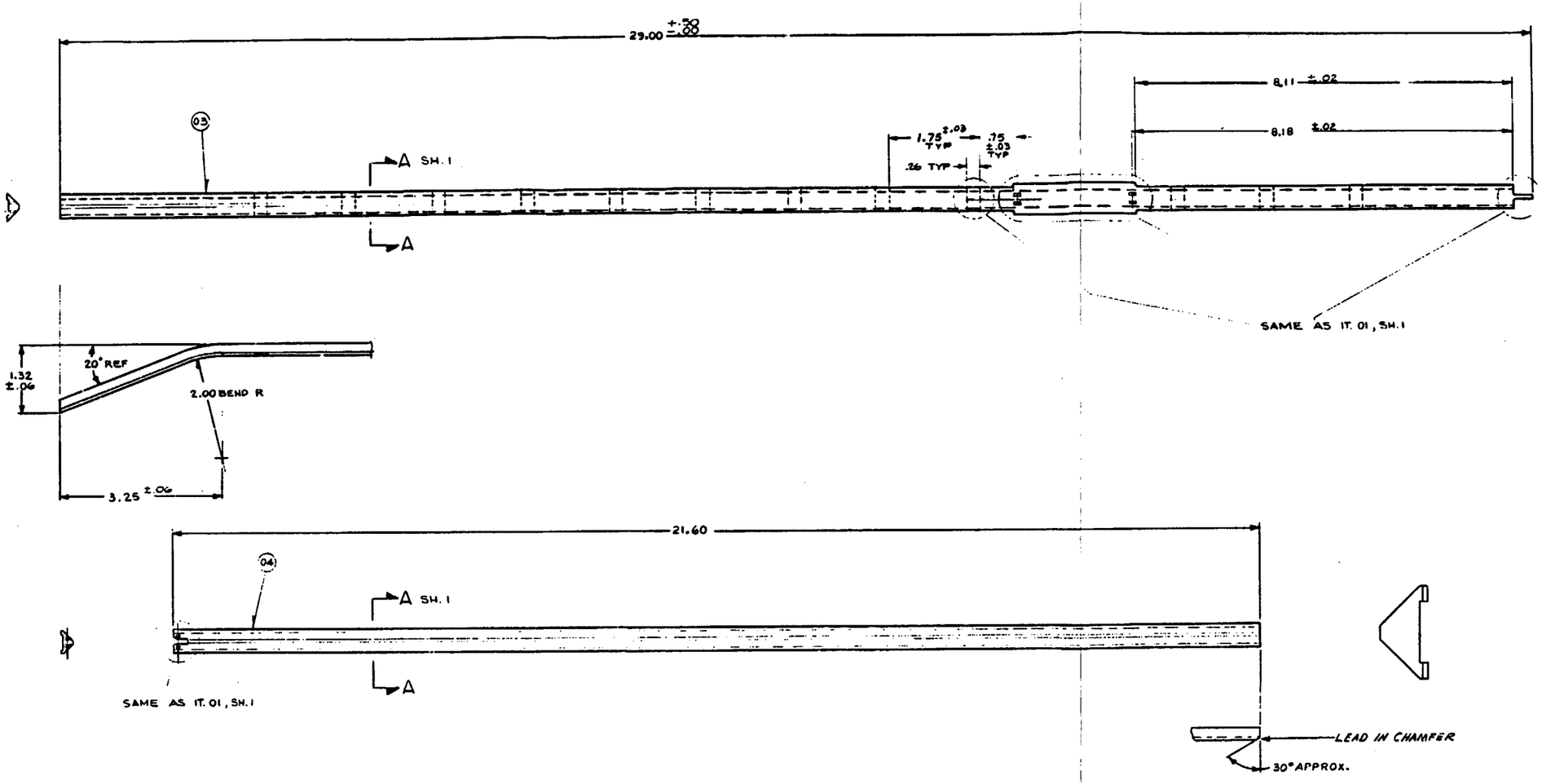

Figure F-5. FLECHT SEASET 21-Rod Bundle Filler Strip (sheet 2 of 2)

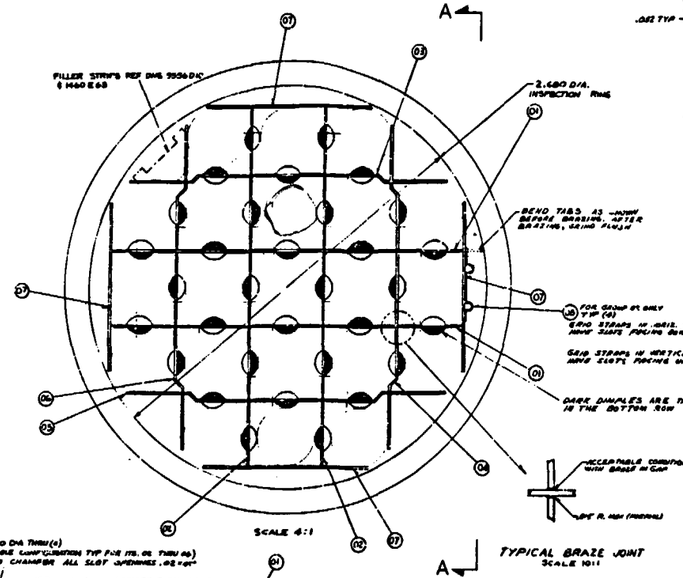

TYPICAL BRAZE JOINT
SCALE 10:1

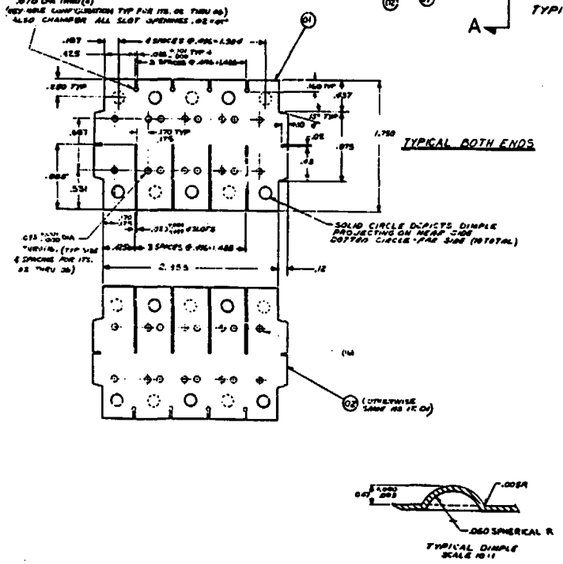

TYPICAL BOTH ENDS

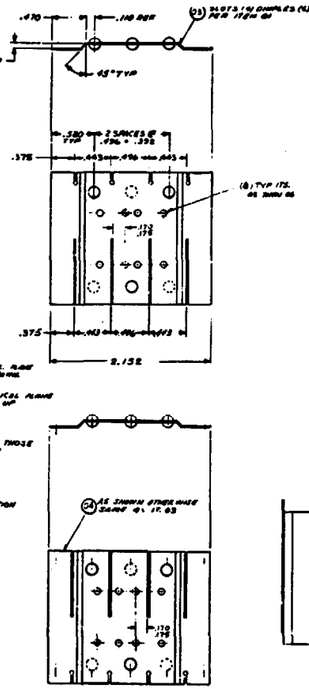

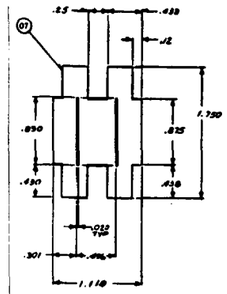

VIEW A-A (ROTATED)

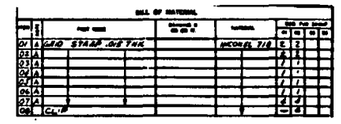

"A" - ALL GRID STRAPS ARE THE SAME HEIGHT, THICKNESS & HAVE THE SAME SHAPE & SIZE IF JUST SIDES, SIMPLE POSITIONS ARE AS SHOWN IF GRID VIEW.

NOTES:
1. BRAZE PER E PROC. SPEC. CAP SYSTEM - DELETE THE AGING CYCLE
2. GRID VIEW MUST HAVE VIEW AN INSPECTION ENVELOPE OF 2.680 DIA

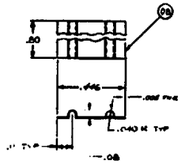

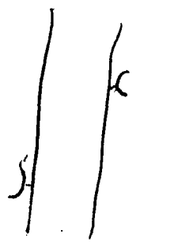

Figure F-6. FLECHT SEASET 21-Rod Bundle Grid Assembly and Details

FORMULA:
$-.748 < X < .748$
$Y = .024 \cos 120.3 \times + .224$

DIM. O-X	DIM. O-Y RADIUS
0	.248
.10	.247
.20	.246
.30	.243
.40	.240
.50	.236
.60	.231
.70	.226
.748	.224

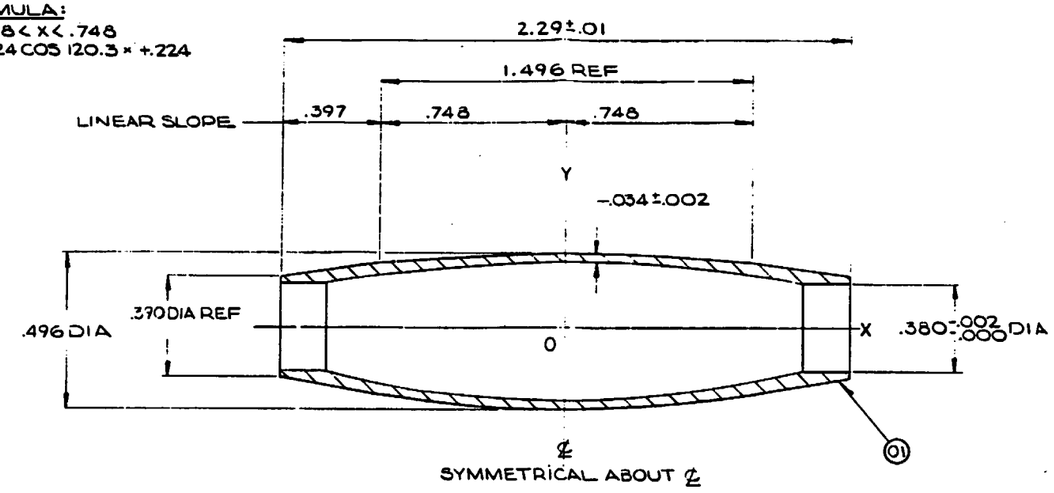

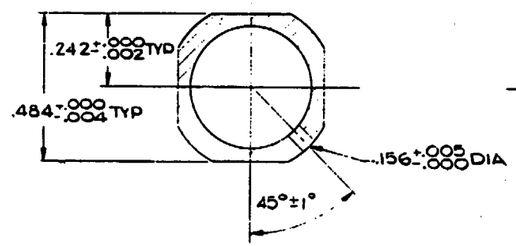

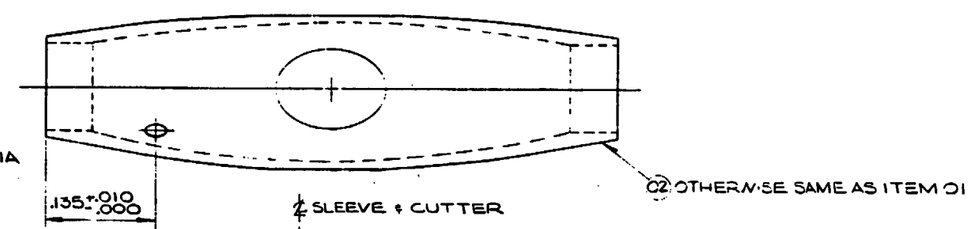

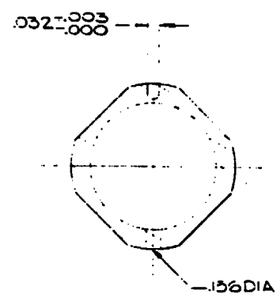

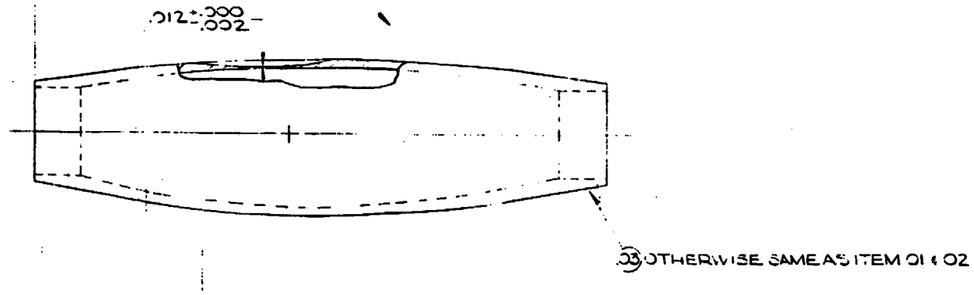

BILL OF MATERIAL								
ITEM	NOTE	PART NAME	DRAWING & SPEC OR ST.	MATERIAL	REQ. PER GROUP			
					01	02	03	04
01		SLEEVE		300 SST	1			
02		SLEEVE		300 SST	1			
03		SLEEVE		300 SST	1			

UNLESS OTHERWISE SPECIFIED THE FOLLOWING TOLERANCES APPLY
THREE PLACE DIMENSIONS ±.005

SEE PROCESS SPECIFICATION NO CAP505128-1 FOR SUPPLEMENTARY MANUFACTURING INFORMATION

Figure F-7. FLECHT SEASET 21-Rod Bundle Flow Blockage Sleeve

BILL OF MATERIAL							
ITEM	NOTE	PART NAME	DRAWING & CB OR PT	MATERIAL	REQ PER GROUP 01	02	03	04
01	C	SLEEVE		304 SST	1			

C – MAKE FROM .500 O.D. x .065 WALL

DIM. O-X	DIM. O-Y
0	.248
.10	.247
.20	.246
.30	.243
.40	.240
.50	.236
.60	.231
.70	.226
.748	.224

FORMULA:
$-.748 < X < .748$
$Y = .024 \cos 120 .8X + .224$

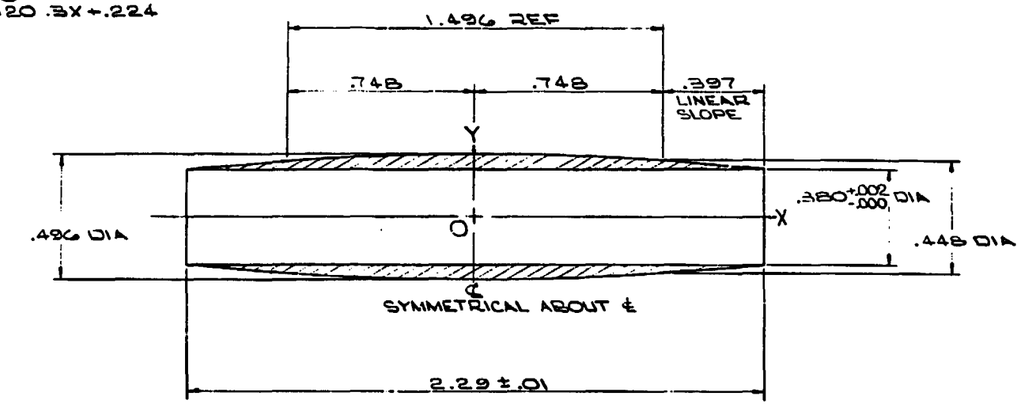

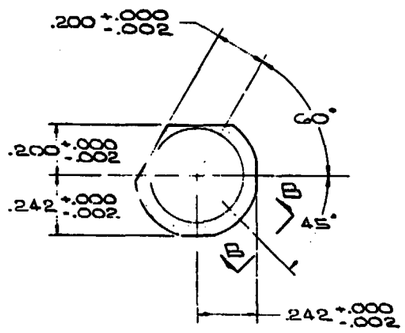

SECTION A-A

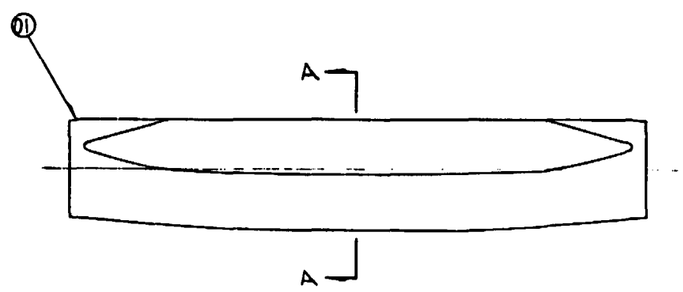

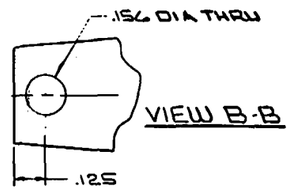

VIEW B-B

Figure F-8. FLECHT SEASET 21-Rod Bundle Corner Flow Blockage Sleeve

BILL OF MATERIAL								
ITEM	NOTE	PART NAME	DRAWING & SUB OR PT	MATERIAL	REQ. PER GROUP			
					01	02	03	04
01	A	SLEEVE			1			

A - MAKE FR 300 SERIES CST

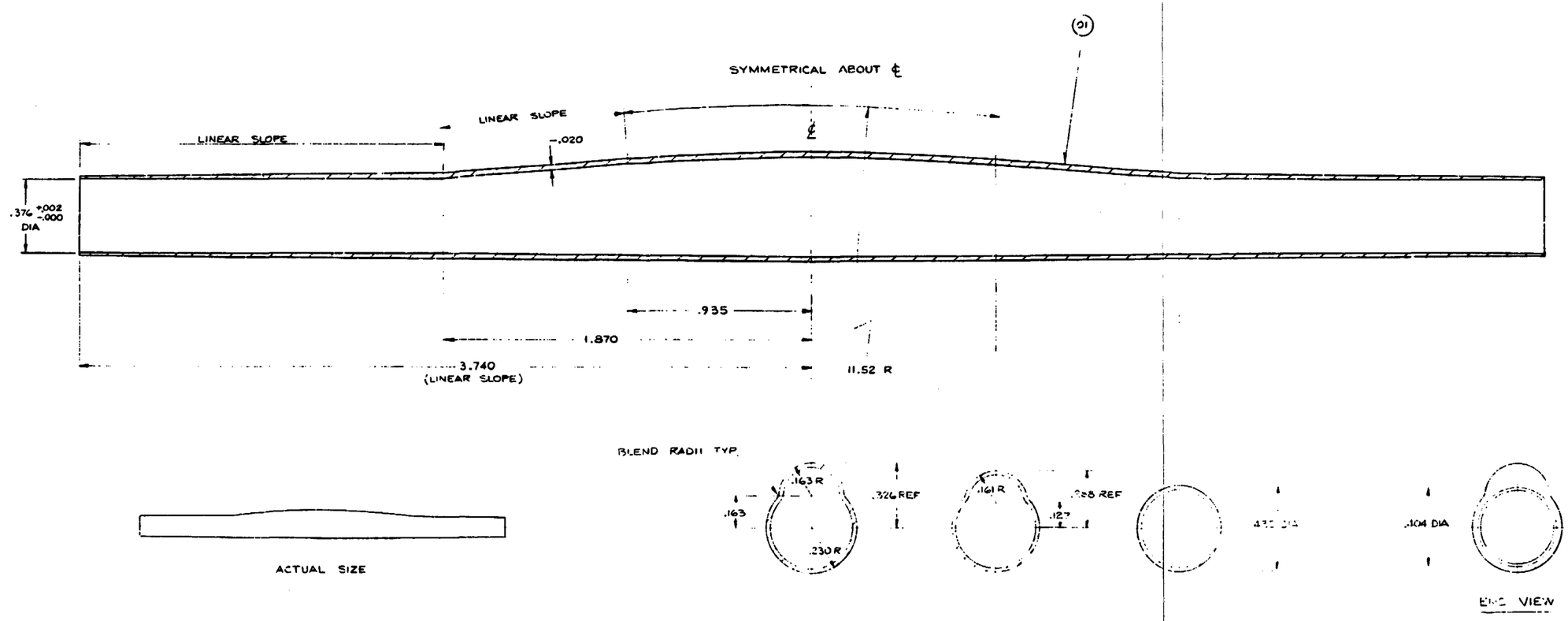

UNLESS OTHERWISE SPECIFIED THE FOLLOWING TOLERANCES APPLY

ALL DIMS. ± .005

STRAIGHTNESS, FLATNESS, PERPENDICULARITY, ROUNDNESS, PARALLELISM, SYMMETRY, AND ANGULARITY TOLERANCES FOR MACHINED SURFACES ARE PERMITTED WITHIN THE PROFILE ESTABLISHED BY THE LIMITS OF SIZE. VARIATIONS IN FORM FOR NONMACHINED FEATURES ARE PERMITTED WITHIN ESTABLISHED CONNECTING ATTACHMENT CONCENTRICITY MUST BE GIVEN TO THE SUM OF THE TOLERANCES OF THE DIAMETERS BEING COMPARED. SURFACE ROUGHNESS IN MICRO .254/.064

ALL EDGES TO CHAMFER .005 - .030 APPROXIMATE RADIUS OR CHAMFER. ALL FILLETS .005 - .020 APPROXIMATE RADIUS.

SCREW THREADS PER ANSI B1.1 PIPE THREADS PER ANSI B2.1 HOLD DIMENSIONS ARE MINIMUM ALL DIMENSIONS CONNECTED TO BE ± .2

SEE PROCESS SPECIFICATION NO CAP595128 FOR SUPPLEMENTARY MANUFACTURING INFORMATION

Figure F-9. FLECHT SEASET 21-Rod Bundle Nonconcentric Flow Blockage Sleeve

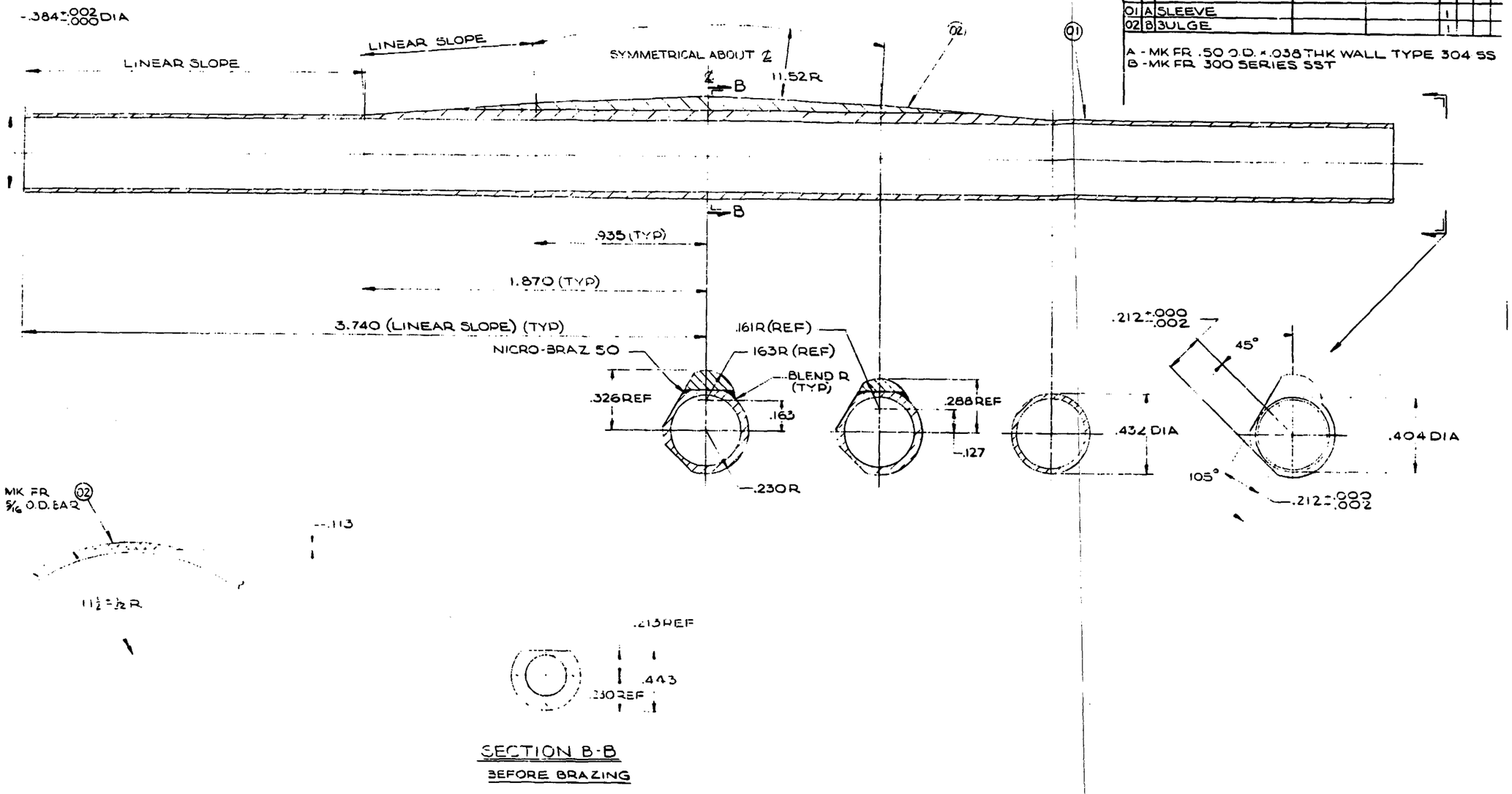

BILL OF MATERIAL								
ITEM	NOTE	PART NAME	DRAWING # OR SPEC #	MATERIAL	REQ. PER GROUP			
					01	02	03	04
01	A	SLEEVE			1			
02	B	BULGE			1			

A - MK FR .50 O.D. x .038 THK WALL TYPE 304 SS
B - MK FR 300 SERIES SST

SECTION B-B
BEFORE BRAZING

Figure F-10. FLECHT SEASET 21-Rod Bundle Corner Flow Blockage Sleeve

BILL OF MATERIAL								
ITEM	NOTE	PART NAME	DRAWING # OR PT.	MATERIAL	REQ. PER GROUP			
					01	02	03	04
01	A	SLEEVE			1			

A - MAKE FR 300 SERIES SST

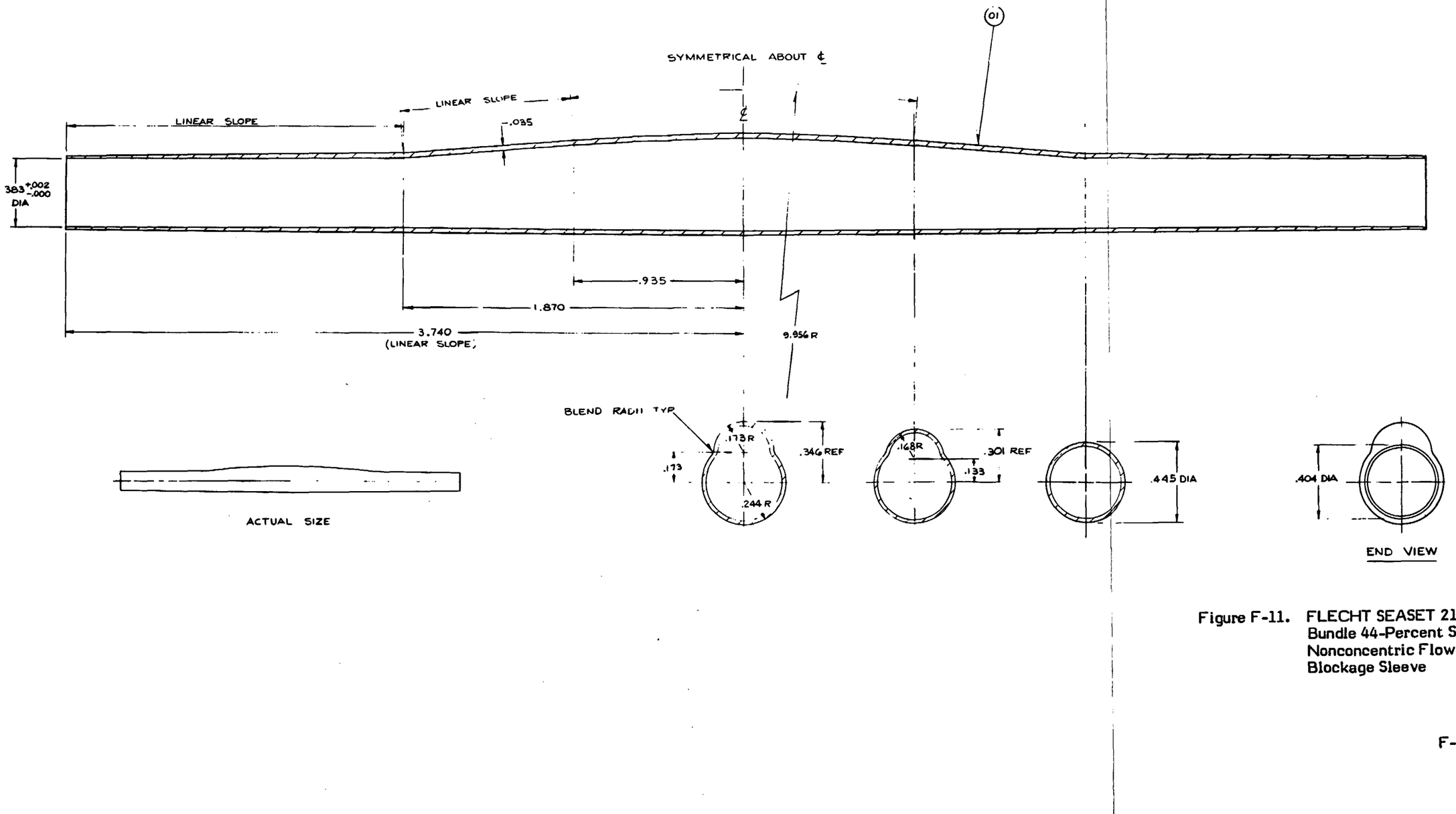

Figure F-11. FLECHT SEASET 21-Rod Bundle 44-Percent Strain Nonconcentric Flow Blockage Sleeve

BILL OF MATERIAL						IDENT CLASS →			
						GROUP NOTE →			
ITEM	NOTE IDENT	PART NAME	(SIZE) REFERENCE INFORMATION	QUI	MAIN DIE CODE PART NUMBER OR REF DWG	2500			
01	B	SLEEVE				1			
02	C	BULGE				1			

B - MK FR .250 STD WT PIPE, TYPE 304 SS
C - MK FR 300 SERIES SST

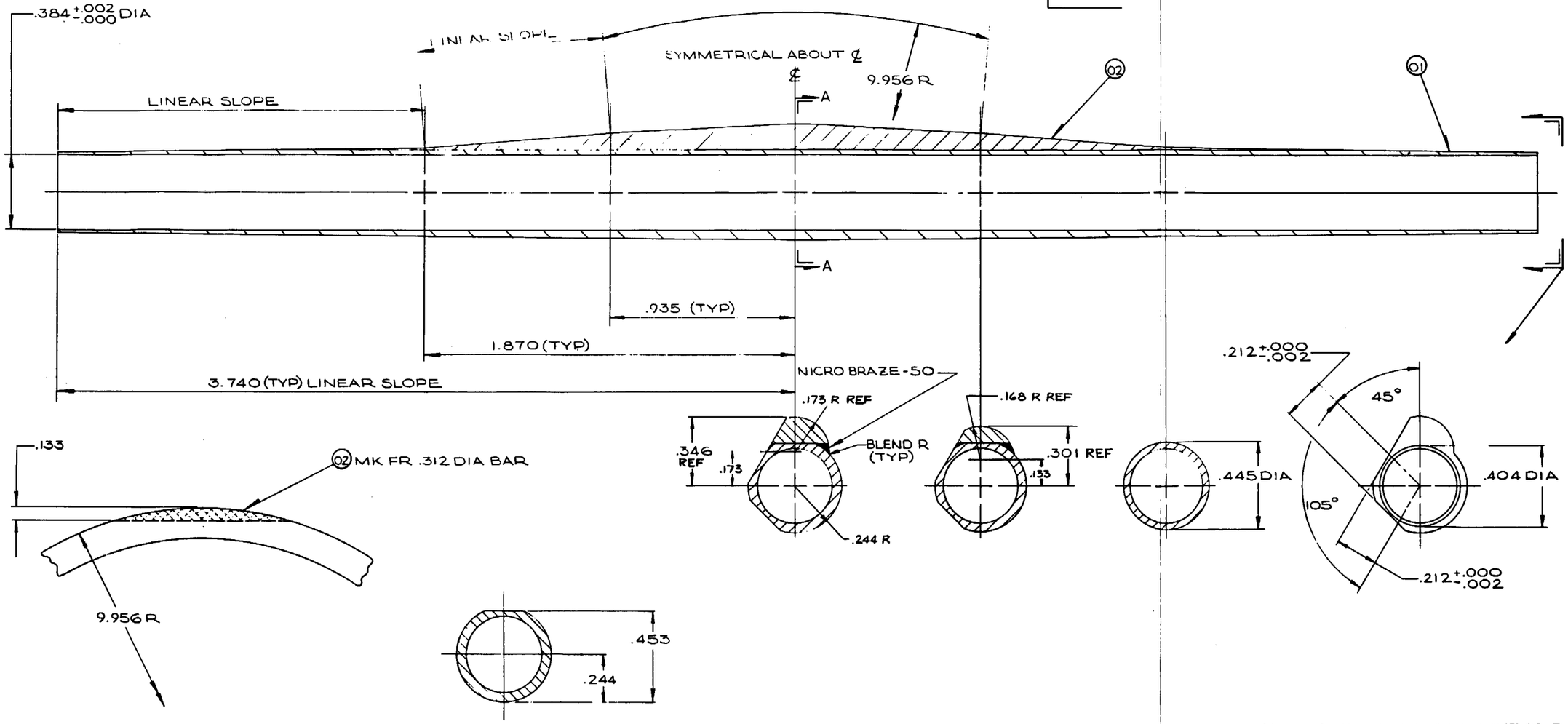

Figure F-12. FLECHT SEASET 21-Rod Bundle 44-Percent Strain Corner Flow Blockage Sleeve

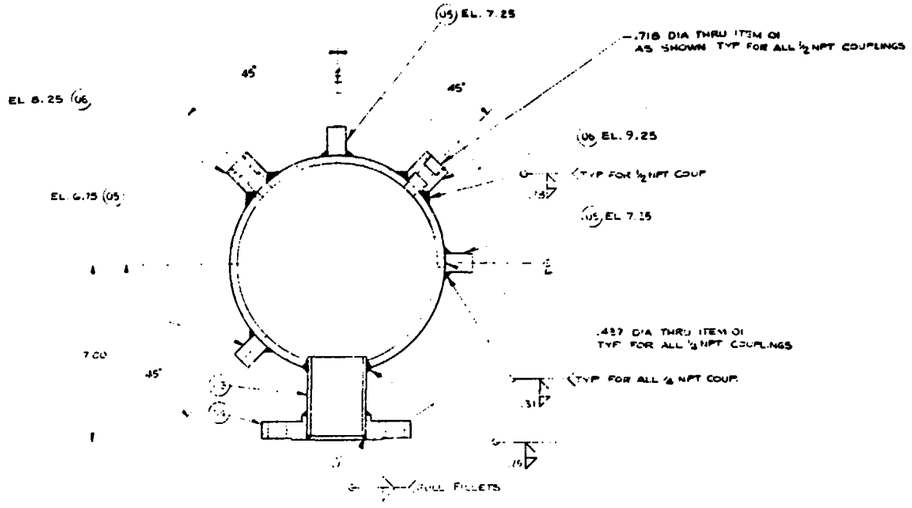

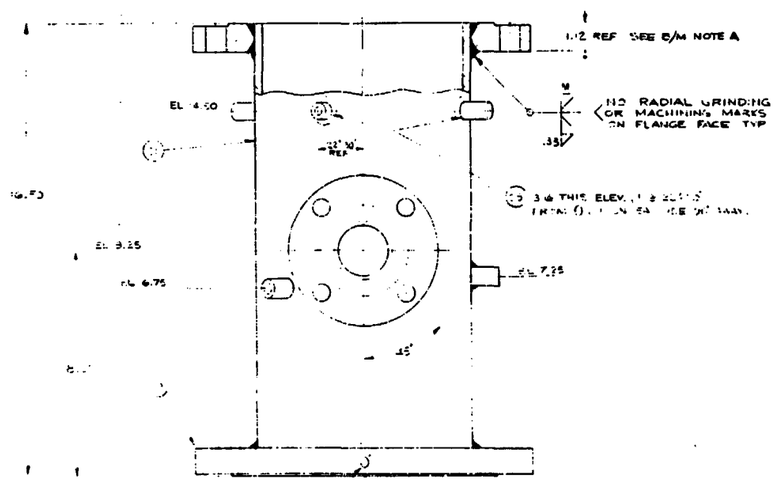

GROUP 1
UPPER PLENUM

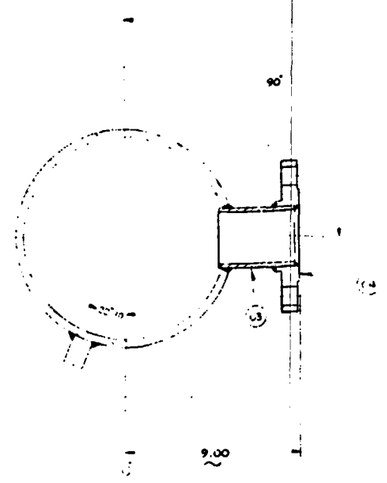

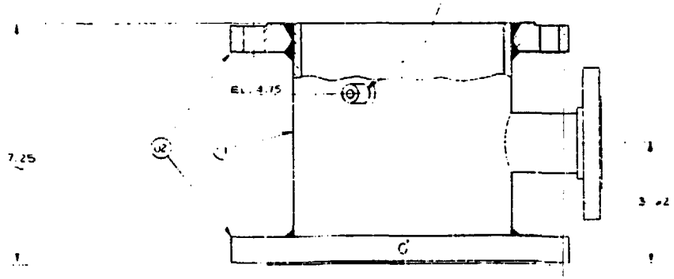

GROUP 2
LOWER PLENUM
(OTHERWISE SAME AS GROUP 1)

BILL OF MATERIAL

ITEM NO.	QTY	PART NAME	DRAWING OR SPEC NO.	MATERIAL	REQ. PER GROUP 01	02	03	04
01	-	PIPE, 8" SCH 40		SA 106 GR B	1			
02	A	FLANGE, 8" 150 LB SLIP ON		A 105 GR II	2	2		
03		PIPE, 2" SCH 40		SA 106 GR B	1	1		
04		FLANGE, 2" 150 LB SLIP ON		A 105 GR II	1	1		
05		½ NPT COUPLING 6000#		SA 105	6	1		
06		¼ NPT COUPLING, 6000#		SA 105	2	-		

A REMOVE BURS BEFORE MACHINING WELD PREP.

NOTES:
1. DESIGN, FABRICATE, TEST & STAMP PER SECT I OF THE ASME BOILER & PRESSURE VESSEL CODE.
2. DESIGN PRESSURE 00 PSIG @ 700°F
3. WELD PER W PROC. SPEC 82127-2V (ALL WELDS FULL PENETRATION EXCEPT ITEM 04)

Figure F-13. FLECHT SEASET 21-Rod Bundle Plenums

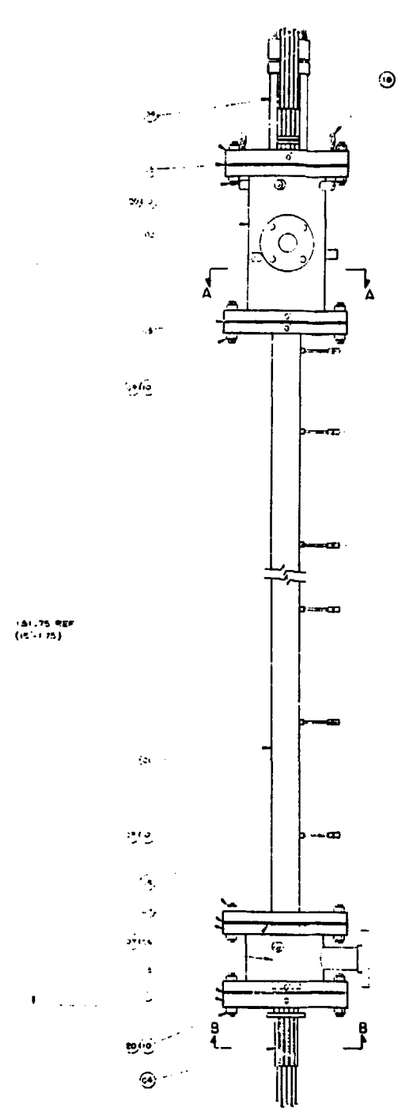

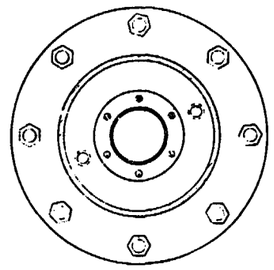

SECTION A-A
HEATER RODS OMITTED

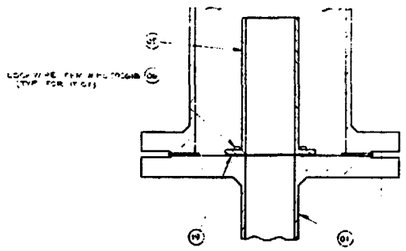

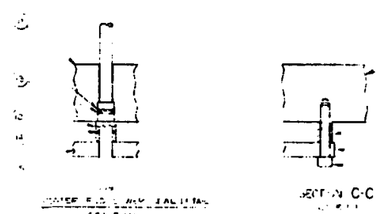

SECTION C-C

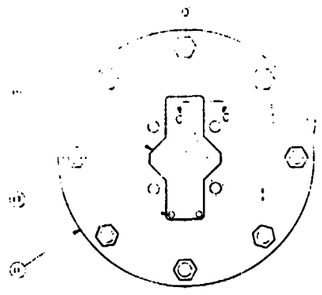

VIEW B-B

ITEM	PART NUMBER	DESCRIPTION	QTY PER ASSY
01	HOUSING	1453 B40 501	1
02	UPPER PLENUM	1453 A48 G01	1
03	LOWER PLENUM	1453 B48 G02	1
04	BUNDLE ASSY	1460E63 G01	1
05	UPPER EXTENSION SLEEVE	1460E59 G01	1
06	.250 SQ LOK-N-K GR 304 NS CAP SCR		16
07	LOWER EXTENSION SLEEVE	1460 B 57 G02	1
08	A GASKET .5" OD 10" CS -15		6
09	STUD .750 ID × 4.50		16
10	NUT HEX .750-10	C 12L	16
11	SEAL B	C 12L	6
12	PIN .98	8766 B49 H01	1
13	D 2 RING .364 ID × .051	1460 L93 H08	21
14	D 11 RING .370 ID × .040	LP152AL C 652-90	42
15	PLATE	S-229 C 652-90	21
16	SPACER	460E59 H13	1
17	L .250 20 LOK-N-K -.38 NS CAP SCR	460E63 H13	4
18	D 6 HS BOLT .375 G		6
19	E GASKET .15 THK	FS 3	2
20	STUD .750 H3 X 8"	DURABLA C 12L	16

A - FLEXITALLIC GASKET CO., CAMDEN, N.J.
B - PARKER SEALS, LEXINGTON, KY
C - CHORTEN A 150 (G S.P. TO 1.38 I.D.)
D REID TOOL SUPPLY CO MUSKEGON HEIGHTS, MICH.
E - MAKE GASKET USING "D" AS TEMPLATE

Figure F-14. FLECHT SEASET 21-Rod Bundle Housing Assembly

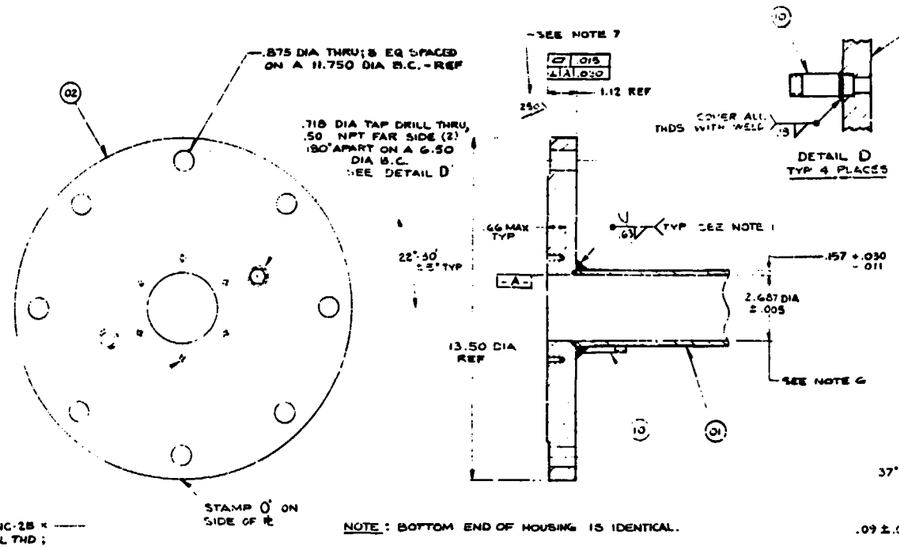

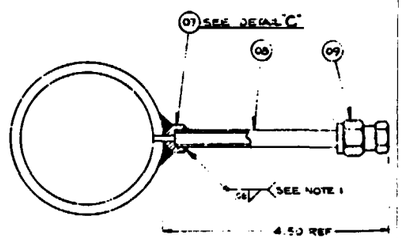

SECTION B-B TYP 13 PLACES

BILL OF MATERIAL

ITEM	QTY	PART NAME	MATERIAL	REQ PER GROUP 01	02	03	04
01	1	TUBE	SA213-TP 304	1			
02	2	FLANGE, 8" 150 LB BLIND	SA182 F 304	2			
03	1	8" 150 LB BLIND FLANGE	C.S. STL	2			
04	A	GASKET	CG-10	2			
05		.750-10 UNC-2A x 5" STUD	C.S. STL	16			
06		.750-10 UNC-2B HEX NUT	C.S. STL	32			
07		BOSS	SA479 GR 304	13			
08		TUBING .250 O.D. x .049 W x 4.00 LG	SA213 TYPE 304	13			
09	B	SWAGELOK CAP	SS-400-C	13			
10		NIPPLE .50 NOM SCH 80 x 6.00	304 SST	14			

A - FLEXITALLIC GASKET CO., CAMDEN, N. J.
B - PGH VALVE & FITTING CO, PGH., PA

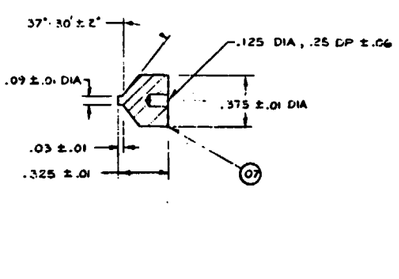

DETAIL 'C'

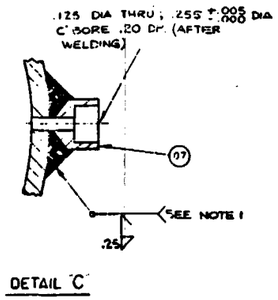

NOTES:
1 - WELD PER W PROC. SPEC. 29261B-1. LIQUID PENETRANT EXAM PER W PROC. SPEC. 595139, QUALITY LEVEL A.
2 - ASSY TO BE FABRICATED PER ASME BOILER CODE SECTION I FOR 80 PSIG @ 1500°F PEAK TEMP @ MID ELEVATION, 1000°F @ FLANGES, 17.02
3 - FLANGES, 17.03 ARE FOR HYDROTEST ONLY. DRILL THRU ON CENTER .718 DIA & TAP .50 NPT.
4 - FINISHED ASSY TO BE STRAIGHT WITHIN .25 OVER ENTIRE LENGTH. NO KINKS PERMITTED.
5 - FINISHED ASSY MUST PASS INSPECTION PLUG OF 2.645 O.D. x 10.00 LG.
6 - VESSEL DIAMETER MAY BE OUT OF ROUND .030 MAX LOCALLY AT WELDED BOSS LOCATIONS, NO WALL THINNING PERMITTED.
7 - IF FLATNESS & PERPINDICULARITY ARE MET AFTER WELDING, NO CUT IS TO BE MADE ON FLANGE SEALING SURFACE. IF MACHINING OF SEALING SURFACE IS REQ'D, A PHONOGRAPHIC SURFACE IS PREFERRED BUT NOT REQ'D. NO RADIAL MACHINING MARKS ARE PERMITTED.

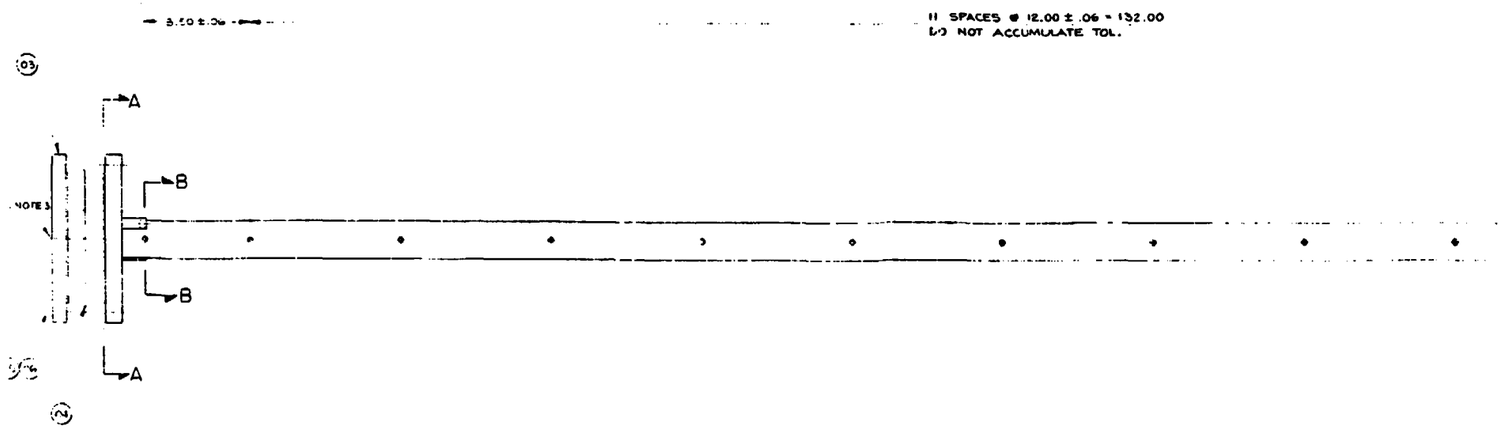

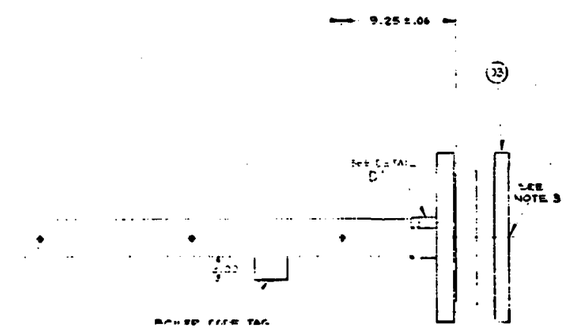

Figure F-15. FLECHT SEASET 21-Rod Bundle Low Mass Housing Detail

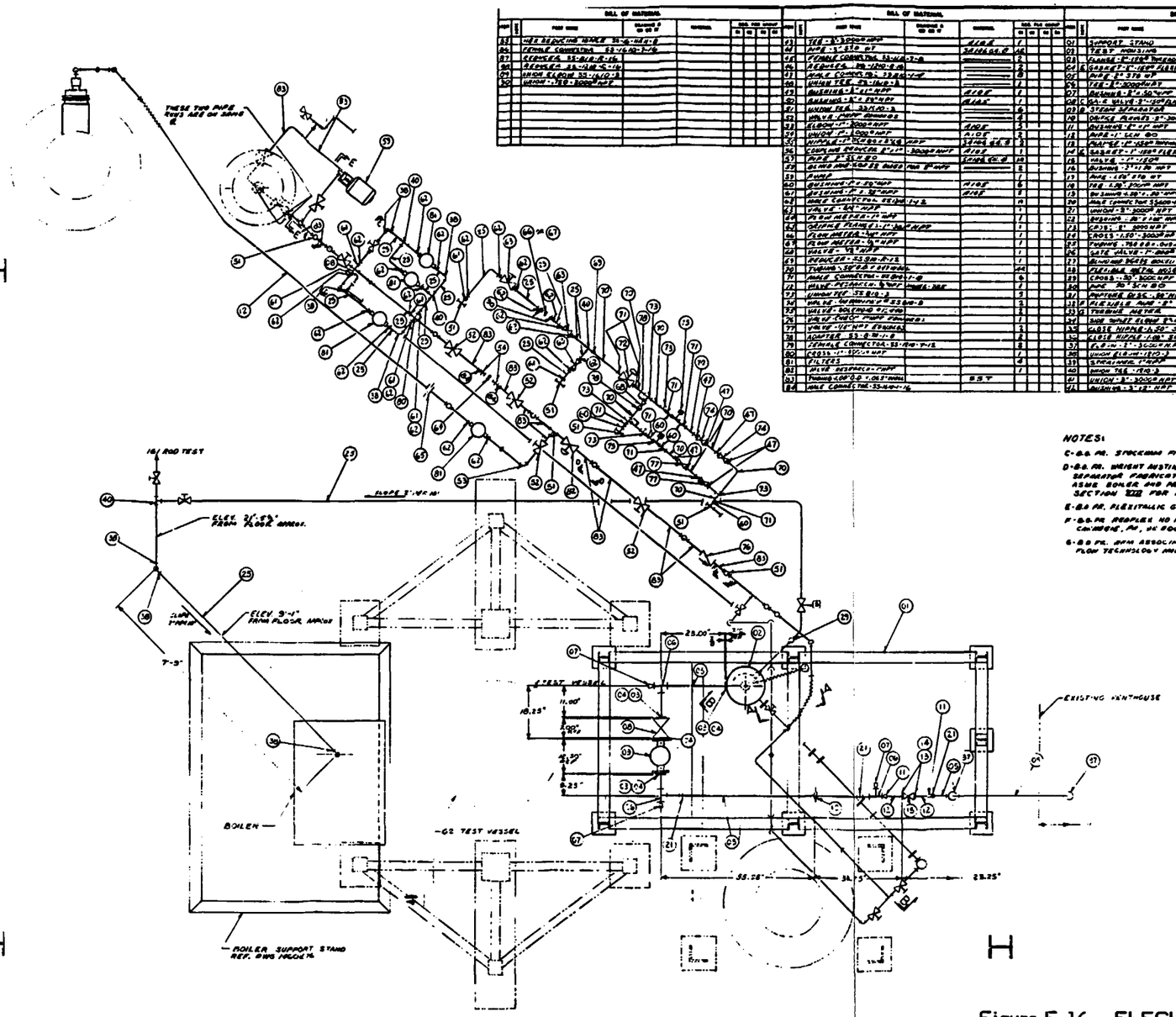

Figure F-16. FLECHT SEASET 21-Rod Bundle Loop Piping (sheet 1 of 3)

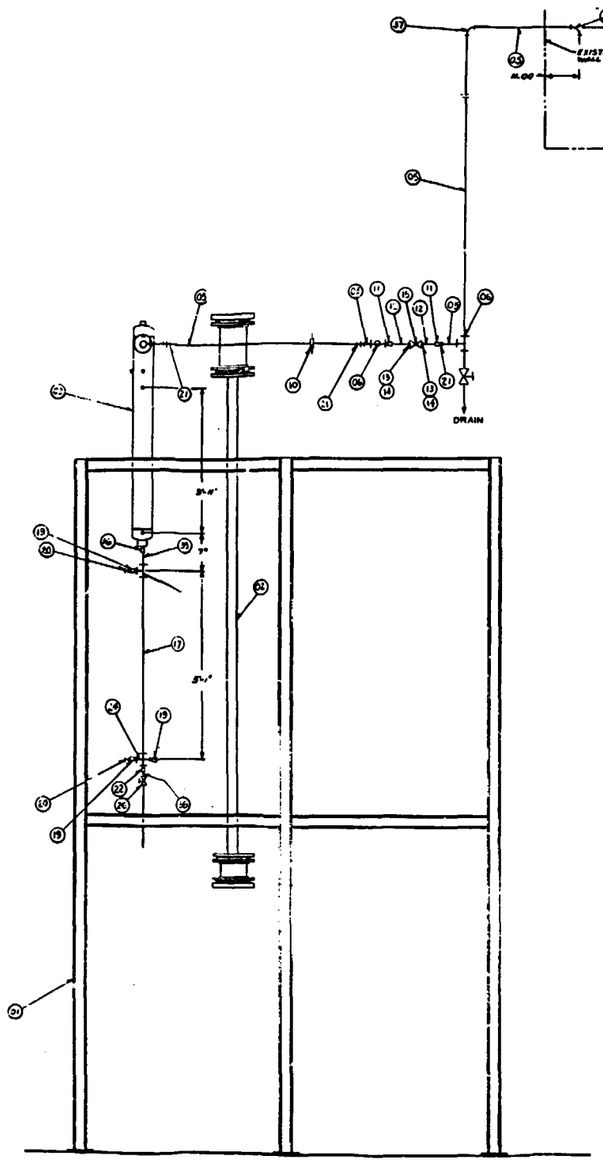

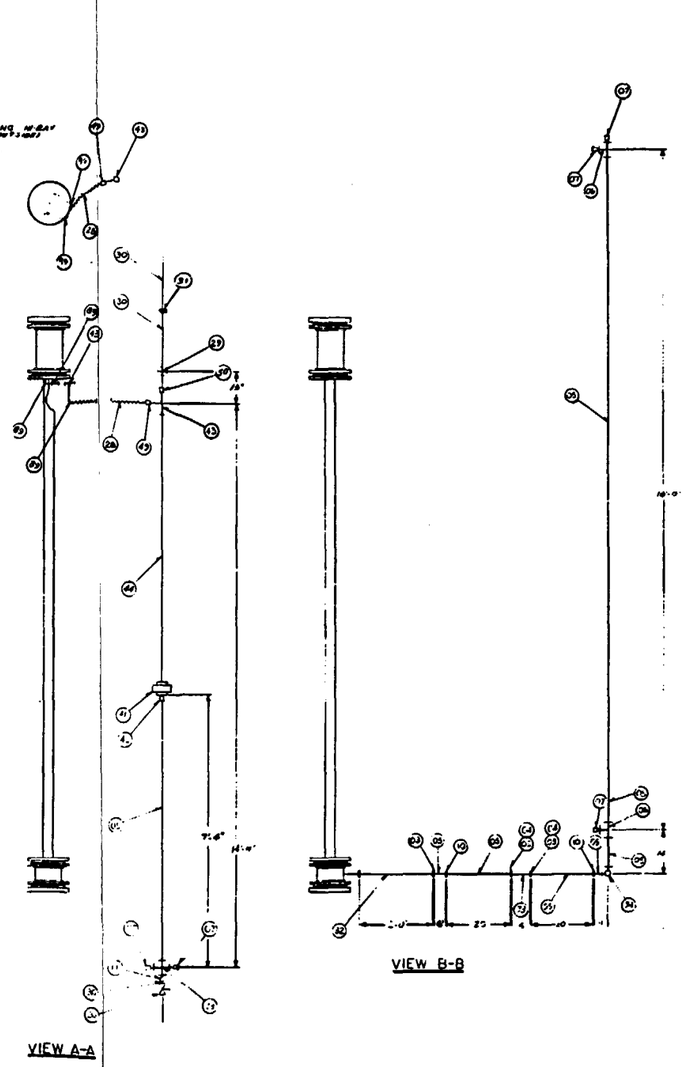

Figure F-16. FLECHT SEASET 21-Rod Bundle Loop Piping (sheet 2 of 3)

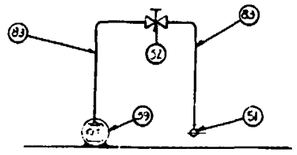

VIEW E-E

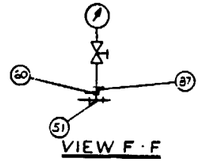

VIEW F-F

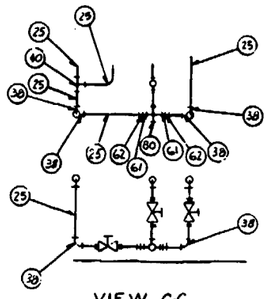

VIEW C-C

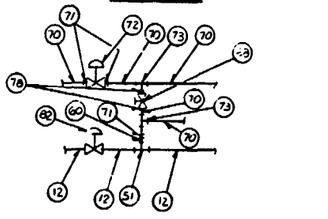

VIEW D-D

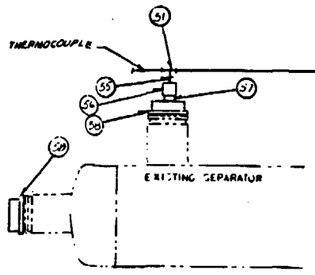

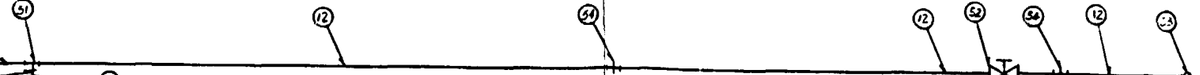

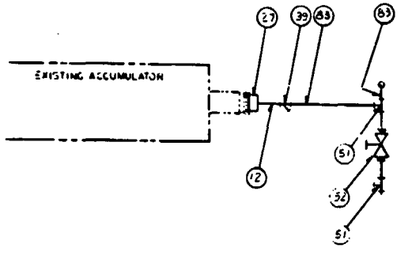

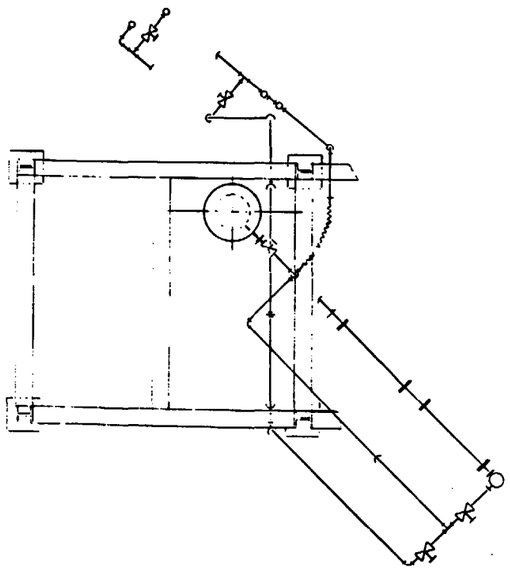

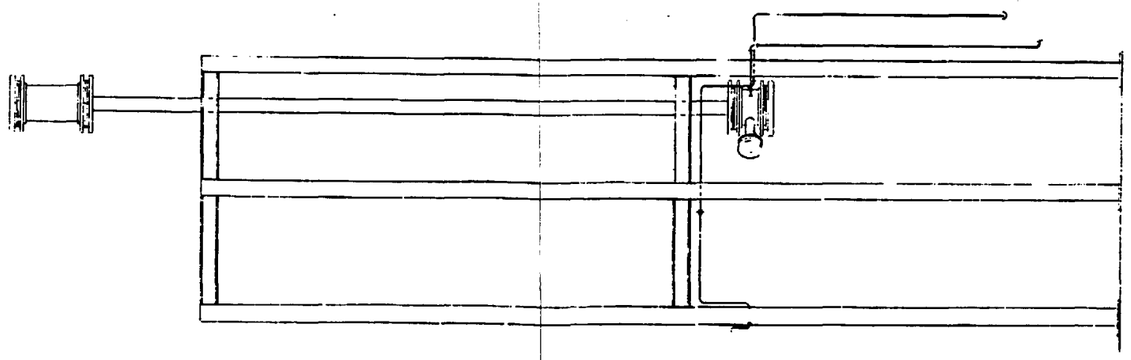

Figure F-16. FLECHT SEASET 21-Rod Bundle Loop Piping (sheet 3 of 3)

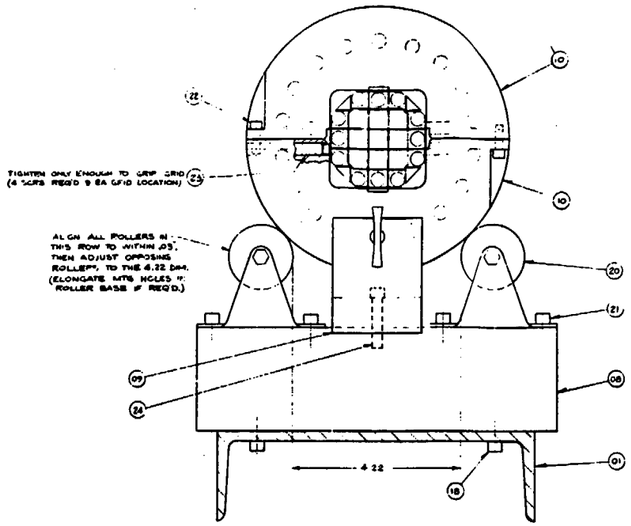

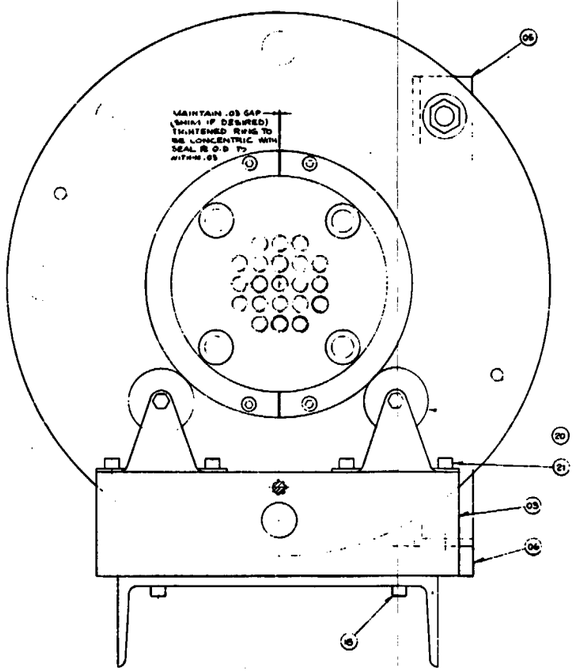

BILL OF MATERIAL

ITEM	QTY	PART NUMBER	DESCRIPTION OR SIZE OF	MATERIAL	REQ PER GROUP A	B	C
01		BASE	14608.47 HOT		1	-	-
02		RING	HO1		1	-	-
03		SUPPORT	HO2		1	-	-
04		SUPPORT	HO3		1	-	-
04A		STRUT	HO4		2	1	-
05		BRACKET	HO5		2	1	-
07		THUMB SCREW	HO9		6	2	-
08		ROLLER SUPPORT	HO6		8	2	-
09		WHEEL	H10		8	2	-
10		FRAME	14608.47 HO8		16	-	-
11	A	THUMB SCREW 1"-14			1	1	-
12		.500-13 UNC 2A x 2.50 LG HEX HD BOLT		C-32%	2	-	-
13		.500-13 UNC-2B HEX NUT			2	-	-
14	E	.250-20 UNC-2A x 1.88 LG SOC HD CAP SCR			4	1	-
15		.750-10 UNC 2A x 6" STUD			1	-	-
16		.750-10 UNC-2B HEX NUT			2	-	-
17		.500-13 UNC-2A x .75 LG 4EX HD BOLT			2	-	-
18		.250-20 UNC-3A x .75 LG SOC HD CAP SCR			23	-	-
19		.500 PLAIN WASHER (LARGE O.D.)			2	-	-
20	B	CASTER 4"-1640-S1			18	-	-
21		.250-20 UNC-2A x .50 LG SOC HD CAP SCR			36	-	-
22		.190-24 UNC 2A x .62 LG S.H. HD CAP SCR			16	-	-
23	A	3/8 SWIVEL PAD AL-3N 3/8"-16			16	-	-
24		.250-20 UNC-2A x 1.25 LG SOC HD CAP SCR			8	-	-

A - REID TOOL SUPPLY CO. MUSKEGON, MICH.
B - COLSON CASTERS, McKEE STEWART EQUIP CORP. PGH, PA.

NOTES:
1 - STRUTS, IT 05 & HARDWARE ITS 12-13-15-16-17-19 & BRACKET IT 06 ARE REQ'D ONLY WHEN FINISHED BUNDLE & STRONG BACK ARE LIFTED & MOVED TO TEST AREA.
2 - SHORTEN A 2" LG SCR TO 1.88 (4 REQ'D)

SEAL PLATE B364D69

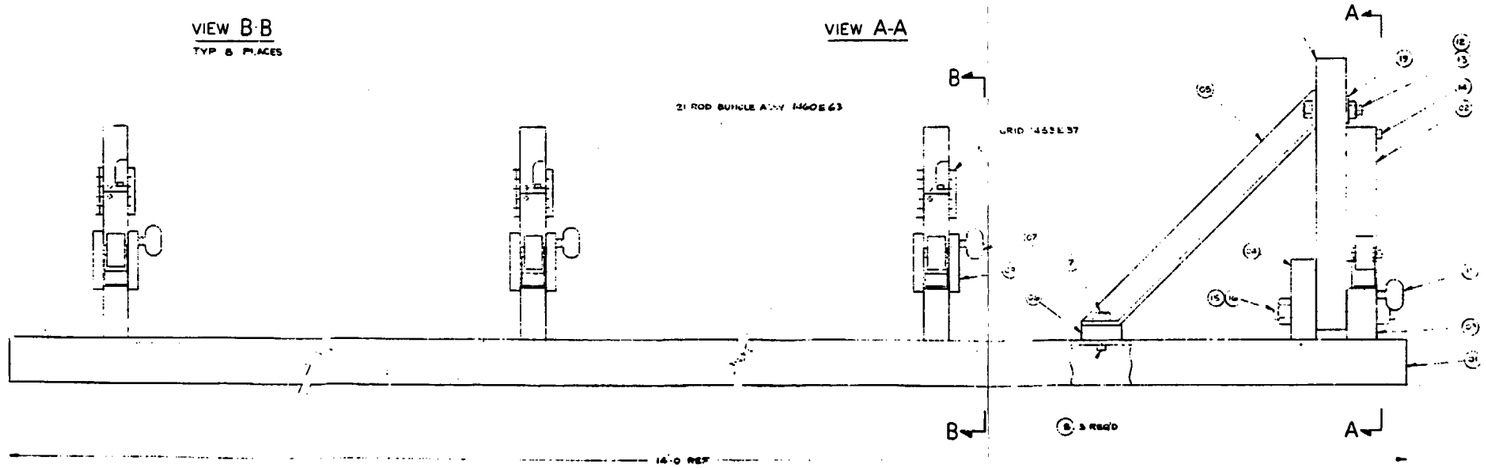

Figure F-17. FLECHT SEASET 21-Rod Bundle Strongback and Assembly Fixture

Channel No.	Location	
1	[illegible]	[illegible]
2	[illegible]	[illegible]
3	[illegible]	[illegible]
4	[illegible]	[illegible]
5	[illegible]	[illegible]
6	[illegible]	[illegible]
7	[illegible]	[illegible]
8	[illegible]	[illegible]
9	[illegible]	[illegible]
10	[illegible]	[illegible]
11	[illegible]	[illegible]
12	Spare	
13	[illegible]	48"
14	[illegible]	48"
15	[illegible]	48"
16	[illegible]	48"
17	[illegible]	60"
18	[illegible]	60"
19	[illegible]	60"
20	[illegible]	60"
21	[illegible]	67"
22	[illegible]	67"
23	[illegible]	67"
24	[illegible]	67"
25	[illegible]	70"
26	[illegible]	70"
27	[illegible]	70"
28	[illegible]	70"
29	[illegible]	70"
30	[illegible]	[illegible]
31	[illegible]	[illegible]
32	[illegible]	[illegible]
33	[illegible]	[illegible]
34	[illegible]	[illegible]
35	[illegible]	[illegible]
36	[illegible]	[illegible]
37	[illegible]	[illegible]
38	[illegible]	[illegible]
39	[illegible]	[illegible]
40	[illegible]	[illegible]
41	[illegible]	[illegible]
42	[illegible]	[illegible]
43	[illegible]	[illegible]
44	[illegible]	[illegible]
45	[illegible]	[illegible]
46	[illegible]	[illegible]
47	Spare	
48	[illegible]	[illegible]
49	[illegible]	[illegible]
50	[illegible]	[illegible]
51	[illegible]	[illegible]
52	[illegible]	[illegible]
53	[illegible]	[illegible]
54	[illegible]	[illegible]
55	Spare	
56	[illegible]	[illegible]
57	[illegible]	[illegible]
58	[illegible]	[illegible]
59	[illegible]	[illegible]
60	[illegible]	[illegible]
61	[illegible]	[illegible]
62	[illegible]	[illegible]
63	[illegible]	[illegible]
64	[illegible]	[illegible]
65	[illegible]	[illegible]
66	[illegible]	[illegible]
67	[illegible]	[illegible]
68	[illegible]	[illegible]
69	[illegible]	[illegible]
70	[illegible]	76"
71	[illegible]	76"
72	[illegible]	[illegible]
73	[illegible]	76"
74	[illegible]	76"
75	[illegible]	76"
76	[illegible]	[illegible]
77	[illegible]	76"
78	[illegible]	76"
79	[illegible]	76"
80	[illegible]	[illegible]
81	[illegible]	[illegible]
82	[illegible]	[illegible]
83	[illegible]	[illegible]
84	[illegible]	77"
85	[illegible]	77"
86	[illegible]	[illegible]
87	[illegible]	77"
88	[illegible]	78"
89	[illegible]	78"
90	[illegible]	78"
91	[illegible]	78"
92	[illegible]	78"
93	[illegible]	78"
94	[illegible]	78"
95	[illegible]	78"

Channel No.	Location	
96	HR T/C-3D	78"
97	HR T/C-4A	78"
98	HR T/C-4C	78"
99	Selective Channel	
100	HR T/C-4E	78"
101	HR T/C-5C	78"
102	Spare	
103	Spare	
104	Spare	
105	Spare	
106	Spare	
107	Spare	
108	Spare	
109	HR T/C-1B	84"
110	HR T/C-1C	84"
111	HR T/C-2B	84"
112	HR T/C-2E	84"
113	HR T/C-3A	84"
114	HR T/C-3B	84"
115	HR T/C-3D	84"
116	HR T/C-4D	84"
117	HR T/C-5B	84"
118	HR T/C-5C	84"
119	HR T/C-1D	90"
120	HR T/C-2B	90"
121	HR T/C-2C	90"
122	HR T/C-2E	90"
123	HR T/C-3A	90"
124	HR T/C-3B	90"
125	HR T/C-3D	90"
126	HR T/C-3E	90"
127	HR T/C04B	90"
128	HR T/C-5C	90"
129	HR T/C-5D	90"
130	HR T/C-1B	96"
131	HR T/C-1C	96"
132	HR T/C-2A	96"
133	HR T/C-2E	96"
134	HR T/C-3A	96"
135	HR T/C-3B	96"
136	HR T/C-3D	96"
137	HR T/C-4D	96"
138	HR T/C-5B	96"
139	HR T/C-5C	96"
140	HR T/C-1B	102"
141	HR T/C-1C	102"
142	HR T/C-1D	102"
143	HR T/C-2C	102"
144	HR T/C-3E	102"
145	HR T/C-4B	102"
146	HR T/C-4D	102"
147	HR T/C-5B	102"
148	HR T/C-5D	102"
149	HR T/C-2A	111"
150	HR T/C-2B	111"
151	HR T/C-2E	111"
152	HR T/C-3A	111"
153	HR T/C-3B	111"
154	HR T/C-3D	111"
155	HR T/C-4A	111"
156	HR T/C-4C	111"
157	HR T/C-4E	111"
158	HR T/C-5C	111"
159	HR T/C-1B	120"
160	HR T/C-1C	120"
161	HR T/C-1D	120"
162	HR T/C-2C	120"
163	HR T/C-3E	120"
164	HR T/C-4B	120"
165	HR T/C-4D	120"
166	HR T/C-5B	120"
167	HR T/C-5D	120"
168	HR T/C-2A	132"
169	HR T/C-4A	132"
170	HR T/C-4C	132"
171	HR T/C-4E	132"
172	HR T/C-1D	138"
173	HR T/C-2C	138"
174	HR T/C-3E	138"
175	HR T/C-5B	138"
176	HR T/C-3D	138"
177	SP T/C-6B	138"
178	SP T/C-11B	132"
179	SP T/C-6A	120"
180	SP T/C-1.C	120"
181	SP T/C-14C	120"
182	SP T/C 5B	111"
183	SP T/C-10A	111"
184	SP T/C-7A	96"
185	SP T/C-8C	96"
186	SP T/C-10C	96"
187	SP T/C-5B	90"
188	SP T/C-7A	90"
189	SP T/C-10C	90"
190	SP T/C-6A	90"

Channel No.	Location	
191	SP T/C-6B	78"
192	SP T/C-11B	78"
193	SP T/C-9B	78"
194	SP T/C-8B	78"
195	SP T/C-7C	74"
196	SP T/C-6B	67"
197	SP T/C-9B	67"
198	SP T/C-11B	67"
199	SP T/C-Spec.	67"
200	SP T/C-10B	59"
201	SP T/C-15B	59"
202	SP T/C-10A	48"
203	SP T/C-10B	18"
204	SPARE	
205	SPARE	
206	SPARE	
207	SPARE	
208	SPARE	
209	SPARE	
210	SPARE	
211	SPARE	
212	SPARE	
213	SPARE	
214	SPARE	
215	SPARE	
216	Spare	
217	Spare	
218	Spare	
219	Spare	
220	Spare	
221	Spare	
222	Spare	
223	Spare	
224	Spare	
225	Spare	
226	Spare	
227	Spare	
228	Spare	
229	Spare	
230	Spare	
231	Spare	
232	Spare	
233	Spare	
234	Spare	
235	Spare	
236	Spare	
237	Spare	
238	Spare	
239	H.I.W. T/C - 270°	2'
240	H.I.W. T/C - 180°	3'
241	H.I.W. T/C - 90°	3'
242	H.I.W. T/C - 270°	3'
243	H.I.W. T/C - 270°	5'
244	H.I.W. T/C - 90°	6'
245	H.I.W. T/C - 270°	6'
246	H.I.W. T/C - 270°	7'
247	H.I.W. T/C - 90°	8'
248	H.I.W. T/C - 270°	8'
249	H.I.W. T/C - 270°	9'
250	H.I.W. T/C - 90°	10'
251	H.I.W. T/C - 270°	10'
252	H.I.W. T/C - 270°	11'
253	HW T/C-90	0'
254	HW T/C-270	0'
255	HW T/C-0	1'
256	HW T/C-180	1'
257	HW T/C-90	2'
258	HW T/C-270	2'
259	HW T/C-0	3'
260	HW T/C-180	3'
261	HW T/C-90	4'
262	HW T/C-270	4'
263	HW T/C-0	5'
264	HW T/C-90	5'
265	HW T/C-180	5'
266	HW T/C-270	5'
267	HW T/C-0	6'
268	HW T/C-90	6'
269	HW T/C-180	6'
270	HW T/C-270	6'
271	HW T/C-0	7'
272	HW T/C-90	7'
273	HW T/C-180	7'
274	HW T/C-270	7'
275	HW T/C-0	8'
276	HW T/C-90	8'
277	HW T/C-180	8'
278	HW T/C-270	8'
279	HW T/C-90	9'
280	HW T/C-270	9'
281	HW T/C-0	10'
282	HW T/C-90	10'
283	HW T/C-180	10'
284	HW T/C-270	10'
285	HW T/C-0	11'

Channel No.	Location	
286	HW T/C-90	11'
287	HW T/C-180	11'
288	HW T/C-270	11'
289	HW T/C-90	12'
290	HW T/C-270	12'
291	Lower Plenum Fluid T/C	
292	Lower Plenum Wall T/C	
293	Upper Plenum Bundle Fluid T/C	
294	Upper Plen. Hsg. Ext. Fl. T/C	
295	Upper Plenum Steam Probe T/C	
296	Upper Plenum Seal Plate T/C	
297	Upper Plenum 90 Wall T/C	
298	Upper Plenum 180 Wall T/C	
299	Upper Plenum 270 Wall T/C	
300	Carryover Tank EL Fluid T/C	
301	Carryover Tank EL Wall T/C	
302	Carryover Tank EL Wall T/C	
303	Steam Separator EL Fluid T/C	
304	Steam Separator EL Wall T/C	
305	Steam Separator EL Wall T/C	
306	Drain Tank EL Fluid T/C	
307	Drain Tank EL Wall T/C	
308	Drain Tank EL	
309	Accumulator EL Fluid T/C	
310	Steam Inj. Sys. EL Fluid T/C	
311	Upper Plenum/Stm.Sep.SteamProbeT/C	
312	Lower Plenum/Stm.Sep. Wall T/C	
313	Stm.Sep/Exhaust Line Stm.ProbeT/C	
314	Stm. Sep/Exhaust Line Wall T/C	
315	Exhaust Line before Orifice Plate- Wall T/C	
316	Exhaust Line before Flow Valve Fluid T/C	
317	Injection Line to Lower Plenum Fluid T/C	
318	Stm. Inj. Sys. Orifice Fluid T/C	
319	Inj. Line to Lower Plenum Fluid T	
320	Crossover Leg after Turbine Meter Fluid T/C	
321	Crossover Leg before Turbine Meter- Fluid T/C	
322	Spare	
323	Spare	
324	Spare	
325	Zone A Primary Power	
326	Zone A Redundant Power	
327	Steam Cooling Power	
328	Spare	
329	Spare	
330	Spare	
331	Turbine Meter 5 gpm	
332	Turbine Meter 1[illegible] gpm	
333	Turbine Meter [illegible] gpm	
334	Bi-directional Turbine Meter	
335	0 to 1 ft. Housing DP	
336	1 to 2 ft. Housing DP	
337	2 to 3 ft. Housing DP	
338	3 to 4 ft. Housing DP	
339	4 to 5 ft. Housing DP	
340	5 to 6 ft. Housing DP	
341	6 to 7 ft. Housing DP	
342	7 to 8 ft. Housing DP	
343	8 to 9 ft. Housing DP	
344	9 to 10 ft. Housing DP	
345	10 to 11 ft. Housing DP	
346	11 to 12 ft. Housing DP	
347	Upper Plenum DP	
348	Overall Housing DP	
349	Carryover Tank DP	
350	Steam Separator DP	
351	Drain Tank DP	
352	Accumulator DP	
353	Exhaust Orifice DP Low Range	
354	Steam Inj. Sys. DP Level	
355	Steam Inj. Sys. Orifice DP	
356	Downcomer/0 ft. El DP	Gravity
357	Downcomer Level DP	Gravity
358	Downcomer to Steam Separator DP	Gravity
359	Upper Plenum to Steam Separator DP	Gravity
360	Exhaust Orifice DP High Range	
361	Exhaust Line Orifice Pressure	
362	Upper Plenum Pressure -Forced Steam Separator Pressure-Gravity	
363	Steam Injection Line Press.	
364	Steam Injection Flow lbs./sec.	

H.R. - HEATER ROD
S.P. - STEAM PROBE
H.S. - HOUSING STEAM
H.W. - HOUSING WALL
H.I.W. - Housing Insulation Wall

Figure F-18. FLECHT SEASET 21-Rod Bundle Computer Data Acquisition System Bundle No. 1

COMPUTER DATA ACQUISITION SYSTEM		
CHANNEL NO.	LOCATION	
1	HR T/C-2A	12"
2	HR T/C-4A	12"
3	HR T/C-4C	12"
4	HR T/C-4E	12"
5	HR T/C-1B	24"
6	HR T/C-1C	24"
7	HR T/C-4D	24"
8	HR T/C-5B	24"
9	HR T/C-2A	39"
10	HR T/C-4A	39"
11	HR T/C-4C	39"
12	HR T/C-4E	39"
13	HR T/C-1B	48"
14	HR T/C-1C	48"
15	HR T/C-4D	48"
16	HR T/C-5B	48"
17	HR T/C-2A	60"
18	HR T/C-4A	60"
19	HR T/C-4C	60"
20	HR T/C-4E	60"
21	HR T/C-2A	67"
22	HR T/C-4A	67"
23	HR T/C-4C	67"
24	HR T/C-4E	67"
25	HR T/C-1B	70"
26	HR T/C-1C	70"
27	HR T/C-2D	70"
28	HR T/C-3C	70"
29	HR T/C-4D	70"
30	HR T/C-5B	70"
31	HR T/C-1D	71"
32	HR T/C-2C	71"
33	HR T/C-2D	71"
34	HR T/C-3C	71"
35	HR T/C-3E	71"
36	HR T/C-4B	71"
37	HR T/C-5D	71"
38	HR T/C-1B	72"
39	HR T/C-1C	72"
40	HR T/C-2B	72"
41	HR T/C-2D	72"
42	HR T/C-2E	72"
43	HR T/C-3A	72"
44	HR T/C-3B	72"
45	HR T/C-3C	72"
46	HR T/C-3D	72"
47	HR T/C-4D	72"
48	HR T/C-5B	72"
49	HR T/C-5C	72"
50	HR T/C-1D	74"
51	HR T/C-2B	74"
52	HR T/C-2C	74"
53	HR T/C-2D	74"
54	HR T/C-2E	74"
55	HR T/C-3A	74"
56	HR T/C-3B	74"
57	HR T/C-3C	74"
58	HR T/C-3D	74"
59	HR T/C-3E	74"
60	HR T/C-4B	74"
61	HR T/C-5C	74"
62	HR T/C-5D	74"
63	HR T/C-1D	75.25"
64	HR T/C-2C	75.25"
65	HR T/C-2D	75.25"
66	HR T/C-3C	75.25"
67	HR T/C-3E	75.25"
68	HR T/C-4B	75.25"
69	HR T/C-5D	75.25"
70	HR T/C-2A	76"
71	HR T/C-2B	76"
72	HR T/C-2D	76"
73	HR T/C-2E	76"
74	HR T/C-3A	76"
75	HR T/C-3B	76"
76	HR T/C-3C	76"
77	HR T/C-3D	76"
78	HR T/C-4A	76"
79	HR T/C-4C	76"
80	HR T/C-4E	76"
81	HR T/C-5C	76"
82	HR T/C-1D	77"
83	HR T/C-2C	77"
84	HR T/C-2D	77"
85	HR T/C-3C	77"
86	HR T/C-3E	77"
87	HR T/C-4B	77"
88	HR T/C-5D	77"
89	HR T/C-2A	78"
90	HR T/C-2B	78"
91	HR T/C-2D	78"
92	HR T/C-2E	78"
93	HR T/C-3A	78"
94	HR T/C-3B	78"
95	HR T/C-3C	78"

COMPUTER DATA ACQUISITION SYSTEM		
CHANNEL NO.	LOCATION	
96	HR T/C-3D	78"
97	HR T/C-4A	78"
98	HR T/C-4C	78"
99	DEFECTIVE CHANNEL	
100	HR T/C-4E	78"
101	HR T/C-5C	78"
102	SPARE	
103	SPARE	
104	SPARE	
105	SPARE	
106	SPARE	
107	SPARE	
108	SPARE	
109	HR T/C-1B	84"
110	HR T/C-1C	84"
111	HR T/C-2B	84"
112	HR T/C-2E	84"
113	HR T/C-3A	84"
114	HR T/C-3B	84"
115	HR T/C-3D	84"
116	HR T/C-4D	84"
117	HR T/C-5B	84"
118	HR T/C-5C	84"
119	HR T/C-1D	90"
120	HR T/C-2B	90"
121	HR T/C-2C	90"
122	HR T/C-2E	90"
123	HR T/C-3A	90"
124	HR T/C-3B	90"
125	HR T/C-3D	90"
126	HR T/C-3E	90"
127	HR T/C-4B	90"
128	HR T/C-5C	90"
129	HR T/C-5D	90"
130	HR T/C-1B	96"
131	HR T/C-1C	96"
132	HR T/C-2B	96"
133	HR T/C-2E	96"
134	HR T/C-3A	96"
135	HR T/C-3B	96"
136	HR T/C-3D	96"
137	HR T/C-4D	96"
138	HR T/C-5B	96"
139	HR T/C-5C	96"
140	HR T/C-1B	102"
141	HR T/C-1C	102"
142	HR T/C-1D	102"
143	HR T/C-2C	102"
144	HR T/C-3E	102"
145	HR T/C-4B	102"
146	HR T/C-4D	102"
147	HR T/C-5B	102"
148	HR T/C-5D	102"
149	HR T/C-2A	111"
150	HR T/C-2B	111"
151	HR T/C-2E	111"
152	HR T/C-3A	111"
153	HR T/C-3B	111"
154	HR T/C-3D	111"
155	HR T/C-4A	111"
156	HR T/C-4C	111"
157	HR T/C-4E	111"
158	HR T/C-5C	111"
159	HR T/C-1B	120"
160	HR T/C-1C	120"
161	HR T/C-1D	120"
162	HR T/C-2C	120"
163	HR T/C-3E	120"
164	HR T/C-4B	120"
165	HR T/C-4D	120"
166	HR T/C-5B	120"
167	HR T/C-5D	120"
168	HR T/C-2A	132"
169	HR T/C-4A	132"
170	HR T/C-4C	132"
171	HR T/C-4E	132"
172	HR T/C-1D	138"
173	HR T/C-2C	138"
174	HR T/C-3E	138"
175	HR T/C-4B	138"
176	HR T/C-5D	138"
177	BF T/C-9B	35"
178	BF T/C-10B	47"
179	BF T/C-15B	58"
180	SP T/C-10B	58"
181	BF T/C-8B	67"
182	SP T/C-SPEC.	67"
183	SP T/C-9B	67"
184	SP T/C-11B	67"
185	BF T/C-6A	77"
186	BF T/C-8A	77"
187	SP T/C-9B	77"
188	SP T/C-7A	77"
189	BF T/C-6B	89"
190	BF T/C-7B	89"

COMPUTER DATA ACQUISITION SYSTEM		
CHANNEL NO.	LOCATION	
191	SP T/C-10C	89"
192	SP T/C-5A	89"
193	BF T/C-8C	97"
194	BF T/C-9B	97"
195	SP T/C-10C	97"
196	BF T/C-5A	109"
197	SP T/C-10A	109"
198	BF T/C-14B	120"
199	SP T/C-6-B	120"
200	SP T/C-15B	120"
201	BF T/C-11E	130"
202	BF T/C-6B	138"
203	BS T/C-2D	73"
204	BS T/C-3C	73"
205	BS T/C-3D	73"
206	BS T/C-4D	73"
207	FS T/C-AØ	72"
208	FS T/C-AØ	84"
209	FS T/C-BØ	60"
210	FS T/C-BØ	78"
211	FS T/C-BØ	84"
212	FS T/C-BØ	111"
213	SPARE	
214	SPARE	
215	SPARE	
216	SPARE	
217	SPARE	
218	SPARE	
219	SPARE	
220	SPARE	
221	SPARE	
222	SPARE	
223	SPARE	
224	SPARE	
225	SPARE	
226	SPARE	
227	SPARE	
228	SPARE	
229	SPARE	
230	SPARE	
231	SPARE	
232	SPARE	
233	SPARE	
234	SPARE	
235	SPARE	
236	SPARE	
237	SPARE	
238	SPARE	
239	H.I.W. T/C-270°	2'
240	H.I.W. T/C-180°	3'
241	H.I.W. T/C-90°	4'
242	H.I.W. T/C-270°	4'
243	H.I.W. T/C-270°	5'
244	H.I.W. T/C-90°	6'
245	H.I.W. T/C-270°	6'
246	H.I.W. T/C-270°	7'
247	H.I.W. T/C-90°	8'
248	H.I.W. T/C-270°	8'
249	H.I.W. T/C-270°	9'
250	H.I.W. T/C-90°	10'
251	H.I.W. T/C-270°	10'
252	H.I.W. T/C-270°	11'
253	HW T/C-90	0'
254	HW T/C-270	0'
255	HW T/C-0	1'
256	HW T/C-180	1'
257	HW T/C-90	2'
258	HW T/C-270	2'
259	HW T/C-0	3'
260	HW T/C-180	3'
261	HW T/C-90	4'
262	HW T/C-270	4'
263	HW T/C-0	5'
264	HW T/C-90	5'
265	HW T/C-180	5'
266	HW T/C-270	5'
267	HW T/C-0	6'
268	HW T/C-90	6'
269	HW T/C-180	6'
270	HW T/C-270	6'
271	HW T/C-0	7'
272	HW T/C-90	7'
273	HW T/C-180	7'
274	HW T/C-270	7'
275	HW T/C-0	8'
276	HW T/C-90	8'
277	HW T/C-180	8'
278	HW T/C-270	8'
279	HW T/C-90	9'
280	HW T/C-270	9'
281	HW T/C-0	10'
282	HW T/C-90	10'
283	HW T/C-180	10'
284	HW T/C-270	10'
285	HW T/C-0	11'

COMPUTER DATA ACQUISITION SYSTEM	
CHANNEL NO.	LOCATION
286	HW T/C-90 11'
287	HW T/C-180 11'
288	HW T/C-270 11'
289	HW T/C-90 12'
290	HW T/C-270 12'
291	LOWER PLENUM FLUID T/C
292	LOWER PLENUM WALL T/C
293	UPPER PLENUM BUNDLE FLUID T/C
294	UPPER PLEN. HSG. EXT. FL. T/C
295	UPPER PLENUM STEAM PROBE T/C
296	UPPER PLENUM SEAL PLATE T/C
297	UPPER PLENUM 90 WALL T/C
298	UPPER PLENUM 180 WALL T/C
299	UPPER PLENUM 270 WALL T/C
300	CARRYOVER TANK EL. FLUID T/C
301	CARRYOVER TANK EL. WALL T/C
302	CARRYOVER TANK EL. WALL T/C
303	STEAM SEPARATOR EL. FLUID T/C
304	STEAM SEPARATOR EL. WALL T/C
305	STEAM SEPARATOR EL. WALL T/C
306	DRAIN TANK EL. FLUID T/C
307	DRAIN TANK EL. WALL T/C
308	DRAIN TANK EL.
309	ACCUMULATOR EL. FLUID T/C
310	STEAM INJ. SYS. EL. FLUID T/C
311	UPPER PLEN/STM. SEP. S.P. T/C
312	UPPER PLEN/STM. SEP. WALL T/C
313	STM. SEP/EXHAUST LINE S.P. T/C
314	STM. SEP/EXHAUST LINE WALL T/C
315	EXHAUST LINE BEFORE ORIFICE PLATE-WALL T/C
316	EXHAUST LINE BEFORE FLOW VALVE FLUID T/C
317	INJ. LINE TO LOWER PLENUM FLUID T/C
318	STM. INJ. SYS. ORIFICE FLUID T/C
319	INJ. LINE TO LOWER PLEN. FLUID T/C
320	CROSSOVER LEG AFTER TURBINE METER-FLUID T/C
321	CROSSOVER LEG BEFORE TURBINE METER-FLUID T/C
322	SPARE
323	SPARE
324	SPARE
325	ZONE A PRIMARY POWER
326	ZONE A REDUNDANT POWER
327	STEAM COOLING POWER
328	SPARE
329	SPARE
330	SPARE
331	TURBINE METER 5 GPM
332	TURBINE METER 15 GPM
333	TURBINE METER 60 GPM
334	BI-DIRECTIONAL TURBINE METER
335	0 TO 1 FT. HOUSING DP
336	1 TO 2 FT. HOUSING DP
337	2 TO 3 FT. HOUSING DP
338	3 TO 4 FT. HOUSING DP
339	4 TO 5 FT. HOUSING DP
340	5 TO 6 FT. HOUSING DP
341	6 TO 7 FT. HOUSING DP
342	7 TO 8 FT. HOUSING DP
343	8 TO 9 FT. HOUSING DP
344	9 TO 10 FT. HOUSING DP
345	10 TO 11 FT. HOUSING DP
346	11 TO 12 FT. HOUSING DP
347	UPPER PLENUM DP
348	OVERALL HOUSING DP
349	CARRYOVER TANK DP
350	STEAM SEPARATOR DP
351	DRAIN TANK DP
352	ACCUMULATOR DP
353	EXHAUST ORIFICE DP LO RANGE
354	STEAM INJ. SYS. DP LEVEL
355	STEAM INJ. SYS. ORIFICE DP
356	DOWNCOMER/0 FT. EL. DP GRAVITY
357	DOWNCOMER LEVEL DP GRAVITY
358	DOWNCOMER TO STEAM SEPARATOR DP GRAVITY
359	UPPER PLENUM TO STEAM SEPARATOR DP GRAVITY
360	EXHAUST ORIFICE DP HIGH RANGE
361	EXHAUST LINE ORIFICE PRESSURE
362	UPPER PLENUM PRESSURE-FORCED STM. SEPARATOR PRESSURE-GRAVITY
363	STEAM INJ. LINE PRESSURE
364	STEAM INJ. FLOW LBS./SEC.

H.R. – HEATER ROD T/C
S.P. – STEAM PROBE T/C
B.S. – BLOCKAGE SLEEVE T/C
H.W. – HOUSING WALL T/C
H.I.W. – HOUSING INSULATION WALL T/C
B.F. – BARE FLUID T/C

Figure F-19. FLECHT SEASET 21-Rod Bundle Computer Data Acquisition System Bundle No. 2

CHANNEL NO.	LOCATION	
1	HR T/C-2A	12"
2	HR T/C-4A	12"
3	HR T/C-4C	12"
4	HR T/C-4E	12"
5	HR T/C-1B	24"
6	HR T/C-1C	24"
7	HR T/C-4D	24"
8	HR T/C-5B	24"
9	HR T/C-2A	39"
10	HR T/C-4A	39"
11	HR T/C-4C	39"
12	HR T/C-4E	39"
13	HR T/C-1B	48"
14	HR T/C-1C	48"
15	HR T/C-4D	48"
16	HR T/C-5B	48"
17	HR T/C-2A	60"
18	HR T/C-4A	60"
19	HR T/C-4C	60"
20	HR T/C-4E	60"
21	HR T/C-2A	67"
22	HR T/C-4A	67"
23	HR T/C-4C	67"
24	HR T/C-4E	67"
25	HR T/C-1B	70"
26	HR T/C-1C	70"
27	HR T/C-2D	70"
28	HR T/C-3C	70"
29	HR T/C-4D	70"
30	HR T/C-5B	70"
31	HR T/C-1D	71"
32	HR T/C-2C	71"
33	HR T/C-2D	71"
34	HR T/C-3C	71"
35	HR T/C-3E	71"
36	HR T/C-4B	71"
37	HR T/C-5D	71"
38	HR T/C-1B	72"
39	HR T/C-1C	72"
40	HR T/C-2B	72"
41	HR T/C-2D	72"
42	HR T/C-2E	72"
43	HR T/C-3A	72"
44	HR T/C-3B	72"
45	HR T/C-3C	72"
46	HR T/C-3D	72"
47	HR T/C-4D	72"
48	HR T/C-5B	72"
49	HR T/C-5C	72"
50	HR T/C-1D	74"
51	HR T/C-2B	74"
52	HR T/C-2C	74"
53	HR T/C-2D	74"
54	HR T/C-2E	74"
55	HR T/C-3A	74"
56	HR T/C-3B	74"
57	HR T/C-3C	74"
58	HR T/C-3D	74"
59	HR T/C-3E	74"
60	HR T/C-4B	74"
61	HR T/C-5C	74"
62	HR T/C-5D	74"
63	HR T/C-1D	75.25"
64	HR T/C-2C	75.25"
65	HR T/C-2D	75.25"
66	HR T/C-3C	75.25"
67	HR T/C-3E	75.25"
68	HR T/C-4B	75.25"
69	HR T/C-5D	75.25"
70	HR T/C-2A	76"
71	HR T/C-2B	76"
72	HR T/C-2D	76"
73	HR T/C-2E	76"
74	HR T/C-3A	76"
75	HR T/C-3B	76"
76	HR T/C-3C	76"
77	HR T/C-3D	76"
78	HR T/C-4A	76"
79	HR T/C-4C	76"
80	HR T/C-4E	76"
81	HR T/C-5C	76"
82	HR T/C-1D	77"
83	HR T/C-2C	77"
84	HR T/C-2D	77"
85	HR T/C-3C	77"
86	HR T/C-3E	77"
87	HR T/C-4B	77"
88	HR T/C-5D	77"
89	HR T/C-2A	78"
90	HR T/C-2B	78"
91	HR T/C-2D	78"
92	HR T/C-2E	78"
93	HR T/C-3A	78"
94	HR T/C-3B	78"
95	HR T/C-3C	78"

CHANNEL NO.	LOCATION	
96	HR T/C-3D	78"
97	HR T/C-4A	78"
98	HR T/C-4C	78"
99	DEFECTIVE CHANNEL	
100	HR T/C-4E	76"
101	HR T/C-5C	78"
102	SPARE	
103	SPARE	
104	SPARE	
105	SPARE	
106	SPARE	
107	SPARE	
108	SPARE	
109	HR T/C-1B	84"
110	HR T/C-1C	84"
111	HR T/C-2B	84"
112	HR T/C-2E	84"
113	HR T/C-3A	84"
114	HR T/C-3B	84"
115	HR T/C-3D	84"
116	HR T/C-4D	84"
117	HR T/C-5B	84"
118	HR T/C-5C	84"
119	HR T/C-1D	90"
120	HR T/C-2B	90"
121	HR T/C-2C	90"
122	HR T/C-2E	90"
123	HR T/C-3A	90"
124	HR T/C-3B	90"
125	HR T/C-3D	90"
126	HR T/C-3E	90"
127	HR T/C-4B	90"
128	HR T/C-5C	90"
129	HR T/C-5D	90"
130	HR T/C-1B	96"
131	HR T/C-1C	96"
132	HR T/C-2B	96"
133	HR T/C-2E	96"
134	HR T/C-3A	96"
135	HR T/C-3B	96"
136	HR T/C-3D	96"
137	HR T/C-4D	96"
138	HR T/C-5B	96"
139	HR T/C-5C	96"
140	HR T/C-1B	102"
141	HR T/C-1C	102"
142	HR T/C-1D	102"
143	HR T/C-2C	102"
144	HR T/C-3E	102"
145	HR T/C-4B	102"
146	HR T/C-4D	102"
147	HR T/C-5B	102"
148	HR T/C-5D	102"
149	HR T/C-2A	111"
150	HR T/C-2B	111"
151	HR T/C-2E	111"
152	HR T/C-3A	111"
153	HR T/C-3B	111"
154	HR T/C-3D	111"
155	HR T/C-4A	111"
156	HR T/C-4C	111"
157	HR T/C-4E	111"
158	HR T/C-5C	111"
159	HR T/C-1B	120"
160	HR T/C-1C	120"
161	HR T/C-1D	120"
162	HR T/C-2C	120"
163	HR T/C-3E	120"
164	HR T/C-4B	120"
165	HR T/C-4D	120"
166	HR T/C-5B	120"
167	HR T/C-5D	120"
168	HR T/C-2A	132"
169	HR T/C-4A	132"
170	HR T/C-4C	132"
171	HR T/C-4E	132"
172	HR T/C-1D	138"
173	HR T/C-2C	138"
174	HR T/C-3E	138"
175	HR T/C-4B	138"
176	HR T/C-5D	138"
177	B.F. T/C-9B	35"
178	B.F. T/C-10B	47"
179	B.F. T/C-15B	58"
180	S.P. T/C-10B	58"
181	B.F. T/C-8B	67"
182	SPARE	
183	S.P. T/C-9B	67"
184	S.P. T/C-11B	67"
185	B.F. T/C-6A	77"
186	B.F. T/C-8A	77"
187	S.P. T/C-9B	77"
188	S.P. T/C-11B	77"
189	B.F. T/C-6C	89"
190	B.F. T/C-7C	89"

CHANNEL NO.	LOCATION	
191	S.P. T/C-10C	89"
192	S.P. T/C-5A	89"
193	B.F. T/C-8C	97"
194	B.F. T/C-9B	97"
195	S.P. T/C-10C	97"
196	B.F. T/C-5A	109"
197	S.P. T/C-10A	109"
198	B.F. T/C-14B	120"
199	S.P. T/C-6B	120"
200	S.P. T/C-15B	120"
201	B.F. T/C-11B	130"
202	B.F. T/C-6B	138"
203	B.S. T/C-4D	73"
204	B.S. T/C-3C	73"
205	B.S. T/C-5B	73"
206	B.S. T/C-3D	73"
207	B.S. T/C-2D	73"
208	B.S. T/C-1C	73"
209	F.S. T/C-BØ	60"
210	F.S. T/C-AØ	72"
211	F.S. T/C-BØ	78"
212	F.S. T/C-BØ	84"
213	F.S. T/C-AØ	84"
214	F.S. T/C-CØ	96"
215	F.S. T/C-BØ	111"
216	F.S. T/C-CØ	120"
217	SPARE	
218	SPARE	
219	SPARE	
220	SPARE	
221	SPARE	
222	SPARE	
223	SPARE	
224	SPARE	
225	SPARE	
226	SPARE	
227	SPARE	
228	SPARE	
229	SPARE	
230	SPARE	
231	SPARE	
232	SPARE	
233	SPARE	
234	SPARE	
235	SPARE	
236	SPARE	
237	SPARE	
238	SPARE	
239	H.I.W. T/C-270°	2'
240	H.I.W. T/C-180°	3'
241	H.I.W. T/C-90°	4'
242	H.I.W. T/C-270°	4'
243	H.I.W. T/C-270°	5'
244	H.I.W. T/C-90°	6'
245	H.I.W. T/C-270°	6'
246	H.I.W. T/C-270°	7'
247	H.I.W. T/C-90°	8'
248	H.I.W. T/C-270°	8'
249	H.I.W. T/C-270°	9'
250	H.I.W. T/C-90°	10'
251	H.I.W. T/C-270°	10'
252	H.I.W. T/C-270°	11'
253	HW T/C-90	0'
254	HW T/C-270	0'
255	HW T/C-0	1'
256	HW T/C-180	1'
257	HW T/C-90	2'
258	HW T/C-270	2'
259	HW T/C-0	3'
260	HW T/C-180	3'
261	HW T/C-90	4'
262	HW T/C-270	4'
263	HW T/C-0	5'
264	HW T/C-90	5'
265	HW T/C-180	5'
266	HW T/C-270	5'
267	HW T/C-0	6'
268	HW T/C-90	6'
269	HW T/C-180	6'
270	HW T/C-270	6'
271	HW T/C-0	7'
272	HW T/C-90	7'
273	HW T/C-180	7'
274	HW T/C-270	7'
275	HW T/C-0	8'
276	HW T/C-90	8'
277	HW T/C-180	8'
278	HW T/C-270	8'
279	HW T/C-90	9'
280	HW T/C-270	9'
281	HW T/C-0	10'
282	HW T/C-90	10'
283	HW T/C-180	10'
284	HW T/C-270	10'
285	HW T/C-0	11'

CHANNEL NO.	LOCATION
286	HW T/C-90 11'
287	HW T/C-180 11'
288	HW T/C-270 11'
289	HW T/C-90 12'
290	HW T/C-270 12'
291	LOWER PLENUM FLUID T/C
292	LOWER PLENUM WALL T/C
293	UPPER PLENUM BUNDLE FLUID T/C
294	UPPER PLEN. HSG. EXT. FL. T/C
295	UPPER PLENUM STEAM PROBE T/C
296	UPPER PLENUM SEAL PLATE T/C
297	UPPER PLENUM 90 WALL T/C
298	UPPER PLENUM 180 WALL T/C
299	UPPER PLENUM 270 WALL T/C
300	CARRYOVER TANK EL. FLUID T/C
301	CARRYOVER TANK EL. WALL T/C
302	CARRYOVER TANK EL. WALL T/C
303	STEAM SEPARATOR EL. FLUID T/C
304	STEAM SEPARATOR EL. WALL T/C
305	STEAM SEPARATOR EL. WALL T/C
306	DRAIN TANK EL. FLUID T/C
307	DRAIN TANK EL. WALL T/C
308	DRAIN TANK EL.
309	ACCUMULATOR EL. FLUID T/C
310	STEAM INJ. SYS. EL. FLUID T/C
311	UPPER PLEN/STM. SEP. S.P. T/C
312	UPPER PLEN/STM. SEP. WALL T/C
313	STM. SEP/EXHAUST LINE S.P. T/C
314	STM. SEP/EXHAUST LINE WALL T/C
315	EXHAUST LINE BEFORE ORIFICE PLATE-WALL T/C
316	EXHAUST LINE BEFORE FLOW VALVE FLUID T/C
317	INJ. LINE TO LOWER PLENUM FLUID T/C
318	STM. INJ. SYS. ORIFICE FLUID T/C
319	INJ. LINE TO LOWER PLEN. FLUID T/C
320	CROSSOVER LEG AFTER TURBINE METER-FLUID T/C
321	CROSSOVER LEG BEFORE TURBINE METER-FLUID T/C
322	SPARE
323	SPARE
324	SPARE
325	ZONE A PRIMARY POWER
326	ZONE A REDUNDANT POWER
327	STEAM COOLING POWER
328	SPARE
329	SPARE
330	SPARE
331	TURBINE METER 5 GPM
332	TURBINE METER 15 GPM
333	TURBINE METER 60 GPM
334	BI-DIRECTIONAL TURBINE METER
335	0 TO 1 FT. HOUSING DP
336	1 TO 2 FT. HOUSING DP
337	2 TO 3 FT. HOUSING DP
338	3 TO 4 FT. HOUSING DP
339	4 TO 5 FT. HOUSING DP
340	5 TO 6 FT. HOUSING DP
341	6 TO 7 FT. HOUSING DP
342	7 TO 8 FT. HOUSING DP
343	8 TO 9 FT. HOUSING DP
344	9 TO 10 FT. HOUSING DP
345	10 TO 11 FT. HOUSING DP
346	11 TO 12 FT. HOUSING DP
347	UPPER PLENUM DP
348	OVERALL HOUSING DP
349	CARRYOVER TANK DP
350	STEAM SEPARATOR DP
351	DRAIN TANK DP
352	ACCUMULATOR DP
353	EXHAUST ORIFICE DP LO RANGE
354	STEAM INJ SYS. DP LEVEL
355	STEAM INJ. SYS. ORIFICE DP
356	DOWNCOMER/0 FT. EL. DP GRAVITY
357	DOWNCOMER LEVEL DP GRAVITY
358	DOWNCOMER TO STEAM SEPARATOR DP GRAVITY
359	UPPER PLENUM T/C STEAM SEPARATOR DP GRAVITY
360	EXHAUST ORIFICE DP HIGH RANGE
361	EXHAUST LINE ORIFICE PRESSURE
362	UPPER PLENUM PRESSURE-FORCED STM. SEPARATOR PRESSURE-GRAVITY
363	STEAM INJ. LINE PRESSURE
364	STEAM INJ. FLOW LBS./SEC.

H.R. – HEATER ROD T/C
S.P. – STEAM PROBE T/C
B.S. – BLOCKAGE SLEEVE T/C
H.W. – HOUSING WALL T/C
H.I.W. – HOUSING INSULATION WALL T/C
B.F. – BARE FLUID T/C

F.S. – FILLER STRIP T/C
AØ - 45°, BØ - 315°, CØ - 240°, DØ - 135° } REFERENCE TO THE HOUSING

Figure F-20. FLECHT SEASET 21-Rod Bundle Computer Data Acquisition System Bundle No. 3

COMPUTER DATA ACQUISITION SYSTEM		
CHANNEL NO.	LOCATION	
1	HR T/C-2A	12"
2	HR T/C-4A	12"
3	HR T/C-4C	12"
4	HR T/C-1C	24"
5	HR T/C-4E	24"
6	HR T/C-5B	24"
7	HR T/C-2A	39"
8	HR T/C-4A	39"
9	HR T/C-4C	39"
10	HR T/C-1C	48"
11	HR T/C-4E	48"
12	HR T/C-5B	48"
13	HR T/C-2A	60"
14	HR T/C-4A	60"
15	HR T/C-4C	60"
16	HR T/C-2A	67"
17	HR T/C-4A	67"
18	HR T/C-4C	67"
19	HR T/C-1C	70"
20	HR T/C-2D	70"
21	HR T/C-3C	70"
22	HR T/C-4D	70"
23	HR T/C-4E	70"
24	HR T/C-5B	70"
25	HR T/C-1D	71"
26	HR T/C-2C	71"
27	HR T/C-2D	71"
28	HR T/C-3C	71"
29	HR T/C-3E	71"
30	HR T/C-4B	71"
31	HR T/C-4D	71"
32	HR T/C-5D	71"
33	HR T/C-1B	72"
34	HR T/C-1C	72"
35	HR T/C-2B	72"
36	HR T/C-2D	72"
37	HR T/C-2E	72"
38	HR T/C-3A	72"
39	HR T/C-3B	72"
40	HR T/C-3C	72"
41	HR T/C-3D	72"
42	HR T/C-4D	72"
43	HR T/C-4E	72"
44	HR T/C-5B	72"
45	HR T/C-5C	72"
46	HR T/C-1B	74"
47	HR T/C-1D	74"
48	HR T/C-2B	74"
49	HR T/C-2C	74"
50	HR T/C-2D	74"
51	HR T/C-2E	74"
52	HR T/C-3A	74"
53	HR T/C-3B	74"
54	HR T/C-3C	74"
55	HR T/C-3D	74"
56	HR T/C-3E	74"
57	HR T/C-4B	74"
58	HR T/C-4D	74"
59	HR T/C-5C	74"
60	HR T/C-5D	74"
61	HR T/C-1D	75.25"
62	HR T/C-2C	75.25"
63	HR T/C-2D	75.25"
64	HR T/C-3C	75.25"
65	HR T/C-3E	75.25"
66	HR T/C-4B	75.25"
67	HR T/C-4D	75.25"
68	HR T/C-5D	75.25"
69	HR T/C-1B	76"
70	HR T/C-2A	76"
71	HR T/C-2B	76"
72	HR T/C-2D	76"
73	HR T/C-2E	76"
74	HR T/C-3A	76"
75	HR T/C-3B	76"
76	HR T/C-3C	76"
77	HR T/C-3D	76"
78	HR T/C-4A	76"
79	HR T/C-4C	76"
80	HR T/C-4D	76"
81	HR T/C-5C	76"
82	HR T/C-1D	77"
83	HR T/C-2C	77"
84	HR T/C-2D	77"
85	HR T/C-3C	77"
86	HR T/C-3E	77"
87	HR T/C-4B	77"
88	HR T/C-4D	77"
89	HR T/C-5D	77"
90	HR T/C-1B	78"
91	HR T/C-2A	78"
92	HR T/C-2B	78"
93	HR T/C-2D	78"
94	HR T/C-2E	78"
95	HR T/C-3A	78"

COMPUTER DATA ACQUISITION SYSTEM		
CHANNEL NO.	LOCATION	
96	HR T/C-3B	78"
97	HR T/C-3C	78"
98	HR T/C-3D	78"
99	DEFECTIVE CHANNEL	
100	HR T/C-4A	78"
101	HR T/C-4C	78"
102	HR T/C-4D	78"
103	HR T/C-5C	78"
104	SPARE	
105	SPARE	
106	SPARE	
107	SPARE	
108	SPARE	
109	HR T/C-1B	84"
110	HR T/C-1C	84"
111	HR T/C-2B	84"
112	HR T/C-2E	84"
113	HR T/C-3A	84"
114	HR T/C-3B	84"
115	HR T/C-3D	84"
116	HR T/C-4E	84"
117	HR T/C-5B	84"
118	HR T/C-5C	84"
119	HR T/C-1B	90"
120	HR T/C-1D	90"
121	HR T/C-2B	90"
122	HR T/C-2C	90"
123	HR T/C-2E	90"
124	HR T/C-3A	90"
125	HR T/C-3B	90"
126	HR T/C-3D	90"
127	HR T/C-3E	90"
128	HR T/C-4B	90"
129	HR T/C-5C	90"
130	HR T/C-5D	90"
131	HR T/C-1B	96"
132	HR T/C-1C	96"
133	HR T/C-2B	96"
134	HR T/C-2E	96"
135	HR T/C-3A	96"
136	HR T/C-3B	96"
137	HR T/C-3D	96"
138	HR T/C-4E	96"
139	HR T/C-5B	96"
140	HR T/C-5C	96"
141	HR T/C-1C	102"
142	HR T/C-1D	102"
143	HR T/C-2C	102"
144	HR T/C-3E	102"
145	HR T/C-4B	102"
146	HR T/C-4E	102"
147	HR T/C-5B	102"
148	HR T/C-5D	102"
149	HR T/C-1B	111"
150	HR T/C-2A	111"
151	HR T/C-2B	111"
152	HR T/C-2E	111"
153	HR T/C-3A	111"
154	HR T/C-3B	111"
155	HR T/C-3D	111"
156	HR T/C-4A	111"
157	HR T/C-4C	111"
158	HR T/C-5C	111"
159	HR T/C-1C	120"
160	HR T/C-1D	120"
161	HR T/C-2C	120"
162	HR T/C-3E	120"
163	HR T/C-4B	120"
164	HR T/C-4E	120"
165	HR T/C-5B	120"
166	HR T/C-5D	120"
167	HR T/C-2A	132"
168	HR T/C-4A	132"
169	HR T/C-4C	132"
170	HR T/C-1D	138"
171	HR T/C-2C	138"
172	HR T/C-3E	138"
173	HR T/C-4B	138"
174	HR T/C-5D	138"
175	SPARE	
176	SPARE	
177	BF T/C-9B	35"
178	BF T/C-10B	47"
179	BF T/C-15B	58"
180	SP T/C-10B	58"
181	BF T/C-8B	67"
182	SP SPEC.	67"
183	SP T/C-9B	67"
184	SP T/C-11B	67"
185	BF T/C-6A	77"
186	BF T/C-8A	77"
187	SP T/C-9B	77"
188	SP T/C-11B	77"
189	BF T/C-6C	89"
190	BF T/C-7C	89"

COMPUTER DATA ACQUISITION SYSTEM		
CHANNEL NO.	LOCATION	
191	SP T/C-10C	89"
192	SP T/C-5A	89"
193	BF T/C-8C	97"
194	BF T/C-9B	97"
195	SP T/C-10C	97"
196	BF T/C-5A	109"
197	SP T/C-10A	109"
198	BF T/C-14B	120"
199	SP T/C-6B	120"
200	SP T/C-15B	120"
201	BF T/C-11B	130"
202	BF T/C-6B	138"
203	BS T/C-4D	70"
204	BS T/C-2E	72"
205	BS T/C-4B	72"
206	BS T/C-1C	73"
207	BS T/C-3B	73"
208	BS T/C-3C	75"
209	FS T/C-BØ	60"
210	FS T/C-AØ	72"
211	FS T/C-BØ	78"
212	FS T/C-BØ	84"
213	FS T/C-AØ	84"
214	FS T/C-CØ	96"
215	FS T/C-BØ	111"
216	FS T/C-CØ	120"
217	SPARE	
218	SPARE	
219	SPARE	
220	SPARE	
221	SPARE	
222	SPARE	
223	SPARE	
224	SPARE	
225	SPARE	
226	SPARE	
227	SPARE	
228	SPARE	
229	SPARE	
230	SPARE	
231	SPARE	
232	SPARE	
233	SPARE	
234	SPARE	
235	SPARE	
236	SPARE	
237	SPARE	
238	SPARE	
239	H.I.W. T/C-270°	2'
240	H.I.W. T/C-180°	3'
241	H.I.W. T/C-90°	4'
242	H.I.W. T/C-270°	4'
243	H.I.W. T/C-270°	5'
244	H.I.W. T/C-90°	6'
245	H.I.W. T/C-270°	6'
246	H.I.W. T/C-270°	7'
247	H.I.W. T/C-90°	8'
248	H.I.W. T/C-270°	8'
249	H.I.W. T/C-270°	9'
250	H.I.W. T/C-90°	10'
251	H.I.W. T/C-270°	10'
252	H.I.W. T/C-270°	11'
253	HW T/C-90	0'
264	HW T/C-270	0'
255	HW T/C-0	1'
256	HW T/C-180	1'
257	HW T/C-90	2'
258	HW T/C-270	2'
259	HW T/C-0	3'
260	HW T/C-180	3'
261	HW T/C-90	4'
262	HW T/C-270	4'
263	HW T/C-0	5'
264	HW T/C-90	5'
265	HW T/C-180	5'
266	HW T/C-270	5'
267	HW T/C-0	6'
268	HW T/C-90	6'
269	HW T/C-180	6'
270	HW T/C-270	6'
271	HW T/C-0	7'
272	HW T/C-90	7'
273	HW T/C-180	7'
274	HW T/C-270	7'
275	HW T/C-0	8'
276	HW T/C-90	8'
277	HW T/C-180	8'
278	HW T/C-270	8'
279	HW T/C-90	9'
280	HW T/C-270	9'
281	HW T/C-0	10'
282	HW T/C-90	10'
283	HW T/C-180	10'
284	HW T/C-270	10'
285	HW T/C-0	11'

COMPUTER DATA ACQUISITION SYSTEM	
CHANNEL NO.	LOCATION
286	HW T/C-90 11'
287	HW T/C-180 11'
288	HW T/C-270 11'
289	HW T/C-90 12'
290	HW T/C-270 12'
291	LOWER PLENUM FLUID T/C
292	LOWER PLENUM WALL T/C
293	UPPER PLENUM BUNDLE FLUID T/C
294	UPPER PLEN. HSG. EXT. FL. T/C
295	UPPER PLENUM STEAM PROBE T/C
296	UPPER PLENUM SEAL PLATE T/C
297	UPPER PLENUM 90 WALL T/C
298	UPPER PLENUM 180 WALL T/C
299	UPPER PLENUM 270 WALL T/C
300	CARRYOVER TANK EL. FLUID T/C
301	CARRYOVER TANK EL. WALL T/C
302	CARRYOVER TANK EL. WALL T/C
303	STEAM SEPARATOR EL. FLUID T/C
304	STEAM SEPARATOR EL. WALL T/C
305	STEAM SEPARATOR EL. WALL T/C
306	DRAIN TANK EL. FLUID T/C
307	DRAIN TANK EL. WALL T/C
308	DRAIN TANK EL.
309	ACCUMULATOR EL. FLUID T/C
310	STEAM INJ. SYS. EL. FLUID T/C
311	UPPER PLEN./STM. SEP. S.P. T/C
312	UPPER PLEN./STM. SEP. WALL T/C
313	STM. SEP./EXHAUST LINE S.P. T/C
314	STM. SEP./EXHAUST LINE WALL T/C
315	EXHAUST LINE BEFORE ORIFICE PLATE-WALL T/C
316	EXHAUST LINE BEFORE FLOW VALVE FLUID T/C
317	INJ. LINE TO LOWER PLENUM FLUID T/C
318	STM. INJ. SYS. ORIFICE FLUID T/C
319	INJ. LINE TO LOWER PLEN. FLUID T/C
320	CROSSOVER LEG AFTER TURBINE METER-FLUID T/C
321	CROSSOVER LEG BEFORE TURBINE METER-FLUID T/C
322	SPARE
323	SPARE
324	SPARE
325	ZONE A PRIMARY POWER
326	ZONE A REDUNDANT POWER
327	STEAM COOLING POWER
328	SPARE
329	SPARE
330	SPARE
331	TURBINE METER 5 GPM
332	TURBINE METER 15 GPM
333	TURBINE METER 60 GPM
334	BI-DIRECTIONAL TURBINE METER
335	0 TO 1 FT. HOUSING DP
336	1 TO 2 FT. HOUSING DP
337	2 TO 3 FT. HOUSING DP
338	3 TO 4 FT. HOUSING DP
339	4 TO 5 FT. HOUSING DP
340	5 TO 6 FT. HOUSING DP
341	6 TO 7 FT. HOUSING DP
342	7 TO 8 FT. HOUSING DP
343	8 TO 9 FT. HOUSING DP
344	9 TO 10 FT. HOUSING DP
345	10 TO 11 FT. HOUSING DP
346	11 TO 12 FT. HOUSING DP
347	UPPER PLENUM DP
348	OVERALL HOUSING DP
349	CARRYOVER TANK DP
350	STEAM SEPARATOR DP
351	DRAIN TANK DP
352	ACCUMULATOR DP
353	EXHAUST ORIFICE DP LO RANGE
354	STEAM INJ. SYS. DP LEVEL
355	STEAM INJ. SYS. ORIFICE DP
356	DOWNCOMER/0 FT. EL. DP GRAVITY
357	DOWNCOMER LEVEL DP GRAVITY
368	DOWNCOMER TO STEAM SEPARATOR DP GRAVITY
359	UPPER PLENUM TO STEAM SEPARATOR DP GRAVITY
360	EXHAUST ORIFICE DP HIGH RANGE
361	EXHAUST LINE ORIFICE PRESSURE
362	UPPER PLENUM PRESSURE-FORCED STM. SEPARATOR PRESSURE-GRAVITY
363	STEAM INJ. LINE PRESSURE
364	STEAM INJ. FLOW LBS./SEC.

H.R. – HEATER ROD T/C
S.P. – STEAM PROBE T/C
B.S. – BLOCKAGE SLEEVE T/C
H.W. – HOUSING WALL T/C
H.I.W. – HOUSING INSULATION WALL T/C
B.F. – BARE FLUID T/C

Figure F-21. FLECHT SEASET 21-Rod Bundle Computer Data Acquisition System Bundle No. 4

COMPUTER DATA ACQUISITION SYSTEM		
CHANNEL NO.	LOCATION	
1	HR T/C-1B	12"
2	HR T/C-2A	12"
3	HR T/C-4C	12"
4	HR T/C-4E	12"
5	HR T/C-1C	24"
6	HR T/C-3B	24"
7	HR T/C-5B	24"
8	HR T/C-1B	39"
9	HR T/C-2A	39"
10	HR T/C-4C	39"
11	HR T/C-4E	39"
12	HR T/C-1C	48"
13	HR T/C-3B	48"
14	HR T/C-5B	48"
15	HR T/C-1B	60"
16	HR T/C-2A	60"
17	HR T/C-4C	60"
18	HR T/C-4E	60"
19	HR T/C-2A	67"
20	HR T/C-2B	67"
21	HR T/C-2C	67"
22	HR T/C-2E	67"
23	HR T/C-4A	67"
24	HR T/C-4B	67"
25	HR T/C-4C	67"
26	HR T/C-4E	67"
27	HR T/C 2C	70"
28	HR T/C-2D	70"
29	HR T/C-3C	70"
30	HR T/C-3D	70"
31	HR T/C-4D	70"
32	HR T/C-1D	71"
33	HR T/C-2E	72"
34	HR T/C-3E	72"
35	HR T/C-4B	72"
36	HR T/C-5C	72"
37	HR T/C-1B	73"
38	HR T/C-2A	73"
39	HR T/C-2D	74"
40	HR T/C-3C	74"
41	HR T/C-4C	74"
42	HR T/C-4D	74"
43	HR T/C-1B	75"
44	HR T/C-1D	75"
45	HR T/C-2E	75"
46	HR T/C-5D	75"
47	HR T/C-1D	76"
48	HR T/C-2B	76"
49	HR T/C-3A	76"
50	HR T/C-3D	76"
51	HR T/C-4A	76"
52	HR T/C-4B	76"
53	HR T/C-4D	76"
54	HR T/C-5C	76"
55	HR T/C-5D	76"
56	HR T/C-1B	77"
57	HR T/C-1C	77"
58	HR T/C-1D	77"
59	HR T/C-2A	77"
60	HR T/C-2C	77"
61	HR T/C-2D	77"
62	HR T/C-3A	77"
63	HR T/C-3B	77"
64	HR T/C-3E	77"
65	HR T/C-5B	77"
66	HR T/C-5D	77"
67	HR T/C-1C	78"
68	HR T/C-2B	78"
69	HR T/C-2E	78"
70	HR T/C-3A	78"
71	HR T/C-3B	78"
72	HR T/C-3C	78"
73	HR T/C-4A	78"
74	HR T/C-4B	78"
75	HR T/C-4C	78"
76	HR T/C-4D	78"
77	HR T/C-4E	78"
78	HR T/C-5D	78"
79	HR T/C-2C	79"
80	HR T/C-2D	79"
81	HR T/C-3A	79"
82	HR T/C-3C	79"
83	HR T/C-3E	79"
84	HR T/C-5C	79"
85	HR T/C-2B	80"
86	HR T/C-3D	80"
87	HR T/C-4A	80"
88	HR T/C-4E	80"
89	HR T/C-5B	80"
90	HR T/C-5C	80"
91	HR T/C-3D	81"
92	HR T/C-3E	82"
93	HR T/C-1C	84"
94	HR T/C-2B	84"
95	HR T/C-2C	84"

COMPUTER DATA ACQUISITION SYSTEM		
CHANNEL NO.	LOCATION	
96	HR T/C-2D	84"
97	HR T/C-3C	84"
98	HR T/C-3D	84"
99	DEFECTIVE CHANNEL	
100	HR T/C-3E	84"
101	HR T/C-4A	84"
102	HR T/C-4D	84"
103	HR T/C-5B	84"
104	HR T/C-5C	84"
105	SPARE	
106	SPARE	
107	SPARE	
108	SPARE	
109	HR T/C-1D	90"
110	HR T/C-2B	90"
111	HR T/C-2C	90"
112	HR T/C-2D	90"
113	HR T/C-2E	90"
114	HR T/C-3A	90"
115	HR T/C-3B	90"
116	HR T/C-3C	90"
117	HR T/C-3D	90"
118	HR T/C-3E	90"
119	HR T/C-4A	90"
120	HR T/C-4B	90"
121	HR T/C-4D	90"
122	HR T/C-5C	90"
123	HR T/C-5D	90"
124	HR T/C-1C	96"
125	HR T/C-2D	96"
126	HR T/C-2E	96"
127	HR T/C-3B	96"
128	HR T/C-3C	96"
129	HR T/C-3D	96"
130	HR T/C-3E	96"
131	HR T/C-4B	96"
132	HR T/C-4D	96"
133	HR T/C-5B	96"
134	HR T/C-5C	96"
135	HR T/C-1C	102"
136	HR T/C-1D	102"
137	HR T/C-2B	102"
138	HR T/C-2C	102"
139	HR T/C-2E	102"
140	HR T/C-3A	102"
141	HR T/C-3B	102"
142	HR T/C-4A	102"
143	HR T/C-4B	102"
144	HR T/C-5B	102"
145	HR T/C-5D	102"
146	HR T/C-1B	111"
147	HR T/C-2A	111"
148	HR T/C-2D	111"
149	HR T/C-3C	111"
150	HR T/C-3D	111"
151	HR T/C-3E	111"
152	HR T/C-4C	111"
153	HR T/C-4D	111"
154	HR T/C-4E	111"
155	HR T/C-5C	111"
156	HR T/C-1C	120"
157	HR T/C-1D	120"
158	HR T/C-2B	120"
159	HR T/C-2C	120"
160	HR T/C-2E	120"
161	HR T/C-3A	120"
162	HR T/C-3B	120"
163	HR T/C-4A	120"
164	HR T/C-4B	120"
165	HR T/C-5B	120"
166	HR T/C-5D	120"
167	HR T/C-1B	132"
168	HR T/C-2A	132"
169	HR T/C-4C	132"
170	HR T/C-4E	132"
171	HR T/C-1D	138"
172	HR T/C-3A	138"
173	HR T/C-5D	138"
174	SPARE	
175	SPARE	
176	SPARE	
177	BF T/C-9B	35"
178	BF T/C-10B	47"
179	BF T/C-13B	58"
180	SP T/C-10B	58"
181	BF T/C-8B	67"
182	SP T/C-SPEC.	67"
183	SP T/C-9B	67"
184	SP T/C-11B	67"
185	BF T/C-6A	77"
186	BF T/C-8A	77"
187	SP T/C-9B	77"
188	SP T/C-11B	77"
189	BF T/C-6C	89"
190	BF T/C-7C	89"

COMPUTER DATA ACQUISITION SYSTEM		
CHANNEL NO.	LOCATION	
191	SP T/C-10C	89"
192	SP T/C-5A	89"
193	BF T/C-8C	97"
194	BF T/C-9B	97"
195	SP T/C-10C	97"
196	BF T/C-5A	109"
197	SP T/C-10A	109"
198	BF T/C-14B	120"
199	SP T/C-6B	120"
200	SP T/C-15B	120"
201	BF T/C-11B	130"
202	BF T/C-6B	138"
203	BS T/C-4D	70"
204	BS T/C-5C	71"
205	BS T/C-2E	71.5"
206	BS T/C-4B	72"
207	BS T/C-3C-A	75"
208	BS T/C-3C-B	75"
209	BS T/C-3C-C	75"
210	FS T/C-BØ	60"
211	FS T/C-AØ	72"
212	FS T/C-BØ	78"
213	FS T/C-BØ	84"
214	FS T/C-AØ	84"
215	FS T/C-CØ	96"
216	FS T/C-BØ	111"
217	SPARE	
218	SPARE	
219	SPARE	
220	SPARE	
221	SPARE	
222	SPARE	
223	SPARE	
224	SPARE	
225	SPARE	
226	SPARE	
227	SPARE	
228	SPARE	
229	SPARE	
230	SPARE	
231	SPARE	
232	SPARE	
233	SPARE	
234	SPARE	
235	SPARE	
236	SPARE	
237	SPARE	
238	SPARE	
239	H.I.W. T/C-270°	2'
240	H.I.W. T/C-180°	3'
241	H.I.W. T/C-90°	4'
242	H.I.W. T/C-270°	4'
243	H.I.W. T/C-270°	5'
244	H.I.W. T/C-90°	6'
245	H.I.W. T/C-270°	6'
246	H.I.W. T/C-270°	7'
247	H.I.W. T/C-90°	8'
248	H.I.W. T/C-270°	8'
249	H.I.W. T/C-270°	9'
250	H.I.W. T/C-90°	10'
251	H.I.W. T/C-270°	10'
252	H.I.W. T/C-270°	11'
253	HW T/C-90	0'
254	HW T/C-270	0'
255	HW T/C-0	1'
256	HW T/C-180	1'
257	HW T/C-90	2'
258	HW T/C-270	2'
259	HW T/C-0	3'
260	HW T/C-180	3'
261	HW T/C-90	4'
262	HW T/C-270	4'
263	HW T/C-0	5'
264	HW T/C-90	5'
265	HW T/C-180	5'
266	HW T/C-270	5'
267	HW T/C-0	6'
268	HW T/C-90	6'
269	HW T/C-180	6'
270	HW T/C-270	6'
271	HW T/C-0	7'
272	HW T/C-90	7'
273	HW T/C-180	7'
274	HW T/C-270	7'
275	HW T/C-0	8'
276	HW T/C-90	8'
277	HW T/C-180	8'
278	HW T/C-270	8'
279	HW T/C-90	9'
280	HW T/C-270	9'
281	HW T/C-0	10'
282	HW T/C-90	10'
283	HW T/C-180	10'
284	HW T/C-270	10'
285	HW T/C-0	11'

COMPUTER DATA ACQUISITION SYSTEM	
CHANNEL NO.	LOCATION
286	HW T/C-90 11'
287	HW T/C-180 11'
288	HW T/C-270 11'
289	HW T/C-90 12'
290	HW T/C-270 12'
291	LOWER PLENUM FLUID T/C
292	LOWER PLENUM WALL T/C
293	UPPER PLENUM BUNDLE FLUID T/C
294	UPPER PLEN. MSG. EXT. FL. T/C
295	UPPER PLENUM STEAM PROBE T/C
296	UPPER PLENUM SEAL PLATE T/C
297	UPPER PLENUM 90 WALL T/C
298	UPPER PLENUM 180 WALL T/C
299	UPPER PLENUM 270 WALL T/C
300	CARRYOVER TANK EL. FLUID T/C
301	CARRYOVER TANK EL. WALL T/C
302	CARRYOVER TANK EL. WALL T/C
303	STEAM SEPARATOR EL. FLUID T/C
304	STEAM SEPARATOR EL. WALL T/C
305	STEAM SEPARATOR EL. WALL T/C
306	DRAIN TANK EL. FLUID T/C
307	DRAIN TANK EL. WALL T/C
308	DRAIN TANK EL.
309	ACCUMULATOR EL. FLUID T/C
310	STEAM INJ. SYS. EL. FLUID T/C
311	UPPER PLEN./STM. SEP S.P. T/C
312	UPPER PLEN./STM. SEP WALL T/C
313	STM. SEP./EXHAUST LINE S.P. T/C
314	STM. SEP./EXHAUST LINE WALL T/C
315	EXHAUST LINE BEFORE ORIFICE PLATE-WALL T/C
316	EXHAUST LINE BEFORE FLOW VALVE FLUID T/C
317	INJ. LINE TO LOWER PLENUM FLUID T/C
318	STM. INJ. SYS. ORIFICE FLUID T/C
319	INJ. LINE TO LOWER PLEN. FLUID T/C
320	CROSSOVER LEG AFTER TURBINE METER-FLUID T/C
321	CROSSOVER LEG BEFORE TURBINE METER-FLUID T/C
322	SPARE
323	SPARE
324	SPARE
325	ZONE A PRIMARY POWER
326	ZONE A REDUNDANT POWER
327	STEAM COOLING POWER
328	SPARE
329	SPARE
330	SPARE
331	TURBINE METER 5 GPM
332	TURBINE METER 15 GPM
333	TURBINE METER 60 GPM
334	BI-DIRECTIONAL TURBINE METER
335	0 TO 1 FT. HOUSING DP
336	1 TO 2 FT. HOUSING DP
337	2 TO 3 FT. HOUSING DP
338	3 TO 4 FT. HOUSING DP
339	4 TO 5 FT. HOUSING DP
340	5 TO 6 FT. HOUSING DP
341	6 TO 7 FT. HOUSING DP
342	7 TO 8 FT. HOUSING DP
343	8 TO 9 FT. HOUSING DP
344	9 TO 10 FT. HOUSING DP
345	10 TO 11 FT. HOUSING DP
346	11 TO 12 FT. HOUSING DP
347	UPPER PLENUM DP
348	OVERALL HOUSING DP
349	CARRYOVER TANK DP
350	STEAM SEPARATOR DP
351	DRAIN TANK DP
352	ACCUMULATOR DP
353	EXHAUST ORIFICE DP LO RANGE
354	STEAM INJ. SYS. DP LEVEL
355	STEAM INJ. SYS. ORIFICE DP
356	DOWNCOMER/0 FT. EL. DP GRAVITY
357	DOWNCOMER LEVEL DP GRAVITY
358	DOWNCOMER TO STEAM SEPARATOR DP GRAVITY
359	UPPER PLENUM TO STEAM SEPARATOR DP GRAVITY
360	EXHAUST ORIFICE DP HIGH RANGE
361	EXHAUST LINE ORIFICE PRESSURE
362	UPPER PLENUM PRESSURE - FORCED & STM. SEPARATOR PRESSURE-GRAVITY
363	STEAM INJ. LINE PRESSURE
364	STEAM INJ. FLOW LBS./SEC.

H.R. – HEATER ROD T/C
S.P. – STEAM PROBE T/C
B.S. – BLOCKAGE SLEEVE T/C
H.W. – HOUSING WALL T/C
H.I.W. – HOUSING INSULATION WALL T/C
B.F. – BARE FLUID T/C

F.S. – FILLER STRIP T/C
AØ = 45° } REFERENCE TO
BØ = 315° } THE HOUSING
CØ = 225° } REFERENCE TO
DØ = 135° } THE HOUSING

BLOCKAGE SLEEVE ORIENTATION
A = 135°
B = 112°
C = 90°

Figure F-22. FLECHT SEASET 21-Rod Bundle Computer Data Acquisition System Bundle No. 5

COMPUTER DATA ACQUISITION SYSTEM		
CHANNEL NO.	LOCATION	
1	HR T/C-4C	12"
2	HR T/C-4E	12"
3	HR T/C-3E	24"
4	HR T/C-1B	39"
5	HR T/C-2A	39"
6	HR T/C-4C	39"
7	HR T/C-1C	48"
8	HR T/C-2C	48"
9	HR T/C-2E	48"
10	HR T/C-3E	48"
11	HR T/C-1B	60"
12	HR T/C-2A	60"
13	HR T/C-4E	60"
14	HR T/C-2A	67"
15	HR T/C-2B	67"
16	HR T/C-4B	67"
17	HR T/C-5C	67"
18	HR T/C-5D	67"
19	HR T/C-3C	70"
20	HR T/C-4A	70"
21	HR T/C-4E	70"
22	HR T/C-5B	70"
23	HR T/C-3D	71"
24	HR T/C-4C	71"
25	HR T/C-4D	72"
26	HR T/C-5B	72"
27	HR T/C-1D	73"
28	HR T/C-2D	73"
29	HR T/C-2E	74"
30	HR T/C-3C	74"
31	HR T/C-4B	74"
32	HR T/C-4D	74"
33	HR T/C-5C	74"
34	HR T/C-1B	75"
35	HR T/C-1D	75"
36	HR T/C-2A	75"
37	HR T/C-2B	75"
38	HR T/C-2C	75"
39	HR T/C-2D	75"
40	HR T/C-3A	75"
41	HR T/C-3B	75"
42	HR T/C-4A	75"
43	HR T/C-4D	75"
44	HR T/C-5B	75"
45	HR T/C-1C	76"
46	HR T/C-1D	76"
47	HR T/C-2E	76"
48	HR T/C-3A	76"
49	HR T/C-3C	76"
50	HR T/C-3D	76"
51	HR T/C-4B	76"
52	HR T/C-4C	76"
53	HR T/C-4D	76"
54	HR T/C-4E	76"
55	HR T/C-5C	76"
56	HR T/C-5D	76"
57	HR T/C-1B	77"
58	HR T/C-1D	77"
59	HR T/C-2A	77"
60	HR T/C-2B	77"
61	HR T/C-2C	77"
62	HR T/C-2D	77"
63	HR T/C-3B	77"
64	HR T/C-5B	77"
65	HR T/C-1C	78"
66	HR T/C-2A	78"
67	HR T/C-2B	78"
68	HR T/C-3A	78"
69	HR T/C-3C	78"
70	HR T/C-3E	78"
71	HR T/C-4A	78"
72	HR T/C-4B	78"
73	HR T/C-4C	78"
74	HR T/C-4D	78"
75	HR T/C-4E	78"
76	HR T/C-5C	78"
77	HR T/C-5D	78"
78	HR T/C-1B	79"
79	HR T/C-1C	79"
80	HR T/C-2C	79"
81	HR T/C-2D	79"
82	HR T/C-2E	79"
83	HR T/C-3A	79"
84	HR T/C-3B	79"
85	HR T/C-3D	79"
86	HR T/C-4B	79"
87	HR T/C-5B	79"
88	HR T/C-5C	79"
89	HR T/C-1B	80"
90	HR T/C-1C	80"
91	HR T/C-2B	80"
92	HR T/C-2D	80"
93	HR T/C-3C	80"
94	HR T/C-3D	80"
95	HR T/C-4A	80"

COMPUTER DATA ACQUISITION SYSTEM		
CHANNEL NO.	LOCATION	
96	HR T/C-4E	80"
97	HR T/C-3E	81"
98	SPARE	
99	SPARE	
100	SPARE	
101	SPARE	
102	SPARE	
103	SPARE	
104	SPARE	
105	SPARE	
106	SPARE	
107	SPARE	
108	SPARE	
109	HR T/C-1C	84"
110	HR T/C-2B	84"
111	HR T/C-2D	84"
112	HR T/C-3C	84"
113	HR T/C-3D	84"
114	HR T/C-3E	84"
115	HR T/C-4A	84"
116	HR T/C-4D	84"
117	HR T/C-5B	84"
118	HR T/C-5D	84"
119	HR T/C-1D	90"
120	HR T/C-2B	90"
121	HR T/C-2C	90"
122	HR T/C-2D	90"
123	HR T/C-2E	90"
124	HR T/C-3A	90"
125	HR T/C-3B	90"
126	HR T/C-3C	90"
127	HR T/C-3D	90"
128	HR T/C-4A	90"
129	HR T/C-4B	90"
130	HR T/C-4D	90"
131	HR T/C-5B	90"
132	HR T/C-5C	90"
133	HR T/C-1C	96"
134	HR T/C-2C	96"
135	HR T/C-2D	96"
136	HR T/C-2E	96"
137	HR T/C-3C	96"
138	HR T/C-3D	96"
139	HR T/C-3E	96"
140	HR T/C-4A	96"
141	HR T/C-4B	96"
142	HR T/C-4D	96"
143	HR T/C-5B	96"
144	HR T/C-5C	96"
145	HR T/C-1C	102"
146	HR T/C-1D	102"
147	HR T/C-2B	102"
148	HR T/C-2C	102"
149	HR T/C-2E	102"
150	HR T/C-3A	102"
151	HR T/C-3B	102"
152	HR T/C-3E	102"
153	HR T/C-4B	102"
154	HR T/C-5C	102"
155	HR T/C-5D	102"
156	HR T/C-1B	111"
157	HR T/C-2A	111"
158	HR T/C-3C	111"
159	HR T/C-3D	111"
160	HR T/C-4A	111"
161	HR T/C-4C	111"
162	HR T/C-4E	111"
163	HR T/C-5B	111"
164	HR T/C-1D	120"
165	HR T/C-3A	120"
166	HR T/C-3B	120"
167	HR T/C-3E	120"
168	HR T/C-4B	120"
169	HR T/C-5D	120"
170	HR T/C-1B	132"
171	HR T/C-2A	132"
172	HR T/C-4C	132"
173	HR T/C-4E	132"
174	HR T/C-1D	138"
175	HR T/C-3A	138"
176	HR T/C-3B	138"
177	BF T/C-9B	35"
178	BF T/C-10B	47"
179	BF T/C-15B	58"
180	SP T/C-10B	58"
181	BF T/C-6B	67"
182	SP T/C-SPEC.	67"
183	SP T/C-9B	67"
184	SP T/C-11B	67"
185	BF T/C-6A	77"
186	BF T/C-8A	77"
187	SP T/C-9B	77"
188	SP T/C-11B	77"
189	BF T/C-6C	89"
190	BF T/C-7C	89"

COMPUTER DATA ACQUISITION SYSTEM		
CHANNEL NO.	LOCATION	
191	SP T/C-10C	89"
192	SP T/C-5A	89"
193	BF T/C-8C	97"
194	SP T/C-9B	97"
195	SP T/C-10C	97"
196	BF T/C-5A	109"
197	SP T/C-10A	109"
198	BF T/C-14B	120"
199	BF T/C-6B	120"
200	SP T/C-15B	120"
201	BF T/C-11B	130"
202	BF T/C-6B	138"
203	BS T/C-4D	70"
204	BS T/C-3A	73"
205	BS T/C-5B	73"
206	BS T/C-2C	75"
207	BS T/C-3CA	75"
208	BS T/C-3CB	75"
209	BS T/C-3CC	75"
210	FS T/C-BØ	60"
211	FS T/C-AØ	72"
212	FS T/C-BØ	78"
213	FS T/C-BØ	84"
214	FS T/C-AØ	84"
215	FS T/C-CØ	96"
216	FS T/C-BØ	111"
217	FS T/C	120"
218	GR T/C	88"
219	SPARE	
220	SPARE	
221	SPARE	
222	SPARE	
223	SPARE	
224	SPARE	
225	SPARE	
226	SPARE	
227	SPARE	
228	SPARE	
229	SPARE	
230	SPARE	
231	SPARE	
232	SPARE	
233	SPARE	
234	SPARE	
235	SPARE	
236	SPARE	
237	SPARE	
238	SPARE	
239	H.I.W. T/C-270°	2'
240	H.I.W. T/C-180°	3'
241	H.I.W. T/C-90°	4'
242	H.I.W. T/C-270°	4'
243	H.I.W. T/C-270°	5'
244	H.I.W. T/C-90°	6'
245	H.I.W. T/C-270°	6'
246	H.I.W. T/C-270°	7'
247	H.I.W. T/C-90°	8'
248	H.I.W. T/C-270°	8'
249	H.I.W. T/C-270°	9'
250	H.I.W. T/C-90°	10'
251	H.I.W. T/C-270°	10'
252	H.I.W. T/C-270°	11'
253	HW T/C-90	0'
254	HW T/C-270	0'
255	HW T/C-0	1'
256	HW T/C-180	1'
257	HW T/C-90	2'
258	HW T/C-270	2'
259	HW T/C-0	3'
260	HW T/C-180	3'
261	HW T/C-90	4'
262	HW T/C-270	4'
263	HW T/C-0	5'
264	HW T/C-90	5'
265	HW T/C-180	5'
266	HW T/C-270	5'
267	HW T/C-0	6'
268	HW T/C-90	6'
269	HW T/C-180	6'
270	HW T/C-270	6'
271	HW T/C-0	7'
272	HW T/C-90	7'
273	HW T/C-180	7'
274	HW T/C-270	7'
275	HW T/C-0	8'
276	HW T/C-90	8'
277	HW T/C-180	8'
278	HW T/C-270	8'
279	HW T/C-90	9'
280	HW T/C-270	9'
281	HW T/C-0	10'
282	HW T/C-90	10'
283	HW T/C-180	10'
284	HW T/C-270	10'
285	HW T/C-0	11'

COMPUTER DATA ACQUISITION SYSTEM		
CHANNEL NO.	LOCATION	
286	HW T/C-90	11'
287	HW T/C-180	11'
288	HW T/C-270	11'
289	HW T/C-90	12'
290	HW T/C-270	12'
291	LOWER PLENUM FLUID T/C	
292	LOWER PLENUM WALL T/C	
293	UPPER PLENUM BUNDLE FLUID T/C	
294	UPPER PLEN. WSG. EXT. FL. T/C	
295	UPPER PLENUM STEAM PROBE T/C	
296	UPPER PLENUM SEAL PLATE T/C	
297	UPPER PLENUM 90 WALL T/C	
298	UPPER PLENUM 180 WALL T/C	
299	UPPER PLENUM 270 WALL T/C	
300	CARRYOVER TANK EL. FLUID T/C	
301	CARRYOVER TANK EL. WALL T/C	
302	CARRYOVER TANK EL. WALL T/C	
303	STEAM SEPARATOR EL. FLUID T/C	
304	STEAM SEPARATOR EL. WALL T/C	
305	STEAM SEPARATOR EL. WALL T/C	
306	DRAIN TANK EL. FLUID T/C	
307	DRAIN TANK EL. WALL T/C	
308	DRAIN TANK EL.	
309	ACCUMULATOR EL. FLUID T/C	
310	STEAM INJ. SYS. EL. FLUID T/C	
311	UPPER PLEN./STM. SEP S.P. T/C	
312	UPPER PLEN./STM. SEP WALL T/C	
313	STM. SEP/EXHAUST LINE S.P. T/C	
314	STM. SEP/EXHAUST LINE WALL T/C	
315	EXHAUST LINE BEFORE ORIFICE PLATE-WALL T/C	
316	EXHAUST LINE BEFORE FLOW VALVE FLUID T/C	
317	INJ. LINE TO LOWER PLENUM FLUID T/C	
318	STM. INJ. SYS. ORIFICE FLUID T/C	
319	INJ. LINE TO LOWER PLEN. FLUID T/C	
320	CROSSOVER LEG AFTER TURBINE METER-FLUID T/C	
321	CROSSOVER LEG BEFORE TURBINE METER-FLUID T/C	
322	SPARE	
323	SPARE	
324	SPARE	
325	ZONE A PRIMARY POWER	
326	ZONE A REDUNDANT POWER	
327	STEAM COOLING POWER	
328	SPARE	
329	SPARE	
330	SPARE	
331	TURBINE METER 5 GPM	
332	TURBINE METER 15 GPM	
333	TURBINE METER 60 GPM	
334	BI-DIRECTIONAL TURBINE METER	
335	0 TO 1 FT. HOUSING DP	
336	1 TO 2 FT. HOUSING DP	
337	2 TO 3 FT. HOUSING DP	
338	3 TO 4 FT. HOUSING DP	
339	4 TO 5 FT. HOUSING DP	
340	5 TO 6 FT. HOUSING DP	
341	6 TO 7 FT. HOUSING DP	
342	7 TO 8 FT. HOUSING DP	
343	8 TO 9 FT. HOUSING DP	
344	9 TO 10 FT. HOUSING DP	
345	10 TO 11 FT. HOUSING DP	
346	11 TO 12 FT. HOUSING DP	
347	UPPER PLENUM DP	
348	OVERALL HOUSING DP	
349	CARRYOVER TANK DP	
350	STEAM SEPARATOR DP	
351	DRAIN TANK DP	
352	ACCUMULATOR DP	
353	EXHAUST ORIFICE DP LO RANGE	
354	STEAM INJ. SYS. DP LEVEL	
355	STEAM INJ. SYS. ORIFICE DP	
356	DOWNCOMER/0 FT. EL. DP GRAVITY	
357	DOWNCOMER LEVEL DP GRAVITY	
358	DOWNCOMER TO STEAM SEPARATOR DP GRAVITY	
359	UPPER PLENUM TO STEAM SEPARATOR DP GRAVITY	
360	EXHAUST ORIFICE DP HIGH RANGE	
361	EXHAUST LINE ORIFICE PRESSURE	
362	UPPER PLENUM PRESSURE-FENCED STM. SEPARATOR PRESSURE-GRAVITY	
363	STEAM INJ. LINE PRESSURE	
364	STEAM INJ. FLOW LBS./SEC.	

H.R. - HEATER ROD T/C
S.P. - STEAM PROBE T/C
B.S. - BLOCKAGE SLEEVE T/C
H.W. - HOUSING WALL T/C
H.I.W. - HOUSING INSULATION WALL T/C
R.F. - RARE FLUID T/C

F.S. - FILLER STRIP T/C
AØ = 45°
BØ = 315° } REFERENCE TO THE HOUSING
CØ = 225°
DØ = 135°

GR - GRID T/C

B.S. - BLOCKAGE SLEEVE REF. @ 3C
A = 135°
B = 120° } REFERENCE TO THE HOUSING
C = 90°

Figure F-23. FLECHT SEASET 21-Rod Bundle Computer Data Acquisition System Bundle No. 6

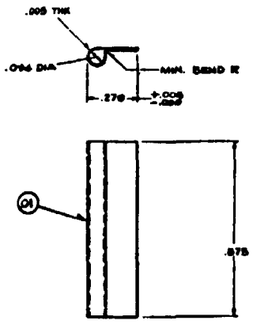

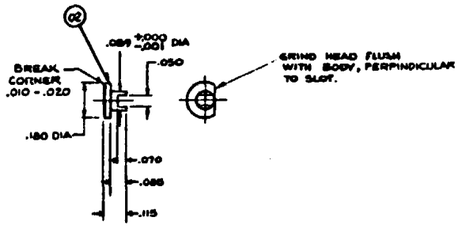

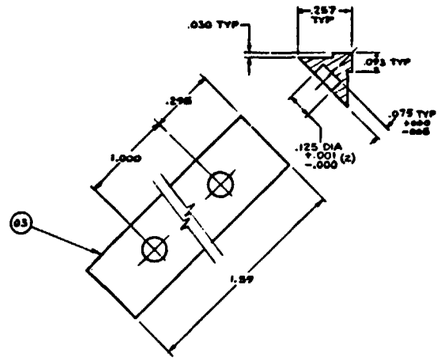

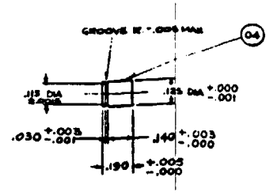

BILL OF MATERIAL

ITEM	QUAN.	PART NAME	DRAWING # OR SPEC #	MATERIAL	SUB ASSY GROUP 01	02	03	04
01		CLIP		304 SST				
02		RIVET						
03		FILLER STRIP SUPPT						
04		FILLER STRIP SUPPT PIN						
05		PROBE HOLDER L.H.-R.H.						
06								
07								
08								
09								
10								
11								
12								
13		PROBE HOLDER L.H.-R.H.		304 SST				
14	A	TEFLON SEAL (HALF)						
15	A	SEAL COMP. (HALF)						
16	B	T/C .020 DIA H 20' CHROMEL-ALUMEL	304 SST UN-GRD					
17		SLEEVE		304 SST				
18								
19								
20								
21								
22								
23								
24								
25		SLEEVE		304 SST				

A - ITEM 14 & 15 ARE COMPONENTS OF CONAX FITTING NO. SPG-100. MODIFY AS SHOWN.
B - C. S. GORDON CO.

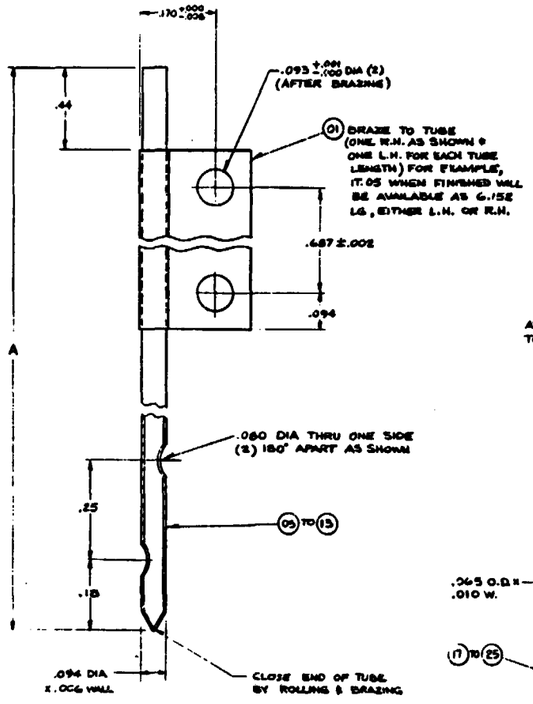

ITEM	A
05	6.16
06	4.15
07	7.15
08	5.15
09	7.90
10	3.15
11	9.75
12	8.75
13	6.75

ITEM	B
17	5.62
18	3.62
19	6.62
20	4.62
21	7.37
22	2.62
23	9.22
24	8.22
25	6.22

AT FINAL ASSY, IT. 05 & 17 GO TOGETHER; IT. 06 & 18, 07 & 19, ETC.

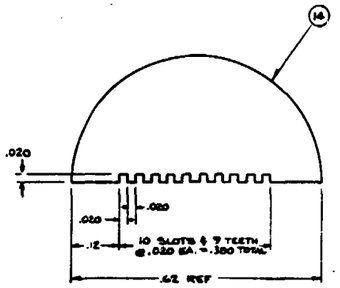

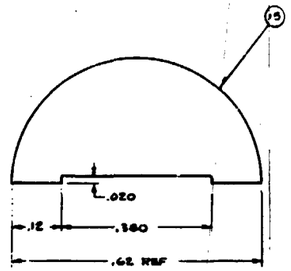

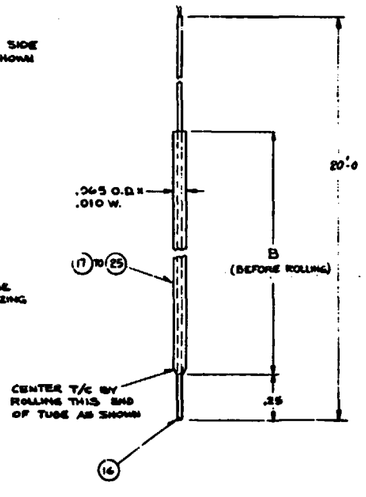

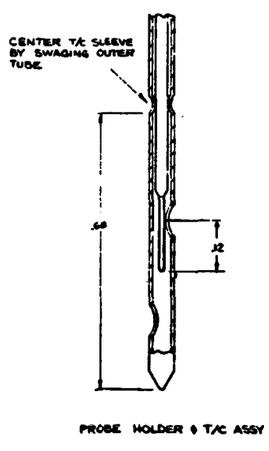

PROBE HOLDER & T/C ASSY

Figure F-24. FLECHT SEASET 21-Rod Bundle Test Instrumentation Components

BILL OF MATERIAL								
ITEM	NOTE	PART NAME	DRAWING & SEE SEC IT.	MATERIAL	REQ. PER GROUP			
					01	02	03	04
01		SEAL PLATE		ASTM 240 XM-19	1			

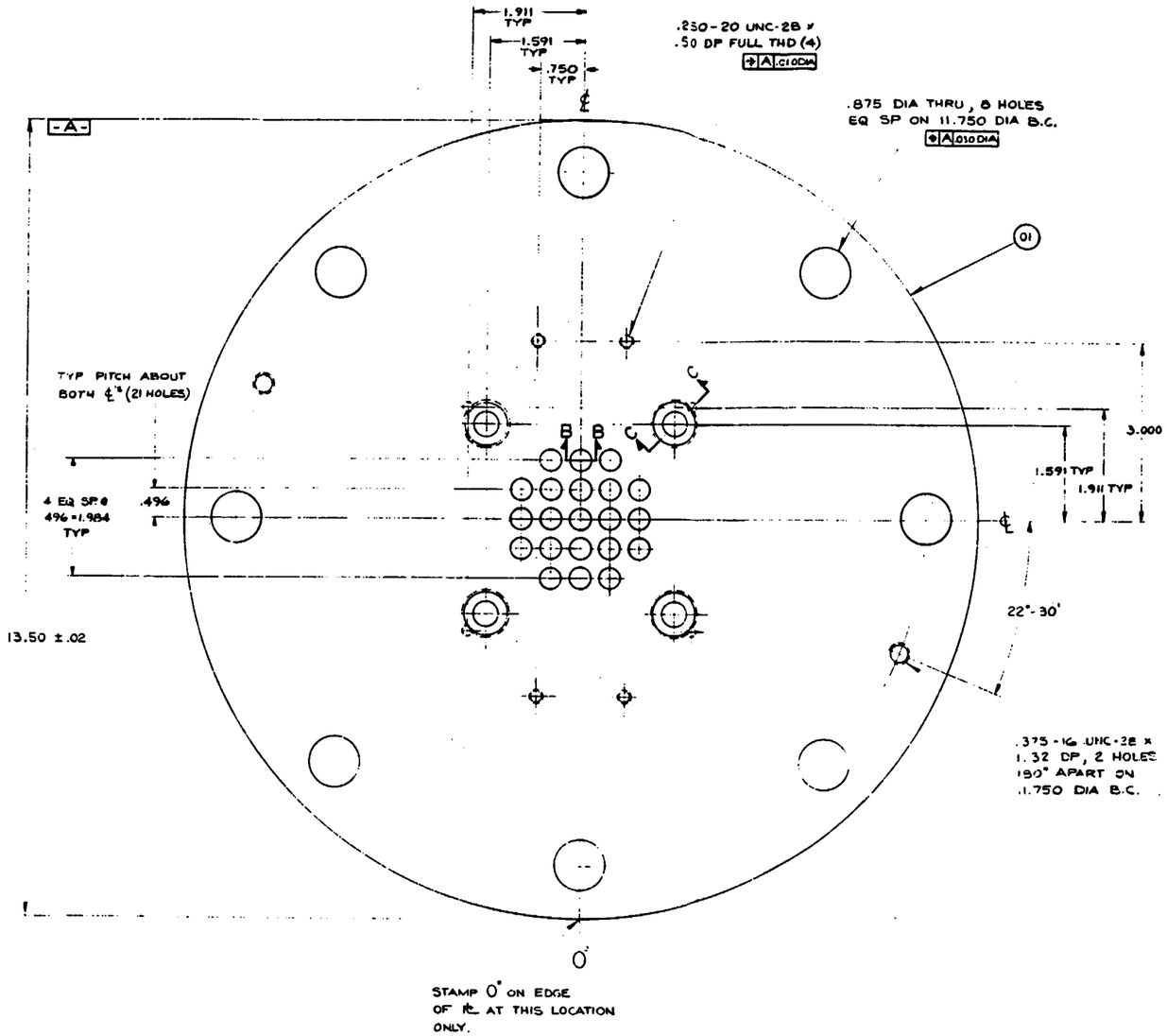

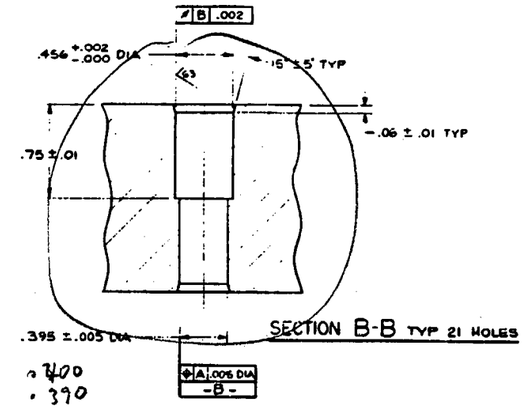

SECTION B-B TYP 21 HOLES

.400
.390

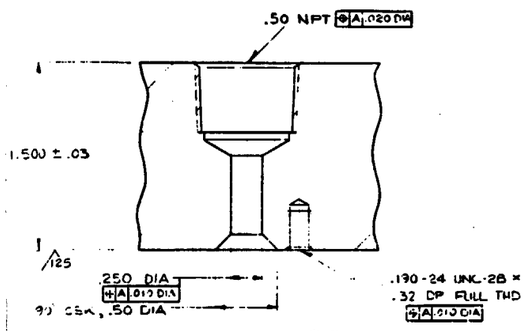

SECTION C-C TYP 4 PLACES

Figure F-25. FLECHT SEASET 21-Rod Bundle Upper and Lower Seal Plate

(07) OTHERWISE SAME AS IT. 01
(06) OTHERWISE SAME AS IT. 03
(05) OTHERWISE SAME AS IT. 02

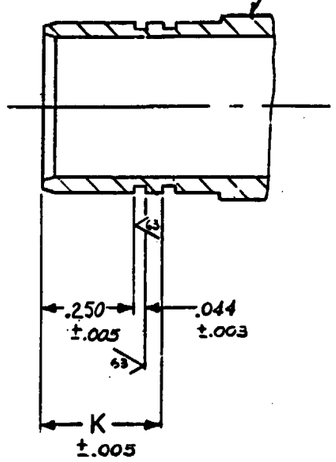

ITEM	B	C	D	E	F	G	H	J	K
01	.500	.975	.451	.410	.380	.435	.485	.100	.325
02	.625	1.100	.451	.410	.380	.435	.485	.250	.325
03	.625	1.100	.351	.310	.280	.335	.385	.100	.325
04	.625	1.100	.451	.410	.377	.435	.485	.250	.250
05	.625	1.100	.451	.410	.380	.435	.485	.250	.325
06	.625	1.100	.351	.310	.280	.335	.385	.100	.325
07	.500	.975	.451	.410	.380	.435	.485	.100	.325
08	.625	.838	.351	.310	.280	.335	.385	.100	.063

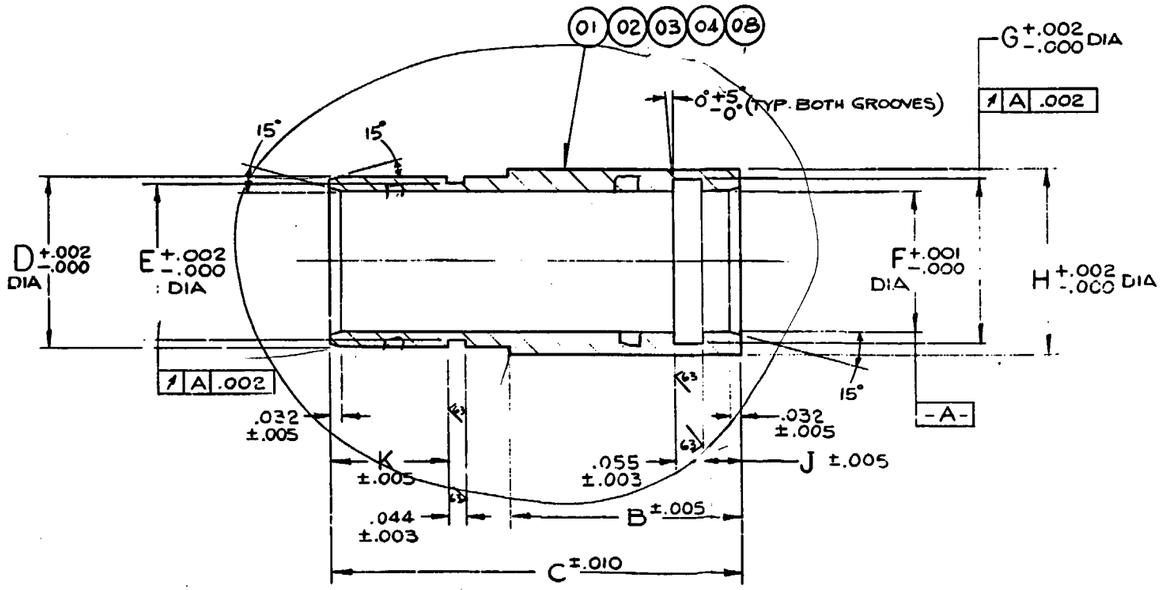

BILL OF MATERIAL

ITEM	NOTE	PART NAME	DRAWING & GR OR IT.	MATERIAL	REQ. PER GROUP 01	02	03	04
01	A	SLEEVE			1			
02	A	SLEEVE			1			
03	A	SLEEVE			1			
04	A	SLEEVE			1			
05	A	SLEEVE			1			
06	A	SLEEVE			1			
07	A	SLEEVE			1			
08	A	SLEEVE			1			

A - MATERIAL - BERYLLIUM COPPER, BERYLCO 33-25, WILLIAMS & CO.

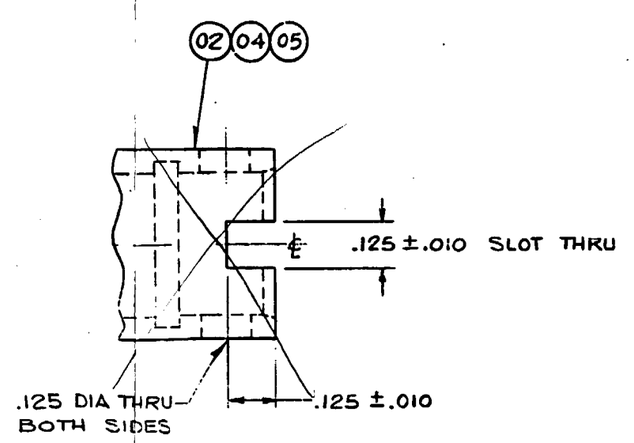

Figure F-26. FLECHT SEASET O-Ring Sleeves

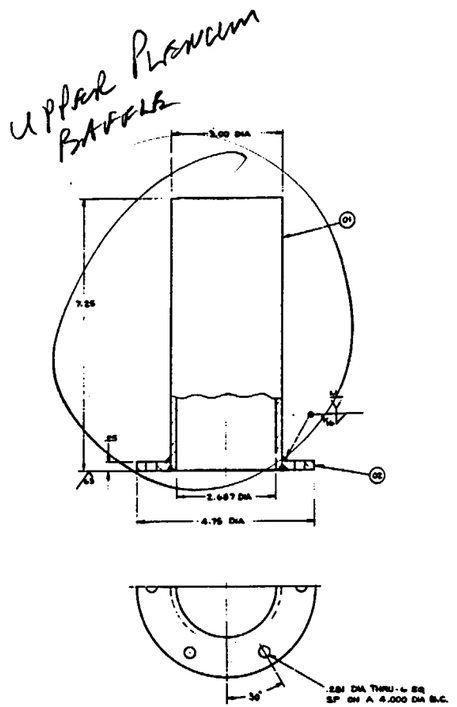

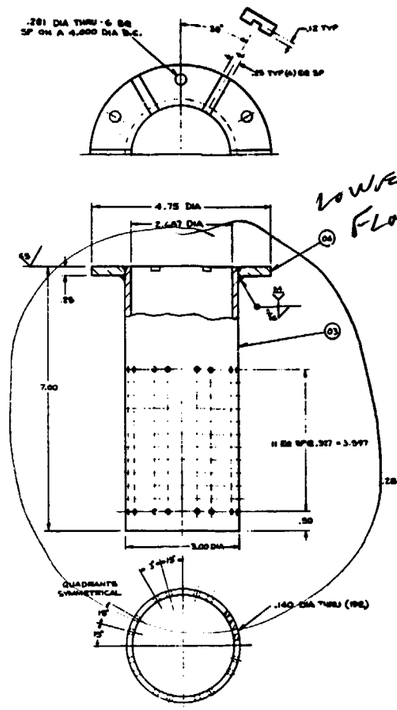

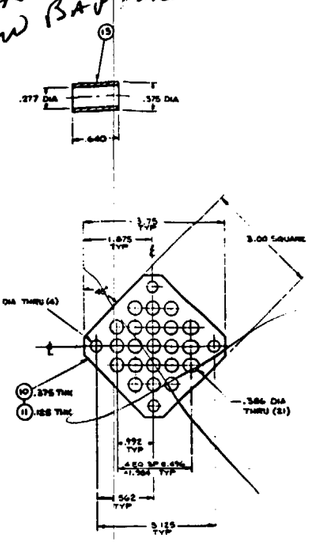

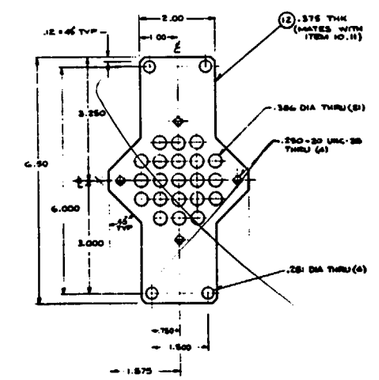

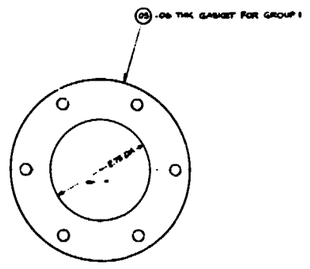

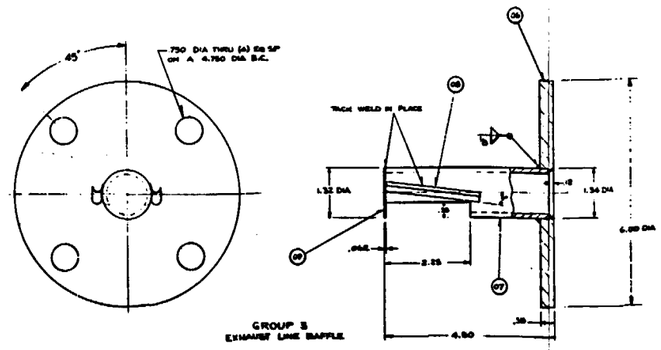

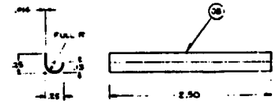

ITEM	QTY	PART NAME	MATERIAL	WEIGHT (LBS) EA	WEIGHT (LBS) TOTAL
01	1	CYLINDER	304 SST		
02	1	BASE	"		
03	1	CYLINDER	"		
04	1	BASE	"		
05	1	GASKET	DURABLA		
06	1	FLANGE	304 SST		
07	1	PIPE 3" SCH 80	"		
08	1	GUYES	INCONEL		
09	1	COVER	304 SST		
10	1	ANTI ROTATION BL	C.S.TL		
11	A/R	GASKET	NEOPRENE		
12	1	ANTI-ROTATION BL	C.S.TL		
13	4	SPACER (25 STG THERU)	C.S.TL		

A - DUROMETER - MED/HARD

Figure F-27. FLECHT SEASET 21-Rod Bundle Details

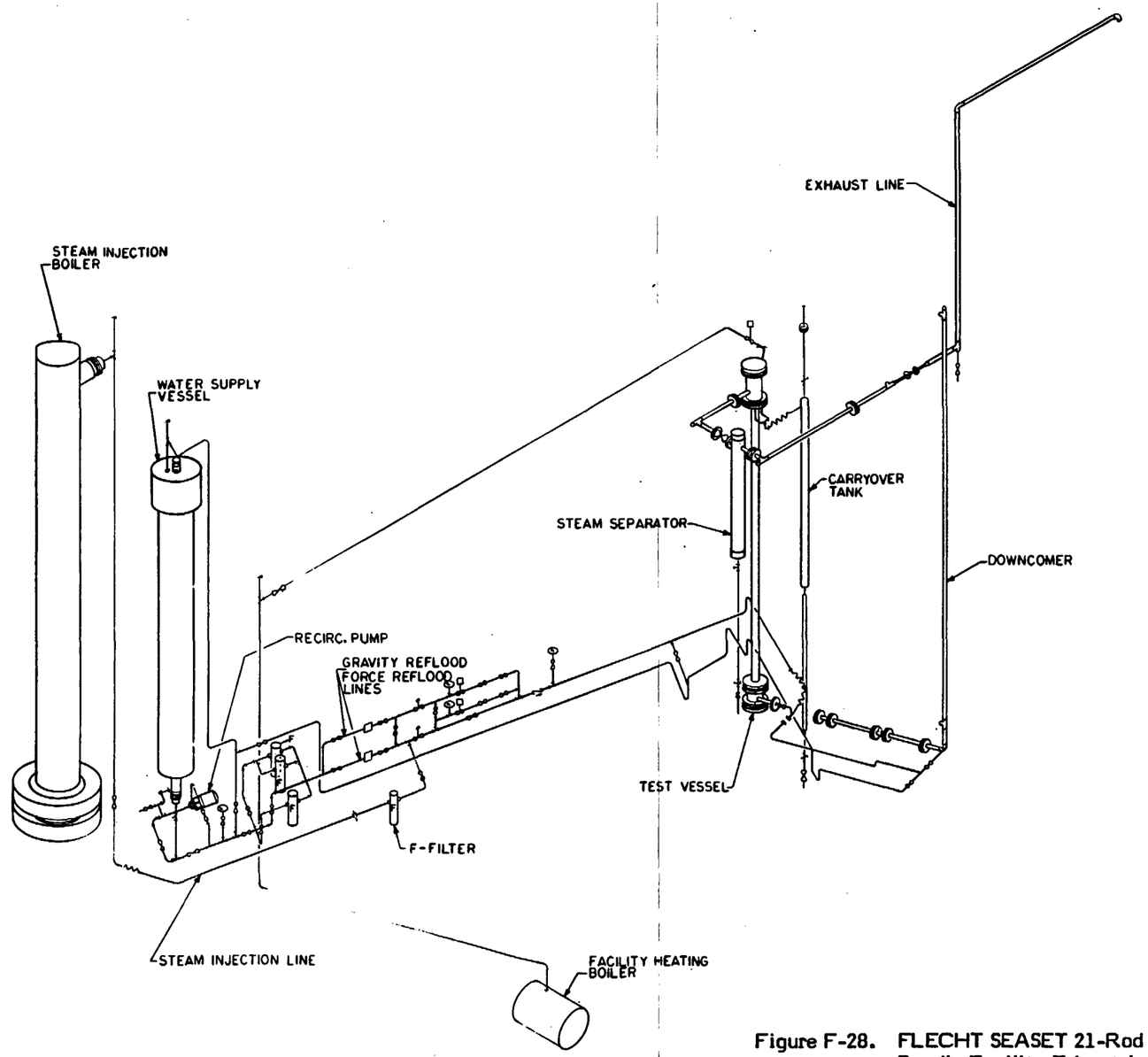

Figure F-28. FLECHT SEASET 21-Rod Bundle Facility Trimetric Diagram

APPENDIX G
BLOCKAGE SLEEVE TESTS

G-1. INTRODUCTION

In the 21-rod bundle task plan,[1] the results from a single-rod reflood test were reported on a nonprototypical, hydro-formed flow blockage sleeve. These tests were conducted to evaluate the method of attaching the blockage sleeve to the heater rod. Another single-rod reflood test was conducted on the prototypical short, concentric flow blockage sleeve, which was instrumented with a 0.51 mm (0.020 in.) diameter thermocouple. This test was conducted to determine the effect of an instrumented blockage sleeve on the heater rod thermal response. The thermocouple lead from the blockage sleeve was routed upstream of the sleeve, along the heater rod, to the nearest grid, and out to the periphery of the bundle. This test showed that the blockage sleeve quenched prior to the time that the heater rod thermocouples quenched, and that the thermal responses of the rod thermocouples were affected. The posttest examination of the blockage sleeve also indicated severe deformation of the sleeve due to the method of instrumenting.

In discussions with persons conducting the FEBA tests, it was learned that the blockage sleeve could be instrumented by routing the thermocouple lead downstream of the sleeve in the flow subchannel without affecting the test data. However, in order to instrument the 21-rod bundle flow blockage sleeves, the thickness of the sleeve was increased from 0.51 mm (0.020 in.) to 0.76 mm (0.030 in.) to provide more material for attaching the thermocouple lead. A third single-rod test was conducted, as described in this appendix, to determine the deformation characteristics of the blockage sleeves to be utilized in the 21-rod bundle test program, and to evaluate the effect of an instrumented blockage sleeve on the thermal response of a heater rod.

---

1. Hochreiter, L. E., et al., "PWR FLECHT SEASET 21-Rod Bundle Flow Blockage Task: Task Plan Report," NRC/EPRI/Westinghouse-5, March 1980.NUREG/CR-1370.

A total of four blockage sleeves were placed in the high-power regions of the heater rod to determine the deformation characteristics of the various sleeve designs. The heater rod with blockage sleeves was subsequently installed in a thin-wall insulated tube. These flow blockage sleeves, shown in figure G-1, are as follows:

-- Short, concentric, thick, instrumented sleeve centered at 1.911 m (75.25 in.)

-- Short, concentric, thin, uninstrumented sleeve centered at 2.011 m (79.19 in.)

-- Short, concentric, thick, uninstrumented sleeve centered at 2.13 m (84 in.)

-- Long, nonconcentric, thick, instrumented sleeve centered at 2.343 m (92.25 in.)

G-2. TEST DESCRIPTION

All four blockage sleeves were annealed for 67 hours at a temperature of 454°C (850°F) prior to testing to relieve the residual stresses. The heater rod was also annealed. The thick sleeves were approximately 0.76 mm (0.030 in.) thick and the thin sleeve was approximately 0.38 mm (0.015 in.) thick. The two instrumented sleeves were slotted at the point of maximum strain to a depth of approximately 0.51 mm (0.020 in.). A 0.081 mm (0.032 in.) diameter, Inconel-sheathed thermocouple was subsequently brazed into this slot on the sleeve. The thermocouple lead was routed downstream of the respective blockage sleeve in the flow subchannel. The thermocouple lead was flattened approximately 0.13 mm (0.005 in.) in the region where it was attached to the blockage sleeve to prevent the thermocouple lead from projecting into the flow stream. This technique, shown in figure G-2, is similar to that utilized by KFK of Germany in its 25-rod bundle FEBA flow blockage experiments.

Each of the blockage sleeves was attached to the heater rod by drilling a 3.17 mm (0.125 in.) diameter hole in the downstream side of the sleeve [3.17 mm (0.125 in.) from the end] and subsequently placing a spot-weld on the rod through the hole in the sleeve. This attachment method was developed and tested in a previous single rod/sleeve test, as reported in the 21-rod bundle task plan.

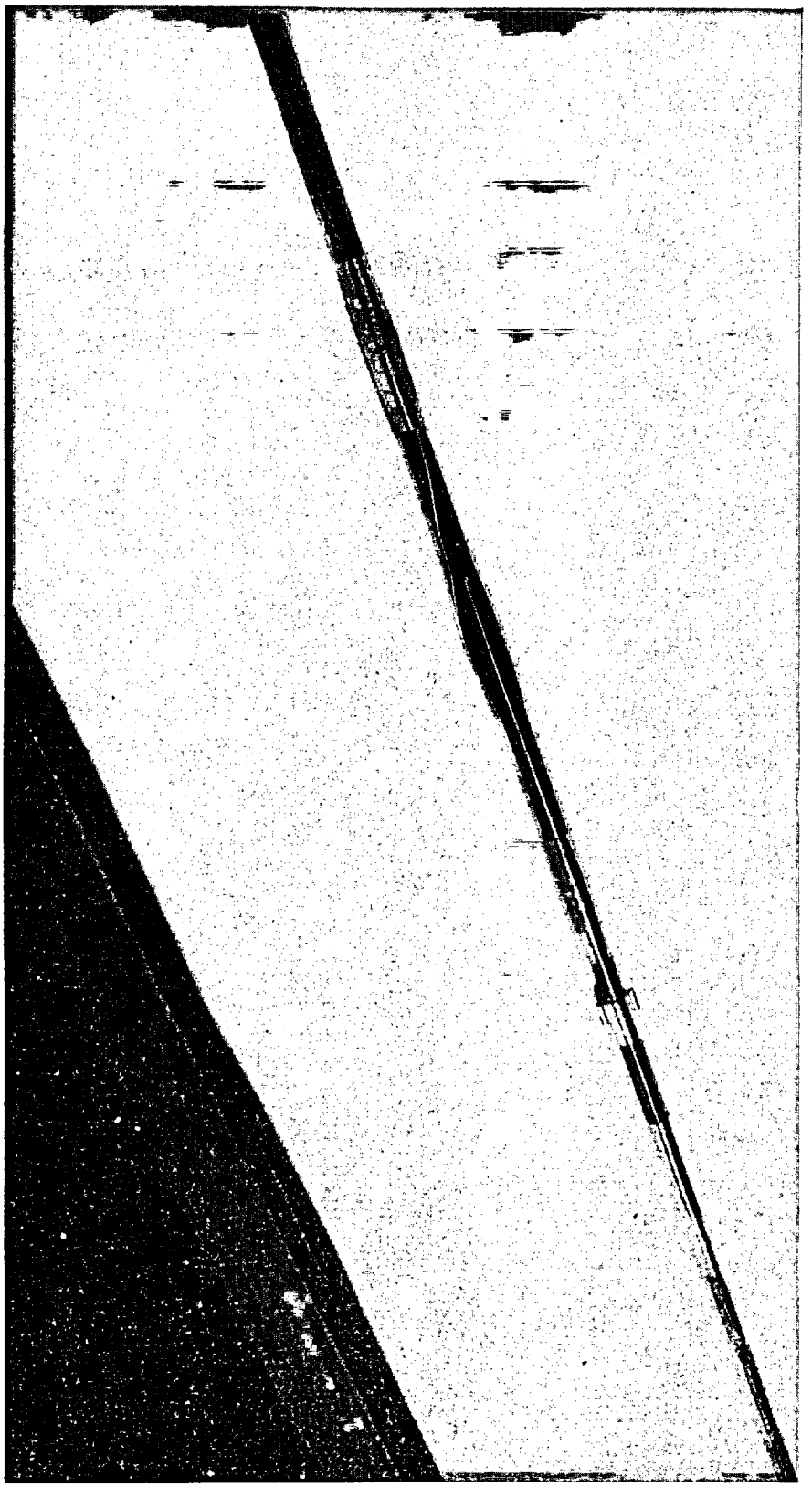

Figure G-1. Flow Blockage Sleeves Used in Blockage Sleeve Tests

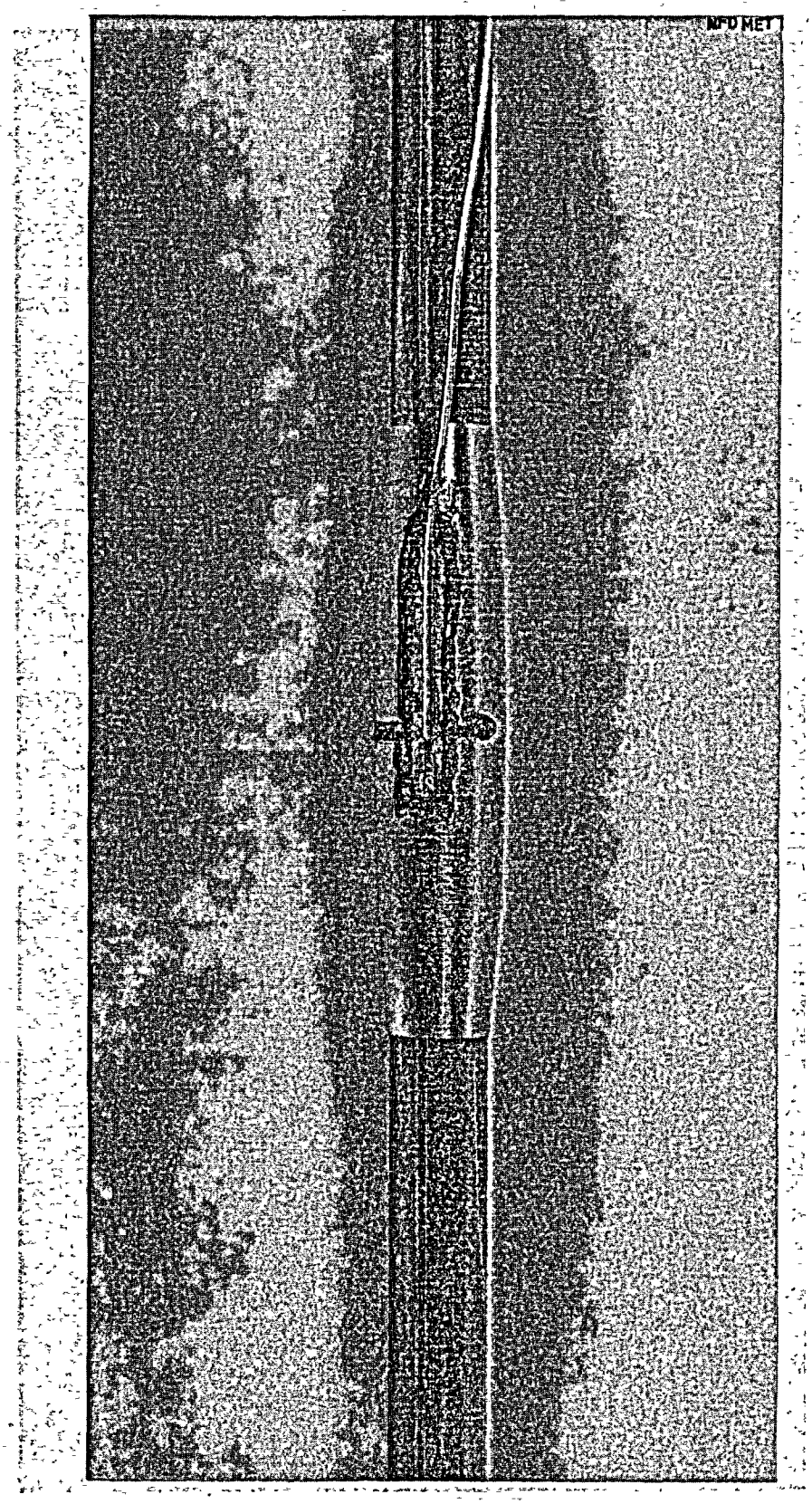

Figure G-2. Thermocouple Lead Attachment

Each of the four blockage sleeves was inspected and measured after every five thermal cycles. To perform this inspection, the heater rod was secured at the top and the insulated housing was subsequently lowered in order to expose all four blockage sleeves. The measurements included the following:

-- Overall sleeve length

-- Diameter of sleeve at 0 and 90 degrees at the center of the sleeve

-- Diameter of sleeve at 0 and 90 degrees at each end of the sleeve

The thermal cycling consisted of an adiabatic heatup period at a rate of 2.3 kw/m (0.7 kw/ft) until the initial clad temperature was achieved; power was subsequently reduced to a rate of 1.8 kw/m (0.55 kw/ft) and flooding was initiated. After 180 seconds of constant flooding, the power was reduced to a rate of 1.4 kw/m (0.42 kw/ft) until all thermocouples had quenched, at which time the power was turned off. The following 25 cycles were conducted:

Cycles	Initial Clad Temperature [°C(°F)]	Flooding Rate [mm/sec (in./sec)]
1-2	538 (1000)	38.1 (1.5)
3-12	1093 (2000)	38.1 (1.5)
13-25	1093 (2000)	20.3 (0.8)

The above thermal cycling was more severe than that observed in the 21-rod bundle tests; therefore it is believed that more deformation would have occurred in these single-rod tests than in the bundle tests.

G-3. TEST RESULTS

The results from the sleeve deformation tests are presented in tables G-1 and G-2 and plotted in figures G-3 and G-4. Figure G-3, which shows the sleeve elongation as a

TABLE G-1

DEFORMATION OF UNINSTRUMENTED BLOCKAGE SLEEVE

Sleeve Description	Time of Measurement	Diameter at Sleeve Center [mm (in.)]		Diameter at Downstream End[a] [mm (in.)]		Diameter at Upstream End[a] [mm (in.)]		Overall Sleeve Length [mm (in.)]
		0°	90°	0°	90°	0°	90°	
Short, thin, uninstrumented sleeve centered at 2.011 m (79.19 in.)	Before test	12.5 (0.493)	12.5 (0.493)	10.7 (0.420)	11.0 (0.432)	10.9 (0.430)	10.9 (0.430)	58.55 (2.305)
	After 5 cycles	12.5 (0.492)	12.5 (0.492)	10.7 (0.421)	10.9 (0.431)	10.8 (0.427)	10.8 (0.426)	58.57 (2.306)
	After 10 cycles	13.1 (0.515)[b]	12.5 (0.492)	10.7 (0.423)	11.1 (0.439)	11.0 (0.434)	11.0 (0.433)	58.70 (2.311)
	After 15 cycles	12.6 (0.497)	12.5 (0.492)	10.8 (0.425)	11.1 (0.437)	10.9 (0.431)	11.0 (0.433)	58.88 (2.318)
	After 20 cycles	12.7 (0.499)	12.6 (0.495)	10.9 (0.429)	11.1 (0.439)	11.1 (0.436)	11.0 (0.432)	59.26 (2.333)
	After 25 cycles	12.7 (0.501)	12.6 (0.497)	11.0 (0.434)	11.1 (0.437)	11.2 (0.441)	11.0 (0.433)	59.61 (2.347)
Short, thick, uninstrumented sleeve centered at 2.13 m (84 in.)	Before test	12.6 (0.496)	12.6 (0.495)	10.6 (0.417)	10.9 (0.431)	11.3 (0.443)	11.1 (0.437)	58.37 (2.298)
	After 5 cycles	12.6 (0.496)	12.6 (0.496)	10.7 (0.422)	11.0 (0.434)	11.0 (0.434)	11.0 (0.433)	58.57 (2.306)
	After 10 cycles	12.6 (0.497)	12.6 (0.497)	10.7 (0.422)	11.1 (0.437)	11.1 (0.436)	11.1 (0.438)	58.88 (2.318)
	After 15 cycles	12.7 (0.499)	12.7 (0.500)	10.8 (0.427)	11.2 (0.442)	11.2 (0.442)	11.2 (0.441)	59.21 (2.331)
	After 20 cycles	12.8 (0.503)	12.8 (0.504)	11.0 (0.433)	11.3 (0.444)	11.3 (0.446)	11.3 (0.445)	59.72 (2.351)
	After 25 cycles	12.7 (0.501)	12.8 (0.505)	11.3 (0.444)	11.4 (0.447)	11.4 (0.448)	11.3 (0.444)	60.20 (2.370)

a. 6.4 mm (0.25 in.) from end of sleeve

b. Measurement made over thermocouple lead from 1.91 m (75.25 in.) instrumented sleeve

TABLE G-2

DEFORMATION OF INSTRUMENTED BLOCKAGE SLEEVES

Sleeve Description	Time of Measurement	Diameter at Sleeve Center[a] [mm (in.)]		Diameter at Downstream End[b] [mm (in.)]		Diameter at Upstream End[b] [mm (in.)]		Overall Sleeve Length [mm (in.)]
		0°	90°	0°	90°	0°	90°	
Short, thick, instrumented sleeve centered at 1.911 m (75.25 in.)	Before test	12.6 (0.496)	12.6 (0.495)	10.9 (0.430)	10.8 (0.427)	10.9 (0.428)	10.9 (0.430)	58.34 (2.297)
	After 5 cycles	12.6 (0.496)	12.5 (0.492)	10.9 (0.430)	10.9 (0.428)	10.9 (0.430)	11.0 (0.433)	58.47 (2.302)
	After 10 cycles	12.6 (0.498)	12.6 (0.495)	10.9 (0.431)	11.0 (0.433)	11.0 (0.432)	11.0 (0.434)	58.70 (2.311)
	After 15 cycles	12.6 (0.497)	12.6 (0.498)	10.9 (0.430)	11.1 (0.437)	11.1 (0.437)	11.1 (0.438)	59.95 (2.321)
	After 20 cycles	12.6 (0.498)	12.8 (0.502)	11.1 (0.437)	11.4 (0.447)	11.3 (0.443)	11.3 (0.444)	59.39 (2.338)
	After 25 cycles	12.6 (0.496)	12.9 (0.506)	11.3 (0.444)	11.5 (0.451)	11.5 (0.452)	11.4 (0.448)	59.92 (2.359)
Long, thick, instrumented sleeve centered at 2.318 m (91. 25 m)	Before test	13.9 (0.548)	11.7 (0.459)	10.4 (0.409)	10.3 (0.405)	10.3 (0.406)	10.3 (0.407)	190.7 (7.506)
	After 5 cycles	13.9 (0.548)	11.6 (0.458)	10.4 (0.408)	10.3 (0.404)	10.4 (0.410)	10.3 (0.407)	190.9 (7.516)
	After 10 cycles	13.9 (0.546)	11.6 (0.457)	10.4 (0.410)	10.4 (0.408)	10.5 (0.413)	10.5 (0.413)	191.4 (7.535)
	After 15 cycles	13.8 (0.542)	11.7 (0.461)	10.5 (0.412)	10.4 (0.410)	10.7 (0.420)	10.6 (0.419)	192.0 (7.559)
	After 20 cycles	13.7 (0.538)	11.8 (0.465)	10.6 (0.416)	10.6 (0.416)	10.9 (0.428)	10.8 (0.426)	192.9 (7.593)
	After 25 cycles	13.6 (0.535)	11.8 (0.464)	10.5 (0.415)	10.6 (0.419)	11.2 (0.439)	11.0 (0.432)	193.7 (7.625)

a. 3.18 mm (0.125 in.) upstream of thermocouple

b. 6.4 mm (0.25 in.) from end of sleeve

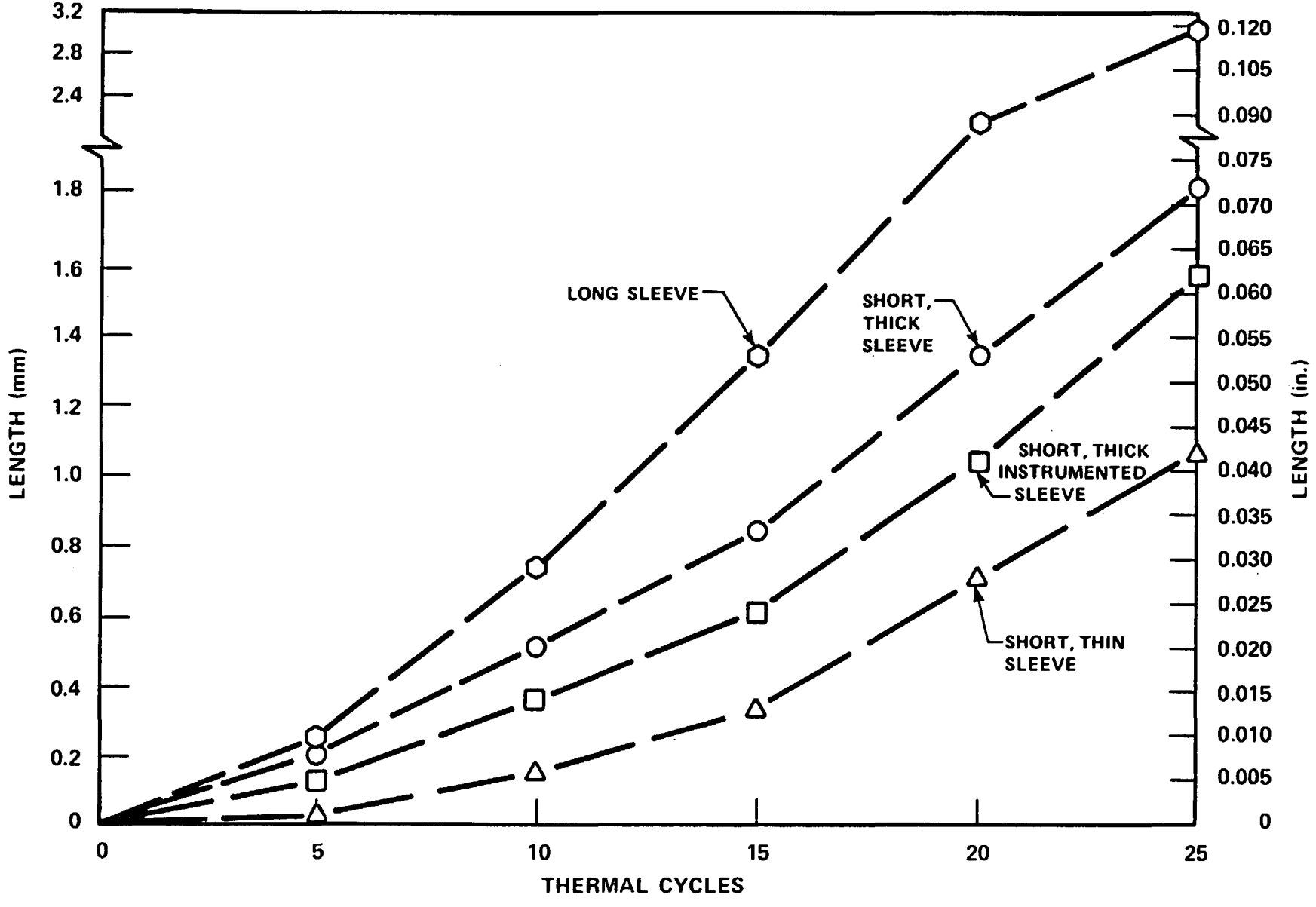

Figure G-3. Sleeve Elongation

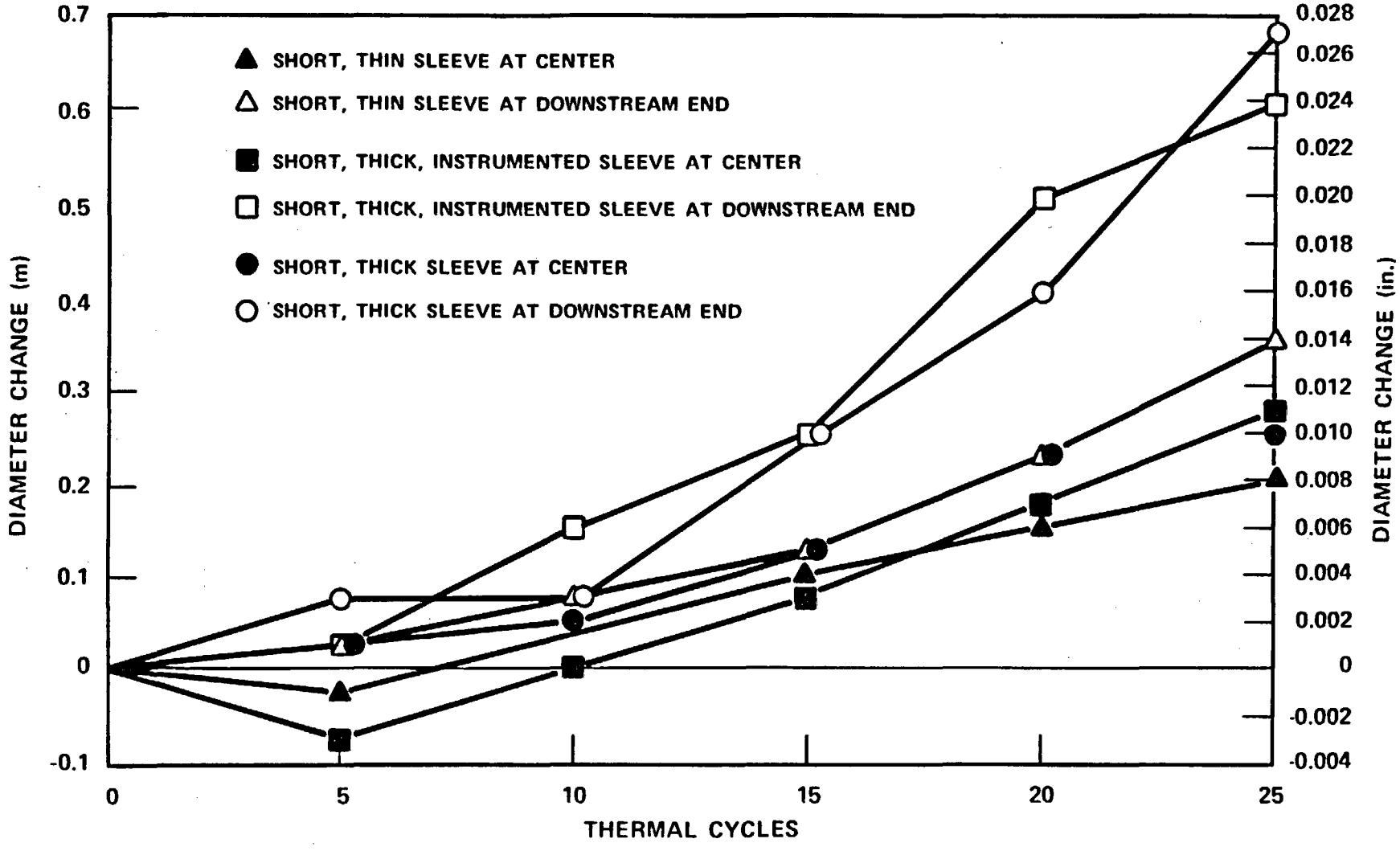

Figure G-4. Sleeve Diameter Changes at Center and Downstream End

function of thermal cycling, indicates that all four sleeves elongated similarly. The long sleeve grew approximately three times as much as the short, thin sleeve; however, the long sleeve is more than three times the length of the short sleeves. Figure G-4, which shows the diametral changes in the short sleeves as a function of thermal cycling, indicates that, radially, all three short sleeves grew similarly. The long sleeve, which is not presented in figure G-4, radially grew the most at the upstream end of the sleeve. At the conclusion of the 15th cycle, a small longitudinal crack of 9.5 mm (0.375 in.) length was detected on the upstream end of the long sleeve. At the conclusion of the 25th cycle and after disassembly, the long sleeve was found to be bowed as shown in figure G-5. After 25 cycles, the physical condition of the three short sleeves, as shown in figures G-6 through G-8, was found to be insignificantly affected by the thermal cycling.

The temperature results from the sleeve instrumentation thermal response tests are shown in figures G-9 through G-12 for the 38.1 mm (1.5 in./sec) flooding rate test (cycle 6) and in figures G-13 through G-16 for the 20.3 mm (0.8 in./sec) flooding rate test (cycle 13). Figure G-9 shows the short, thick instrumented sleeve temperature transient as well as the heater rod and housing wall temperatures at the 1.911 m (75.25 in.) elevation. The sleeve quenched at approximately 205 seconds, approximately 115 seconds later than the sleeve quenched in the previous instrumented blockage sleeve test. Figure G-10 shows the temperature transient for the heater rod thermocouples immediately upstream and downstream of the blockage sleeve. Figure G-11 shows the long instrumented sleeve temperature transient at the 2.343 m (92.25 in.) elevation as well as the heater rod and housing wall temperatures at the 2.318 m (91.25 in.) elevation and the heater rod temperature at the 2.165 m (85.25 in.) elevation. Figure G-12, which shows the quench curve for all cycle 6 thermocouples, indicates that the blockage sleeves did not prematurely quench.

Figures G-13 through G-16 provide the same information described above for the 13th cycle, which was the first 20.3 mm (0.8 in./sec) flooding rate test. The long blockage sleeve thermocouple and the housing wall thermocouple at the 2.318 m (91.25 in.) elevation consistently quenched earlier than the 2.165 m (85.25 in.) elevation heater rod thermocouple for the 20.3 mm (0.8 in./sec) flooding rate tests. It is believed that the long, nonconcentric blockage sleeve and thermocouple came into contact with the

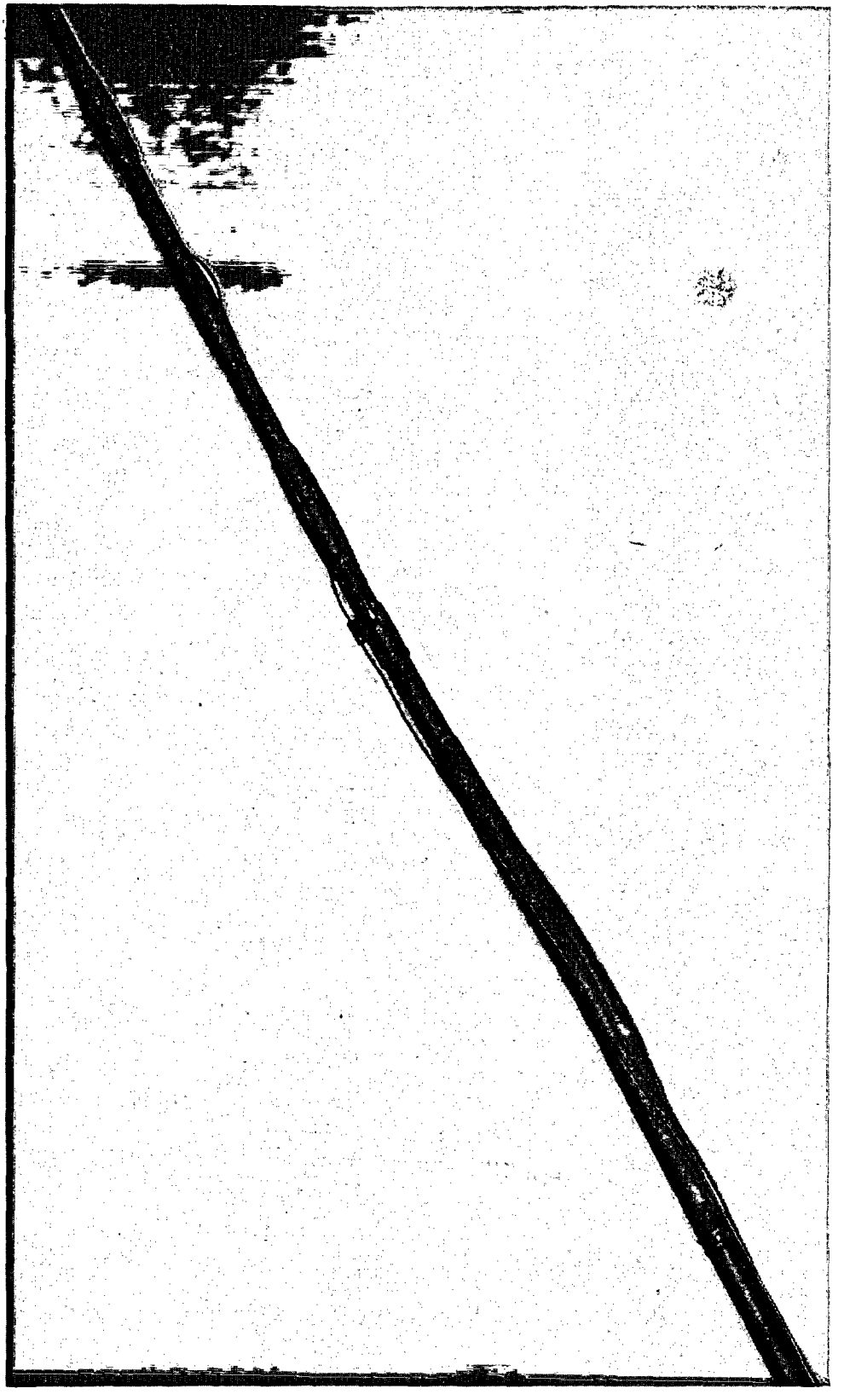

Figure G-5. Long Sleeve After 25 Cycles

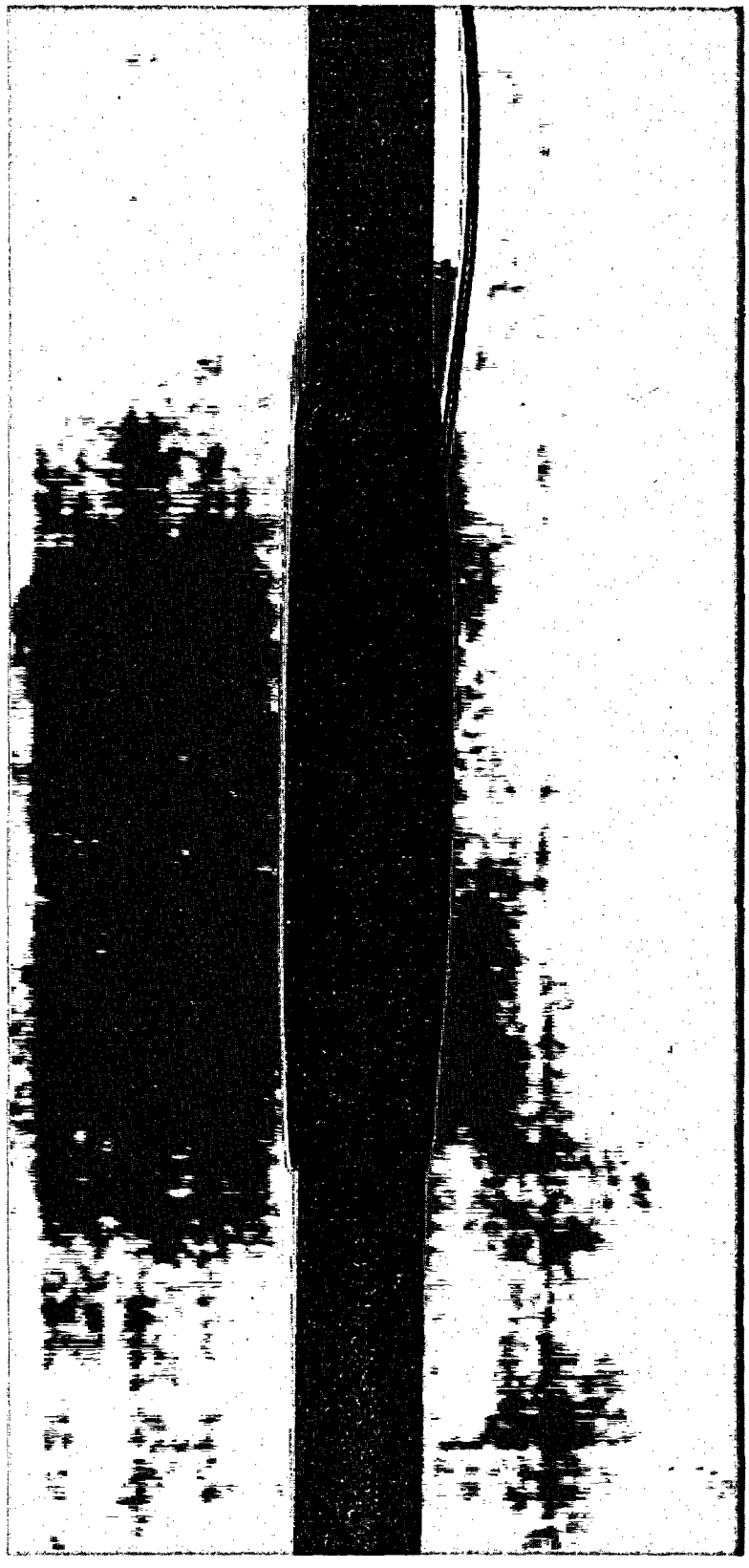

Figure G-6. Short, Thick Sleeve After 25 Cycles

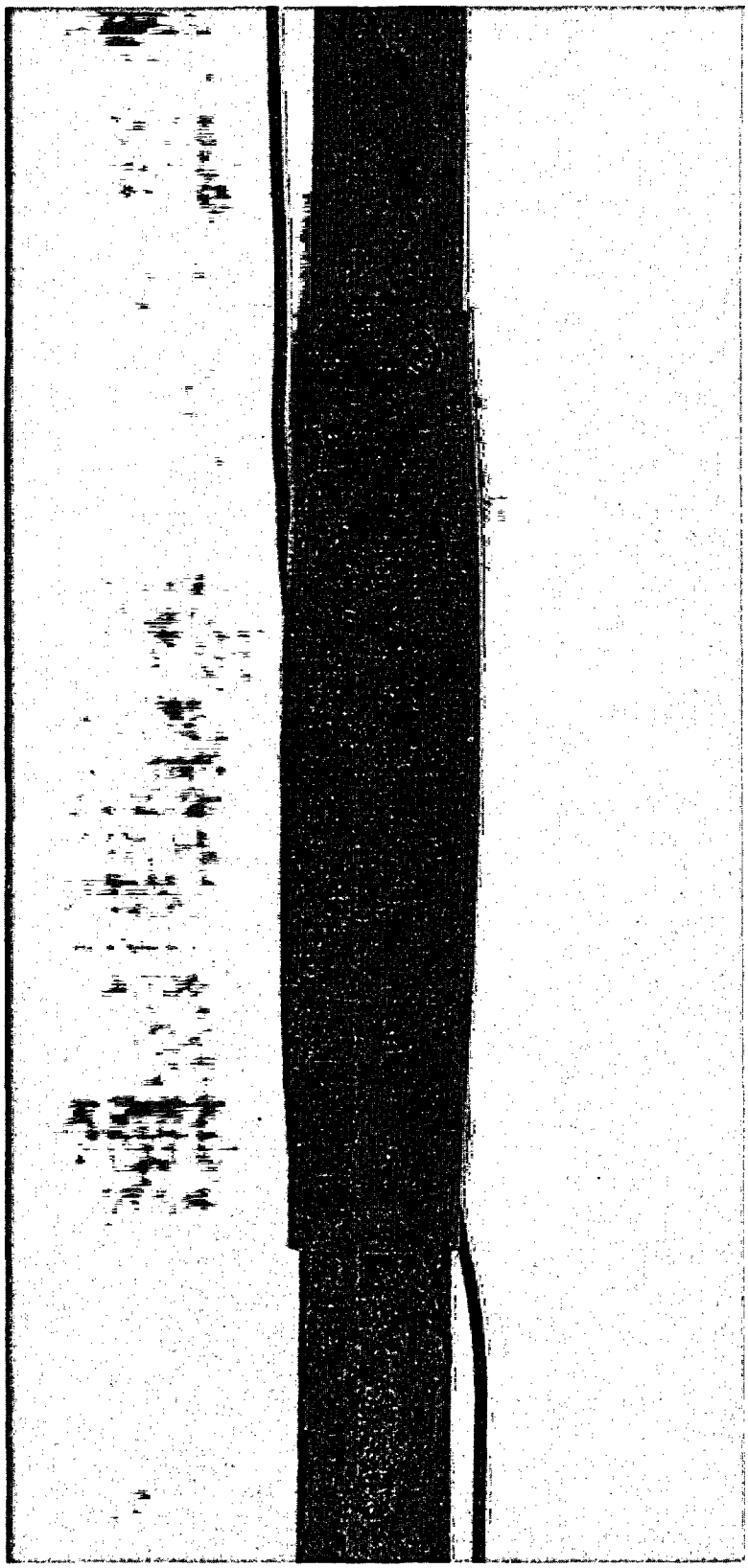

Figure G-7. Short, Thick Instrumented Sleeve After 25 Cycles

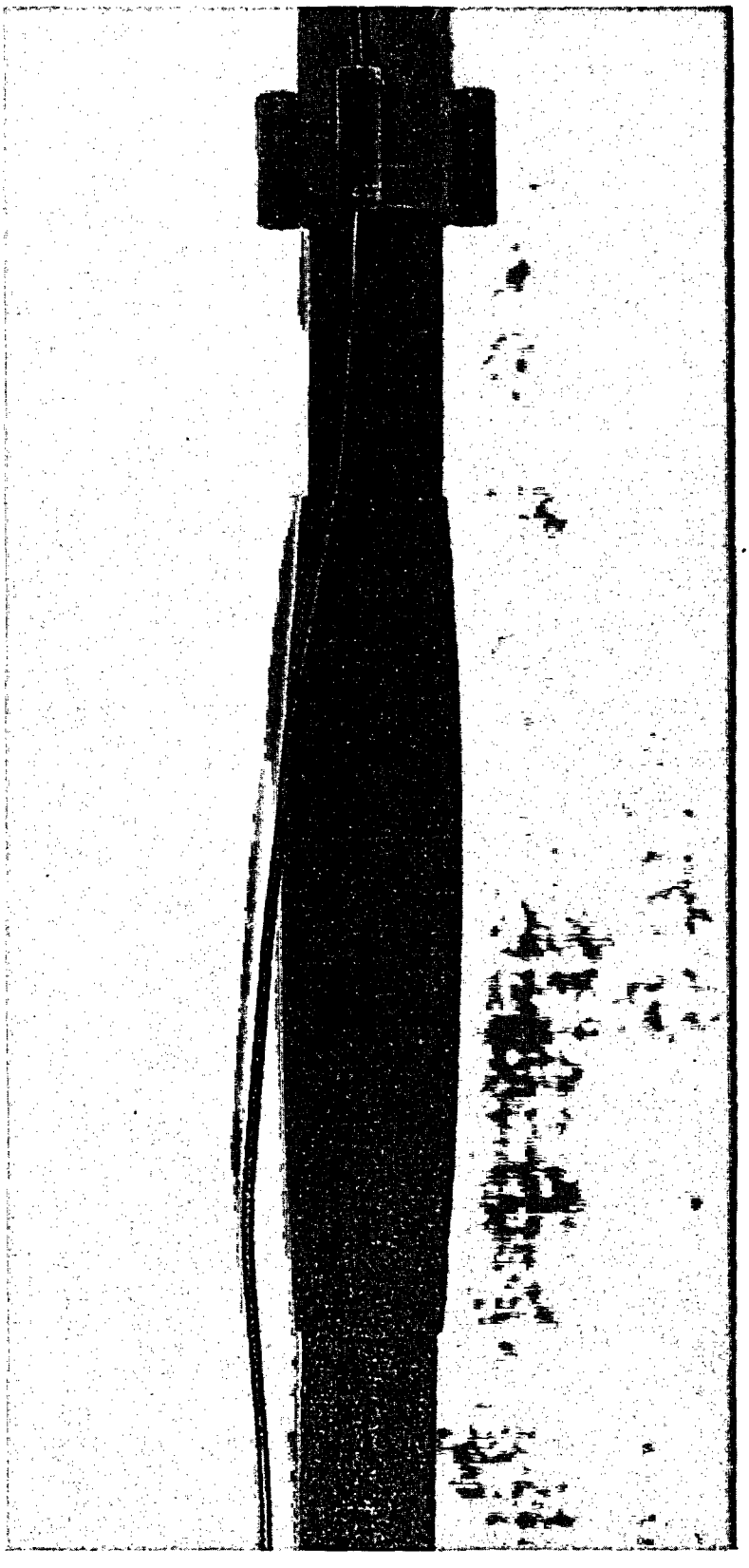

Figure G-8. Short, Thin Sleeve After 25 Cycles

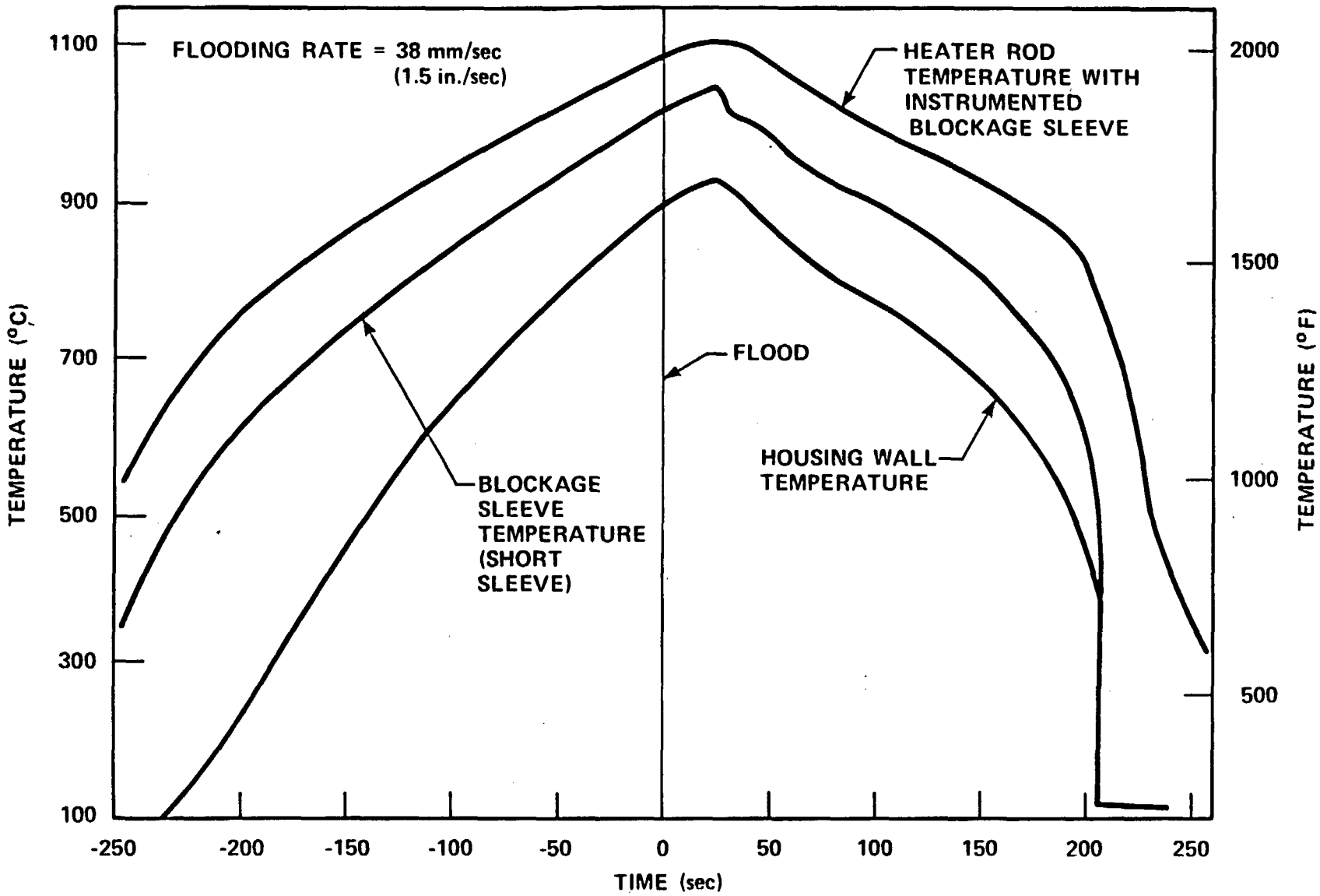

Figure G-9. Heater Rod, Wall, and Blockage Sleeve Temperatures at 1.911 m (75.25 in.), Cycle 6

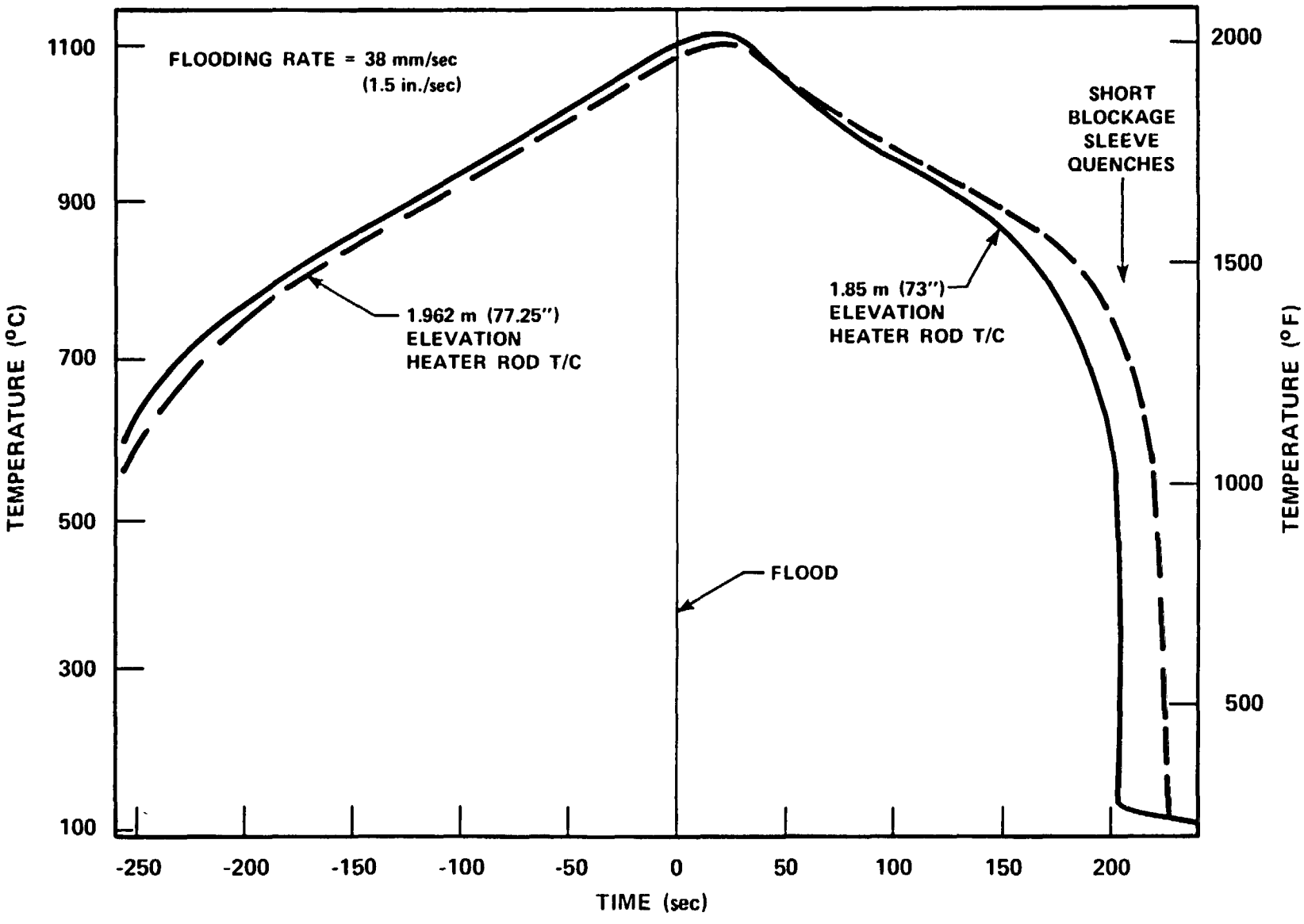

Figure G-10. Heater Rod Temperatures at 1.85 and 1.962 m (73 and 77.25 in.), Cycle 6

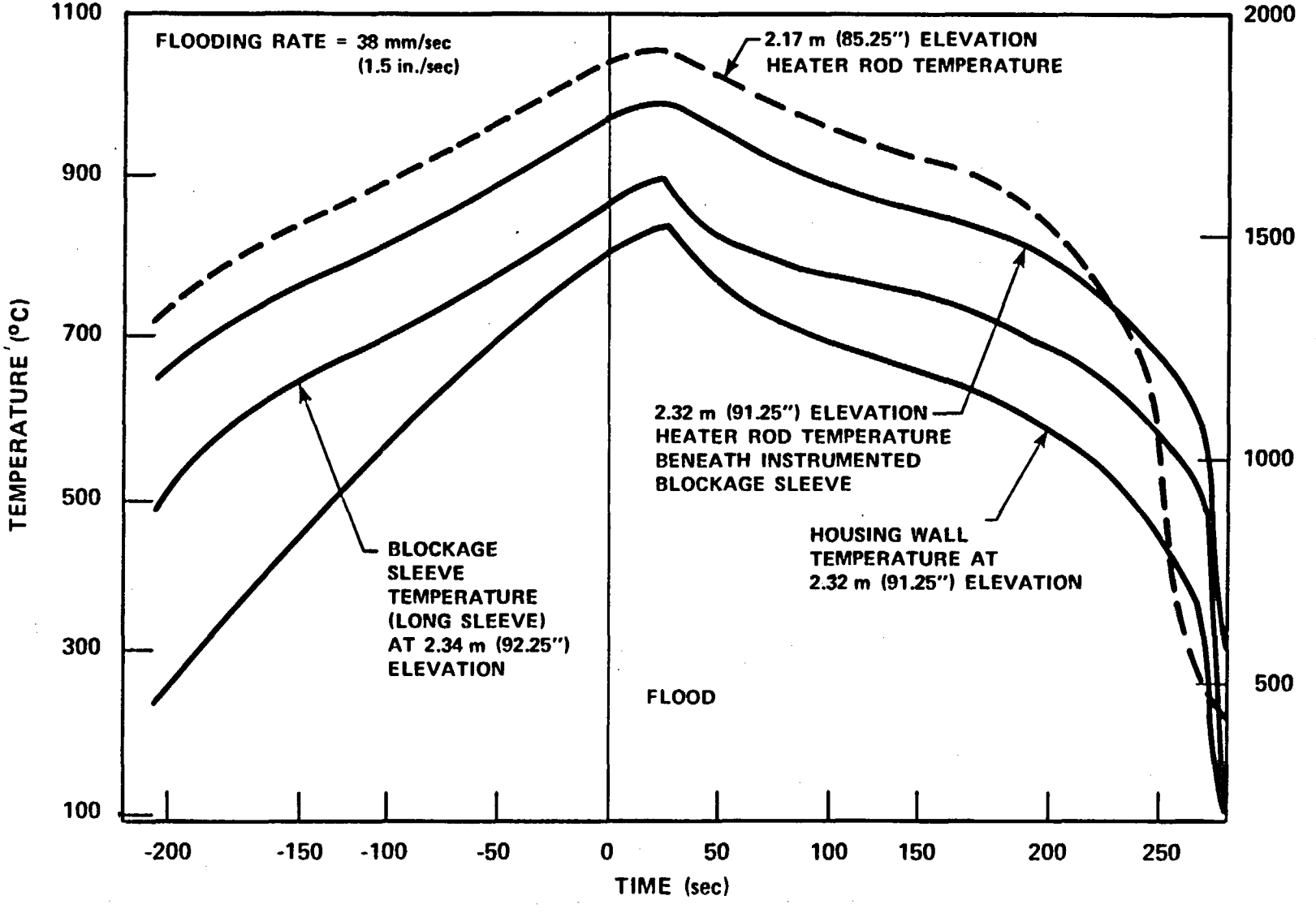

Figure G-11. Heater Rod and Wall Temperatures at 2.318 m (91.25 in.); Heater Rod Temperature at 2.165 m (85.25 in.); and Long Blockage Sleeve Temperature at 2.343 m (92.25 in.), Cycle 6

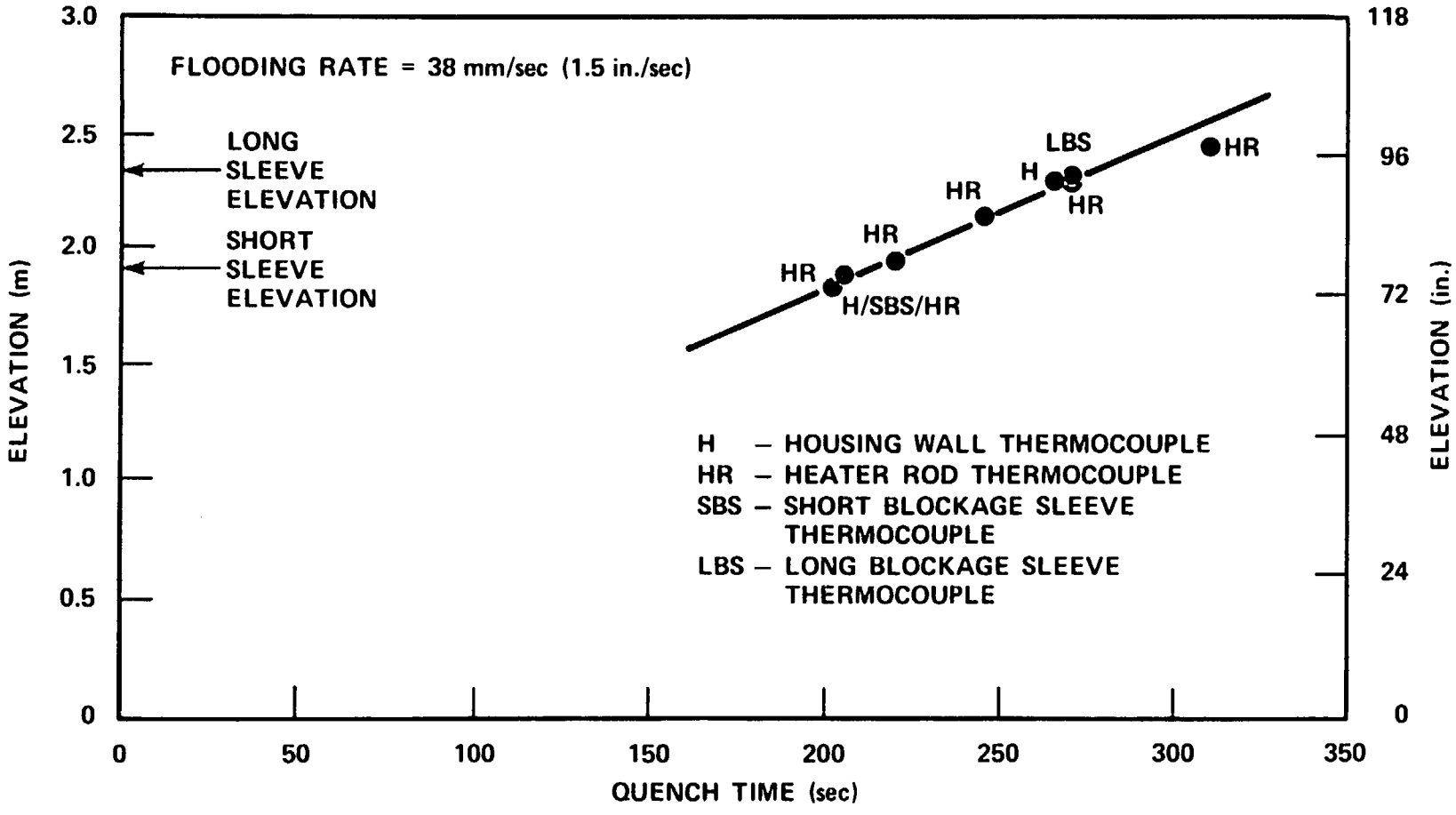

Figure G-12. Quench Curve for Sleeve Deformation and Instrumentation Test, Cycle 6

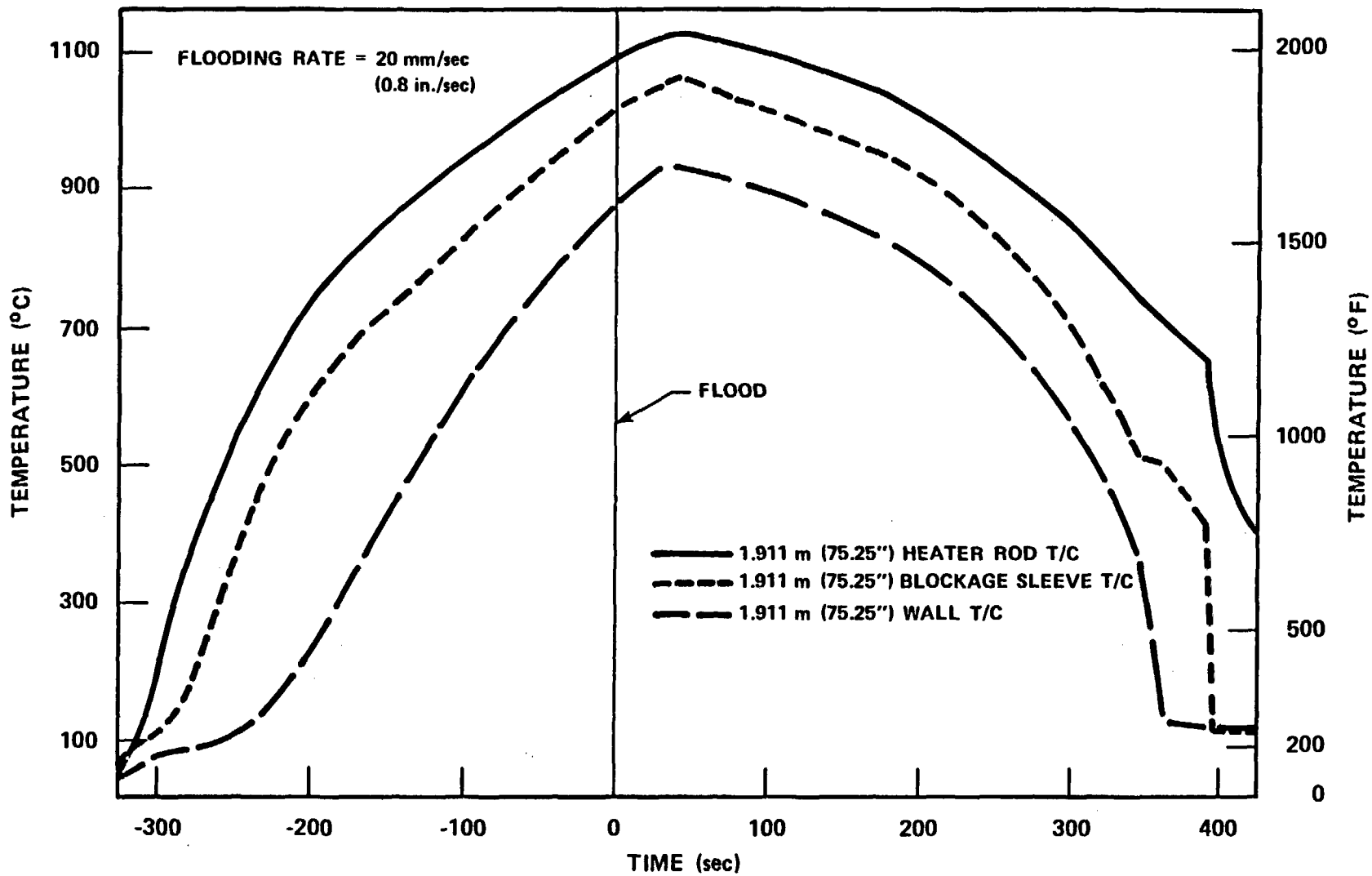

Figure G-13. Heater Rod, Wall, and Blockage Sleeve Temperatures at 1.911 m (75.25 in.), Cycle 13

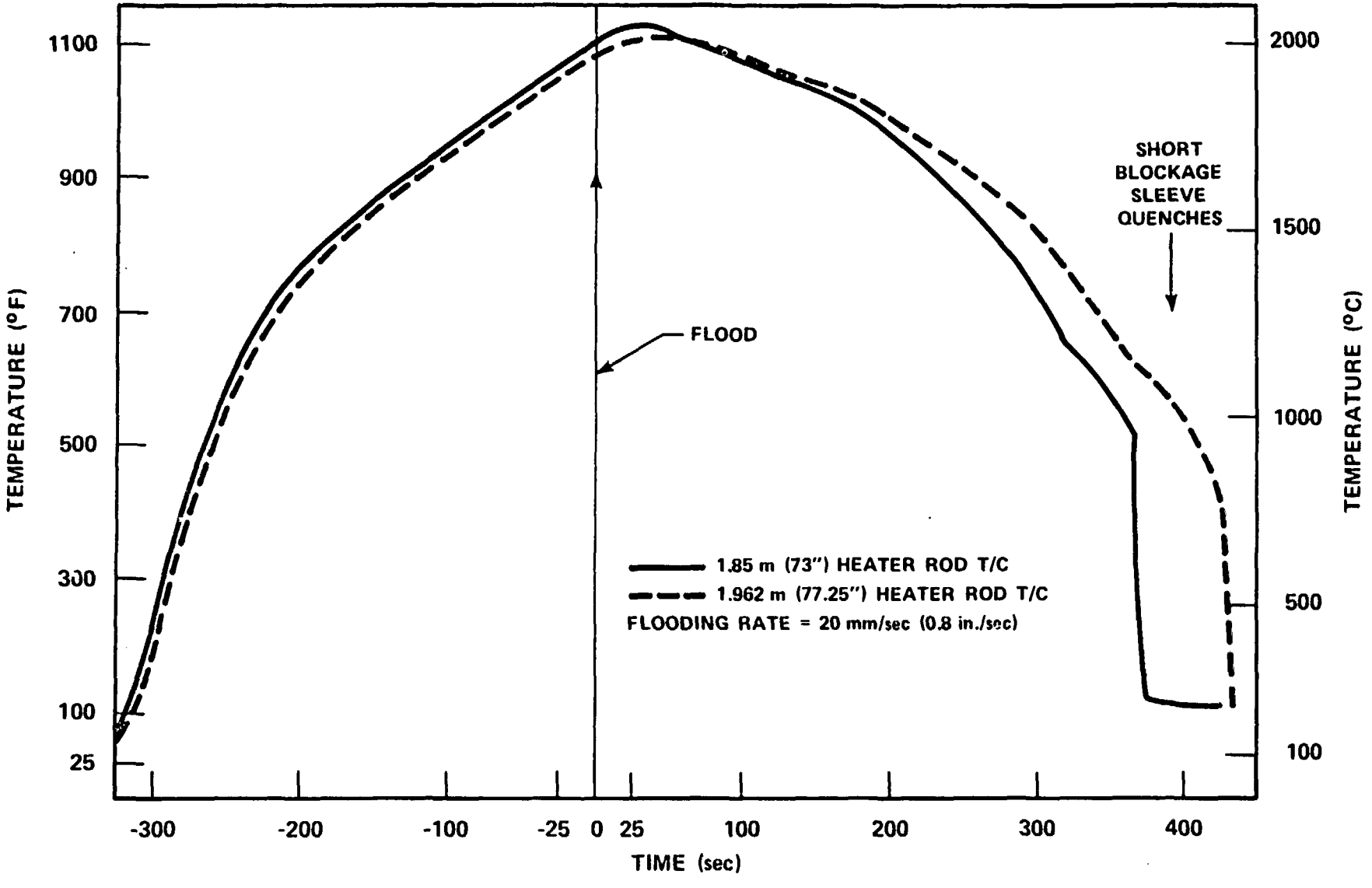

Figure G-14. Heater Rod Temperatures at 1.85 and 1.962 m (73 and 77.25 in.), Cycle 13

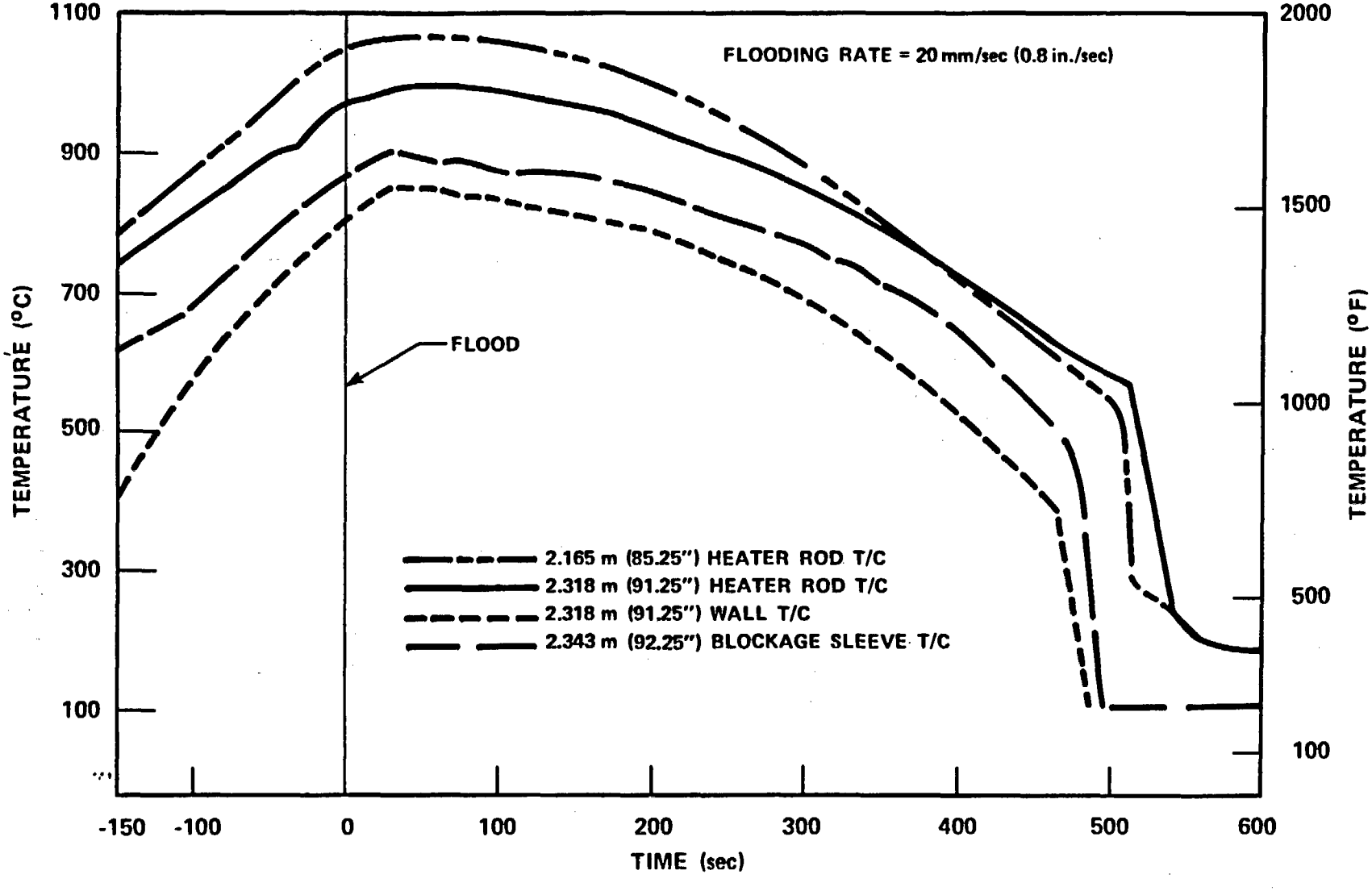

Figure G-15. Heater Rod and Wall Temperatures at 2.318 m (91.25 in.); Heater Rod Temperature at 2.165 m (85.25 in.); and Long Blockage Sleeve Temperature at 2.343 m (92.25 in.), Cycle 13

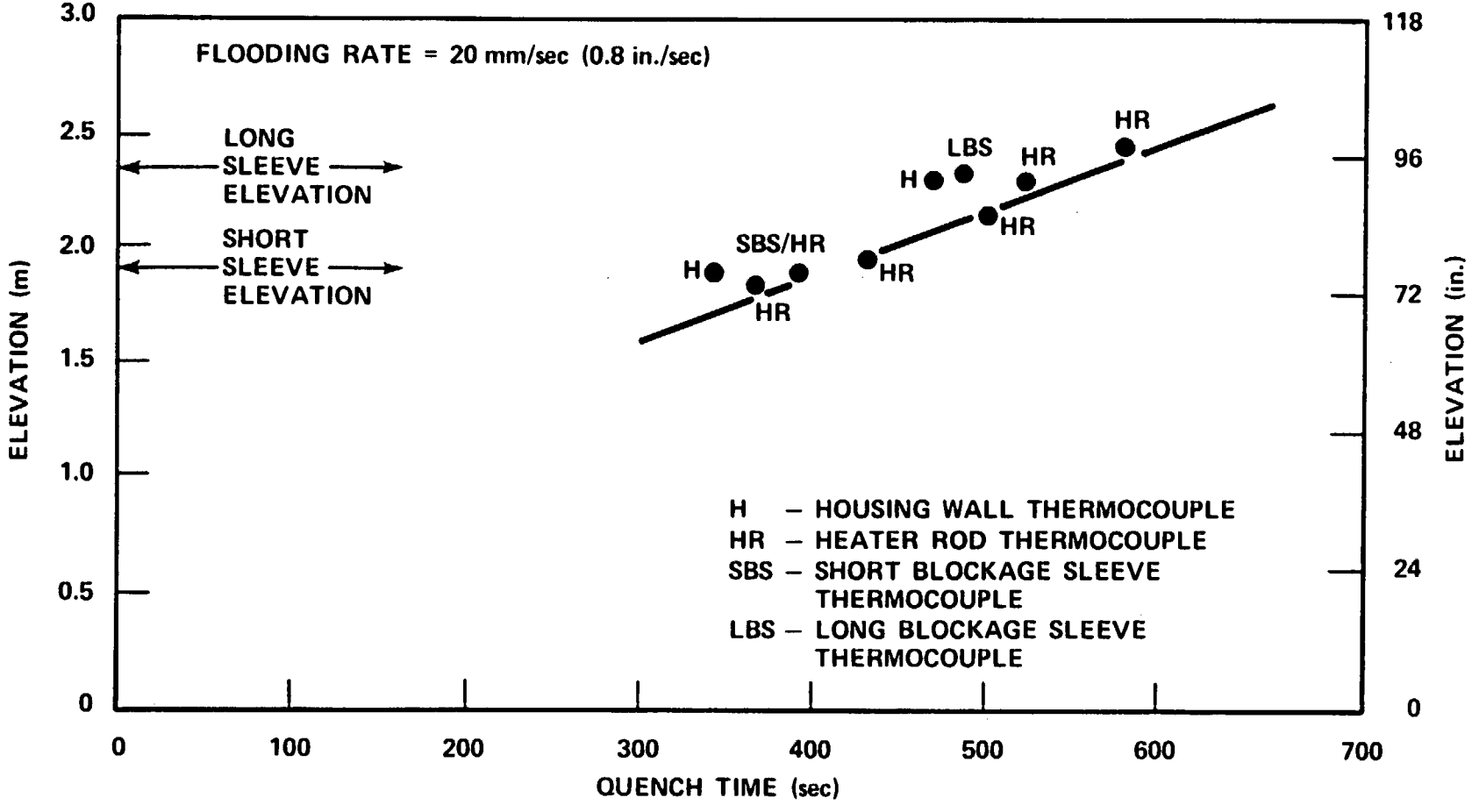

Figure G-16. Quench Curve for Sleeve Deformation and Instrumentation Test, Cycle 13

housing wall during these long-duration tests. If the rod were centered within the housings, there would be only a 1.98 mm (0.078 in.) gap between the sleeve and the housing.

The sequence of quenching was consistent from cycle to cycle, although the quench times varied by as much as ±15 percent for the 20.3 mm/sec (0.8 in./sec) flooding rate tests. This variation was attributed to the manual control of the facility.

The quench curve for the previous single-rod test described in paragraph G-1 is shown in figure G-17. This figure shows that the quench time for the instrumented short, thin sleeve is much earlier than the heater rod thermocouple quench times.

All the thermocouples survived the 25 cycles except for the two housing wall thermocouples. The 1.911 m (75.25 in.) elevation wall thermocouple failed after the 15th cycle and the 2.318 m (91.25 in.) elevation wall thermocouple failed after the 20th cycle. To quantitatively assess the environment to which a thermocouple was subjected, the integral of the time-temperature curve for that thermocouple was calculated. The temperature data for the heater rod thermocouple between the short, thick instrumented sleeve and the short, thin sleeve at the 1.962 m (77.25 in.) elevation was analyzed based on the integral of the time-temperature curve when the rod temperature was above 538°C (1000°F). The respective 161-rod unblocked bundle data for those 14 reflood tests planned for the 21-rod bundle were analyzed to determine the life expectancy required. Table G-3 summarizes these results.

G-4. CONCLUSIONS

It was concluded that the method utilized to instrument the short, thick blockage sleeve did not affect the thermal response of the heater rod and that the short, thick instrumented blockage sleeve had an acceptable amount of deformation in these severe single-rod tests. The integral of the time-temperature curve indicates that the blockage sleeve thermocouples would survive the planned 21-rod bundle test matrix.

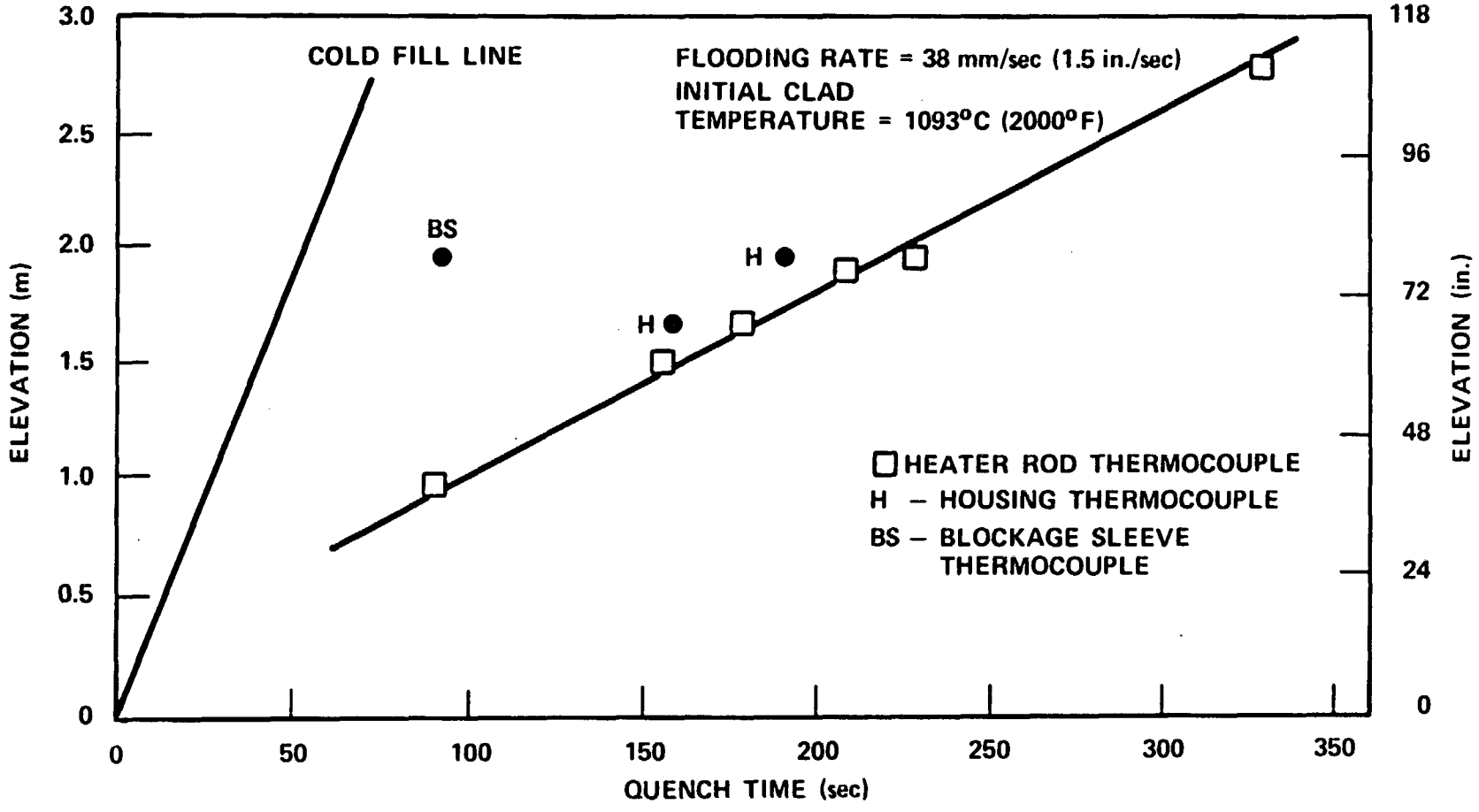

Figure G-17. Quench Curve for the Single-Rod Test with Instrumented Short, Thin Sleeve, Cycle 6

TABLE G-3

THERMOCOUPLE LIFE EXPECTANCY

Test and Cycle	Integral of Time-Temperature Curve [°C-sec (°F-sec)]	Integral of Time-Temperature Curves for 14 Planned Reflood Matrix Tests [°C-sec (°F-sec)]
38.1 mm/sec (1.5 in./sec) flooding rate test, cycle 6	1.7×10^5 (3.0×10^5)	--
20.3 mm/sec (0.8 in./sec) flooding rate test, cycle 13	2.3×10^5 (4.2×10^5)	--
Total[a]	4.70×10^6 (8.46×10^6) [1.962 m (77.25 in.) rod thermocouple]	1.71×10^6 (3.07×10^6) [1.83m (72 in.) rod thermocouple]

a. It was assumed that the integral of the time-temperature curve was approximately the same for each of the respective cycles; therefore, the total is equal to 10 cycles x 3.0×10^5 °F-sec + 13 cycles x 4.2×10^5 °F-sec.

However, it was found that the long, nonconcentric sleeve bowed significantly on the side opposite the sleeve bulge. The bowing of the long sleeve was attributed to the tight fit between the sleeve and the heater rod. It was postulated that the sleeve grew axially with the heater rod as the rod temperature increased, but as the temperature decreased and the heater rod contracted, the sleeve did not contract and a compressive force was placed on the sleeve which subsequently bowed the weaker side of the sleeve.

Another test was conducted on the long, nonconcentric blockage sleeve to determine the amount of bowing attributable to the thermal cycling. The long sleeve was mounted on a short length of tubing, heated to approximately 1093°C (2000°F), cooled in air, and subsequently quenched at a temperature of approximately 816°C (1500°F) in a hot water bath. After every five cycles, the sleeve was cooled to room temperature and measured for bow. The measured amount of bow was found to be less than that measured from the single-rod tests.

The posttest visual examination of the 21-rod blocked bundles revealed that the flow blockage sleeves retained their nominal shape and, generally, the blockage sleeve thermocouples survived the testing. (There was one failed blockage sleeve thermocouple out of a total of 30 thermocouples in all five blocked bundles.) The long, nonconcentric blockage sleeve on the center heater rod was removed from configuration F and subsequently inspected. It was found that the posttest dimensions of the long, nonconcentric sleeve were within the tolerance limitations allowed for manufacturing.

APPENDIX H
BUNDLE GEOMETRY ANALYSIS

H-1. INTRODUCTION

The posttest examination of the 21-rod bundle revealed that in all six bundles, the pin connecting the filler rods broke at the midplane elevation. The filler rods were found to be bowed into the bundle; this subsequently caused some heater rod bow on the periphery of the bundle. The lower grid assembly, which consisted of the lower three grids and respective filler rods, was subsequently separated from the upper grid assembly by approximately 25 to 51 mm (1 to 2 in.) for each bundle. The heater rod bow observed in the posttest examination was limited to the bundle midplane, where the filler rods had separated. The remainder of the bundle was observed to be essentially unchanged from its nominal pretest geometry, except for heater rod and filler rod surface oxidation. Observations and measurements concerning posttest bundle geometry are listed in table H-1. Photographs of the center section for each bundle are shown in figures H-1 through H-6.

The first two bundles were cast in epoxy by ORNL and subsequently sliced in 25 to 51 mm (1 to 2 in.) thick cross sections. Each cross section was photographed, as shown in figures H-7 and H-8 for the 1.85 m (73 in.) elevation. For configuration A, the subchannel flow areas were calculated and input into COBRA. The posttest geometry flow was subsequently compared to the nominal pretest flow. The flow variation from nominal geometry to posttest geometry is shown in figure H-9 for the subchannel surrounding the center rod. This subchannel shows a maximum flow variation of less than 15 percent.

TABLE H-1

POSTTEST BUNDLE GEOMETRY OBSERVATIONS

Configuration	Distance Lower Grid Assembly Dropped [mm (in.)]	Visual Observations of Posttest Bundle Geometry
A	51 (2)	Greatest heater rod bow of all six bundles. The thermocouple leads for steam probes below 1.70 m (67 in.), which were attached to the fillers, were broken at the filler separation.
B	64 (2.5)[a]	Heater rod bow was not as great as in configuration A.
C	3.18 (0.125)	Least heater rod bow of all six bundles, since the coplanar blockage prevented filler rods from bowing into the heater rods
D	19 (0.75)	Heater rod bow was approximately the same amount as in configuration B.
E	25. (1.0)	Heater rod bow was approximately the same amount as in configuration B.
F	76 (3.0)[a]	Heater rod bow was approximately the same amount as in configuration B.

a. The lower grid assembly could drop a maximum distance of 51 mm (2 in.), since mechanical restraints were installed in the lower plenum prior to configuration B testing. It was assumed that at least 13 mm (0.5 in.) in configuration B and at least 25 mm (1 in.) in configuration F was attributed to drag induced in removing the bundle from the housing.

Figure H-1. Posttest Photograph of Configuration A Midplane

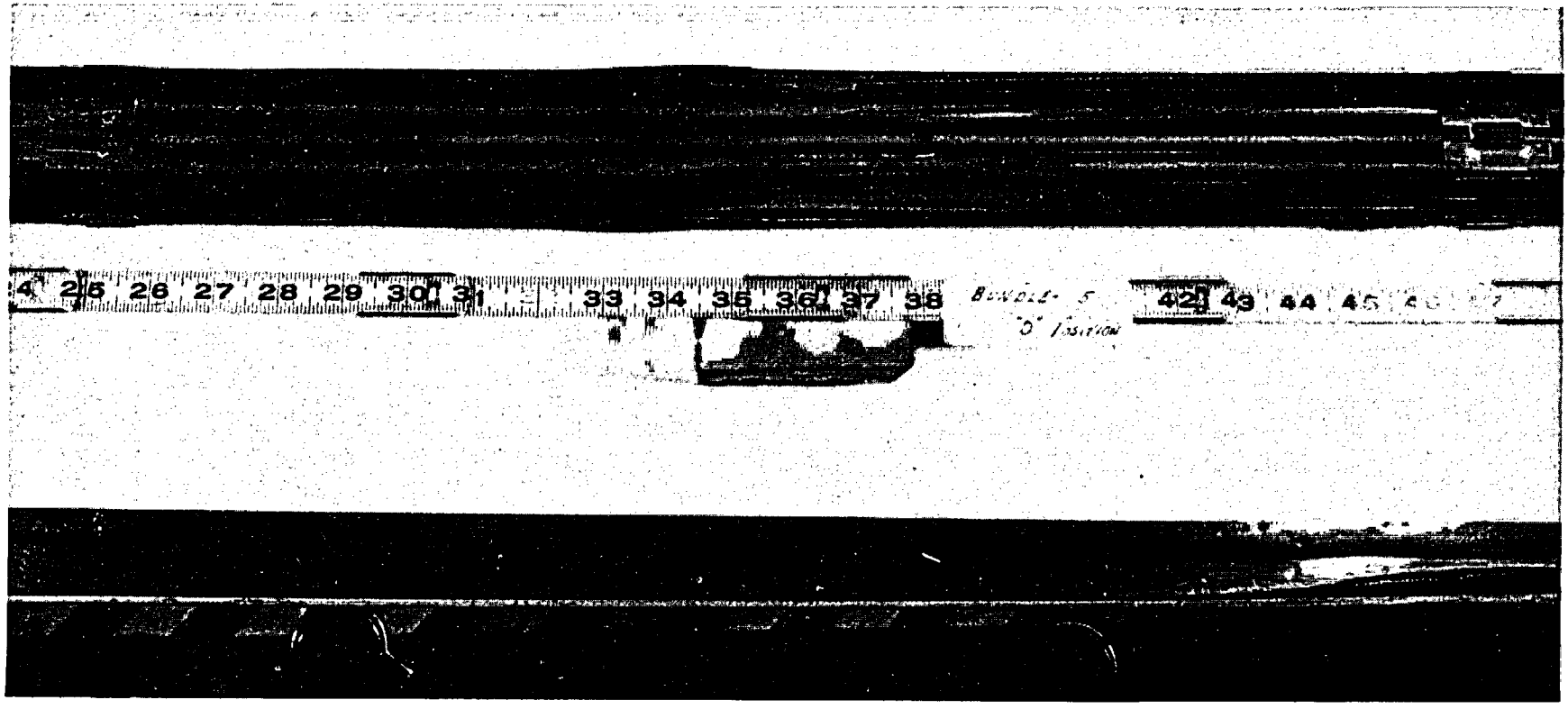

Figure H-5. Posttest Photograph of Configuration E Midplane

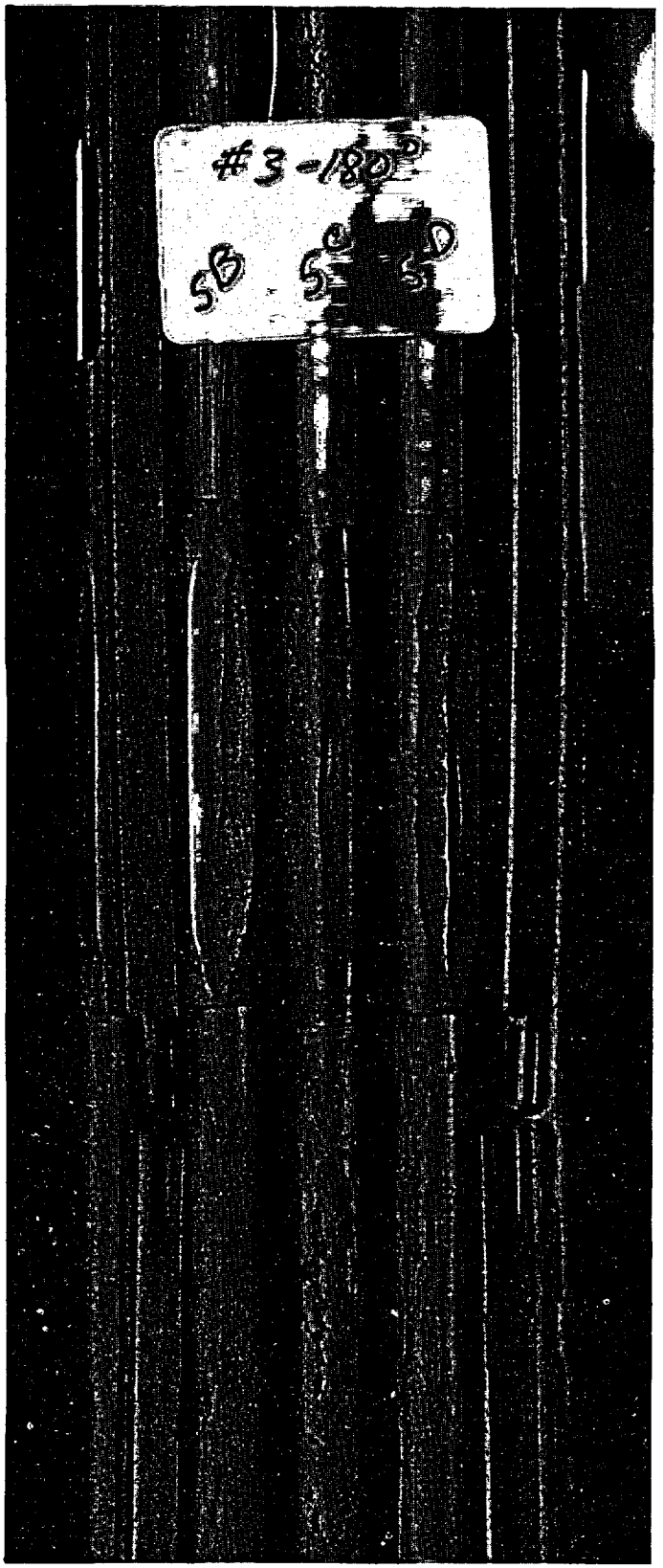

Figure H-3. Posttest Photograph of Configuration C Midplane

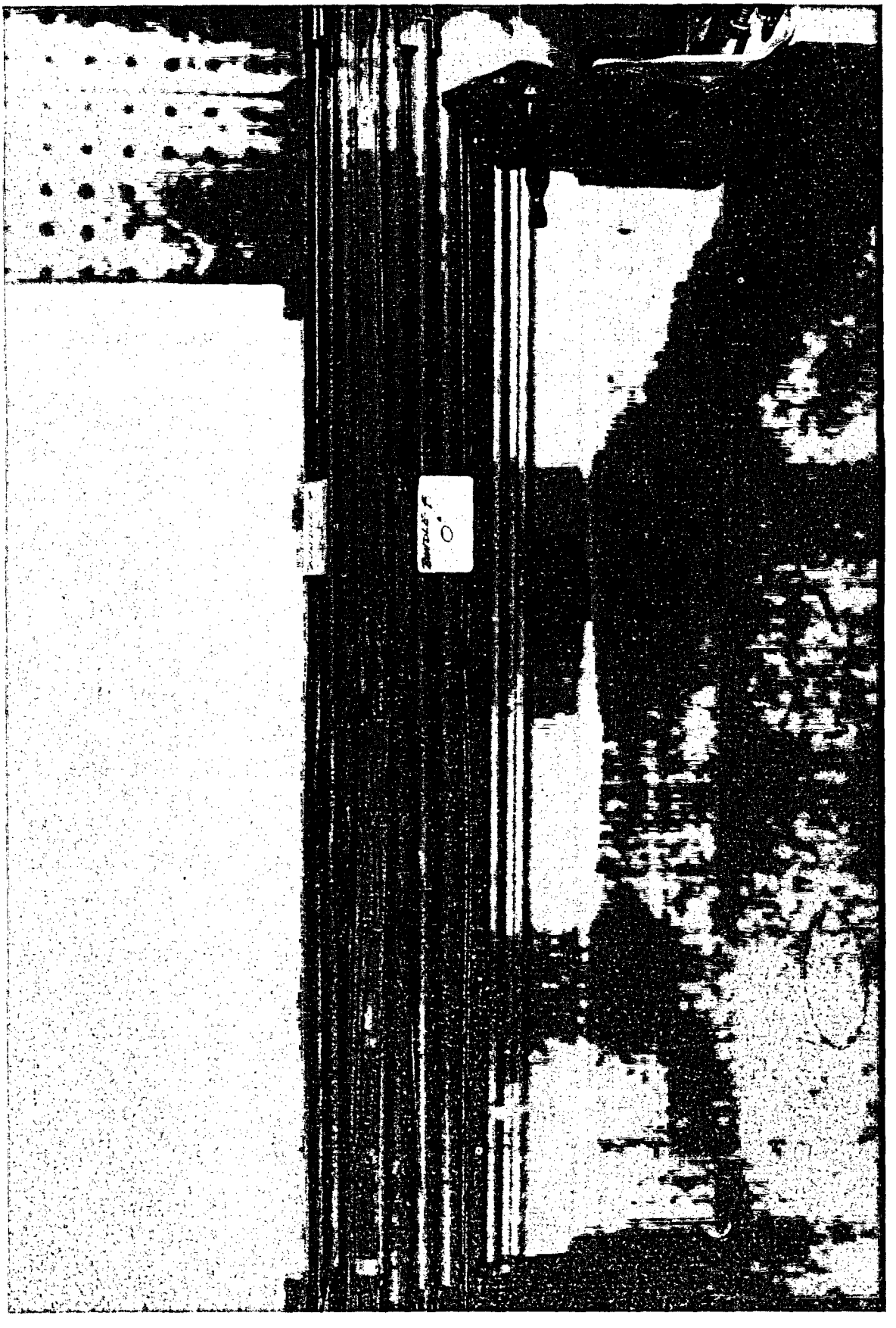

Figure H-4. Posttest Photograph of Configuration D Midplane

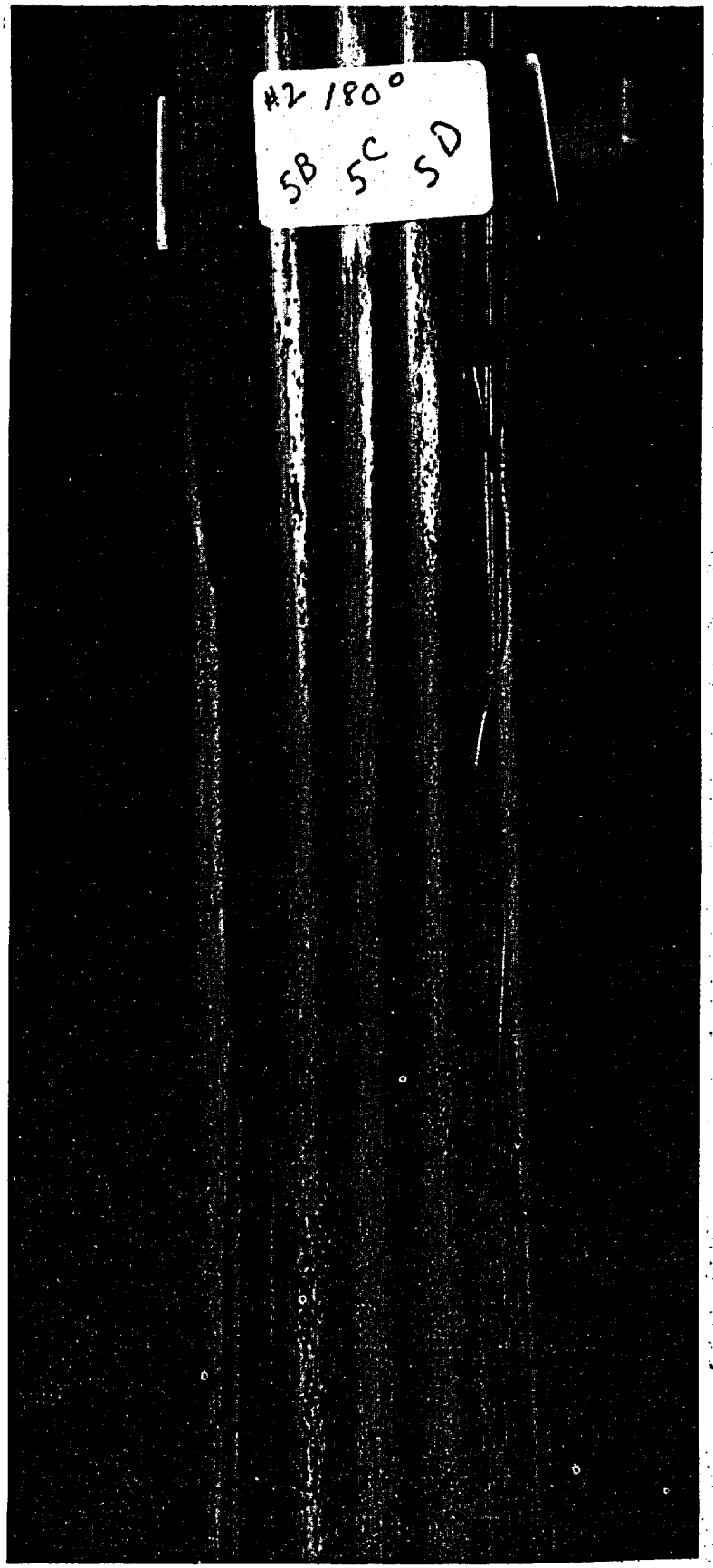

Figure H-2. Posttest Photograph of Configuration B Midplane

Figure H-6. Posttest Photograph of Configuration F Midplane

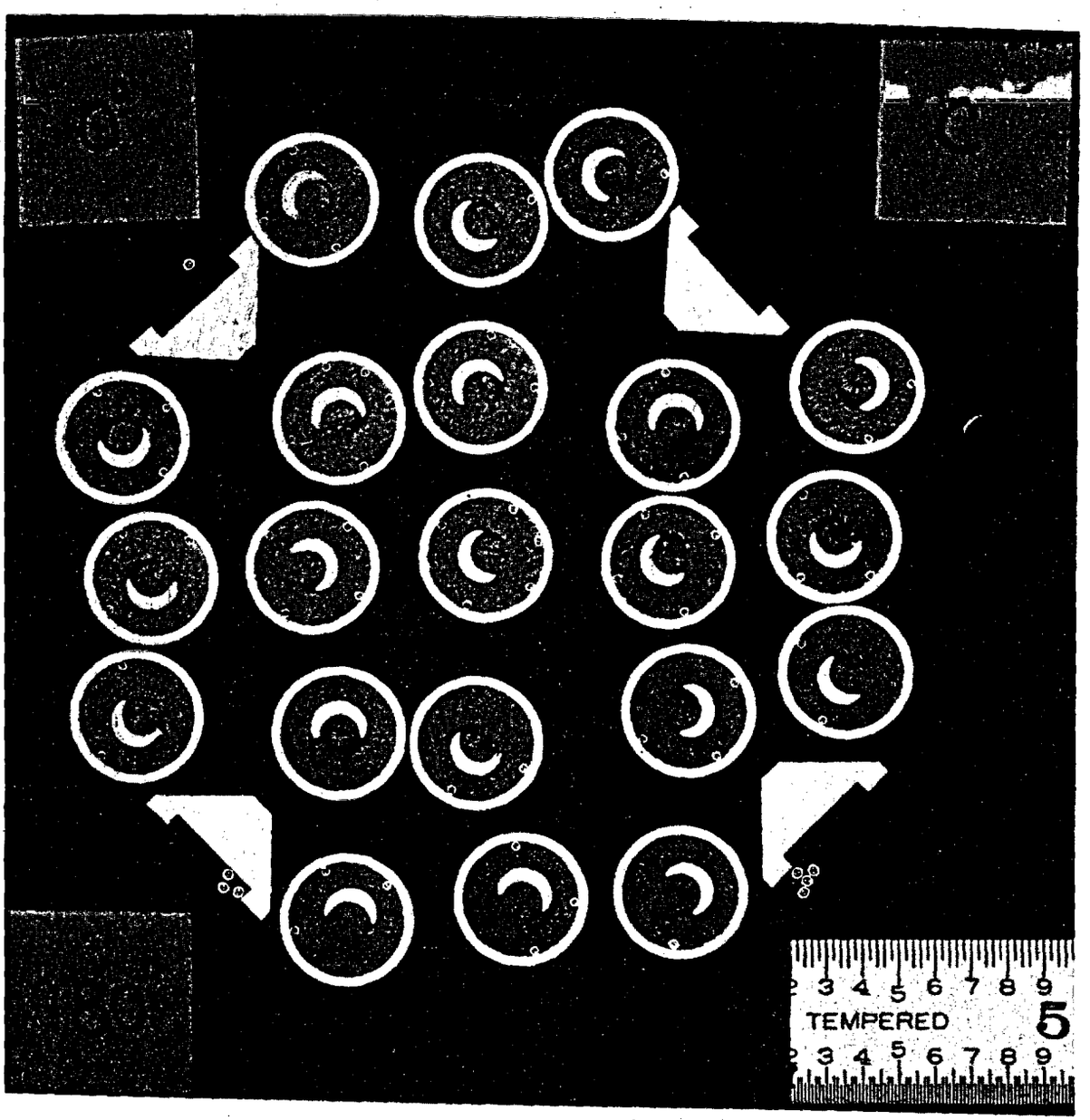

Figure H-7. Configuration A Cross Section at 1.85 m (73 in.) Elevation

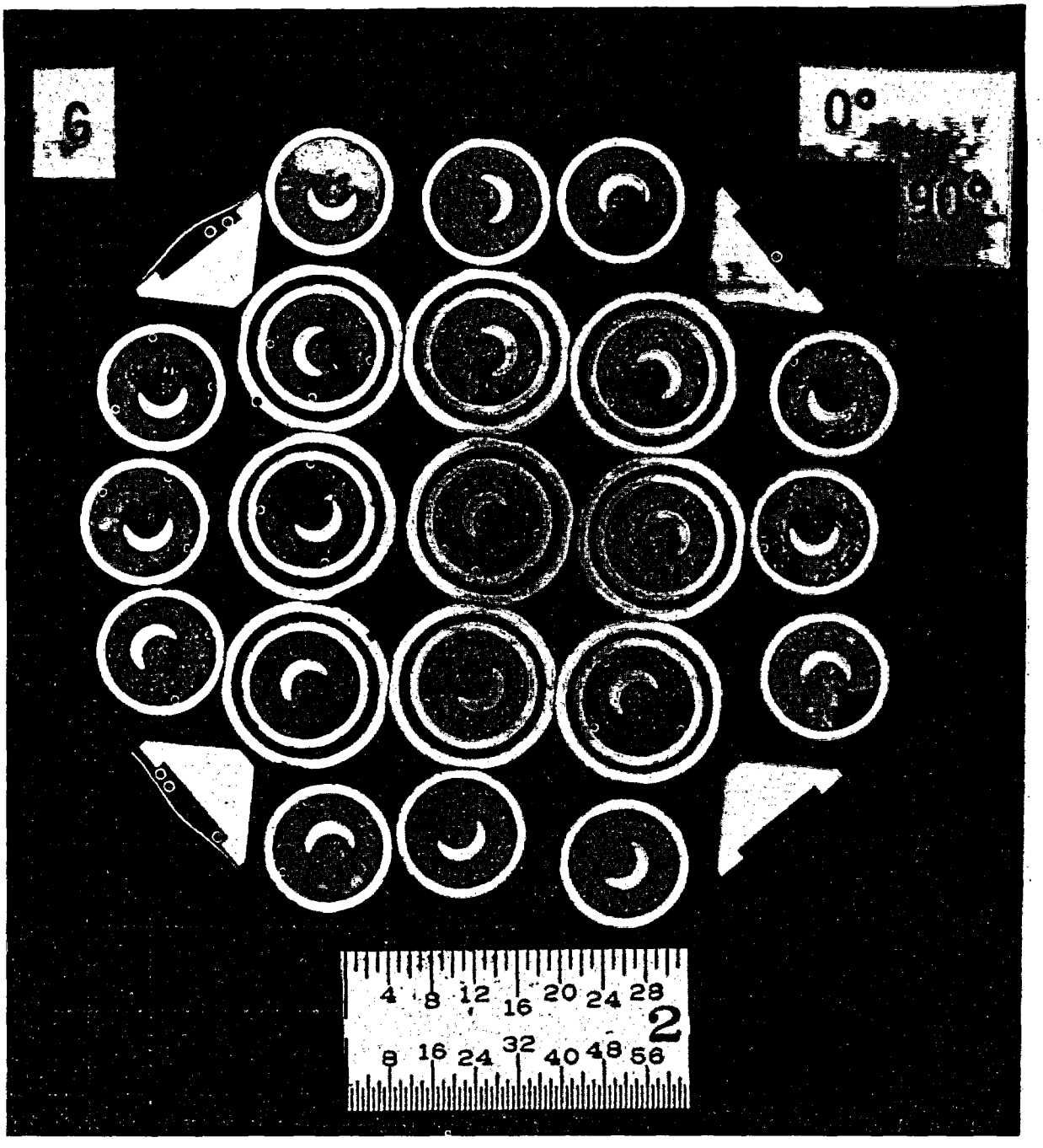

Figure H-8. Configuration B Cross Section at 1.85 m (73 in.) Elevation

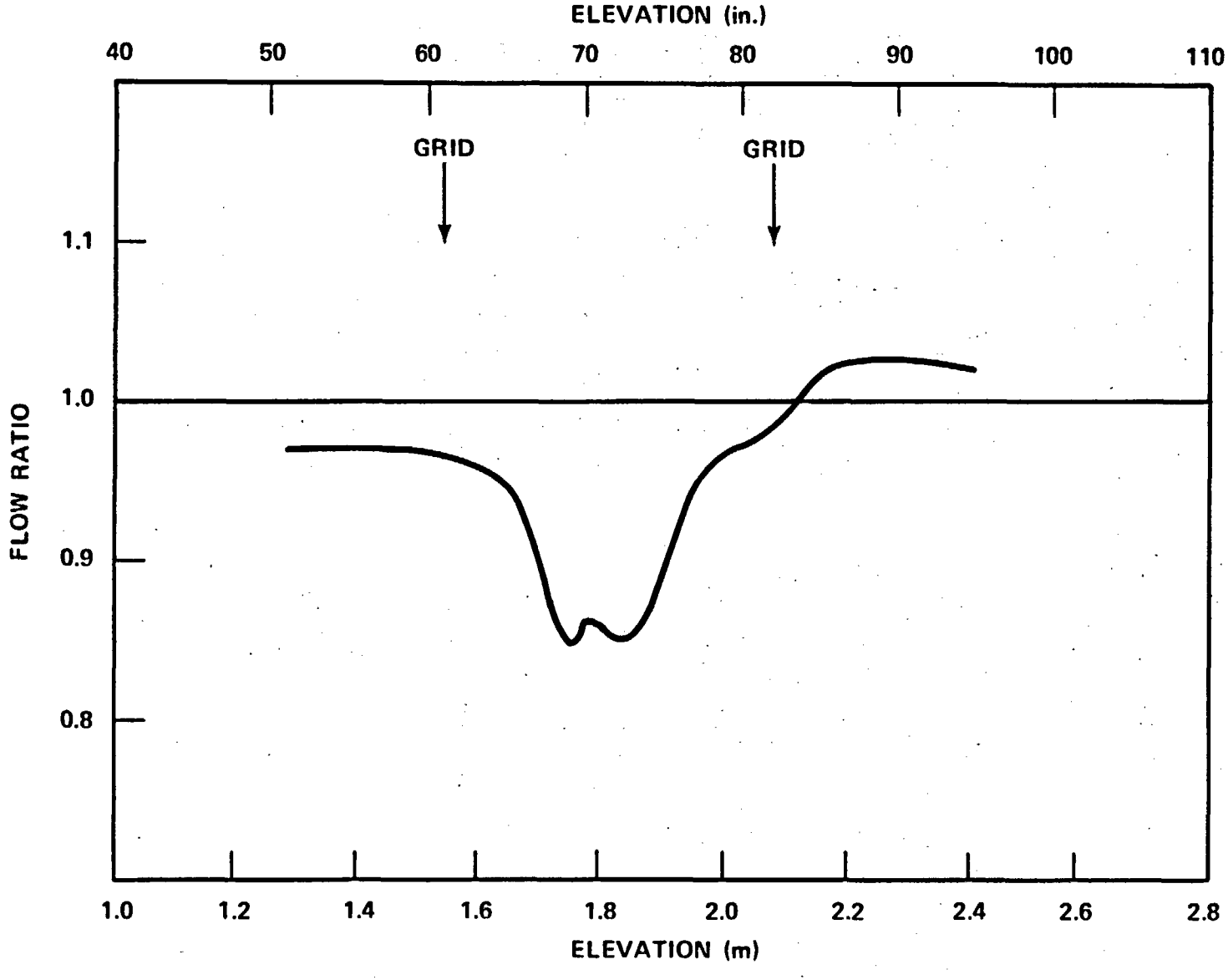

Figure H-9. Ratio of Posttest Geometry Flow to Pretest Geometry Flow for Center Heater Rod in Configuration A From COBRA-IV-I Code

The posttest examination of the bundle does not, however, provide an explanation for the geometry variation during the course of testing or for the geometry during a high-temperature reflood test. The heater rod temperature and heat transfer data from the repeat tests were subsequently evaluated to determine whether the bundle geometry affected the bundle thermal response.

H-2. REPEAT TEST TEMPERATURE ANALYSIS

The repeat test data from each of the six 21-rod bundles were evaluated to determine the effect of filler rod and heater rod bowing at the bundle midplane on the bundle thermal response. Insofar as experimentally possible, at least three tests were conducted at the same boundary and initial conditions at regular intervals during the forced reflood testing. However, in configurations D and E, the first repeat tests both had high initial injection flow rates. Although the first repeat test could not be utilized, an additional repeat test was conducted immediately after the third repeat test in these two bundles. This fourth repeat test was conducted to isolate the effects of "pure" data repeatability. Pure data repeatability represents a measure of the bundle's thermal response variation for successive tests under the same initial and boundary conditions. A fifth repeat test (run 42415E) was conducted in configuration E, to determine the effect of the power step at flood initiation (see paragraph M-12). A fourth and a fifth repeat test were conducted in configuration F because of the additional forced reflood tests that were conducted in place of the gravity reflood tests. The forced reflood tests had much higher temperatures and could have produced additional heater rod bowing.

The nominal test conditions for each of the repeat tests were as follows:

-- Flooding rate - 27.9 mm/sec (1.1 in./sec)

-- Peak initial linear power - 2.4 kw/m (0.78 kw/ft)

-- Initial clad temperature - 871°C (1600°F)

-- System pressure - 0.28 MPa (40 psia)

-- Inlet subcooling - 78°C (140°F)

-- Average initial housing temperature at 1.83 m (72 in.) elevation - 510°C (950°F)

The following lists the respective valid repeat tests for each of the six bundles and the sequential order in which they were conducted; the second and third numbers in the test run number refer to the sequential cycle number:

	Sequential Order and Test Number				
Bundle	First	Second	Third	Fourth	Fifth
A	42430A	42907A	43715A	-	-
B	41907B	42415B	42915B	-	-
C	42107C	42715C	43315C	-	-
D		42615D	43115D	43215D	-
E		41515E	42215E	42315E	42415E
F	41807F	42215F	42915F	43915F	44015F

The average initial housing temperature and housing axial temperature distribution could not be exactly controlled because of the method of heating the housing. The bundle was power-pulsed twice to a peak rod temperature of 649°C (1200°F), which subsequently heated the housing by radiation and convection. The bundle was then heated to a temperature of 871°C (1600°F), at which time reflood was initiated. The average initial housing temperatures at the 1.83 m (72 in.) elevation at time of reflood for each of the above repeat tests are compared below:

	Average Initial Housing Temperature at 1.83 m (72 in.) Elevation for Sequential Tests Listed Above [°C (°F)]				
Bundle	First	Second	Third	Fourth	Fifth
A	501 (933)	490 (914)	534 (994)	-	-
B	533 (992)	531 (988)	529 (985)	-	-
C	498 (929)	503 (938)	514 (957)	-	-
D	-	501 (933)	511 (951)	516 (960)	-
E	-	517 (962)	515 (959)	509 (949)	503 (947)
F	502 (936)	504 (939)	523 (974)	527 (980)	529 (984)

From the posttest bundle examination, it was learned that the grid assembly separated at the midplane and moved down. In moving down, the grids nominally located at 1.04 and 1.57 m (41 and 62 in.) covered up the heater rod thermocouples at 0.99 and 1.57 m (39 and 60 in.), respectively, and provided a substantially lower temperature response in the thermocouples. As shown in figures H-10 through H-17, the 0.99 and 1.52 m (39 and 60 in.) thermocouples for configurations A and B provided a much lower temperature measurement from test to test. This effect would be expected with a grid covering the respective thermocouple. The thermocouples at 0.61 and 1.22 m (24 and 48 in.) did not exhibit this same thermal behavior. The thermocouples for configuration C (figures H-18 through H-21) do not show as much of a temperature change from test to test, since the lower grid assembly only moved down 3.18 mm (0.125 in.). A similar comparison could not be effectively performed for configurations D and E, since the first repeat test was invalid; however, similar responses were found in configuration F. From the comparisons of configuration A and B thermocouple responses, it was concluded that the filler separation and some lower grid assembly movement occurred between the first and second repeat tests, since the largest temperature differential occurs between these two tests. Although there was very little difference between the second and third repeat tests, it was concluded that some lower grid assembly movement could still occur. The grids are approximately 44.4 mm (1.75 in.) long and there would be no measurable difference as long as the thermocouple was within the length of the grid.

The eight steam probes at 1.70 m (67 in.) and below all failed in configuration A between the second and third repeat tests. These failures were attributed to the fact that the thermocouple lead was attached to the filler rods, and broke after being elongated when the filler rods separated and moved down. In configurations B through F, these thermocouple leads were rerouted out the bottom of the bundle to prevent similar instrumentation failures.

H-3. REPEAT TEST HEAT TRANSFER ANALYSIS AS A FUNCTION OF TIME

To assess the combined effects of heater rod bow, rod surface degradation, and boundary condition repeatability, the heat transfer coefficient ratio between repeat tests was calculated as a function of time. The heat transfer coefficient ratios for only those

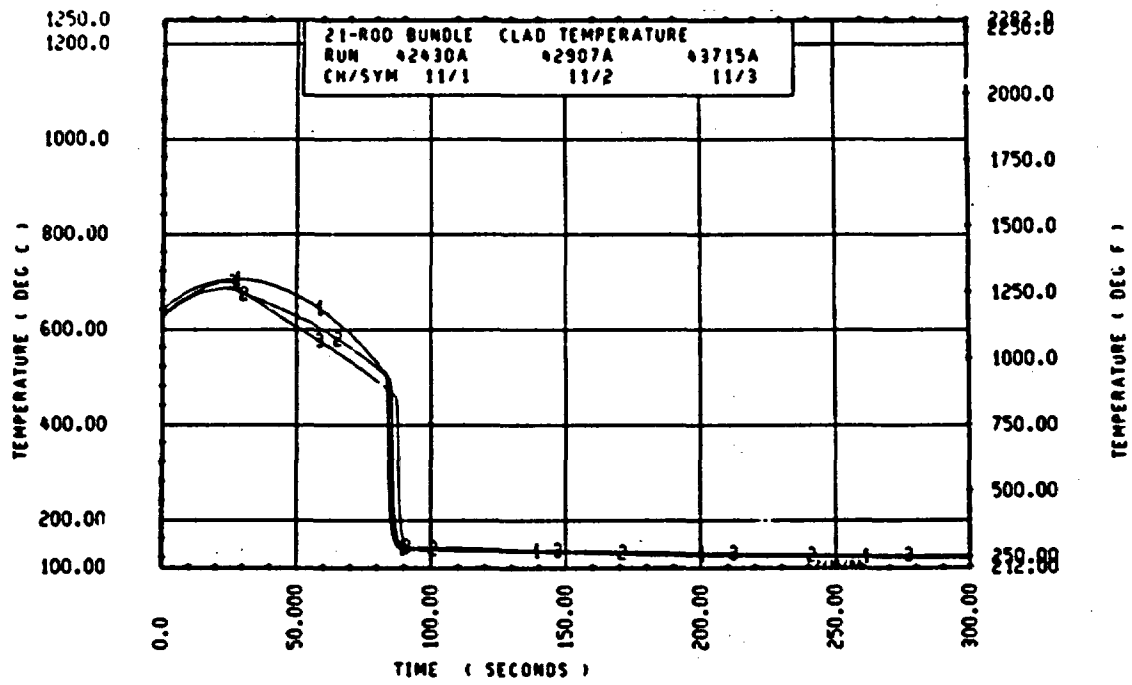

Figure H-10. Temperature Transient, Rod 4C, 0.99 m (39 in.) Elevation (Configuration A)

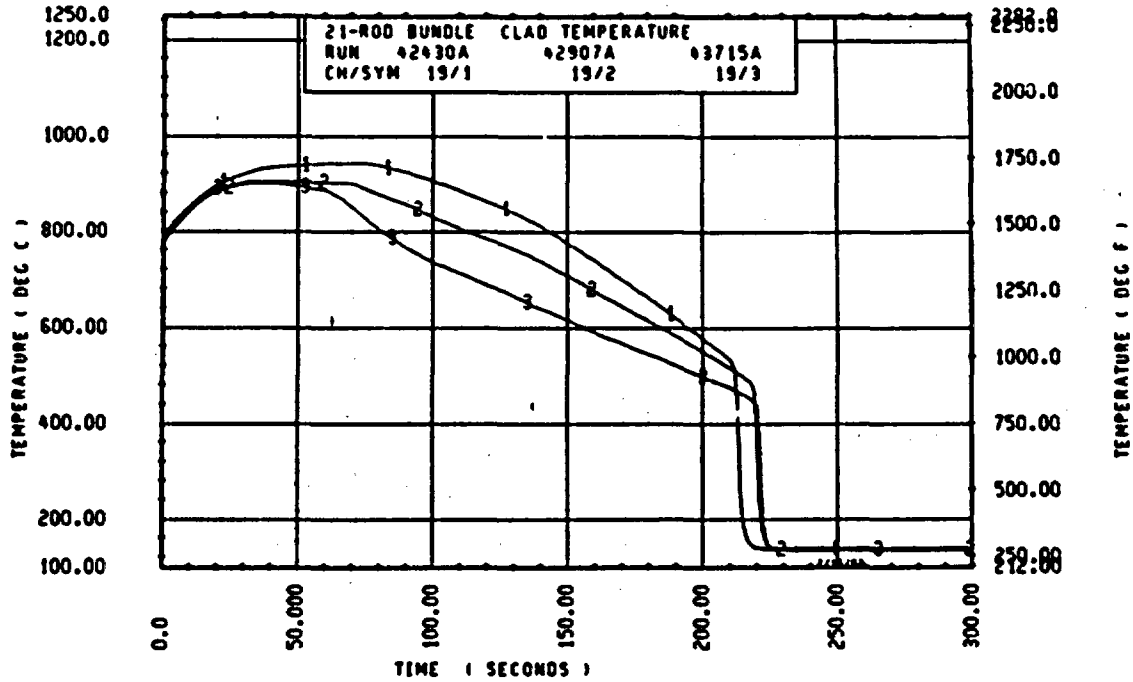

Figure H-11. Temperature Transient, Rod 4C, 1.52 m (60 in.) Elevation (Configuration A)

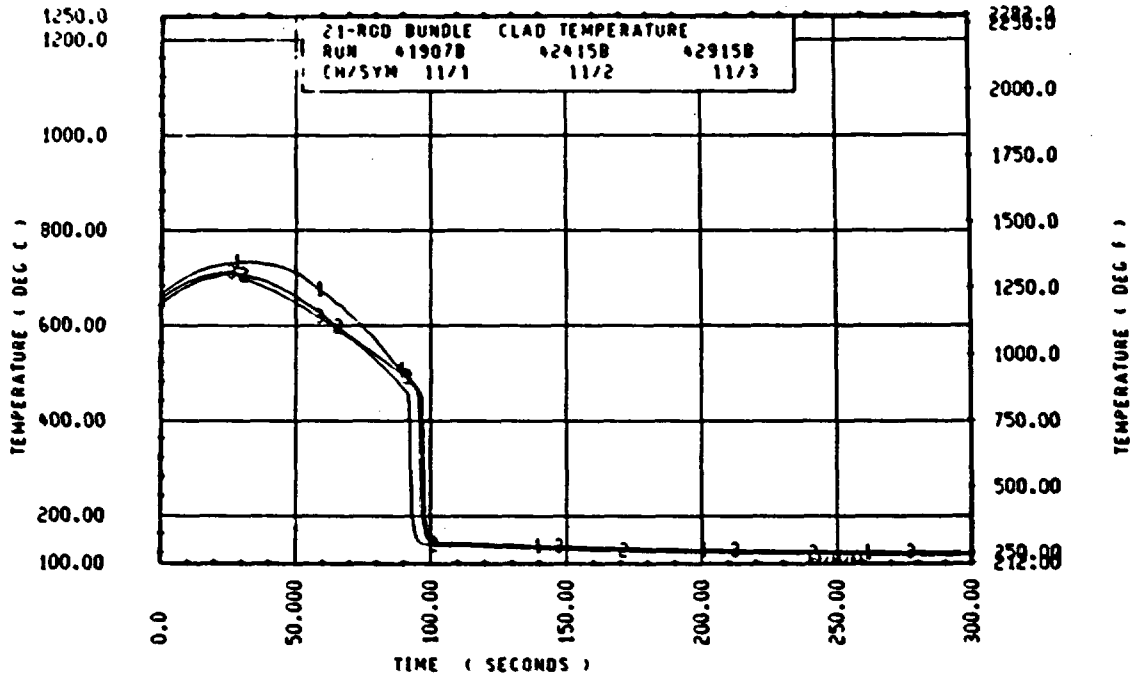

Figure H-12. Temperature Transient, Rod 4C, 0.99 m (39 in.) Elevation (Configuration B)

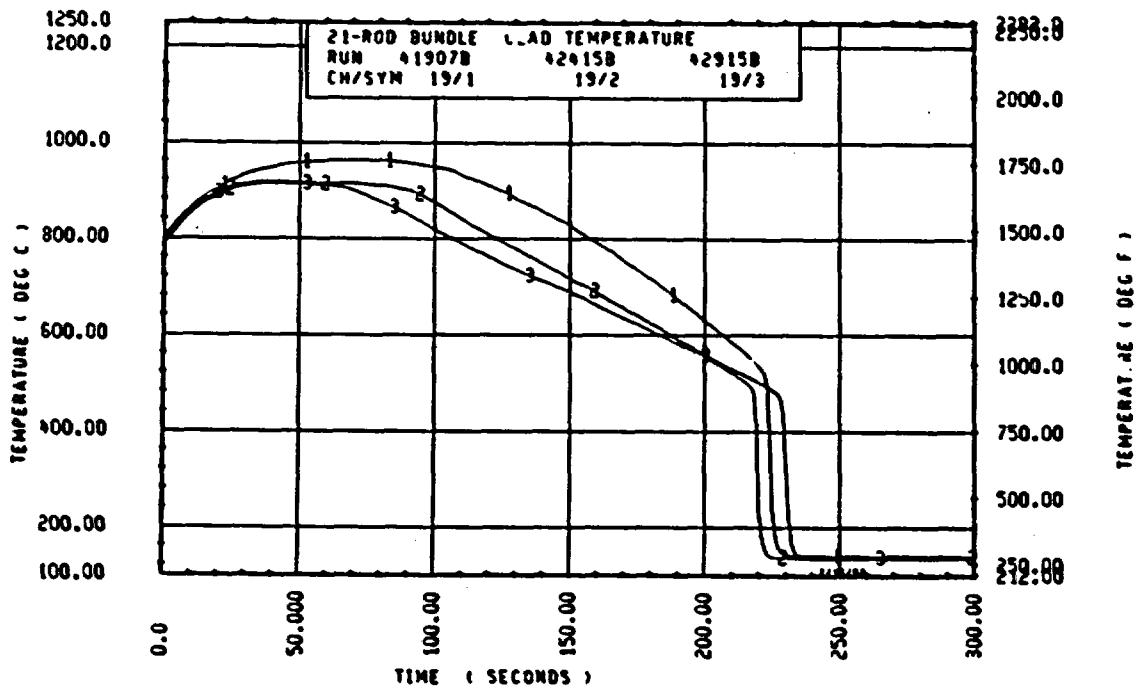

Figure H-13. Temperature Transient, Rod 4C, 1.52 m (60 in.) Elevation (Configuration B)

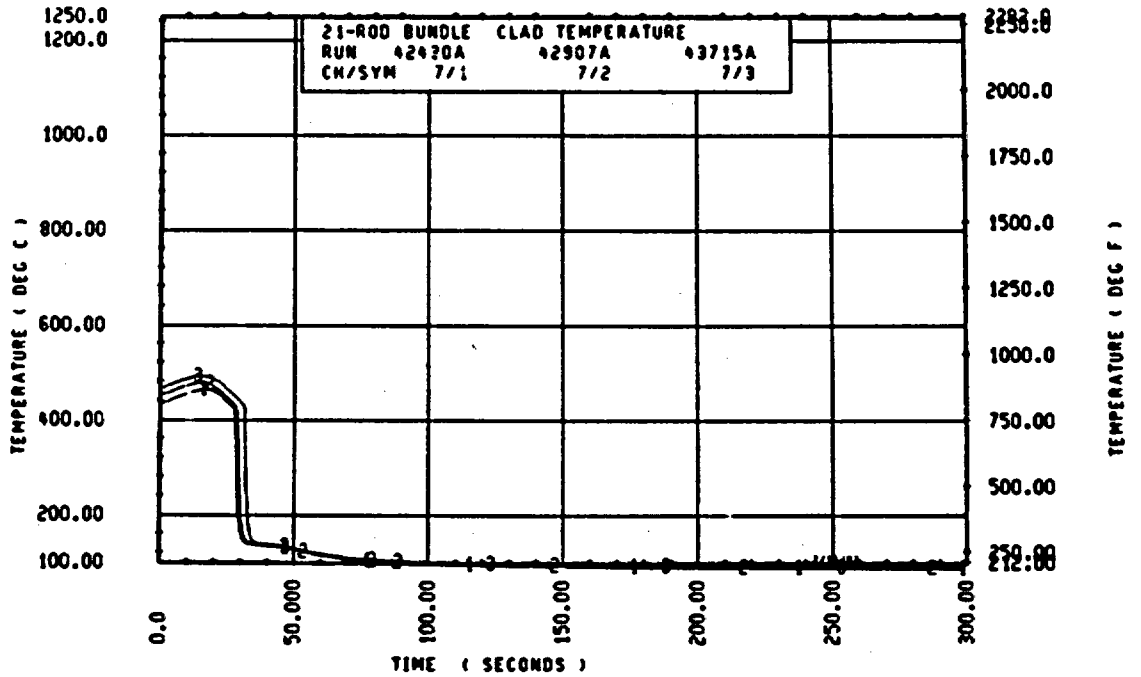

Figure H-14. Temperature Transient, Rod 4D, 0.61 m (24 in.) Elevation (Configuration A)

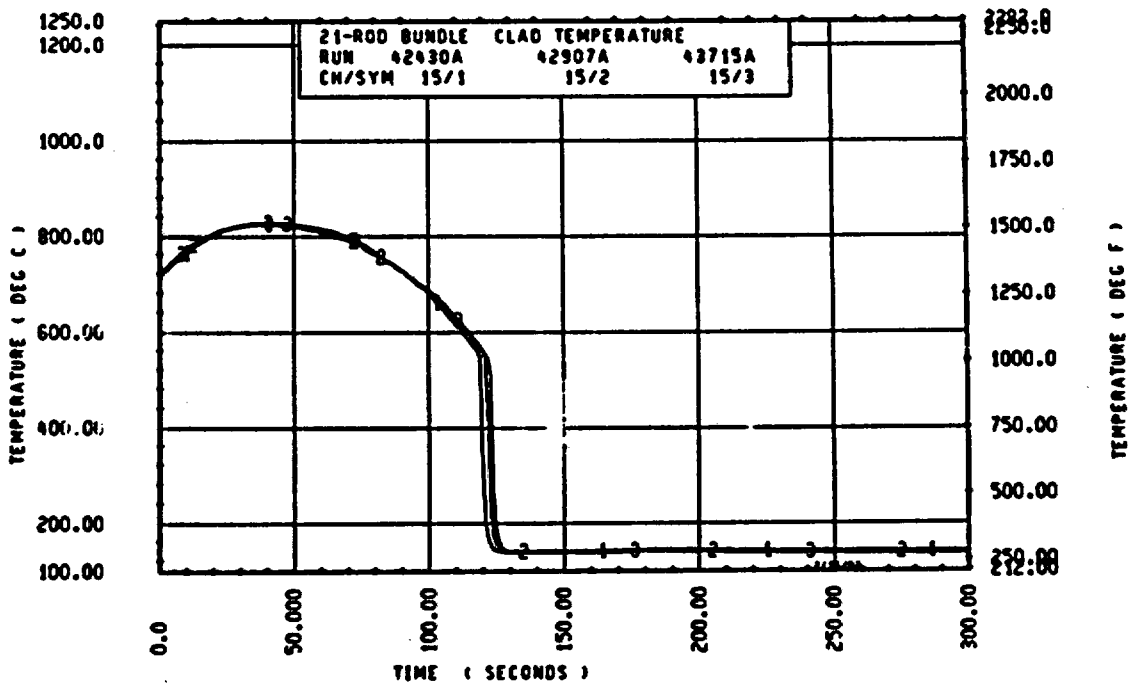

Figure H-15. Temperature Transient, Rod 4D, 1.22 m (48 in.) Elevation (Configuration A)

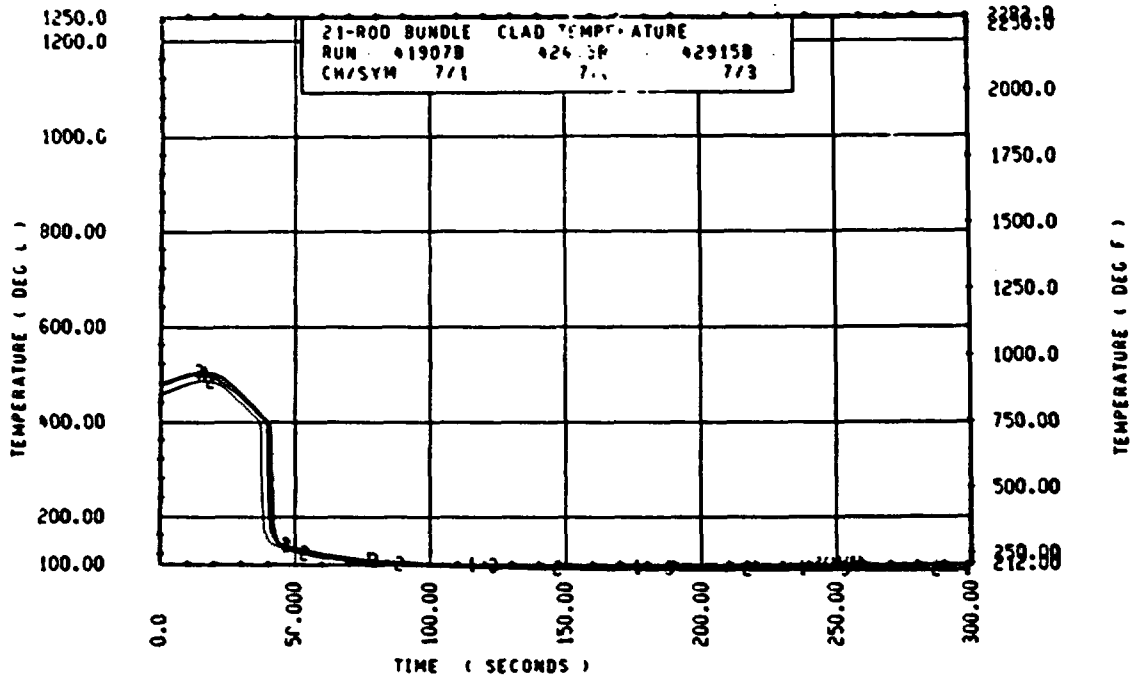

Figure H-16. Temperature Transient, Rod 4D, 0.61 m (24 in.) Elevation (Configuration B)

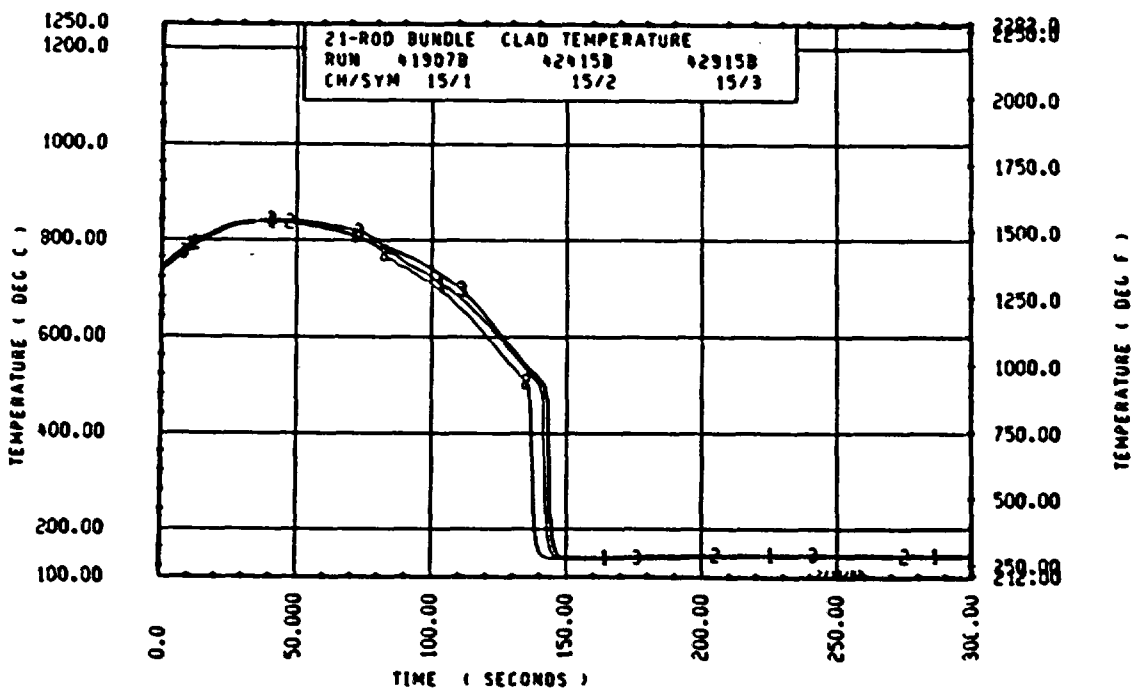

Figure H-17. Temperature Transient, Rod 4D, 1.22 m (48 in.) Elevation (Configuration B)

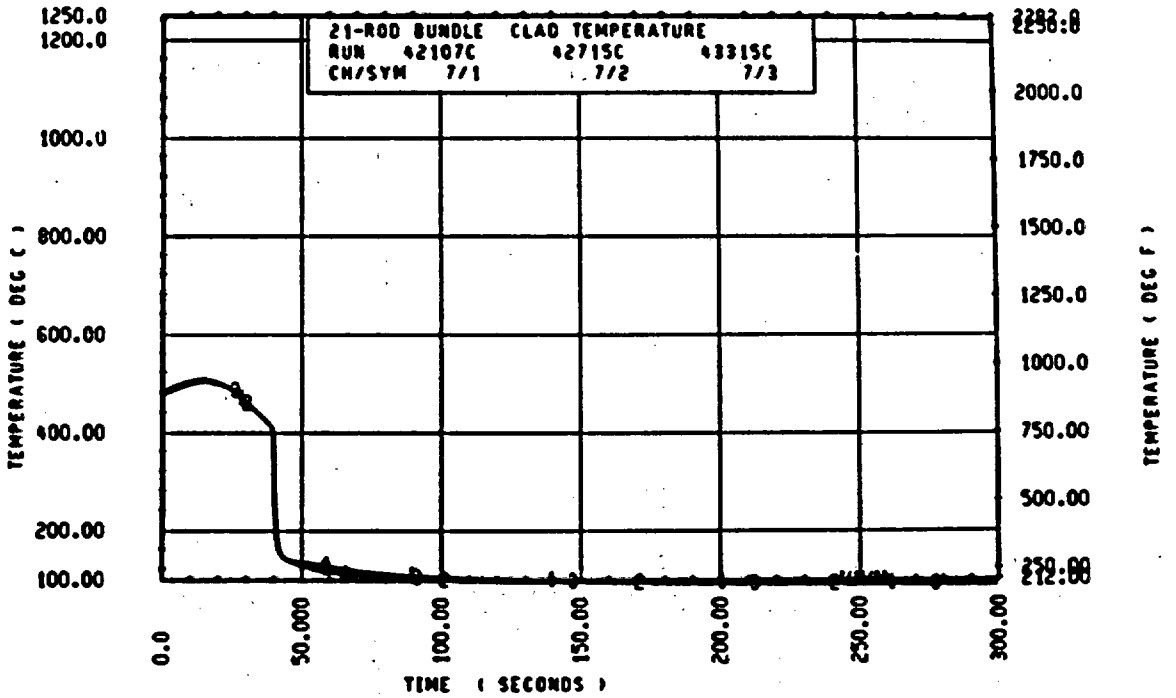

Figure H-18. Temperature Transient, Rod 4D, 0.61 m (24 in.) Elevation (Configuration C)

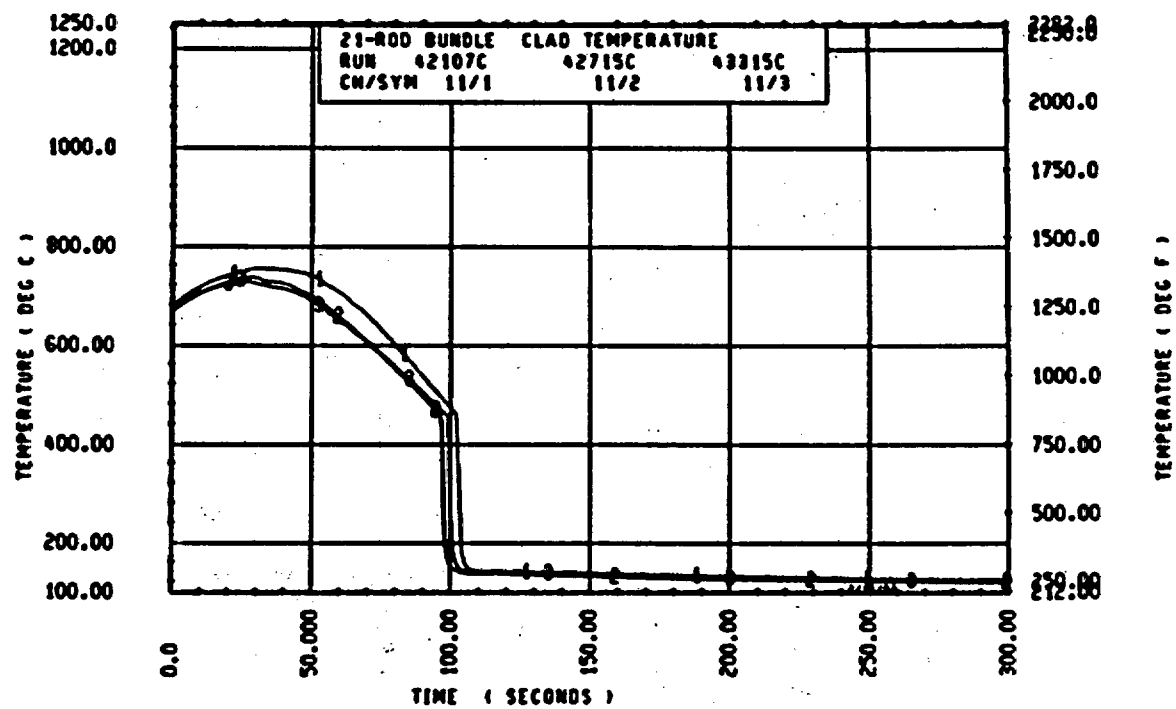

Figure H-19. Temperature Transient, Rod 4C, 0.99 m (39 in.) Elevation (Configuration C)

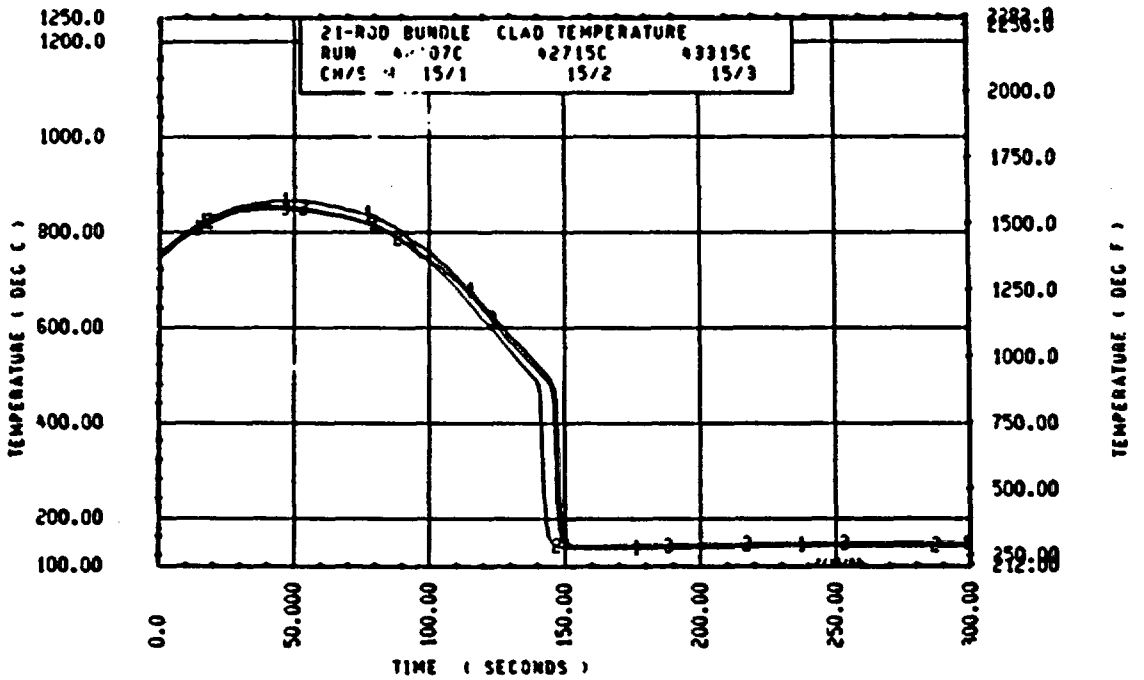

Figure H-20. Temperature Transient, Rod 4D, 1.22 m (48 in.) Elevation (Configuration C)

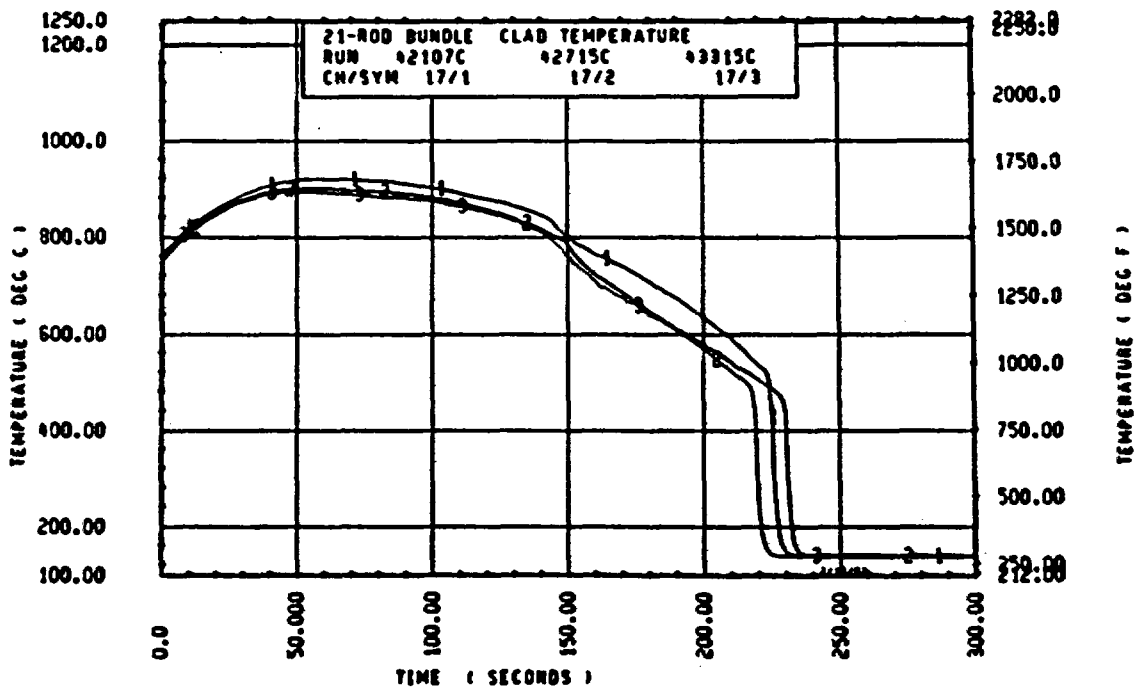

Figure H-21. Temperature Transient, Rod 4C, 1.52 m (60 in.) Elevation (Configuration C)

heater rod thermocouples in the bundle midplane of 1.70 to 2.03 m (67 to 80 in.) were calculated, since the posttest bundle examination revealed that the rod bow occurred only in the bundle midplane. An example of the heat transfer coefficient ratio for the center rod (rod 3C) in configuration A for the first and third repeat tests is shown in figure H-22. The averages and standard deviations for each midplane heat transfer coefficient ratio were subsequently calculated with respect to time. The means of the heat transfer coefficient ratio averages and standard deviations were finally calculated for all respective midplane thermocouples.

The mean standard deviations of the heat transfer coefficient ratios were calculated for the first and third repeat tests of configurations A, B, C, and F, and for the third and fourth repeat tests of configurations D and E. The first and third repeat tests in configurations A, B, C, and F represent the greatest interval between repeat tests; the third and fourth repeat tests in configurations D and E represent the least interval between repeat tests, since these were successive tests. A comparison of these results, shown as a function of time in figure H-23, indicates that the data with the greatest potential for variation (configuration A, B, C, and F tests) were not significantly different from the data with the least potential for variation (configuration D and E tests). These curves represent the average of all the midplane thermocouples. Most of the data initially decrease with time, to a time of approximately 150 seconds, and then increase with time. This early response is attributed to both the low absolute value and the rapidly changing value of the heat transfer coefficient. A small, rapidly changing heat transfer coefficient would be more affected by differences in test conditions and bundle geometry than the heat transfer coefficient later in time when the heat transfer has increased and stabilized. The increase late in time is attributed to the approach of the quench front, when the heat transfer coefficient again begins to increase significantly.

Some of the differences between bundles shown in figure H-23 were attributed to the actual test conditions for the different configurations. In configuration A, the flooding rate and the 1.83 m (72 in.) housing temperatures for the first repeat test were approximately 2 percent and 6 to 10 percent, respectively, less than those for the third repeat test. In configuration B, the flooding rate for the first repeat test was approximately 2 percent higher than that for the third repeat test. In configuration C, the flooding

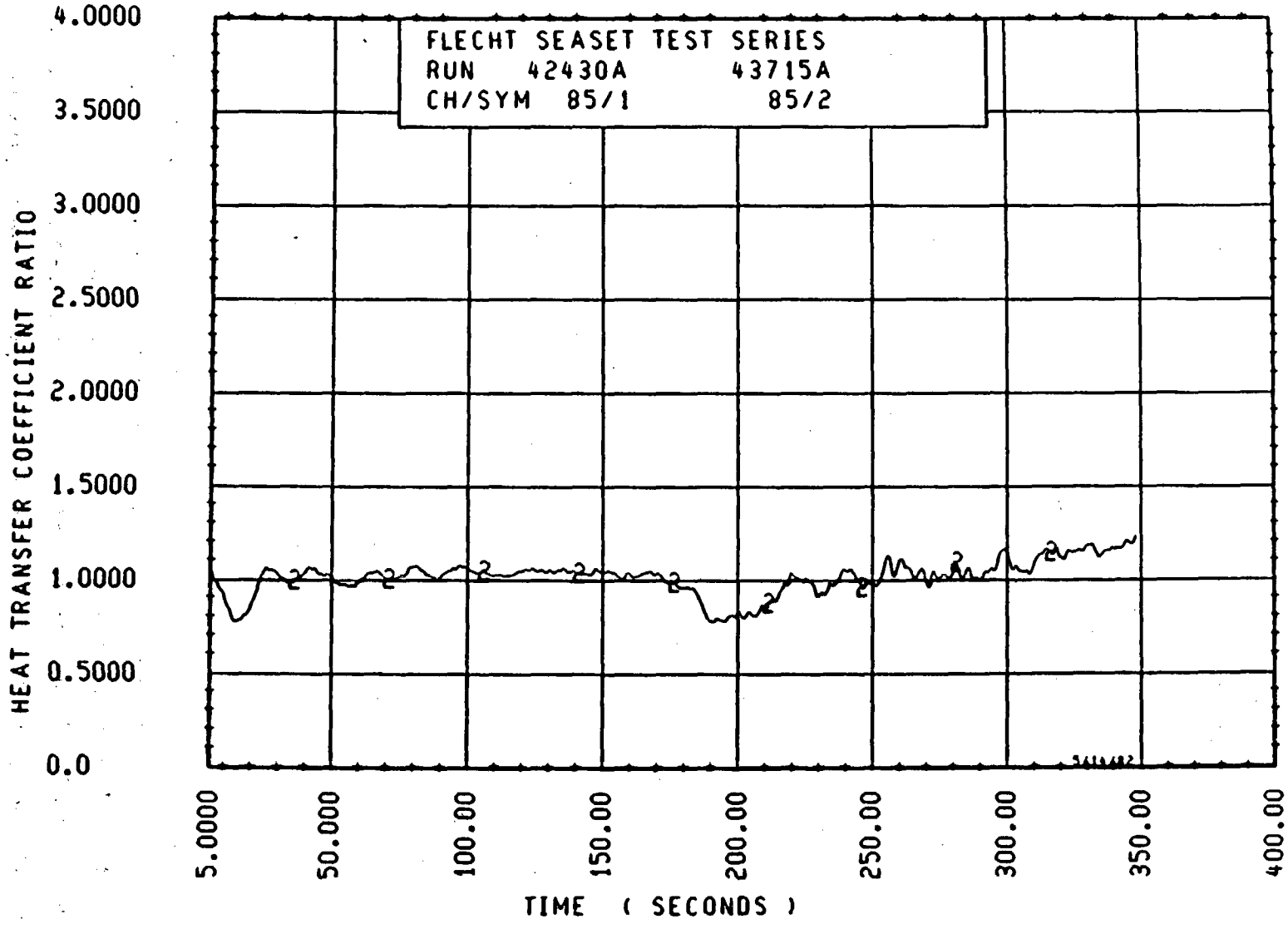

Figure H-22. Heat Transfer Coefficient Ratio Versus Time, Rod 3C, 1.96 m (77 in.) Elevation

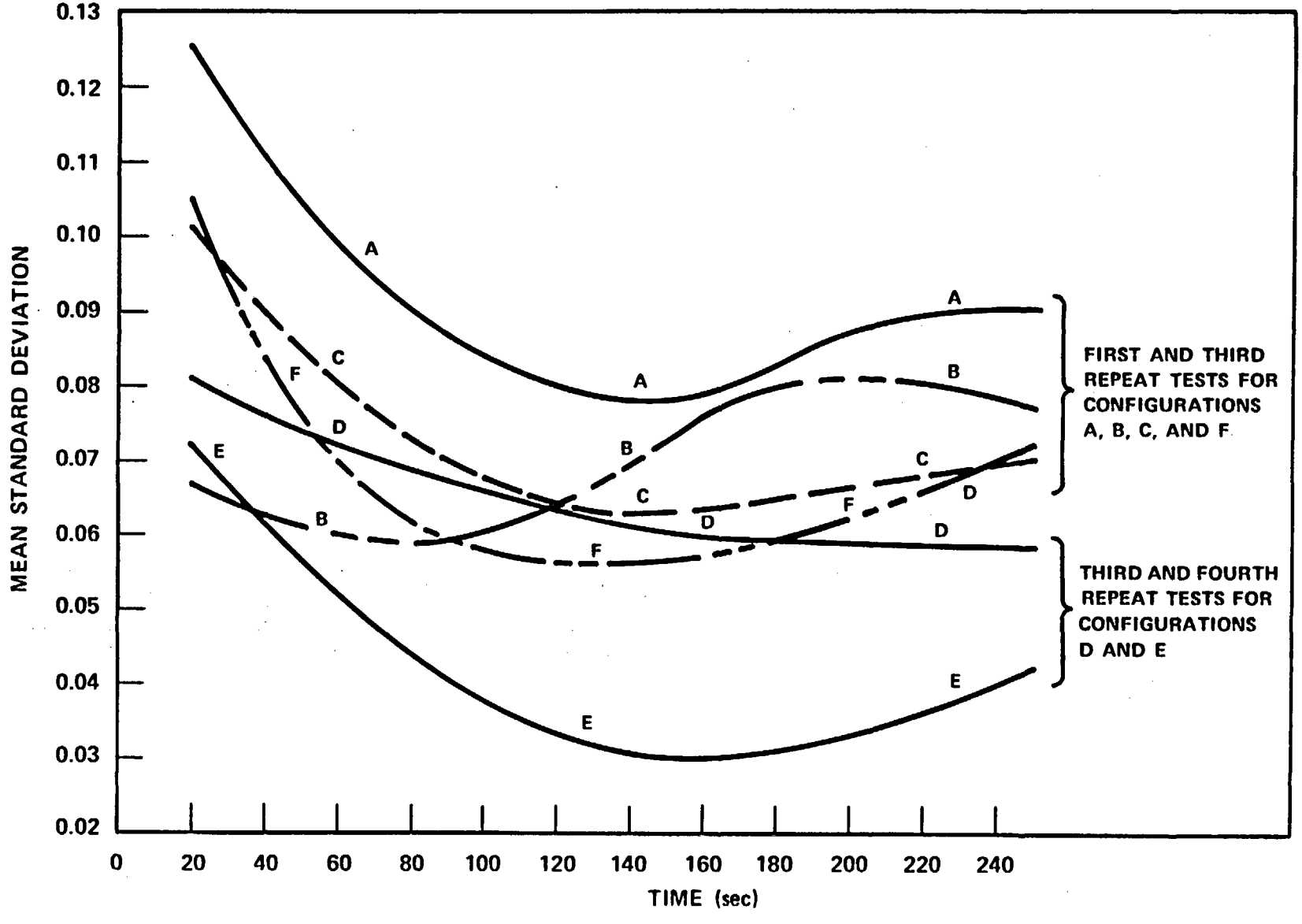

Figure H-23. Mean Standard Deviations of Heat Transfer Coefficient Ratios

rate for the first repeat test was approximately 4.5 percent lower than that for the third repeat test for the first 50 seconds of the transient. However, in the tests for configurations D and E, the test conditions were repeated better than in the tests for configurations A, B, and C. In configuration D, the flooding rate for the third repeat test was approximately 1.5 percent less than that for the fourth repeat test for the first 70 seconds of the transient, but the bundle power for the third repeat test was approximately 0.7 percent higher than that for the fourth repeat test. In configuration E, there was less than ±0.5 percent variation in the flooding rate between the third and fourth repeat tests.

Therefore, it was concluded that the results in figure H-23 were influenced by the as-run test conditions as well as the bundle geometry.

H-4. REPEAT TEST HEAT TRANSFER ANALYSIS FOR SECOND AND THIRD REPEAT TESTS

To provide a relative comparison among all six bundles, the mean standard deviations for the second and third repeat tests were calculated for the time frame of 20 to 250 seconds, as shown in figure H-24. This figure shows variations from bundle to bundle which were inconsistent with the posttest bundle examination. In particular, configuration C had the least amount of rod bow and configuration A had the greatest amount of rod bow, but both had approximately the same mean standard deviation. However, a close examination of the test data provides some consistency with the posttest observations.

Configuration C had a relatively large mean standard deviation of 0.0530 (figure H-24) for the following two reasons. During the first 50 seconds of the reflood transient, there was approximately a 4-percent difference between the second and third repeat tests in the flooding rate. Late in the transient (approximately 150 to 200 seconds), a sharp decrease in the temperature response for 13 thermocouples on rods 1D, 2D, and 2E provided a large standard deviation. This temperature decrease, as shown in figure H-25 for rod 2E at 1.93 m (76 in.), occurred in both tests but at different times, thereby providing a large heat transfer coefficient ratio during this time frame (figure H-26). By neglecting these 13 thermocouples in the calculation, the mean standard

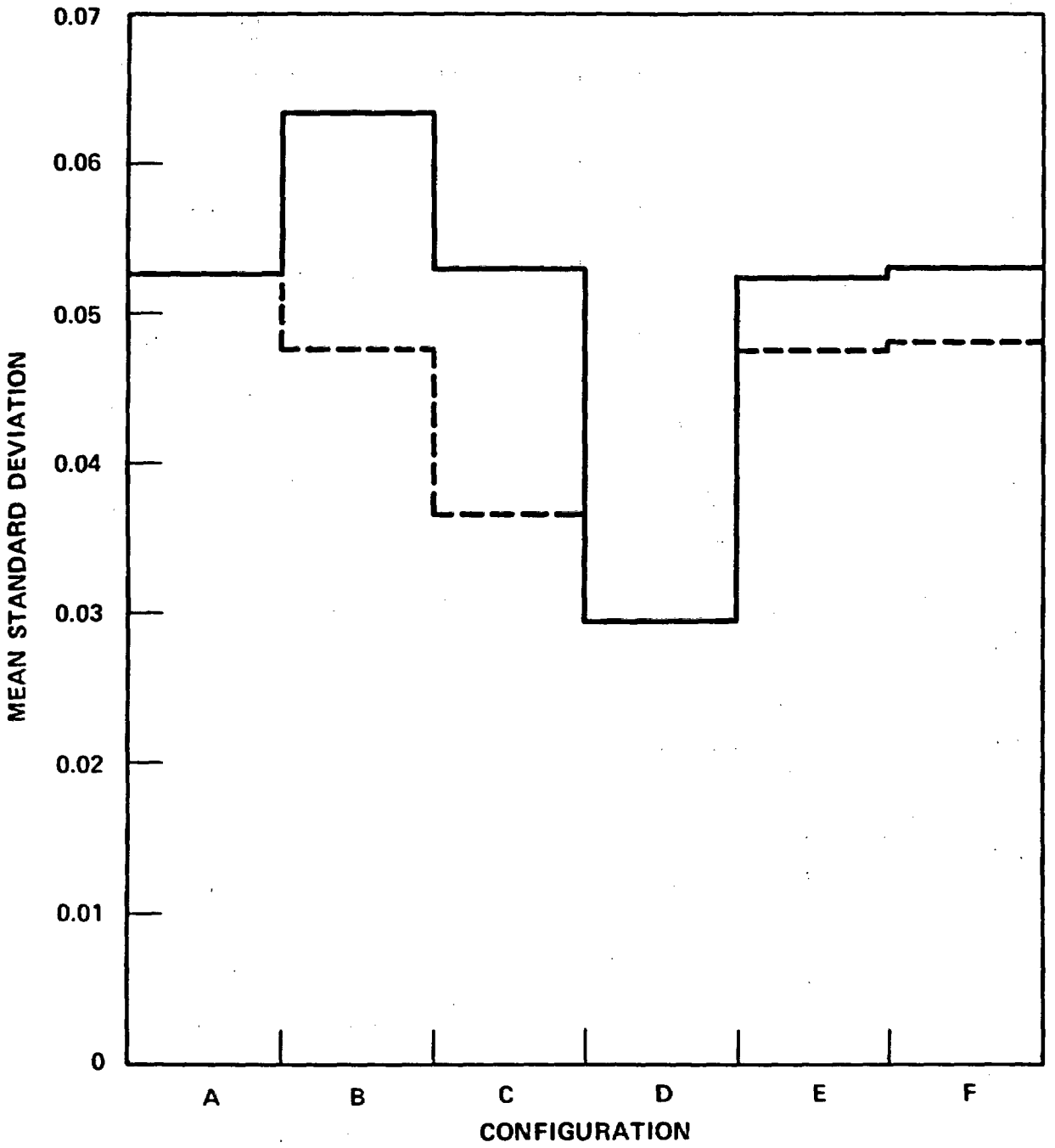

Figure H-24. Mean Standard Deviation Between Second and Third Repeat Tests for 20 to 250 Seconds

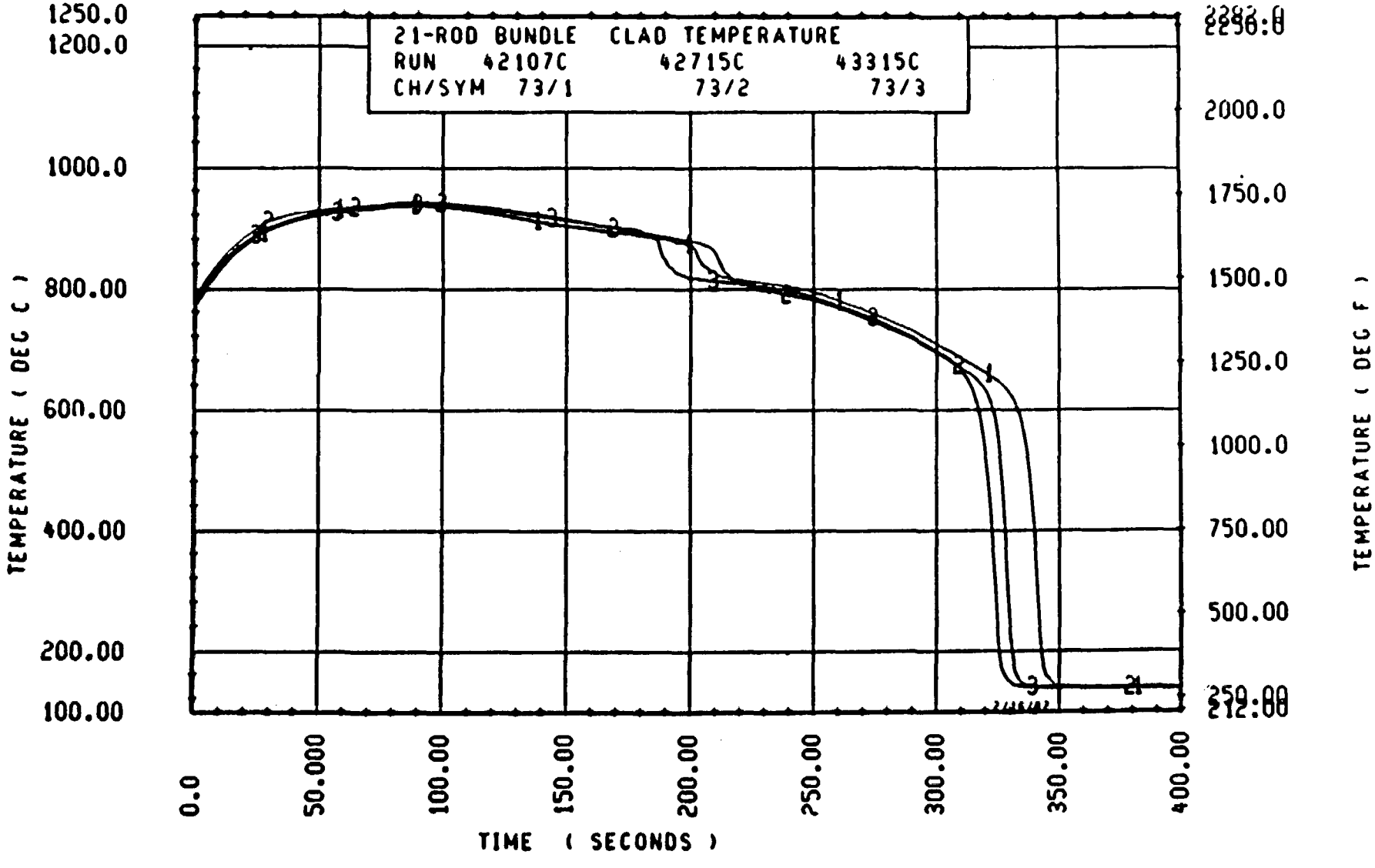

Figure H-25. Temperature Transient, Rod 2E, 1.961 m (77.2 in.) Elevation

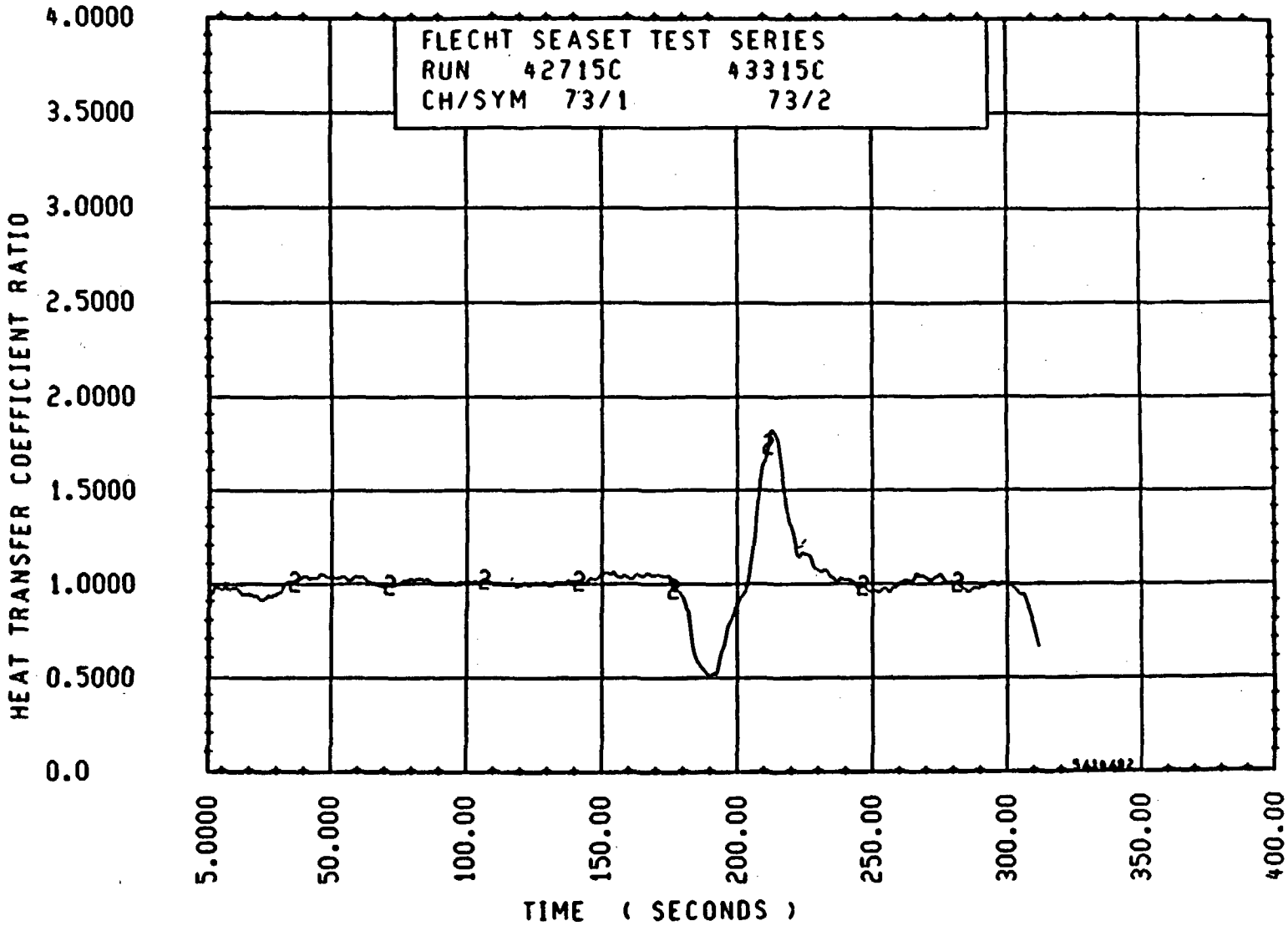

Figure H-26. Heat Transfer Coefficient Ratio Versus Time, Rod 2E, 1.961 m (77.2 in.) Elevation

deviation was reduced from a value of 0.0530 to 0.0383 for the remaining 64 thermocouples, as shown by the dashed line in figure H-24. The sharp temperature decrease in these heater rod thermocouples is attributed to quenching of the filler rods.

In configuration D, the test conditions which directly affected the bundle thermal response, such as flooding rate, power, and housing temperature, were very well duplicated between the second and third repeat tests. Also, a large number of thermocouples (23) in the blockage zone had failed in configuration D; this subsequently reduced the data base to 62 thermocouples. However, it was the good duplication of test conditions which provided the low mean standard deviation of 0.0296.

In configuration B, the test conditions were duplicated very well between the second and third repeat tests, but there were 14 thermocouples which exhibited the same thermal behavior as in configuration C. Elimination of these 14 thermocouples in the calculation reduced the mean standard deviation from 0.0633 to 0.0474 for the remaining 64 thermocouples, as shown by the dashed line in figure H-24.

In configuration A, the test conditions between the second and third repeat tests were not duplicated very well. The flooding rate was approximately 3.5 percent lower and the 1.83 m (72 in.) housing temperatures were approximately 10 percent lower for the second repeat test during the entire transient. However, there were no thermocouples which provided the significantly large standard deviations calculated for configurations B and C. The sharp temperature decreases which were also measured in configuration A occurred at essentially the same time for the two repeat tests. Therefore, the calculated mean standard deviation of 0.0527 need not be corrected.

In configuration E, the test conditions between the second and third repeat tests were duplicated very well. The flooding rate was only about 1 percent lower for the second repeat test during the entire transient. The bundle power and the 1.83 m (72 in.) housing temperatures were exactly the same for both tests. There were three thermocouples in configuration E which provided significantly large standard deviations because of the sharp temperature decrease which occurred at slightly different times

for the two repeat tests. Elimination of these three thermocouples reduced the mean standard deviation from 0.0514 to 0.0475 for the 68 thermocouples, as shown by the dashed line in figure H-24.

In configuration F, the flooding rate was approximately 2 percent lower for the second repeat test during the entire test, but the power was approximately 0.75 percent higher for the second repeat test. There were six thermocouples which provided significantly high average standard deviations because of the sharp temperature decrease occurring at slightly different times in the two repeat tests. Elimination of these six thermocouples reduced the average standard deviation from 0.0529 to 0.0481 for the remaining 78 thermocouples, as shown by the dashed line in figure H-24.

The average heat transfer coefficient ratio for all six bundles (figure H-27) indicates that the average heat transfer coefficient ratio variation was no greater than ± 2.5 percent from bundle to bundle.

H-5. CONCLUSIONS

Based on the repeat test heat transfer data, it has been concluded that the effect of heater rod bow was approximately the same as the effect of data repeatability. Both effects were insignificant relative to the flow blockage effects early in time (to approximately turnaround time as shown by the enhancement factors in paragraph 6-4). Therefore, there is no need to consider the effect of rod bow in the blockage data evaluation. The effects of rod bow, boundary conditions, and rod surface degradation could not be separated in this analysis.

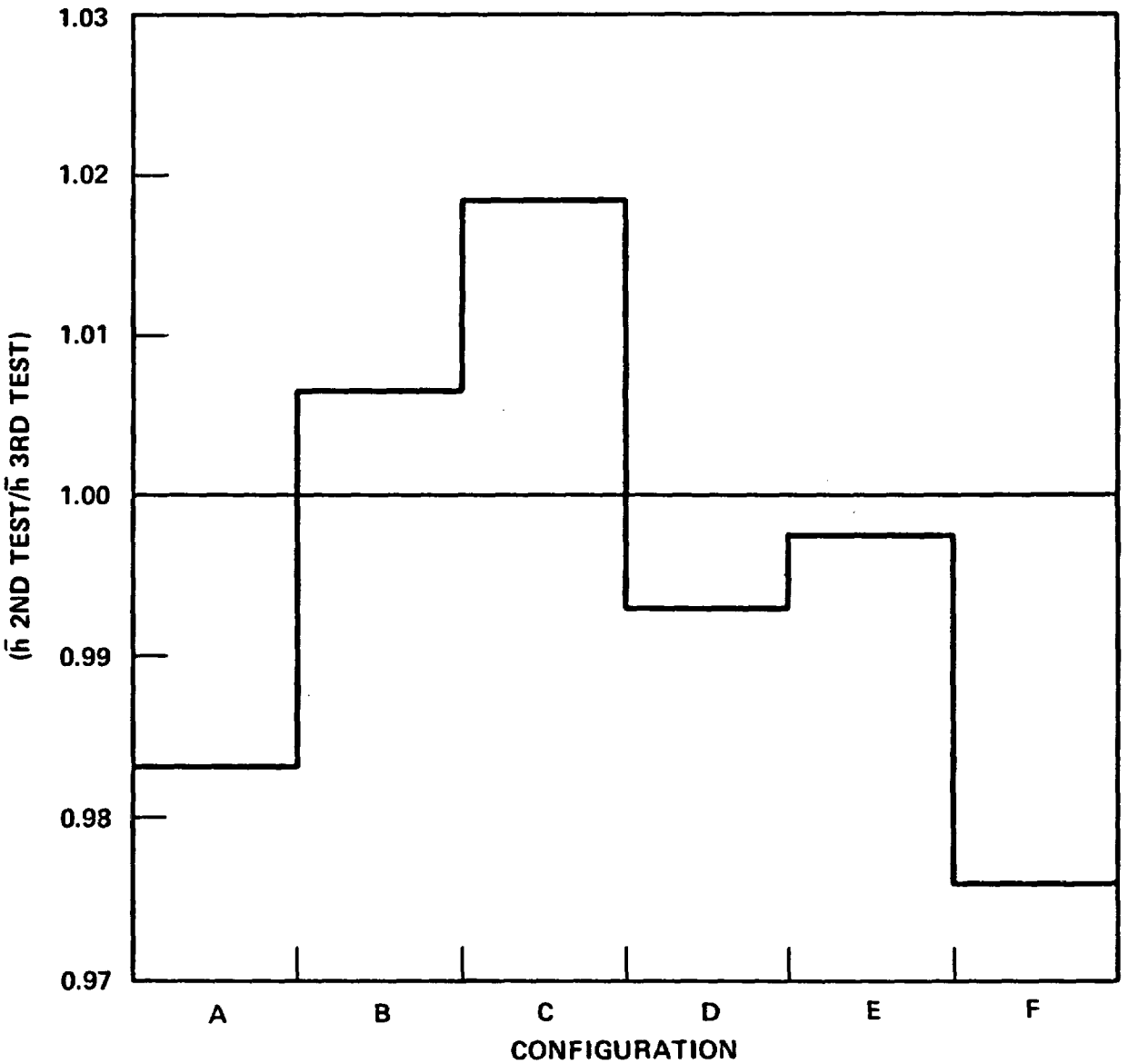

Figure H-27. Average Heat Transfer Coefficient Ratio for Second and Third Tests Between 20 and 250 Seconds

APPENDIX I
HEATER ROD HEAT CONDUCTION ANALYSIS

I-1. INTRODUCTION

The effect of axial and azimuthal heat conduction on the thermal response of the FLECHT SEASET heater rods was investigated utilizing the TAP-A computer code. This investigation was undertaken to determine the following:

- The effect of axial heat conduction on the heater rod thermocouples with a quenched flow blockage sleeve

- The effect of azimuthal heat conduction on the measured heater rod temperatures

The flow blockage sleeve on a heater rod, as postulated prior to testing, could quench much earlier than the heater rod. Subsequently the axial conduction in the heater rod could affect the thermocouples immediately upstream and downstream of the quenched blockage sleeve. Since the thermocouple temperature data were reduced by a one-dimensional computer code (DATAR), if significant axial heat conduction effects were present, the thermocouple data could not be properly reduced to obtain a heat transfer coefficient.

The subchannel blockage was expected to provide subchannel-to-subchannel flow variations and, subsequently, azimuthal heat transfer variations. The thermocouple data could not be properly evaluated if significant azimuthal temperature variations existed in the heater rod, unless the azimuthal location of the heater rod thermocouples could be determined accurately.

I-2. AXIAL HEAT CONDUCTION ANALYSIS AND RESULTS

A two-dimensional TAP-A code model of a heater rod with and without a flow blockage sleeve was set up to investigate the response of the clad immediately downstream of a "stationary" quench front. This stationary quench front was simulated by increasing the outside film coefficient over a certain portion of the heater rod. In reality, the quench front travels at a velocity of approximately 2.5 mm/sec (0.10 in./sec) at the midplane for a 28 mm/sec (1.1 in./sec) flooding rate test.

The TAP-A code heater rod models were 76 mm (3 in.) long and 9.50 mm (0.374 in.) in diameter, and consisted of three radial nodes and 300 axial nodes of 0.25 mm (0.010 in.) thickness. The three radial nodes in the heater rod model consisted of a Kanthal heating element, boron nitride insulation, and stainless steel clad. The unblocked heater rod model is shown in figure I-1. The blockage sleeve was simulated by a 0.51 mm (0.020 in.) thick, 17.5 mm (0.69 in.) long tapered cylinder and a 0.51 mm (0.020 in.) thick, 10.9 mm (0.43 in.) long uniform cylinder, as shown in figure I-2. In the variable-width gap between the heater rod and the blockage sleeve, simultaneous radiation and conduction was provided through the steam. The remainder of the sleeve was assumed to be in perfect contact with the heater rod. The emissivity of the rod and the sleeve were both assumed to be 0.50, since minimal surface oxidation occurs beneath the sleeve. The properties of all the materials were input into the code as a function of temperature.

Each of the models was subjected to a typical reflood transient starting at an initial clad temperature of approximately 951°C (1600°F). Although the power was held constant throughout the transient at a rate of 2.3 kw/m (0.70 kw/ft), the heat transfer coefficient provided for a typical reflood temperature transient. The steam coolant temperature was assumed to be 100°C (212°F).

The 18 mm (0.69 in.) long portion of the blockage sleeve which protruded into the flow stream was assumed to quench (by subjection to a large outside film coefficient). The remainder of the sleeve and the heater rod downstream of the sleeve were subjected to the nominal outside film coefficient. Both of these film coefficients are shown in figure I-3. The unblocked heater rod model was subjected to essentially the same

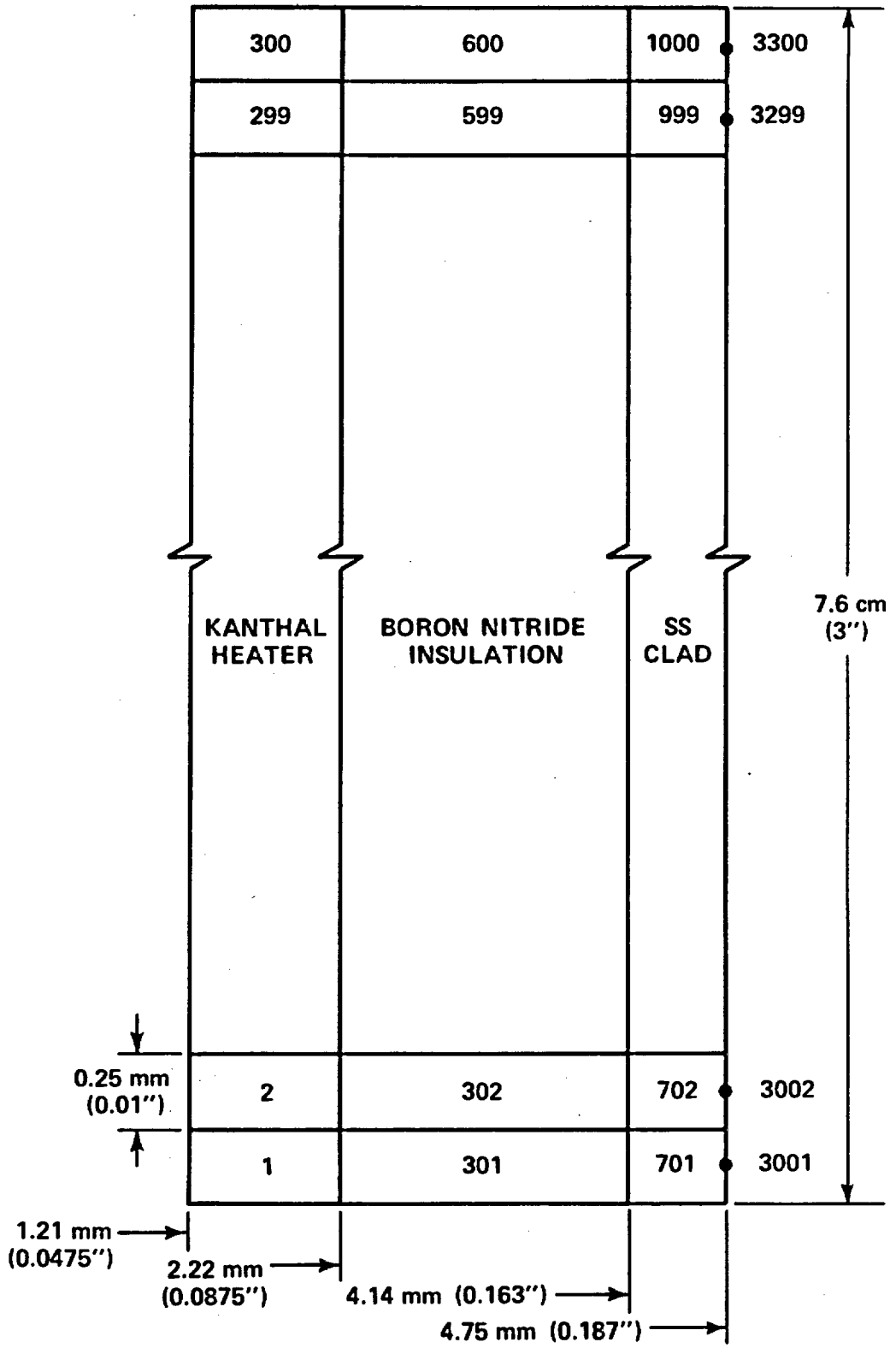

Figure I-1. TAP-A Unblocked Heater Rod Model

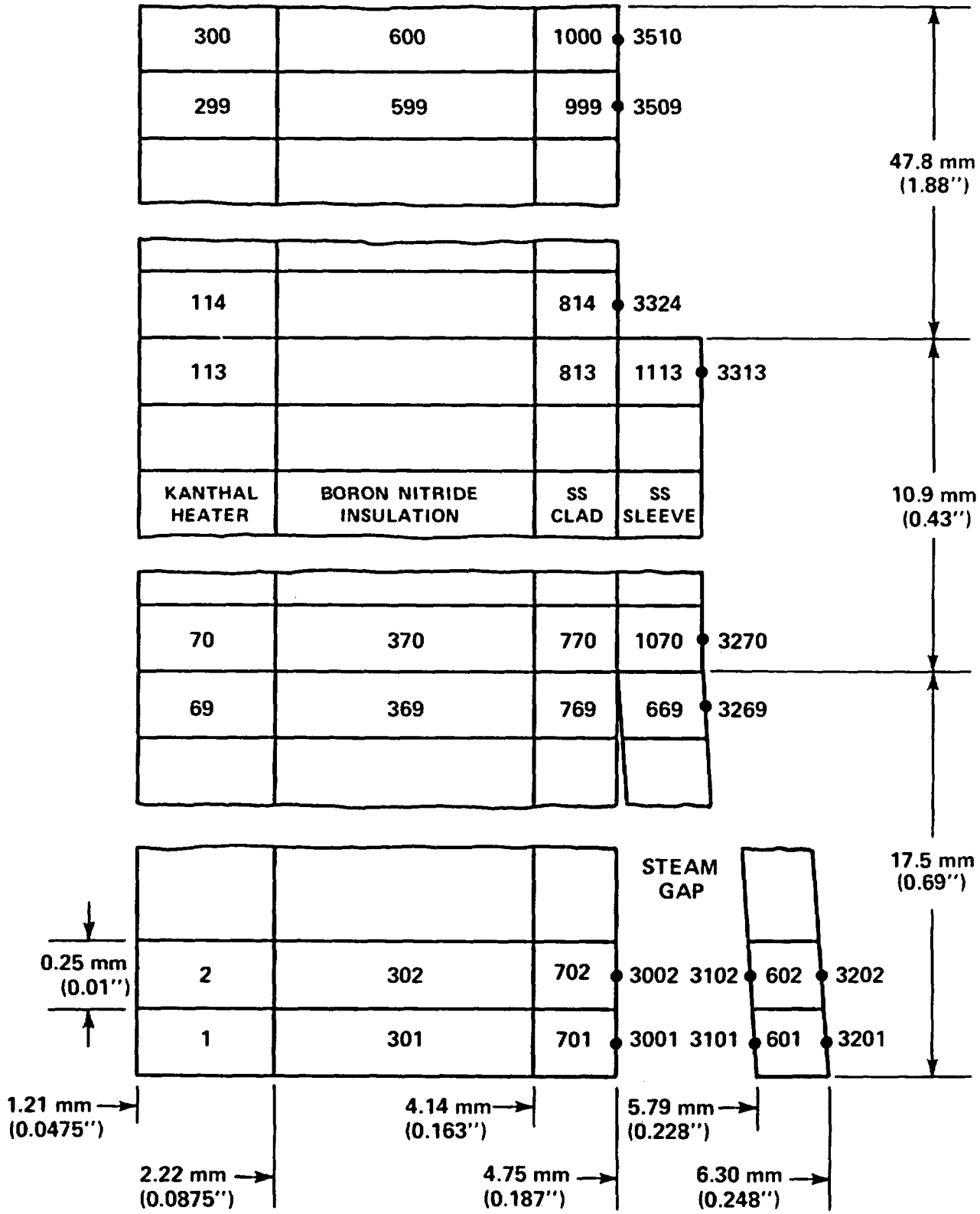

Figure I-2. TAP-A Heater Rod and Blockage Sleeve Model

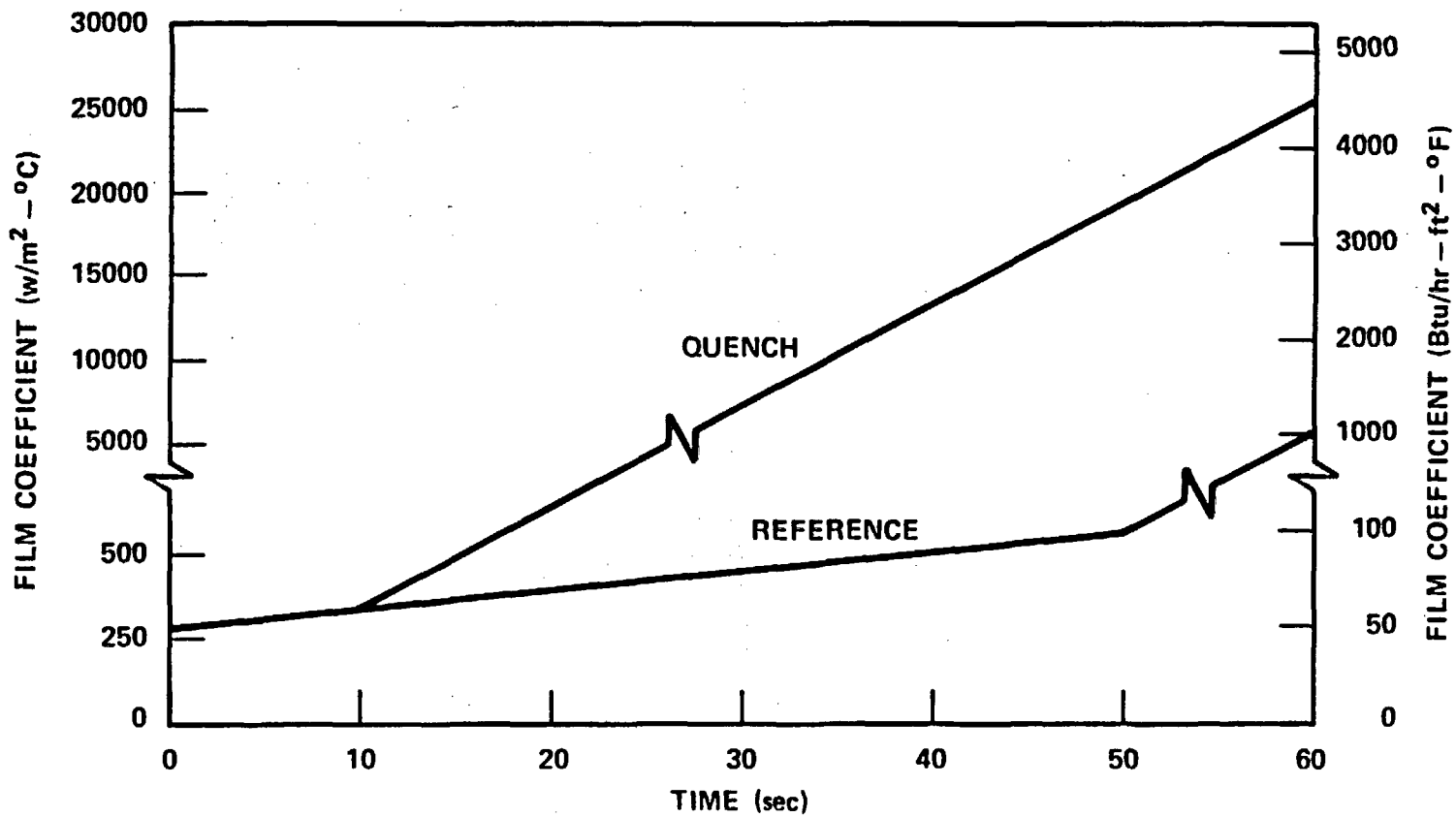

Figure I-3. Unblocked Heater Rod Film Coefficients
$[T_q = 432^{o}C\ (810^{o}F)]$

boundary conditions; however, the clad quench temperatures of the two models were slightly different. The effect of clad quench temperature on heater rod thermal response was also investigated by varying the time during the reflood transient when the large film coefficient was imposed. The following shows the clad quench temperatures for both models:

	Clad Quench Temperature [°C (°F)]	
Rod Model	Case 1	Case 2
Unblocked	432 (810)	335 (635)
Blocked	446 (835)	341 (645)

The results for the unblocked rod are shown in figures I-4 through I-8 for the two clad quench temperatures of 432°C and 335°C (810°F and 635°F). The axial clad temperature distribution for the 432°C (810°F) quench temperature case at 10 and 40 seconds after quench is shown in figure I-5. The ratio of axial to radial heat flow in the clad is shown in figure I-6 at 10 and 40 seconds after quench for the 432°C (810°F) quench temperature case. The locations of the rod thermocouples corresponding to 25 mm (1 in.) minimum spacing are shown in the figures. As shown in figure I-6, the ratio of axial conduction to radial convection is at a maximum of approximately 30 right at the quench front. Axial conduction in the clad is quickly felt, such that there is a 10-percent effect at 10 seconds after quench at approximately 25 mm (1 in.) downstream of the quench front. This corresponds to a velocity of approximately 2.5 mm/sec (0.10 in./sec), which is equal to the velocity of a traveling quench front. However, it requires another 30 seconds for a 10-percent effect to be felt at another 15 mm (0.60 in.) downstream, which is much slower than the velocity of the traveling quench front. The ratio of axial to radial heat flow in the clad for the 335°C (635°F) quench temperature is shown in figure I-8 at 10 and 40 seconds after quench. The axial conduction in an unblocked rod appears to be a weak function of the quench temperature.

The results for the rod with the blockage sleeve are shown in figures I-9 through I-16 for the two clad quench temperatures of 446°C and 341°C (835°F and 645°F). The

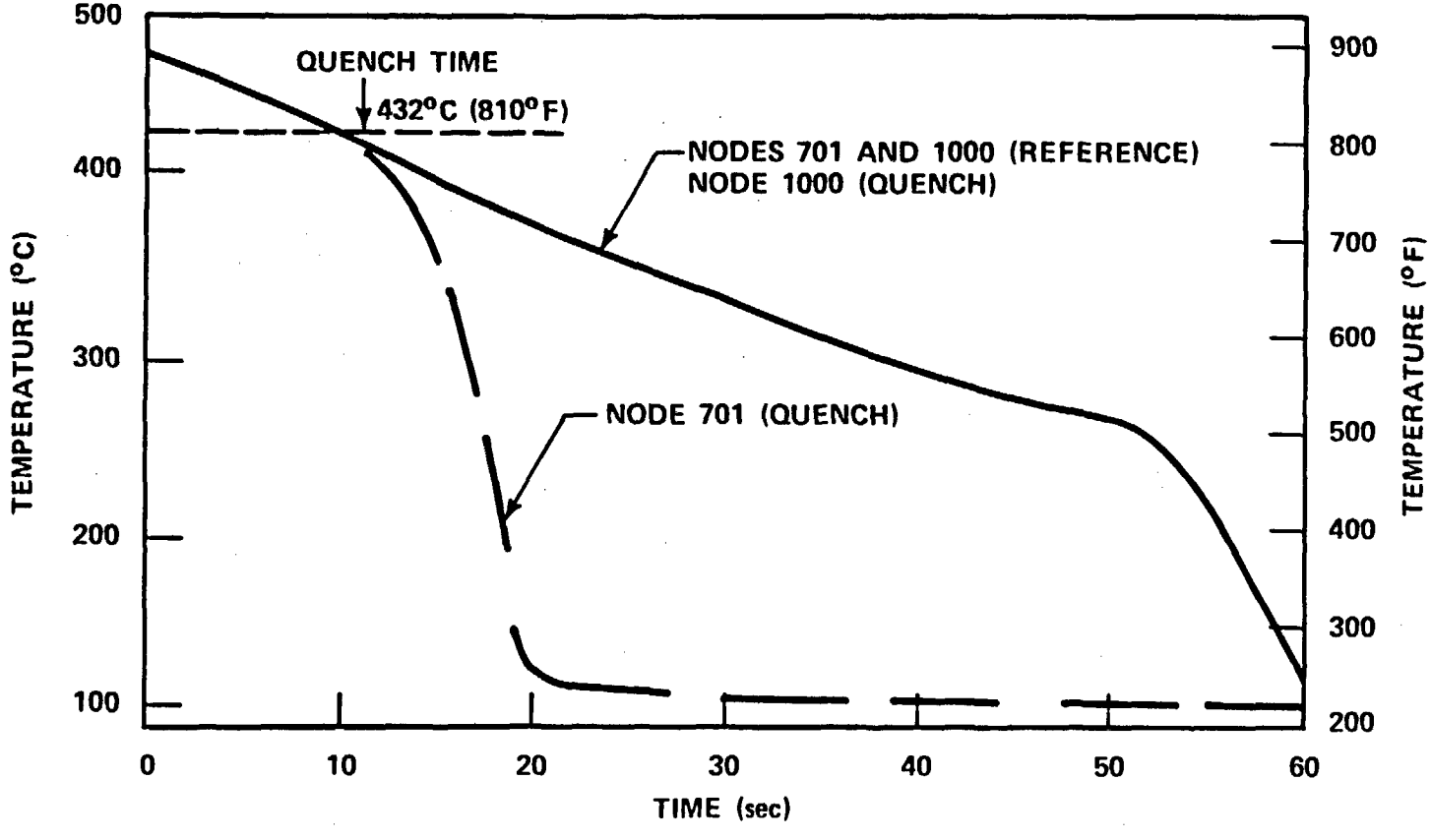

Figure I-4. Unblocked Heater Rod Clad Temperature [T_q = 432°C (810°F)]

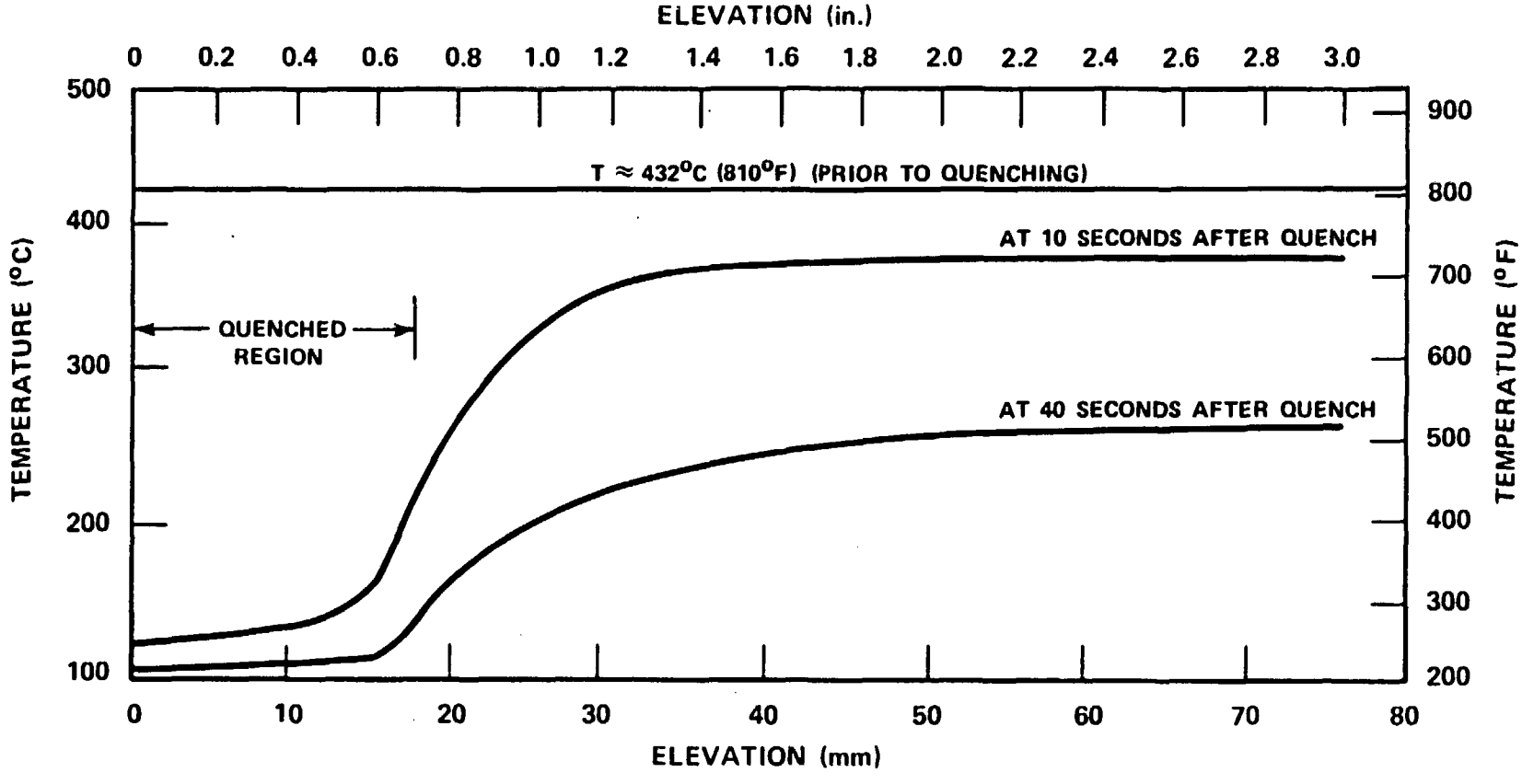

Figure I-5. Axial Clad Temperature Distribution for Unblocked Rod

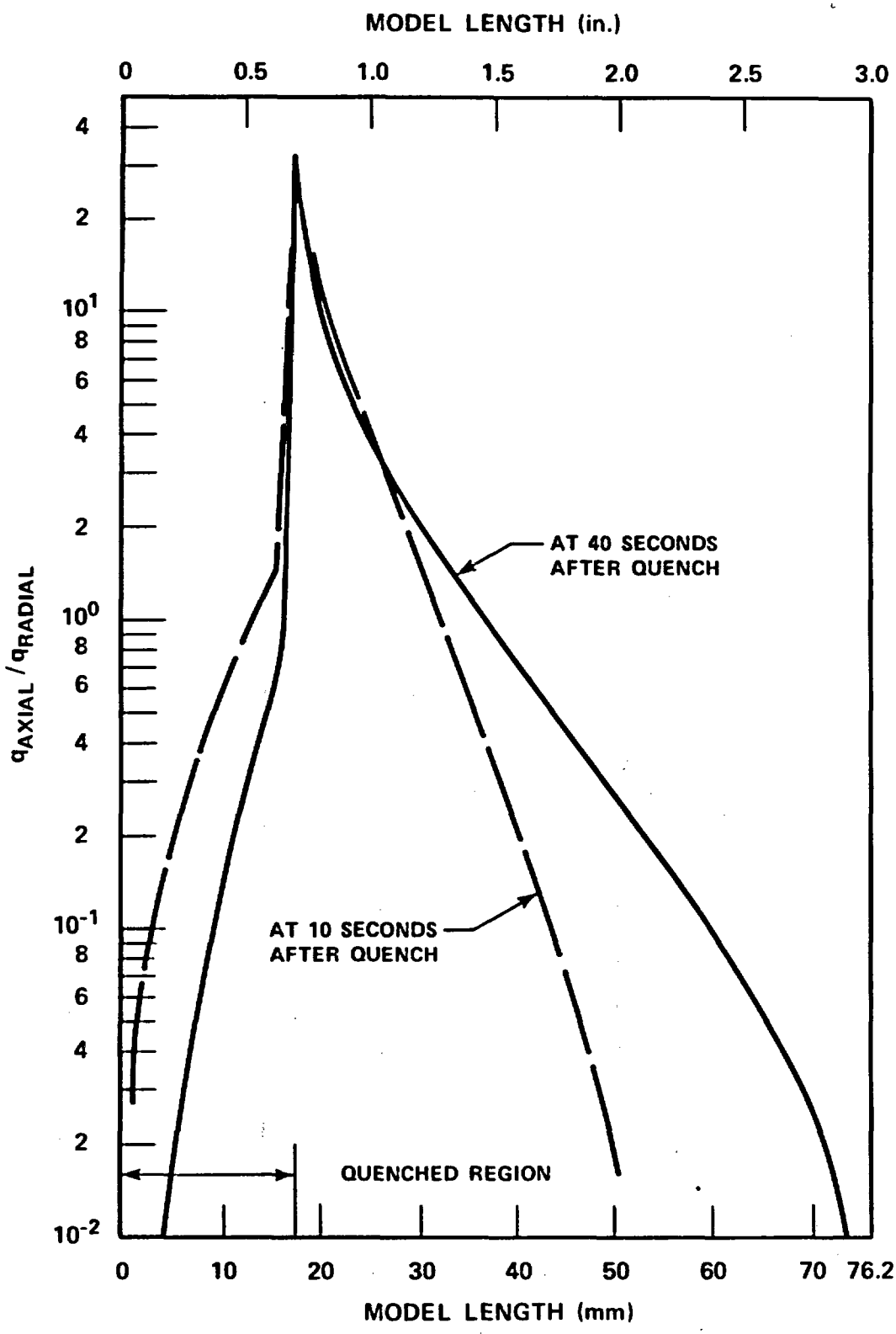

Figure I-6. Ratio of Axial to Radial Heat Flow in Unblocked Rod [T_q = 432°C (810°F)]

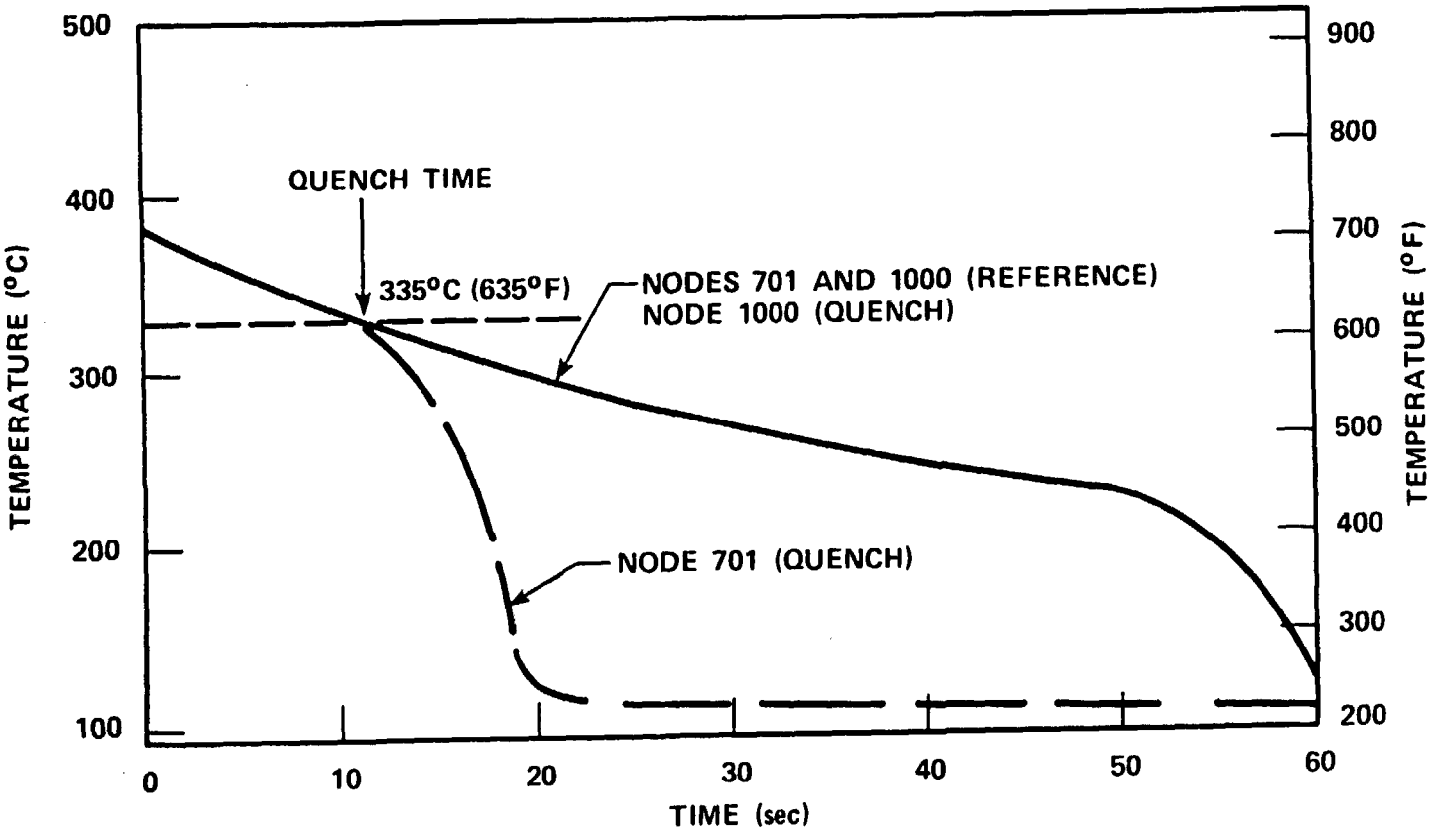

Figure I-7. Unblocked Heater Rod Clad Temperature [T_q = 335°C (635°F)]

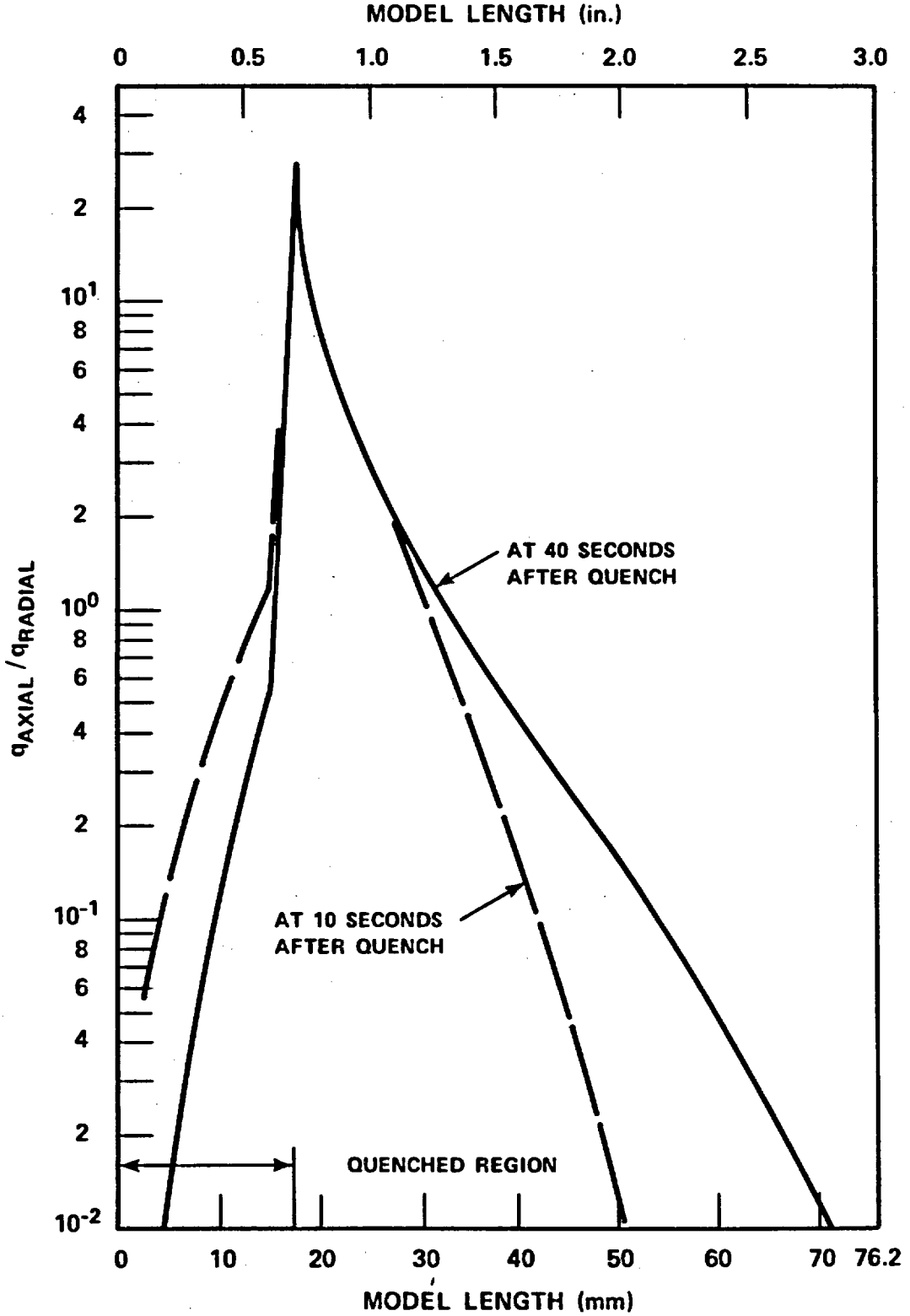

Figure I-8. Ratio of Axial to Radial Heat Flow in Unblocked Rod [T_q = 335°C (635°F)]

axial clad and sleeve temperature distributions for the 446°C (835°F) quench temperature case at 10 and 40 seconds after quench are shown in figures I-10 and I-11, respectively. The ratio of axial to radial heat flow in the clad and in the sleeve are shown in figures I-12 and I-13 at 10 and 40 seconds after quench, respectively, for the 446°C (835°F) quench temperature case.

As shown in figures I-12 and I-13, the ratio of axial conduction to radial convection in the sleeve is at a maximum of approximately 30 right at the quench front. The effect of axial conduction in the sleeve is less than 10 percent at approximately 5 mm (0.20 in.) downstream of the quenched region of the sleeve. The ratio of axial conduction to radial heat flow in the clad is approximately 1 at the quench front. The thermal resistance of the steam gap between the rod and the sleeve limits the axial conduction in the clad beneath the quenched sleeve. The response of the sleeve and the clad while in perfect contact with each other is shown to be the same. At the end of the sleeve, the ratio of axial to radial heat flow in the clad is 0.03 at 10 seconds after quench and 0.65 at 40 seconds after quench, as shown in figures I-12 and I-13, respectively. A 10-percent effect in the clad at 40 seconds after quench is felt at 14 mm (0.55 in.) downstream of the sleeve.

The ratios of axial to radial heat flow in the clad and sleeve for a quench temperature of 341°C (645°F) are shown in figures I-15 and I-16 at 10 and 40 seconds, respectively. The same general response occurs in both the sleeve and clad at the 341°C (645°F) quench temperature as at the 446°C (835°F) quench temperature, except that the effect of axial conduction is much less. A 10-percent effect in the clad at 40 seconds after quench is felt at only 1 mm (0.05 in.) downstream of the sleeve. The axial conduction in a rod with a quenched blockage sleeve appears to be a strong function of the quench temperature.

I-3. CONCLUSIONS FROM AXIAL CONDUCTION ANALYSIS

It was found that the effect of axial conduction was greater for the unblocked heater rod than for the blocked heater rod for the quench temperatures investigated. This difference in thermal response is attributed to the insulating effect of the blockage sleeve on the heater rod. However, as the quench temperature increases, it is expected

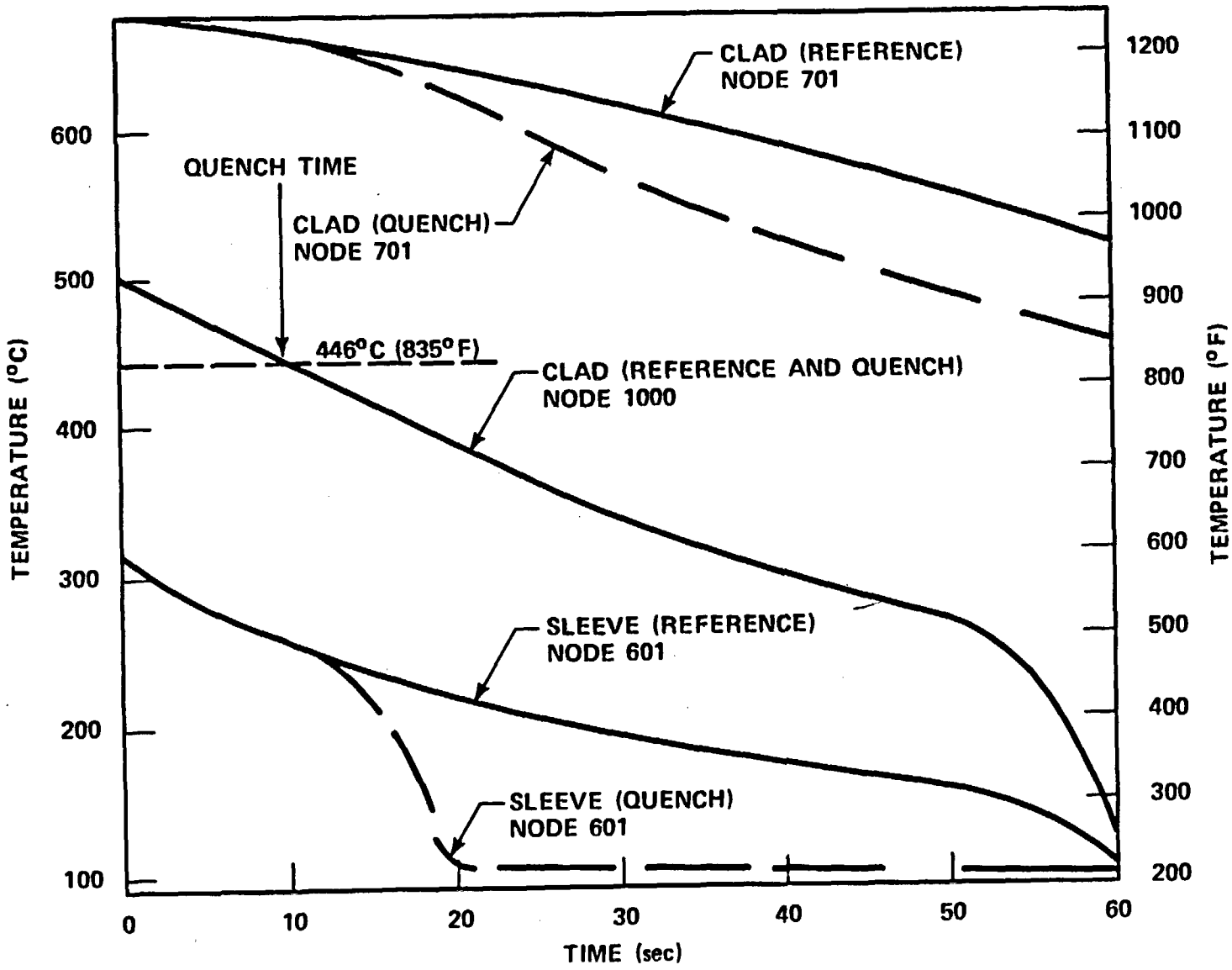

Figure I-9. Blocked Heater Rod Clad Temperature
$[T_q = 446^{\circ}C\ (835^{\circ}F)]$

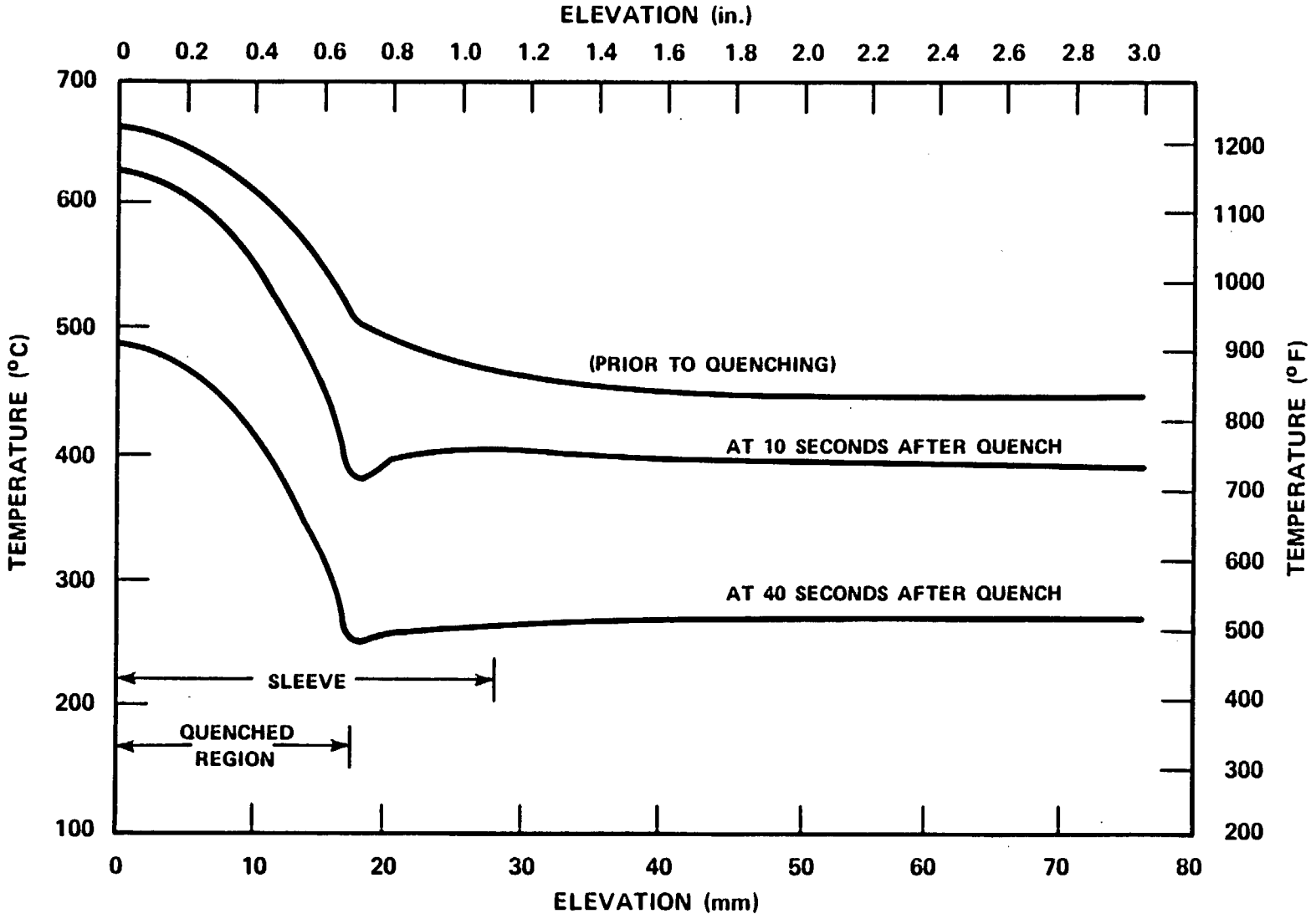

Figure I-10. Axial Clad Temperature Distribution for Blocked Rod

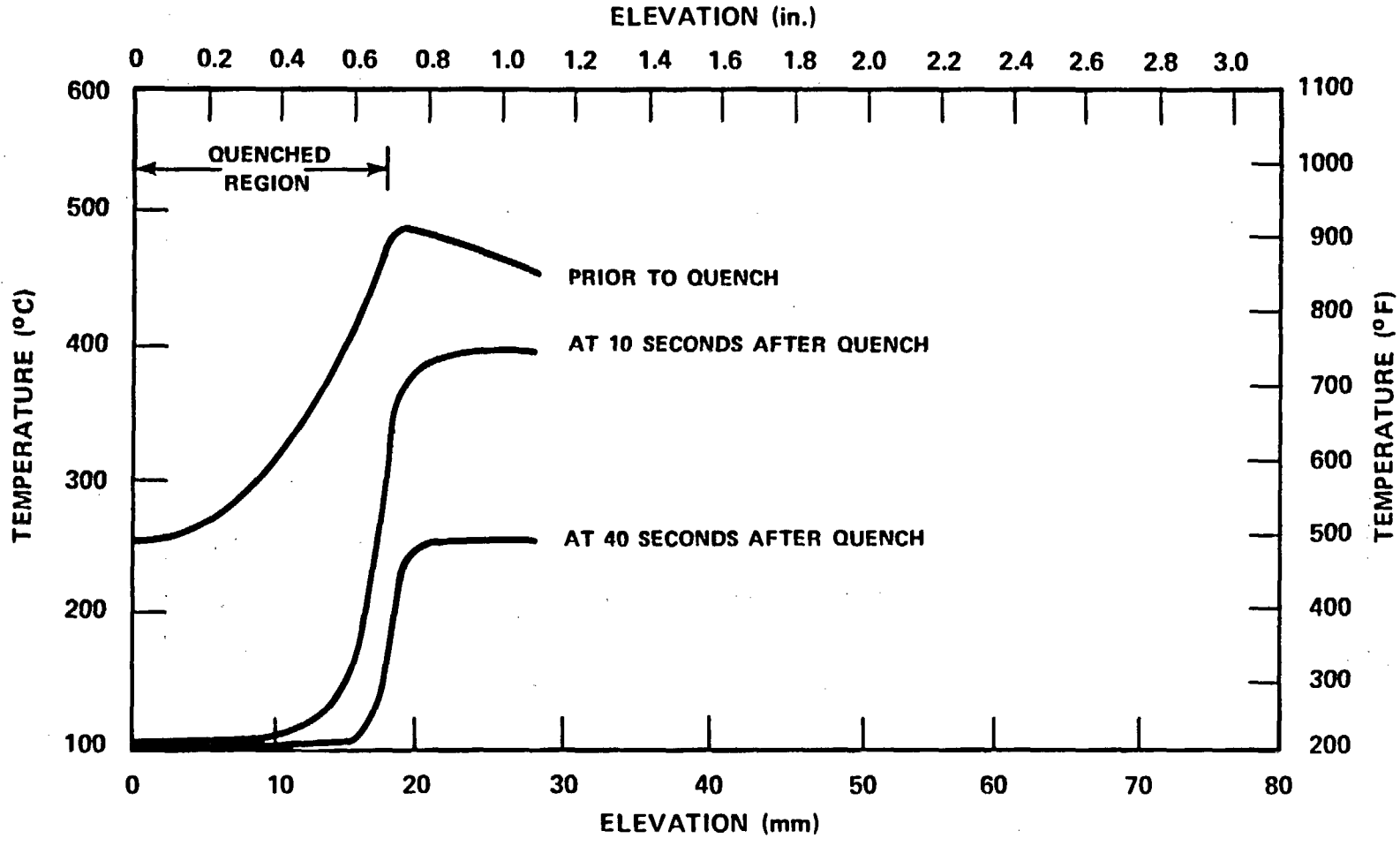

Figure I-11. Axial Sleeve Temperature Distribution for Blocked Rod at 40 Seconds

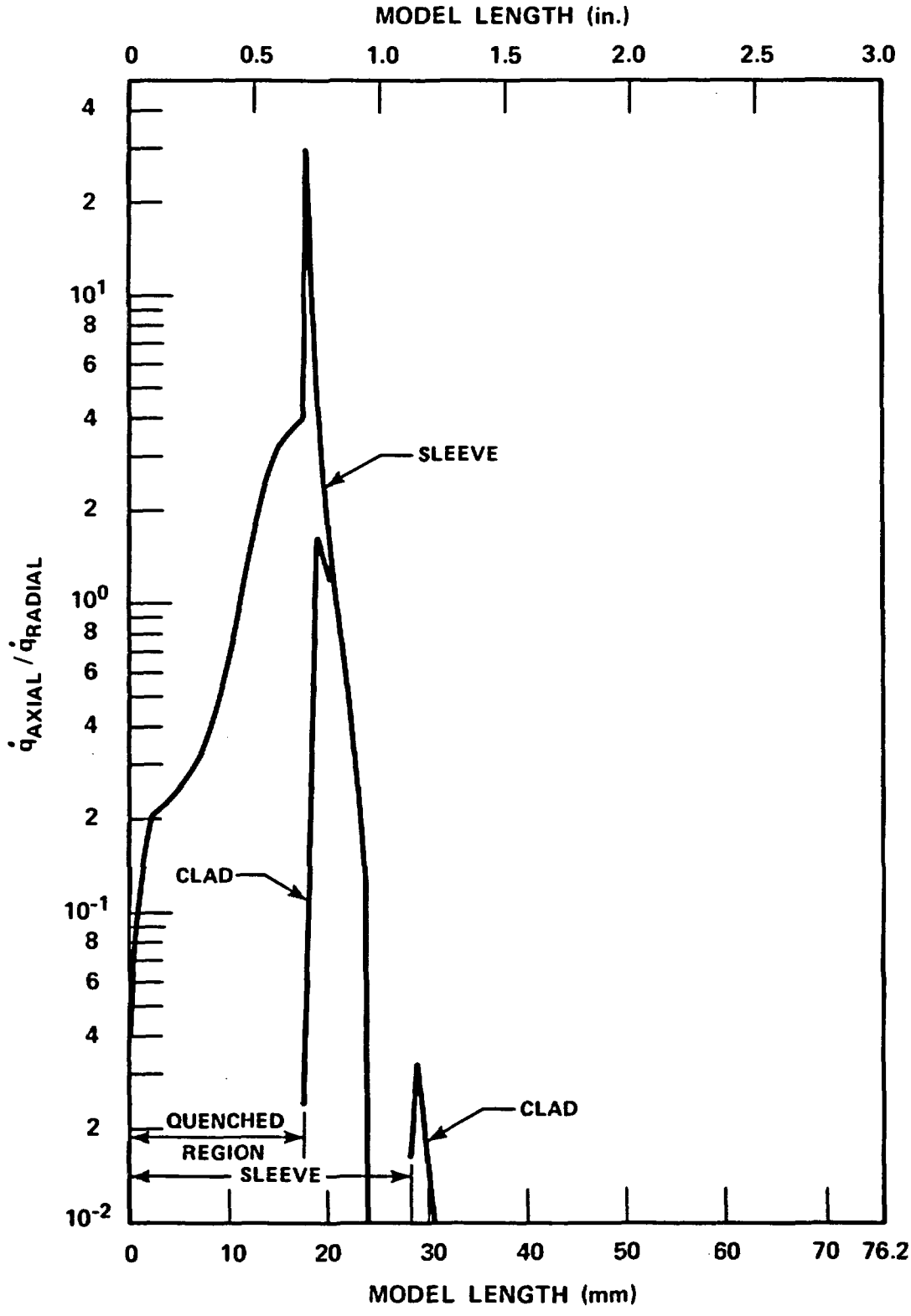

Figure I-12. Ratio of Axial to Radial Heat Flow in Blocked Rod at 10 Seconds $\left[T_q = 446^{\circ}C\ (835^{\circ}F)\right]$

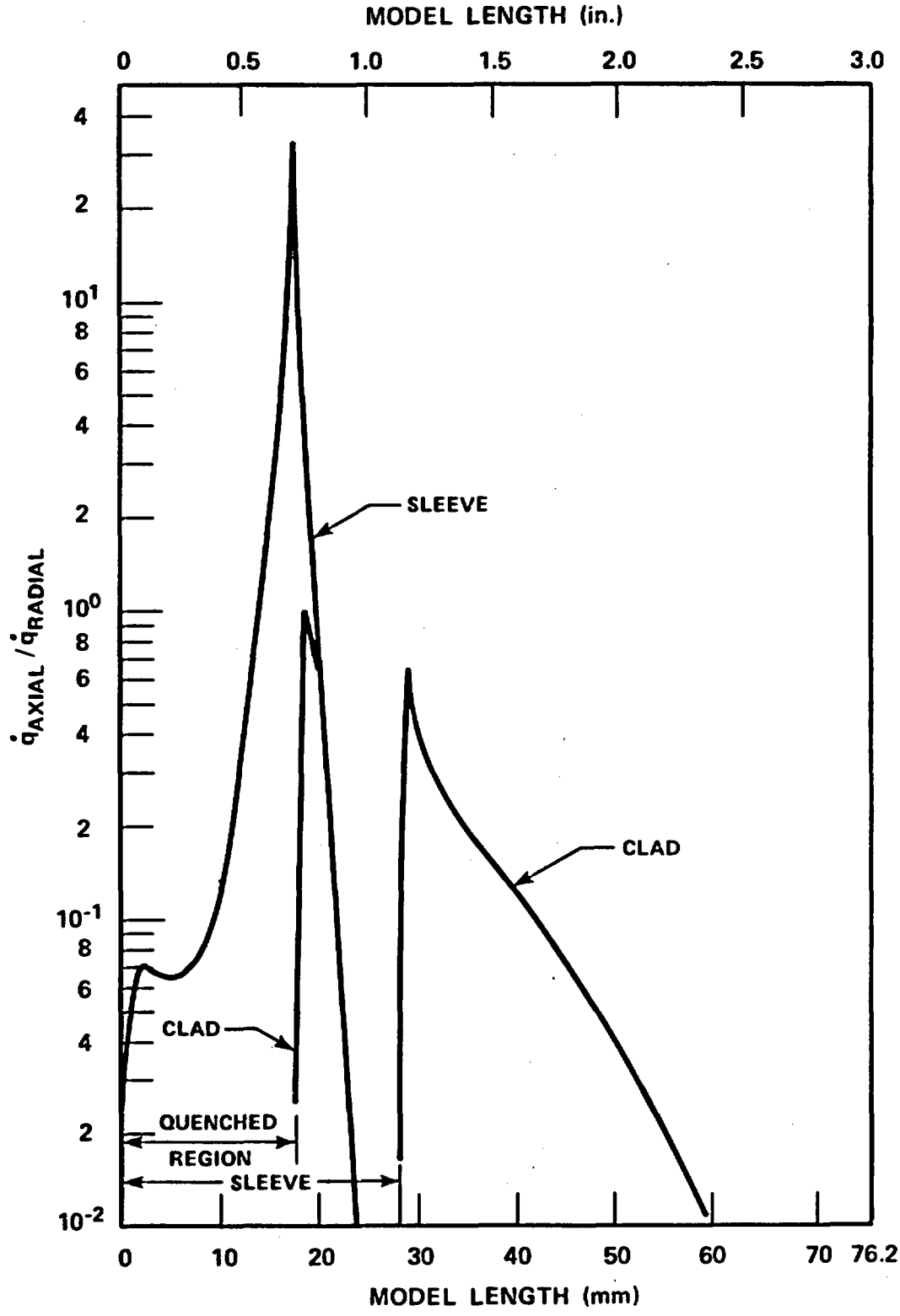

Figure I-13. Ratio of Axial to Radial Heat Flow in Blocked Rod at 40 Seconds [T_q = 446°C (835°F)]

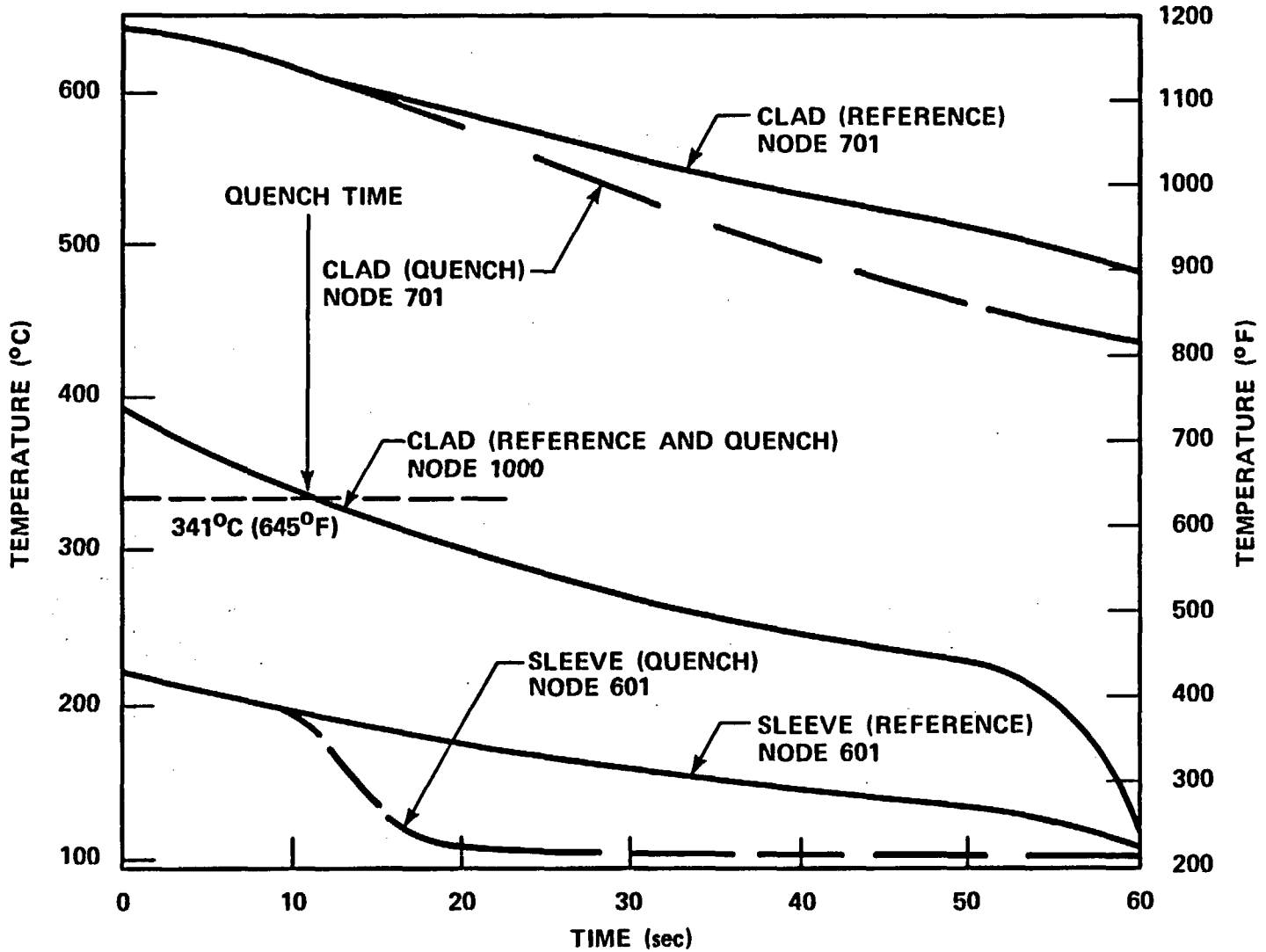

Figure I-14. Blocked Heater Rod Clad Temperature
[T_q = 341°C (645°F]

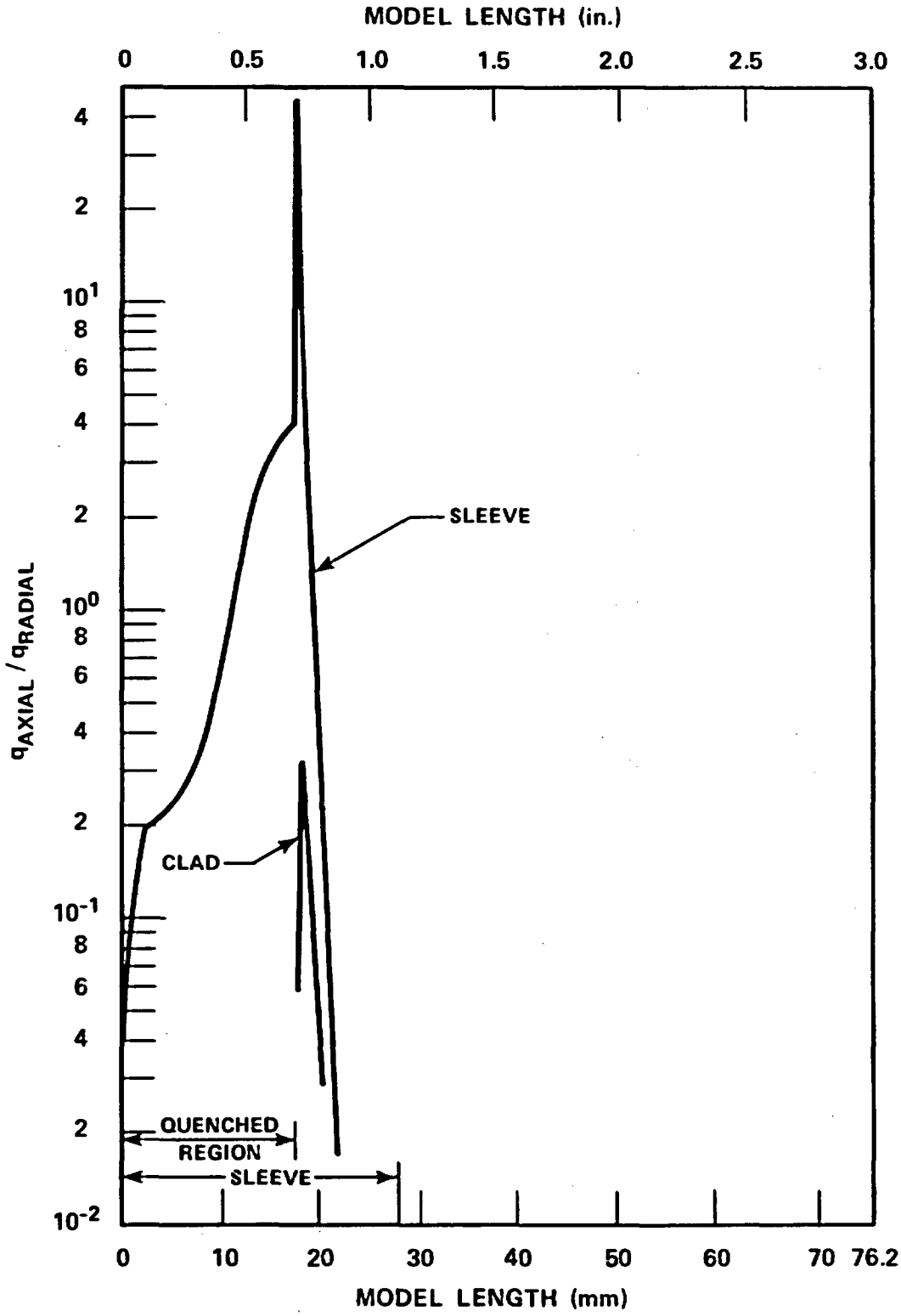

Figure I-15. Ratio of Axial to Radial Heat Flow in Blocked Rod at 10 Seconds $\left[T_q = 341^{\circ}C\ (645^{\circ}F)\right]$

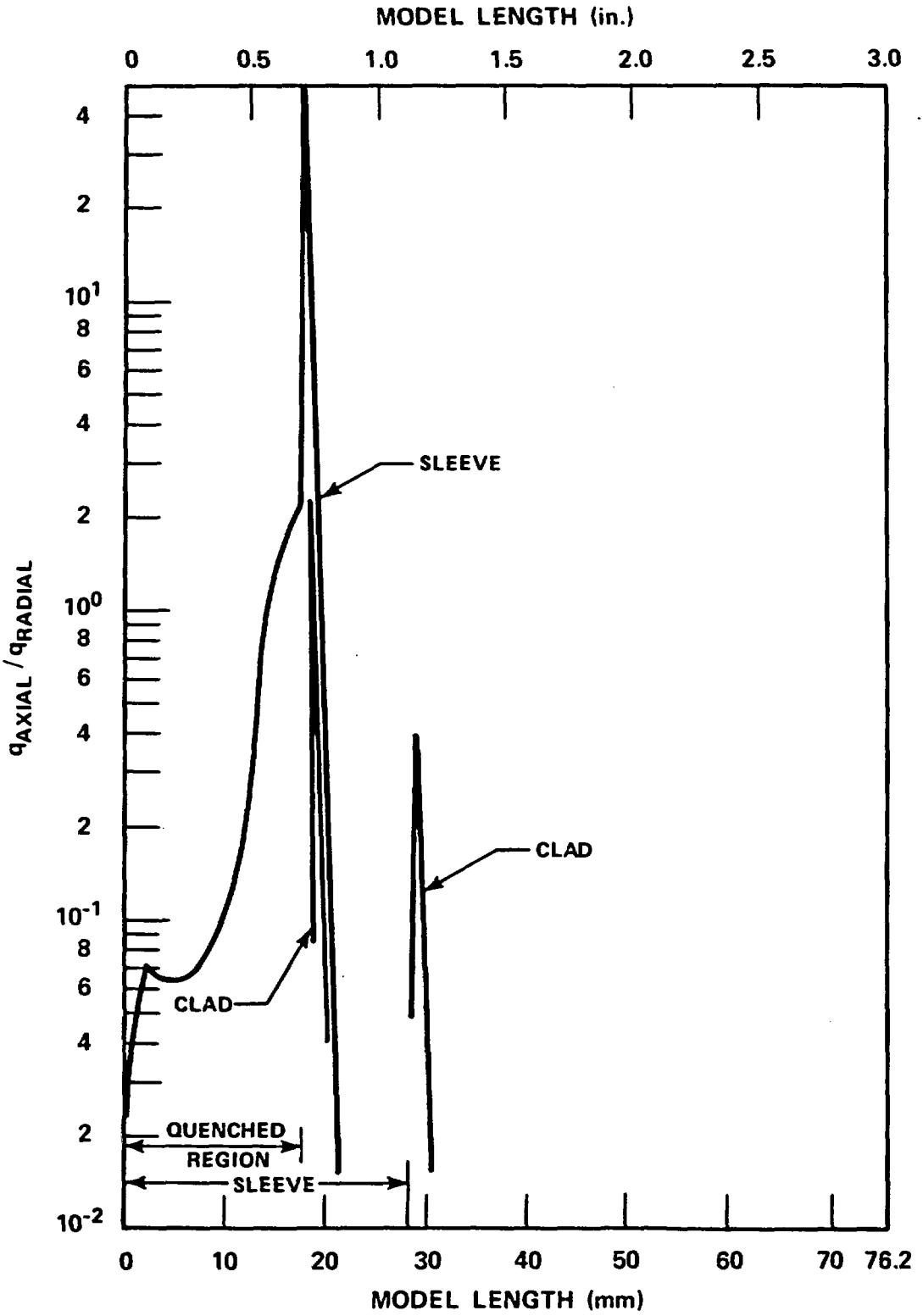

Figure I-16. Ratio of Axial to Radial Heat Flow in Blocked Rod at 40 Seconds [T_q = 341°C (645°F)]

that the effect of the axial conduction will be greater in the blocked rod than in the unblocked rod, since radiation will dominate conduction in the steam gap between the rod and the sleeve, and will increase the heat transfer from the rod to the sleeve.

Since this analysis was based on a stationary quench front, it is believed that conservative results have been obtained for an unblocked rod. In the presence of a traveling quench front at a velocity of approximately 2 mm/sec (0.10 in./sec), a heater rod thermocouple at 50 mm (2 in.) downstream of the quench front would be affected sooner by the quench front than by axial conduction, as shown in figure I-17, assuming that a ratio of axial to radial heat flow of 0.10 is acceptable. A heater rod thermocouple at approximately 25 mm (1 in.) downstream of the quench front would be affected at about the same time by the quench front and by axial conduction for the range of quench temperatures investigated.

However, in the flow blockage test program, it was anticipated that the hollow blockage sleeve attached to the heater rod could quench prior to the arrival of the traveling quench front. In this case, axial heat conduction through the clad could affect the heater rod thermocouples immediately upstream and downstream of the sleeve. As shown in figure I-17 at a time of 40 seconds after the sleeve quenches, as far as 25 mm (1 in.) downstream of the quenched sleeve, the heater rod clad is affected for a clad quench temperature of 446°C (835°F) and at 12 mm (0.50 in.) for a clad temperature of 341°C (645°F). This result indicates that axial conduction is a strong function of the clad quench temperature in this range of temperatures for a rod with a quenched blockage sleeve.

Two clad quench temperatures were investigated for both the unblocked rod and the blocked rod. The effect of axial conduction was projected for higher clad quench temperatures based on a linear relationship between the two known quench temperatures, as shown in figures I-18 and I-19 for an unblocked rod and a rod with a quenched sleeve, respectively. Figure I-18 shows that the effect of axial conduction in an unblocked rod is fairly independent of the clad quench temperature, especially at 10 seconds after quench. For a rod with a quenched blockage sleeve, the projected effect of axial conduction as a function of the clad quench temperature (figure I-19) is fairly significant.

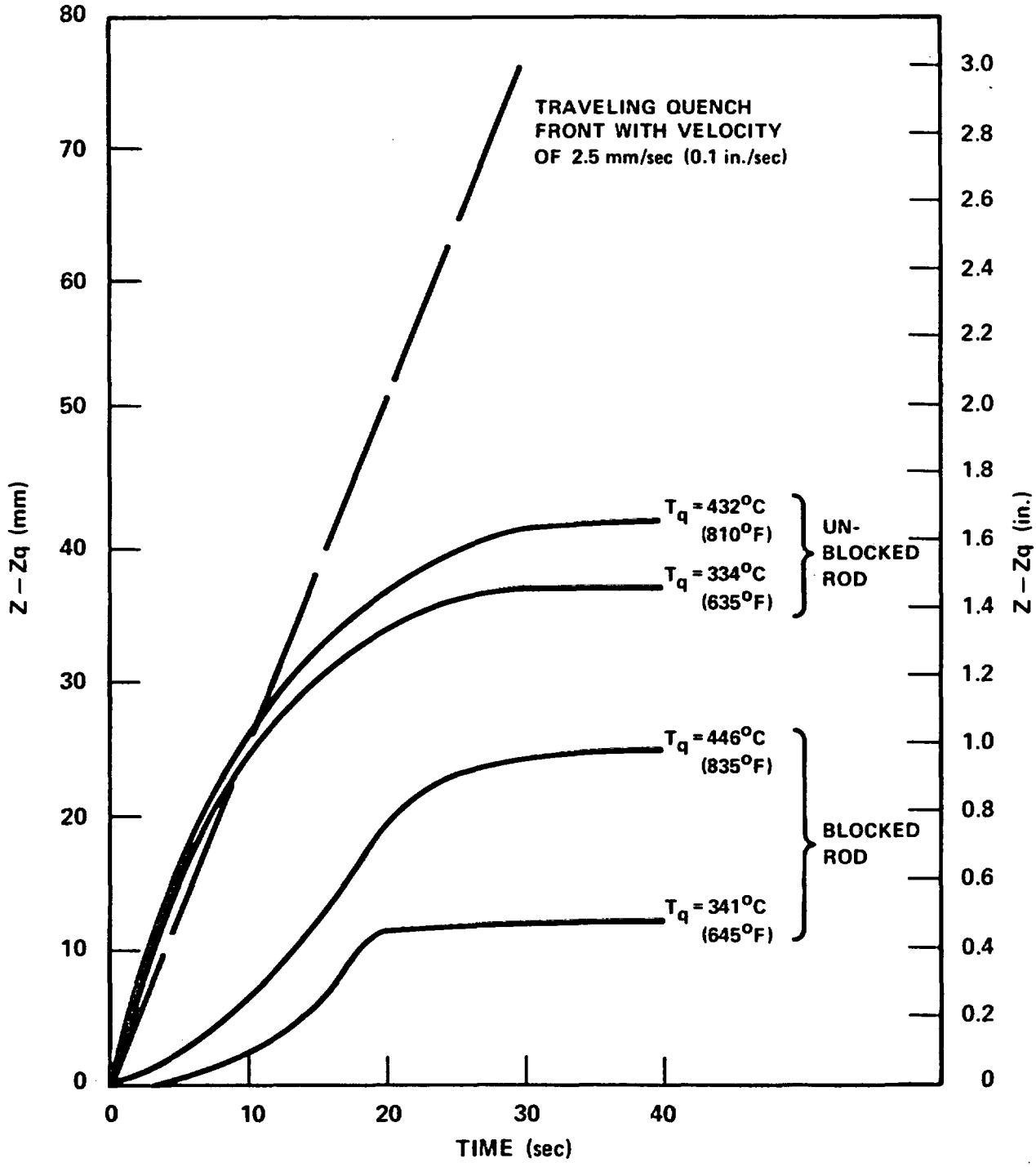

Figure I-17. Effect of Traveling Quench Front on Downstream Heater Rod Thermocouples

I-4. MEASURED BLOCKAGE SLEEVE QUENCH TIMES AND TEMPERATURES

A review of the measured clad temperatures underneath the short, concentric flow blockage sleeves indicates that the clad temperature at the time the sleeve quenched was approximately 593°C to 704°C (1100°F to 1300°F), as shown for rod 3C for bundles B, C, and D in figure I-20. Although this measured clad temperature was higher than that utilized in the axial heat conduction analysis, the blockage sleeves did not prematurely quench in the tests. The blockage sleeves quenched at approximately the same time as the unblocked heater rod thermocouples at the same elevation, as shown below by quench times for the 23 mm/sec (0.9 in./sec) flooding rate test in configuration B (run 42306B). This behavior was observed for all the blocked bundles in the 21-rod bundle test program; therefore, there was no problem associated with premature quenching of flow blockage sleeves.

Heater Rod Thermocouple Location [m (in.)]	Blockage Sleeve Thermocouple Location [m (in.)]	Quench Time (sec)	
		Heater Rod	Blockage Sleeve
3A 1.83 (72)	2D 1.85 (73)	385	398
1C 1.83 (72)	3C 1.85 (73)	393	393
2E 1.83 (72)	3D 1.85 (73)	398	389
5B 1.83 (72)	4D 1.85 (73)	401	403
5C 1.83 (72)		385	

I-5. AZIMUTHAL HEAT CONDUCTION ANALYSIS AND RESULTS

A two-dimensional TAP-A code model of a heater rod was set up to investigate the response of the clad when subjected to an azimuthal heat transfer variation. This azimuthal heat transfer variation could be caused by subchannel flow blockage, which provides flow variations in adjacent subchannels.

The TAP-A code heater rod model (figure I-21) was 9.50 mm (0.374 in.) in diameter and consisted of 6 radial nodes and 48 azimuthal nodes, each of which was 0.042π radians

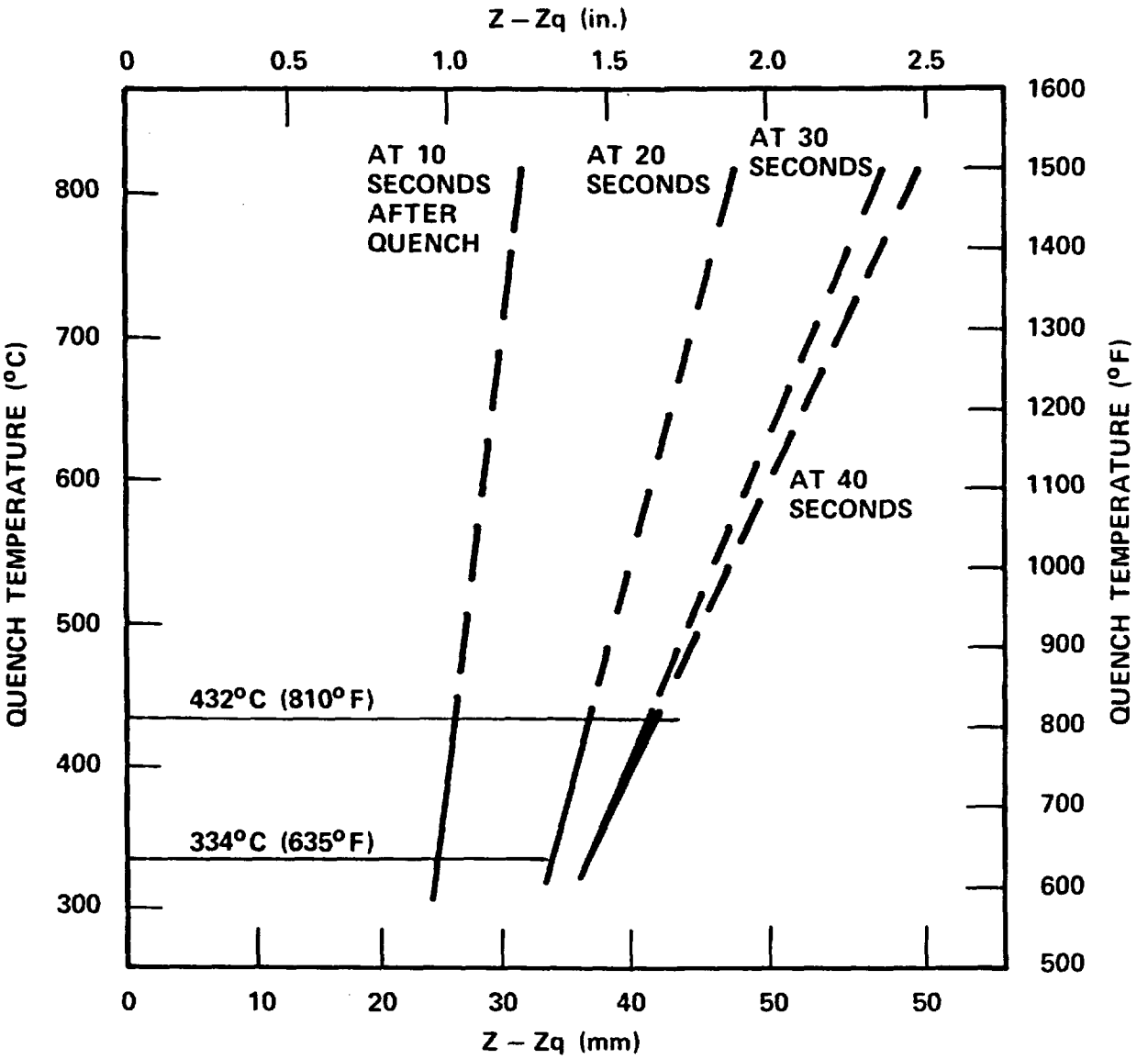

Figure I-18. Projected Effect of a Stationary Quench Front on Unblocked Heater Rod for $q_{axial}/q_{radial} = 0.10$

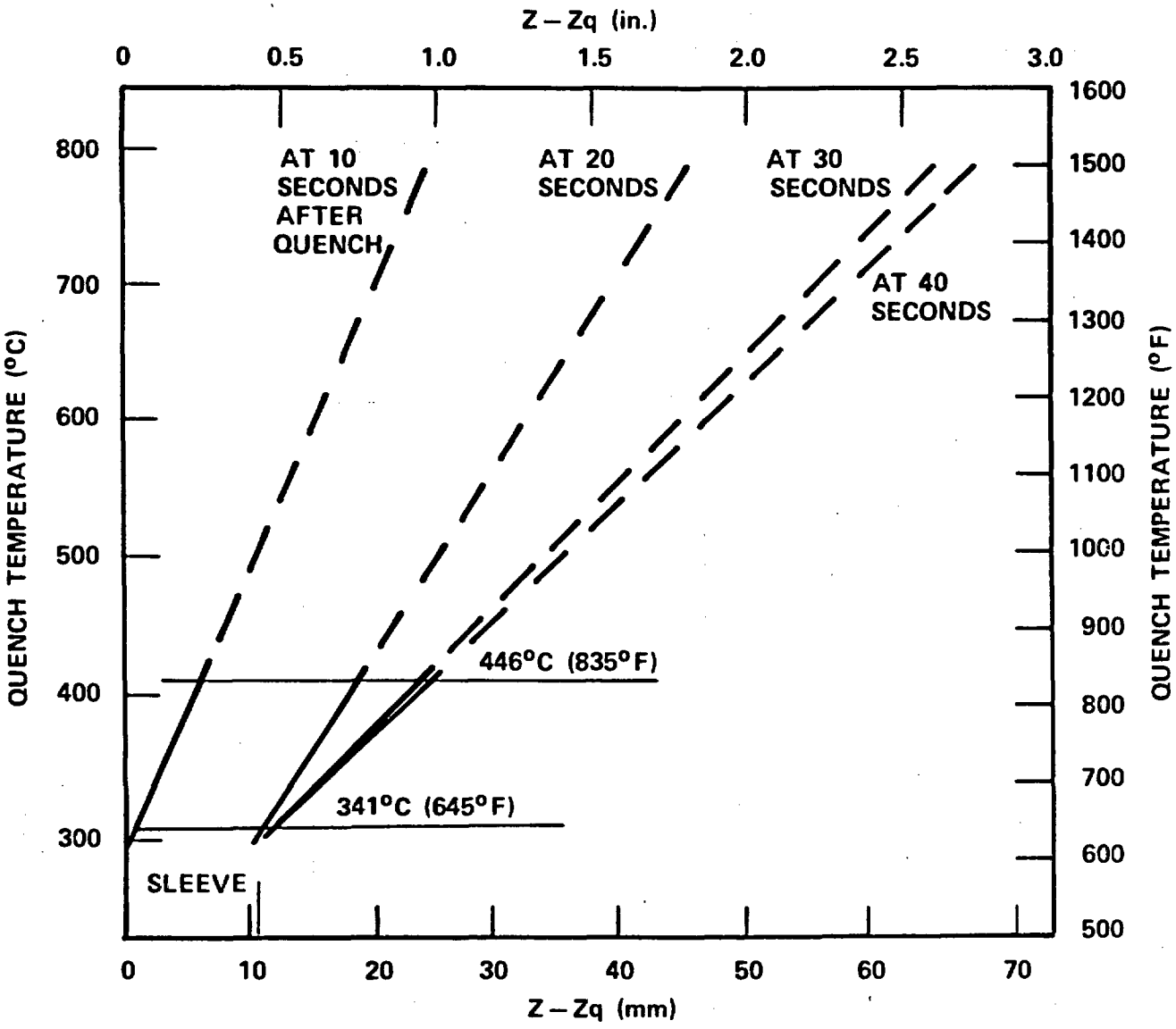

Figure I-19. Projected Effect of a Quenched Blockage Sleeve on Downstream Rod for $q_{axial}/q_{radial} = 0.10$

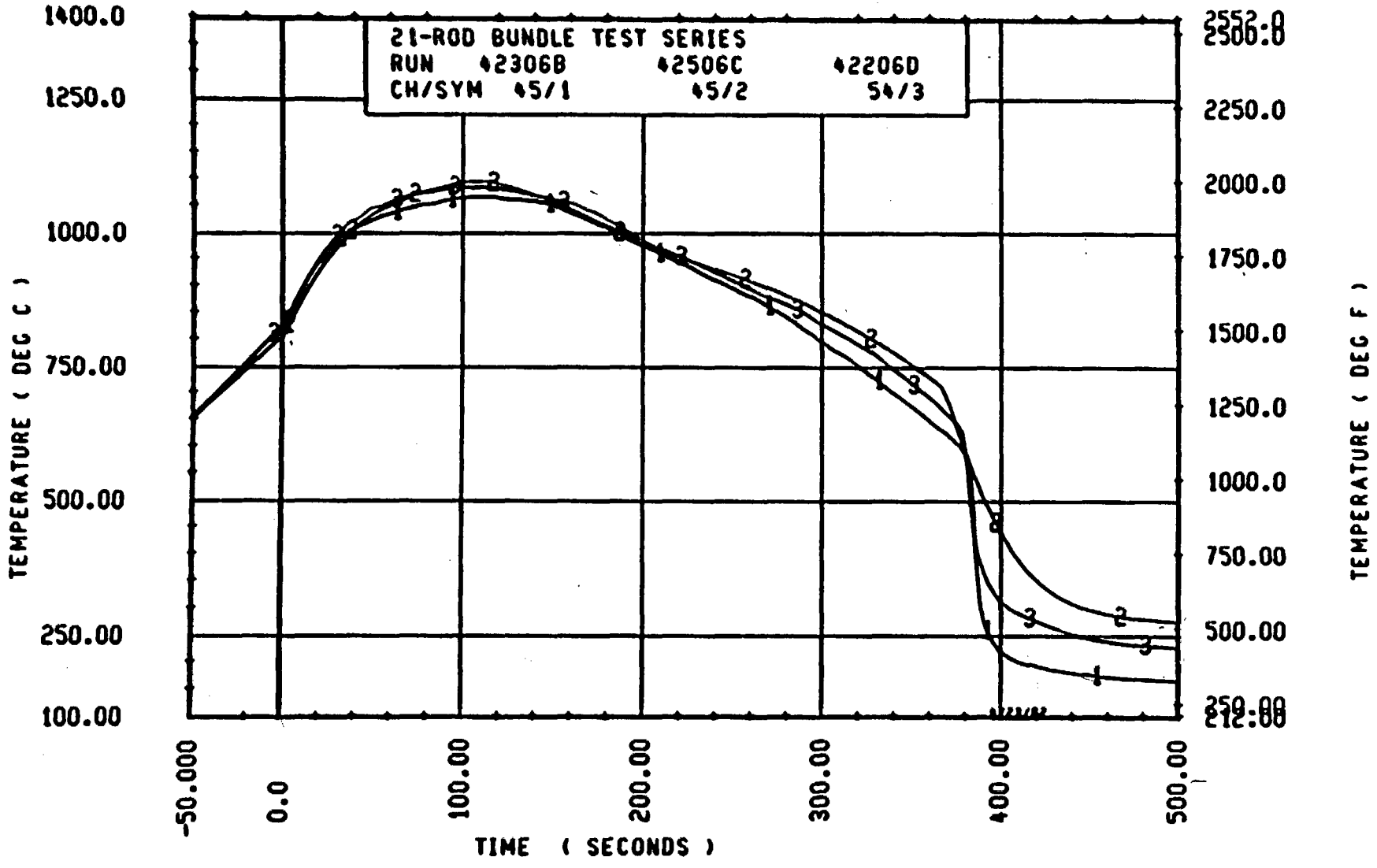

Figure I-20. Temperature Transient, Rod 3C, Configurations B, C, and D

(7.5 degrees). The six radial nodes consisted of a center node of boron nitride insulation, a heating element node of both boron nitride and Kanthal (coil heater), three nodes of boron nitride insulation, and a cladding node of stainless steel.

The model was divided into eight 45-degree slices, each of which had six azimuthal nodes and a corresponding outside film coefficient. The properties of all the materials were input into the code as a function of temperature.

The model was initially subjected to a typical reflood transient starting at an initial clad temperature of approximately 851°C (1600°F) with a uniform azimuthal outside film coefficient, as shown in figure I-22. The power was reduced from an initial linear power of 2.3 kw/m (0.70 kw/ft) as a function of time according to the ANS + 20 percent power decay curve. The steam coolant temperature was assumed to be 131°C (267°F).

Since the azimuthal variation in the heat transfer coefficient was not exactly known, several assumptions were made with respect to the magnitude of and respective heater rod area for the heat transfer coefficient. In considering a flow-centered subchannel with high flow, as shown in figure I-23, it was assumed that only the middle 45-degree section or 12.5 percent of the heater rod facing the subchannel would have a higher heat transfer coefficient. The remaining 315-degree section or 87.5 percent of the surface area was subjected to the nominal heat transfer coefficient. From a review of the 21-rod bundle blockage heat transfer data, the blocked heat transfer coefficient could be as much as approximately 100 percent greater than the unblocked heat transfer immediately after flood initiation and subsequently decrease to the nominal value by approximately the turnaround time. This variation in heat transfer coefficient, as shown in figure I-22, was applied to the heater rod as a best estimate of the conditions which could exist in adjacent subchannels of the same bundle. A 50-percent variation in the transient heat transfer coefficient was also investigated, as shown in figure I-22.

The results of this analysis are shown in figures I-24 and I-25. Figure I-24 shows the average cladding temperature as a function of time for the cases with the uniform and nonuniform heat transfer coefficients. Figure I-25 shows the maximum cladding temperature differential as a function of time for the two cases. These figures show that the azimuthal temperature difference is a very strong function of the heat transfer

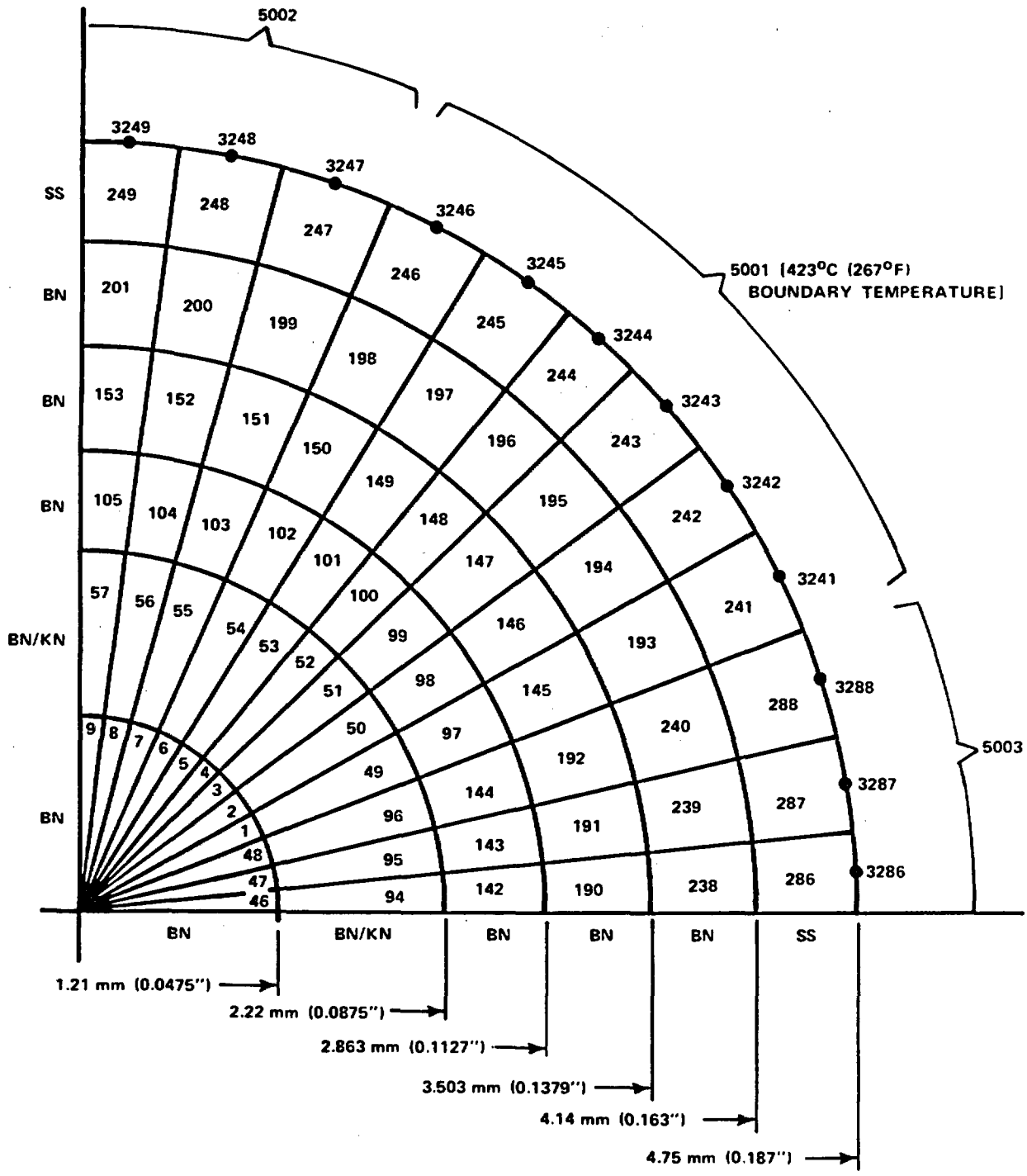

Figure I-21. Two-Dimensional TAP-A Model of Heater Rod

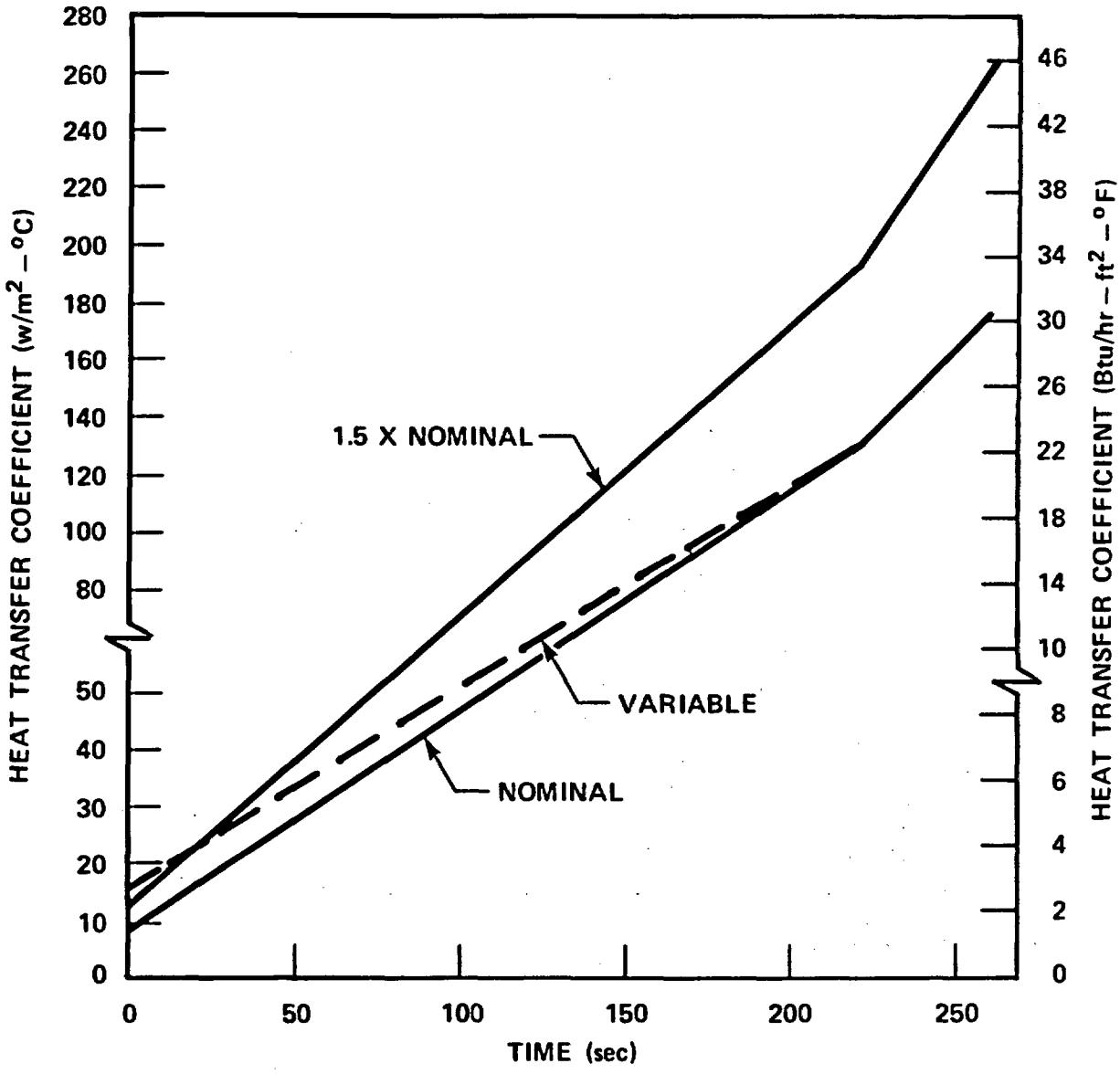

Figure I-22. Typical Reflood Heat Transfer Coefficient, TAP-A Azimuthal Heat Conduction Model

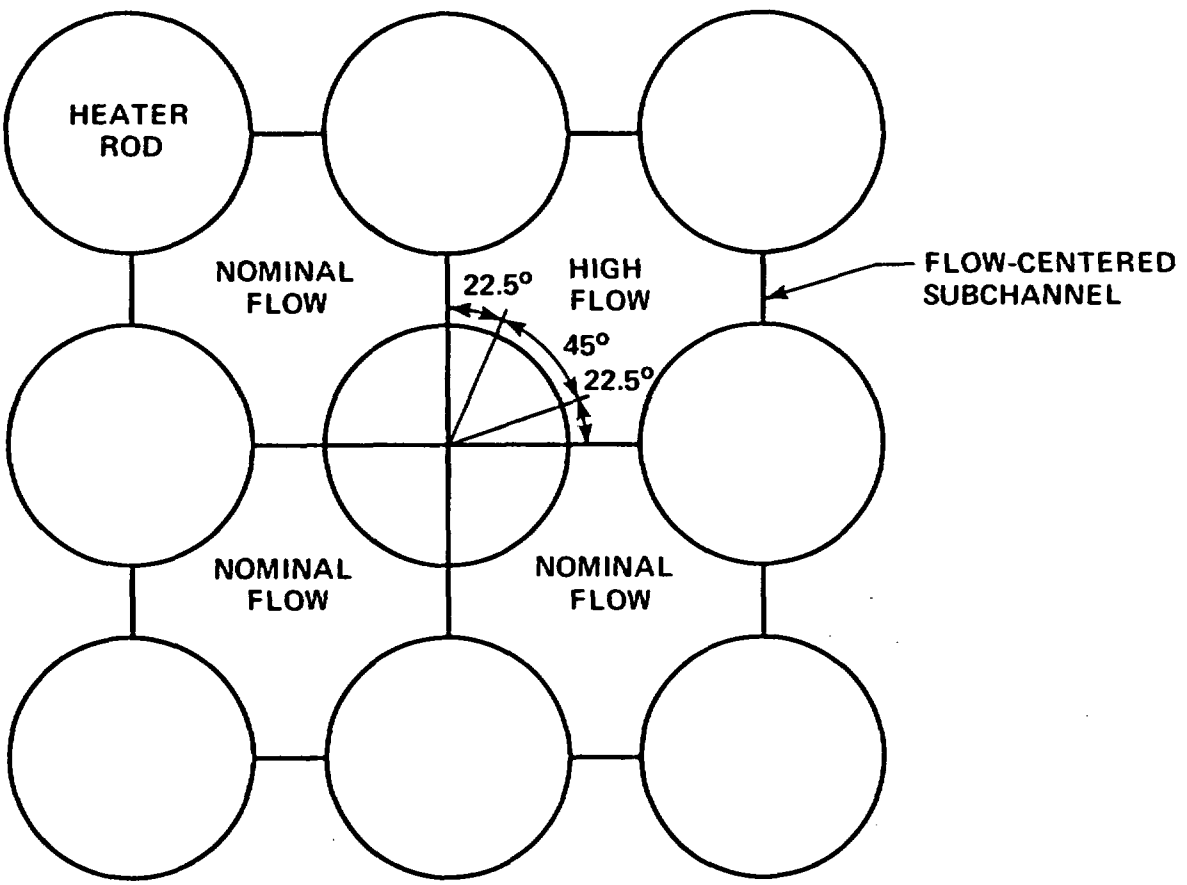

Figure I-23. Flow Subchannels

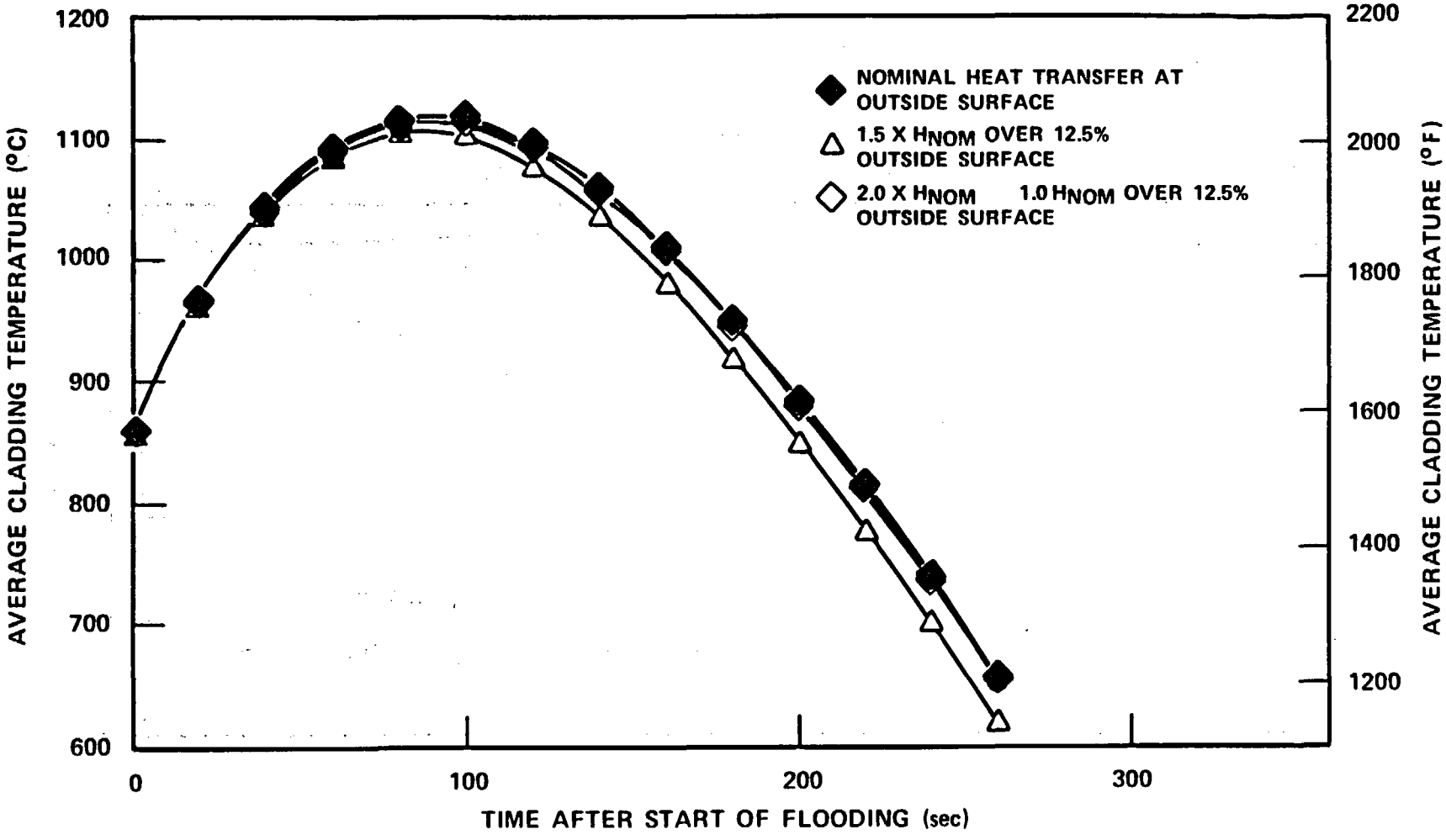

Figure I-24. Average Cladding Temperature Versus Time

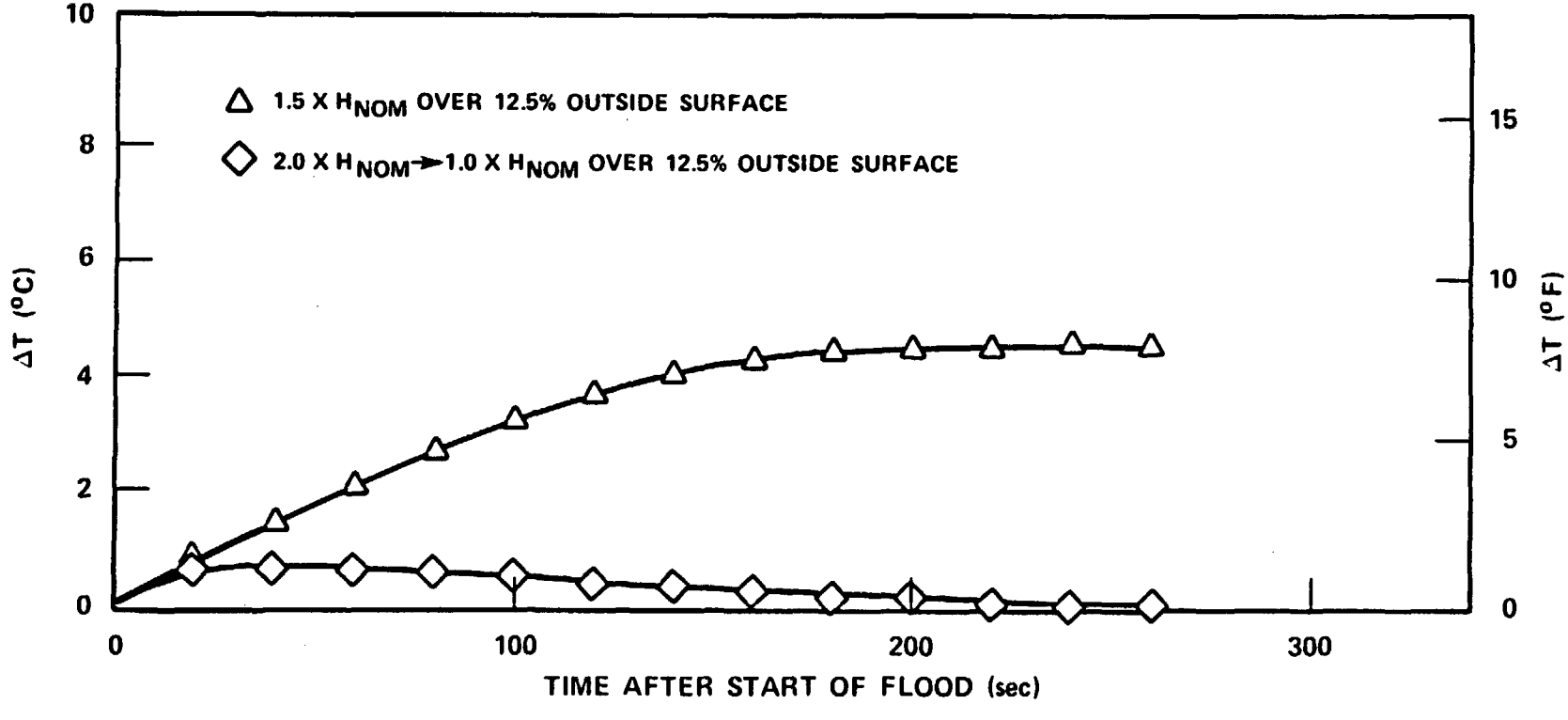

Figure I-25. Maximum Cladding Temperature Differential Versus Time

coefficient. However, for the best-estimate heat transfer coefficient, the maximum temperature differential is only 0.69°C (1.25°F), which is less than the uncertainty of the measurement.

I-6. CONCLUSIONS FROM AZIMUTHAL HEAT CONDUCTION ANALYSIS

From the above results, it was concluded that the azimuthal temperature variations in the reflood tests would be insignificant, and therefore knowledge of the azimuthal location of heater rod thermocouples was not required. Furthermore, it was concluded that the heater rod responds to the flow in the surrounding four subchannels such that the COBRA-IV-I code subchannel results could be averaged to provide rod-centered subchannel results.

APPENDIX J
SELF-ASPIRATING STEAM PROBE PERFORMANCE

J-1. INTRODUCTION

A new type of steam probe was required for the 21-rod bundle task because of the lack of thimble tubes typically utilized, as in the unblocked bundle task,[1] for measuring superheated steam temperature in a nonequilibrium mixture.

The same measurement technique was utilized for the 21-rod bundle probe as for the unblocked bundle probe. The technique utilized was to separate the superheated steam flow from the entrained droplets as quickly as possible and over the shortest flow path. The significant difference between the unblocked bundle steam probe and the 21-rod bundle steam probe was that the former aspirates to atmospheric pressure, thereby providing a significant pressure drop for flow through the probe; the latter depends on a frictional pressure drop across the steam probe length as the driving force for steam flow.

J-2. THERMAL ANALYSIS OF STEAM PROBE

The thermocouple junction was placed midway between the two diametrically opposed flow holes, to minimize the inside frictional losses and to provide maximum radiation

1. Loftus, M. J., et al., "PWR FLECHT SEASET Unblocked Bundle, Forced and Gravity Reflood Task Data Report," NRC/EPRI/Westinghouse-7, June 1980. NUREG/CR-1532, Vols. 1 and 2.

shielding and protection from water droplets. The following schematic diagram of the steam probe shows the parameters involved in this hydraulic model:

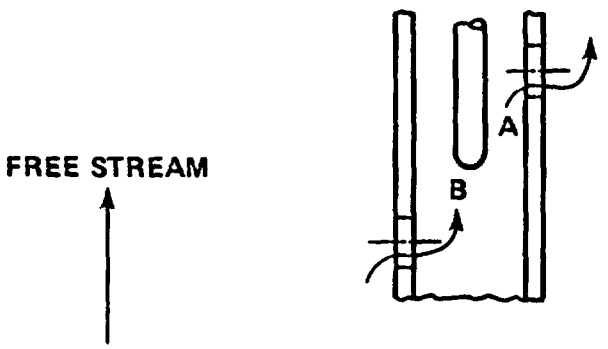

In parallel flow paths, the pressure drops across both flow paths are equal:

$$\Delta P_{\text{free stream}} = \Delta P_{\text{steam probe}} \tag{J-1}$$

The pressure drop in the free stream is assumed to be attributable to bundle frictional pressure losses:

$$\Delta P_{\text{free stream}} = \left(\frac{fL}{D_f}\right)\left(\frac{\rho V^2_{\text{free stream}}}{2\, g_c}\right) \tag{J-2}$$

The pressure drop in the steam probe is attributed to the entrance, exit, and frictional pressure losses in regions A and B, as illustrated in the above sketch:

$$\Delta P_{\text{steam probe}} = \Delta P_{\text{region A}} + \Delta P_{\text{region B}} \tag{J-3}$$

where

$$\Delta P_{\text{region A}} = \left(K_{SA} + \frac{f_{SA}L/2}{D_{SA}}\right)\left(\frac{\rho V_{SA}^2}{2g_c}\right) \tag{J-4}$$

$$\Delta P_{\text{region B}} = \left(K_{SB} + \frac{f_{SB}L/2}{D_{SB}}\right)\left(\frac{\rho V_{SB}^2}{2g_c}\right) \tag{J-5}$$

Therefore, assuming constant vapor density,

$$\left(\frac{fL}{D_h}\right)V_{\text{free stream}}^2 = \left(K_{SA} + \frac{f_{SA}L/2}{D_{SA}}\right)V_{SA}^2 + \left(K_{SB} + \frac{f_{SB}L/2}{D_{SB}}\right)V_{SB}^2 \tag{J-6}$$

where

f = friction factor = 64/Re
D_h = hydraulic diameter of bundle = 0.00832 m (0.0273 ft)
K_{SA} = shield exit pressure loss coefficient = 1.0 (maximum)
K_{SB} = shield entrance pressure loss coefficient = 0.5 (maximum)
D_{SA} = hydraulic diameter of region A = D_S - 0.81 mm (0.032 in.)
D_{SB} = hydraulic diameter of region B = D_S
D_S = inside diameter of shield = 2.08 mm (0.082 in.)
L = distance between flow holes = 6.4 mm (0.25 in.)

By applying the continuity equation within the probe,

$$V_{SA}A_{SA} = V_{SB}A_{SB} \tag{J-7}$$

equation (J-6) can be solved for the maximum velocity, V_{SA}, in the shield. Assuming the steam velocity in the free stream to be 12.2 m/sec (40 ft/sec),[1,2] the steam velocity across the thermocouple was calculated to be 0.41 m/sec (1.33 ft/sec). It should be noted that the free stream velocity utilized in this analysis represents a low estimate and that an increase in this velocity will also increase the velocity through the shield.

The temperature measured by the thermocouple within the steam probe was adversely affected by the radiation heat transfer from the surrounding high-temperature heater rods. A sufficient steam flow through the probe is required to "cool" the thermocouple to the temperature of the steam. The following calculation was performed to determine the cooling effectiveness of the steam flow, as previously calculated.

An energy balance[3] on the shield yields the following heat flow equation:

$$\underset{\text{by convection}}{\dot{q}_{\text{shield to steam}}} + \underset{\text{by radiation}}{\dot{q}_{\text{shield to thermocouple}}} = \underset{\text{by radiation}}{\dot{q}_{\text{rod to shield}}} \qquad \text{(J-8)}$$

An energy balance[3] on the thermocouple junction, which is assumed to be at the same temperature as the thermocouple sheath, yields the following:

$$\underset{\text{by convection}}{\dot{q}_{\text{thermocouple junction to steam}}} = \underset{\text{by radiation}}{\dot{q}_{\text{shield to thermocouple junction}}} \qquad \text{(J-9)}$$

The previous five terms are defined as follows:

$$\underset{\text{by convection}}{\dot{q}_{\text{shield to steam}}} = h(T_{\text{shield}} - T_{\text{steam}}) \qquad \text{(J-10)}$$

---

1. Lilly, G. P., et al., "PWR FLECHT Cosine Low Flooding Rate Test Series Evaluation Report," WCAP-8838, March 1977.

2. Lilly, G.P., et al., "PWR FLECHT Skewed Profile Low Flooding Rate Test Series Evaluation Report," WCAP-9183, November 1977.

3. Steady-state conditions are assumed in this calculation, because of the slow response of the system during reflood.

where $h = \left[(hA)_{outside} + (hA)_{inside}\right]_{shield\ to\ steam}$

$$\dot{q}_{\substack{shield\ to\ thermocouple \\ by\ radiation}} = \frac{A_{T/C}\sigma\left(T_{SH}^4 - T_{T/C}^4\right)}{\left(\frac{1 - \epsilon_{SH}}{\epsilon_{SH}}\right)\left(\frac{A_{T/C}}{A_{SH}}\right) + \frac{1}{\epsilon_{T/C}}} \tag{J-11}$$

$$\dot{q}_{\substack{rod\ to\ shield \\ by\ radiation}} = A_{SH}\,\epsilon_{SH}\,\sigma\left(T_R^4 - T_{SH}^4\right) \tag{J-12}$$

since $A_{SH} << A_{rod}$.

$$\dot{q}_{\substack{thermocouple\ junction \\ to\ steam\ by\ radiation}} = \bar{h}_{\substack{thermocouple \\ junction \\ to\ steam}} A_{T/C\ junction}\,(T_{T/C} - T_{STM}) \tag{J-13}$$

$$\dot{q}_{\substack{shield\ to\ thermocouple \\ junction\ by\ radiation}} = A_{T/C\ junction}\,\sigma\,\epsilon_{T/C}\left(T_{SH}^4 - T_{T/C}^4\right) \tag{J-14}$$

The outside film coefficient for the shield was determined by the following correlation for laminar flow over a plane surface:[1]

$$\bar{h}_{\substack{shield\ to \\ steam}} = \frac{K}{L}\left(0.664\ Re_L^{1/2} Pr^{1/3}\right) \tag{J-15}$$

The inside film coefficient for the shield was determined by the following correlation[1] for laminar flow inside a cylindrical pipe:

$$\bar{h}_{\substack{shield\ to \\ steam}} = \frac{K}{D}\,1.86\left(Re\ Pr\ \frac{D}{L}\right)^{1/3} \tag{J-16}$$

1. Chapman, A. J., Heat Transfer, 3rd edition, Macmillan, New York, 1974.

The thermocouple junction was assumed to be a sphere in an open flow stream; therefore the film coefficient was determined by the following correlation:[1]

$$\bar{h}_{\substack{\text{thermocouple}\\ \text{junction to}\\ \text{steam}}} = \frac{K}{D}\left(2 + 0.03\ Pr^{0.33}Re^{0.59} + 0.35\ Pr^{0.356}Re^{0.58}\right) \qquad \text{(J-17)}$$

The respective heat transfer areas are as follows:

-- Shield outside area - 4.75×10^{-5} m^2 (5.11×10^{-4} ft^2)

-- Shield inside area - 4.15×10^{-5} m^2 (4.47×10^{-4} ft^2)

-- Thermocouple junction area - 1.03×10^{-6} m^2 (1.11×10^{-5} ft^2)

-- Thermocouple sheath area - 9.38×10^{-6} m^2 (1.01×10^{-4} ft^2)

The steam properties were assumed constant at a temperature of 760°C (1400°F). The emissivities of the shield and the thermocouple were assumed to be 0.8.[2]

The following equations (in metric units) were developed from the preceding energy balances in equations (J-8) and (J-9) and respective correlations:

$$T_{SH} + 2.212 \times 10^{-11}\,(T_{SH} + 273)^4 = T_{T/C} + 14.12 \times 10^{-11}\,(T_{T/C} + 273)^4 + 7.99 \times 10^{-11}\,(T_R + 273)^4 \qquad \text{(J-18)}$$

$$T_{STM} = T_{T/C} - 7.35 \times 10^{-11}\,(T_{SH} + 273)^4 - (T_{T/C} + 273)^4 \qquad \text{(J-19)}$$

---

1. Kutateladze, S. S., Fundamentals of Heat Transfer, 2nd edition, Academic Press, New York, 1963.

2. McAdams, W. H., Heat Transmission, 3rd edition, McGraw-Hill, New York, 1954.

In English engineering units, the above equations are

$$T_{SH} + 3.792 \times 10^{-11} (T_{SH} + 460)^4 = T_{T/C} + 2.421 \times 10^{-11} (T_{T/C} + 460)^4 + 1.372 \times 10^{-11} (T_R - 460)^4 \quad \text{(J-20)}$$

$$T_{STM} = T_{T/C} - 1.26 \times 10^{-11}\left[(T_{SH} + 460)^4 - (T_{T/C} + 460)^4\right] \quad \text{(J-21)}$$

The above two equations contain four unknown temperatures: shield, thermocouple, rod, and steam. Therefore, rod temperatures of 982°C, 1093°C, and 1204°C (1800°F, 2000°F, and 2200°F) were assumed, as well as various thermocouple and shield temperatures, to satisfy the above equations. The ratios of the thermocouple temperature to the steam temperature for the three rod temperatures are shown in figure J-1 as a function of the steam temperature. As shown by this figure, relatively small errors, 4 percent and less, are introduced in this steam temperature measurement technique for the expected range of operation.(1) The error in the temperature measurement is increased by approximately 1 percent for an increase of 0.1 in the emissivity of both the shield and the thermocouple, and similarly, is decreased approximately 1 percent for a decrease of 0.1 in the emissivity. The error in the temperature measurement is rather insensitive to the film coefficient. A ±50-percent change in the film coefficient results in approximately a $\mp$1.5-percent change in the temperature measurement error.

J-3. TESTS OF SELF-ASPIRATING STEAM PROBE

Several tests were conducted to evaluate the thermal response of the self-aspirating steam probe prior to its installation in the 21-rod bundle. The first test utilized a single-rod reflood facility in which the self-aspirating steam probe was placed in the flow annulus between the heater rod and the thin wall housing. An unshielded

1. Rosal, E. R., et al., "FLECHT Low Flooding Rate Skewed Test Series Data Report," WCAP-9108, May 1977.

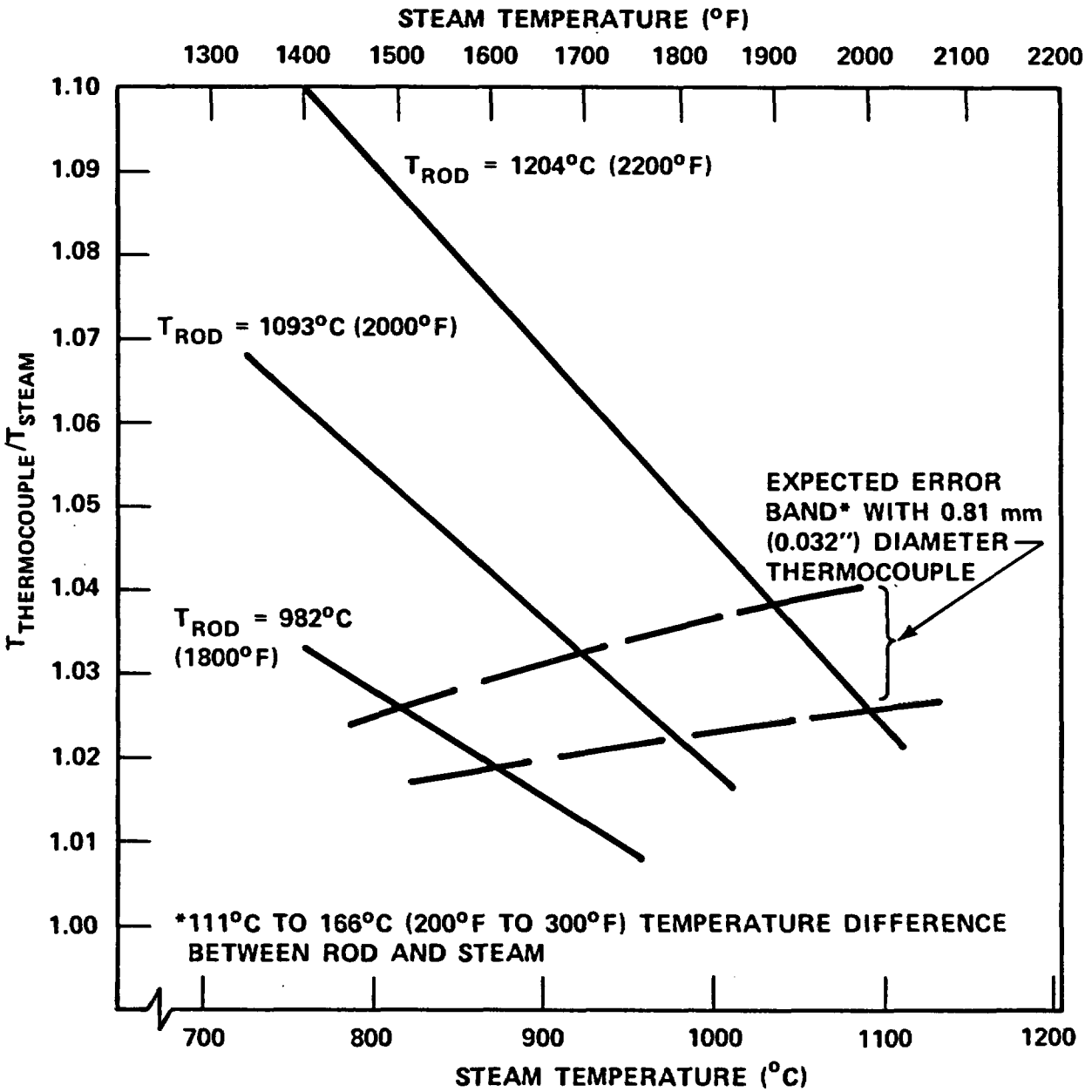

Figure J-1. Steam Probe Measurement Error With 0.81 mm (0.032 in.) Diameter Thermocouple

thermocouple was also placed in the flow annulus on the other side of the heater rod at the same elevation. A flooding rate of 38 mm/sec (1.5 in./sec) was initiated when the heater rod temperature reached 1093°C (2000°F).

The heater rod temperature, housing temperature, steam probe temperature, and unshielded thermocouple temperature transients are shown in figure J-2. By performing an energy balance on the unshielded thermocouple as follows, assuming the thermocouple can be modeled as a sphere,

$$\dot{q}_{\substack{\text{radiation}\\ \text{from rod}\\ \text{to T/C}}} + \dot{q}_{\substack{\text{radiation}\\ \text{from}\\ \text{housing}\\ \text{to T/C}}} = \dot{q}_{\substack{\text{convection}\\ \text{from T/C}\\ \text{to steam}}} + \dot{q}_{\substack{\text{stored}\\ \text{in T/C}}} \tag{J-22}$$

$$F_{R\text{-}T/C}\, A_{T/C}\, \sigma\varepsilon\left(T_R^4 - T_{T/C}^4\right) + F_{H\text{-}T/C}\, A_{T/C}\, \sigma\varepsilon\left(T_H^4 - T_{T/C}^4\right) = h_{T/C\text{-}STM} A \left(T_{T/C} - T_{STM}\right) + \bar{\rho} C_p \frac{dT_{T/C}}{dt} \tag{J-23}$$

and knowing the rod temperature, housing temperature, and thermocouple temperature, the actual steam temperature, T_{STM}, was calculated and subsequently compared to the temperature measured by the self-aspirating steam probe. The rod-to-thermocouple shape factor, $F_{R\text{-}T/C}$, was initially assumed to be 0.5 but was changed to 0.33 to achieve good comparison between the calculated and measured steam temperatures prior to flood. The housing-to-thermocouple shape factor, $F_{H\text{-}T/C}$, was assumed to be 1. These results, also shown in figure J-2, indicate that the steam temperature as measured by the steam probe is within a few percent of the actual steam temperature.

The second test conducted to evaluate the thermal response of the self-aspirating steam probe consisted of placing the respective probe in the 161-rod unblocked bundle of the FLECHT SEASET program. The self-aspirating steam probe was placed at the 2.74 m (108 in.) elevation by replacing a view port with a blank flange to which the steam probe was subsequently attached. The self-aspirating steam probe was located within several rod rows of two thimble tube aspirating steam probes. These thimble

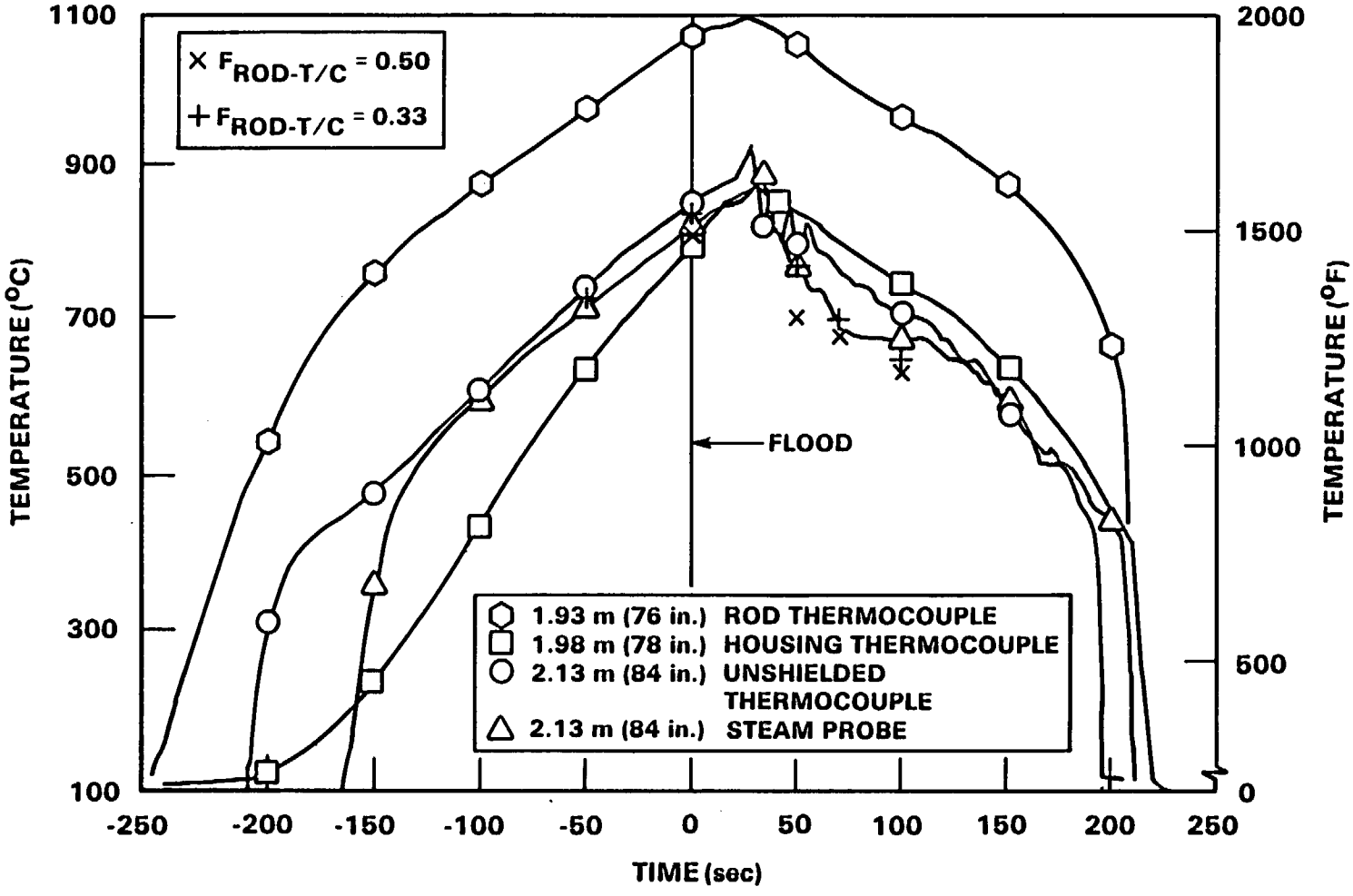

Figure J-2. Self-Aspirating Steam Probe Single-Rod Test Results

tube steam probes were in approximately symmetrical positions. Two tests at constant flooding rates of 25 mm/sec (1 in./sec) and 38 mm/sec (1.5 in./sec) were conducted at 871°C (1600°F) initial clad temperature and 2.3 kw/m (0.70 kw/ft) peak initial power.

The comparisons of the self-aspirating steam probe and the thimble tube steam probes for the two reflood tests are shown in figures J-3 and J-4 for the 25 mm/sec (1 in./sec) and 38 mm/sec (1.5 in./sec) flooding rate tests, respectively. These figures show that the self-aspirating steam probe measures a vapor temperature which is between the vapor temperature measured by the two thimble tube aspirating steam probes. Also shown in these figures is a heater rod temperature near the steam probes.

J-4. REVIEW OF 21-ROD BUNDLE STEAM PROBE DATA

The self-aspirating steam probe and unshielded thermocouple were placed in symmetrical subchannels in the first 21-rod bundle at the three elevations shown in figures J-5 through J-7. (These figures include the respective computer channel numbers for the instruments.) The steam temperature as measured by each instrument and adjacent heater rod temperatures for the 22 mm/sec (0.9 in./sec) forced flooding rate test at the 1.98, 2.29, and 3.05 m (78, 90, and 120 in.) elevations are shown in figures J-5, J-6, and J-7, respectively. These figures generally indicate similar temperature responses for the self-aspirating steam probe and unshielded thermocouple. The response of each instrument was consistent with the adjacent measured heater rod temperatures. The unshielded thermocouple tends to measure greater temperature oscillations than the self-aspirating steam probe, as would be expected because of the protection from water droplets which the shield provides to the steam probe. However, the self-aspirating steam probe typically quenches before the unshielded thermocouple because of the shield trapping water droplets during the low steam flow at the end of the test. These results are fairly consistent with variation in the flooding rate for the unblocked bundle configuration.

In subsequent bundles, the number of unshielded thermocouples was increased and, consequently, the number of self-aspirating steam probes was reduced. This substitution was made since the response of the two instruments was similar and the rod

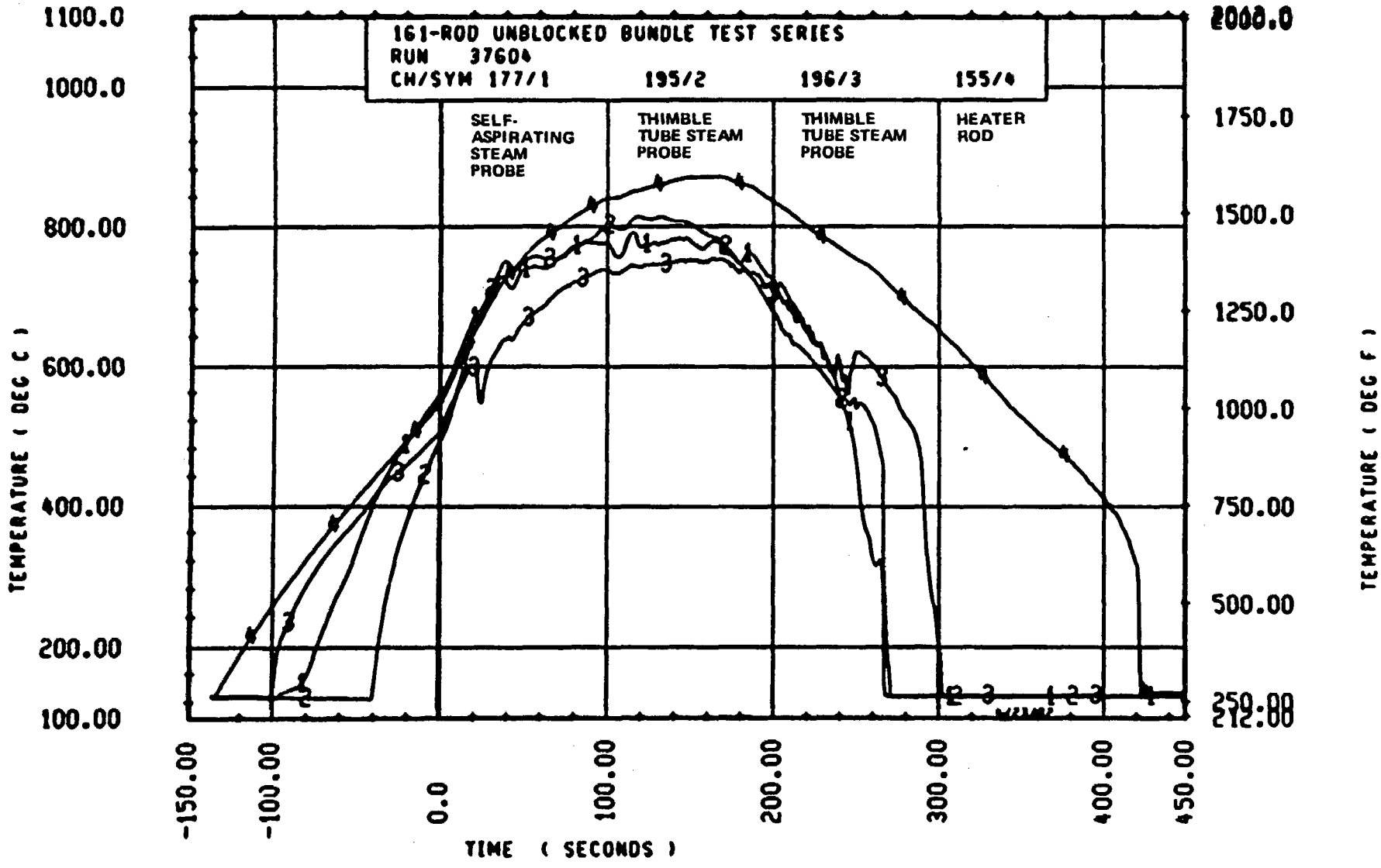

Figure J-3. Self-Aspirating Steam Probe Unblocked Bundle Test Results, 25.4 mm/sec (1 in./sec) Flooding Rate

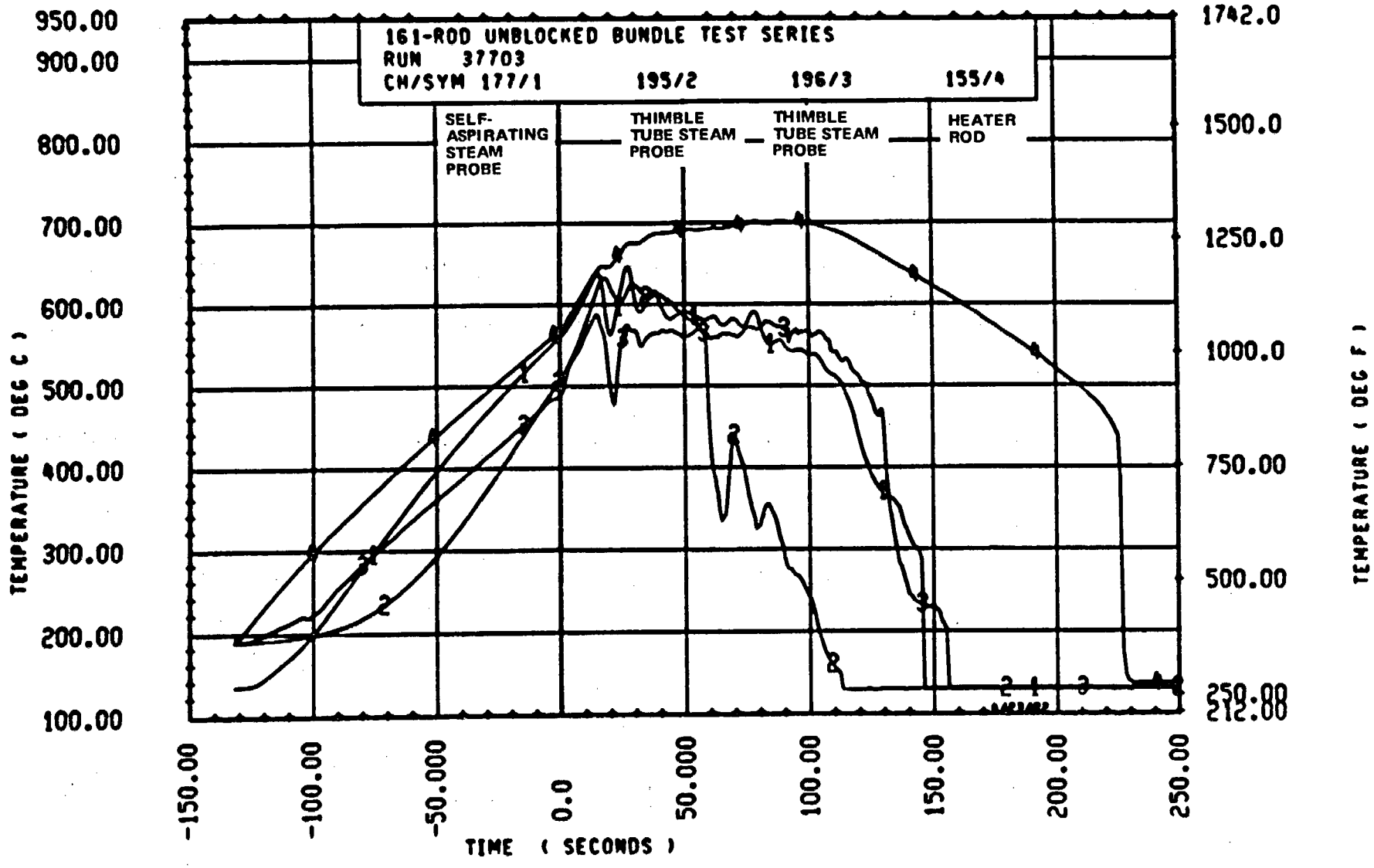

Figure J-4. Self-Aspirating Steam Probe Unblocked Bundle Test Results, 38.1 mm/sec (1.5 in./sec) Flooding Rate

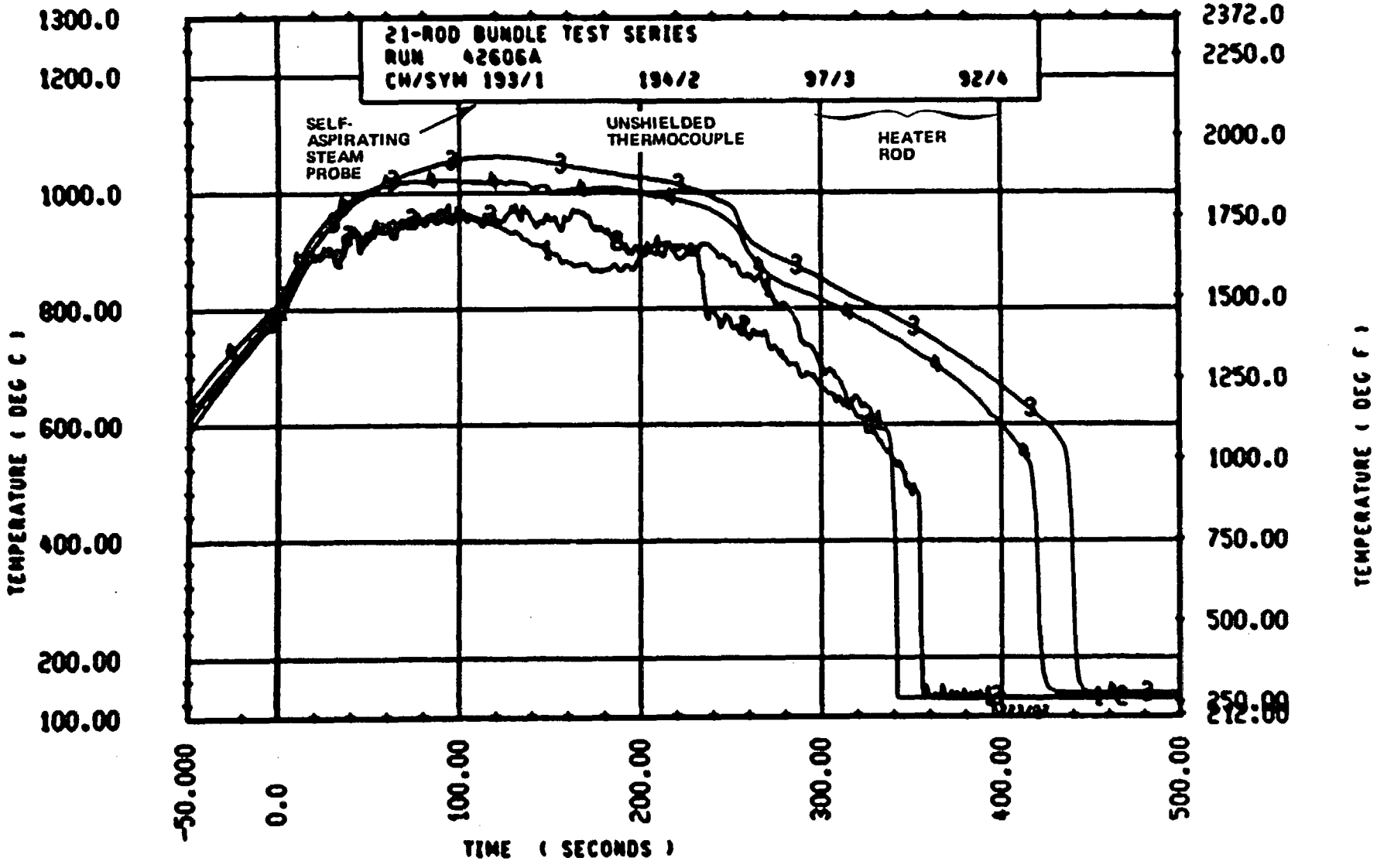

Figure J-5. Self-Aspirating Steam Probe 21-Rod Bundle Test Results, 1.98 m (78 in.) Elevation

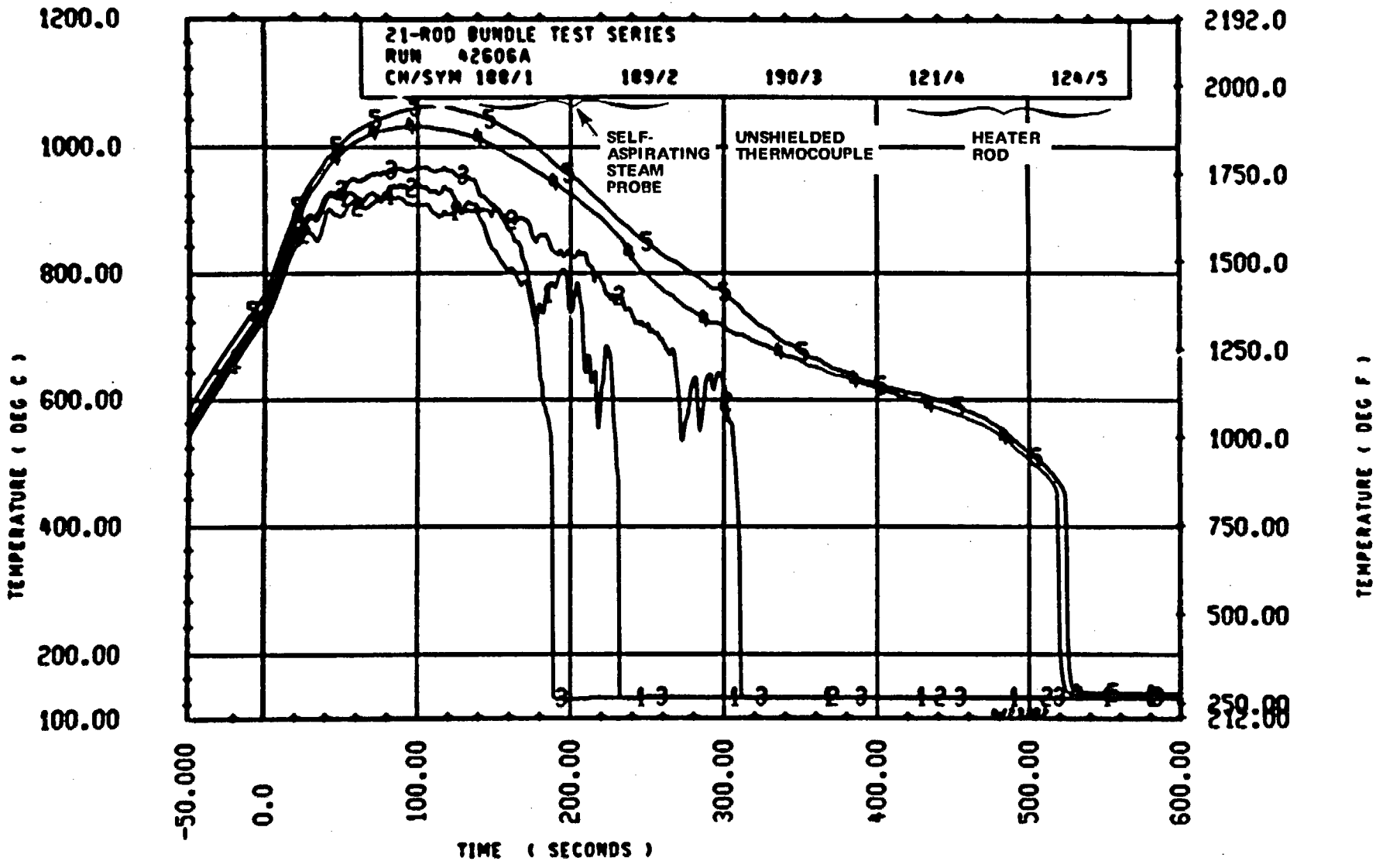

Figure J-6. Self-Aspirating Steam Probe 21-Rod Bundle Test Results, 2.29 m (90 in.) Elevation

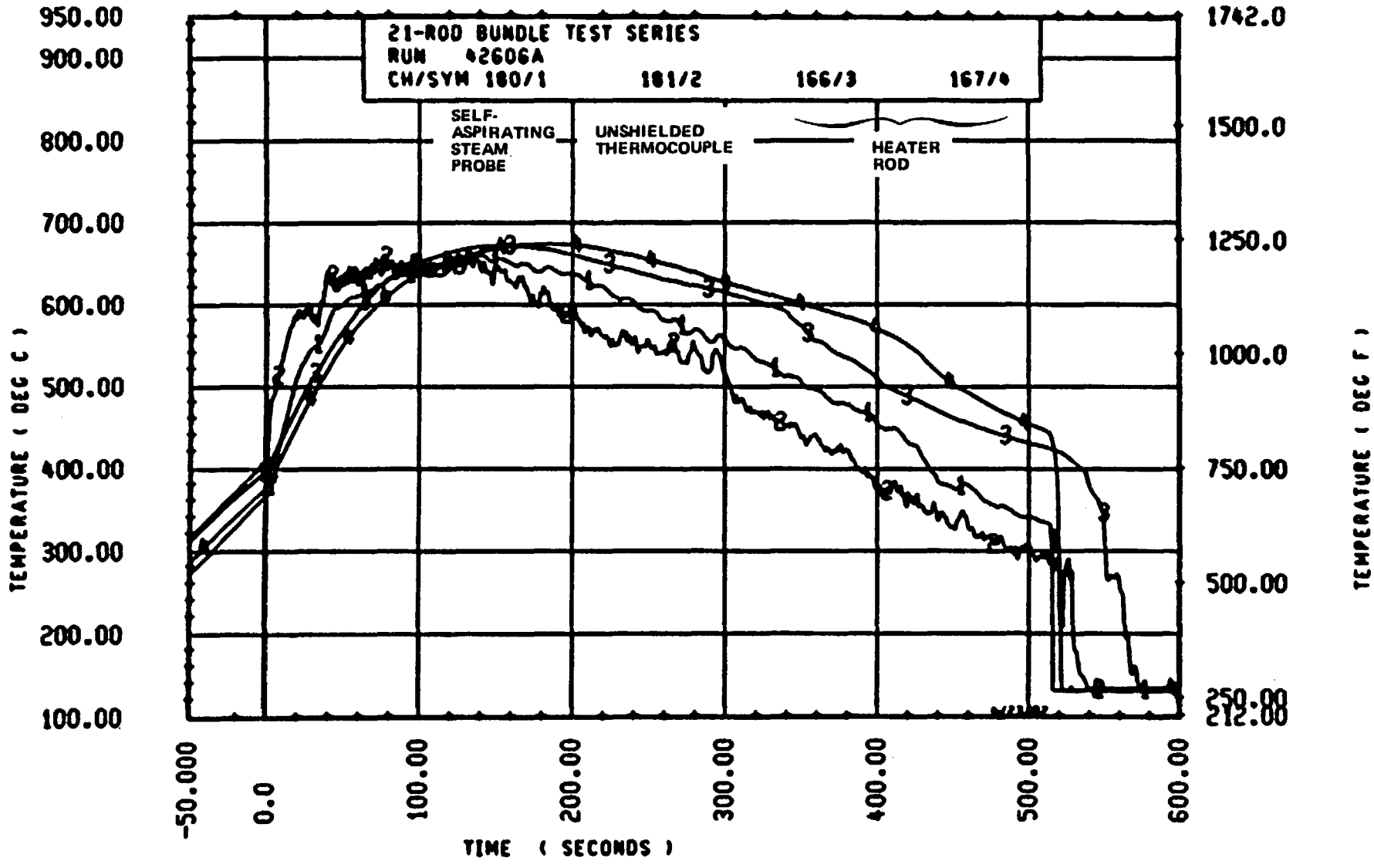

Figure J-7. Self-Aspirating Steam Probe 21-Rod Bundle Test Results, 3.05 m (120 in.) Elevation

temperatures were much lower than expected in the unblocked configuration, such that radiation effects were smaller. The differences in steam temperature instrumentation among six bundles are listed in table J-1.

The self-aspirating steam probes and unshielded thermocouples quenched prior to the heater rod thermocouples, as would be expected. However, there was a significant difference in quench times among the temperature instruments. The steam probes and unshielded thermocouple were attached to the grid straps and pointed in both the upstream and downstream directions. The instrumentation which pointed in the downstream direction quenched much earlier than the instrumentation which pointed in the upstream direction. The quench times for the steam temperature instruments and the heater rods for runs 42430A and 41907B are shown in figures J-8 and J-9, respectively. This phenomenon is attributed to a quench front moving up the instrument from the grid. This quench front may simply be water droplets which wet the grid and are subsequently swept along the instruments by the steam flow.

The temperature measurements of those instruments downstream of a grid appear to be unaffected by the premature quench. The quench temperatures for the steam temperature instrumentation downstream of the grid, as shown in figure J-10, indicate that the instrumentation quenches at a relatively high temperature. Therefore, the steam temperature data from all the instrumentation can be utilized in the evaluation of the blockage data.

J-5. CONCLUSIONS

The self-aspirating steam probe performed satisfactorily although the test conditions, specifically the heater rod temperatures, were much lower than originally expected. The self-aspirating steam probe was initially designed to be shielded from the radiation heat transfer of the high-temperature heater rods and quenching by the water droplets. The unshielded thermocouples performed better than originally anticipated, perhaps also because of the lower heater rod temperatures, and/or the evaporation and breakup of water droplets in the blockage zone, which subsequently limited the probability of quenching by the water droplets.

TABLE J-1

STEAM TEMPERATURE INSTRUMENTATION

Subchannel	Configuration A		Configurations B-F	
	Instrumentation Type,[a] Computer Channel No.	Elevation [m (in.)]	Instrumentation Type,[a] Computer Channel No.	Elevation [m (in.)]
9	SP, 203	0.97 (38)	BF, 177	0.89 (35)
10	SP, 202	1.22 (48)	BF, 178	1.19 (47)
15	SP, 201	1.50 (59)	BF, 179	1.47 (58)
10	SP, 200	1.50 (59)	SP, 180	1.47 (58)
Per[b]	SP, 199	1.70 (67)	BF, 182	1.70 (67)
11	SP, 198	1.70 (67)	SP, 184	1.70 (67)
9	SP, 197	1.70 (67)	SP, 183	1.70 (67)
8	SP, 196	1.70 (67)	BF, 181	1.70 (67)
7	SP, 195	1.88 (74)	-	-
8	BF, 194	1.98 (78)	BF, 186	1.96 (77)
9	SP, 193	1.98 (78)	SP, 187	1.96 (77)
11	SP, 192	1.98 (78)	SP, 188	1.96 (77)
6	SP, 191	1.98 (78)	BF, 185	1.96 (77)
6	BF, 190	2.29 (90)	BF, 189	2.26 (89)
10	SP, 189	2.29 (90)	SP, 191	2.26 (89)
7	SP, 188	2.29 (90)	BF, 190	2.26 (89)
5	SP, 187	2.29 (90)	SP, 192	2.26 (89)
10	SP, 186	2.44 (96)	SP, 195	2.46 (97)
8	SP, 185	2.44 (96)	BF, 193	2.46 (97)
9	SP, 184	2.44 (96)	BF, 194	2.46 (97)
10	SP, 183	2.82 (111)	SP, 197	2.77 (109)
5	SP, 182	2.82 (111)	BF, 196	2.77 (109)
14	BF, 181	3.05 (120)	BF, 198	3.05 (120)
15	SP, 180	3.05 (120)	SP, 200	3.05 (120)
6	SP, 179	3.05 (120)	SP, 199	3.05 (120)
11	SP, 178	3.35 (132)	BF, 201	3.30 (130)
6	SP, 177	3.51 (138)	BF, 202	3.51 (138)

a. SP = steam probe
BF = bare fluid thermocouple

b. Per = peripheral subchannel

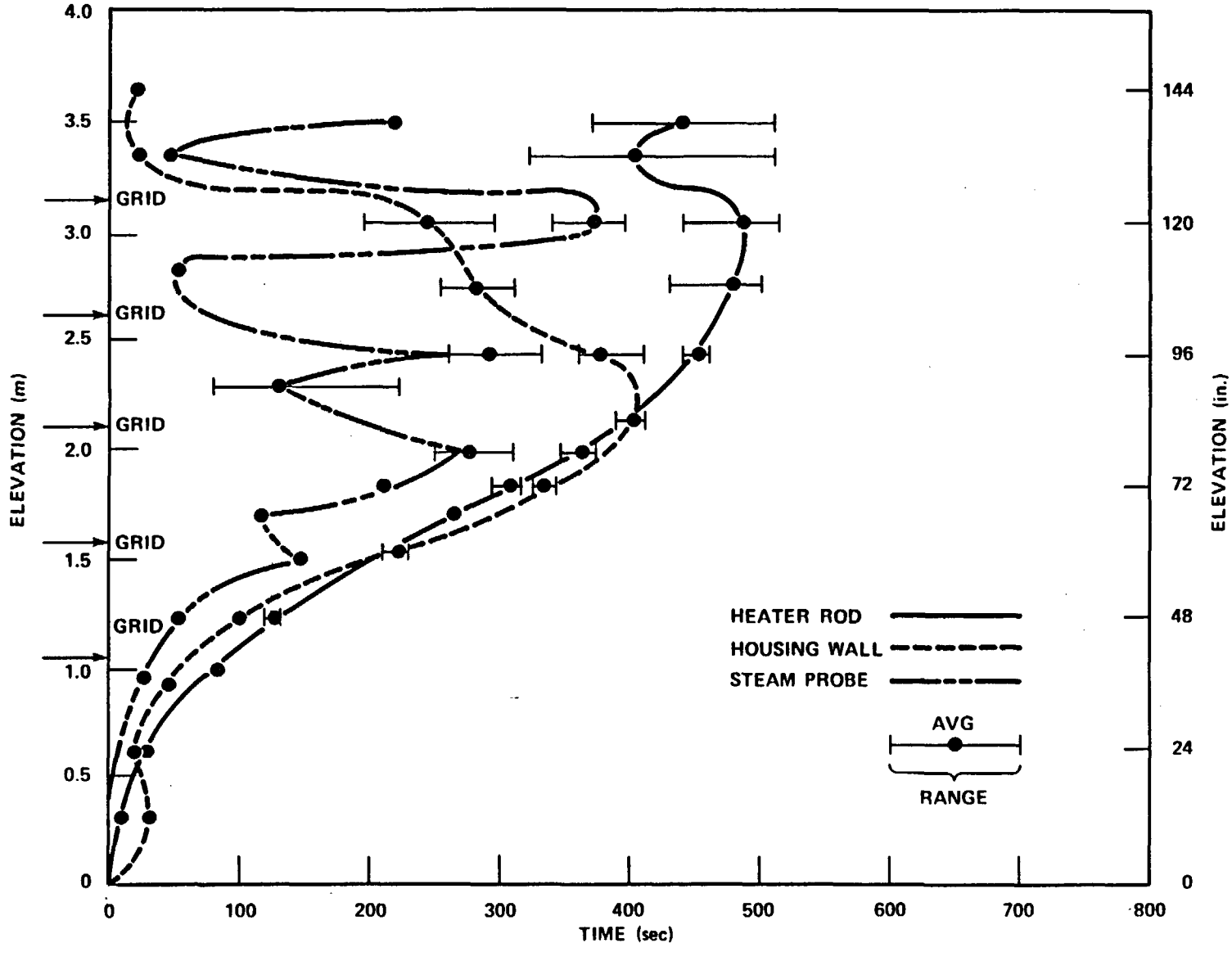

Figure J-8. Quench Curve for Rods, Housing, and Steam Probe, Run 42430A

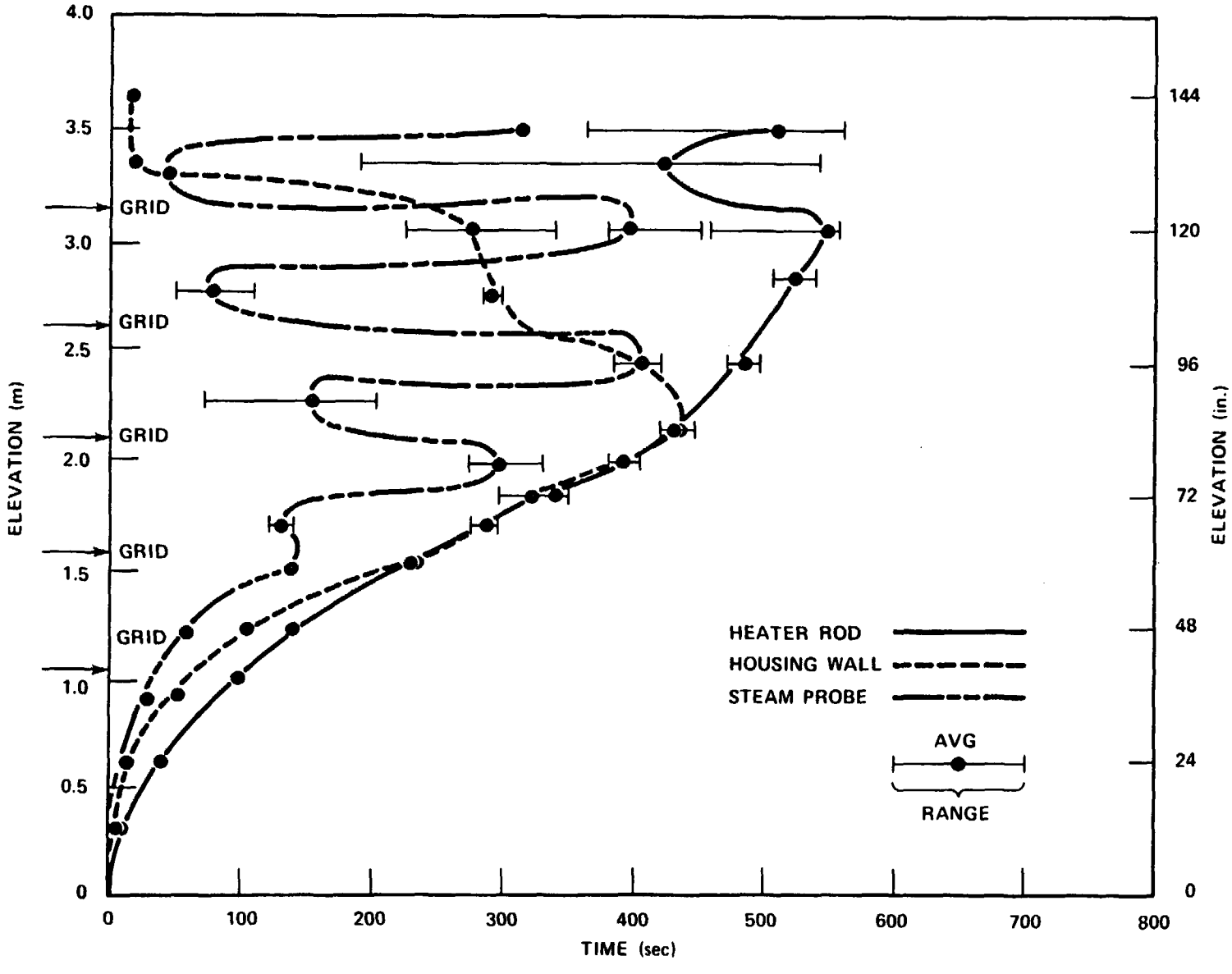

Figure J-9. Quench Curve for Rods, Housing, and Steam Probe, Run 41907B

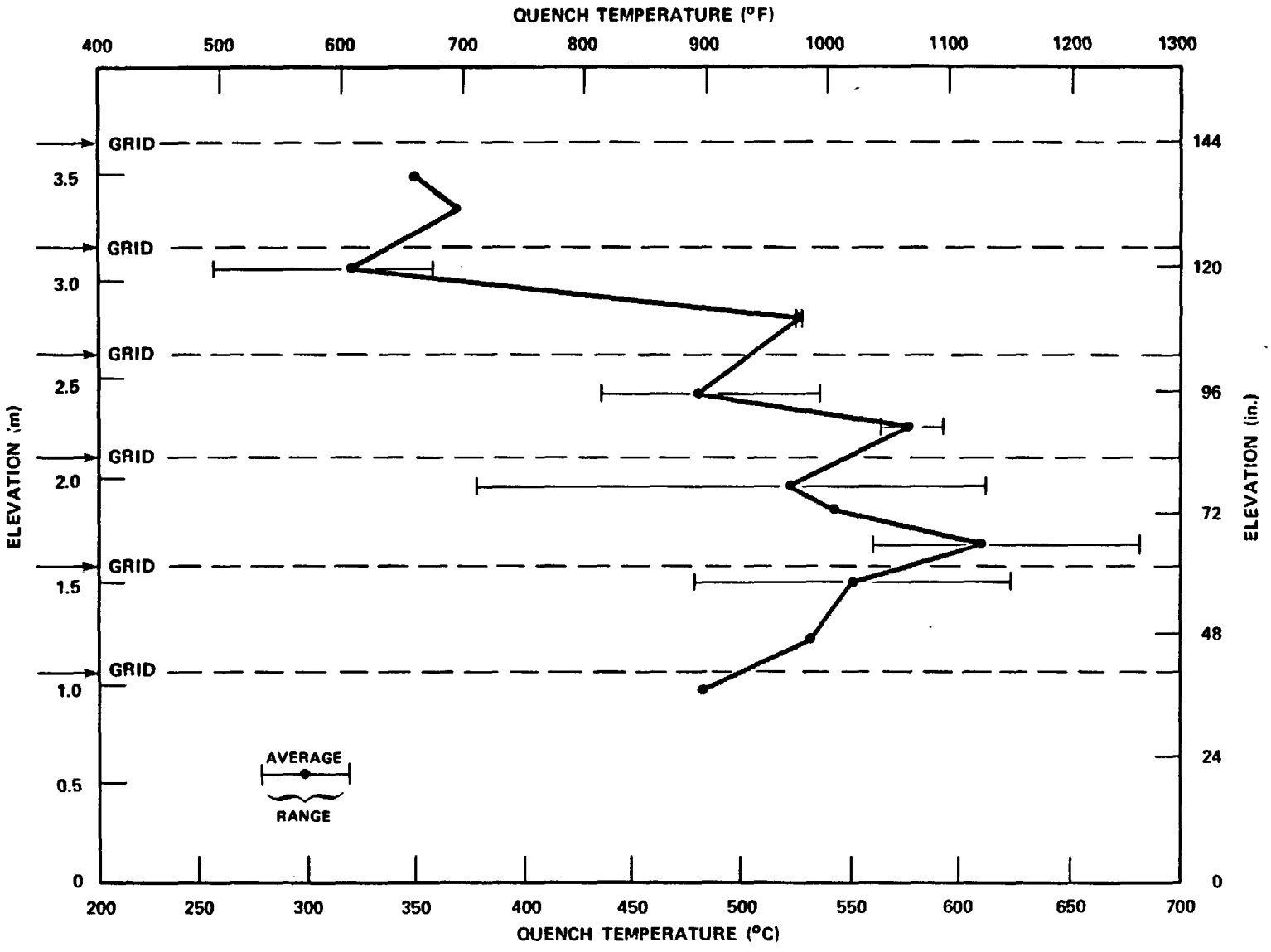

Figure J-10. Steam Probe Quench Temperature Versus Elevation, Run 42430A

NRC FORM 335 (7-77) U.S. NUCLEAR REGULATORY COMMISSION

BIBLIOGRAPHIC DATA SHEET

1. REPORT NUMBER *(Assigned by DDC)*
NUREG/CR-2444, Vol.1
EPRI NP-2014
WCAP-9992

4. TITLE AND SUBTITLE *(Add Volume No., if appropriate)*
PWR FLECHT SEASET 21-Rod Bundle Flow Blockage Task Data and Analysis Report, NRC/EPRI/Westinghouse Report No. 11. Main Report and Appendices A-J.

2. *(Leave blank)*

3. RECIPIENT'S ACCESSION NO.

7. AUTHOR(S)
M. J. Loftus, L. E. Hochreiter, N. Lee, M.F. McGuire, A. H. Wenzel, M. M. Valkovic

5. DATE REPORT COMPLETED
MONTH June YEAR 1982

9. PERFORMING ORGANIZATION NAME AND MAILING ADDRESS *(Include Zip Code)*
Westinghouse Electric Corporation
Nuclear Energy Systems
Post Office Box 355
Pittsburgh, Pennsylvania 15230

DATE REPORT ISSUED
MONTH September YEAR 1982

6. *(Leave blank)*

8. *(Leave blank)*

12. SPONSORING ORGANIZATION NAME AND MAILING ADDRESS *(Include Zip Code)*
U.S. Nuclear Regulatory Commission
Office of Nuclear Regulatory Research
Division of Accident Evaluation
Washington, D. C. 20555

Electric Power Research Institute
3412 Hillview Ave.
Palo Alto, CA 94303

10. PROJECT/TASK/WORK UNIT NO.

11. CONTRACT NO.
B6204

13. TYPE OF REPORT
Technical

PERIOD COVERED *(Inclusive dates)*
July 1981 - July 1982

15. SUPPLEMENTARY NOTES

14. *(Leave blank)*

16. ABSTRACT *(200 words or less)*

This report presents data and limited analysis from the 21-Rod Bundle Flow Blockage Task of the Full-Length Emergency Cooling Heat Transfer Sep rate Effects and Systems Effects Test Program (FLECHT-SEASET). The tests consisted of forced and gravity reflooding tests utilizing electrical heater rods with a cosine axial power profile to simulate PWR nuclear core fuel rod arrays. Steam cooling and hydraulic characteristics tests were also conducted. These tests were utilized to determine effects of various flow blockage configurations (shapes and distributions) on reflooding behavior, to aid in development/assessment of computational models on predicting reflooding behavior of flow blockage configurations, and to screen flow blockage configurations for future 163-rod flow blockage bundle tests.

17. KEY WORDS AND DOCUMENT ANALYSIS

17a. DESCRIPTORS

17b. IDENTIFIERS/OPEN-ENDED TERMS

18. AVAILABILITY STATEMENT
Unlimited

19. SECURITY CLASS *(This report)*
Unclassified

21. NO. OF PAGES

20. SECURITY CLASS *(This page)*
Unclassified

22. PRICE
$

NRC FORM 335 (7-77)

UNITED STATES
NUCLEAR REGULATORY COMMISSION
WASHINGTON, D.C. 20555

OFFICIAL BUSINESS
PENALTY FOR PRIVATE USE, $300

FOURTH CLASS MAIL
POSTAGE & FEES PAID
USNRC
WASH. D. C
PERMIT No G-67